KINETIC STUDIES AND MECHANISMS OF REDUCTION OF IRON(III) AND MANGANESE(III) COMPLEXES OF BIS(SALICYLIDENE)PHENYLENEDIAMINE BY SOME REDUCTANTS IN MIXED AQUEOUS AND SURFACTANT MEDIUM

BY

ISMAILA IBRAHIM

DEPARTMENT OF CHEMISTRY,
FACULTY OF PHYSICAL SCIENCE,
AHMADU BELLO UNIVERSITY,
ZARIA, NIGERIA

DECEMBER, 2021

KINETIC STUDIES AND MECHANISMS OF REDUCTION OF IRON(III) AND MANGANESE(III) COMPLEXES OF BIS(SALICYLIDENE)PHENYLENEDIAMINE BY SOME REDUCTANTS IN MIXED AQUEOUS AND SURFACTANT MEDIUM

BY

Ismaila IBRAHIM
B. Sc. (ABU, 2012), M. Sc. (ABU, 2016)
P16PSCH9024

A THESIS SUBMITTED TO THE SCHOOL OF POSTGRADUATE STUDIES, AHMADU BELLO UNIVERSITY, IN PARTIAL FULFILLMENT OF THE REQUIREMENTS FOR THE AWARD OF A DOCTOR OF PHILOSOPHY DEGREE IN INORGANIC CHEMSTRY

DEPARTMENT OF CHEMISTRY,
FACULTY OF PHYSICAL SCIENCES,
AHMADU BELLO UNIVERSITY,
ZARIA, NIGERIA

DECEMBER, 2021

DECLARATION

I declare that the work in this thesis entitled "Kinetic studies and mechanisms of reduction of iron(III) and manganese(III) complexes of bis(salicylidene)phenylenediamine by some reductants in mixed aqueous and surfactant medium" has been carried out by me in the Department of Chemistry of Ahmadu Bello University, Zaria. The information derived from the literature has been duly acknowledged in the text and a list of references provided. No part of this thesis was previously presented for another degree or diploma at this or any other institution.

Ismaila IBRAHIM _____ _____

Signature Date

CERTIFICATION

This thesis entitled "**Kinetic studies and mechanisms of reduction of iron(III) and manganese(III) complexes of bis(salicylidene)phenylenediamine by some reductants in mixed aqueous and surfactant medium**" by Ismaila IBRAHIM meets the regulations governing the award of the degree of Doctor of Philosophy in Inorganic Chemistry of Ahmadu Bello University, and is approved for its contribution to knowledge and literary presentation.

Prof. S. O. Idris	_____	_____
Chairman, Supervisory Committee	Signature	Date
Dr. I. Abdulkadir	_____	_____
Member, Supervisory Committee	Signature	Date
Dr. A. D. Onu	_____	_____
Member, Supervisory Committee	Signature	Date
Prof. G. I. Ndukwe	_____	_____
Head of Department	Signature	Date
Prof. A. A. Sani	_____	_____
Dean, School of Postgraduate Studies	Signature	Date

DEDICATION

This work is dedicated to my parents, Mallam Sani B. Ibrahim and Hulera Ibrahim, may Allah (S.W.T) reward them abundantly! Amen.

ACKNOWLEDGEMENT

All praise is to Almighty Allah, the Creator and Sustainer of the universe for sparing my life, guarding and guiding me throughout this research work. All Glory is due to Him, The Lord of the Day of Judgement. May His Peace and Blessings be onto His Noble Prophet (S. A. W), the Seal of Prophets.

My profound gratitude goes to my resourceful supervisors, Prof. S. O. Idris, Dr. I. Abdulkadir and Dr. A. D. Onu for their invaluable suggestions, expertise, counseling and intellectual contributions to the success of this work. I also acknowledge their support, motivation, encouragement, guidance, training and mentorship.

I would like to thank the Head of Department, Prof. G. I. Ndukwe, and also Prof. E. B. Agbaji, Prof. A. Uzairu, Prof. A. O. Oyewale, Prof. M. S. Sallau, Dr. G. A. Shallangwa, Dr. J. D. Habila, Dr. H. Ibahim, Dr. S. Uba, Dr. A. B. Aliyu, Dr. Z. N. Garba, Dr. Z. I. Yashim, Dr.(Mrs) O.R.A Iyun, Mrs S. A. Hamza and the entire staff of the Department for their support and encouragement. I wish to also thank Mr. S. K. Musa, the Departmental Chief Technologist, the entire Departmental Technical staff and members of staff of Multi User Science Research Laboratory, Ahmadu Bello University Zaria for their assistance.

I also wish to acknowledge the the management of Petroleum Technology Development Fund (PTDF), for sponsoring the programme under PTDF Local Scholarship Scheme (LSS-PhD) number PTDF/ED/LSS/PHD/II/0346/19.

My sincere appreciation goes to my Dad, Mallam Sani B. Ibrahim, my Mum, Hulera Ibrahim and the entire members of my family. I must thank them for among others, the moral and spiritual upbringing, support and encouragement, without which I could not have reached this height.

I also wish to thank Dr Isah Adamu of Niger State Universal Basic Education Board (NSUBEB), for his support and encouragement. Also acknowledged are Dr. B. Anweting, Dr. A. Busari, Dr. B. Myek, Dr. A. Adetoro, Dr. M. T. Ibrahim, Dr. A. B. Umar, Mr. N. Oladunni, Mrs. S. Abdulsalam, Mrs. M. Imam, Mr. A. Haruna, Dr. A. Usman, Mr. I. U. Nkole, Mr. Z. Y. Ibrahim, Mr. Y. Ahmed, Mr. S. Ilyasu, Mr. U. Hassan, Mr. M. Ibrahim and Mr. L. Upahi.

May the blessings of Almighty Allah be on all the people that contributed towards the success of my research in Ahmadu Bello University, Zaria.

ABSTRACT

The kinetics of reduction of N,N′-phenylenebis(salicylideneiminato)iron(III) ($[Fe(salphen)]^+$) at 435 nm by thioglycolic acid, oxalic acid, hypophosphorous acid and hydrogen peroxide and reduction of N,N′-phenylenebis(salicylideneiminato)manganese(III) ($[Mn(salphen)]^+$) at 450 nm by hydrogen peroxide, thioglycolic acid, thioglycol, thiocyanate ion, thiosemicarbazide and thiodiglycol were studied in mixed aqueous and surfactant medium under pseudo-first order conditions. A stoichiometry of 1:1 was obtained for $[Fe(salphen)]^+$ – TSH reaction while 2:1 (complex:reductant) was obtained for $[Fe(salphen)]^+ – H_3PO_2$ and $[Fe(salphen)]^+ – H_2O_2$ reactions and 2:3 (complex:reductant) for $[Fe(salphen)]^+ – H_2C_2O_4$ reaction. Also, a stoichiometry of 1:1 was obtained for $[Mn(salphen)]^+$ – TSH, $[Mn(salphen)]^+$ – RSH, and $[Mn(salphen)]^+ – SCN^-$ reactions while 2:1 (complex:reductant) was obtained for $[Mn(salphen)]^+ – H_2O_2$, $[Mn(salphen)]^+ – H_2NNHCSNH_2$ and $[Mn(salphen)]^+ – S(CH_2CH_2OH)_2$ reactions. The reactions were first order in [oxidant] and [reductant] in all the systems. The $[Fe(salphen)]^+$-TSH, $[Fe(salphen)]^+ – H_2C_2O_4$, $[Fe(salphen)]^+ – H_3PO_2$, $[Mn(salphen)]^+$ – TSH, $[Mn(salphen)]^+ – SCN^-$ and $[Mn(salphen)]^+ – H_2NNHCSNH_2$ reactions were independent of $[H^+]$ while $[Fe(salphen)]^+ – H_2O_2$, $[Mn(salphen)]^+ – H_2O_2$ and $[Mn(salphen)]^+ – S(CH_2CH_2OH)_2$ reactions showed an inverse $[H^+]$ dependence with non-zero intercept but $[Mn(salphen)]^+$ – RSH reaction showed a positive $[H^+]$ dependence. The reactions conform to the following rate equations:

$$\frac{-d[Msalphen^+]}{dt} = k_2[M(salphen)^+][A]$$

$$\frac{-3}{2}\frac{d[Fesalphen^+]}{dt} = k_2[Fe(salphen)^+][H_2C_2O_4]$$

$$\frac{-1}{2}\frac{d[Msalphen^+]}{dt} = k_2[M(salphen)^+][B]$$

$$\frac{-1}{2}\frac{d[Msalphen^+]}{dt} = (a + \frac{b}{[H^+]})[M(salphen)^+][C]$$

$$\frac{-d[Mnsalphen^+]}{dt} = (e + f[H^+])[Mn(salphen)^+][RSH]$$

where M = Fe or Mn, A = TSH or SCN^-, B = H_3PO_2 or $H_2NNHCSNH_2$ and C = H_2O_2 or $S(CH_2CH_2OH)_2$

The rates of reactions displayed a negative salt effect in $[Fe(salphen)]^+$ – H_2O_2, $[Mn(salphen)]^+$ – H_2O_2, $[Mn(salphen)]^+$ – SCN^- and $[Mn(salphen)]^+$ – $S(CH_2CH_2OH)_2$ reactions respectively, a positive salt effect in $[Mn(salphen)]^+$ – RSH reaction and a zero salt effect in $[Fe(salphen)]^+$ – TSH, $[Fe(salphen)]^+$ – H_3PO_2, $[Fe(salphen)]^+$ – $H_2C_2O_4$, $[Mn(salphen)]^+$ – TSH and $[Mn(salphen)]^+$ – $H_2NNHCSNH_2$ reactions respectively. Added ion catalysis/ or inhibition was observed in all the reactions studied except the reaction of $[Fe(salphen)]^+$ with $H_2C_2O_4$ where neither catalysis nor reaction inhibition was observed. There was no evidence of an intermediate complex of significant stability for all the reactions except the reactions of H_2O_2 with $[Fe(salphen)]^+$ and $[Mn(salphen)]^+$ where it was observed from Michaelis-Menten plot. Free radicals were detected in all the reactions except the reaction of $H_2C_2O_4$ with $[Fe(salphen)]^+$. The reaction rates were catalysed/ or inhibited in the presence of surfactants (SDS and CTAB) and Piszkiewicz model was used to analyze the results which indicated the existence of significant electrostatic and hydrophobic interactions between the metal complexes and the pre-micellar aggregates of the surfactants. Based on the results obtained, outersphere mechanistic pathway is proposed for all the reactions under investigation.

TABLE OF CONTENTS

	Page
Cover Page	i
Fly Leaf	ii
Title Page	iii
Declaration	iv
Certification	v
Dedication	vi
Acknowledgement	vii
Abstract	viii
Table of Contents	x
List of Tables	xv
List of Figures	xix
List of Schemes	xxviii
List of Appendices	xxix
Abbreviations	xxx
CHAPTER ONE	
1.0 INTRODUCTION	**1**
1.1 Statement of the Research Problem	**3**
1.2 Justification of the Study	**5**
1.3 Aim and Objectives of the Research	**6**
CHAPTER TWO	
2.0 LITERATURE REVIEW	**8**

2.1 Reactions of N,N′-Phenylenebis(salicylideneiminato)iron(III) and Manganese(III) Complexes 8

2.2 Reactions of Thioglycolic Acid 11

2.3 Reactions of Oxalic Acid 12

2.4 Reactions of Hypophosphorous Acid 14

2.5 Reactions of Hydrogen Peroxide 15

2.6 Reactions of Thioglycol 17

2.7 Reactions of Thiocyanate Ion 19

2.8 Reactions of Thiosemicarbazide 21

2.9 Reactions of Thiodiglycol 22

2.10 Reactions of Sodium Dodecyl Sulphate 25

2.11 Reactions of Cetyltrimethylammonium Bromide 26

CHAPTER THREE

3.0 MATERIALS AND METHODS 28

3.1 Materials 28

3.1.1 Chemical and reagents 28

3.1.2 Equipment 29

3.1.3 Preparation of DMSO:H_2O (1:4 v/v) mixed solution 29

3.1.4 Preparation of stock thioglycolic acid solution 29

3.1.5 Preparation of stock oxalic acid solution 29

3.1.6 Preparation of hypophosphorous acid stock solution 29

3.1.7 Preparation of sodium thiosulphate solution 30

3.1.8 Preparation of stock hydrogen peroxide solution 30

3.1.9 Preparation of stock thioglycol solution 30

3.1.10 Preparation of stock potassium thiocyanate solution 30

3.1.11 Preparation of stock thiosemicarbazide solution 30

3.1.12 Preparation of stock thiodiglycol solution 31

3.1.13 Preparation of stock sodium dodecyl sulphate solution 31

3.1.14 Preparation of stock cetyltrimethylammonium bromide solution 31

3.1.15 Preparation of stock sodium chloride solution 31

3.1.16 Preparation of stock sodium carbonate solution 31

3.1.17 Preparation of hydrochloric acid stock solution 31

3.1.18 Preparation of stock salt solutions 32

3.2 Methods 32

3.2.1 Synthesis of Fe(III) and Mn(III) – salphen complexes 32

3.2.2 Stoichiometry 34

3.2.3 Products analysis 36

3.2.4 Determination of reactions order 37

3.2.5 Determination of effect of acid on the reactions rate 37

3.2.6 Determination of effect of ionic strength and dielectric constant 38

3.2.7 Determination of effect of added of ions 38

3.2.8 Determination of effect of temperature on the reactions rate 38

3.2.9 Test for intermediate complex formation 39

3.2.10 Test for free radicals 39

3.2.11 Determination of critical micelle concentration 39

3.2.12 Determination of effect of surfactant concentrations on the reactions rate 39

CHAPTER FOUR

4.0 RESULTS 41

4.1 Synthesis of Fe(III) and Mn(III) – salphen complexes 41

4.2 Stoichiometric Studies 41

4.3 Products Analysis 42

4.4 Order of the Reactions 54

4.5 Effect of Acid on the Reactions Rate 86

4.6 Effect of Changes in Ionic Strength and Dielectric Constant on the Reactions Rate 95

4.7 Effect of Added Ions on the Reactions Rate 101

4.8 Effect of Temperature on the Reactions Rate 154

4.9 Test for Intermediate Complex Formation 154

4.9.1 Spectrophotometric test 154

4.9.2 Michaelis – Menten plots 154

4.10 Free radicals 215

4.11 Effect of Surfactants on the Reactions Rate 215

4.11.1 Critical micelle concentration 215

4.11.2 Influence of surfactants on the reactions rate 215

CHAPTER FIVE

5.0 DISCUSSIONS 248

5.1 Synthesis of $[Fe(salphen)]^+$ and $[Mn(salphen)]^+$ Ions 248

5.2 Reactions of TSH with $[Fe(salphen)]^+$ and $[Mn(salphen)]^+$ 249

5.3 Reaction of $H_2C_2O_4$ with $[Fe(salphen)]^+$ 254

5.4 Reaction of H_3PO_2 with $[Fe(salphen)]^+$ 258

5.5 Reactions of H_2O_2 with $[Fe(salphen)]^+$ and $[Mn(salphen)]^+$ 262

5.6 Reaction of RSH with $[Mn(salphen)]^+$ 268

5.7 Reaction of SCN^- with $[Mn(salphen)]^+$ 271

5.8 Reaction of $H_2NNHCSNH_2$ with $[Mn(salphen)]^+$ 275

5.9 Reaction of $S(CH_2CH_2OH)_2$ with $[Mn(salphen)]^+$ 280

5.10 Reaction Rate in the Presence of Surfactants 285

5.10.1 Critical micelle concentration of surfactants 285

5.10.2 Kinetic model for the effect of surfactants on the reactions rate 286

5.10.3 Reaction mechanism in the presence of surfactants 289

CHAPTER SIX

6.0 SUMMARY, CONCLUSION AND RECOMMENDATIONS 295

6.1 Summary 295

6.2 Conclusion 296

6.3 Recommendations 297

REFERENCES 298

APPENDICES 322

LIST OF TABLES

4.1	Pseudo-first order and second order rate constants for the reaction of $[Fe(salphen)]^+$ and TSH	75
4.2	Pseudo-first order and second order rate constants for the reaction of $[Fe(salphen)]^+$ and $H_2C_2O_4$	76
4.3	Pseudo-first order and second order rate constants for the reaction of $[Fe(salphen)]^+$ and H_3PO_2	77
4.4	Pseudo-first order and second order rate constants for the reaction of $[Fe(salphen)]^+$ and H_2O_2	78
4.5	Pseudo-first order and second order rate constants for the reaction of $[Mn(salphen)]^+$ and H_2O_2	79
4.6	Pseudo-first order and second order rate constants for the reaction of $[Mn(salphen)]^+$ and TSH	80
4.7	Pseudo-first order and second order rate constants for the reaction of $[Mn(salphen)]^+$ and RSH	81
4.8	Pseudo-first order and second order rate constants for the reaction of $[Mn(salphen)]^+$ and SCN^-	82
4.9	Pseudo-first order and second order rate constants for the reaction of $[Mn(salphen)]^+$ and $H_2NNHCSNH_2$	83
4.10	Pseudo-first order and second order rate constants for the reaction of $[Mn(salphen)]^+$ and $S(CH_2CH_2OH)_2$	84
4.11	Acid dependence effect on the rate of reaction of $[Mn(salphen)]^+$ and TSH	87
4.12	Acid dependence effect on the rate of reaction of $[Fe(salphen)]^+$ and TSH	88
4.13	Acid dependence effect on the rate of reaction of $[Fe(salphen)]^+$ and $H_2C_2O_4$	89
4.14	Acid dependence effect on the rate of reaction of $[Fe(salphen)]^+$ and H_3PO_2	90
4.15	Effect of dielectric constant on the rate of reaction of $[Fe(salphen)]^+$ and TSH	102
4.16	Effect of dielectric constant on the rate of reaction of $[Fe(salphen)]^+$ and $H_2C_2O_4$	103

4.17	Effect of dielectric constant on the rate of reaction of $[Fe(salphen)]^+$ and H_3PO_2	104
4.18	Effect of dielectric constant on the rate of reaction of $[Fe(salphen)]^+$ and H_2O_2	105
4.19	Effect of dielectric constant on the rate of reaction of $[Mn(salphen)]^+$ and TSH	106
4.20	Effect of dielectric constant on the rate of reaction of $[Mn(salphen)]^+$ and H_2O_2	107
4.21	Effect of dielectric constant on the rate of reaction of $[Mn(salphen)]^+$ and SCN^-	108
4.22	Effect of dielectric constant on the rate of reaction of $[Mn(salphen)]^+$ and $H_2NNHCSNH_2$	109
4.23	Effect of dielectric constant on the rate of reaction of $[Mn(salphen)]^+$ and $S(CH_2CH_2OH)_2$	110
4.24	Effect of dielectric constant on the rate of reaction of $[Mn(salphen)]^+$ and RSH	111
4.25	Effect of added cations on the rate of reaction of $[Fe(salphen)]^+$ and $H_2C_2O_4$	118
4.26	Effect of added cations on the rate of reaction of $[Fe(salphen)]^+$ and TSH	119
4.27	Effect of added cations on the rate of reaction of $[Fe(salphen)]^+$ and H_3PO_2	120
4.28	Effect of added cations on the rate of reaction of $[Fe(salphen)]^+$ and H_2O_2	121
4.29	Effect of added cations on the rate of reaction of $[Mn(salphen)]^+$ and TSH	122
4.30	Effect of added cations on the rate of reaction of $[Mn(salphen)]^+$ and $H_2NNHCSNH_2$	123
4.31	Effect of added cations on the rate of reaction of $[Mn(salphen)]^+$ and H_2O_2	124
4.32	Effect of added cations on the rate of reaction of $[Mn(salphen)]^+$ and RSH	125
4.33	Effect of added cations on the rate of reaction of $[Mn(salphen)]^+$ and SCN^-	126

4.34	Effect of added cations on the rate of reaction of $[Mn(salphen)]^+$ and $S(CH_2CH_2OH)_2$	127
4.35	Effect of added anions on the rate of reaction of $[Fe(salphen)]^+$ and $H_2C_2O_4$	146
4.36	Effect of added anions on the rate of reaction of $[Fe(salphen)]^+$ and TSH	147
4.37	Effect of added anions on the rate of reaction of $[Fe(salphen)]^+$ and H_3PO_2	148
4.38	Effect of added anions on the rate of reaction of $[Fe(salphen)]^+$ and H_2O_2	149
4.39	Effect of added anions on the rate of reaction of $[Mn(salphen)]^+$ and TSH	150
4.40	Effect of added anions on the rate of reaction of $[Mn(salphen)]^+$ and RSH	151
4.41	Effect of added anions on the rate of reaction of $[Mn(salphen)]^+$ and SCN^-	152
4.42	Effect of added anions on the rate of reaction of $[Mn(salphen)]^+$ and $H_2NNHCSNH_2$	153
4.43	Effect of added anions on the rate of reaction of $[Mn(salphen)]^+$ and H_2O_2	155
4.44	Effect of added anions on the rate of reaction of $[Mn(salphen)]^+$ and $S(CH_2CH_2OH)_2$	156
4.45	Temperature dependent rate constants and activation parameters for the reaction of $[Fe(salphen)]^+$ and TSH	175
4.46	Temperature dependent rate constants and activation parameters for the reaction of $[Fe(salphen)]^+$ and $H_2C_2O_4$	176
4.47	Temperature dependent rate constants and activation parameters for the reaction of $[Fe(salphen)]^+$ and H_3PO_2	177
4.48	Temperature dependent rate constants and activation parameters for the reaction of $[Fe(salphen)]^+$ and H_2O_2	178
4.49	Temperature dependent rate constants and activation parameters for the reaction of $[Mn(salphen)]^+$ and H_2O_2	179

4.50	Temperature dependent rate constants and activation parameters for the reaction of $[Mn(salphen)]^+$ and TSH	180
4.51	Temperature dependent rate constants and activation parameters for the reaction of $[Mn(salphen)]^+$ and RSH	181
4.52	Temperature dependent rate constants and activation parameters for the reaction of $[Mn(salphen)]^+$ and SCN^-	182
4.53	Temperature dependent rate constants and activation parameters for the reaction of $[Mn(salphen)]^+$ and $H_2NNHCSNH_2$	183
4.54	Temperature dependent rate constants and activation parameters for the reaction of $[Mn(salphen)]^+$ and $S(CH_2CH_2OH)_2$	184
4.55	Variation of specific conductance of surfactant with surfactant concentration	216
4.56	Surfactant dependent rate constants and Piszkiewicz parameters for the reaction of $[Fe(salphen)]^+$ and TSH	223
4.57	Surfactant dependent rate constants and Piszkiewicz parameters for the reaction of $[Fe(salphen)]^+$ and $H_2C_2O_4$	224
4.58	Surfactant dependent rate constants and Piszkiewicz parameters for the reaction of $[Mn(salphen)]^+$ and TSH	225
4.59	Surfactant dependent rate constants and Piszkiewicz parameters for the reaction of $[Mn(salphen)]^+$ and SCN^-	226
4.60	Surfactant dependent rate constants and Piszkiewicz parameters for the reaction of $[Mn(salphen)]^+$ and $S(CH_2CH_2OH)_2$	227
4.61	Surfactant dependent rate constants and Piszkiewicz parameters for the reaction of $[Fe(salphen)]^+$ and H_2O_2	229
4.62	Surfactant dependent rate constants and Piszkiewicz parameters for the reaction of $[Mn(salphen)]^+$ and H_2O_2	230
4.63	Surfactant dependent rate constants and Piszkiewicz parameters for the reaction of $[Mn(salphen)]^+$ and RSH	231

LIST OF FIGURES

4.1	Plot of absorbance versus mole ratio for the reaction of $[Fe(salphen)]^+$ and TSH	43
4.2	Plot of absorbance versus mole ratio for the reaction of $[Fe(salphen)]^+$ and $H_2C_2O_4$	44
4.3	Plot of absorbance versus mole ratio for the redox reaction of $[Fe(salphen)]^+$ and H_3PO_2	45
4.4	Plot of absorbance versus mole ratio for the redox reaction of $[Fe(salphen)]^+$ and H_2O_2	46
4.5	Plot of absorbance versus mole ratio for the redox reaction of $[Mn(salphen)]^+$ and H_2O_2	47
4.6	Plot of absorbance versus mole ratio for the redox reaction of $[Mn(salphen)]^+$ and TSH	48
4.7	Plot of absorbance versus mole ratio for the redox reaction of $[Mn(salphen)]^+$ and RSH	49
4.8	Plot of absorbance versus mole ratio for the redox reaction of $[Mn(salphen)]^+$ and SCN^-	50
4.9	Plot of absorbance versus mole ratio for the redox reaction of $[Mn(salphen)]^+$ and $H_2NNHCSNH_2$	51
4.10	Plot of absorbance versus mole ratio for the redox reaction of $[Mn(salphen)]^+$ and $S(CH_2CH_2OH)_2$	52
4.11	Typical pseudo-first order plot for the redox reaction of $[Fe(salphen)]^+$ and TSH	55
4.12	Typical pseudo-first order plot for the redox reaction of $[Fe(salphen)]^+$ and $H_2C_2O_4$	56
4.13	Typical pseudo-first order plot for the redox reaction of $[Fe(salphen)]^+$ and H_3PO_2	57
4.14	Typical pseudo-first order plot for the redox reaction of $[Fe(salphen)]^+$ and H_2O_2	58
4.15	Typical pseudo-first order plot for the redox reaction of $[Mn(salphen)]^+$ and H_2O_2	59
4.16	Typical pseudo-first order plot for the redox reaction of $[Mn(salphen)]^+$ and TSH	60

4.17	Typical pseudo-first order plot for the redox reaction of $[Mn(salphen)]^+$ and RSH	61
4.18	Typical pseudo-first order plot for the redox reaction of $[Mn(salphen)]^+$ and SCN^-	62
4.19	Typical pseudo-first order plot for the redox reaction of $[Mn(salphen)]^+$ and $H_2NNHCSNH_2$	63
4.20	Typical pseudo-first order plot for the redox reaction of $[Mn(salphen)]^+$ and $S(CH_2CH_2OH)_2$	64
4.21	Plot of log k_1 versus log [TSH] for the redox reaction of $[Fe(salphen)]^+$ and TSH	65
4.22	Plot of log k_1 versus log $[H_2C_2O_4]$ for the redox reaction of $[Fe(salphen)]^+$ and $H_2C_2O_4$	66
4.23	Plot of log k_1 versus log $[H_3PO_2]$ for the redox reaction of $[Fe(salphen)]^+$ and H_3PO_2	67
4.24	Plot of log k_1 versus log $[H_2O_2]$ for the redox reaction of $[Fe(salphen)]^+$ and H_2O_2	68
4.25	Plot of log k_1 versus log $[H_2O_2]$ for the redox reaction of $[Mn(salphen)]^+$ and H_2O_2	69
4.26	Plot of log k_1 versus log [TSH] for the redox reaction of $[Mn(salphen)]^+$ and TSH	70
4.27	Plot of log k_1 versus log [RSH] for the redox reaction of $[Mn(salphen)]^+$ and RSH	71
4.28	Plot of log k_1 versus log $[SCN^-]$ for the redox reaction of $[Mn(salphen)]^+$ and SCN^-	72
4.29	Plot of log k_1 versus log $[H_2NNHCSNH_2]$ for the redox reaction of $[Mn(salphen)]^+$ and $H_2NNHCSNH_2$	73
4.30	Plot of log k_1 versus log $[S(CH_2CH_2OH)_2]$ for the redox reaction of $[Mn(salphen)]^+$ and $[S(CH_2CH_2OH)_2]$	74
4.31	Plot of k_2 versus $1/[H^+]$ for the redox reaction of $[Fe(salphen)]^+$ and H_2O_2	91
4.32	Plot of k_2 versus $1/[H^+]$ for the redox reaction of $[Mn(salphen)]^+$ and H_2O_2	92
4.33	Plot of k_2 versus $1/[H^+]$ for the redox reaction of	93

	$[Mn(salphen)]^+$ and $S(CH_2CH_2OH)_2$	
4.34	Plot of k_2 versus $[H^+]$ for the redox reaction of $[Mn(salphen)]^+$ and RSH	94
4.35	Plot of log k_2 versus √I for for the redox reaction of $[Fe(salphen)]^+$ and H_2O_2	96
4.36	Plot of log k_2 versus √I for for the redox reaction of $[Mn(salphen)]^+$ and H_2O_2	97
4.37	Plot of log k_2 versus √I for for the redox reaction of $[Mn(salphen)]^+$ and SCN^-	98
4.38	Plot of log k_2 versus √I for for the redox reaction of $[Mn(salphen)]^+$ and $S(CH_2CH_2OH)_2$	99
4.39	Plot of log k_2 versus √I for for the redox reaction of $[Mn(salphen)]^+$ and RSH	100
4.40	Plot of log k_2 versus 1/D for the redox reaction of $[Fe(salphen)]^+$ and H_2O_2	112
4.41	Plot of log k_2 versus 1/D for the redox reaction of $[Mn(salphen)]^+$ and H_2O_2	113
4.42	Plot of log k_2 versus 1/D for the redox reaction of $[Mn(salphen)]^+$ and SCN^-	114
4.43	Plot of log k_2 versus 1/D for the redox reaction of $[Mn(salphen)]^+$ and $H_2NNHCSNH_2$	115
4.44	Plot of log k_2 versus 1/D for the redox reaction of $[Mn(salphen)]^+$ and $S(CH_2CH_2OH)_2$	116
4.45	Plot of log k_2 versus 1/D for the redox reaction of $[Mn(salphen)]^+$ and RSH	117
4.46	Plot of k_2 versus $[Mg^{2+}]$ for the redox reaction of $[Fe(salphen)]^+$ and TSH	128
4.47	Plot of k_2 versus $[Ca^{2+}]$ for the redox reaction of $[Fe(salphen)]^+$ and TSH	129
4.48	Plot of k_2 versus $[Mg^{2+}]$ for the redox reaction of $[Fe(salphen)]^+$ and H_3PO_2	130
4.49	Plot of k_2 versus $[Ca^{2+}]$ for the redox reaction of $[Fe(salphen)]^+$ and H_3PO_2	131
4.50	Plot of k_2 versus $[Mg^{2+}]$ for the redox reaction of	132

	$[Fe(salphen)]^+$ and H_2O_2	
4.51	Plot of k_2 versus $[Ca^{2+}]$ for the redox reaction of $[Fe(salphen)]^+$ and H_2O_2	133
4.52	Plot of k_2 versus $[Mg^{2+}]$ for the redox reaction of $[Mn(salphen)]^+$ and TSH	134
4.53	Plot of k_2 versus $[Ca^{2+}]$ for the redox reaction of $[Mn(salphen)]^+$ and TSH	135
4.54	Plot of k_2 versus $[Mg^{2+}]$ for the redox reaction of $[Mn(salphen)]^+$ and $H_2NNHCSNH_2$	136
4.55:	Plot of k_2 versus $[Ca^{2+}]$ for the redox reaction of $[Mn(salphen)]^+$ and $H_2NNHCSNH_2$	137
4.56	Plot of k_2 versus $[Mg^{2+}]$ for the redox reaction of $[Mn(salphen)]^+$ and H_2O_2	138
4.57	Plot of k_2 versus $[Ca^{2+}]$ for the redox reaction of $[Mn(salphen)]^+$ and H_2O_2	139
4.58	Plot of k_2 versus $[Mg^{2+}]$ for the redox reaction of $[Mn(salphen)]^+$ and RSH	140
4.59	Plot of k_2 versus $[K^+]$ for the redox reaction of $[Mn(salphen)]^+$ and RSH	141
4.60	Plot of k_2 versus $[Mg^{2+}]$ for the redox reaction of $[Mn(salphen)]^+$ and SCN^-	142
4.61	Plot of k_2 versus $[Ca^{2+}]$ for the redox reaction of $[Mn(salphen)]^+$ and SCN^-	143
4.62	Plot of k_2 versus $[Mg^{2+}]$ for the redox reaction of $[Mn(salphen)]^+$ and $S(CH_2CH_2OH)_2$	144
4.63	Plot of k_2 versus $[Ca^{2+}]$ for the redox reaction of $[Mn(salphen)]^+$ and $S(CH_2CH_2OH)_2$	145
4.64	Plot of k_2 versus $[NO_3^-]$ for the redox reaction of $[Fe(salphen)]^+$ and TSH	157
4.65	Plot of k_2 versus $[CH_3COO^-]$ for the redox reaction of $[Fe(salphen)]^+$ and TSH	158
4.66	Plot of k_2 versus $[NO_3^-]$ for the redox reaction of $[Fe(salphen)]^+$ and H_3PO_2	159
4.67	Plot of k_2 versus $[CH_3COO^-]$ for the redox reaction of	160

	$[Fe(salphen)]^+$ and H_3PO_2	
4.68	Plot of k_2 versus $[NO_3^-]$ for the redox reaction of $[Fe(salphen)]^+$ and H_2O_2	161
4.69	Plot of k_2 versus $[HCOO^-]$ for the redox reaction of $[Fe(salphen)]^+$ and H_2O_2	162
4.70	Plot of k_2 versus $[NO_3^-]$ for the redox reaction of $[Mn(salphen)]^+$ and TSH	163
4.71	Plot of k_2 versus $[HCOO^-]$ for the redox reaction of $[Mn(salphen)]^+$ and TSH	164
4.72	Plot of k_2 versus $[NO_3^-]$ for the redox reaction of $[Mn(salphen)]^+$ and RSH	165
4.73	Plot of k_2 versus $[SO_4^{2-}]$ for the redox reaction of $[Mn(salphen)]^+$ and RSH	166
4.74	Plot of k_2 versus $[NO_3^-]$ for the redox reaction of $[Mn(salphen)]^+$ and SCN^-	167
4.75	Plot of k_2 versus $[HCOO^-]$ for the redox reaction of $[Mn(salphen)]^+$ and SCN^-	168
4.76	Plot of k_2 versus $[NO_3^-]$ for the redox reaction of $[Mn(salphen)]^+$ and $H_2NNHCSNH_2$	169
4.77	Plot of k_2 versus $[HCOO^-]$ for the redox reaction of $[Mn(salphen)]^+$ and $H_2NNHCSNH_2$	170
4.78	Plot of k_2 versus $[NO_3^-]$ for the redox reaction of $[Mn(salphen)]^+$ and H_2O_2	171
4.79	Plot of k_2 versus $[HCOO^-]$ for the redox reaction of $[Mn(salphen)]^+$ and H_2O_2	172
4.80	Plot of k_2 versus $[SO_4^{2-}]$ for the redox reaction of $[Mn(salphen)]^+$ and $S(CH_2CH_2OH)_2$	173
4.81	Plot of k_2 versus $[HCOO^-]$ for the redox reaction of $[Mn(salphen)]^+$ and $S(CH_2CH_2OH)_2$	174
4.82	Plot of $\ln\left(\frac{k_2}{T}\right)$ versus $\left(\frac{1}{T}\right)$ for the reaction of $[Fe(salphen)]^+$ and TSH	185
4.83	Plot of $\ln\left(\frac{k_2}{T}\right)$ versus $\left(\frac{1}{T}\right)$ for the reaction of $[Fe(salphen)]^+$ and $H_2C_2O_4$	186

4.84 Plot of $\ln\left(\frac{k_2}{T}\right)$ versus $\left(\frac{1}{T}\right)$ for the reaction of $[Fe(salphen)]^+$ and H_3PO_2 187

4.85 Plot of $\ln\left(\frac{k_2}{T}\right)$ versus $\left(\frac{1}{T}\right)$ for the reaction of $[Fe(salphen)]^+$ and H_2O_2 188

4.86 Plot of $\ln\left(\frac{k_2}{T}\right)$ versus $\left(\frac{1}{T}\right)$ for the reaction of $[Mn(salphen)]^+$ and H_2O_2 189

4.87 Plot of $\ln\left(\frac{k_2}{T}\right)$ versus $\left(\frac{1}{T}\right)$ for the reaction of $[Mn(salphen)]^+$ and TSH 190

4.88 Plot of $\ln\left(\frac{k_2}{T}\right)$ versus $\left(\frac{1}{T}\right)$ for the reaction of $[Mn(salphen)]^+$ and RSH 191

4.89 Plot of $\ln\left(\frac{k_2}{T}\right)$ versus $\left(\frac{1}{T}\right)$ for the reaction of $[Mn(salphen)]^+$ and SCN^- 192

4.90 Plot of $\ln\left(\frac{k_2}{T}\right)$ versus $\left(\frac{1}{T}\right)$ for the reaction of $[Mn(salphen)]^+$ and $H_2NNHCSNH_2$ 193

4.91 Plot of $\ln\left(\frac{k_2}{T}\right)$ versus $\left(\frac{1}{T}\right)$ for the reaction of $[Mn(salphen)]^+$ and $S(CH_2CH_2OH)_2$ 194

4.92 Plot for spectrophotometric test for the redox reaction of $[Fe(salphen)]^+$ and TSH 195

4.93 Plot for spectrophotometric test for the redox reaction of $[Fe(salphen)]^+$ and $H_2C_2O_4$ 196

4.94 Plot for spectrophotometric test for the redox reaction of $[Fe(salphen)]^+$ and H_3PO_2 197

4.95 Plot for spectrophotometric test for the redox reaction of $[Fe(salphen)]^+$ and H_2O_2 198

4.96 Plot for spectrophotometric test for the redox reaction of $[Mn(salphen)]^+$ and H_2O_2 199

4.97 Plot for spectrophotometric test for the redox reaction of $[Mn(salphen)]^+$ and TSH 200

4.98 Plot for spectrophotometric test for the redox reaction of $[Mn(salphen)]^+$ and SCN^- 201

4.99 Plot for spectrophotometric test for the redox reaction 202

of $[Mn(salphen)]^+$ and $H_2NNHCSNH_2$

4.100 Plot for spectrophotometric test for the redox reaction of $[Mn(salphen)]^+$ and $S(CH_2CH_2OH)_2$ 203

4.101 Plot for spectrophotometric test for the redox reaction of $[Mn(salphen)]^+$ and RSH 204

4.102 Michaelis-Menten plot for the redox reaction of $[Fe(salphen)]^+$ and TSH 205

4.103 Michaelis-Menten plot for the redox reaction of $[Fe(salphen)]^+$ and $H_2C_2O_4$ 206

4.104 Michaelis-Menten plot for the redox reaction of $[Fe(salphen)]^+$ and H_3PO_2 207

4.105 Michaelis-Menten plot for the redox reaction of $[Mn(salphen)]^+$ and TSH 208

4.106 Michaelis-Menten plot for the redox reaction of $[Mn(salphen)]^+$ and RSH 209

4.107 Michaelis-Menten plot for the redox reaction of $[Mn(salphen)]^+$ and SCN^- 210

4.108 Michaelis-Menten plot for the redox reaction of $[Mn(salphen)]^+$ and $H_2NNHCSNH_2$ 211

4.109 Michaelis-Menten plot for the redox reaction of $[Mn(salphen)]^+$ and $S(CH_2CH_2OH)_2$ 212

4.110 Michaelis-Menten plot for the redox reaction of $[Fe(salphen)]^+$ and H_2O_2 213

4.111 Michaelis-Menten plot for the redox reaction of $[Mn(salphen)]^+$ and H_2O_2 214

4.112 Plot of specific conductance against [SDS] in water 217

4.113 Plot of specific conductance against [SDS] in H_2O/DMSO (4:1), 0.6 mol dm^{-3} NaCl and 1×10^{-4} mol dm^{-3} $[Fe(salphen)^+]$ 218

4.114 Plot of specific conductance against [SDS] in H_2O/DMSO (4:1), 0.6 mol dm^{-3} NaCl and 1×10^{-4} mol dm^{-3} $[Mn(salphen)^+]$ 219

4.115 Plot of specific conductance against [CTAB] in water 220

4.116	Plot of specific conductance against [CTAB] in H_2O/DMSO (4:1), 0.6 mol dm^{-3} NaCl and 1×10^{-4} mol dm^{-3} $[Fe(salphen)^+]$	221
4.117	Plot of specific conductance against [CTAB] in H_2O/DMSO (4:1), 0.6 mol dm^{-3} NaCl and 1×10^{-4} mol dm^{-3} $[Mn(salphen)^+]$	222
4.118	Plot of k_ψ against [SDS] fitted into the Piszkiewicz's equation for the reaction of $[Fe(salphen)]^+$ and TSH	232
4.119	Plot of k_ψ against [CTAB] fitted into the Piszkiewicz's equation for the reaction of $[Fe(salphen)]^+$ and TSH	233
4.120	Plot of k_ψ against [SDS] fitted into the Piszkiewicz's equation for the reaction of $[Fe(salphen)]^+$ and $H_2C_2O_4$	234
4.121	Plot of k_ψ against [CTAB] fitted into the Piszkiewicz's equation for the reaction of $[Fe(salphen)]^+$ and $H_2C_2O_4$	235
4.122	Plot of k_ψ against [SDS] fitted into the Piszkiewicz's equation for the reaction of $[Fe(salphen)]^+$ and H_2O_2	236
4.123	Plot of k_ψ against [CTAB] fitted into the Piszkiewicz's equation for the reaction of $[Fe(salphen)]^+$ and H_2O_2	237
4.124	Plot of k_ψ against [SDS] fitted into the Piszkiewicz's equation for the reaction of $[Mn(salphen)]^+$ and H_2O_2	238
4.125	Plot of k_ψ against [CTAB] fitted into the Piszkiewicz's equation for the reaction of $[Mn(salphen)]^+$ and H_2O_2	239
4.126	Plot of k_ψ against [SDS] fitted into the Piszkiewicz's equation for the reaction of $[Mn(salphen)]^+$ and TSH	240
4.127	Plot of k_ψ against [CTAB] fitted into the Piszkiewicz's equation for the reaction of $[Mn(salphen)]^+$ and TSH	241
4.128	Plot of k_ψ against [SDS] fitted into the Piszkiewicz's equation for the reaction of $[Mn(salphen)]^+$ and RSH	242
4.129	Plot of k_ψ against [CTAB] fitted into the Piszkiewicz's equation for the reaction of $[Mn(salphen)]^+$ and RSH	243
4.130	Plot of k_ψ against [SDS] fitted into the Piszkiewicz's equation for the reaction of $[Mn(salphen)]^+$ and SCN^-	244
4.131	Plot of k_ψ against [CTAB] fitted into the Piszkiewicz's equation for the reaction of $[Mn(salphen)]^+$ and SCN^-	245

4.132 Plot of k_ψ against [SDS] fitted into the Piszkiewicz's equation for the reaction of $[Mn(salphen)]^+$ and $S(CH_2CH_2OH)_2$ 246

4.133 Plot of k_ψ against [CTAB] fitted into the Piszkiewicz's equation for the reaction of $[Mn(salphen)]^+$ and $S(CH_2CH_2OH)_2$ 247

LIST OF SCHEMES

3.1	Reaction of salicylaldehyde and o-phenylenediamine to give N,N′-bis(salicylidene)phenylenediamine	33
3.2	Reaction of N,N′-bis(salicylidene)phenylenediamine to give N,N′-phenylenebis(salicylideneiminato)iron(III), [Fe(salphen)]Cl	33
5.1	Distribution of reactants between aqueous phase and micellar pseudophase	287
5.2	Model showing probable location of reactants in micellar pseoudophase	290

LIST OF APPENDICES

I	FTIR spectrum of salphen	321
II	FTIR spectrum of $[Fe(salphen)]^+$	322
III	FTIR spectrum of $[Mn(salphen)]^+$	323
IV	FTIR spectrum of the product of reaction of TSH and $[Fe(salphen)]^+$	324
V	FTIR spectrum of the product of reaction of TSH and $[Mn(salphen)]^+$	325
VI	FTIR spectrum of the product of reaction of RSH and $[Mn(salphen)]^+$	326
VII	FTIR spectrum of the product of reaction of $S(CH_2CH_2OH)_2$ and $[Mn(salphen)]^+$	327

ABBREVIATIONS

Abbreviation	Definition
A_t	Absorbance at time
A_∞	Absorbance at infinity
AR	Analar reagent
BDH	British drug house
CTAB	Cetyltrimethylammonium bromide
CMC	Critical micelle concentration
D	Dielectric constant
DNA	Deoxyribonucleic acid
EPR	Electron paramagnetic resonance
E_a	Activation energy
FTIR	Fourier transformed infrared
$[Fe(salphen)]^+$	N,N′-phenylenebis(salicylideneiminato)iron(III)
$\Delta G^{\ddagger}$	Gibb's energy of activation
h	Planck's constant
$\Delta H^{\ddagger}$	Enthalpy of activation
k_1	Pseudo – first order rate constant
k_2	Second order rate constant
k_w	Second order rate constant in the absence of surfactant
k_ψ	Second order rate constant in the presence of surfactant
$k_{\Psi exp}$	Experimentally determined second order rate constant in the presence of surfactant

Abbreviation	**DEFINITION**
$k_{\Psi cal}$	Calculated second order rate constant in the presence of surfactant
k_B	Boltzmann's constant
K	Equilibrium constant
$[Mn(salphen)]^+$	N,N′-phenylenebis(salicylideneiminato)-manganese(III)
R	Molar gas constant
RA	Reducing agent
Redox	Reduction – oxidation
RNA	Ribonucleic acid
RSH	Thioglycol
$\Delta S^{\ddagger}$	Entropy of activation
SDS	Sodium dodecyl sulphate
$[S_f]$	Surfactant concentration
Salen	Bis(salicylidene)ethylenediamine
Salphen	Bis(salicylidene)phenylenediamine
t	Time
T	Temperature
TSH	Thioglycolic acid
UV – visible	Ultra violet – visible
μ	Ionic strength
λ_{max}	Wavelength of maximum absorption

CHAPTER ONE

1.0 INTRODUCTION

Organic molecules containing imine groups, commonly known as Schiff bases, are of great interest to inorganic chemists due to their wide range of applications such as molecular ferromagnet designs, catalysis, biological modeling and preparation of liquid crystals (Rodriguez *et al*., 1997; Ramade *et al*., 1997; Miyasaka *et al*., 1998; Hoshino, 1998; Pinkowicz *et al*., 2015; Sukhikh and Vostrikova, 2017).

Schiff bases besides their diverse applications, also play a key role as chelating ligands in main group metal and transition metal coordination chemistry. This is due to their ease of synthesis, stability under a variety of oxidative and reductive conditions and the structural versatility (Ziessel, 2001; Cozzi, 2004; Gupta and Sutar, 2008; Costes *et al*., 2008; Ran *et al*., 2010; Orio *et al*., 2010).

Undoubtedly, salen type ligands are receiving more attention among all the Schiff bases due to their ease of preparation from the condensation of a diamine with salicylaldehyde or its derivatives (Subrata *et al*., 2012). Ligands categorized under this class consist of two imine nitrogen and two phenolic oxygen donors that usually coordinate to the metal ion (Ahmad *et al*., 2020).

The chemistry of mononuclear and dinuclear iron(III) complexes has also continued to receive a lot of attention (Fernandez *et al*., 2004). This is mainly due to the fact that iron plays a key role in physiological processes (Herold, 2004). Redox processes involving iron(III) have been followed with keen interest especially as regards biomimetic processes involving haeme and non-haeme iron(III) complexes (Smelkal *et al*., 1996; Brausam and Van-Eldik, 2004). In this regard iron(III)-imine complexes have received special attention

and various mechanistic studies involving iron(III) complexes have been carried out (Anweting *et al*., 2017; Busari *et al*., 2019; Anweting *et al*., 2020; Busari *et al*., 2021; Nkole *et al*., 2021a; Nkole *et al*., 2021b)

Manganese complexes have also been of interest due to their role in biological redox processes and catalytic disproportionation of the superoxide ion, O^{2-}. Examples are the manganese-containing superoxide dimustase (Mn-SOD), catalase and the oxygen evolving complex in photosynthesis II in green plants (Matshushita and Shono, 1981; Pecoraro *et al*., 1994; Waldo and Penner-Hahn, 1995; Zouni *et al*., 2001). In photosystem II, a tetranuclear manganese cluster has been identified by many spectroscopic measurements and crystal structure analysis as the active catalyst for the oxidation of water to oxygen. However, the exact mechanism has remained in speculation (Zouni *et al*., 2001; Umena *et al*., 2011).

As such, the application of manganese model systems would be far reaching and extensive studies of the coordination chemistry and reactivity of manganese(III) can provide useful insight into the functional role of this transition metal ion in biological systems (Gangopadhyay *et al*., 1994a).

In addition, the study of the effect of surfactant micelles on reaction rates has also been a subject of great interest (Warren *et al*., 2006; Senapati *et al*., 2011; Akram *et al*., 2014; Yadav *et al*., 2016; Kumar *et al*., 2016; Ogunlusi *et al*., 2016). Surfactants are known to form stable aggregates (micelles) in water above the critical micelle concentration (CMC) (Nagarajan and Ruckenstein, 1991; Patist *et al*., 2001). The rates of chemical reactions are known to be altered or modified by micelles (Owoyomi *et al*., 2007). The existence of micellar aggregates of substrate and surfactant at concentrations below the

CMC of the surfactant has also been recognized (Sánchez *et al*., 1997; Hadgiivanova and Diamant, 2007; Zaheer, 2009).

Many mechanistic studies of electron transfer processes in surfactant solutions have been reported to show varied surfactant effects on reaction rates ranging from inhibition to activation; and in some cases, alteration of the reaction mechanism (Tanaka *et al*., 1979; Larson *et al*., 2000; Shen, 2001). These effects are strongly dependent on the charges on the redox partners and the nature of the surfactant head group (Tachiyashiki and Yamatera, 1986; Ige and Soriyan, 1986).

Surfactant chain length has also been reported to contribute to the surfactant effect on reaction rates (Lombardo *et al*., 2006; Mohareb *et al*., 2006; Astray *et al*., 2011). Such influence has been attributed to the presence of hydrophobic and electrostatic forces and for a given set of reaction, the observed rate of reaction depends on the extent of association between the reactants and micellar aggregate (Sugumar *et al*., 2015; Joshi *et al*., 2016). The kinetics of reactions in micellar solutions can be accounted for qualitatively by considering the electrostatic and hydrophobic interactions between micelles and reactants, transition states and products (Ogunlusi *et al*., 2016).

1.1 Statement of the Research Problem

Metallo-salens have been extensively used as catalysts for a broad range of transition metal catalysis reactions including epoxidation of olefins, hydroxylation, lactide polymerisation and asymmetric ring opening of epoxides (Srinivasan *et al*., 1986; Jacobsen *et al*., 1990; Jacobsen *et al*., 1991; Canali and Sherrington, 1999; Jacobsen, 2000). The significance of these tetradentate N_2O_2 ligands and their transition metal complexes as catalysts, has attracted attention, being relevant for their applications particularly on the development of agrochemical and pharmaceutical industries (Ribeiro *et al*., 2004).

Similarly, biological chemists have also exploited the oxidative nature of metallo-salens for developing novel chemical nucleases that modify nucleic acids (Bhattacharya and Mandal, 1996; Routier *et al*., 1996; Muller *et al*., 1999; Czlapinski and Sheppard, 2001; Doctrow *et al*., 2002). Various metallo-salen complexes are also implicated in hydrolytic cleavage of DNA and RNA (Komiyama *et al*., 1999; Prema *et al*., 2007).

It has been demonstrated that Fe(III) and Mn(III)-salen and salphen cause damage to DNA *in vitro* and also induces efficient apoptosis *in vivo* (Woldemariam and Mandal, 2008; Ansari *et al*., 2009a; Ansari *et al*., 2009b). It was also demonstrated that Fe(III) and Mn(III)-salen and salphen complexes affect cell viability and induce nuclear fragmentation and apoptosis in breast cancer (MCF7) cells. These complexes also induce caspase-3/7 activation and release of cytochrome c from the mitochondria to cytosol, suggesting the involvement of the mitochondrial pathway of apoptosis (Ansari et al., 2009a; Ansari *et al*., 2009b; Ansari *et al*., 2011).

As DNA interacting molecules find potential applications in novel anti-tumour therapy, intense research efforts are being invested towards developing novel DNA/RNA modifiers and in understanding their molecular mechanisms of action (Cohen and Lippard, 2001; Barnes and Lippard, 2004; Ott and Gust, 2007). In general, redox active agents that damage DNA *in vitro* are assumed to exhibit apoptotic activities in live cells by inducing oxidative stress and/or DNA damage (Cohen and Lippard, 2001; Wang, 2001; Valko *et al*., 2004; Boerner and Zaleski, 2005; Danford *et al*., 2005).

Metallo-salens with diverse structures and redox characteristics are shown to produce reactive oxygen species under oxidative/reducing environments and damage to DNA/RNA *in vitro* (Czlapinski and Sheppard, 2001; Doctrow *et al*., 2002; Shrivastava *et al*., 2004). For example, iron and copper-salen derivatives produce hydroxyl radicals in the

presence of dithiothreitol and damage DNA (Routier *et al*., 1999; Rokita and Burrows, 2001). Furthermore, various metal-salens and derivative complexes have been implicated in efficient asymmetric catalysis and in catalyzing the hydrolytic cleavage of DNA and RNA (Komiyama *et al*., 1999; Wiznycia *et al*., 2005; Prema *et al*., 2007).

Similarly, kinetic micellar effect is a change in reaction rate constant due to the presence of surfactant micelles in solution (Dwars *et al*., 2005; Buurma, 2009; Romsted, 2012) which are helpful in studying reaction mechanisms (Laguta *et al*., 2018a). Reports have shown that metal complexes of aromatic diimines exhibit unique interaction with hydrophobic solutes in aqueous solutions because of the hydrophobicity of the ligands (Yokoyama, *et al*., 1995; Rajendran *et al*., 1997).

The presence of π-electrons in the hydrophobic salphen ligands make the electrostatic and hydrophobic interaction between the complexes and the surfactants contribution to the reaction rate interesting for investigation (Ogunlusi *et al*., 2016). The influence of surfactants in reaction rate are also important in pharmaceutical formulations (Katre *et al*., 2013).

However, despite several applications of $[Fe(salphen)]^+$ and $[Mn(salphen)]^+$ complexes with regards to their redox properties, kinetics and mechanisms of their redox reactions are very scanty.

1.2 Justification of the Study

The complexes, N,N′-phenylenebis(salicylideneiminato)iron(III), $[Fe(salphen)]^+$, and N,N′-phenylenebis(salicylideneiminato)manganese(III), $[Mn(salphen)]^+$ are very versatile with lots of their applications centered around their redox properties. Yet there is scarcity of information on the kinetics and mechanisms of their redox reactions. The present study is undertaken to obtain kinetic data with a view of gaining insight into the

mechanistic pathway of the redox reactions of these complexes. The data that would be generated from these redox reactions will complement the much needed kinetic information which would further explain their redox properties and hence may give more information on how to improve on the diverse applications of the redox partners.

Furthermore, the study is used as a mimic of some biochemical processes and would assist in understanding the interplay of the various factors that can influence the reaction rates and also explain the kinetic data using a suitable micellar kinetic model. The cooperativity index and binding constants would provide additional information on the mode of interaction between surfactants and the metal complexes.

The thermodynamic parameters that would be obtained would provide additional information on the influence of temperature on the reactions. In addition, the kinetic data generated and the proposed mechanisms would contribute to conceptual development of mechanism of redox reactions of iron(III) and manganese(III) complexes.

1.3 Aim and Objectives of the Study

The aim of this study is to determine the kinetics of redox reactions of N,N′-phenylenebis(salicylideneiminato)iron(III), $[Fe(salphen)]^+$ and N,N′-phenylenebis(salicylideneiminato)manganese(III), $[Mn(salphen)]^+$ complexes and some reducing agents in mixed aqueous and surfactant medium and propose plausible mechanisms for the reactions. The objectives of this study are to:

i. synthesize and characterize N,N′-phenylenebis(salicylideneiminato)iron(III) and N,N′-phenylenebis(salicylideneiminato)manganese(III) complexes;
ii. determine the stoichiometry and order of the reactions;
iii. determine the effect of changes in hydrogen ion concentration, ionic strength, added ions and dielectric constant of the medium on the reaction rates;

iv. generate thermodynamic parameters for the reactions;

v. determine the effect of surfactant concentration on the reactions rate; the catalytic factor (k_ψ/k_w) or inhibition factor (k_w/k_ψ), cooperativity index and binding constants.

CHAPTER TWO

2.0 LITERATURE REVIEW

2.1 Reactions of N,N′-Phenylenebis(salicylideneiminato)iron(III) and Manganese(III) Complexes

The complexes, $[Fe(salphen)]^+$ and $[Mn(salphen)]^+$, are dark brown in colour and are derived from the reaction of bis(salicylidene)phenylenediamine (salphen) with $FeCl_3$ and $Mn(CH_3COO)_3$ respectively in methanol (Ansari *et al*., 2009a; Ansari *et al*., 2009b; Ansari *et al*., 2011). Iron plays a unique role in biological systems, as enzymes containing iron are of crucial importance in electron transfer reactions and in the activation and transport of small molecules, such as molecular oxygen (Natarajan *et al*., 2005). Managanese complexes have also been of interest in biological redox processes including catalytic disproportionation of superoxide ion, O_2^-. Examples are the manganese-containing superoxide dismutase (Mn-SOD) and the oxygen evolving photosynthesis II in green plants (Matsushita and Shono, 1981).

Studies have demonstrated that Fe(III) and Mn(III)-salen and salphen complexes induced efficient apoptosis in cultured human cells. The nature of the substituents and the space between diamino groups play critical roles in determining the apoptotic activities of the complexes (Ansari *et al*., 2009a; Ansari *et al*., 2009b; Ansari *et al*., 2011).

Salem (1994) studied the kinetics of the reaction between $[Mn^{III}(saltm)Br]$ complex (saltm = N,N'-bis(salicylidene)propylenediamine) and hydrogen peroxide in a pH range 5.05 – 7.29 in both aqueous and micellar sodium dodecyl sulphate (SDS) solution. First order dependence in both reactants was observed with a significant reaction inhibition recorded with increasing acidity of the reaction medium and increasing SDS concentration.

A mechanism involving manganese(IV) and a peroxo-intermediate was proposed with the subsequent release of $OH^{\bullet}$ radicals at the rate determining step.

In the same vain, the kinetics of the reduction of manganese(III) complex of trans-cyclohexane-1,2-diamine-N,N,N',N'-tetraacetate ($cdta^{4-}$) by thioglycolic acid and glutathione respectively were investigated at 30 ºC in aqueous media in the pH range of 2.0 - 10.33 with varying reductant concentrations at constant ionic strength, $\mu = 0.20\ C^2$ mol dm^{-3} ($NaClO_4$). The reactions were first order in both complex and reductants according to the rate law as shown in equation 2.1;

$$\frac{-d[Mn^{III}(cdta)^{-}]}{dt} = k_2[Mn^{III}(cdta)^{-}][reductant] \qquad 2.1$$

The reactions occured via inner-sphere mechanism due to the formation of an inner-sphere associated complex, which decomposed unimolecularly before electron transfer from the thiols to the oxidant. Free radicals participated in the reactions and the oxidation products of the thiols were dithiodiglycolic acid and glutathione disulphide respectively (Gangopadhyay *et al*., 1994b).

The kinetics and mechanism of the reduction of $[Fe(salen)(H_2O)_2]^{+}$, by L-ascorbic acid was studied under pseudo first order conditions at 28.5 ± 0.3 ºC and 515 nm. First order dependence was observed in both reactants and the reaction was acid catalysed, whereas varying the ionic strength and dielectric constant of the medium did not affect the reaction rate. An inner-sphere mechanism was proposed as the reaction pathway (Alioke *et al*., 2012).

However, Atiga *et al*. (2014) reported a proton-coupled outer-sphere electron transfer mechanism in the reduction of μ-adi-di(N,N′-bis(salicylidene)ethylenediaminatoiron(III)) complex, [Fe_2adi], by dithionate ion, $S_2O_6^{2-}$, in

aqueous perchloric acid. The results indicated a first order dependence in [Fe_2adi] but a zeroth-order dependence in [$S_2O_6^{2-}$] whereas spectrophotometric titrations indicated the reduction of one mole of the complex by a mole of the reductant. The reaction rate increased with increasing [H^+], decreased with increasing dielectric constant, but was unaltered by increasing ionic strength of the medium. The results also show that addition of ions such as CH_3COO^- and Mg^{2+} ions had no effect on the reaction rate, an indication of a probable intramolecular electron transfer in $Fe_2adiH_2^{2+}$ in the rate-determining step.

The presence of free radicals and the formation of an inner-sphere complex were inferred in the kinetics of oxidation of glyoxylic acid (HGl) by $Mn^{III}(salen)(OH_2)_2^+$ (H_2salen = N,N-bis(salicylidene)ethane-1,2-diamine) investigated in the pH range of 1.83 - 6.10 and at μ = 0.3 C^2 mol dm^{-3} ($NaClO_4$). Formic acid, CO_2 and Mn^{II} were identified as the reaction products from a reaction stoichiometry where 2 moles of $Mn^{III}(salen)(OH_2)_2^+$ were reduced per mole of glyoxylic acid. The reaction involved fast equilibrium pre-association of $Mn^{III}(salen)(OH_2)^{2+}$ with HGl and its conjugate base Gl^- forming the corresponding inner-sphere complex followed by the slow electron transfer steps (Kar *et al*., 2014).

Redox reaction of adipato bridged iron(III)salen complex, [$(Fe(salen))_2$adi] with dithionite ion, $S_2O_4^{2-}$, was carried out in aqueous perchloric acid at 29 ± 1 °C. Spectrophotometric titrations indicated the reduction of one mole of [$(Fe(salen))_2$adi] per mole of $S_2O_4^{2-}$ and sulphur(IV) oxide was proposed as the oxidation product of $S_2O_4^{2-}$ ion. First order dependence in [$(Fe(salen))_2$adi] and [$S_2O_4^{2-}$] was observed in the reaction and the reaction rate increased with increase in [H^+] but was unaffected by changes in ionic strength, dielectric constant of the medium and added ions. An inner-sphere electron transfer was proposed as the reaction pathway (Ukoha *et al*., 2015).

Recently, Jena *et al*. (2018) investigated the reaction of trans-Mn^{III}(salophen)$(OH_2)^{2+}$ and bioxalate (HOX^-) in aqueous medium and reported the rapid equilibration of the reactants to trans-Mn^{III}(salophen)(OH_2)(HOX) followed by an acid dissociation equilibrium to an aqua-mono oxalate complex which obeyed second order kinetics satisfying 2:1 stoichiometry with reaction products of Mn^{II} and CO_2. Polymerisation was not induced by acrylamide monomer and it was observed that H_2OX was a better reducing agent than HOX^-.

The redox reactions of the oxalato complexes indicated the significance of H-bonding interaction, supporting a proton controlled electron transfer process (PCET) (Huynh and Meyer, 2007). Reports have also indicated that the Mn^{III}(salophen/salen) complexes may be good substitutes for Oxalo Oxidase (OXO) enzyme for improving oxalates in plants and animal biochemistry (Jena *et al*., 2018).

2.2 Reactions of Thioglycolic Acid

Thioglycolic acid (TSH) also called mercaptoacetic acid, $HSCH_2COOH$, is the simplest and industrially most important mercaptocarboxylic acid which has two reactive centers; the mercapto group and the carboxyl group. The compound forms salts of the carboxyl and mercapto groups, esters, amides, anilides, thioethers, and so on (Rippel and Hoechst, 2012). Many biological functions of thiol-containing compounds are governed by their easy oxidation (Jocelyn, 1972; Friedman, 1973).

The strongly reducing nature of mercaptoacetic acid is of importance both in investigations of biochemical redox and enzyme systems and in industrial applications such as cold-waving preparations and modification of wool (Rippel and Hoechst, 2012).

Sun and Stanbury (2002) reported the oxidation of thioglycolic acid by $[IrCl_6]^{2-}$ in aqueous solution at 25 ºC and found the reaction to be highly susceptible to trace metal-ion

catalysis. Suppressing this catalysis was effective using bathophenanthrolinedisulphonate (bathophen), which allowed studying the direct oxidation process. Although a disulphide was produced as a reaction product in the absence of bathophen, a mixture of a disulphide and a sulphonate were produced in its presence. In both cases, Ir(IV) was reduced to $[IrCl_6]^{3-}$. The reaction displayed first order dependence in both Ir(IV) and thioglycolic acid and the result shows a complex pH dependence due to the diprotic nature of thioglycolic acid.

In order to account for the product mixture, Sun and Stanbury (2002) proposed a mechanism in which RSO_3^- was produced in a series of steps originating with the oxidation of $RS^\bullet$ by $[IrCl_6]^{2-}$, while RSSR was produced by association of $RS^\bullet$ with thioglycolic acid to generate $RSSR^{\bullet-}$ and oxidation of $RSSR^{\bullet-}$ by $[IrCl_6]^{2-}$.

In another study, Mandal *et al*. (2015) reported the reduction of $[(en)(dien)Co^{III}(O_2)Co^{III}(en)(dien)]^{5+}$ by thioglycolic acid ($HSCH_2COOH$) to $[(en)(dien)Co^{III}(\mu\text{-}O_2)Co^{III}(en)(dien)]^{4+}$ in an acidic media ($[H^+]$ = 0.01– 0.06 mol dm^{-3}). Thiolate anion was proposed as the reactive form of the reductant as observed from the decrease in reaction rate with increasing ionic strength and $[H^+]$ of the media and a disulphide was analysed as the reduction product of thioglycolic acid.

2.3 Reactions of Oxalic Acid

Oxalic acid is the simplest dicarboxylic acid, with the formula HO_2CCO_2H. It is a much stronger acid than acetic acid and is also a strong reducing agent (Khan *et al*., 1998). Its conjugate base, the oxalate dianion ($C_2O_4^{2-}$), is a chelating agent for many metals; for example in the drug oxaliplatin, the anion chelates platinum(II) (Ehrsson *et al*., 2002). Oxalic acid and oxalates can be oxidised by permanganate in an autocatalytic reaction (Kovacs *et al*., 2004).

The kinetics of oxidation of oxalic acid by BiF_6^- was investigated in $HClO_4$ and HF mixture and the reaction rate followed first order kinetics in Bi(V) and oxalic acid. The reaction was $[H^+]$ independent and addition of HF and F^- had no effect on the reaction rate whereas the rate decreased with an increase in ionic strength of the reaction medium. The results indicated the formation of an intermediate complex through hydrogen bonding interaction between BiF_6^- and oxalic acid prior to electron transfer (Prasad *et al*., 2007).

Similarly, Banerji *et al*. (2009) reported an inner-sphere oxidation of 5 moles of oxalic acid by 2 moles of permanganate in the reaction of oxalic acid with bis(pyridine) silver permanganate in aqueous acetic acid. The participation of free radicals in the reaction was unlikely whereas the formation of carbon dioxide and Mn(II) as reaction products were confirmed. The reaction was first order each with respect to permanganate and oxalic acid and was catalysed by hydrogen ions. An intercept was obtained from the Michaelis-Menten plot supporting a reaction mechanism involving the formation of an intermediate.

Furthermore, the kinetics of micellar catalysed oxidation of oxalic acid by N-bromophthalimide was studied in perchloric acid at 308 K. The order of reaction with respect to [oxalic acid], [oxidant], and $[H^+]$ were fractional, first and negative fractional order respectively. Increase in the concentration of cetyltrimethylammonium bromide increased the reaction rate whereas ionic strength and added ions (Cl^- and Br^-) had no effect on the rate but the rate decreased with increasing dielectric constant of the medium. A positive cooperativity (n = 1.15) was obtained indicating a significant interaction between cetyltrimethylammonium bromide and oxalic acid (Katre *et al*., 2012).

Recently, Peng and Guo (2020) also studied the reduction of Cr(VI) by oxalic acid at 70 ºC and at high acid (H_2SO_4) concentration. The reduced product, Cr(III), was in the form ($Cr(HC_2O_4)_3$), which displayed a negative effect on the reduction process. However,

the high reaction temperature and high acidic medium destroyed the stable structure of the complex compound to release oxalate, and facilitated the reduction of Cr(VI) to Cr(III). The results indicated a alternative approach for Cr(VI) reduction and demonstrated potential future applications in wastewater treatment.

2.4 Reactions of Hypophosphorous Acid

Hypophosphorous acid, H_3PO_2 is an oxyacid of phosphorus (Mehrotra, 2013). It has phosphorus in an oxidation state of +1 and is a powerful reducing agent (Greenwood and Earnshaw, 1997). The acid has been found to be a better reducing agent than phosphorous acid (Mohammed *et al*., 2017) and it is been used for the formulation of pharmaceuticals, discolouration of polymers and water treatment (Mehrotra, 2013).

Most electron transfer reactions of hypophosphorous acid proceed by mechanisms involving tautometric forms of hypophosphorous acid in aqueous solution. Reversible tautometric shift is catalysed by acid between the predominant inactive tautomer, $HOP(O)H_2$ and the minor active tautomer $HP(OH)_2$ which is followed by reaction of the active form with the oxidant (Mohammed, *et al*., 2017).

Similarly, reactions of H_3PO_2 are reported to involve radical formation such as $HPO_2^{\bullet-}$, $HPO_3^{\bullet-}$, or $^{\bullet}PO_3^{2-}$, which can be generated in aqueous solutions by interaction of H_3PO_2 with Ti^{III} or hydrogen peroxide (Beckwith, 1972).

The reaction of H_3PO_2 and $[CoW_{12}O_{40}]^{5-}$ in HCl has been studied. A reversible rate determining step led to the formation of the hypophosphorous acid radical ($H_2P^{\bullet}O_2$), which rapidly reacted with the complex to form H_3PO_3 (Ayoko, 1990).

Other researchers have studied the kinetics of the oxidation of neutral red (NR^+), by hypophosphorous acid (H_3PO_2), in aqueous perchloric acid medium under pseudo-first order conditions at 23 ± 1°C, $[H^+] = 1.0 \times 10^{-2}$ mol dm^{-3}, $\mu = 0.1$ C^2 mol dm^{-3} ($NaClO_4$) and

λ_{max} = 525 nm. The reaction was first order in $[NR^+]$ and $[H_3PO_2]$. The reaction was acid independent and displayed a zero Bronsted-Debye salt effect. There was no evidence of formation of an intermediate complex of significant stability and free radicals were absent in the reaction. The results suggested an outer sphere mechanism for the reaction (Ibrahim *et al*., 2016).

Similarly, Mohammed *et al*. (2017) reported the reduction of diaquotetrakis(2,2'-bipyridine)-µ-oxodiruthenium(III), $[(H_2O)_2(bipy)_4Ru_2O]_4^+$, by H_3PO_2 in aqueous acidic medium at ionic strength = 0.5 C^2 mol dm^{-3} ($NaClO_4$), $[H^+] = 5.0 \times 10^{-2}$ mol dm^{-3} and temperature = 31 ± 1 ºC. The stoichiometry of the reaction showed that 1 mole of $[(H_2O)_2(bipy)_4Ru_2O]_4^+$ was reduced per mole of H_3PO_2. The reaction was first order with respect to both $[(H_2O)_2(bipy)_4Ru_2O_4^+]$ and $[H_3PO_2]$, hence second order overall. Variations in the ionic strength and dielectric constant of the reaction medium had no effect on the rate. Similarly, the addition of various ions to the reaction medium did not affect the rate. Free radicals were identified in the reaction by a polymerisation test and spectroscopic information and Michaelis–Menten plots suggested the absence of an intermediate complex prior to electron transfer. The reduction product of $[(H_2O)_2(bipy)_4Ru_2O]_4^+$ and the oxidation product of H_3PO_2 were $[(H_2O)_2(bipy)_2Ru]^{2+}$ and H_3PO_3 respectively. The results proposed that the reaction occurred through an outer sphere pathway.

2.5 Reactions of Hydrogen Peroxide

Hydrogen peroxide, H_2O_2, is a very pale blue, clear liquid which is slightly more viscous than water (Housecroft and Sharpe, 2005). It is an environmentally friendly oxidant used as bleaching agent in textiles, personal care products and also in wastewater treatment (O'Neil, 2013). It is also used in food processing industry as chlorine-free bleaching and sterilizing agents, although its consumption in high concentration (0.05 %

w/w) according to U.S. FDA regulations (U.S. FDA, 2011) can cause food poisoning (Lu *et al*, 2011; Linley *et al*., 2012). Concentrated hydrogen peroxide is also used as a propellant in rockets (Hill, 2001).

Hydrogen peroxide is formed in human and animals as a short-lived product in biochemical processes and is toxic to cells. The toxicity is due to oxidation of proteins, membrane lipids and DNA by the peroxide ions. A class of biological enzymes called SOD (superoxide dismutase) is developed in nearly all living cells as an important antioxidant agent (Löffler and Petrides, 1988).

Luo *et al*. (2005) examined the reaction kinetics of L-cysteine (CSH) with hydrogen peroxide (H_2O_2) in aqueous buffers (in the absence of metal ions) over a wide range of pH (pH 4–13) and at varying ratios of initial reactant concentrations. The disappearance of CSH and H_2O_2 and appearance of cystine (CSSC) versus time were monitored by reverse-phase high performance liquid chromatography (HPLC). It was observed that the reaction of CSH with H_2O_2 in the absence of metal ions (Cu^{2+}) is quantitatively consistent with a two-step nucleophilic reaction mechanism involving rate-determining nucleophilic attack of thiolate anion on the unionized H_2O_2 to generate cysteine sulphenic acid (CSOH) as an intermediate. The results indicated that the generation of the reactive sulphenic acid intermediate and are of biological importance because these reactions may regulate a wide array of cellular processes.

In another investigation, Skounas *et al*. (2010) reported the catalytic decomposition of H_2O_2 by complexes of copper(II) with polymers such as alanine (PAla) and glycylglycine (PGlygly) in alkaline condition. The observed trend in catalytic efficiency was PGlygly > Pala, due to the differences in the modes of complexation and the adopted

conformations of the macromolecules upon complexation. A reaction mechanism was proposed which involved the reduction of Cu(II) to Cu(I) in the rate determining step.

Moreover, Impert *et al*. (2012) reported that the oxidation of trispicolinatoruthenate(II) complex by hydrogen peroxide gave mertrispicolinatoruthenium(III) in acidic solution. Kinetics of the reaction was studied under a large excess of H_2O_2 at constant pH. The rate of the reaction decreases with increasing pH and was completely retarded in alkaline media. The reaction was perceived to occur through the picolinato chelate ring opening followed by substitution of the coordinated water by H_2O_2 and a two-electron intramolecular ruthenium(II) oxidation. The results show a slower rate of the trispicolinatoruthenate(II) oxidation by hydrogen peroxide or dioxygen than the mertrispicolinatoruthenium(III) reduction by bioreductants such as cytochrome cII or cobalt(II) reductants.

Onu *et al*. (2015) have also studied the the reduction of H_2O_2 by aminocarboxylactocobaltate(II) complex ($[CoHEDTAOH_2]^-$) in aqueous medium at T = 29 ± 1˚C, μ = 0.50 C^2 mol dm^{-3} ($NaClO_4$) and $[H^+] = 1 \times 10^{-3}$ mol dm^{-3}. It was observed that 2 moles of the complex were oxidised per mole of H_2O_2 and the reaction displayed first order dependence in the concentrations of the reductant and oxidant and inverse acid dependence. The reaction was insensitive to changes in ionic strength of the medium suggesting interaction of charged and uncharged species at the activated complex. The Michaelis-Menten plot was linear without intercept, which suggested the absence of intermediate complex. The results obtained were in favour of the occurrence of outer-sphere mechanism.

2.6 Reactions of Thioglycol

Thioglycol (RSH) also called 2-mercaptoethanol, $HOCH_2CH_2SH$, is a colourless liquid with an unpleasant odour. It is miscible in water and nearly all common organic

solvents. It is produced by reaction of hydrogen sulphide gas and ethylene oxide (Roy, 2005). The compound is used as intermediate for the synthesis of polyvinylchlorides (PVC) heat stabilizers and as a chain transfer agent in the manufacture of PVC.

It is also used to produce dispersants, fibers, textiles, dyes and pharmaceuticals. Furthermore, it is used as a component of corrosion inhibitors and ore floatation agent. Low molecular weight thiols or their esters such as thioglycol, 1-thioglycerol and dithiothreitol denatures protein by reducing disulphide linkages leading to tautomerization and breaking up of quaternary protein structure (Shen *et al*., 2010).

Goswami *et al*. (2004) carried out kinetic investigation on the reductions of $[L^1Mn^{IV}(O)_2Mn^{III}L^1]$ (L^1 = 1,4,7,10-tetraazacyclododecane) and $[L^2Mn^{IV}(O)_2Mn^{III}L^2]$ (L^2 = 1,4,8,11-tetraazacyclotetradecane) by 2-mercaptoethanol (RSH) in aqueous buffer at 30 ± 0.1 ºC. The reactions were slow but significantly catalysed by copper(II) ions. The reactions were highly influenced by acid variation of the medium and the observed kinetics suggested the significance of $[Cu(RSH)]^{2+}$ and $[Cu(RS)]^{+}$ for the reaction between $[L^1Mn^{IV}(O)_2Mn^{III}L^1]$ and RSH. The reduction of $[L^2Mn^{IV}(O)_2Mn^{III}L^2]$ by the thiol was complex and rationalized considering two equilibria involving the catalyst (Cu^{2+}) and the reductant. The pH rate profile suggested the importance of both the μ-O protonated $[Mn^{III}(O)(OH)Mn^{IV}]$ and the deprotonated $[Mn^{III}(O)_2Mn^{IV}]$ forms of the oxidant, $[L^2Mn^{IV}(O)_2Mn^{III}L^2]$ in the reaction. The

results indicated the dominance of an outer-sphere pathway.

Similary, Chakraborty *et al*. (2013) reported the oxidation of 2-mercaptoethanol and L-cysteine by an aqueous solution of $[Mn^{IV}{}_3(\mu\text{-}O)_4(phen)_4(H_2O)_2]^{4+}$ (phen = 1,10-phenanthroline) in the pH range 2.2–4.0 to their respective disulphides, itself being reduced to $[Mn(phen)_3]^{2+}$ in the presence of excess 1,10-phenanthroline. The observed rate

constants in H_2O were lower in D_2O media and a proton-coupled single electron transfer step was proposed. The result indicated that the deprotonated oxidant reacted faster than the protonated species in oxidising both the thiols.

Other researchers (Shanmugaprabha *et al*., 2016) have carried out kinetic investigation on the oxidation of 2-mercaptoethanol and 2-mercaptoethylamine by heteropoly 11-tungsto-1-vanadophosphate anion, $[PV^{V}W_{11}O^{40}]^{4-}$, in aqueous perchloric acid at 25 ºC. Electron paramagnetic resonance (EPR) and optical studies showed that $[PV^{V}W_{11}O_{40}]^{4-}$ was reduced to the one-electron anion, $[PV^{IV}W_{11}O_{40}]^{5-}$, while the thiols were oxidised to their corresponding disulphides, RSSR. Spectrophotometric titrations showed 1:1 reaction stoichiometries. At constant pH, the reactions showed simple second order kinetics with first order dependence of rate on both [oxidant] and [thiol]. The reaction rate increased with increasing pH and plots of k_2 versus $\frac{1}{[H^+]}$ were linear with intercepts, showing that both the undissociated thiol (RSH) and thiolate ion (RS^-) were reactive. Generation of $RS^{\bullet}$ from RSH occured via a separated concerted proton–electron transfer mechanism (Shanmugaprabha *et al*., 2016).

2.7 Reactions of Thiocyanate Ion

Thiocyanate ion, (SCN^-), is the conjugate base of thiocyanic acid. It is analogous to the cyanate ion, (OCN^-), where oxygen is replaced by sulphur. It is also one of the pseudohalides, due to its similarity to the reactions of halide ions. Organic and transition metal derivatives of thiocyanate ion can exist as linkage isomers. In thiocyanates, the organic group (or metal ion) is attached to sulphur, R−S−C≡N, has a S–C single bond and a C≡N triple bond. However, in isothiocyanates, the substituent is attached to nitrogen, R−N=C=S, has a S=C double bond and a C=N double bond (Guy, 1977).

Organic thiocyanates are valuable building blocks in organic chemistry and they allow access to various sulphur containing functional groups (Castanheiro *et al*., 2016). Thiocyanate is known to be an important part in the biosynthesis of hypothiocyanite ion by a lactoperoxidase which functions as an antimicrobial agent in host defense (Conner *et al*., 2007; Pedemonte *et al*., 2007). Thiocyanate ion has antioxidant properties that include the ability to protect cells against oxidising agents such as hypochlorous acid (HOCl) and repair protein chloramines. The diverse properties of thiocyanate ion both as host defense and antioxidant agent make it a potentially useful therapeutic agent (Joshua and Brian, 2012).

It has been shown that the complete absence of thiocyanate or reduced thiocyanate in the human body (cystic fibrosis) is damaging to the human host defense system (Moskwa *et al*., 2007; Minarowski *et al*., 2008; Xu *et al*., 2009). It is a potent inhibitor of iodide transport and is a competitive substrate for the thyroid peroxidase but it does not appear to be concentrated in the thyroid. Blockage of the iodide trapping mechanism has a disruptive effect on the thyroid-pituitary axis, similar to iodine deficiency (Klaassen, 2001).

Industrial applications of thiocyanates include photography, printing, textiles, dyeing, medicines, freezing mixtures, manufacture of synthetic dyestuffs, sulphocyanides, thioureas and mustard oil. It is also as an analytical reagent. Thus, the reactions of thiocyanate ions are of interest due to their medicinal and biological importance as well as their analytical and industrial applications (Nandibewoor *et al*., 2000).

Previous reports indicated that zinc(II), cobalt(II) and copper(II) ions form a stable anion, $[M(SCN)_4]^{2-}$, with thiocyanate, which interacted with methylene blue to form an ion-pair, $MB_2[M(SCN)_4]$, and turned methylene blue violet. The kinetics of formation of

ternary complexes were therefore studied using stopped-flow technique and the study provided an alternative method for the spectrophotometric determination of Co(II) and Zn(II) ions (Jonnalagadda and Gollapalli, 2008).

Nandibewoor *et al*. (2000) studied the oxidation of thiocyanate by periodate in alkaline media and observed a very slow reaction in the absence of a catalyst but was significantly catalysed in the presence of Ru^{III}. The reaction products were OCN^-, SO_4^{2-} and IO_3^- from a reaction stoichiometry that indicated the consumption of 4 moles of IO_4^- per mole of SCN^-. Changes in the concentration of alkali did not alter the reaction rate whereas a decrease in rate was recorded with an increase in ionic strength of the reaction medium. A first order dependence each in $[Ru^{III}]$ and $[IO_4^-]$ while a half order dependence in $[SCN^-]$ were obtained in the reaction. The mechanism for the reaction was illustrated by the formation of an adduct between Ru^{III} and SCN^- which reacted with IO_4^- at the rate determining step for electron transfer.

In another investigation, Kalmar *et al*. (2013) reported a mechanistic investigation on the multistep oxidation of excess SCN^- with peroxomonosulphate ion (HSO_5^-) in the pH range of 6.5 – 13.5. The intermediate detected under the reaction condition was $OSCN^-$ and an evaluation of the estimated activation parameters of the elementary steps showed that the oxidations of SCN^- as and the consecutive oxidation of $OSCN^-$ by HSO_5^- occurred through $2e^-$ transfer steps rather than $1e^-$ transfer.

2.8 Reactions of Thiosemicarbazide

Thiosemicarbazide, $H_2NCSNHNH_2$, is similar to thiourea, H_2NCSNH_2, but with an additional NH center and their complexes are effective antibacterial agents (Sorouraddin et al., 2005). They form coordination bonds to metal ions which may involve

thiosemicarbazide as either a neutral ligand or as a deprotonated ligand (El-Gammal *et al*., 2014). They are also used in heterocyclic synthesis (Metwally *et al*., 2011).

Thiosemicarbazide and its derivatives are useful intermediates and subunits for the development of molecules having pharmaceutical or biological interest (Metwally *et al*., 2011). They also have potent biological activity (Hong *et al*., 2004) particularly as antimicrobial and antifungal agent (Yamagushi *et al*., 2009). The biological activities of thiosemicarbazides could be enhanced by the functional groups on the parent aldehyde or ketone (Ferrari *et al*., 2001). It is also good as a potential antitumour agent (Ferrari *et al*., 1999; Ali *et al*., 2001; Gielen, 2003), antimalarial and antiviral agents (Alsop *et al*., 2005), ulcer inhibitory, radioprotectory, anticonvulsant and anticancer agents (Singh *et al*., 2006).

Oxidation of these thiosemicarbazides by various oxidants like ferricyanide (Llewellyn, 2014), ferric ion (Ratnam and Anipindi 2012), N-chloro-3-methyl-2,6-diphenylpiperidin-4-one (Ramalingam *et al*., 2009), bromate (Jonnalagadda *et al*., 2002), manganese(III) (Sherigara *et al*., 1994), hydrogen peroxide (Gowda and Vasireddy, 1990) and by haloamines (Gowda and Bhat, 1987; Gowda and Rao, 1988; Gowda and Sherigara, 1989; Gowda *et al*., 1991), N-chlorobenzamide (Nayak and Gowda, 1992), Cobalt(III) (Prakash *et al*., 1992), Vanadium(V) (Kandpal *et al*., 1996), ruthenium(III) (Das-Karfa *et al*., 2010), $[Mn^{IV}Mo_9O_{32}]^{6-}$ (More *et al*., 2018), Cu^{2+} (Chattopadhyay and Mak, 2000) have been carried out with the major products of oxidation given as carbon dioxide, hydrogen sulphide, nitrogen species, cyanide and sulphate except in case of ferric ion where the product is disulphide (Ratnam and Anipindi 2012; Llewellyn, 2014) and Ru(III) with a bridged product, $[(tap)_2Ru(\mu\text{-}O)(\mu\text{-}tsc)Ru(tap)_2]^{2+}$ (Das-Karfa *et al*., 2010).

2.9 Reactions of Thiodiglycol

Thiodiglycol or bis(2-hydroxyethyl) sulphide, $(HOC_2H_4)_2S$, is the primary hydrolysis product of sulphur mustard $(ClC_2H_4)_2S$ (a chemical warfare agent, CWA) (Munro *et al*., 1999) both in its deliberate destruction and environmental degradation (Ashmore and Nathanail, 2008). It is also a starting material for the production of sulphur mustard (Sokołowski and Konopski, 2007). Thiodiglycol has been used as a marker and considered a proof of the use of mustard gas (Caballero *et al*., 2018).

The organic compound is also used as a solvent in antifreeze solutions, a dyestuff for printing and in the textile industry, an antioxidant, a vulcanizing agent, an intermediate for other commodities, and a costabilizer in the production of polyvinyl chloride (Veriansyah *et al*., 2006). It is relatively non-toxic (Watson, and Griffin, 1992) despite having a similar structure and physical properties as sulphur mustard (Veriansyah *et al*., 2006) and thus also used as a model organic sulphur compound. Thiodiglycol has high thermal and chemical stability and as such severe conditions are necessary for its remediation. It is also resistant to hydrolysis and photolysis (Lee and Allen, 1998; Veriansyah *et al*., 2006).

Sulphur mustard is cytotoxic and is also a carcinogenic and mutagenic alkylating agent and its destruction has mainly been through incineration or neutralization, both very expensive processes, while bioremediation offers a very advantageous alternative method because of its minimal environmental impact and its cost effectiveness. Biodegradation of mustard gas has not been achieved under laboratory conditions due to its toxicity to micro-organisms (Munro *et al*., 1999). A two-step process for the destruction of mustard gas has already been conceived and developed: the first step lies in the chemical hydrolysis of the gas (Harvey *et al*., 1998) or the chemical treatment of mustard–lewisite mixtures (Boronin

et al., 2000), and the second step the biodegradation of the detoxification product, thiodiglycol. Although thiodiglycol has a lower toxicity, it has to be destroyed and not left to accumulate in the environment (Dell'Amico *et al*., 2009).

It was demonstrated that sulphur mustard from stockpile storage containers could be quickly hydrolyzed with water at 90 °C (Kim *et al*., 1997). Since two equivalents of HC1 are produced in this reaction, the product is neutralized with NaOH upon cooling. This reaction yields 90–95% thiodiglycol which is non-toxic, readily biodegradable, and miscible in water (Harvey *et al.*, 1997; Harvey *et al*., 1998). However, because thiodiglycol is reversibly converted to sulphur mustard in the presence of concentrated HCl, it is classified as a Schedule Two Compound in the Chemical Weapons Convention and has to be further processed (U.S. Arms Control and Disarmament Agency, 1993; Kim *et al*., 1997; Medvedeva *et al*., 2008).

If thiodiglycol was not degraded during hydrolysis, it may react with mustard gas or it intermediates to form more toxic thiodiglycol aggregates and derivatives (Munro *et al*., 1999; Medvedeva *et al*., 2008), or even react with degradation product to reverse the pathway of mustard gas degradation (Brevett *et al*., 2009).

The source of environmental thiodiglycol is not limited to the hydrolysis of mustard gas as it is also commercially exploited in textile dyeing, ink, and in printing solvents. It also has applications in chemical synthesis as a building block. Therefore, environmental contamination could also occur by accidental release, or through chemical synthesis waste water streams (Toups *et al*., 2010).

Ogata and Sawaki, (1963) examined the catalytic activities of some inorganic compounds for the hydrogen peroxide oxidation of thiodiglycol (TDG) in aqueous media at 25 °C and at a pH of 4.7. The order of catalytic activity was $Na_2MoO_4 \approx Na_2WO_4 >>$

H_2SeO_3 > NH_4VO_3 ≈ Na_2TeO_4 ≈ $UO_2(OAc)_2$ ≈ $Cu(OAc)_2$. The kinetic studies of the reaction with sodium molybdate as a catalyst indicated the probable oxidation of thiodiglycol by dihydroperoxymolybdate, $HMoO_6^-$, formed rapidly from Na_2MoO_4 and hydrogen peroxide. An increase in reaction rate was reported with decreasing pH, which was attributed to the transformation of $HMoO_6^-$ to H_2MoO_6, an indication of both forms being reactive.

In another investigation, Variansyah *et al*. (2006) studied the hydrothermal rate of decomposition thiodiglycol in an isothermal continuous tubular reactor under supercritical water conditions at the temperature range of 386 to 528 °C and a pressure of 25 MPa. The conversion of thiodiglycol was monitored by analyzing the total organic carbon (TOC) content of the liquid effluent samples and the reported reaction products were H_2S, CO, CH_4, CO_2, C_2H_4, C_2H_6 and H_2SO_4.

2.10 Reactions of Sodium Dodecyl Sulphate

Sodium dodecyl sulphate (SDS), also known as sodium lauryl sulphate (SLS), is a synthetic organic compound with the molecular formula $CH_3(CH_2)_{11}SO_4Na$. It is an anionic surfactant used in many cleaning and hygiene products and is commonly used as a component for lysing cells during RNA extraction and/or DNA extraction, and for denaturing proteins in preparation for electrophoresis in the SDS-PAGE technique. Along with sodium dodecylbenzene sulphonate and Triton X-100, aqueous solutions of SDS are popular for dispersing or suspending nanotubes, such as carbon nanotubes (CNTs) (Islam, 2003).

The periodate oxidation of bis-(1,10-phenanthroline)-dicyano iron(II), $[Fe(C_{12}H_8N_2)(CN)_2]$, in SDS surfactant was studied in aqueous and acidic medium. The redox reaction was catalysed in H_2SO_4 acid and the catalytic factor was much lower in

absence of acid. The higher rates in acid-micelle solution are the reverse to what was observed in surfactant-free medium where acid inhibited the reaction. The results were interpreted in terms of electrostatic attraction between the protonated species and the anionic surfactant aggregates (Soriyan *et al*., 2008).

Similarly, the base hydrolysis of malachite green (MG^+) was studied in aqueous solution of mixed surfactants of sodium dodecyl sulphate (SDS) and Triton X-100 (TX-100). The results show that the SDS/TX-100 system compositions has relatively significant influence on the rate constant of the base hydrolysis of MG^+ when compared to the reaction in the respective single surfactant systems (Soriyan *et al*., 2009).

In addition, the electron transfer reaction between $[Fe(bipy)_3]^{2+}$ and $[Co(CN)_5N_3]^{3-}$ has been investigated in aqueous solutions of SDS, Triton X-100 and SDS/Triton X-100 mixtures. SDS inhibited the electron transfer reaction while Triton X-100 showed no significant effect on the reaction. Binding parameters were obtained using Piszkiewicz model with cooperativity index n = 2.184 in the presence of SDS. Binary mixture of surfactants Triton X-100/SDS inhibited the reaction at low concentrations of Triton X-100 with relative rate enhancement as the mixture becomes richer in Triton X-100. The results were explained in terms of strong electrostatic and/or hydrophobic interactions between the surfactants and the substrates (Ogunlusi *et al*., 2013).

2.11 Reactions of Cetyltrimethylammonium Bromide

Cetyltrimethylammonium bromide (CTAB) also known as hexadecyltrimethylammonium bromide and cetrimonium bromide is a quaternary ammonium surfactant with the molecular formula $[(C_{16}H_{33})N(CH_3)_3]Br$. It is one of the components of the antiseptic, cetrimide (Laemmli, 1970). The cetrimonium (hexadecyltrimethylammonium) cation is an effective antiseptic agent against bacteria and

fungi. It is also one of the main components of some buffers for the extraction of DNA (Clarke, 2009). It has been widely used in synthesis of gold nanoparticles and mesoporous silica nanoparticles and also in hair conditioning products.

The alkaline fading of brilliant green (a triphenylmethane dye) was examined in aqueous solutions of dodecyltrimethylammonium bromide (DTAB), didodecyldimethylammonium bromide (DDAB) and cetyltrimethylammonium bromide (CTAB) at 25 °C. The pseudo-first order rate constant variation with surfactant concentration showed a sigmoid shaped curve, which is analogous to the positive cooperativity in enzymatic reactions. The catalytic factors k_ψ/k_w of 1.8, 11.9 and 30.4 were obtained for DDAB, DTAB and CTAB respectively. The data obtained fitted the Pieszkiewicz model with the value of the cooperativity index, n, greater than unity in all cases, but less than the number of surfactant molecules found in micelle, which indicated the presence of pre-micelle aggregates (Owoyomi *et al*., 2007).

Similarly, the redox reaction between tris(1,10-phenanthroline)iron(II), $[Fe(phen)_3]^{2+}$, and azidopentacyanocobaltate(III), $[Co(CN)_5N_3]^{3-}$ was investigated in three cationic surfactants: dodecyltrimethylammonium bromide (DTAB), tetradecyltrimethylammonium bromide (TTAB) and cetyltrimethylammonium bromide (CTAB) in the presence of 0.1 mol dm^{-3} NaCl at 35 °C. Second order rate constant in the absence and presence of surfactant, k_w and k_ψ were determined and inhibition factors, k_w/k_ψ followed the trend CTAB > TTAB > DTAB with respect to the surfactant concentrations used. Electron transfer rate was inhibited by the surfactants with premicelllar activity. The magnitudes of the binding constants obtained suggested significant electrostatic and hydrophobic interactions. Activation parameters $\Delta H^{\ddagger}$, $\Delta S^{\ddagger}$, and E_a had larger positive values in the presence of surfactants than in surfactant-free medium. The electron transfer was

proposed to proceed via outer-sphere mechanism in the presence of the surfactants (Ogunlusi *et al*., 2016).

CHAPTER THREE

3.0 MATERIALS AND METHODS

3.1 Materials

3.1.1 Chemicals and reagents

All chemicals and reagents used in this work are analar grade and were used without further purification except otherwise stated. The chemicals used include o-phenylenediamine (BDH), salicylaldehyde (Merck), methanol (Merck), anhydrous iron(III) chloride (SureChem), manganese(II) acetate tetrahydrate (Loba Chemie), lead(1V) oxide (BDH), acetic acid (Riedel-deHaen), DMSO (JHD), thioglycolic acid (BDH, 92.12 g mol^{-1}, 98 %, density 1.33 g cm^{-3}), oxalic acid dihydrate (JHD, 126.07 g mol^{-1}), hypophosphorous acid (Sigma-Aldrich, 66.0 g mol^{-1}, 50 %, density 1.21 g cm^{-3}), sodium thiosulphate pentahydrate (Kermel, 248.17 g mol^{-1}), hydrogen peroxide (BDH, 34.015 g mol^{-1}, 30 %, density 1.11 g cm^{-3}), thioglycol (Merck, 78.13 g mol^{-1}, 98 %, density 1.114 g cm^{-3}), potassium thiocyanate (BDH, 97.181 g mol^{-1}), thiosemicarbazide (Kem Light, 91.14 g mol^{-1}), thiodiglycol (BDH, 122.19 g mol^{-1}, 97 %, density 1.18 g cm^{-3}), sodium dodecyl sulphate (BDH, 288.38 g mol^{-1}), cetyltrimethylammonium bromide (PureChem, 364.46 g mol^{-1}), sodium chloride (JHD, 58.44 g mol^{-1}), sodium carbonate (BDH, 105.99 g mol^{-1}), hydrochloric acid (BDH, 36.46 g mol^{-1}, 36.5 %, density 1.18 g cm^{-3}), sodium nitrate (BDH, 84.99 g mol^{-1}), sodium sulphate (Kermel, 142.04 g mol^{-1}), potassium chloride (BDH, 74.55 g mol^{-1}), sodium acetate (BDH, 82.03 g mol^{-1}), sodium formate (Hopkin and Williams, 68.01 g mol^{-1}), calcium chloride (BDH, 110.99 g mol^{-1}) and magnesium chloride hexahydrate (BDH, 203.30 g mol^{-1}).

3.1.2 Equipment

The rates of the reactions were monitored by following the rate of decrease in absorbance of the reactions on a Corning 253 colourimeter. All weighings were done using Mettler Toledo MS-TS analytical balance. Conductivity measurements were carried out with a HANNA HI 4321 conductivity meter.

3.1.3 Preparation of DMSO:H_2O (1:4 v/v) mixed solution

Mixed solution (DMSO:H_2O; 1:4 v/v) was prepared by measuring 50 cm^3 of DMSO (JHD) using a measuring cylinder into a 250 cm^3 volumetric flask and made up to the mark with distilled water.

3.1.4 Preparation of stock thioglycolic acid solution

Stock solution of thioglycolic acid, $HSCH_2COOH$, (1.0 mol dm^{-3}) was prepared by transferring 7.07 cm^3 of 98 % $HSCH_2COOH$ solution (BDH, 92.12 g mol^{-1}, density 1.33 g cm^{-3}) into a 100 cm^3 volumetric flask and made up to the mark with distilled water.

3.1.5 Preparation of stock oxalic acid solution

Stock solution of oxalic acid ($H_2C_2O_4$) (0.5 mol dm^{-3}) was prepared by dissolving 3.15 g of $H_2C_2O_4.2H_2O$ (JHD, 126.07 g mol^{-1}) in a 100 cm^3 volumetric flask with distilled water and was standardised titrimetically using standard sodium hydroxide (NaOH) solution.

3.1.6 Preparation of hypophosphorous acid stock solution

Stock solution of hypophosphorous acid, H_3PO_2, (0.5 mol dm^{-3}) was prepared by transferring 2.73 cm^3 of 50 % H_3PO_2 solution (Sigma-Aldrich, 66.0 g mol^{-1}, density 1.21 g cm^{-3}) into a 50 cm^3 volumetric flask and made up to the mark with distilled water and was standardised titrimetically using standard NaOH solution.

3.1.7 Preparation of sodium thiosulphate solution

A solution of sodium thiosulphate, $Na_2S_2O_3$, (1.0 mol dm^{-3}) was prepared by dissolving 24.82 g of $Na_2S_2O_3.5H_2O$ (Kermel, 248.17 g mol^{-1}) in a 100 cm^3 volumetric flask and made up to the mark with distilled water.

3.1.8 Preparation of stock hydrogen peroxide solution

Stock solution of hydrogen peroxide, H_2O_2, (1.0 mol dm^{-3}) was prepared by transferring 10.21 cm^3 of 30 % H_2O_2 solution (BDH, 34.015 g mol^{-1}, density 1.11 g cm^{-3}) into a 100 cm^3 volumetric flask and made up to the mark with distilled water and was standardised titrimetically using sodium thiosulphate (Vogel, 2000).

3.1.9 Preparation of stock thioglycol solution

Stock solution of thioglycol, $HSCH_2CH_2OH$, (1.0 mol dm^{-3}) was prepared by transferring 7.16 cm^3 of 98 % $HSCH_2CH_2OH$ solution (Merck, 78.13 g mol^{-1}, density 1.114 g cm^{-3}) into a 100 cm^3 volumetric flask and made up to the mark with distilled water.

3.1.10 Preparation of stock potassium thiocyanate solution

Stock solution of potassium thiocyanate, KSCN, (1.0 mol dm^{-3}) was prepared by dissolving 9.718 g of KSCN (BDH, 97.181 g mol^{-1}) in a 100 cm^3 volumetric flask with distilled water and standardised gravimetrically.

3.1.11 Preparation of stock thiosemicarbazide solution

Stock solution of thiosemicarbazide, $H_2NNHCSNH_2$, (1.0 mol dm^{-3}) was prepared by dissolving 9.114 g of $H_2NNHCSNH_2$ (Kem Light, 91.14 g mol^{-1}) in a 100 cm^3 volumetric flask and made up to the mark with mixed solution (DMSO:H_2O; 1:4 v/v).

3.1.12 Preparation of stock thiodiglycol solution

Stock solution of thiodiglycol, $S(CH_2CH_2OH)_2$, (2.0 mol dm^{-3}) was prepared by transferring 21.35 cm^3 of 97 % $S(CH_2CH_2OH)_2$ solution (BDH, 122.19 g mol^{-1}, density 1.18 g cm^{-3}) into a 100 cm^3 volumetric flask and made up to the mark with distilled water.

3.1.13 Preparation of stock sodium dodecyl sulphate solution

Stock solution of sodium dodecyl sulphate (SDS) (0.1 mol dm^{-3}) was prepared by dissolving 1.44 g of SDS (BDH, 288.38 g mol^{-1}) in a 50 cm^3 volumetric flask with distilled water.

3.1.14 Preparation of stock cetyltrimethylammonium bromide solution

Stock solution of cetyltrimethylammonium bromide **(**CTAB) (0.1 mol dm^{-3}) was prepared by dissolving 1.82 g of CTAB (PureChem, 364.46 g mol^{-1}) in a 50 cm^3 volumetric flask with distilled water.

3.1.15 Preparation of stock sodium chloride solution

Stock solution of sodium chloride, NaCl, (1.5 mol dm^{-3}) was prepared by dissolving 21.92 g NaCl (JHD, 58.44 g mol^{-1}) in a 250 cm^3 volumetric flask with distilled water and standardized gravimetrically.

3.1.16 Preparation of stock sodium carbonate solution

Stock solution of sodium carbonate, Na_2CO_3, (0.2 mol dm^{-3}) was prepared by dissolving 2.12 g Na_2CO_3 (BDH, 105.99 g mol^{-1}) in a 100 cm^3 volumetric flask and made up to the mark with distilled water.

3.1.17 Preparation of hydrochloric acid stock solution

Stock solution of hydrochloric acid, HCl, (0.2 mol dm^{-3}) was prepared by transferring 4.24 cm^3 of 36.5 % HCl solution (BDH, 36.46 g mol^{-1}, density 1.18 g cm^{-3})

into a 250 cm^3 volumetric flask, made up to the mark with distilled water and was standardized volumetrically using Na_2CO_3 and methyl orange as indicator (Vogel, 2000).

3.1.18 Preparation of stock salt solutions

Stock solutions (0.5 mol dm^{-3}) of sodium nitrate, $NaNO_3$, (BDH, 84.99 g mol^{-1}), sodium sulphate, Na_2SO_4, (Kermel, 142.04 g mol^{-1}), potassium chloride, KCl, (BDH, 74.55 g mol^{-1}), sodium acetate, CH_3COONa, (BDH, 82.03 g mol^{-1}), sodium formate, HCOONa, (Hopkin and Williams, 68.01 g mol^{-1}), calcium chloride, $CaCl_2$, (BDH, 110.99 g mol^{-1}) and magnesium chloride, $MgCl_2.6H_2O$, (BDH, 203.30 g mol^{-1}) were prepared by dissolving 4.25 g, 7.10 g, 3.73 g, 4.10 g, 3.40 g, 5.55 g and 10.17 g respectively of each salt in a 100 cm^3 volumetric flask with distilled water and standardized gravimetrically.

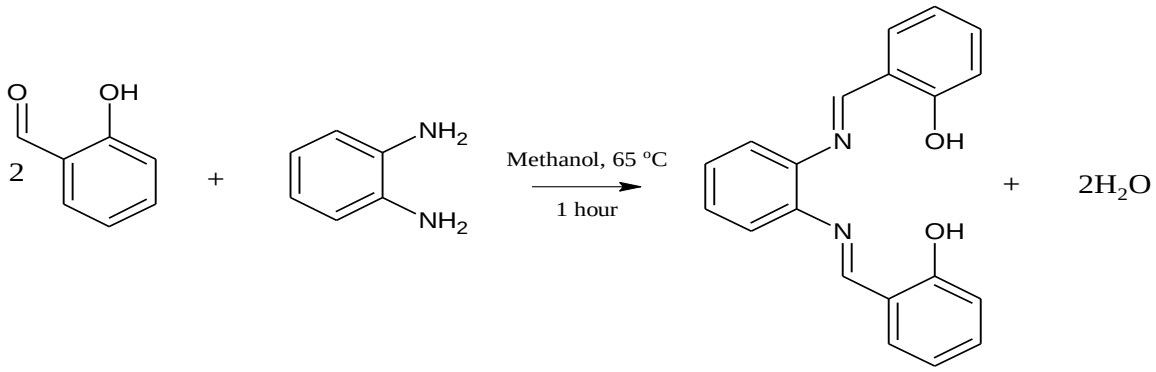
3.2 Methods

3.2.1 Synthesis of Fe(III) and Mn(III) – salphen complexes

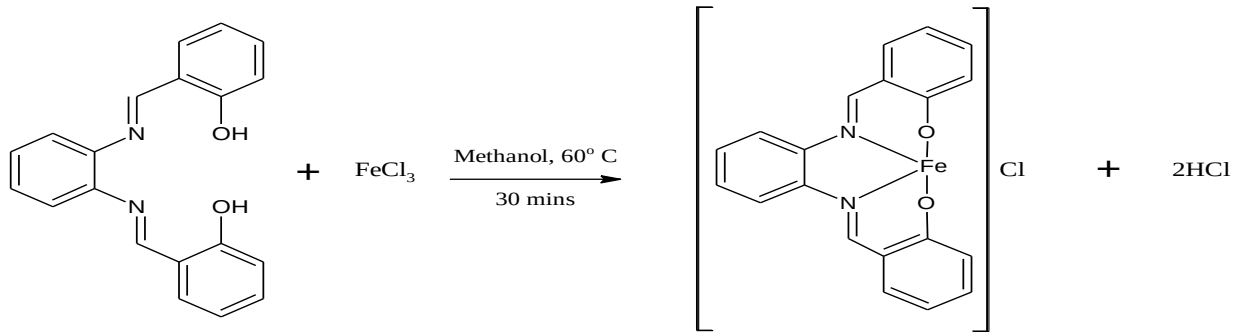
The ligand, bis(salicylidene)phenylenediamine, and the Fe(III) and Mn(III) complexes, [Fe(salphen)]Cl and [Mn(salphen)](CH_3COO), were synthesized and characterized according to the literature (Ansari *et al*., 2009a; Ansari *et al*., 2009b; Ansari *et al*., 2011). The ligand was prepared by refluxing o-phenylenediamine (BDH, 1.71 g, 15.8 mmol) with salicylaldehyde (Merck, 3.3 cm^3, 31.6 mmol) in methanol (Merck, 30 cm^3) for 1 hour. The precipitate was cooled and filtered after which it was washed with methanol and then dried in a desiccator. The reaction step is shown as Scheme 3.1.

The complex, [Fe(salphen)]Cl, was prepared by stirring a mixture of the Schiff base (0.78g, 2.5 mmol) with anhydrous iron(III) chloride (SureChem, 0.4 g, 2.5 mmol) in methanol (20 cm^3) at 60 °C for 30 minutes. The mixture was then kept at room temperature overnight to precipitate out the complex. The product was recrystallized from methanol and dried in a desiccator (Ansari *et al*., 2011). The reaction step is shown as Scheme 3.2.

$Mn(CH_3COO)_3$ was prepared by stirring a mixture of manganese(II) acetate tetrahydrate (Loba Chemie, 7.35 g, 30 mmol) and lead(1V) oxide (BDH, 2.39 g, 10 mmol) in acetic acid (Riedel-deHaen, 75 cm^3) at 50-60 °C until the black lead(IV) oxide dissolved. The resulting dark brown solution was kept overnight. Dark red coloured crystals which formed were filtered off by suction and recrystallized from acetic acid and dried in a desiccator (Gündüz *et al*., 1994).



Scheme 3.1: **Reaction of salicylaldehyde and o-phenylenediamine to give N,N′-Bis(salicylidene)phenylenediamine**



Scheme 3.2: **Reaction of N,N′-bis(salicylidene)phenylenediamine to give N,N′ phenylenebis(salicylideneiminato)iron(III), [Fe(salphen)]Cl**

The complex, [Mn(salphen)](CH_3COO), was prepared by stirring a mixture of the Schiff base (2.04g, 6.5 mmol) with $Mn(CH_3COO)_3$ (1.73 g, 6.5 mmol) in methanol (40 ml) at 60 °C for 30 minutes, then keeping the mixture at room temperature overnight to

precipitate out the complex. The product was recrystallized from methanol and dried in a desiccator (Ansari *et al*., 2009b).

The ligand and the complexes were characterized by UV-Visible and FTIR analyses. The molar conductivities of [Fe(salphen)]Cl and [Mn(salphen)](CH_3COO) were determined in 2.0×10^{-4} mol dm^{-3} and 1.0×10^{-4} mol dm^{-3} (DMSO:H_2O; 1:4 v/v) solutions respectively.

Stock solutions of $[Fe(salphen)]^+$ (4.83×10^{-3} mol dm^{-3}) and $[Mn(salphen)]^+$ (4.85×10^{-3} mol dm^{-3}) were prepared by accurately weighing and transferring 0.0196 g and 0.0225 g of the complexes respectively into a 10 cm^3 volumetric flask and dissolved with 2 cm^3 of DMSO. The solutions were made up to the mark with distilled water.

3.2.2 Stoichiometry

The stoichiometry of each of the reactions were determined by spectrophotometric titration using the mole ratio method (Onu *et al*., 2016). The concentrations of $[Fe(salphen)]^+$ and $[Mn(salphen)]^+$ complex were kept constant while that of the reductants were varied at different mole ratios as follows:

i. For $[Fe(salphen)]^+$ - TSH reaction; $[Fe(salphen)^+] = 2.0 \times 10^{-4}$ mol dm^{-3}, [TSH] = $(0.25 – 3.5) \times 10^{-4}$ mol dm^{-3}, $\mu = 0.2$ C^2 mol dm^{-3}, D = 76.88, T = 26 ± 1°C and λ_{max} = 435 nm

ii. For $[Fe(salphen)]^+$ - $H_2C_2O_4$ reaction; $[Fe(salphen)^+] = 2.0 \times 10^{-4}$ mol dm^{-3}, $[H_2C_2O_4] = (0.25 – 3.5) \times 10^{-4}$ mol dm^{-3}, $\mu = 0.2$ C^2 mol dm^{-3}, D = 76.06, T = 26 ± 1°C and λ_{max} = 435 nm

iii. For $[Fe(salphen)]^+$ - H_3PO_2 reaction; $[Fe(salphen)^+] = 2.0 \times 10^{-4}$ mol dm^{-3}, $[H_3PO_2] = (0.25 – 3.5) \times 10^{-4}$ mol dm^{-3}, $\mu = 0.2\ C^2$ mol dm^{-3}, D = 76.68, T = 26 ± 1°C and λ_{max} = 435 nm

iv. For $[Fe(salphen)]^+$ - H_2O_2 reaction; $[Fe(salphen)^+] = 1.0 \times 10^{-4}$ mol dm^{-3}, $[H_2O_2] = (0.25 – 3.5) \times 10^{-4}$ mol dm^{-3}, $\mu = 0.6\ C^2$ mol dm^{-3}, $[H^+] = 2.0 \times 10^{-5}$ mol dm^{-3}, D = 78.12, T = 28 ± 1°C and λ_{max} = 435 nm

v. For $[Mn(salphen)]^+$ - H_2O_2 reaction; $[Mn(salphen)^+] = 1.0 \times 10^{-4}$ mol dm^{-3}, $[H_2O_2] = (0.25 – 3.5) \times 10^{-4}$ mol dm^{-3}, $\mu = 0.2\ C^2$ mol dm^{-3}, $[H^+] = 2.0 \times 10^{-5}$ mol dm^{-3}, D = 76.82, T = 30 ± 1°C and λ_{max} = 450 nm

vi. For $[Mn(salphen)]^+$ - TSH reaction; $[Mn(salphen)^+] = 1.0 \times 10^{-4}$ mol dm^{-3}, [TSH] = $(0.25 – 3.5) \times 10^{-4}$ mol dm^{-3}, $\mu = 0.6\ C^2$ mol dm^{-3}, D = 77.98, T = 32 ± 1°C and λ_{max} = 450 nm

vii. For $[Mn(salphen)]^+$ - RSH reaction; $[Mn(salphen)^+] = 1.0 \times 10^{-4}$ mol dm^{-3}, [RSH] = $(0.25 – 3.5) \times 10^{-4}$ mol dm^{-3}, $\mu = 0.6\ C^2$ mol dm^{-3}, $[H^+] = 4.0 \times 10^{-5}$ mol dm^{-3}, D = 78.19, T = 28 ± 1°C and λ_{max} = 450 nm

viii. For $[Mn(salphen)]^+$ - SCN^- reaction; $[Mn(salphen)^+] = 1.0 \times 10^{-4}$ mol dm^{-3}, $[SCN^-] = (0.25 – 3.5) \times 10^{-4}$ mol dm^{-3}, $\mu = 0.6\ C^2$ mol dm^{-3}, $[H^+] = 4.0 \times 10^{-5}$ mol dm^{-3}, D = 78.12, T = 28 ± 1°C and λ_{max} = 450 nm

ix. For $[Mn(salphen)]^+$ - $H_2NNHCSNH_2$ reaction; $[Mn(salphen)^+] = 1.0 \times 10^{-4}$ mol dm^{-3}, $[H_2NNHCSNH_2] = (0.25 – 3.5) \times 10^{-4}$ mol dm^{-3}, $\mu = 0.6\ C^2$ mol dm^{-3}, $[H^+] = 2.0 \times 10^{-5}$ mol dm^{-3}, D = 75.10, T = 28 ± 1°C and λ_{max} = 450 nm

x. For $[Mn(salphen)]^+$ - $S(CH_2CH_2OH)_2$ reaction; $[Mn(salphen)^+] = 1.0 \times 10^{-4}$ mol dm^{-3}, $[S(CH_2CH_2OH)_2] = (0.25 – 3.5) \times 10^{-4}$ mol dm^{-3}, $\mu = 0.6$ C^2 mol dm^{-3}, $[H^+] = 2.0 \times 10^{-5}$ mol dm^{-3}, D = 66.60, T = 50 ± 1°C and λ_{max} = 450 nm

The reactions were allowed to go to completion and the absorbance were recorded at 435 nm and 450 nm for reactions of $[Fe(salphen)]^+$ and $[Mn(salphen)]^+$ respectively. The stoichiometries of the reactions were determined from the points of inflexion on the graphs of plots of absorbances against mole ratios (Idris *et al*., 2015).

3.2.3 Products analysis

At the completion of the reactions, the reaction mixtures were analyzed for organic and inorganic products formed in each system as follows:

(a) For reactions of $[Fe(salphen)]^+$, a $KMnO_4$ solution was added to the final reaction product of $[Fe(salphen)]^+$ and reductants to confirm the presence of Fe^{2+}, the reduction product of Fe^{3+} (Mifsud, 2009).

(b) The presence of CO_2, the oxidation product of $H_2C_2O_4$, was confirmed using lime water ($Ca(OH)_2$) (Svehla and Sivasankar, 2012).

(c) The product of oxidation of hypophosphorous acid was determined by the addition of saturated sodium molybdate solution to the reaction product (Yusuf *et al*., 2004; Mohammed *et al*., 2017).

(d) For reactions of $[Mn(salphen)]^+$, 1 drop of test sample was diluted with 0.5 cm^3 concentrated H_2SO_4 after which 0.2 g of KIO_4 was added and the solution was gently warmed to confirm the presence of Mn^{2+}, the reduction product of Mn^{3+} (Nazarenko, 2004).

(e) For SCN^- reaction, SO_4^{2-} ion, was detected by addition of $BaCl_2$ solution to the reaction product followed by excess dilute HCl while CN^- ion was detected by addition of $S_2O_3^{2-}$ solution to the reaction product followed by $FeCl_3$ (Svehla and Sivasankar, 2012).

(f) For $H_2NNHCSNH_2$ reaction, SO_4^{2-} ion, was detected by addition of $BaCl_2$ solution to the reaction product followed by excess dilute HCl. CN^- ion was detected by addition of $S_2O_3^{2-}$ followed by $FeCl_3$. Also, NH_4^+ ion was detected by adding 1 cm^3 of 0.1 mol dm^{-3} NaOH solution to the reaction product in a tube and a moistened red litmus paper was placed at the tip of the tube which was then gently heated (Svehla and Sivasankar, 2012).

(g) For TSH, RSH and $S(CH_2CH_2OH)_2$ reactions, the reaction products were extracted six times with diethyl ether. The combined ether extracts were dried with anhydrous Na_2SO_4 and allowed to dry. FTIR analyses were carried out on the products.

3.2.4 Determination of reactions order

The rates of the reactions were studied by monitoring the decrease in absorbance of the reaction mixture at its λ_{max} using Corning Colourimeter 253. All kinetic measurements were carried out under pseudo-first order conditions with respective reductant concentrations in at least 10-fold excess of the oxidant concentration. Ionic strength as well as $[H^+]$ were maintained constant for each system unless otherwise stated. The pseudo – first order plots of log $(A_t - A_\infty)$ against time were made (where A_t and A_∞ are absorbances at time, t and infinity respectively). The slopes from the plots gave the pseudo – first order rate constants, k_1. The second order rate constants, k_2, were determined as k_1/[reductant] (Myek *et al*., 2017).

3.2.5 Determination of effect of acid on the reactions rate

The effect of varying hydrogen ion concentration on the reaction rates was investigated by keeping the concentrations of the oxidant, reductants and ionic strength constant while that of the hydrogen ion was varied. Order of the reaction with respect to acid concentration was obtained as the slope of the plot of log k_1 against log $[H^+]$. Variation of acid dependent second order rate constants, k_2 with $[H^+]$ were obtained by plotting k_2 against $[H^+]$ or $\frac{1}{[H^+]}$ respectively (Idris *et al*., 2015).

3.2.6 Determination of effect of ionic strength and dielectric constant

The ionic strength of the reaction mixture were varied while maintaining the concentrations of the oxidant, reductant and hydrogen ion constant (Hamza *et al*., 2012). The effect of dielectric constant (D) on the reaction rate was investigated by carrying out the reactions in medium of varying dielectric constants. The medium dielectric constants were varied using a binary solvent mixture of water and DMSO while keeping all other conditions constant (Liou and Wang, 2000).

3.2.7 Determination of effect of added of ions

The effect of added ions on the reaction rate were investigated by the addition of $(1.0 – 30.0) \times 10^{-3}$ mol dm^{-3} solutions of ions (Ca^{2+}, Mg^{2+}, K^+, CH_3COO^-, $HCOO^-$, NO_3^- or SO_4^{2-}) while maintaining the oxidant, reductant and hydrogen ion concentrations and ionic strength constant (Mohammed *et al.,* 2016).

3.2.8 Determination of effect of temperature on the reactions rate

The influence of temperature on the reaction rates both in the presence and absence of surfactant were studied in the range 298 – 317 K using a thermostated water bath. The reactant solutions were equilibrated at the temperature of the water bath, mixed and quickly

transferred into the colourimeter to measure the change in absorbance with time. The temperature dependence data were analyzed using Eyring's plot of $\ln\left(\frac{k_2}{T}\right)$ versus $\left(\frac{1}{T}\right)$ (Espenson, 1981) as indicated in equation 3.1. The Gibb's free energy and activation energy for the reactions were calculated using equations 3.2 and 3.3 respectively (Ogunlusi *et al*., 2016).

$$\ln\left(\frac{k_2}{T}\right) = \ln\left(\frac{k_B}{h}\right) + \frac{\Delta S^{\ddagger}}{R} - \frac{\Delta H^{\ddagger}}{R}\left(\frac{1}{T}\right) \quad 3.1$$

$$\Delta G^{\ddagger} = \Delta H^{\ddagger} - T\Delta S^{\ddagger} \quad 3.2$$

$$Ea = \Delta H^{\ddagger} + RT \quad 3.3$$

where k_2 = second order rate constant, T = Kelvin temperature, k_B = Boltzmann's constant, h = Planck's constant, $\Delta S^{\ddagger}$ entropy of activation, $\Delta H^{\ddagger}$ = enthalpy of activation, *A* = pre-exponential factor (constant), E_a = Activation energy, $\Delta G^{\ddagger}$ = Gibb's energy of activation and R = Molar Gas constant.

3.2.9 Test for intermediate complex

The spectra of the reaction mixtures were obtained after the commencement of the reaction. These were compared with the spectra of the iron(III) and manganese(III) complexes over a wavelength range of 400 – 700 nm. Michaelis-Menten plots of $1/k_1$ versus 1/[reductant] were carried out (Onu *et al*., 2015).

3.2.10 Test for free radicals

Test for free radicals were investigated by addition of acrylamide to partially reacting mixtures followed by excess methanol (Abdulsalam *et al*., 2016).

3.2.11 Determination of critical micelle concentration

The critical micelle concentration (CMC) of the surfactants were determined by measuring the specific conductivities of various concentrations of the surfactant solutions.

The conductivity meter was calibrated using 0.01 mol dm^{-3} KCl solution. The breakpoint in the conductivity-concentration profile was taken as the CMC (Olanrewaju *et al*., 2011).

3.2.12 Determination of effect of surfactant concentrations on the reactions rate

The redox reactions were investigated in separate surfactant solutions of SDS and CTAB at varying concentrations while maintaining the concentrations of the oxidant, reductant, hydrogen ion and ionic strength constant. The pseudo – first order plots of log $(A_t - A_\infty)$ against time were made and from the slopes of the plots, the pseudo – first order rate constants, k_1 were obtained. The second order rate constants, k_ψ, were determined as k_1/[reductant]. From the results, the catalytic factor (k_ψ/k_w), were determined as the ratio of the second order rate constant in the presence of surfactant (k_ψ) to the second order rate constant in the absence of surfactant (k_w), whereas the inhibition factor (k_w/k_ψ), were determined as the ratio of the second order rate constant in the absence of surfactant (k_w) to the second order rate constant in the presence of surfactant (k_ψ) (where $k_w = k_2$ = second order rate constant in the absence of surfactant) (Ogunlusi *et al*., 2016).

CHAPTER FOUR

4.0 RESULTS

4.1 Synthesis of Fe(III) and Mn(III) – salphen complexes

The yield of the ligand, [Fe(salphen)]Cl, $Mn(CH_3COO)_3$ and [Mn(salphen)](CH_3COO) obtained were 4.29 g (86%), 0.47 g (47%), 3.62 g (68%) and 2.11 g (70%) respectively. From the FTIR (ATR, cm^{-1}) spectra of the Ligand, peaks were observed at 3050, 2591, 1608, 1558, 1470, 1447, 1399, 1360, 1274, 1189, 1149, 1101, 908, 752, 639, 580 and 499 cm^{-1} (Appendix I) while peaks were observed at 1602, 1577, 1533, 1461, 1439, 1378, 1312, 1195, 1146, 1126, 922, 871, 811, 749, 613, 536, 508 and 475 cm^{-1} from the spectra of $[Fe(salphen)]^+$ (Appendix II). Similary, from the spectra of $[Mn(salphen)]^+$, peaks were observed at 1604, 1575, 1531, 1460, 1431, 1405, 1375, 1313, 1190, 1144, 1127, 1026, 926, 873, 809, 771, 751, 628, 608, 539, 505, 446 cm^{-1} (Appendix III).

The molar conductivity of $[Fe(salphen)]^+$ was found to be 145 S cm^2 mol^{-1} with specific conductance of 29.0×10^{-6} S cm^{-1} while that of $[Mn(salphen)]^+$ was 112 S cm^2 mol^{-1} with specific conductance of 11.20×10^{-6} S cm^{-1}.

4.2 Stoichiometric Studies

Stoichiometric studies showed that one mole of $[Fe(salphen)]^+$ was consumed by one mole of TSH whereas two moles of $[Fe(salphen)]^+$ were consumed by one mole each of H_3PO_2 and H_2O_2 but by three moles of $H_2C_2O_4$. The results also showed that one mole of $[Mn(salphen)]^+$ was consumed by one mole of each of TSH, RSH and SCN^- whereas two

moles of $[Mn(salphen)]^+$ were consumed by one mole each of H_2O_2, $H_2NNHCSNH_2$ and $S(CH_2CH_2OH)_2$. The titration curves used to determine the reaction stoichiometries are presented in Figures 4.1 – 4.10. The overall equations for the redox reactions can therefore be represented by equations 4.1 – 4.10.

$$2[Fe(salphen)]^+ + 2[TSH] \longrightarrow 2[Fe(salphen)] + TSST + 2H^+ \quad 4.1$$

$$2[Fe(salphen)]^+ + 3H_2C_2O_4 + O_2 \longrightarrow 2[Fe(salphen)] + 6CO_2 + 2H_2O + 2H^+ \quad 4.2$$

$$2[Fe(salphen)]^+ + H_3PO_2 + H_2O \longrightarrow 2[Fe(salphen)] + H_3PO_3 + 2H^+ \quad 4.3$$

$$2[Fe(salphen)]^+ + H_2O_2 \longrightarrow 2[Fe(salphen)] + O_2 + 2H^+ \quad 4.4$$

$$2[Mn(salphen)]^+ + H_2O_2 \longrightarrow 2[Mn(salphen)] + O_2 + 2H^+ \quad 4.5$$

$$2[Mn(salphen)]^+ + 2[TSH] \longrightarrow 2[Mn(salphen)] + TSST + 2H^+ \quad 4.6$$

$$2[Mn(salphen)]^+ + 2[RSH] \longrightarrow 2[Mn(salphen)] + RSSR + 2H^+ \quad 4.7$$

$$2[Mn(salphen)]^+ + 2[SCN^-] \longrightarrow 2[Mn(salphen)] + (SCN)_2 \quad 4.8$$

Thiocyanogen, $(SCN)_2$, undergoes further hydrolysis according to equation 4.9 to give the final products.

$$4H_2O + 3(SCN)_2 \longrightarrow 7H^+ + 5SCN^- + HCN + SO_4^{2-} \quad 4.9$$

$$2[Mn(salphen)]^+ + H_2NNHCSNH_2 + 3H_2O + \tfrac{1}{2}O_2 \longrightarrow 2[Mn(salphen)] + SO_4^{2-} + CN^- + 2NH_4^+ + 3H^+ \quad 4.10$$

$$2[Mn(salphen)]^+ + S(CH_2CH_2OH)_2 + H_2O \longrightarrow 2[Mn(salphen)] + O{=}S(CH_2CH_2OH)_2 + 2H^+ \quad 4.11$$

4.3 Products Analysis

The results of possible products are as follows:

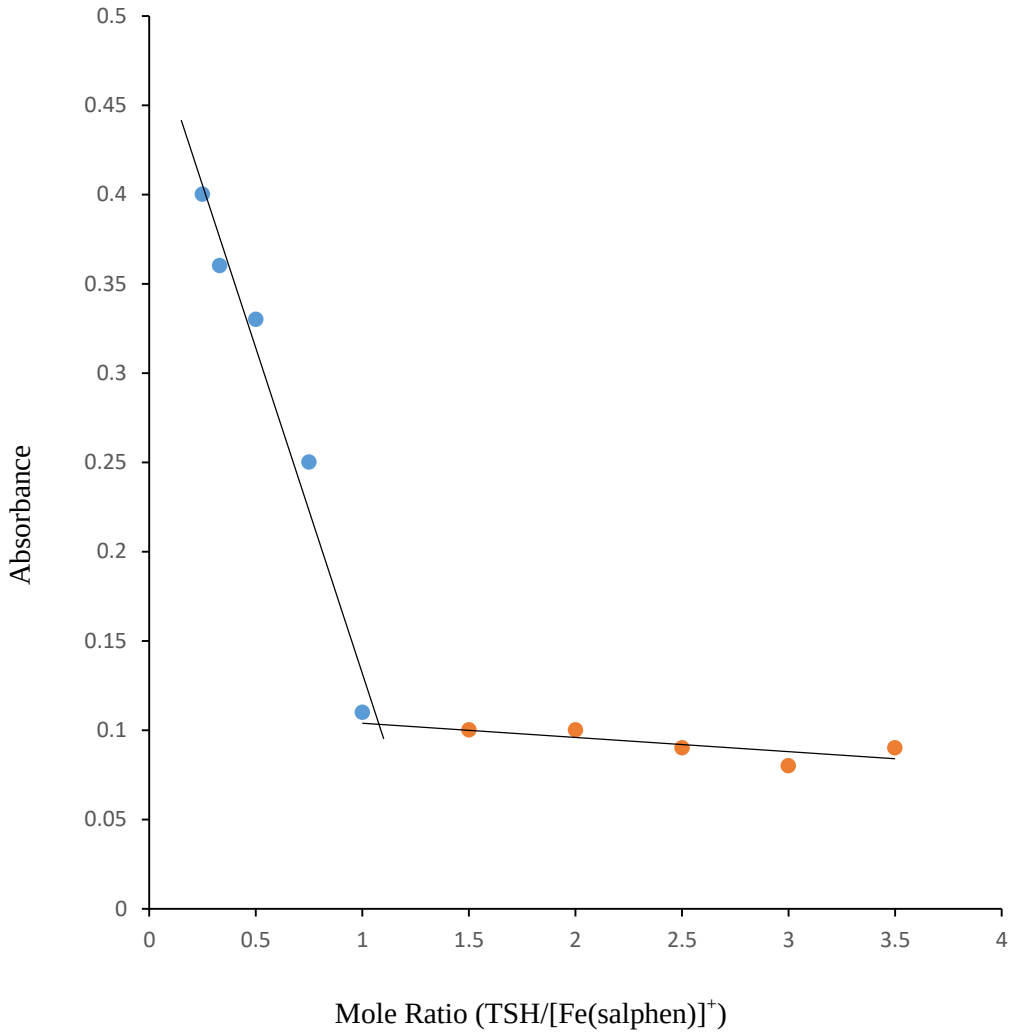


Figure 4.1: **Plot of absorbance versus mole ratio for the redox reaction of $[Fe(salphen)]^+$ and TSH at $[Fe(salphen)^+] = 2.0 \times 10^{-4}$ mol dm^{-3}, $\mu = 0.2$ C^2 mol dm^{-3}, D = 76.88, T = 26 ± 1 °C and λ_{max} = 435 nm**

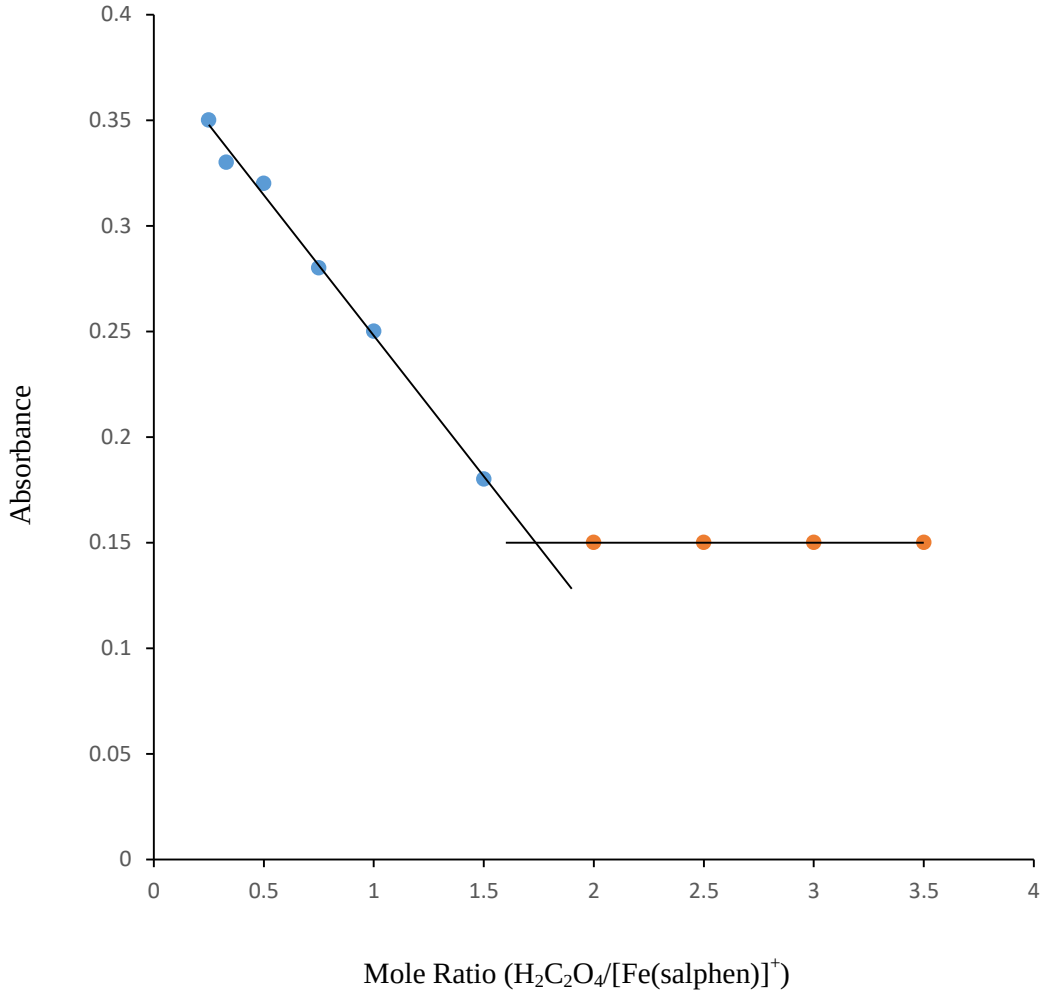


Figure 4.2: **Plot of absorbance versus mole ratio for the redox reaction of [Fe(salphen)]$^+$ and $H_2C_2O_4$ at [Fe(salphen)$^+$] = 2.0 × 10^{-4} mol dm^{-3}, μ = 0.2 C^2 mol dm^{-3}, D = 76.06, T = 26 ± 1 °C and λ_{max} = 435 nm**

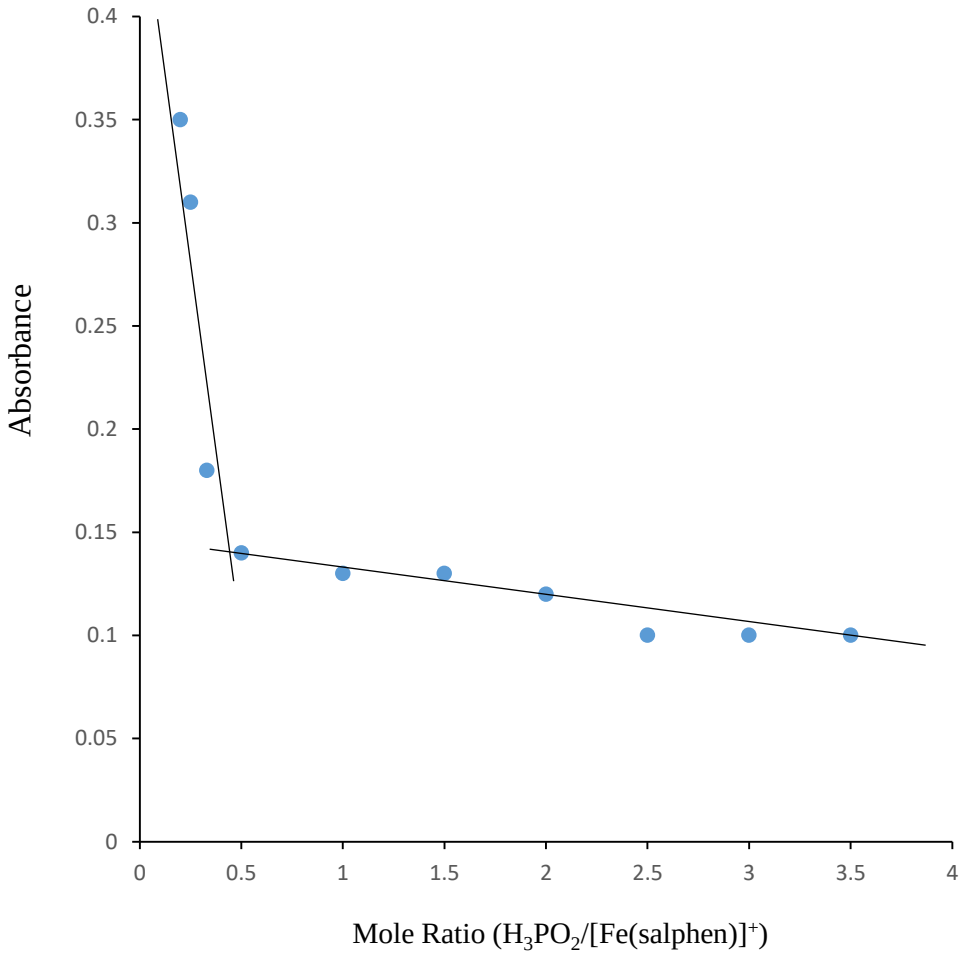


Figure 4.3: **Plot of absorbance versus mole ratio for the redox reaction of $[Fe(salphen)]^+$ and H_3PO_2 at $[Fe(salphen)^+] = 2.0 \times 10^{-4}$ mol dm^{-3}, μ = 0.2 C^2 mol dm^{-3}, D = 76.68, T = 26 ± 1°C and λ_{max} = 435 nm**

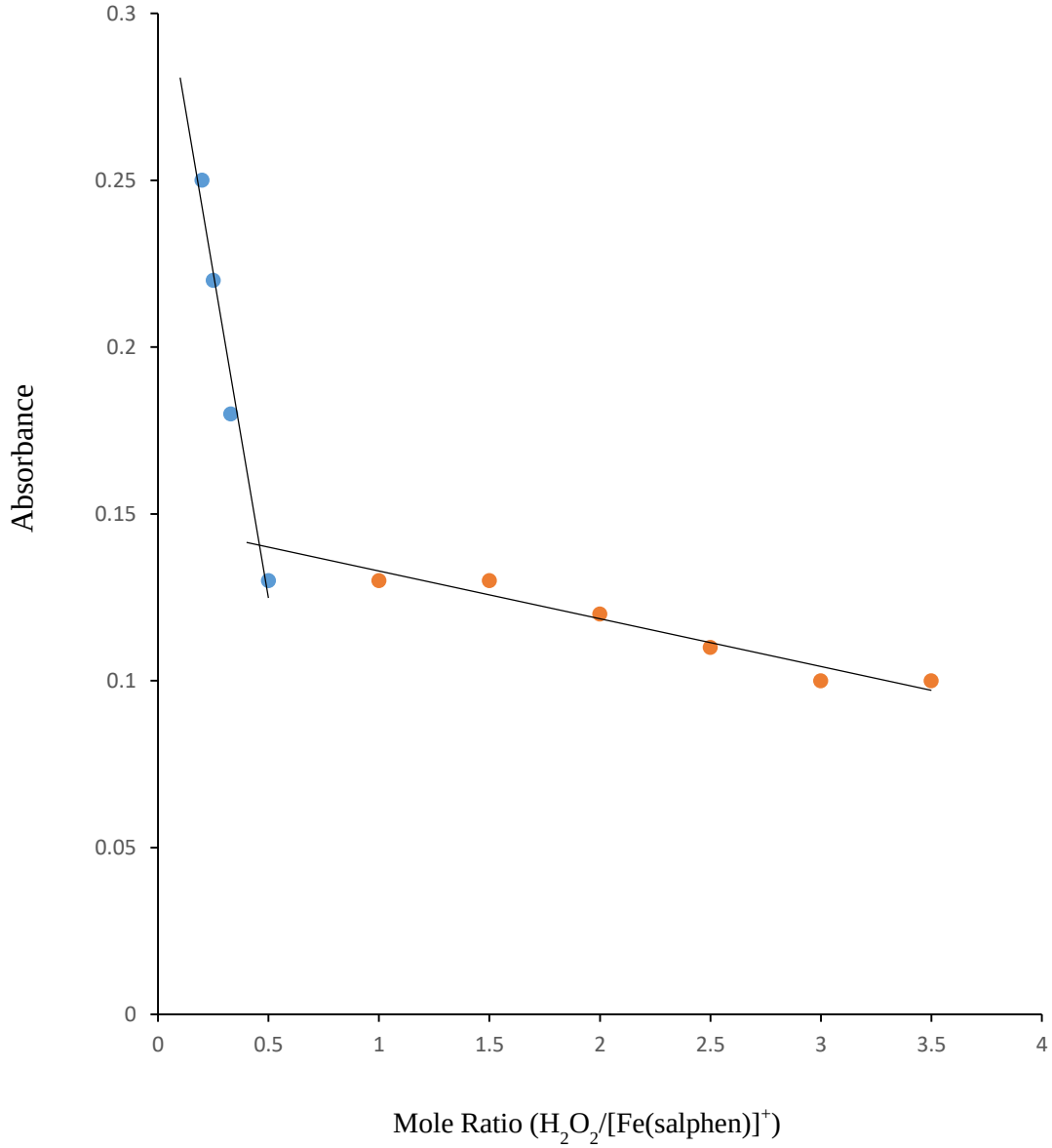


Figure 4.4: **Plot of absorbance versus mole ratio for the redox reaction of $[Fe(salphen)]^+$ and H_2O_2 at $[Fe(salphen)^+] = 1.0 \times 10^{-4}$ mol dm^{-3}, μ = 0.6 C^2 mol dm^{-3}, $[H^+] = 2.0 \times 10^{-5}$ mol dm^{-3}, D = 78.12, T = 28 ± 1°C and λ_{max} = 435 nm**

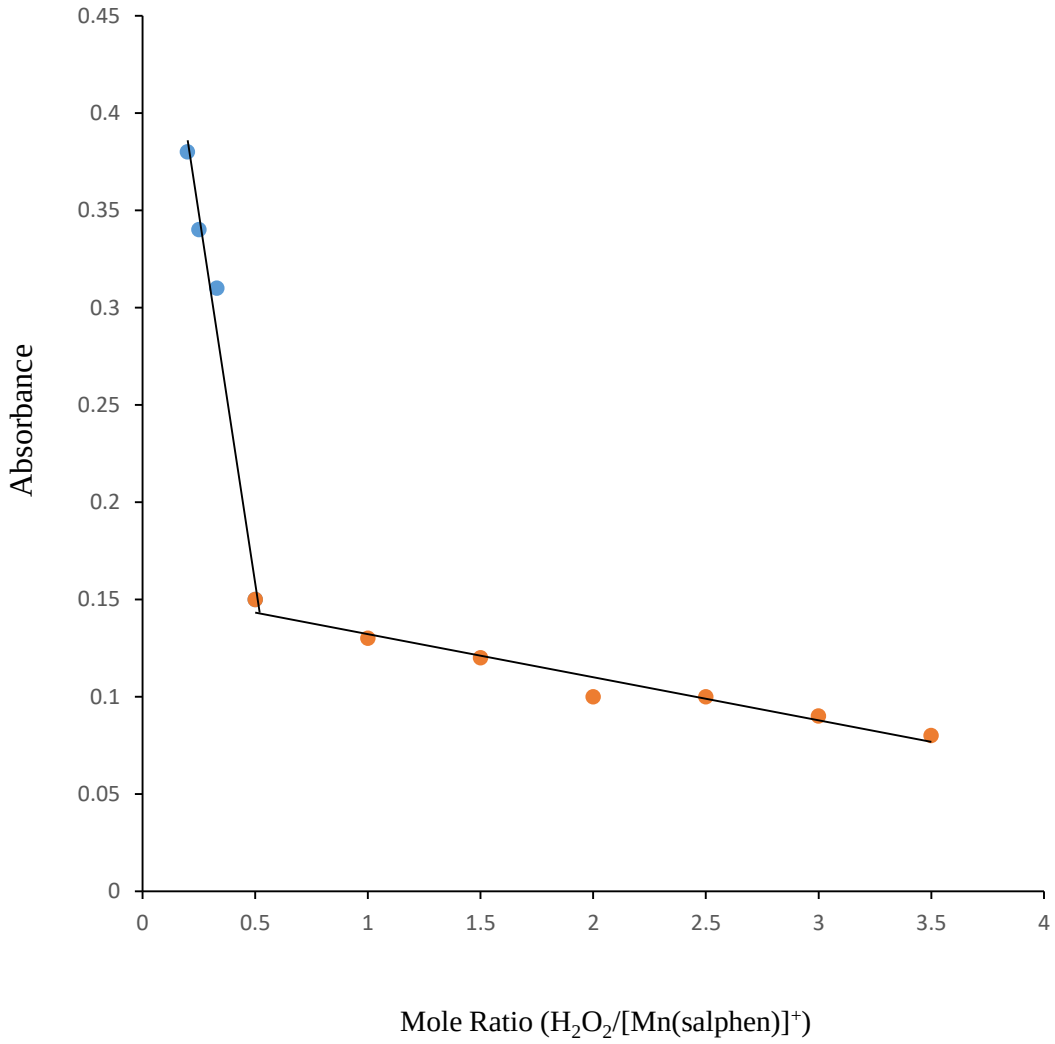


Figure 4.5: **Plot of absorbance versus mole ratio for the redox reaction of [Mn(salphen)]$^+$ and H_2O_2 at [Mn(salphen)$^+$] = 1.0×10^{-4} mol dm^{-3}, μ = 0.2 C^2 mol dm^{-3}, [H$^+$] = 2.0×10^{-5} mol dm^{-3}, D = 76.82, T = 30 ± 1°C and λ_{max} = 450 nm**

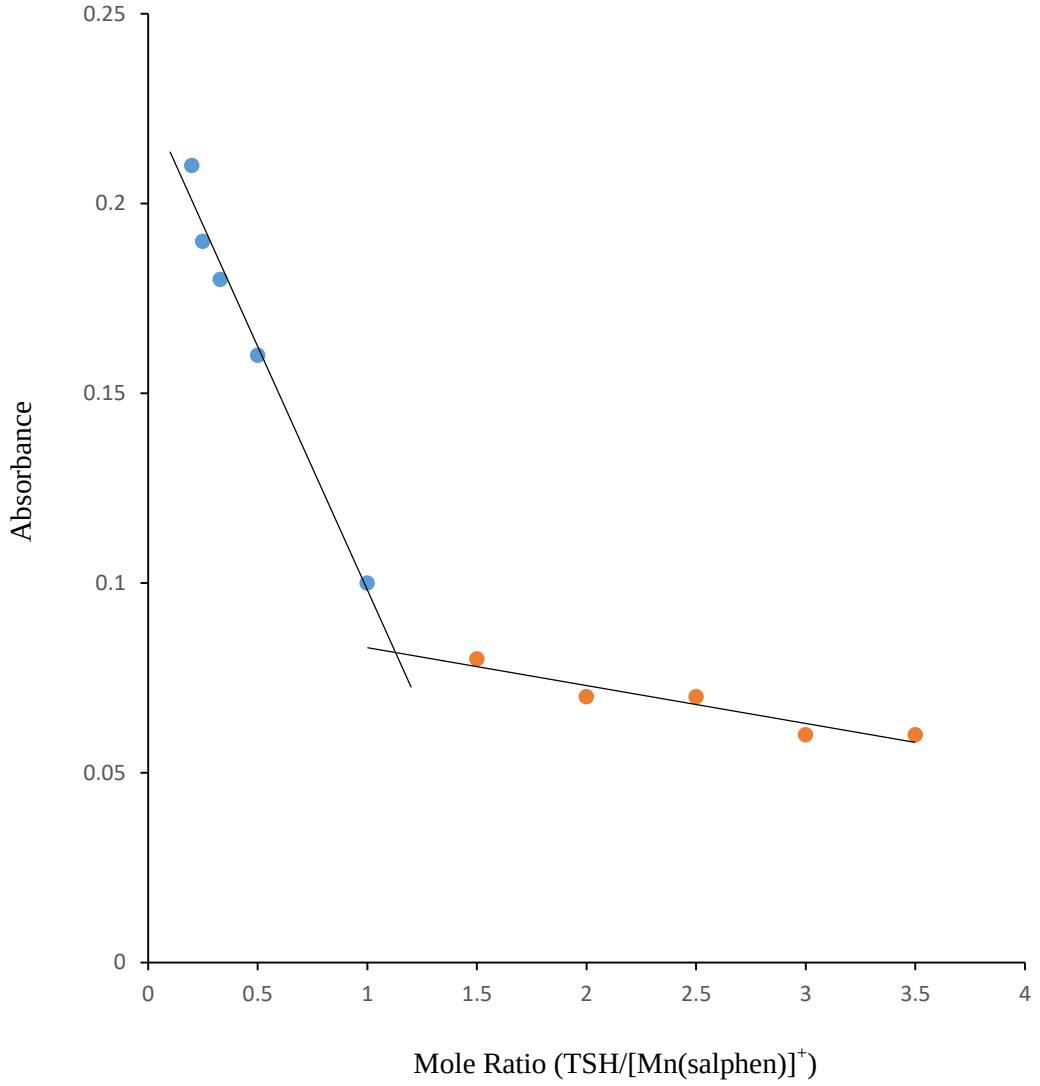


Figure 4.6: **Plot of absorbance versus mole ratio for the redox reaction of $[Mn(salphen)]^+$ and TSH at $[Mn(salphen)^+] = 1.0 \times 10^{-4}$ mol dm^{-3}, μ = 0.6 C^2 mol dm^{-3}, D = 77.98, T = 32 ± 1°C and λ_{max} = 450 nm**

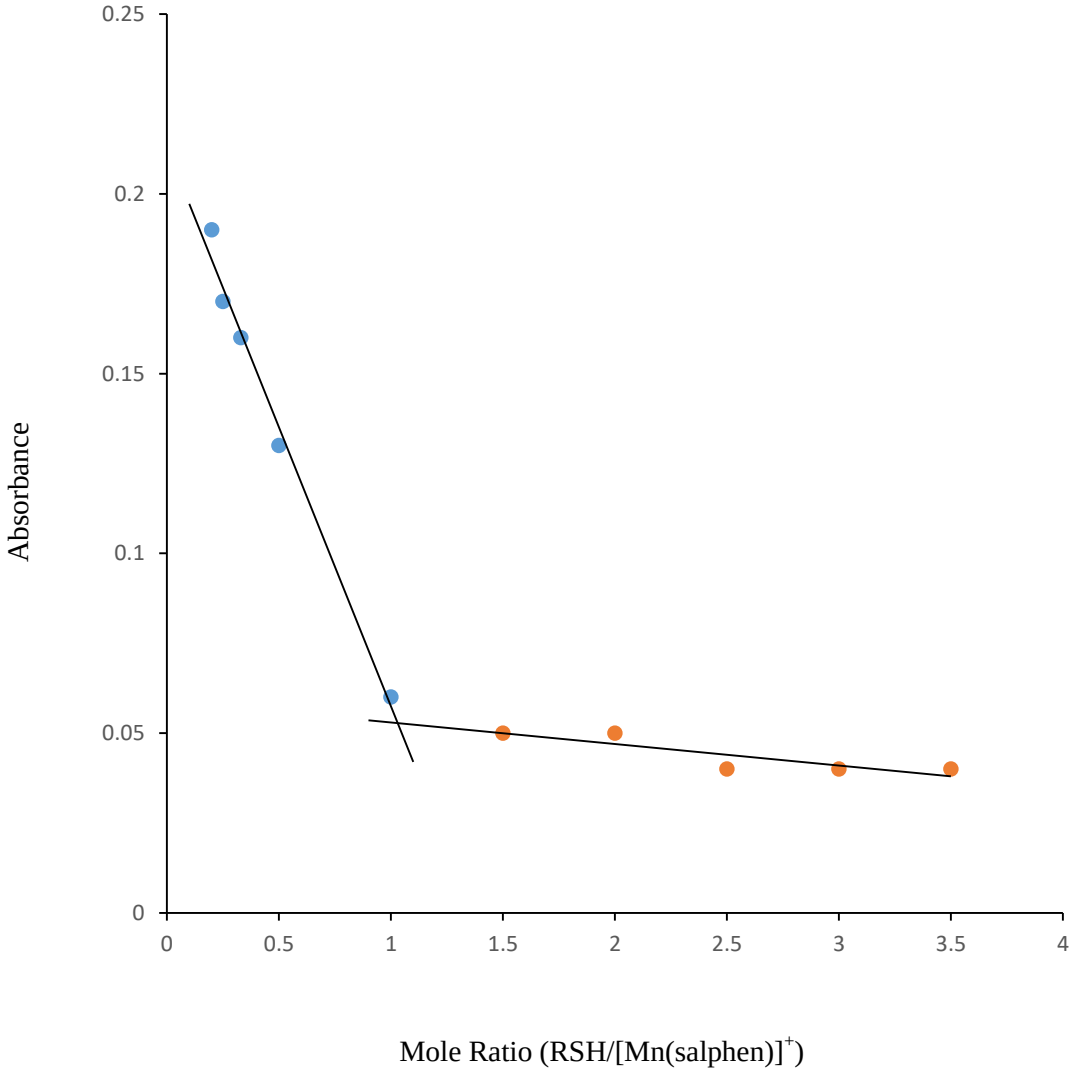


Figure 4.7: **Plot of absorbance versus mole ratio for the redox reaction of $[Mn(salphen)]^+$ and RSH at $[Mn(salphen)^+] = 1.0 \times 10^{-4}$ mol dm^{-3}, μ = 0.6 C^2 mol dm^{-3}, $[H^+] = 4.0 \times 10^{-5}$ mol dm^{-3}, D = 78.19, T = 28 ± 1°C and λ_{max} = 450 nm**

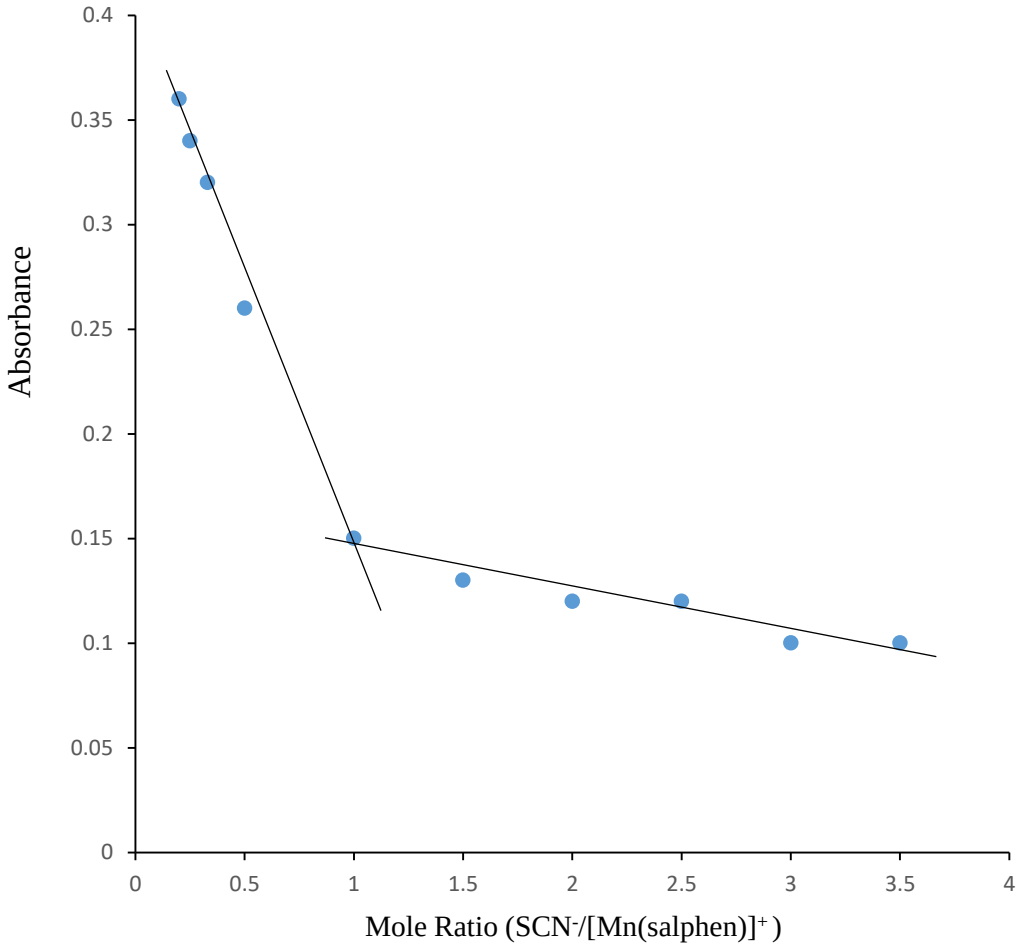


Figure 4.8: **Plot of absorbance versus mole ratio for the redox reaction of $[Mn(salphen)]^{+}$ and SCN^{-} at $[Mn(salphen)^{+}] = 1.0 \times 10^{-4}$ mol dm^{-3}, $\mu = 0.6$ C^2 mol dm^{-3}, $[H^{+}] = 4.0 \times 10^{-5}$ mol dm^{-3}, D = 78.12, T = 28 ± 1°C and λ_{max} = 450 nm**

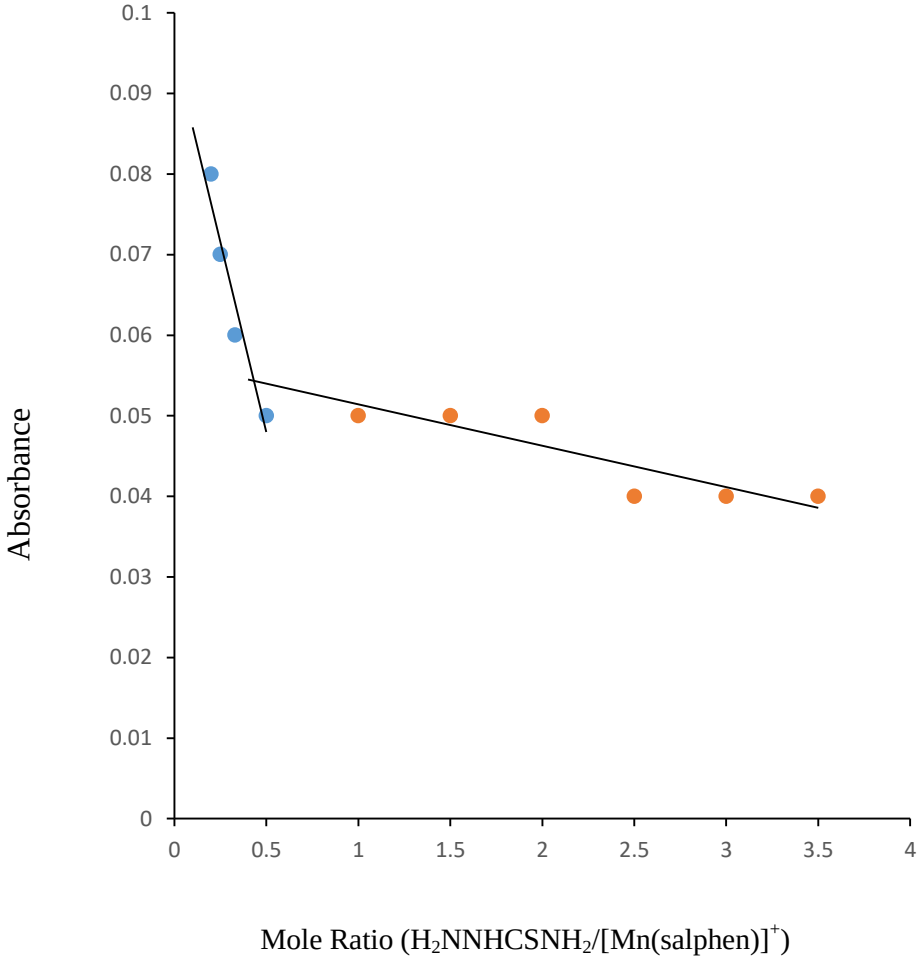


Figure 4.9: **Plot of absorbance versus mole ratio for the redox reaction of $[Mn(salphen)]^+$ and $H_2NNHCSNH_2$ at $[Mn(salphen)^+] = 1.0 \times 10^{-4}$ mol dm^{-3}, μ = 0.6 C^2 mol dm^{-3}, $[H^+] = 2.0 \times 10^{-5}$ mol dm^{-3}, D = 75.10, T = 28 ± 1°C and λ_{max} = 450 nm**

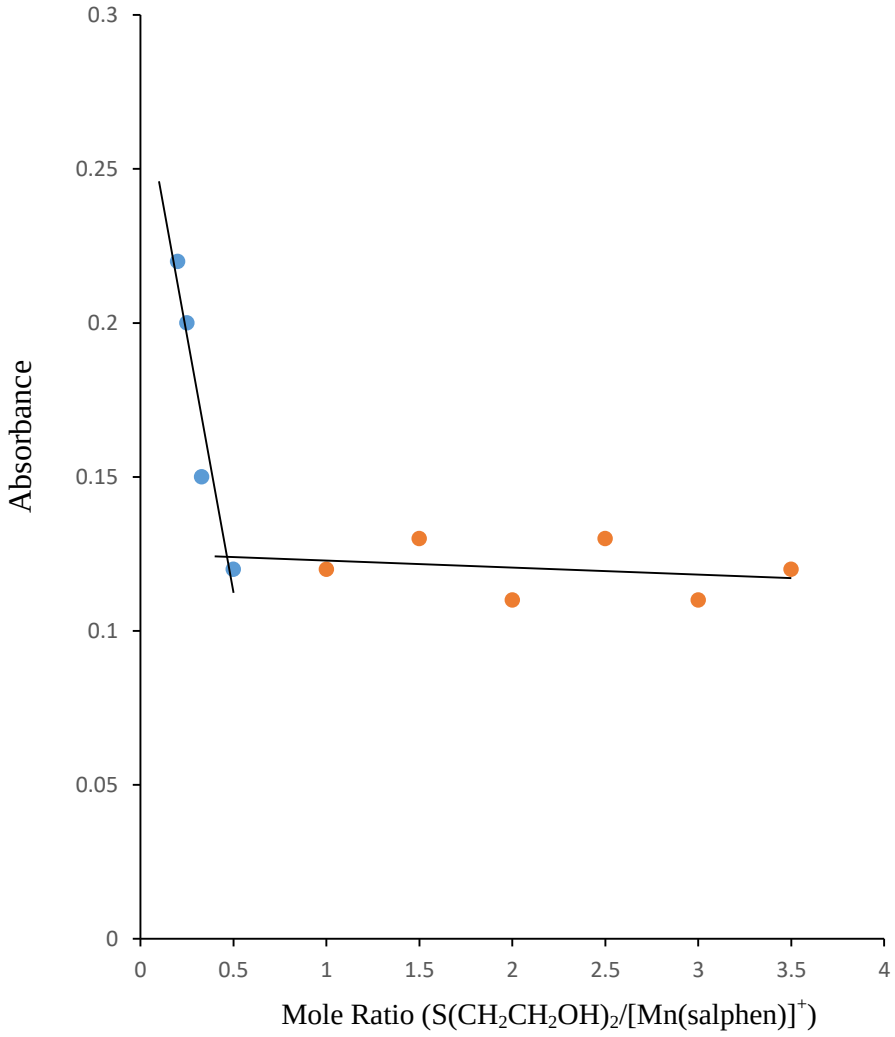


Figure 4.10: Plot of absorbance versus mole ratio for the redox reaction of $[Mn(salphen)]^+$ and $S(CH_2CH_2OH)_2$ at $[Mn(salphen)^+] = 1.0 \times 10^{-4}$ mol dm^{-3}, $\mu = 0.6$ C^2 mol dm^{-3}, $[H^+] = 2.0 \times 10^{-5}$ mol dm^{-3}, D = 66.60, T = 50 ± 1°C and λ_{max} = 450 nm

a) A brown precipitate of Fe_2O_3 was observed, indicating that the formation of Fe_2O_3 was as a result of $KMnO_4$ oxidation of the Fe^{2+} complex formed during the reduction of $[Fe(salphen)]^+$ (Mifsud, 2009).

b) The presence of CO_2 was confirmed using lime water, $Ca(OH)_2$, which turned milky (Svehla and Sivasankar, 2012).

c) No precipitate of sodium phosphomolybdate was observed when a solution of sodium molybdate was added to the product of H_3PO_2 - $[Fe(salphen)]^+$ reaction, indicating that H_3PO_4 was not produced (as a reaction product). Hence, the presence of H_3PO_3 was inferred as the product of H_3PO_2 oxidation (Yusuf *et al*., 2004; Mohammed *et al*., 2017).

d) The appearance of characteristic purple colour of MnO_4^- after the reaction solution was acidified with H_2SO_4 and KIO_4 was added shows the presence of Mn^{2+} (Nazarenko, 2004).

e) In SCN^- - $[Mn(salphen)]^+$ reaction, the formation of a white precipitate of $BaSO_4$, insoluble in excess dilute HCl was observed, when $BaCl_2$ solution was added to the reaction product. The precipitate was an indication of the presence of SO_4^{2-} ion. The formation of a blood red complex of $Fe(SCN)_3$ when $S_2O_3^{2-}$ solution was added to the reaction product followed by $FeCl_3$ indicated the presence of CN^- ion (Svehla and Sivasankar, 2012).

f) In $H_2NNHCSNH_2$ - $[Mn(salphen)]^+$ reaction, the formation of a white precipitate of $BaSO_4$, insoluble in excess dilute HCl was observed, when $BaCl_2$ solution was added to the reaction product indicated the presence of SO_4^{2-} ion. The formation of a blood red complex of $Fe(SCN)_3$ when $S_2O_3^{2-}$ solution was added to the reaction product followed by $FeCl_3$ indicated the presence of CN^- ion (Svehla and

Sivasankar, 2012) and the change in colour of moist red litmus paper to blue from ammonia fumes when NaOH solution was added to reaction product confirmed the presence of NH_3 from NH_4^+ ion (Svehla and Sivasankar, 2012).

g) In the reaction of $[Fe(salphen)]^+$ with TSH, $HSCH_2COOH$, bands can be observed from the FTIR spectra at 2916 cm^{-1}, 1679 cm^{-1}, 1257 cm^{-1} and 562 cm^{-1} while in the reaction of $[Mn(salphen)]^+$ with TSH, bands were observed at 2917 cm^{-1}, 1681 cm^{-1}, 1258 cm^{-1} and 562 cm^{-1} (Appendix IV and V). Also, in the reaction of $[Mn(salphen)]^+$ with RSH, $HSCH_2CH_2OH$, bands were observed at 3309 cm^{-1}, 1042 cm^{-1} and 481 cm^{-1} (Appendix VI) while in the reaction of $[Mn(salphen)]^+$ with $S(CH_2CH_2OH)_2$, bands were observed at 3334 cm^{-1}, 1040 cm^{-1} and 1007 cm^{-1} (Appendix VII).

4.4 Order of the Reactions

The results of the kinetic study were obtained by plotting $\log(A_t - A_\infty)$ against time t. Typical plots are shown in Figures 4.11 – 4.20. The order of the reactions were determined by plotting log k_1 against log of [TSH], $[H_2C_2O_4]$, $[H_3PO_2]$ and $[H_2O_2]$ in their reactions with $[Fe(salphen)]^+$ (Figures 4.21 – 4.24) and log of $[H_2O_2]$, [TSH], [RSH], $[SCN^-]$, $[H_2NNHCSNH_2]$ and $[S(CH_2CH_2OH)_2]$ in their reactions with $[Mn(salphen)]^+$ (Figures 4.25 – 4.30). The slopes obtained were 0.98, 1.04, 1.00 and 0.92 indicating first order dependence in [TSH], $[H_2C_2O_4]$ $[H_3PO_2]$ and $[H_2O_2]$ in their reactions with $[Fe(salphen)]^+$ and slopes of 0.93, 0.99, 0.97, 0.98, 0.99 and 0.97 indicating first order dependence in $[H_2O_2]$, [TSH], [RSH], $[SCN^-]$, $[H_2NNHCSNH_2]$ and $[S(CH_2CH_2OH)_2]$ in their reactions with $[Mn(salphen)]^+$.

The pseudo-first order rate constants, k_1 determined from the graphs are presented in Tables 4.1 – 4.10. The values of second order rate constants k_2, determined as

k_1/[reductant] in the reactions of TSH, $H_2C_2O_4$, H_3PO_2 and H_2O_2 with $[Fe(salphen)]^+$ respectively (Tables

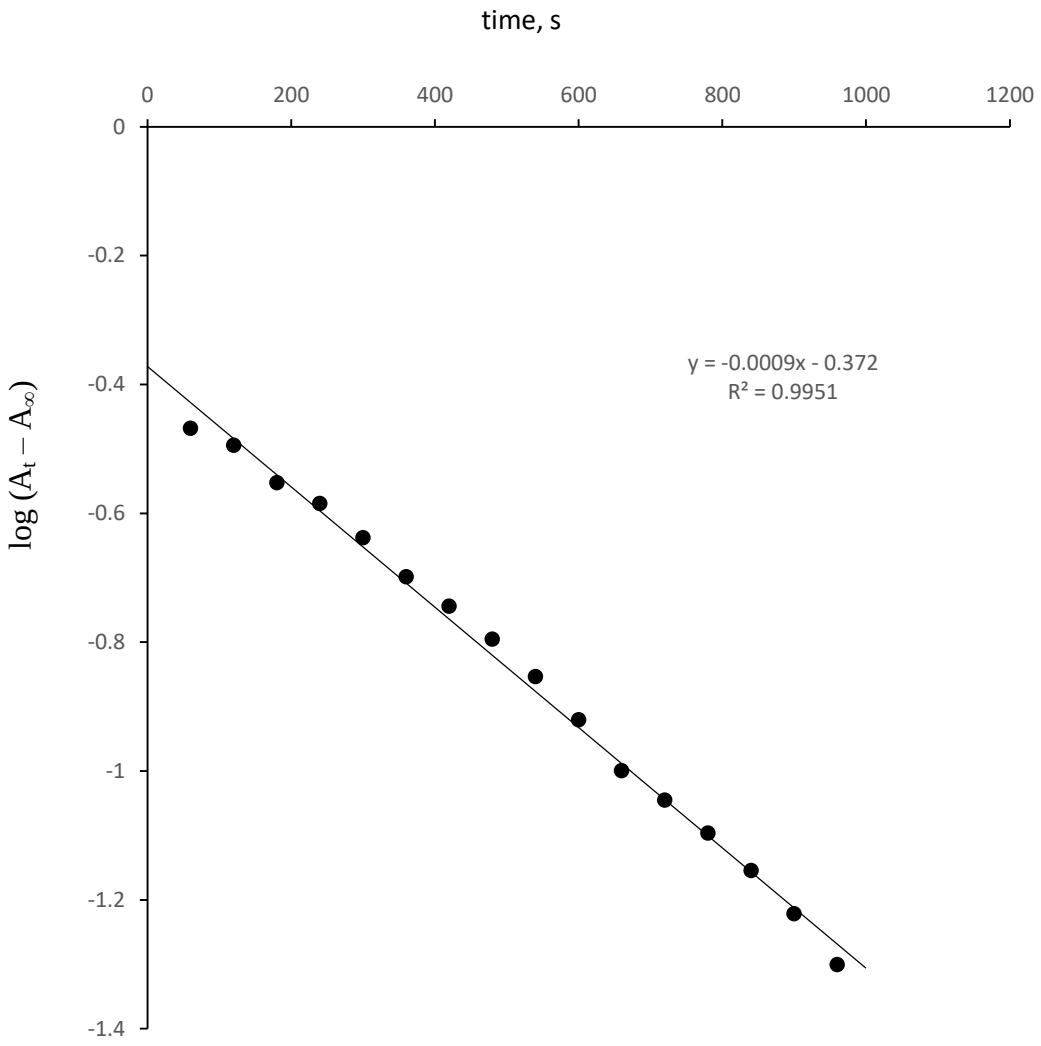


Figure 4.11: Typical pseudo-first order plot for the redox reaction of $[Fe(salphen)]^+$ and TSH at $[Fe(salphen)^+] = 2.0 \times 10^{-4}$ mol dm^{-3}, [TSH] = 0.15 mol dm^{-3}, μ = 0.2 C^2 mol dm^{-3}, D = 76.88, T = 26 ± 1°C and λ_{max} = 435 nm

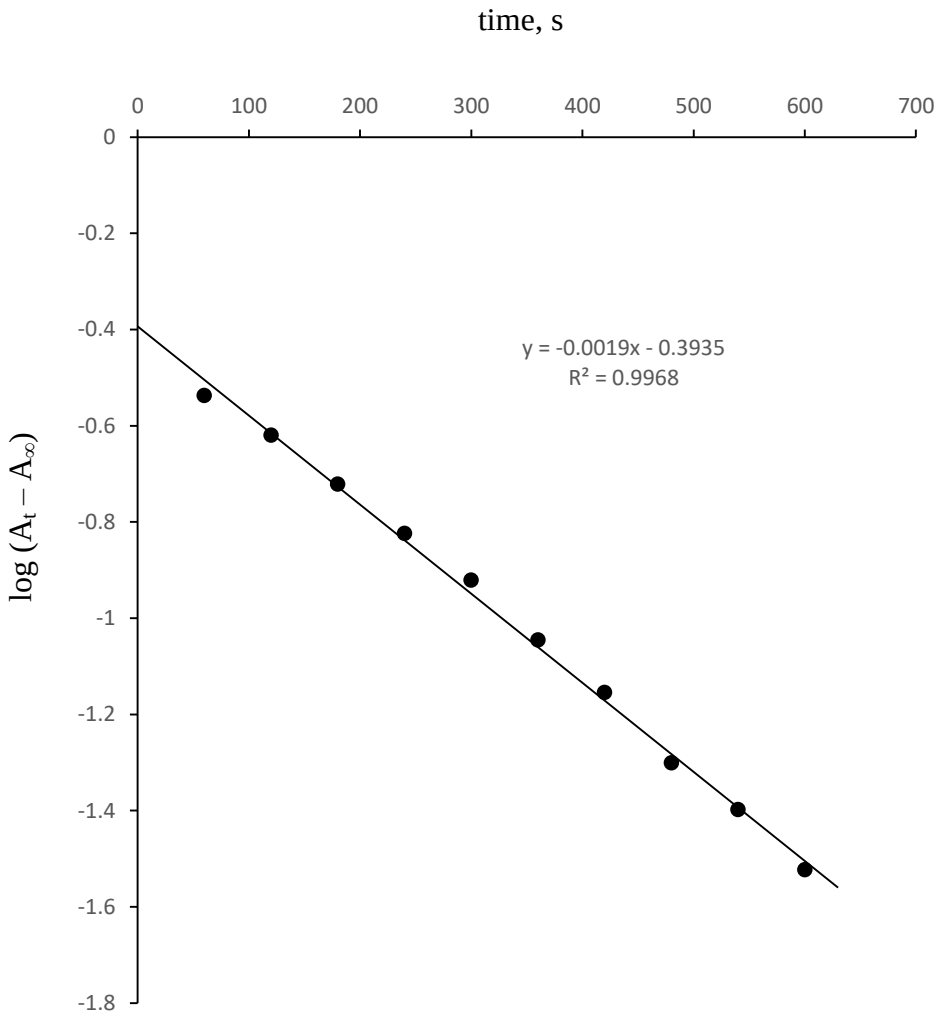


Figure 4.12: Typical pseudo-first order plot for the redox reaction of $[Fe(salphen)]^{+}$ and $H_2C_2O_4$ at $[Fe(salphen)^{+}] = 2.0 \times 10^{-4}$ mol dm^{-3}, $[H_2C_2O_4] = 6.0 \times 10^{-3}$ mol dm^{-3}, $\mu = 0.2$ C^2 mol dm^{-3}, D = 76.06, T = 26 ± 1°C and λ_{max} = 435 nm

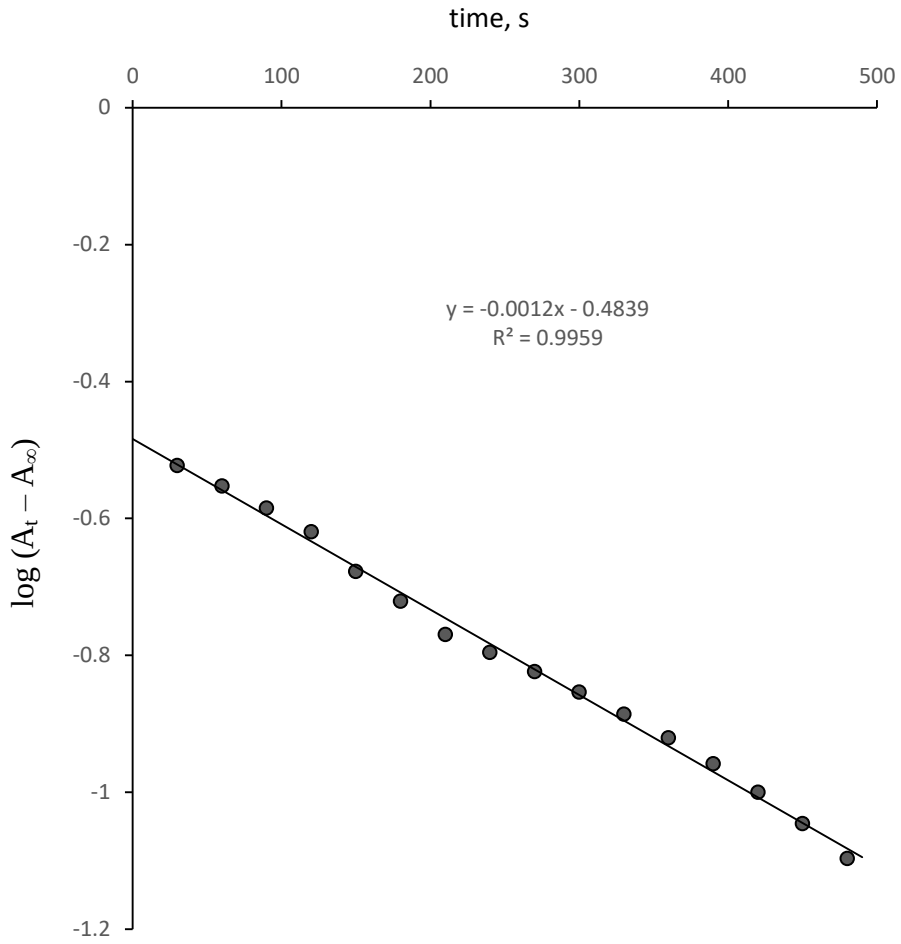


Figure 4.13: Typical pseudo-first order plot for the redox reaction of $[Fe(salphen)]^+$ and H_3PO_2 at $[Fe(salphen)^+] = 2.0 \times 10^{-4}$ mol dm^{-3}, $[H_3PO_2] = 0.13$ mol dm^{-3}, $\mu = 0.2$ C^2 mol dm^{-3}, D = 76.68, T = 26 ± 1°C and $\lambda_{max} = 435$ nm

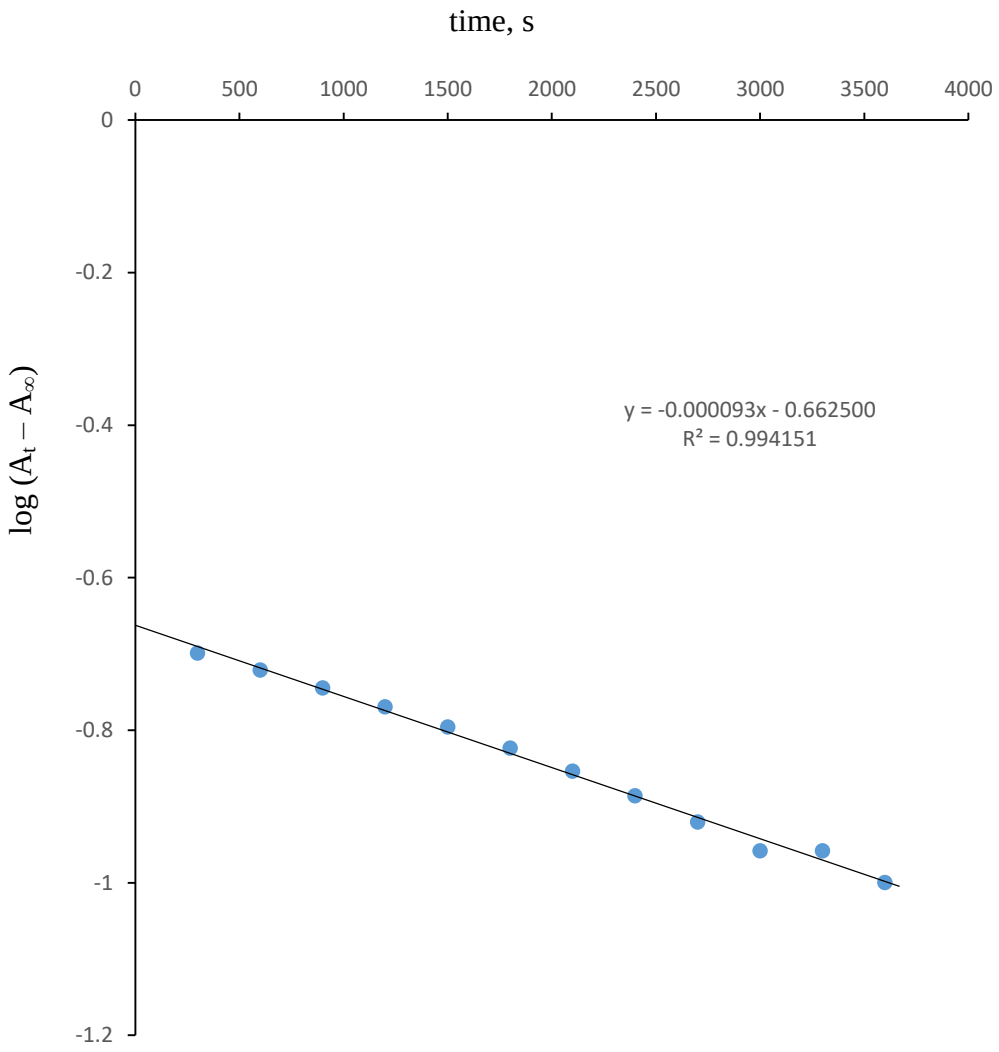


Figure 4.14: Typical pseudo-first order plot for the redox reaction of $[Fe(salphen)]^{+}$ and H_2O_2 at $[Fe(salphen)^{+}] = 1.0 \times 10^{-4}$ mol dm^{-3}, $[H_2O_2] = 0.42$ mol dm^{-3}, $\mu = 0.6$ C^2 mol dm^{-3}, $[H^{+}] = 2.0 \times 10^{-5}$ mol dm^{-3}, D = 78.12, T = 28 ± 1°C and λ_{max} = 435 nm

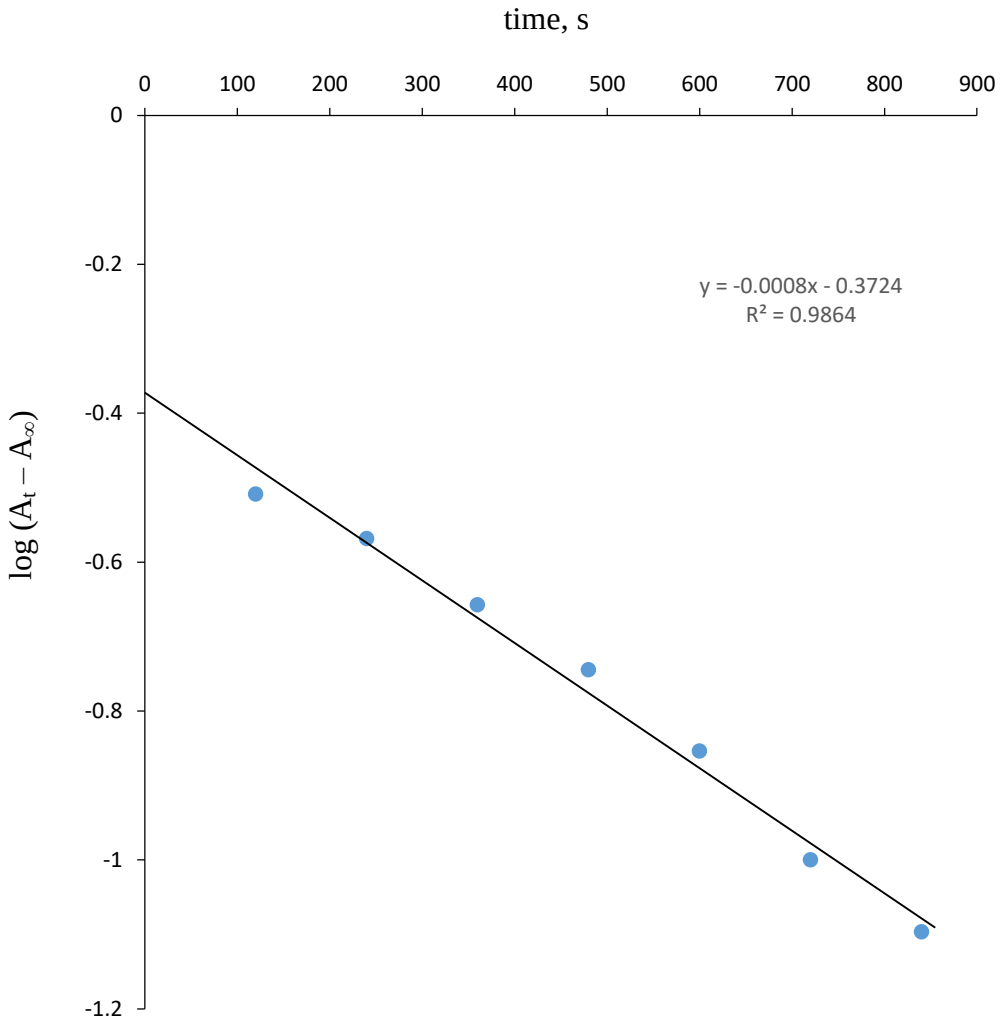


Figure 4.15: Typical pseudo-first order plot for the redox reaction of $[Mn(salphen)]^+$ and H_2O_2 at $[Mn(salphen)^+] = 1.0 \times 10^{-4}$ mol dm^{-3}, $[H_2O_2] = 0.15$ mol dm^{-3}, $\mu = 0.2$ C^2 mol dm^{-3}, $[H^+] = 2.0 \times 10^{-5}$ mol dm^{-3}, D = 76.82, T = 30 ± 1°C and λ_{max} = 450 nm

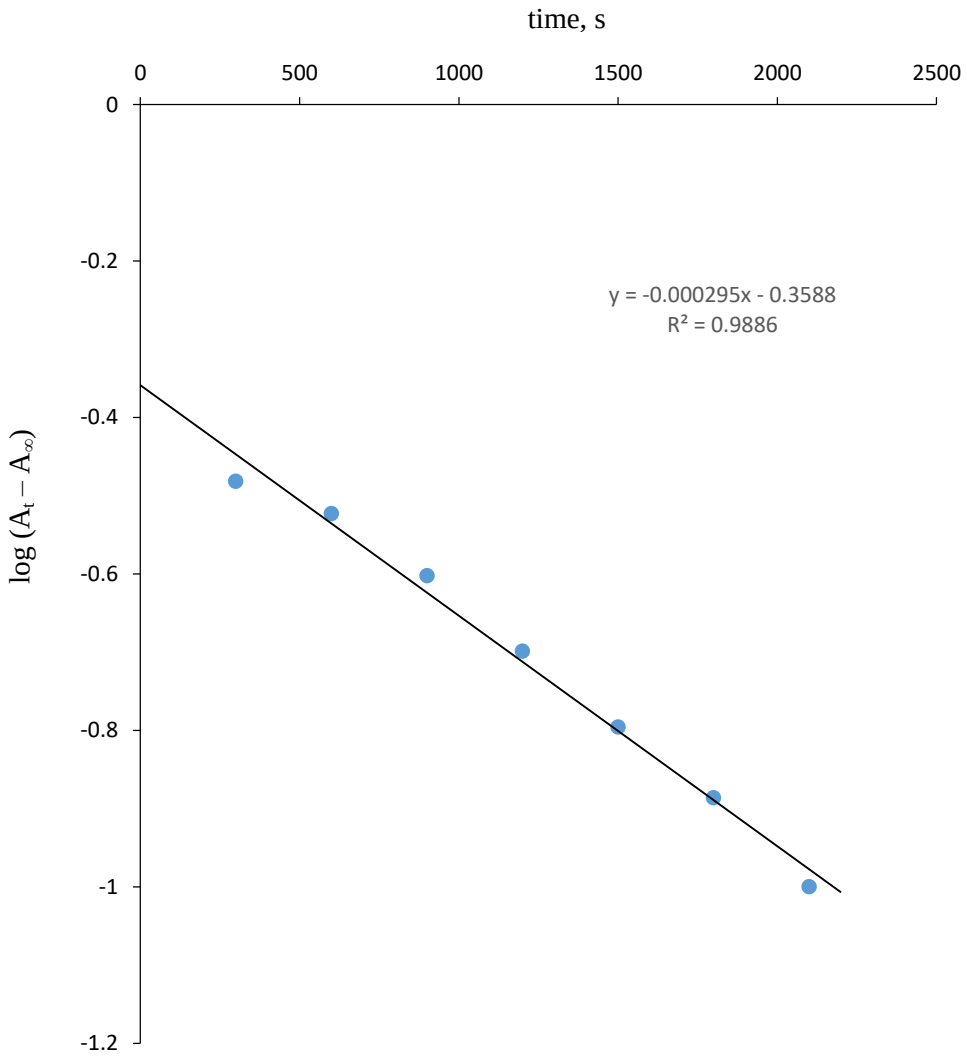


Figure 4.16: Typical pseudo-first order plot for the redox reaction of $[Mn(salphen)]^+$ and TSH at $[Mn(salphen)^+] = 1.0 \times 10^{-4}$ mol dm^{-3}, [TSH] = 0.42 mol dm^{-3}, μ = 0.6 C^2 mol dm^{-3}, D = 77.98, T = 32 ± 1°C and λ_{max} = 450 nm

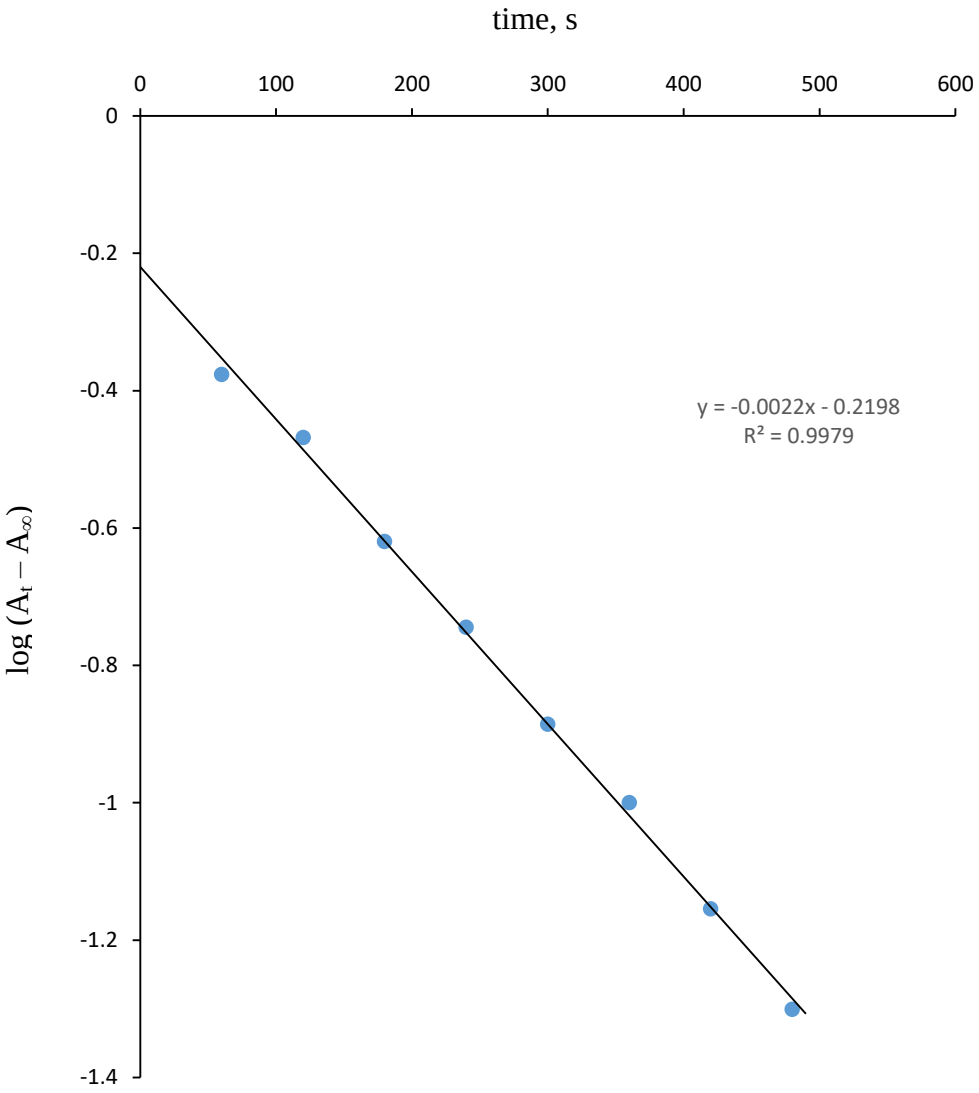


Figure 4.17: Typical pseudo-first order plot for the redox reaction of $[Mn(salphen)]^+$ and RSH at $[Mn(salphen)^+] = 1.0 \times 10^{-4}$ mol dm^{-3}, [RSH] = 0.4 mol dm^{-3}, μ = 0.6 C^2 mol dm^{-3}, $[H^+] = 4.0 \times 10^{-5}$ mol dm^{-3}, D = 78.19, T = 28 ± 1°C and λ_{max} = 450 nm

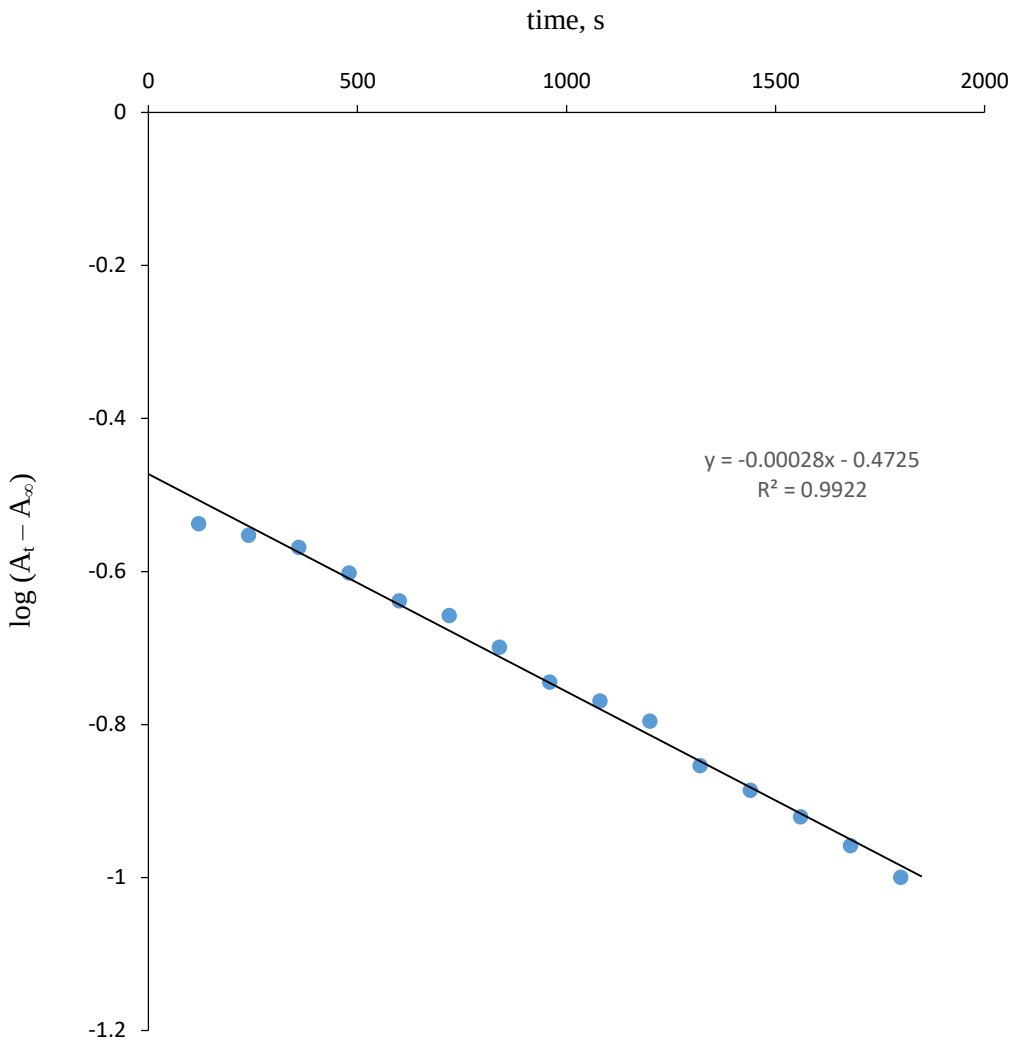


Figure 4.18: Typical pseudo-first order plot for the redox reaction of $[Mn(salphen)]^+$ and SCN^- at $[Mn(salphen)^+] = 1.0 \times 10^{-4}$ mol dm^{-3}, $[SCN^-] = 0.42$ mol dm^{-3}, $\mu = 0.6$ C^2 mol dm^{-3}, $[H^+] = 4.0 \times 10^{-5}$ mol dm^{-3}, D = 78.12, T = 28 ± 1 °C and λ_{max} = 450 nm

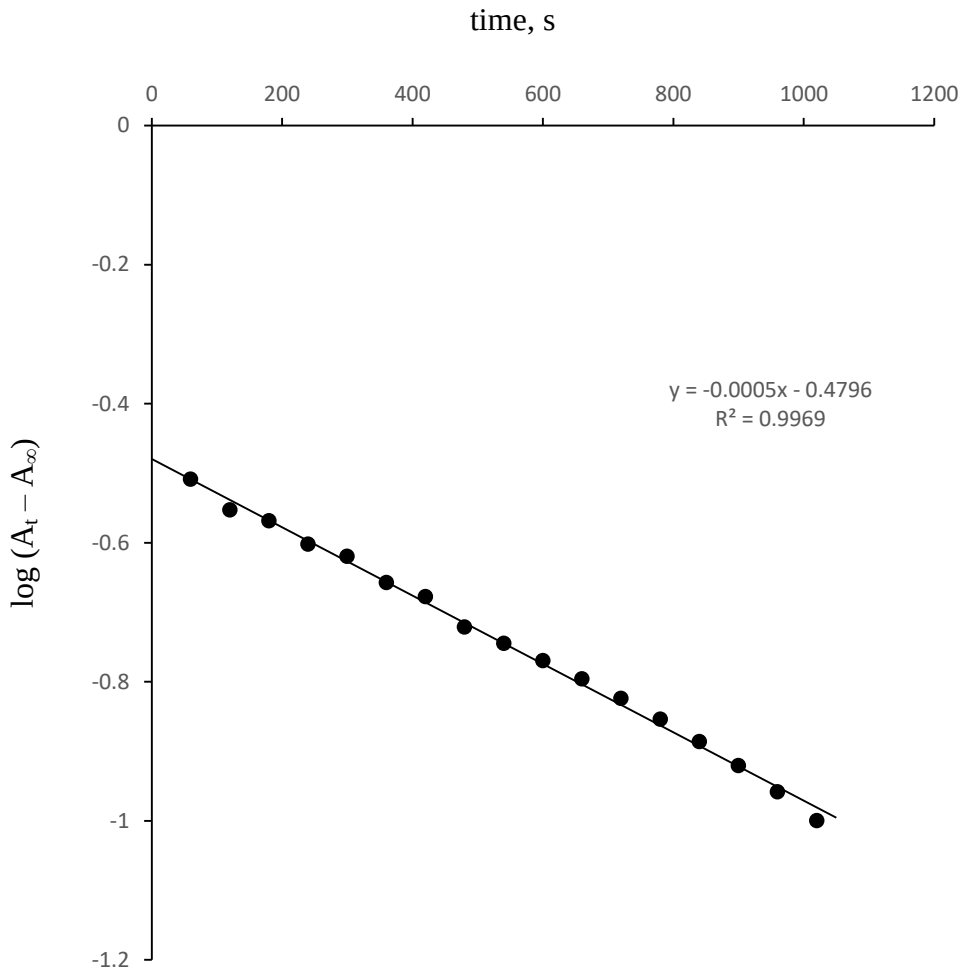


Figure 4.19: Typical pseudo-first order plot for the redox reaction of $[Mn(salphen)]^+$ and $H_2NNHCSNH_2$ at $[Mn(salphen)^+] = 1.0 \times 10^{-4}$ mol dm^{-3}, $[H_2NNHCSNH_2] = 0.28$ mol dm^{-3}, $\mu = 0.6$ C^2 mol dm^{-3}, $[H^+] = 2.0 \times 10^{-5}$ mol dm^{-3}, D = 75.10, T = 28 ± 1 °C and λ_{max} = 450 nm

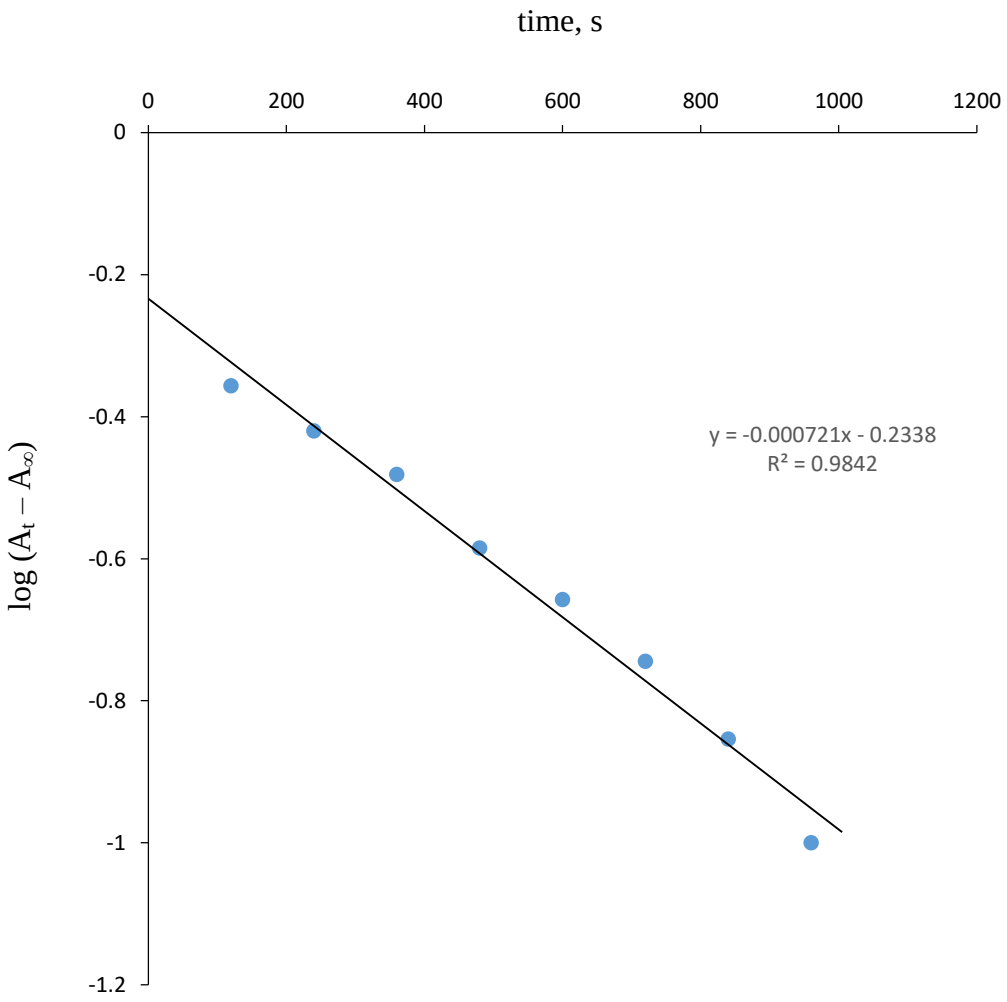


Figure 4.20: Typical pseudo-first order plot for the redox reaction of $[Mn(salphen)]^+$ and $S(CH_2CH_2OH)_2$ at $[Mn(salphen)^+] = 1.0 \times 10^{-4}$ mol dm^{-3}, $[S(CH_2CH_2OH)_2] = 0.40$ mol dm^{-3}, $\mu = 0.6$ C^2 mol dm^{-3}, $[H^+] = 2.0 \times 10^{-5}$ mol dm^{-3}, D = 66.60, T = 50 ± 1 °C and $\lambda_{max} = 450$ nm

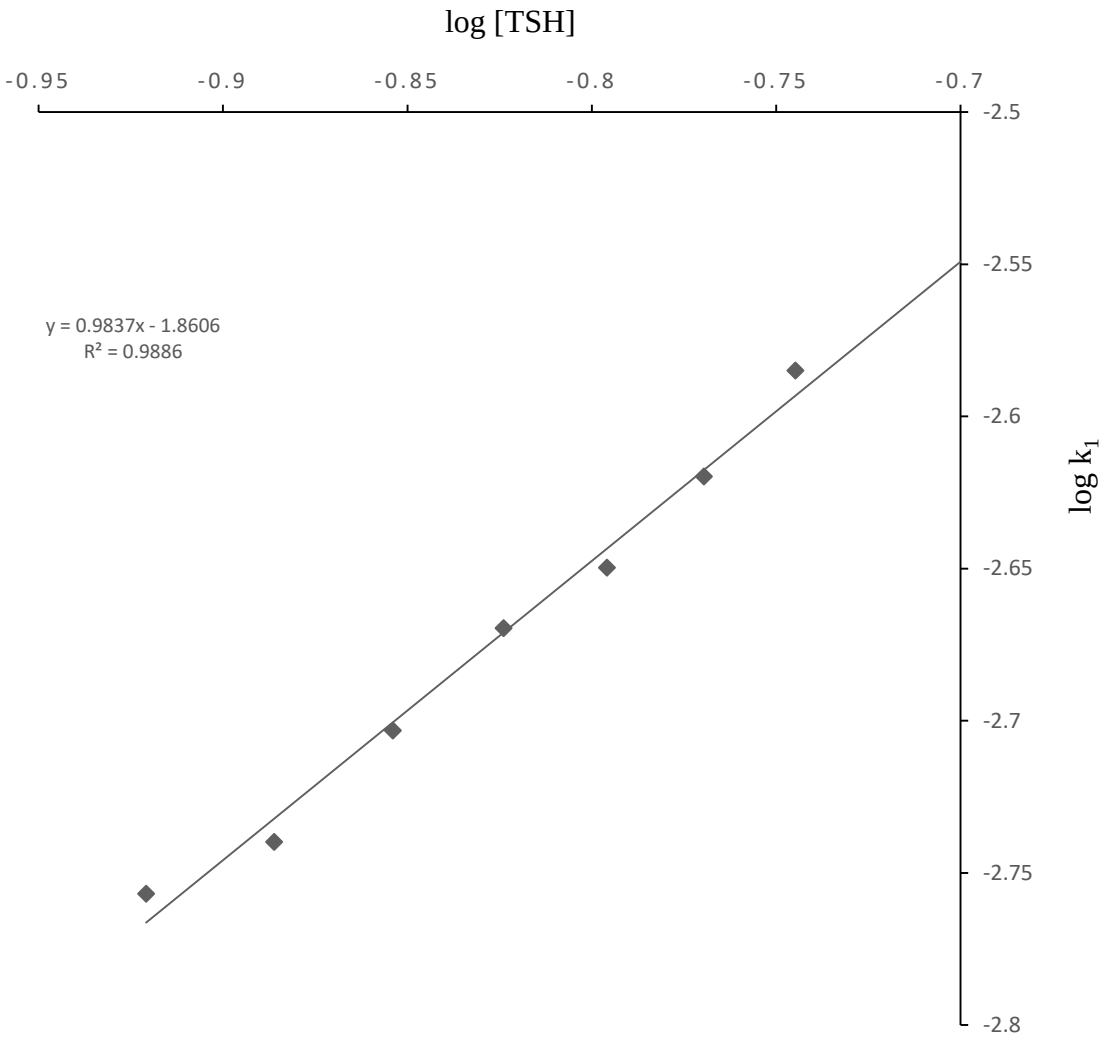


Figure 4.21: Plot of log k_1 versus log [TSH] for the redox reaction of $[Fe(salphen)]^+$ and TSH at $[Fe(salphen)^+] = 2.0 \times 10^{-4}$ mol dm^{-3}, $\mu = 0.2$ C^2 mol dm^{-3}, D = 76.88, T = 26 ± 1°C and λ_{max} = 435 nm

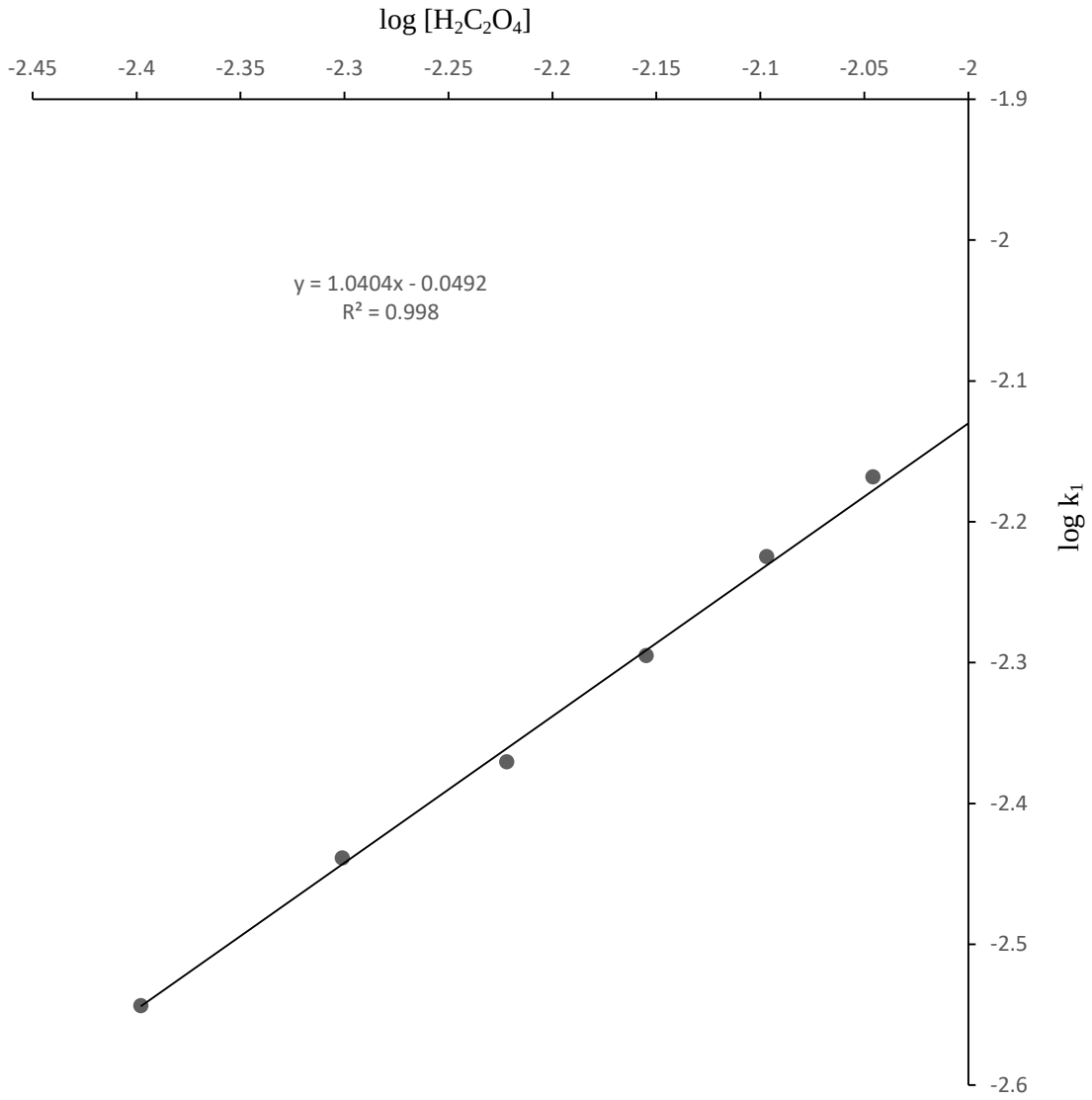


Figure 4.22: Plot of log k_1 versus log $[H_2C_2O_4]$ for the redox reaction of $[Fe(salphen)]^+$ and $H_2C_2O_4$ at $[Fe(salphen)^+] = 2.0 \times 10^{-4}$ mol dm^{-3}, μ = 0.2 C^2 mol dm^{-3}, D = 76.06, T = 26 ± 1°C and λ_{max} = 435 nm

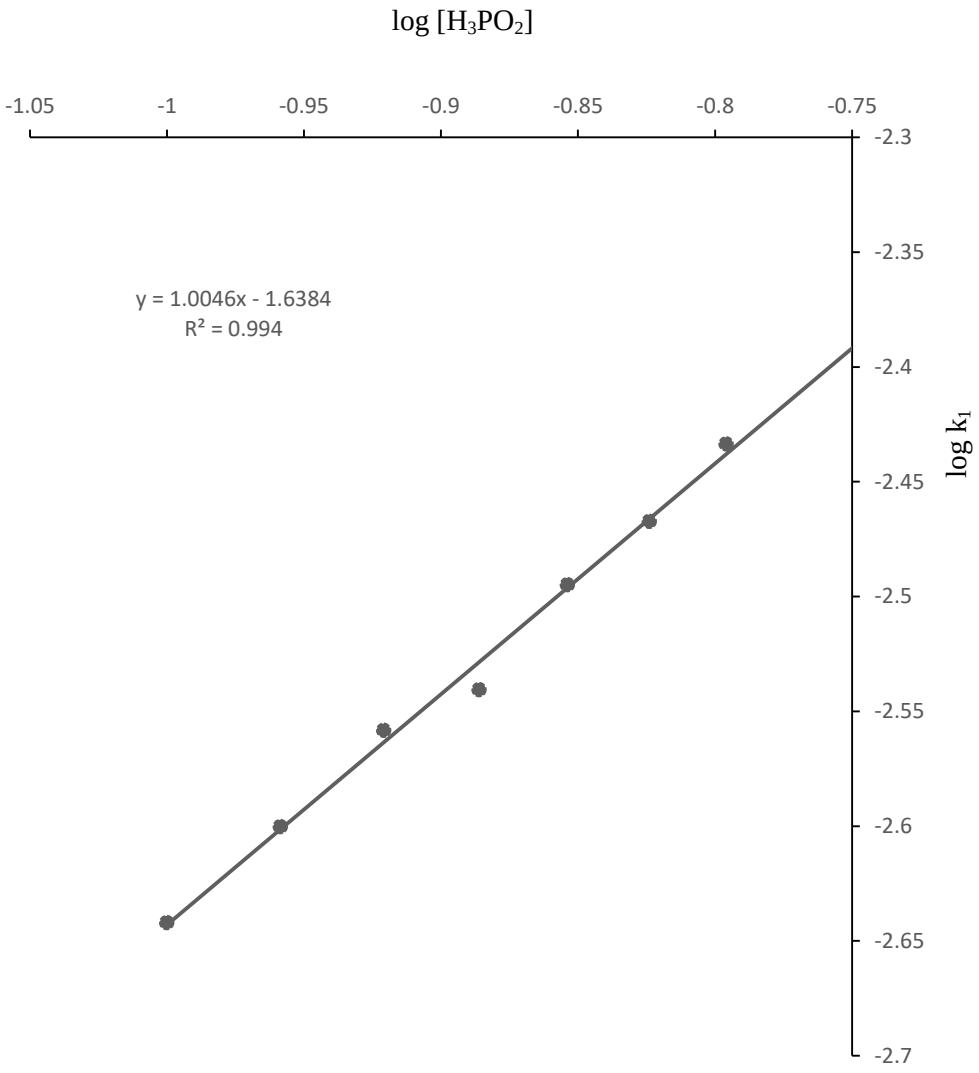


Figure 4.23: Plot of log k_1 versus log $[H_3PO_2]$ for the redox reaction of $[Fe(salphen)]^+$ and H_3PO_2 at $[Fe(salphen)^+] = 2.0 \times 10^{-4}$ mol dm^{-3}, μ = 0.2 C^2 mol dm^{-3}, D = 76.68, T = 26 ± 1°C and λ_{max} = 435 nm

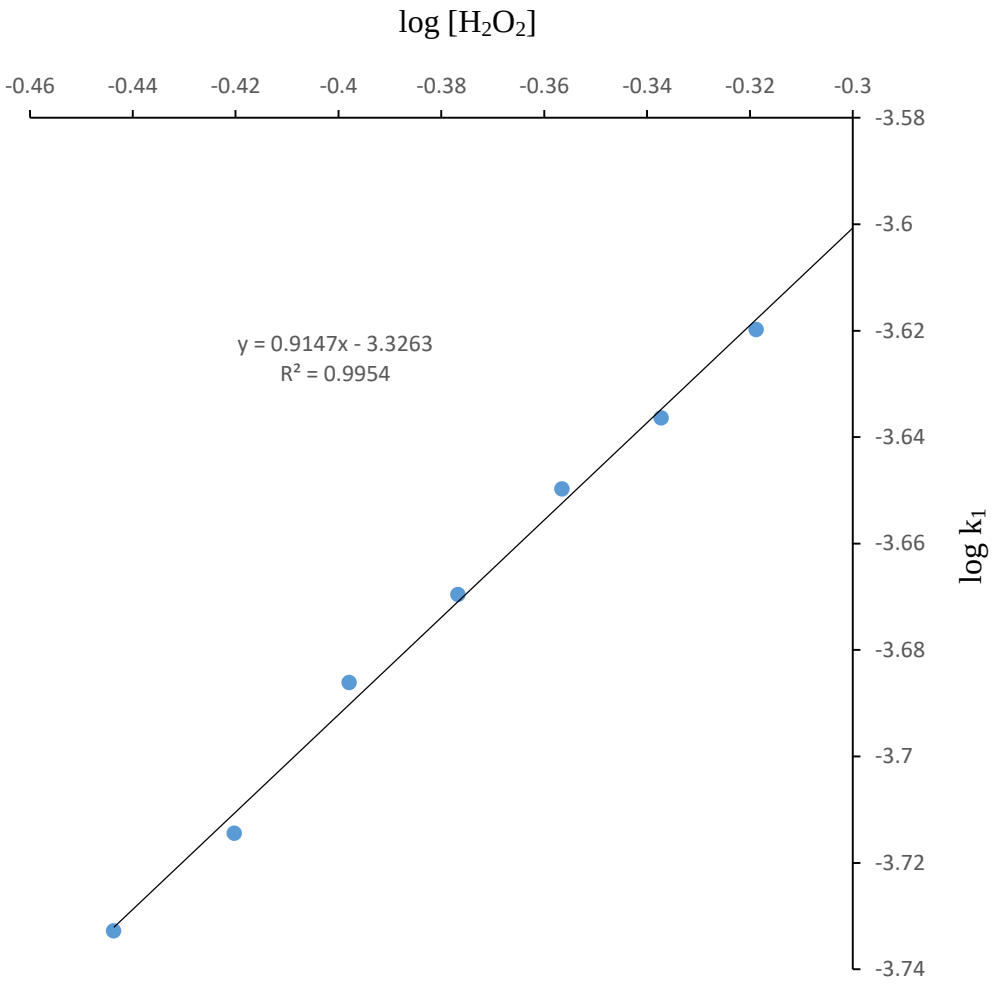


Figure 4.24: Plot of log k_1 versus log $[H_2O_2]$ for the redox reaction of $[Fe(salphen)]^+$ and H_2O_2 at $[Fe(salphen)^+] = 1.0 \times 10^{-4}$ mol dm^{-3}, μ = 0.6 C^2 mol dm^{-3}, $[H^+] = 2.0 \times 10^{-5}$ mol dm^{-3}, D = 78.12, T = 28 ± 1°C and λ_{max} = 435 nm

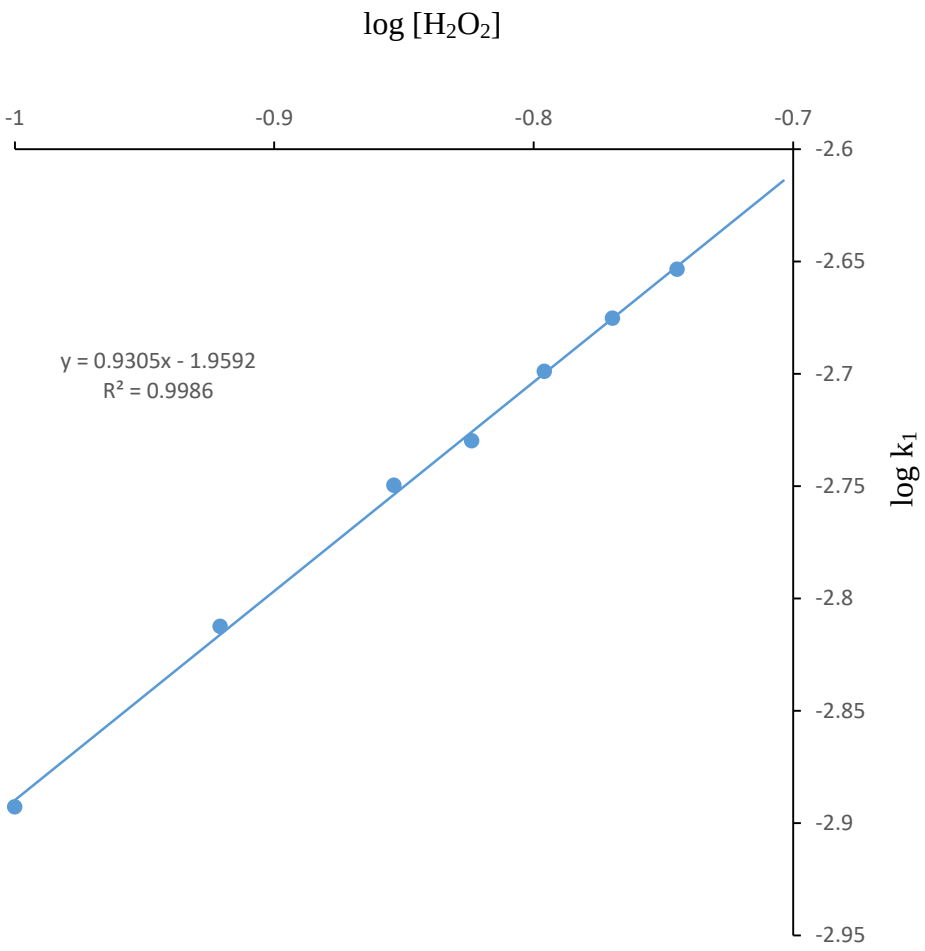


Figure 4.25: Plot of log k_1 versus log $[H_2O_2]$ for the redox reaction of $[Mn(salphen)]^+$ and H_2O_2 at $[Mn(salphen)^+] = 1.0 \times 10^{-4}$ mol dm^{-3}, μ = 0.2 C^2 mol dm^{-3}, $[H^+] = 2.0 \times 10^{-5}$ mol dm^{-3}, D = 76.82, T = 30 ± 1°C and λ_{max} = 450 nm

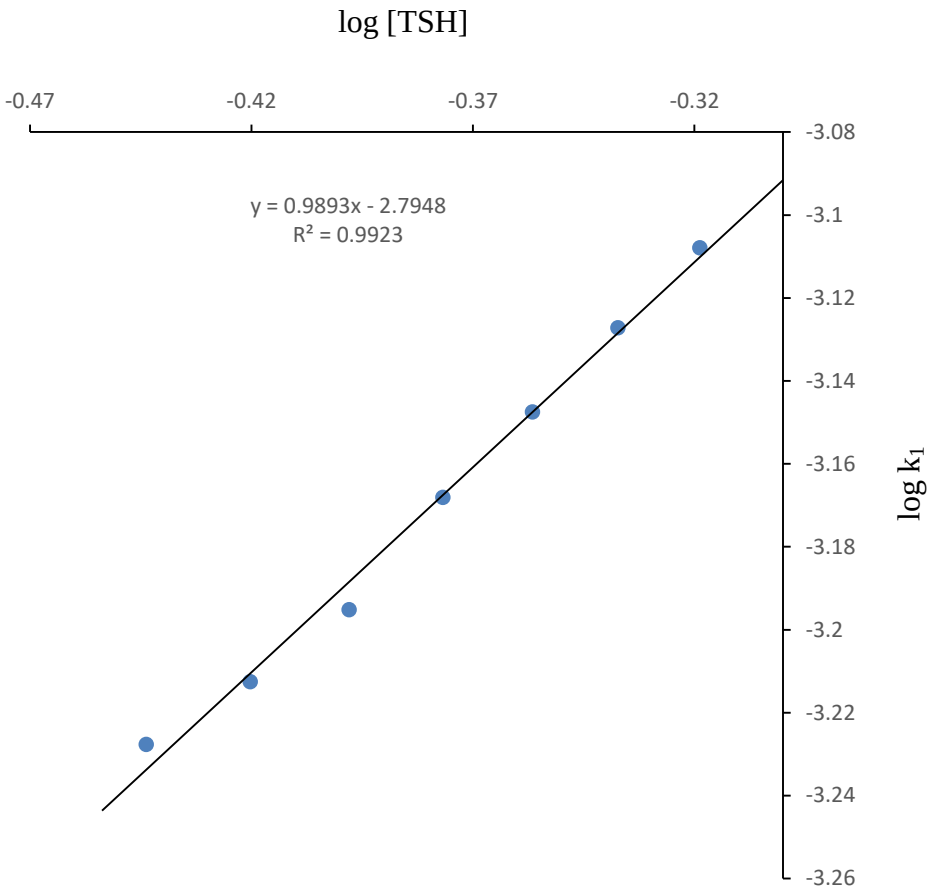


Figure 4.26: Plot of log k_1 versus log [TSH] for the redox reaction of $[Mn(salphen)]^+$ and TSH at $[Mn(salphen)^+] = 1.0 \times 10^{-4}$ mol dm^{-3}, $\mu = 0.6$ C^2 mol dm^{-3}, D = 77.98, T = 32 ± 1°C and λ_{max} = 450 nm

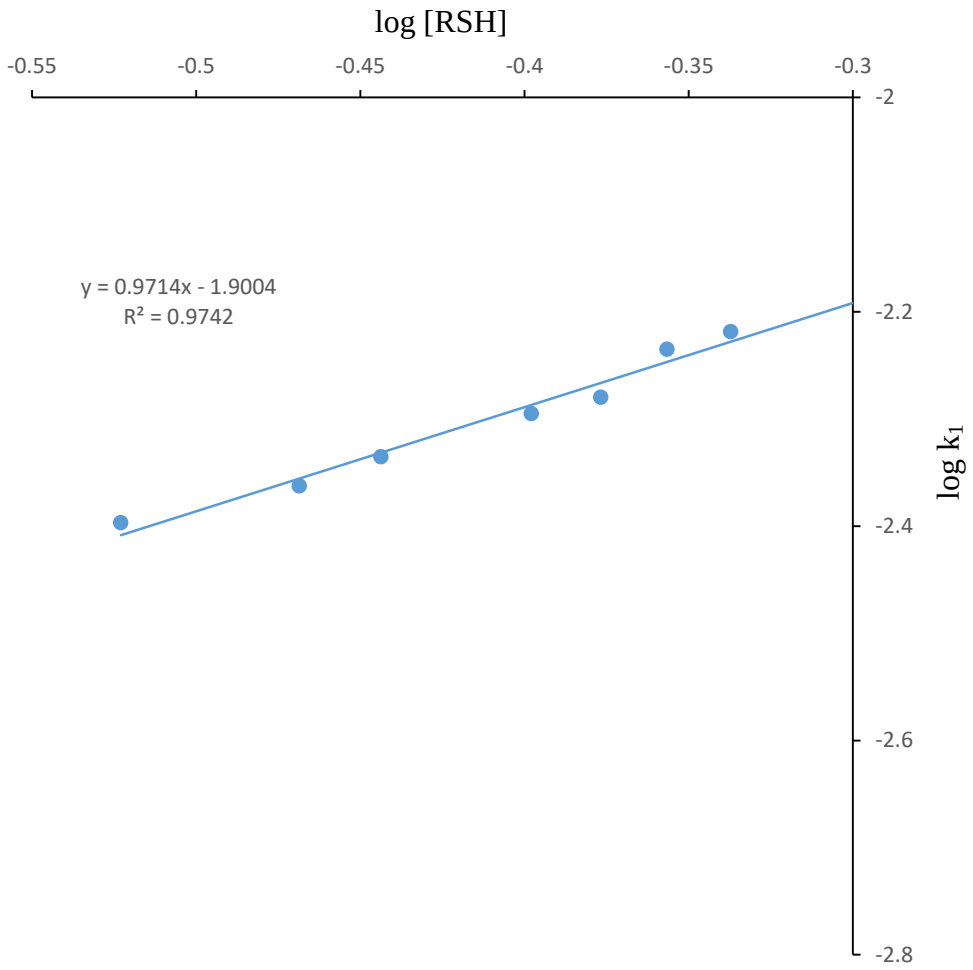


Figure 4.27: Plot of log k_1 versus log [RSH] for the redox reaction of $[Mn(salphen)]^+$ and RSH at $[Mn(salphen)^+] = 1.0 \times 10^{-4}$ mol dm^{-3}, $\mu = 0.6$ C^2 mol dm^{-3}, D = 78.19, T = 28 ± 1 °C and λ_{max} = 450 nm

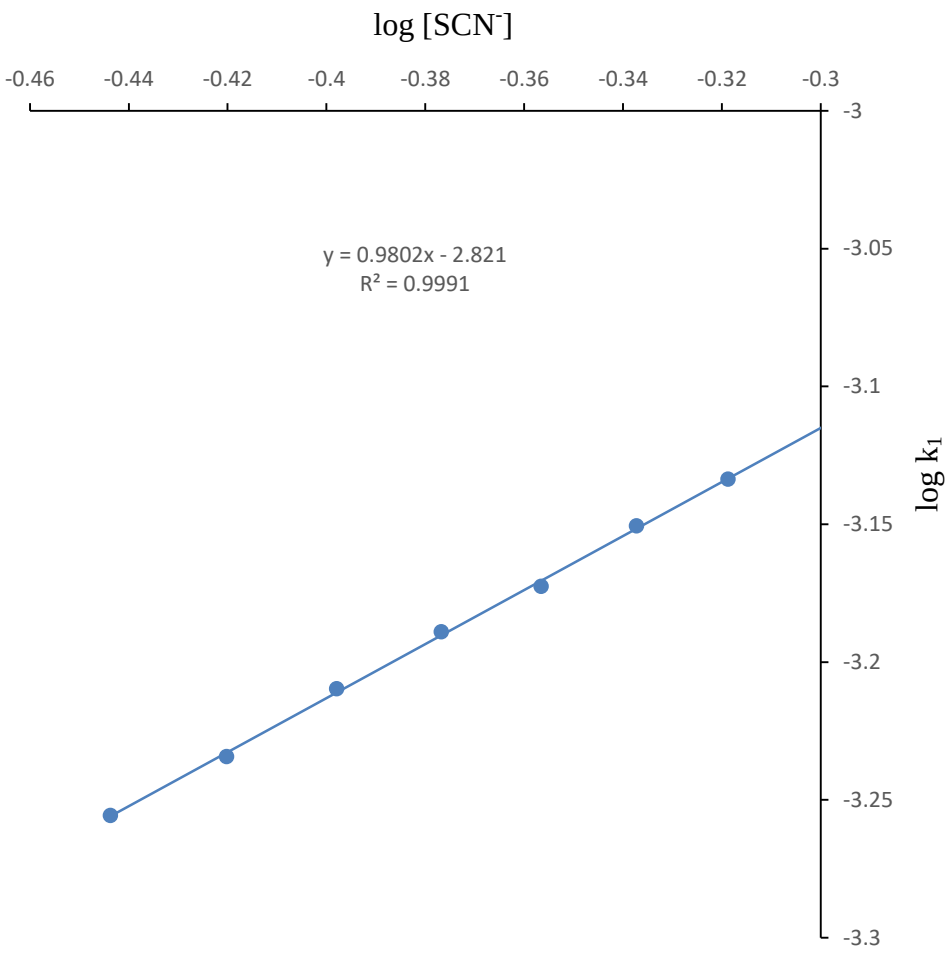


Figure 4.28: Plot of log k_1 versus log [SCN^-] for the redox reaction of $[Mn(salphen)]^+$ and SCN^- at $[Mn(salphen)^+] = 1.0 \times 10^{-4}$ mol dm^{-3}, $\mu = 0.6$ C^2 mol dm^{-3}, $[H^+] = 4.0 \times 10^{-5}$ mol dm^{-3}, D = 78.12, T = 28 ± 1 °C and λ_{max} = 450 nm

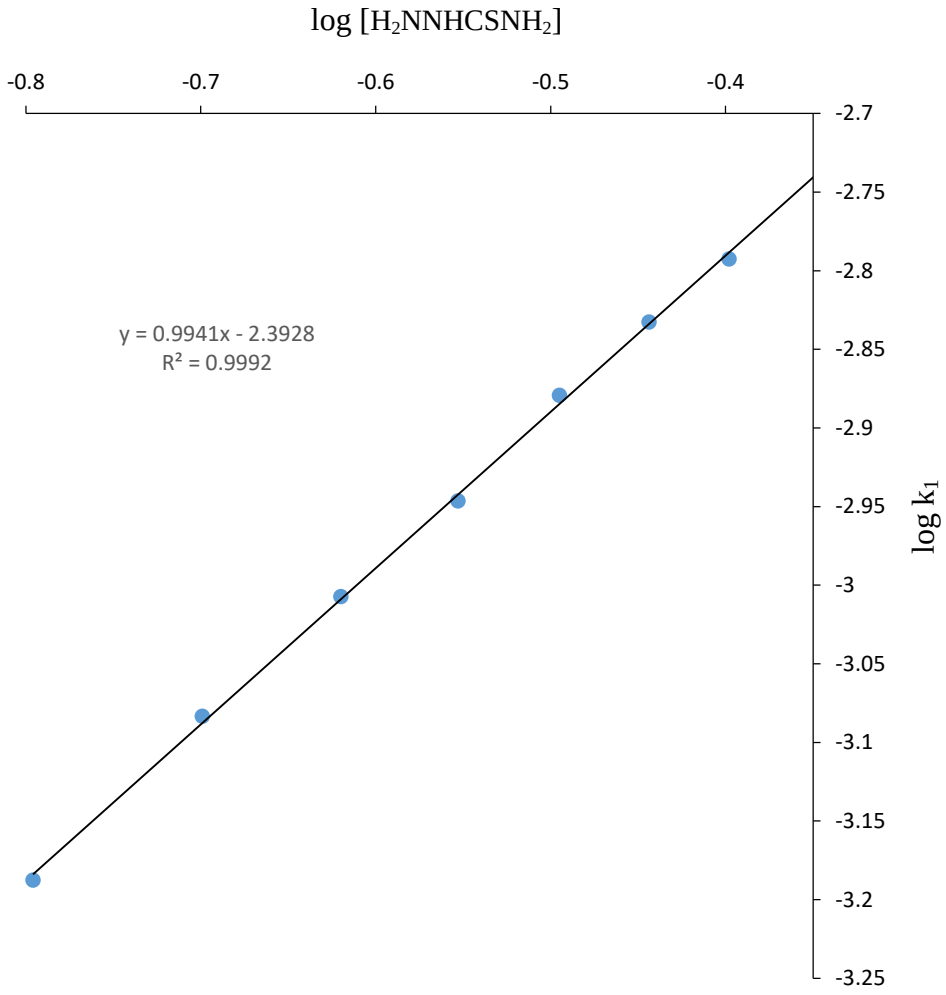


Figure 4.29: Plot of log k_1 versus log [$H_2NNHCSNH_2$] for the redox reaction of [Mn(salphen)]$^+$ and $H_2NNHCSNH_2$ at [Mn(salphen)$^+$] = 1.0 × 10^{-4} mol dm^{-3}, μ = 0.6 C^2 mol dm^{-3}, [H^+] = 2.0 × 10^{-5} mol dm^{-3}, D = 75.10, T = 28 ± 1°C and λ_{max} = 450 nm

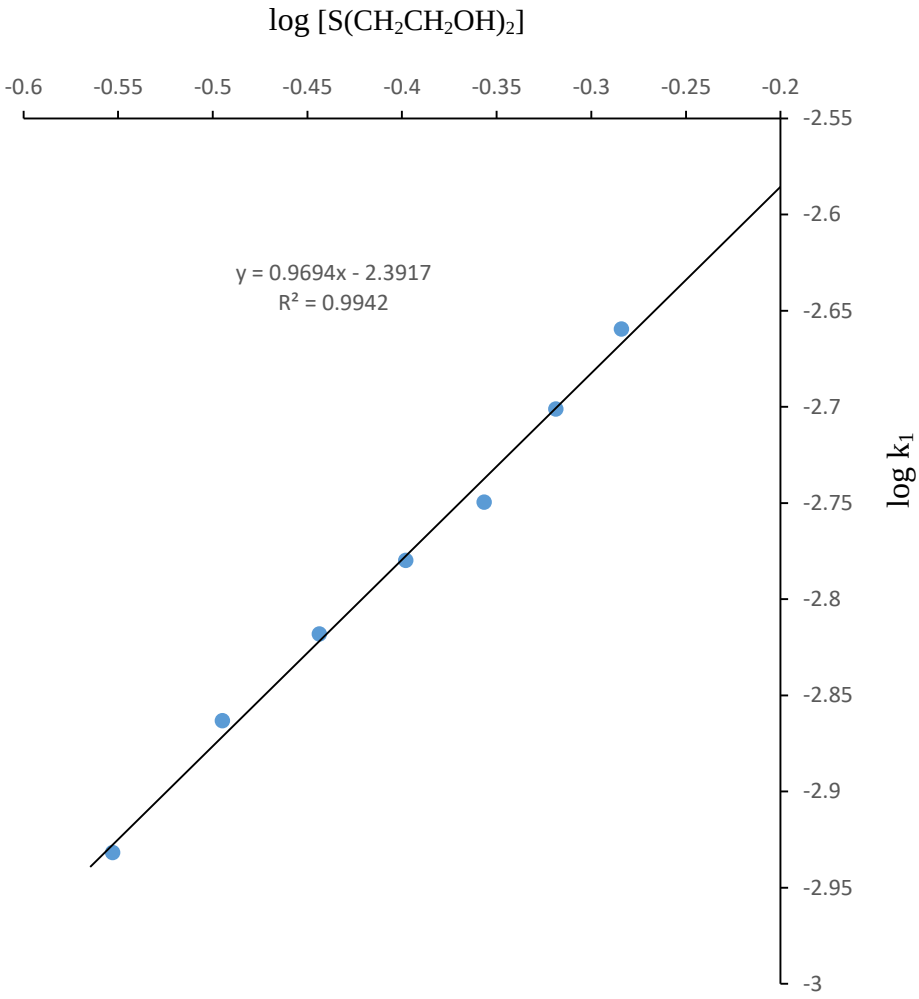


Figure 4.30: Plot of log k_1 versus log $[S(CH_2CH_2OH)_2]$ for the redox reaction of $[Mn(salphen)]^+$ and $[S(CH_2CH_2OH)_2]$ at $[Mn(salphen)^+] = 1.0 \times 10^{-4}$ mol dm^{-3}, $\mu = 0.6$ C^2 mol dm^{-3}, $[H^+] = 2.0 \times 10^{-5}$ mol dm^{-3}, T = 50 ± 1 °C and λ_{max} = 450 nm

Table 4.1: Pseudo-first order and second order rate constants for the reaction of $[Fe(salphen)]^+$ and TSH at $[Fe(salphen)^+] = 2.0 \times 10^{-4}$ mol dm^{-3}, D = 76.88, T = 26 ± 1°C and λ_{max} = 435 nm

[TSH], mol dm^{-3}	μ, C^2 mol dm^{-3}	10^3 k_1, s^{-1}	10^2 k_2, dm^3 mol^{-1} s^{-1}
0.12	0.20	1.75	1.46
0.13	0.20	1.82	1.40
0.14	0.20	1.98	1.41
0.15	0.20	2.14	1.43
0.16	0.20	2.24	1.40
0.17	0.20	2.40	1.41
0.18	0.20	2.60	1.44
0.15	0.18	2.16	1.44
0.15	0.20	2.12	1.41
0.15	0.25	2.17	1.45
0.15	0.30	2.14	1.43
0.15	0.40	2.10	1.40
0.15	0.50	2.16	1.44
0.15	0.60	2.14	1.43

Table 4.2: Pseudo-first order and second order rate constants for the reaction of $[Fe(salphen)]^+$ and $H_2C_2O_4$ at $[Fe(salphen)^+] = 2.0 \times 10^{-4}$ mol dm^{-3}, D = 76.06, T = 26 ± 1°C and λ_{max} = 435 nm

10^3 $[H_2C_2O_4]$, mol dm^{-3}	μ, C^2 mol dm^{-3}	10^3 k_1, s^{-1}	10 k_2, dm^3 mol^{-1} s^{-1}
4.00	0.20	2.86	7.15
5.00	0.20	3.64	7.28
6.00	0.20	4.26	7.10
7.00	0.20	5.07	7.24
8.00	0.20	5.96	7.45
9.00	0.20	6.79	7.54
11.00	0.20	8.06	7.33
6.00	0.18	4.28	7.13
6.00	0.20	4.26	7.10
6.00	0.24	4.29	7.15
6.00	0.28	4.27	7.12
6.00	0.32	4.30	7.17
6.00	0.36	4.29	7.15
6.00	0.40	4.26	7.10

Table 4.3: Pseudo-first order and second order rate constants for the reaction of $[Fe(salphen)]^+$ and H_3PO_2 at $[Fe(salphen)^+] = 2.0 \times 10^{-4}$ mol dm^{-3}, D = 76.68, T = 26 ± 1°C and λ_{max} = 435 nm

$[H_3PO_2]$, mol dm^{-3}	μ, C^2 mol dm^{-3}	$10^3 k_1$, s^{-1}	$10^2 k_2$, dm^3 mol^{-1} s^{-1}
0.10	0.20	2.28	2.28
0.11	0.20	2.51	2.28
0.12	0.20	2.77	2.30
0.13	0.20	2.88	2.22
0.14	0.20	3.20	2.29
0.15	0.20	3.41	2.27
0.16	0.20	3.69	2.30
0.13	0.18	2.90	2.23
0.13	0.20	2.88	2.22
0.13	0.24	2.92	2.25
0.13	0.28	2.90	2.23
0.13	0.32	2.83	2.18
0.13	0.36	2.95	2.27
0.13	0.40	2.86	2.20

Table 4.4: Pseudo-first order and second order rate constants for the reaction of $[Fe(salphen)]^+$ and H_2O_2 at $[Fe(salphen)^+] = 1.0 \times 10^{-4}$ mol dm^{-3}, $[H^+] = 2.0 \times 10^{-5}$ mol dm^{-3}, D = 78.12, T = 28 ± 1°C and λ_{max} = 435 nm

$[H_2O_2]$, mol dm^{-3}	μ, C^2 mol dm^{-3}	10^5 $[H^+]$, mol dm^{-3}	10^3 k_1, s^{-1}	10^2 k_2, dm^3 mol^{-1} s^{-1}
0.10	0.20	2.00	1.28	1.28
0.12	0.20	2.00	1.54	1.28
0.14	0.20	2.00	1.78	1.27
0.15	0.20	2.00	1.86	1.24
0.16	0.20	2.00	2.00	1.25
0.17	0.20	2.00	2.11	1.24
0.18	0.20	2.00	2.22	1.23
0.15	0.20	2.00	1.87	1.25
0.15	0.25	2.00	1.52	1.01
0.15	0.27	2.00	1.34	0.89
0.15	0.30	2.00	1.27	0.85
0.15	0.35	2.00	1.08	0.72
0.15	0.40	2.00	0.99	0.66
0.15	0.45	2.00	0.92	0.61
0.15	0.20	2.00	1.86	1.24
0.15	0.20	3.00	1.24	0.83
0.15	0.20	4.00	1.08	0.72
0.15	0.20	5.00	0.92	0.61
0.15	0.20	6.00	0.83	0.55

Table 4.5: Pseudo-first order and second order rate constants for the reaction of $[Mn(salphen)]^+$ and H_2O_2 at $[Mn(salphen)^+] = 1.0 \times 10^{-4}$ mol dm^{-3}, D = 76.82, T = 30 ± 1°C and λ_{max} = 450 nm

$[H_2O_2]$, mol dm^{-3}	10 μ, C^2 mol dm^{-3}	10^5 $[H^+]$, mol dm^{-3}	10^4 k_1, s^{-1}	10^4 k_2, dm^3 mol^{-1} s^{-1}
0.36	0.60	2.00	1.85	5.14
0.38	0.60	2.00	1.93	5.08
0.40	0.60	2.00	2.06	5.15
0.42	0.60	2.00	2.14	5.10
0.44	0.60	2.00	2.24	5.09
0.46	0.60	2.00	2.31	5.02
0.48	0.60	2.00	2.40	5.00
0.42	0.50	2.00	2.52	6.00
0.42	0.60	2.00	2.15	5.12
0.42	0.70	2.00	1.96	4.67
0.42	0.80	2.00	1.73	4.12
0.42	0.90	2.00	1.57	3.74
0.42	1.00	2.00	1.32	3.14
0.42	0.60	2.00	2.15	5.12
0.42	0.60	4.00	1.36	3.24
0.42	0.60	6.00	1.04	2.48
0.42	0.60	8.00	0.78	1.86
0.42	0.60	10.00	0.62	1.48

Table 4.6: Pseudo-first order and second order rate constants for the reaction of $[Mn(salphen)]^+$ and TSH at $[Mn(salphen)^+] = 1.0 \times 10^{-4}$ mol dm^{-3}, D = 77.98, T = 32 ± 1°C and λ_{max} = 450 nm

[TSH], mol dm^{-3}	μ, C^2 mol dm^{-3}	10^4 k_1, s^{-1}	10^3 k_2, dm^3 mol^{-1} s^{-1}
0.36	0.60	5.92	1.64
0.38	0.60	6.13	1.61
0.40	0.60	6.38	1.60
0.42	0.60	6.79	1.62
0.44	0.60	7.12	1.62
0.46	0.60	7.46	1.62
0.48	0.60	7.80	1.63
0.42	0.50	6.75	1.61
0.42	0.60	6.79	1.62
0.42	0.70	6.73	1.60
0.42	0.80	6.86	1.63
0.42	0.90	6.72	1.60
0.42	1.00	6.77	1.61

Table 4.7: Pseudo-first order and second order rate constants for the reaction of $[Mn(salphen)]^+$ and RSH at $[Mn(salphen)^+] = 1.0 \times 10^{-4}$ mol dm^{-3}, D = 78.19, T = 28 ± 1 °C and λ_{max} = 450 nm

[RSH], mol dm^{-3}	μ, C^2 mol dm^{-3}	10^5 [H$^+$], mol dm^{-3}	10^3 k_1, s^{-1}	10^2 k_2, dm^3 mol^{-1} s^{-1}
0.30	0.60	4.00	4.01	1.34
0.34	0.60	4.00	4.34	1.28
0.36	0.60	4.00	4.62	1.28
0.40	0.60	4.00	5.07	1.27
0.42	0.60	4.00	5.25	1.25
0.44	0.60	4.00	5.82	1.32
0.46	0.60	4.00	6.04	1.31
0.40	0.50	4.00	4.40	1.10
0.40	0.60	4.00	5.02	1.26
0.40	0.70	4.00	5.55	1.39
0.40	0.80	4.00	6.52	1.63
0.40	0.90	4.00	7.39	1.85
0.40	1.00	4.00	8.01	2.00
0.40	0.60	1.00	1.20	0.30
0.40	0.60	2.00	3.00	0.75
0.40	0.60	3.00	3.64	0.91
0.40	0.60	4.00	5.08	1.27
0.40	0.60	6.00	6.40	1.60
0.40	0.60	8.00	7.76	1.94
0.40	0.60	10.00	10.23	2.56

Table 4.8: Pseudo-first order and second order rate constants for the reaction of $[Mn(salphen)]^+$ and SCN^- at $[Mn(salphen)^+] = 1.0 \times 10^{-4}$ mol dm^{-3}, D = 78.12, T = 28 ± 1°C and λ_{max} = 450 nm

$[SCN^-]$, mol dm^{-3}	μ, C^2 mol dm^{-3}	10^5 $[H^+]$, mol dm^{-3}	10^4 k_1, s^{-1}	10^3 k_2, dm^3 mol^{-1} s^{-1}
0.36	0.60	4.00	5.55	1.54
0.38	0.60	4.00	5.83	1.53
0.40	0.60	4.00	6.17	1.54
0.42	0.60	4.00	6.47	1.54
0.44	0.60	4.00	6.72	1.53
0.46	0.60	4.00	7.07	1.54
0.48	0.60	4.00	7.35	1.53
0.42	0.50	4.00	6.52	1.55
0.42	0.60	4.00	6.47	1.54
0.42	0.70	4.00	5.90	1.40
0.42	0.80	4.00	5.41	1.29
0.42	0.90	4.00	5.00	1.19
0.42	1.00	4.00	4.30	1.02
0.42	0.60	1.00	6.42	1.53
0.42	0.60	2.00	6.40	1.52
0.42	0.60	4.00	6.45	1.54
0.42	0.60	6.00	6.47	1.54
0.42	0.60	8.00	6.53	1.55
0.42	0.60	10.0	6.47	1.54

Table 4.9: Pseudo-first order and second order rate constants for the reaction of $[Mn(salphen)]^+$ and $H_2NNHCSNH_2$ at $[Mn(salphen)^+] = 1.0 \times 10^{-4}$ mol dm^{-3}, D = 75.10, T = 28 ± 1 °C and λ_{max} = 450 nm

$[SCN^-]$, mol dm^{-3}	μ, C^2 mol dm^{-3}	10^5 $[H^+]$, mol dm^{-3}	10^4 k_1, s^{-1}	10^3 k_2, dm^3 mol^{-1} s^{-1}
0.36	0.60	4.00	5.55	1.54
0.38	0.60	4.00	5.83	1.53
0.40	0.60	4.00	6.17	1.54
0.42	0.60	4.00	6.47	1.54
0.44	0.60	4.00	6.72	1.53
0.46	0.60	4.00	7.07	1.54
0.48	0.60	4.00	7.35	1.53
0.42	0.50	4.00	6.52	1.55
0.42	0.60	4.00	6.47	1.54
0.42	0.70	4.00	5.90	1.40
0.42	0.80	4.00	5.41	1.29
0.42	0.90	4.00	5.00	1.19
0.42	1.00	4.00	4.30	1.02
0.42	0.60	1.00	6.42	1.53
0.42	0.60	2.00	6.40	1.52
0.42	0.60	4.00	6.45	1.54
0.42	0.60	6.00	6.47	1.54
0.42	0.60	8.00	6.53	1.55
0.42	0.60	10.0	6.47	1.54

Table 4.10: Pseudo-first order and second order rate constants for the reaction of $[Mn(salphen)]^+$ and $S(CH_2CH_2OH)_2$ at $[Mn(salphen)^+] = 1.0 \times 10^{-4}$ mol dm^{-3}, D = 66.60, T = 50 ± 1°C and λ_{max} = 450 nm

$[H_2NNHCSNH_2]$, mol dm^{-3}	μ, C^2 mol dm^{-3}	10^5 $[H^+]$, mol dm^{-3}	10^4 k_1, s^{-1}	10^3 k_2, dm^3 mol^{-1} s^{-1}
0.16	0.60	2.00	6.49	4.06
0.20	0.60	2.00	8.25	4.13
0.24	0.60	2.00	9.83	4.10
0.28	0.60	2.00	11.31	4.04
0.32	0.60	2.00	13.20	4.13
0.36	0.60	2.00	14.70	4.08
0.40	0.60	2.00	16.12	4.03
0.28	0.40	2.00	11.22	4.01
0.28	0.50	2.00	11.31	4.04
0.28	0.60	2.00	11.28	4.03
0.28	0.70	2.00	11.40	4.07
0.28	0.80	2.00	11.28	4.03
0.28	0.90	2.00	11.33	4.05
0.28	0.60	1.00	11.31	4.04
0.28	0.60	2.00	11.40	4.07
0.28	0.60	4.00	11.31	4.04
0.28	0.60	6.00	11.28	4.03
0.28	0.60	8.00	11.33	4.05
0.28	0.60	10.00	11.40	4.07

$[S(CH_2CH_2OH)_2]$, mol dm^{-3}	μ, C^2 mol dm^{-3}	10^5 $[H^+]$, mol dm^{-3}	10^4 k_1, s^{-1}	10^3 k_2, dm^3 mol^{-1} s^{-1}
0.28	0.60	2.00	11.70	4.18
0.32	0.60	2.00	13.70	4.28
0.36	0.60	2.00	15.20	4.22
0.40	0.60	2.00	16.60	4.15
0.44	0.60	2.00	17.80	4.05
0.48	0.60	2.00	19.90	4.15
0.52	0.60	2.00	21.90	4.21
0.40	0.50	2.00	18.50	4.63
0.40	0.60	2.00	16.62	4.16
0.40	0.70	2.00	14.23	3.56
0.40	0.80	2.00	10.80	2.70
0.40	0.90	2.00	8.96	2.24
0.40	1.00	2.00	7.88	1.97
0.40	0.60	1.00	18.90	4.73
0.40	0.60	2.00	16.60	4.15
0.40	0.60	4.00	14.50	3.63
0.40	0.60	6.00	13.80	3.45
0.40	0.60	8.00	13.30	3.33
0.40	0.60	10.00	12.70	3.18

4.1 – 4.4) and in the reactions of H_2O_2, TSH, RSH, SCN^-, $H_2NNHCSNH_2$ and $S(CH_2CH_2OH)_2$ with $[Mn(salphen)]^+$ respectively (Tables 4.5 – 4.10) were fairly constant. Based on these results, the rate equations are represented by equations 4.12 – 4.21.

$$\frac{-d[Fe(salphen)^+]}{dt} = k_2[Fe(salphen)^+][TSH] \quad 4.12$$

where $k_2 = (1.42 \pm 0.02) \times 10^{-2}$ dm^3 mol^{-1} s^{-1}

$$\frac{-3}{2}\frac{d[Fe(salphen)^+]}{dt} = k_2[Fe(salphen)^+][H_2C_2O_4] \quad 4.13$$

where $k_2 = (7.29 \pm 0.16) \times 10^{-1}$ dm^3 mol^{-1} s^{-1}

$$\frac{-1}{2}\frac{d[Fe(salphen)^+]}{dt} = k_2[Fe(salphen)^+][H_3PO_2] \quad 4.14$$

where $k_2 = (2.28 \pm 0.03) \times 10^{-2}$ dm^3 mol^{-1} s^{-1}

$$\frac{-1}{2}\frac{d[Fe(salphen)^+]}{dt} = k_2[Fe(salphen)^+][H_2O_2] \quad 4.15$$

where $k_2 = (5.08 \pm 0.06) \times 10^{-4}$ dm^3 mol^{-1} s^{-1}

$$\frac{-1}{2}\frac{d[Mn(salphen)^+]}{dt} = k_2[Mn(salphen)^+][H_2O_2] \quad 4.16$$

where $k_2 = (1.26 \pm 0.02) \times 10^{-2}$ dm^3 mol^{-1} s^{-1}

$$\frac{-d[Mn(salphen)^+]}{dt} = k_2[Mn(salphen)^+][TSH] \quad 4.17$$

where $k_2 = (1.62 \pm 0.02) \times 10^{-3}$ dm^3 mol^{-1} s^{-1}

$$\frac{-d[Mn(salphen)^+]}{dt} = k_2[Mn(salphen)^+][RSH] \quad 4.18$$

where $k_2 = (1.29 \pm 0.03) \times 10^{-2}$ dm^3 mol^{-1} s^{-1}

$$\frac{-d[Mn(salphen)^+]}{dt} = k_2[Mn(salphen)^+][SCN^-] \quad 4.19$$

where $k_2 = (1.54 \pm 0.01) \times 10^{-3}$ dm^3 mol^{-1} s^{-1}

$$\frac{-1}{2}\frac{d[Mn(salphen)^+]}{dt} = k_2[Mn(salphen)^+][H_2NNHCSNH_2] \quad 4.20$$

where $k_2 = (4.08 \pm 0.04) \times 10^{-3}$ dm^3 mol^{-1} s^{-1}

$$\frac{-1}{2}\frac{d[Mn(salphen)^+]}{dt} = k_2[Mn(salphen)^+][S(CH_2CH_2OH)_2] \quad 4.21$$

where $k_2 = (4.18 \pm 0.07) \times 10^{-3}$ dm^3 mol^{-1} s^{-1}

4.5 Effect of Acid on the Reactions Rate

Acid inhibition was observed in the reaction of H_2O_2 with $[Fe(salphen)]^+$ (Table 4.4) and in the reactions of H_2O_2 (Table 4.5) and $S(CH_2CH_2OH)_2$ (Table 4.10) with $[Mn(salphen)]^+$ whereas the reaction of RSH with $[Mn(salphen)]^+$ was catalysed by $[H^+]$ as presented in Table 4.7. The slopes obtained from the plots of log k_1 versus log $[H^+]$ were -0.76 in H_2O_2 – $[Fe(salphen)]^+$ reaction, -0.72, -0.17 and +0.87 in the reactions of H_2O_2, $S(CH_2CH_2OH)_2$ and RSH with $[Mn(salphen)]^+$. The reactions rate were independent of $[H^+]$ in the reactions of SCN^- (Table 4.8), $H_2NNHCSNH_2$ (Table 4.9) and TSH (Table 4.11) with $[Mn(salphen)]^+$ and in the reactions of TSH (Table 4.12), $H_2C_2O_4$ (Table 4.13) and H_3PO_2 (Table 4.14) with $[Fe(salphen)]^+$.

Plots of k_2 versus $\frac{1}{[H^+]}$ in the H_2O_2 – $[Fe(salphen)]^+$ reaction (Figure 4.31), H_2O_2 – $[Mn(salphen)]^+$ (Figure 4.32) and $S(CH_2CH_2OH)_2$ – $[Mn(salphen)]^+$ reaction (Figure 4.33) and plot of k_2 versus $[H^+]$ in the RSH – $[Mn(salphen)]^+$ reaction (Figure 4.34) were linear with intercepts. The observed acid dependence effect can be expressed as:

Table 4.11: Acid dependence effect on the rate of reaction of $[Mn(salphen)]^+$ and TSH at $[Mn(salphen)^+] = 1.0 \times 10^{-4}$ mol dm^{-3}, [TSH] = 0.42 mol dm^{-3}, $\mu = 0.6\ C^2$ mol dm^{-3}, D = 77.98, T = 32 ± 1°C and λ_{max} = 450 nm

10^5 $[H^+]$, mol dm^{-3}	10^4 k_1, s^{-1}	10^3 k_2, dm^3 mol^{-1} s^{-1}
0.00	6.79	1.62
1.00	6.86	1.63
2.00	6.75	1.61
4.00	6.84	1.63
6.00	6.86	1.63
8.00	6.68	1.59
10.0	6.72	1.60

Table 4.12: Acid dependence effect on the rate of reaction of $[Fe(salphen)]^+$ and TSH at $[Fe(salphen)^+] = 2.0 \times 10^{-4}$ mol dm^{-3}, [TSH] = 0.15 mol dm^{-3}, μ = 0.2 C^2 mol dm^{-3}, D = 76.88, T = 26 ± 1°C and λ_{max} = 435 nm

10^5 [H^+], mol dm^{-3}	10^3 k_1, s^{-1}	10^2 k_2, dm^3 mol^{-1} s^{-1}
0.00	2.14	1.43
1.00	2.10	1.40
2.00	2.13	1.42
4.00	2.16	1.44
6.00	2.12	1.41
8.00	2.16	1.44
10.00	2.13	1.42

Table 4.13: Acid dependence effect on the rate of reaction of $[Fe(salphen)]^+$ and $H_2C_2O_4$ at $[Fe(salphen)^+] = 2.0 \times 10^{-4}$ mol dm^{-3}, $[H_2C_2O_4] = 6.0 \times 10^{-3}$ mol dm^{-3}, $\mu = 0.2$ C^2 mol dm^{-3}, D = 76.06, T = 26 ± 1°C and λ_{max} = 435 nm

10^5 [H^+], mol dm^{-3}	10^3 k_1, s^{-1}	10 k_2, dm^3 mol^{-1} s^{-1}
0.00	4.27	7.12
1.00	4.29	7.15
2.00	4.28	7.13
4.00	4.26	7.10
6.00	4.29	7.15
8.00	4.27	7.12
10.00	4.28	7.13

Table 4.14: Acid dependence effect on the rate of reaction of $[Fe(salphen)]^{+}$ and H_3PO_2 at $[Fe(salphen)^{+}] = 2.0 \times 10^{-4}$ mol dm^{-3}, $[H_3PO_2] = 0.13$ mol dm^{-3}, $\mu = 0.2$ C^2 mol dm^{-3}, D = 76.68, T = 26 ± 1 °C and λ_{max} = 435 nm

10^5 $[H^+]$, mol dm^{-3}	10^3 k_1, s^{-1}	10^2 k_2, dm^3 mol^{-1} s^{-1}
0.00	2.88	2.22
1.00	2.86	2.20
2.00	2.86	2.20
4.00	2.92	2.25
6.00	2.90	2.23
8.00	2.88	2.22
10.00	2.92	2.25

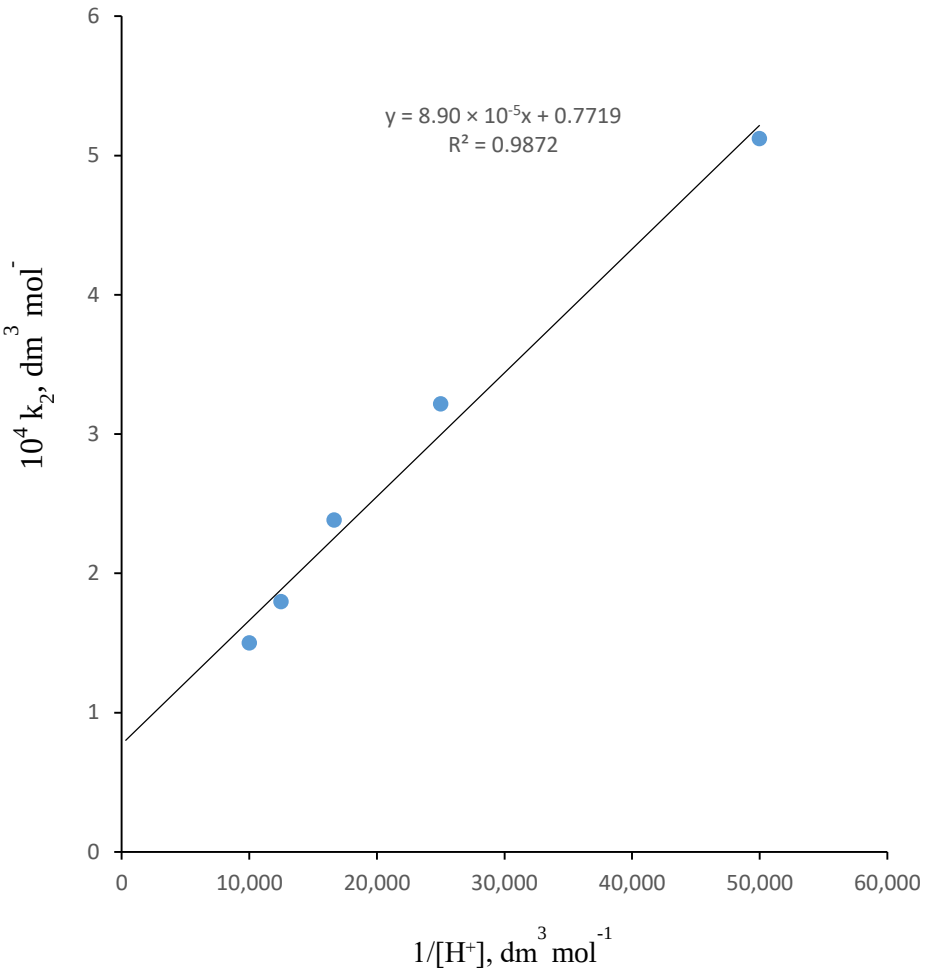


Figure 4.31: Plot of 10^4 k_2 versus $1/[H^+]$ for the redox reaction of $[Fe(salphen)]^+$ and H_2O_2 at $[Fe(salphen)^+] = 1.0 \times 10^{-4}$ mol dm^{-3}, $[H_2O_2] = 0.42$ mol dm^{-3}, $\mu = 0.6$ C^2 mol dm^{-3}, $[H^+] = 2.0 \times 10^{-5}$ mol dm^{-3}, D = 78.12, T = 28 ± 1 °C and λ_{max} = 435 nm

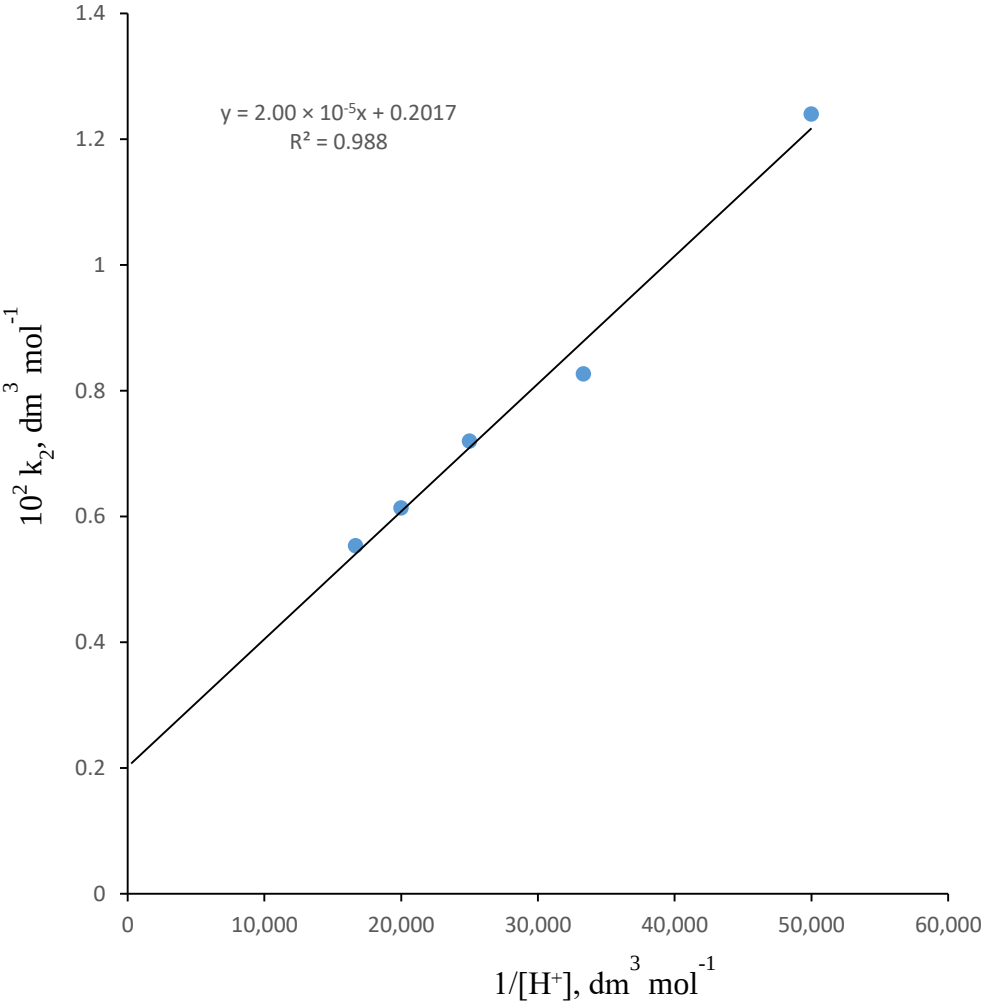


Figure 4.32: Plot of 10^2 k_2 versus $1/[H^+]$ for the redox reaction of $[Mn(salphen)]^+$ and H_2O_2 at $[Mn(salphen)^+] = 1.0 \times 10^{-4}$ mol dm^{-3}, $[H_2O_2] = 0.15$ mol dm^{-3}, $\mu = 0.2$ C^2 mol dm^{-3}, $[H^+] = 2.0 \times 10^{-5}$ mol dm^{-3}, D = 76.82, T = 30 ± 1 °C and λ_{max} = 450 nm

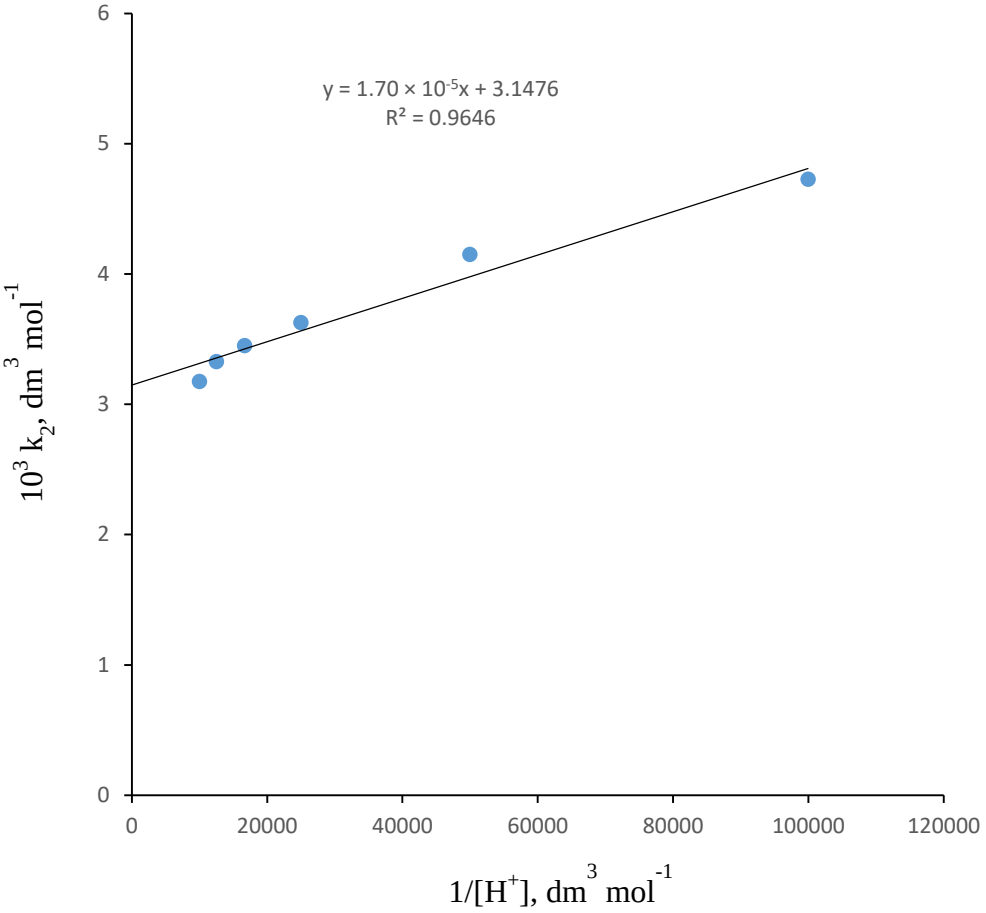


Figure 4.33: Plot of 10^3 k_2 versus $1/[H^+]$ for the redox reaction of $[Mn(salphen)]^+$ and $S(CH_2CH_2OH)_2$ at $[Mn(salphen)^+]$ = 1.0 × 10^{-4} mol dm^{-3}, $[S(CH_2CH_2OH)_2]$ = 0.40 mol dm^{-3}, μ = 0.6 C^2 mol dm^{-3}, D = 66.60, T = 50 ± 1 °C and λ_{max} = 450 nm

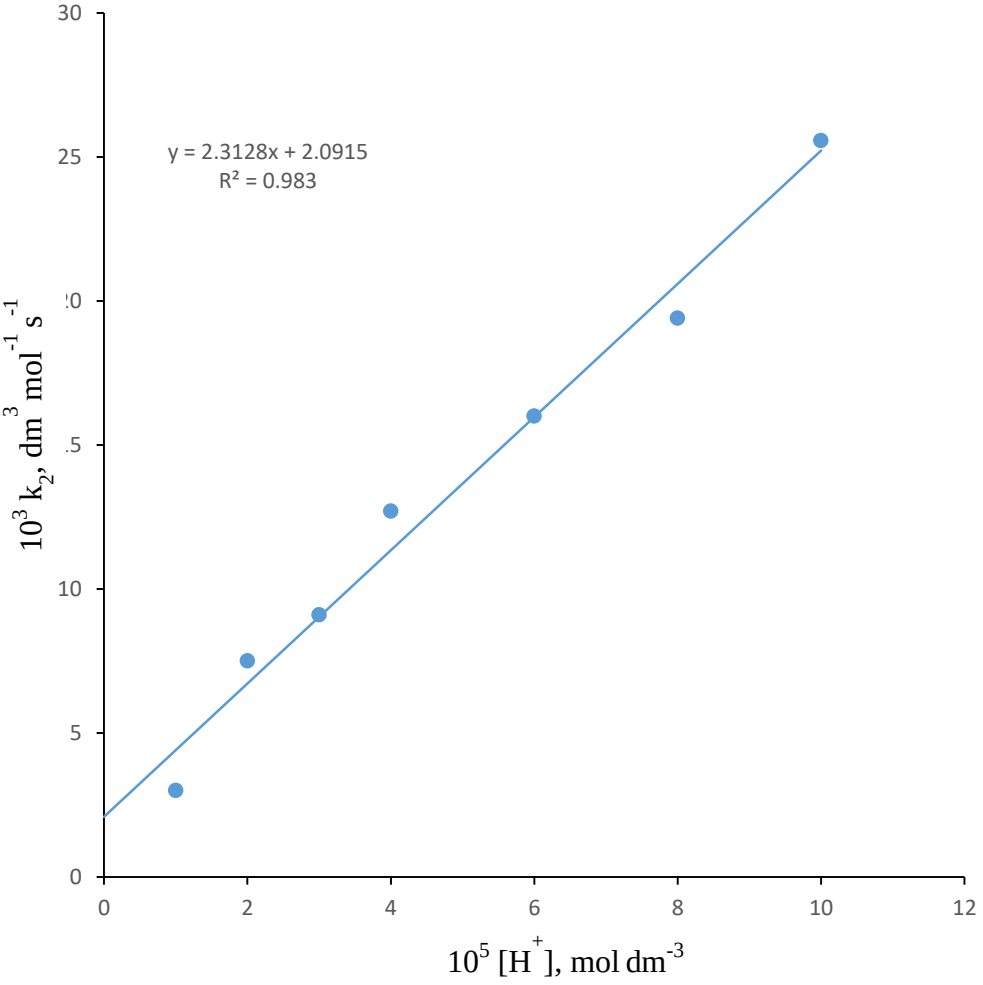


Figure 4.34: Plot of 10^3 k_2 versus 10^5 [H^+] for the redox reaction of [Mn(salphen)]$^+$ and RSH at [Mn(salphen)$^+$] = 1.0×10^{-4} mol dm^{-3}, [RSH] = 0.4 mol dm^{-3}, μ = 0.6 C^2 mol dm^{-3}, D = 78.19, T = 28 ± 1°C and λ_{max} = 450 nm

$$k_2 = a + \frac{b}{[H^+]} \quad 4.22$$

where $a = 8.90 \times 10^{-5}$ dm^3 mol^{-1} s^{-1}, $b = 7.72 \times 10^{-1}$ s^{-1}, for H_2O_2 – [Fe(salphen)]$^+$ reaction

$$k_2 = c + \frac{d}{[H^+]} \quad 4.23$$

where $c = 2.00 \times 10^{-5}$ dm^3 mol^{-1} s^{-1}, $d = 2.02 \times 10^{-1}$ s^{-1}, for H_2O_2 – [Mn(salphen)]$^+$ reaction

$$k_2 = e + \frac{f}{[H^+]} \quad 4.24$$

where $e = 1.70 \times 10^{-5}$ dm^3 mol^{-1} s^{-1}, $f = 3.15$ s^{-1}, for $S(CH_2CH_2OH)_2$ – [Mn(salphen)]$^+$ reaction

$$k_2 = g + h[H^+] \quad 4.25$$

where $g = 2.31$ dm^3 mol^{-1} s^{-1}, $h = 2.09$ dm^6 mol^{-2} s^{-1}, for RSH – [Mn(salphen)]$^+$ reaction.

4.6 Effect of Changes in Ionic Strength and Dielectric Constant on the Reactions Rate

Increase in ionic strength of the reaction medium had no effect on the reactions rate of TSH, $H_2C_2O_4$ and H_3PO_2 reactions with [Fe(salphen)]$^+$ (Tables 4.1 – 4.3) while the rate decreased in H_2O_2 – [Fe(salphen)]$^+$ reaction (Table 4.4) in the concentration range investigated. Increase in ionic strength also had no effect on the reactions rate of TSH (Table 4.6) and $H_2NNHCSNH_2$ (Table 4.9) reactions with [Mn(salphen)]$^+$, while the rate decreased in H_2O_2 (Table 4.5), SCN^- (Table 4.8) and $S(CH_2CH_2OH)_2$ (Table 4.10) reactions with [Mn(salphen)]$^+$ but the rate increased in RSH – [Mn(salphen)]$^+$ reaction (Table 4.7). The slope obtained from the plot of log k_2 against $\sqrt{\mu}$ was -0.91 in H_2O_2 – [Fe(salphen)]$^+$ reaction (Figure 4.35) whereas slopes of -1.34, -0.76, -1.35 and 0.92 were obtained in the

reactions of H_2O_2, SCN^-, $S(CH_2CH_2OH)_2$ and RSH with $[Mn(salphen)]^+$ (Figures 4.36 – 4.39).

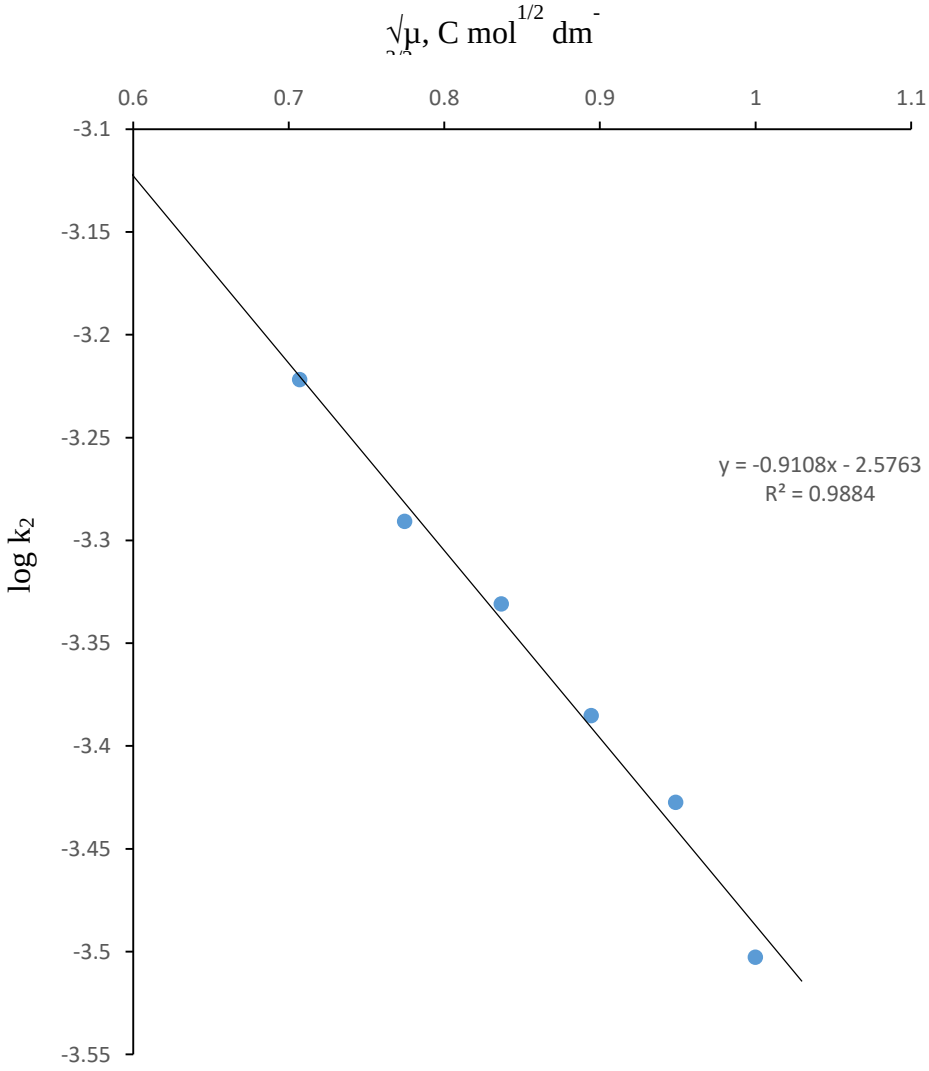


Figure 4.35: Plot of log k_2 versus √I for the redox reaction of $[Fe(salphen)]^+$ and H_2O_2 at $[Fe(salphen)^+] = 1.0 \times 10^{-4}$ mol dm^{-3}, $[H_2O_2] = 0.42$ mol dm^{-3}, $[H^+] = 2.0 \times 10^{-5}$ mol dm^{-3}, D = 78.12, T = 28 ± 1°C and λ_{max} = 435 nm

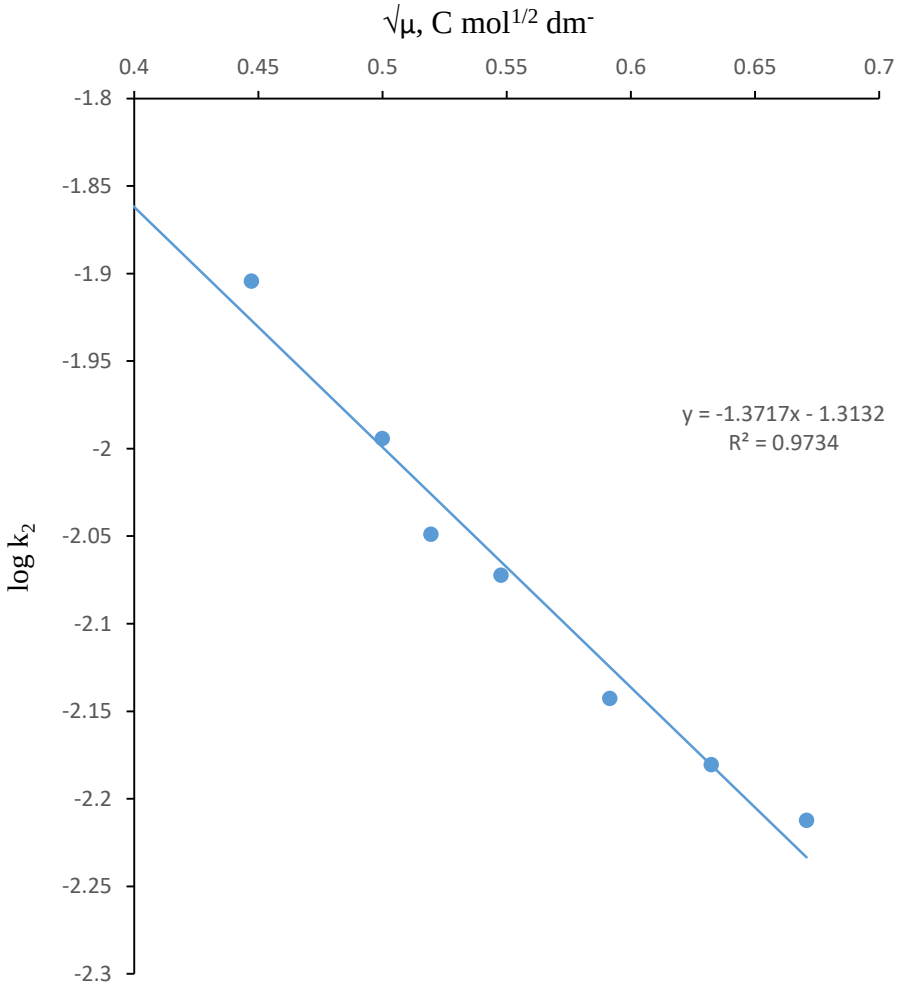


Figure 4.36: Plot of log k_2 versus √I for the redox reaction of $[Mn(salphen)]^+$ and H_2O_2 at $[Mn(salphen)^+] = 1.0 \times 10^{-4}$ mol dm^{-3}, $[H_2O_2] = 0.15$ mol dm^{-3}, $[H^+] = 2.0 \times 10^{-5}$ mol dm^{-3}, D = 76.82, T = 30 ± 1°C and λ_{max} = 450 nm

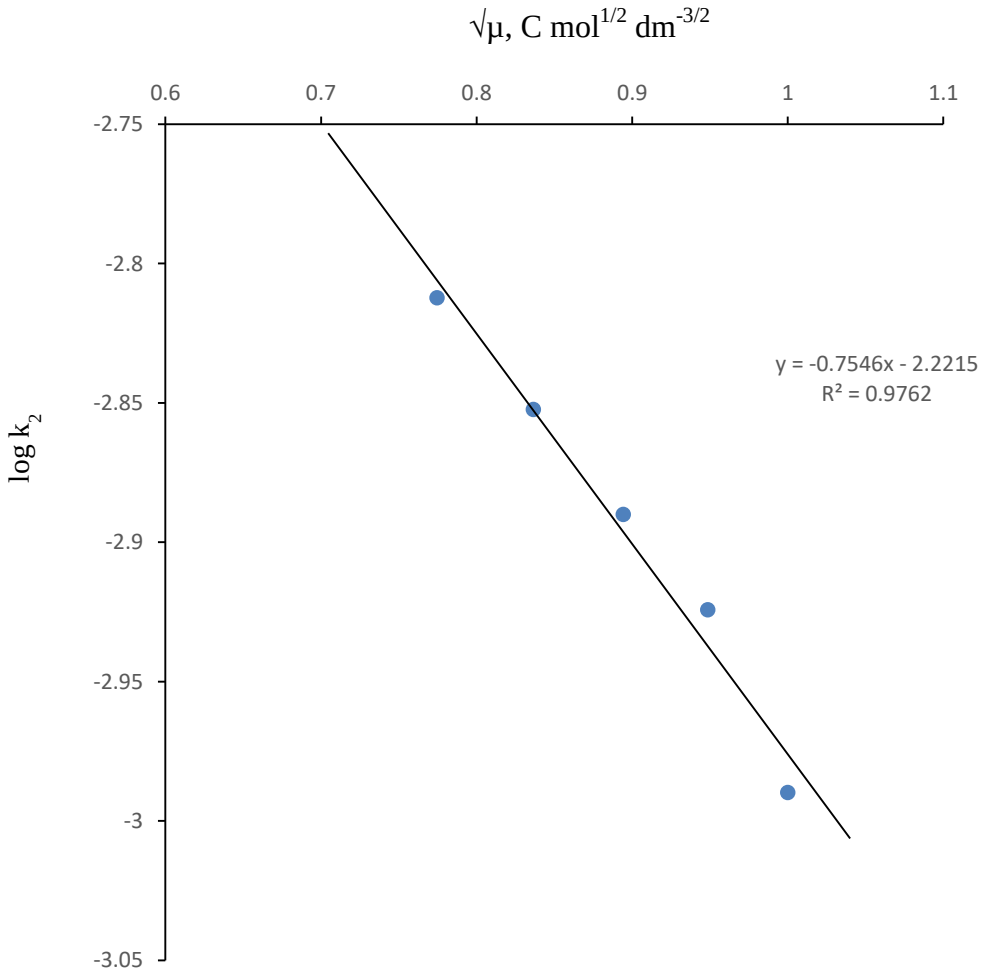


Figure 4.37: Plot of log k_2 versus √I for the redox reaction of $[Mn(salphen)]^+$ and SCN^- at $[Mn(salphen)^+] = 1.0 \times 10^{-4}$ mol dm^{-3}, $[SCN^-] = 0.42$ mol dm^{-3}, $[H^+] = 4.0 \times 10^{-5}$ mol dm^{-3}, D = 78.12, T = 28 ± 1°C and λ_{max} = 450 nm

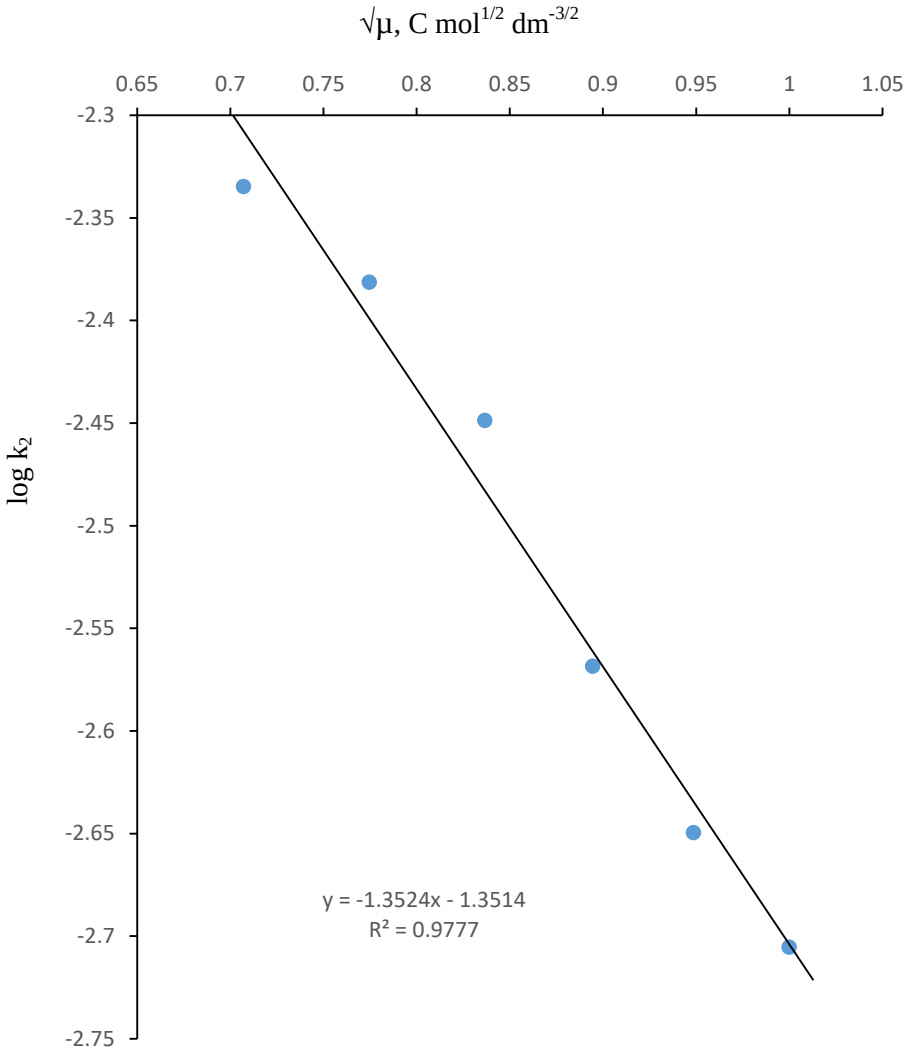


Figure 4.38: **Plot of log k_2 versus √I for the redox reaction of $[Mn(salphen)]^+$ and $S(CH_2CH_2OH)_2$ at $[Mn(salphen)^+] = 1.0 \times 10^{-4}$ mol dm^{-3}, $[S(CH_2CH_2OH)_2] = 0.40$ mol dm^{-3}, $[H^+] = 2.0 \times 10^{-5}$ mol dm^{-3}, D = 66.60, T = 50 ± 1°C and λ_{max} = 450 nm**

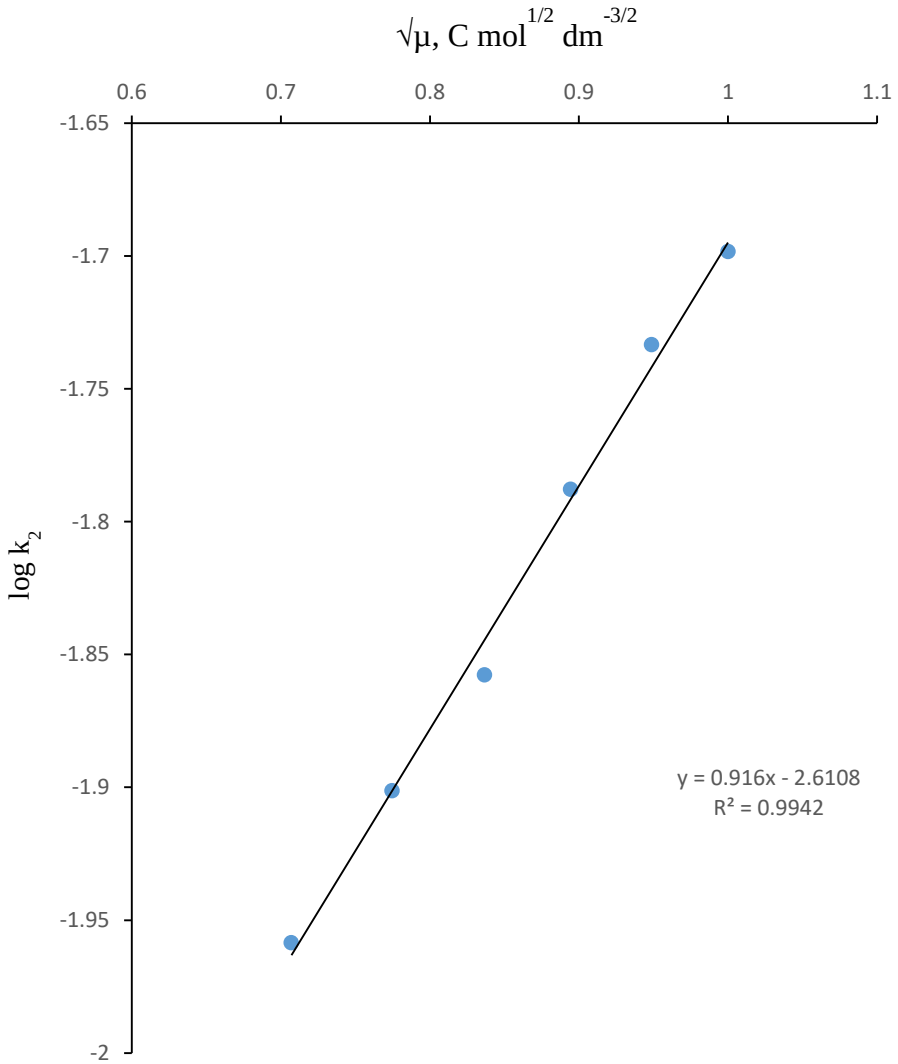


Figure 4.39: Plot of log k_2 versus √I for the redox reaction of $[Mn(salphen)]^+$ and RSH at $[Mn(salphen)^+] = 1.0 \times 10^{-4}$ mol dm^{-3}, [RSH] = 0.4 mol dm^{-3}, $[H^+] = 4.0 \times 10^{-5}$ mol dm^{-3}, D = 78.19, T = 28 ± 1°C and λ_{max} = 450 nm

Decrease in the dielectric constant of the reaction medium had no effect on the reaction rate of TSH, $H_2C_2O_4$ and H_3PO_2 reactions with $[Fe(salphen)]^+$ (Tables 4.15 – 4.17) while the rate decreased in H_2O_2 - $[Fe(salphen)]^+$ reaction (Table 4.18). Similarly, decreasing the dielectric constant of the reaction medium had no effect effect on the reaction rate of TSH - $[Mn(salphen)]^+$ reaction (Table 4.19) whereas the rate decreased in H_2O_2, SCN^-, $H_2NNHCSNH_2$ and $S(CH_2CH_2OH)_2$ reactions with $[Mn(salphen)]^+$ (Tables 4.20 – 4.23) but

an increase in the rate was observed in RSH – $[Mn(salphen)]^+$ reaction (Table 4.24). Plots of log k_2 against 1/D are presented for H_2O_2 – $[Fe(salphen)]^+$ reaction (Figure 4.40) and for the reactions of H_2O_2, SCN^-, $H_2NNHCSNH_2$, $S(CH_2CH_2OH)_2$ and RSH with $[Mn(salphen)]^+$ (Figures 4.41 – 4.45).

4.7 Effect of Added Ions on the Reactions Rate

Increase in concentration of added cations (Mg^{2+}, Ca^{2+} and K^+) had no effect effect on the rate of $H_2C_2O_4$ – $[Fe(salphen)]^+$ reaction (Table 4.25), whereas the rate increased in TSH, H_3PO_2 and H_2O_2 reactions with $[Fe(salphen)]^+$ (Tables 4.26 – 4.28) and in the reactions of TSH and $H_2NNHCSNH_2$ with $[Mn(salphen)]^+$ (Tables 4.29 and 4.30). The reaction rate was however decreased with increasing cation concentration in the reactions of H_2O_2, RSH, SCN^- and $S(CH_2CH_2OH)_2$ with $[Mn(salphen)]^+$ (Tables 4.31 – 4.34). Plots of ion dependent second order rate constant, k_2, versus concentrations of cations, [X] are presented in Figures 4.46 – 4.63.

Increasing concentrations of added anions (SO_4^{2-}, NO_3^-, CH_3COO^- and $HCOO^-$) had no effect effect on the rate of $H_2C_2O_4$ – $[Fe(salphen)]^+$ reaction (Table 4.35) while the rate increased in TSH, H_3PO_2 and H_2O_2 reactions with $[Fe(salphen)]^+$ (Tables 4.36 – 4.38) and

TSH, RSH, SCN^- and $H_2NNHCSNH_2$ reactions with $[Mn(salphen)]^+$ (Tables 4.39 – 4.42).

Table 4.15: Effect of dielectric constant on the rate of reaction of $[Fe(salphen)]^+$ and TSH at $[Fe(salphen)^+] = 2.0 \times 10^{-4}$ mol dm^{-3}, [TSH] = 0.15 mol dm^{-3}, μ = 0.2 C^2 mol dm^{-3}, T = 26 ± 1°C and λ_{max} = 435 nm

D	10^2 1/D	10^3 k_1, s^{-1}	10^2 k_2, dm^3 mol^{-1} s^{-1}
76.88	1.30	2.16	1.44
74.69	1.34	2.14	1.43
73.59	1.36	2.17	1.45
72.49	1.38	2.14	1.43
71.40	1.40	2.12	1.41
69.20	1.45	2.16	1.44
67.01	1.49	2.10	1.40

Table 4.16: Effect of dielectric constant on the rate of reaction of $[Fe(salphen)]^+$ and $H_2C_2O_4$ at $[Fe(salphen)^+] = 2.0 \times 10^{-4}$ mol dm^{-3}, $[H_2C_2O_4] = 6.0 \times 10^{-3}$ mol dm^{-3}, $\mu = 0.2$ C^2 mol dm^{-3}, $T = 26 \pm 1^{\circ}C$ and $\lambda_{max} = 435$ nm

D	10^2 1/D	10^3 k_1, s^{-1}	10 k_2, dm^3 mol^{-1} s^{-1}
76.06	1.32	4.30	7.17
74.96	1.33	4.29	7.15
73.87	1.35	4.32	7.20
72.77	1.37	4.26	7.10
71.67	1.40	4.28	7.13
70.57	1.42	4.33	7.22
69.48	1.44	4.28	7.13

Table 4.17: Effect of dielectric constant on the rate of reaction of $[Fe(salphen)]^{+}$ and H_3PO_2 at $[Fe(salphen)^{+}] = 2.0 \times 10^{-4}$ mol dm^{-3}, $[H_3PO_2] = 0.13$ mol dm^{-3}, $\mu = 0.2\ C^2$ mol dm^{-3}, $T = 26 \pm 1^{\circ}C$ and $\lambda_{max} = 435$ nm

D	10^2 1/D	$10^3 k_1$, s^{-1}	$10^2 k_2$, $dm^3\ mol^{-1}\ s^{-1}$
76.68	1.30	2.92	2.25
75.58	1.32	2.88	2.22
74.48	1.34	2.90	2.23
73.39	1.36	2.83	2.18
72.29	1.38	2.95	2.27
71.19	1.41	2.92	2.25
70.09	1.43	2.86	2.20

Table 4.18: Effect of dielectric constant on the rate of reaction of $[Fe(salphen)]^+$ and H_2O_2 at $[Fe(salphen)^+] = 1.0 \times 10^{-4}$ mol dm^{-3}, $[H_2O_2] = 0.42$ mol dm^{-3}, $\mu = 0.6\ C^2$ mol dm^{-3}, $[H^+] = 2.0 \times 10^{-5}$ mol dm^{-3}, T = 28 ± 1°C and λ_{max} = 435 nm

D	10^2 1/D	10^4 k_1, s^{-1}	10^4 k_2, dm^3 mol^{-1} s^{-1}
78.12	1.28	2.15	5.12
77.02	1.30	1.98	4.71
75.92	1.32	1.64	3.91
74.83	1.34	1.37	3.26
73.73	1.36	1.00	2.38

Table 4.19: Effect of dielectric constant on the rate of reaction of $[Mn(salphen)]^+$ and TSH at $[Mn(salphen)^+] = 1.0 \times 10^{-4}$ mol dm^{-3}, [TSH] = 0.42 mol dm^{-3}, $\mu = 0.6\ C^2$ mol dm^{-3}, T = 32 ± 1°C and λ_{max} = 450 nm

D	10^2 1/D	10^4 k_1, s^{-1}	10^3 k_2, dm^3 mol^{-1} s^{-1}
77.98	1.28	6.75	1.61
76.88	1.30	6.79	1.62
75.79	1.32	6.89	1.64
74.69	1.34	6.75	1.61
73.59	1.36	6.79	1.62
72.49	1.38	6.86	1.63
71.40	1.40	6.75	1.61

Table 4.20: Effect of dielectric constant on the rate of reaction of $[Mn(salphen)]^+$ and H_2O_2 at $[Mn(salphen)^+] = 1.0 \times 10^{-4}$ mol dm^{-3}, $[H_2O_2] = 0.15$ mol dm^{-3}, $\mu = 0.2\ C^2$ mol dm^{-3}, $[H^+] = 2.0 \times 10^{-5}$ mol dm^{-3}, T = 30 ± 1°C and λ_{max} = 450 nm

D	10^2 1/D	10^3 k_1, s^{-1}	10^2 k_2, dm^3 mol^{-1} s^{-1}
76.82	1.30	1.84	1.23
75.72	1.32	1.15	0.77
74.62	1.34	0.97	0.65
73.52	1.36	0.85	0.57
72.43	1.38	0.74	0.49

Table 4.21: Effect of dielectric constant on the rate of reaction of $[Mn(salphen)]^+$ and SCN^- at $[Mn(salphen)^+] = 1.0 \times 10^{-4}$ mol dm^{-3}, $[SCN^-] = 0.42$ mol dm^{-3}, $\mu = 0.6\ C^2$ mol dm^{-3}, $[H^+] = 4.0 \times 10^{-5}$ mol dm^{-3}, T = 28 ± 1°C and λ_{max} = 450 nm

D	10^2 1/D	10^4 k_1, s^{-1}	10^3 k_2, dm^3 mol^{-1} s^{-1}
78.12	1.28	6.47	1.54
77.84	1.29	5.18	1.23
77.57	1.29	3.68	0.88
77.30	1.29	2.13	0.51
77.02	1.29	1.13	0.27

Table 4.22: Effect of dielectric constant on the rate of reaction of $[Mn(salphen)]^+$ and $H_2NNHCSNH_2$ at $[Mn(salphen)^+] = 1.0 \times 10^{-4}$ mol dm^{-3}, $[H_2NNHCSNH_2] = 0.28$ mol dm^{-3}, $\mu = 0.6\ C^2$ mol dm^{-3}, $[H^+] = 2.0 \times 10^{-5}$ mol dm^{-3}, T = 28 ± 1°C and $\lambda_{max} = 450$ nm

D	10^2 1/D	10^4 k_1, s^{-1}	10^3 k_2, dm^3 mol^{-1} s^{-1}
75.10	1.33	11.40	4.07
74.00	1.35	10.41	3.72
72.91	1.37	9.90	3.54
71.81	1.39	8.98	3.21
70.71	1.41	8.59	3.07

Table 4.23: Effect of dielectric constant on the rate of reaction of $[Mn(salphen)]^+$ and $S(CH_2CH_2OH)_2$ at $[Mn(salphen)^+] = 1.0 \times 10^{-4}$ mol dm^{-3}, $[S(CH_2CH_2OH)_2] = 0.40$ mol dm^{-3}, $\mu = 0.6$ C^2 mol dm^{-3}, $[H^+] = 2.0 \times 10^{-5}$ mol dm^{-3}, T = 50 ± 1°C and λ_{max} = 450 nm

D	10^2 1/D	10^4 k_1, s^{-1}	10^3 k_2, dm^3 mol^{-1} s^{-1}
66.60	1.50	16.60	4.15
65.76	1.52	14.50	3.63
64.92	1.54	12.70	3.18
63.23	1.58	9.47	2.37
61.54	1.63	6.96	1.74
59.85	1.67	5.46	1.37

Table 4.24: Effect of dielectric constant on the rate of reaction of $[Mn(salphen)]^+$ and RSH at $[Mn(salphen)^+] = 1.0 \times 10^{-4}$ mol dm^{-3}, [RSH] = 0.40 mol dm^{-3}, $\mu = 0.6\ C^2$ mol dm^{-3}, $[H^+] = 4.0 \times 10^{-5}$ mol dm^{-3}, T = 28 ± 1°C and λ_{max} = 450 nm

D	10^2 1/D	10^3 k_1, s^{-1}	10^2 k_2, dm^3 mol^{-1} s^{-1}
78.19	1.28	5.07	1.27
77.64	1.29	5.51	1.38
77.09	1.30	6.50	1.63
76.54	1.31	7.62	1.91
75.99	1.32	9.70	2.43
75.44	1.33	11.17	2.79

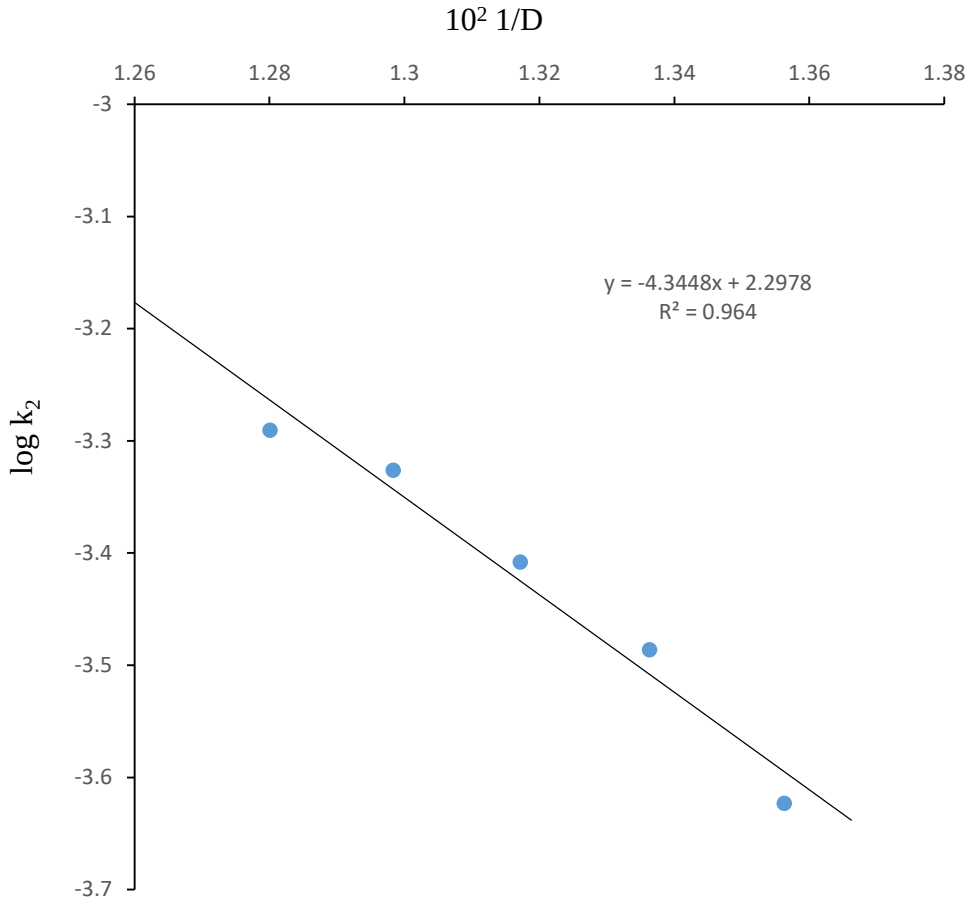


Figure 4.40: Plot of log k_2 versus 10^2 1/D for the redox reaction of $[Fe(salphen)]^+$ and H_2O_2 at $[Fe(salphen)^+] = 1.0 \times 10^{-4}$ mol dm^{-3}, $[H_2O_2] = 0.42$ mol dm^{-3}, $\mu = 0.6$ C^2 mol dm^{-3}, $[H^+] = 2.0 \times 10^{-5}$ mol dm^{-3}, T = 28 ± 1°C and λ_{max} = 435 nm

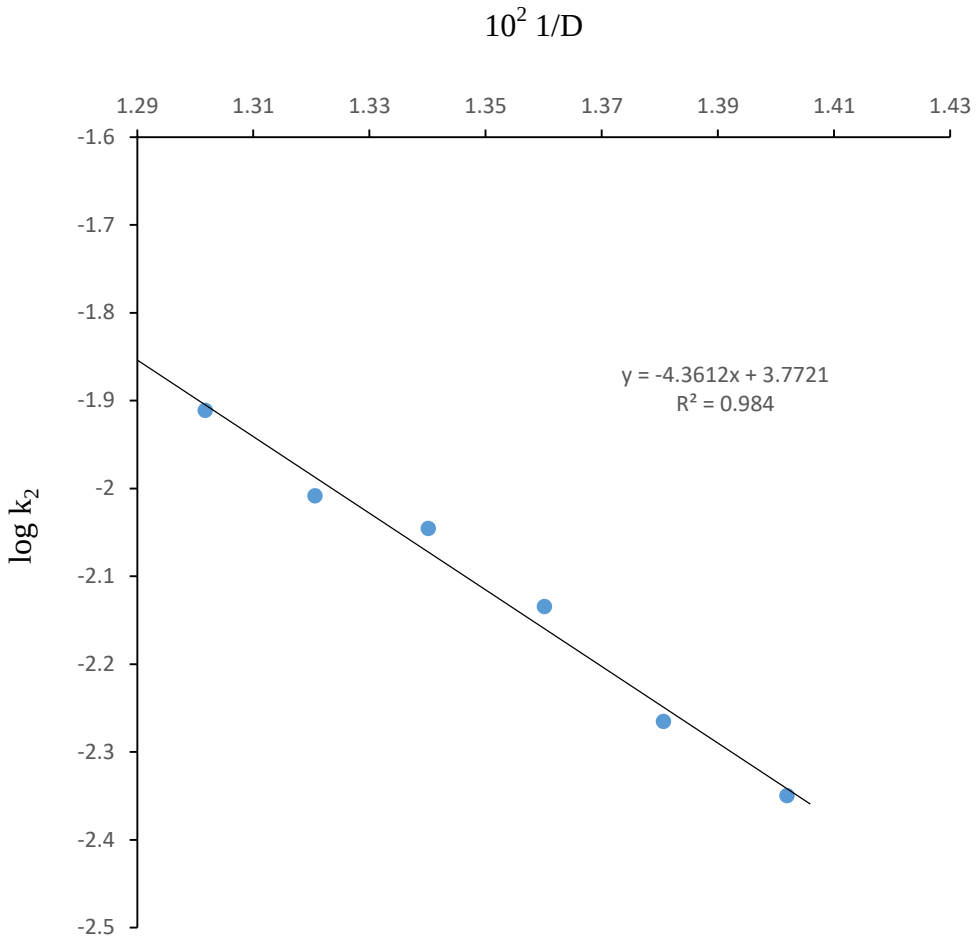


Figure 4.41: Plot of log k_2 versus 10^2 1/D for the redox reaction of $[Mn(salphen)]^+$ and H_2O_2 at $[Mn(salphen)^+] = 1.0 \times 10^{-4}$ mol dm^{-3}, $[H_2O_2] = 0.15$ mol dm^{-3}, $\mu = 0.2$ C^2 mol dm^{-3}, $[H^+] = 2.0 \times 10^{-5}$ mol dm^{-3}, T = 30 ± 1°C and λ_{max} = 450 nm

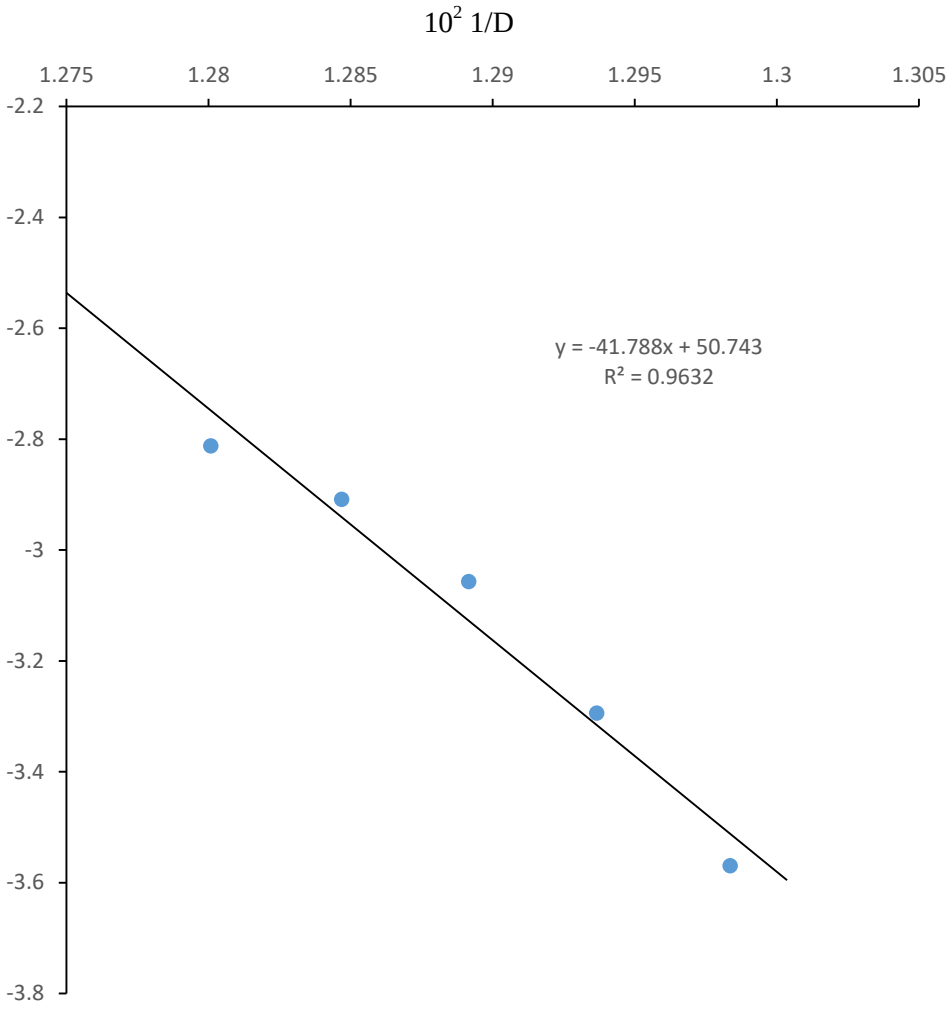


Figure 4.42: Plot of log k_2 versus 10^2 1/D for the redox reaction of $[Mn(salphen)]^+$ and SCN^- at $[Mn(salphen)^+] = 1.0 \times 10^{-4}$ mol dm^{-3}, $[SCN^-] = 0.42$ mol dm^{-3}, $\mu = 0.6$ C^2 mol dm^{-3}, $[H^+] = 4.0 \times 10^{-5}$ mol dm^{-3}, T = 28 ± 1°C and $\lambda_{max} = 450$ nm

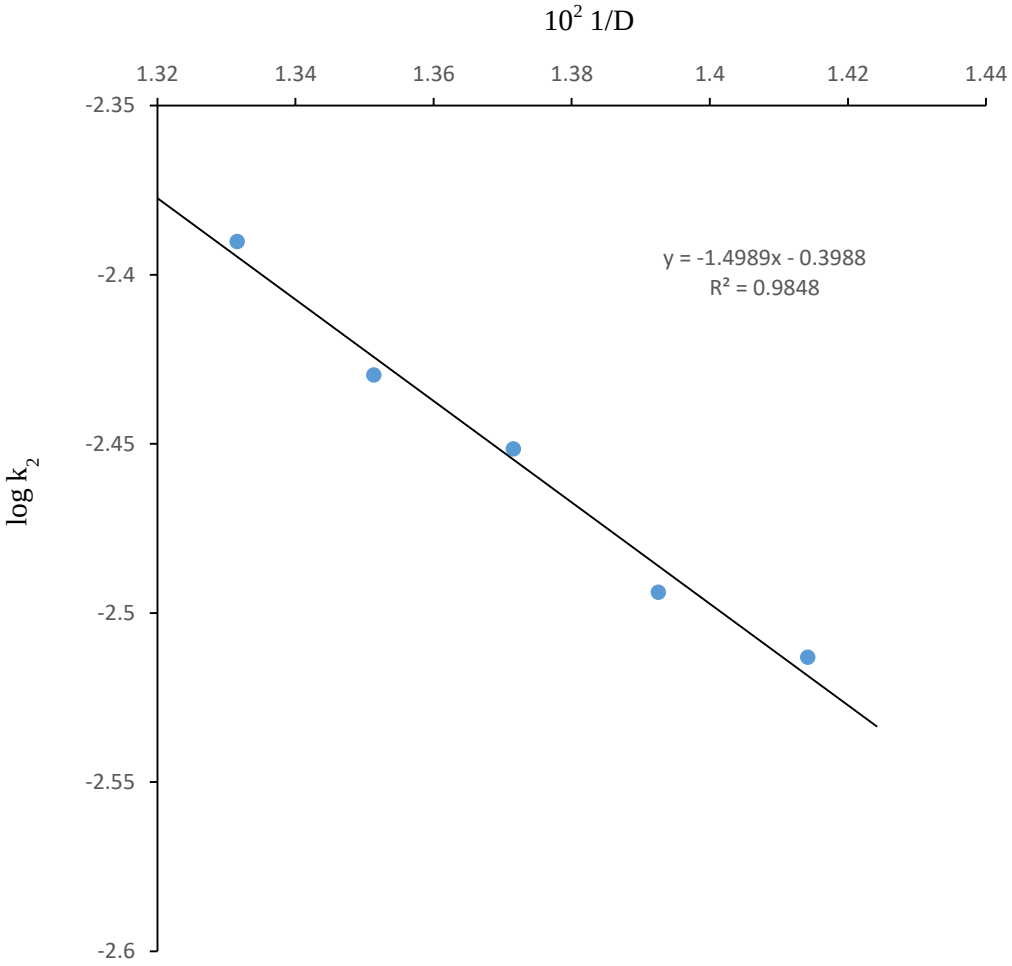


Figure 4.43: Plot of log k_2 versus 10^2 1/D for the redox reaction of $[Mn(salphen)]^+$ and $H_2NNHCSNH_2$ at $[Mn(salphen)^+] = 1.0 \times 10^{-4}$ mol dm^{-3}, $[H_2NNHCSNH_2] = 0.28$ mol dm^{-3}, $\mu = 0.6$ C^2 mol dm^{-3}, $[H^+] = 2.0 \times 10^{-5}$ mol dm^{-3}, T = 28 ± 1°C and $\lambda_{max} = 450$ nm

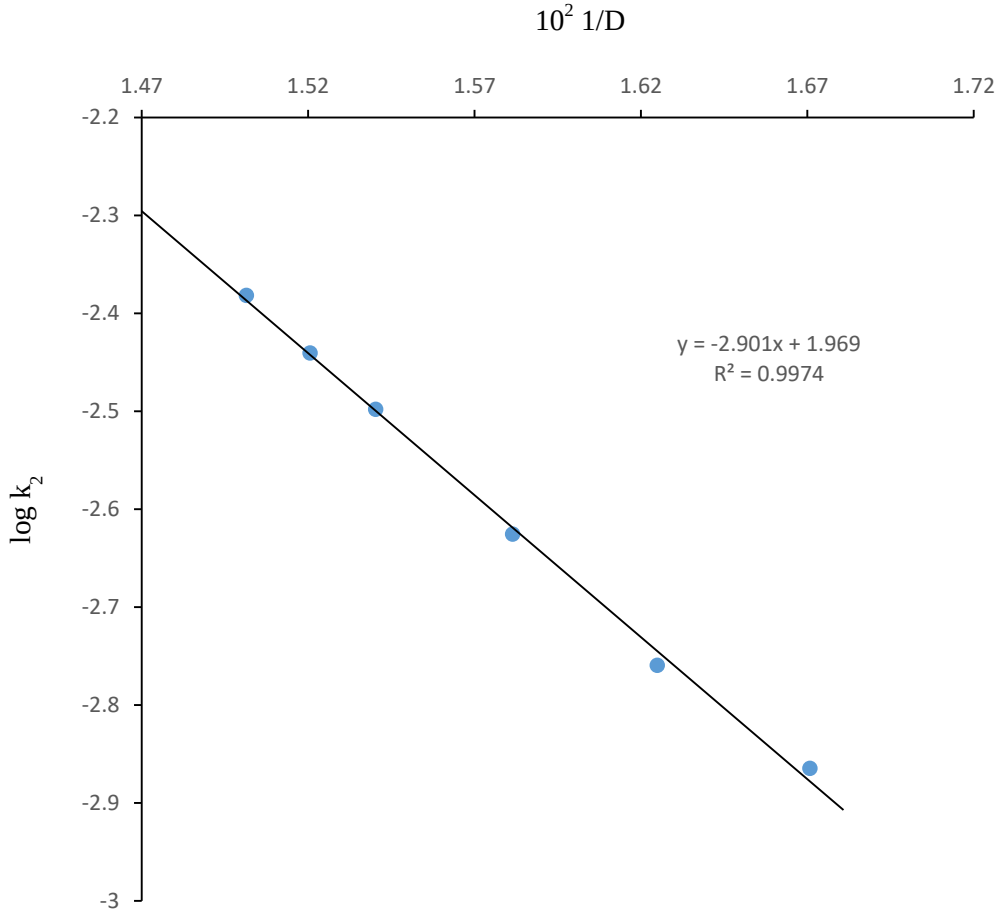


Figure 4.44: Plot of log k_2 versus 10^2 1/D for the redox reaction of $[Mn(salphen)]^+$ and $S(CH_2CH_2OH)_2$ at $[Mn(salphen)^+] = 1.0 \times 10^{-4}$ mol dm^{-3}, $[S(CH_2CH_2OH)_2] = 0.40$ mol dm^{-3}, $\mu = 0.6$ C^2 mol dm^{-3}, $[H^+] = 2.0 \times 10^{-5}$ mol dm^{-3}, T = 50 ± 1°C and λ_{max} = 450 nm

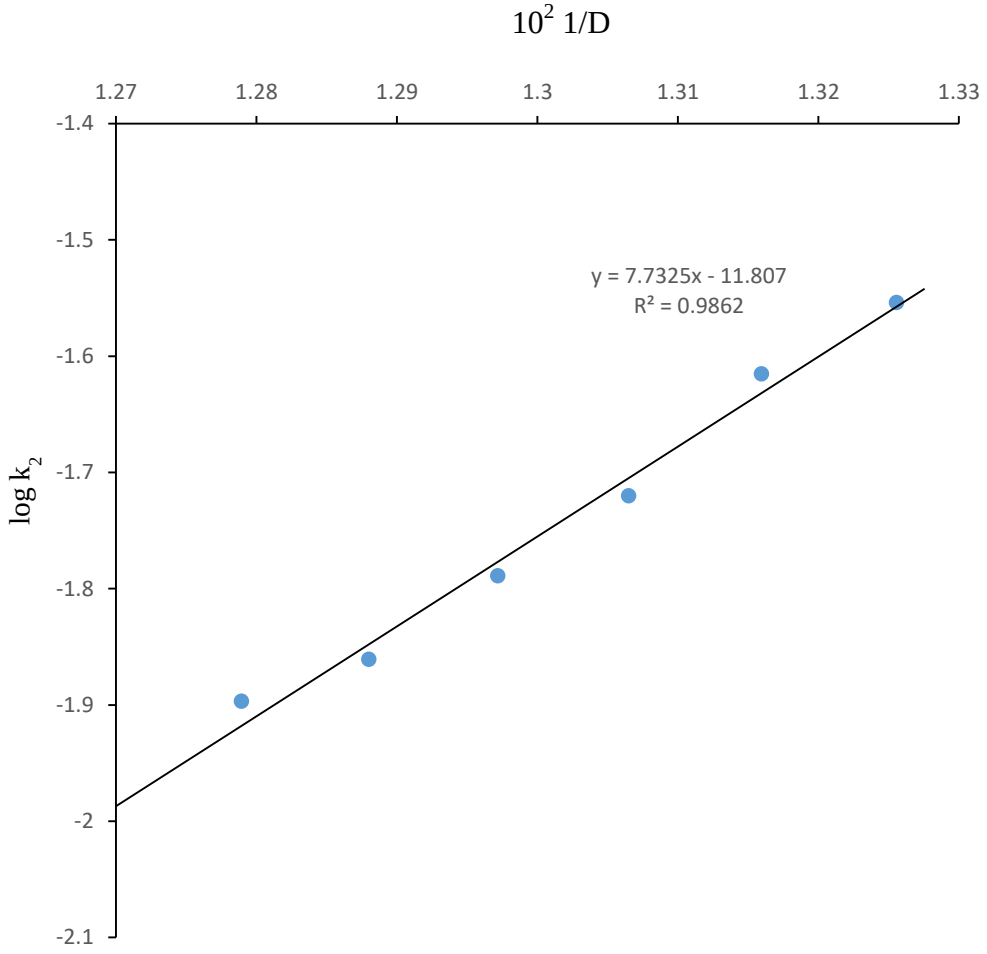


Figure 4.45: Plot of log k_2 versus 10^2 1/D for the redox reaction of $[Mn(salphen)]^+$ and RSH at $[Mn(salphen)^+]$ = 1.0×10^{-4} mol dm^{-3}, [RSH] = 0.4 mol dm^{-3}, μ = 0.6 C^2 mol dm^{-3}, T = 28 ± 1°C and λ_{max} = 450 nm

Table 4.25: Effect of added cations on the rate of reaction $[Fe(salphen)]^+$ and $H_2C_2O_4$ at $[Fe(salphen)^+] = 2.0 \times 10^{-4}$ mol dm^{-3}, $[H_2C_2O_4] = 6.0 \times 10^{-3}$ mol dm^{-3}, $\mu = 0.2$ C^2 mol dm^{-3}, D = 76.06, T = 26 ± 1°C and λ_{max} = 435 nm

[X]	10^3 [X], mol dm^{-3}	$10^3 k_1$, s^{-1}	$10\ k_2$, dm^3 mol^{-1} s^{-1}
Mg^{2+}	0.00	4.26	7.10
	1.00	4.30	7.17
	2.00	4.29	7.15
	3.00	4.29	7.15
	4.00	4.26	7.10
	5.00	4.27	7.12
	6.00	4.28	7.14
K^+	0.00	4.27	7.12
	1.00	4.29	7.15
	2.00	4.28	7.13
	3.00	4.26	7.10
	4.00	4.25	7.08
	5.00	4.27	7.12
	6.00	4.26	7.10

Table 4.26: Effect of added cations on the rate of reaction $[Fe(salphen)]^+$ and TSH at $[Fe(salphen)^+] = 2.0 \times 10^{-4}$ mol dm^{-3}, [TSH] = 0.15 mol dm^{-3}, μ = 0.2 C^2 mol dm^{-3}, D = 76.88, T = 26 ± 1°C and λ_{max} = 435 nm

[X]	10^3 [X], mol dm^{-3}	$10^3 k_1$, s^{-1}	$10^2 k_2$, dm^3 mol^{-1} s^{-1}
Mg^{2+}	0.0	2.16	1.44
	1.0	2.24	1.49
	2.0	2.28	1.52
	3.0	2.33	1.55
	4.0	2.37	1.58
	6.0	2.46	1.64
	8.0	2.55	1.70
Ca^{2+}	0.0	2.15	1.43
	1.0	2.19	1.46
	2.0	2.24	1.49
	3.0	2.28	1.52
	4.0	2.31	1.54
	6.0	2.39	1.59
	8.0	2.43	1.62

Table 4.27: Effect of added cations on the rate of reaction $[Fe(salphen)]^+$ and H_3PO_2 at $[Fe(salphen)^+] = 2.0 \times 10^{-4}$ mol dm^{-3}, $[H_3PO_2] = 0.13$ mol dm^{-3}, $\mu = 0.2$ C^2 mol dm^{-3}, D = 76.68, T = 26 ± 1°C and λ_{max} = 435 nm

[X]	10^3 [X], mol dm^{-3}	$10^3 k_1$, s^{-1}	$10^2 k_2$, dm^3 mol^{-1} s^{-1}
Mg^{2+}	0.0	2.90	2.23
	1.0	3.04	2.34
	2.0	3.13	2.41
	3.0	3.32	2.55
	4.0	3.64	2.80
	5.0	3.96	3.05
	6.0	4.28	3.29
Ca^{2+}	0.0	2.88	2.22
	1.0	2.95	2.27
	2.0	3.41	2.62
	3.0	3.43	2.64
	4.0	3.94	3.03
	5.0	4.19	3.22
	6.0	4.26	3.32

Table 4.28: Effect of added cations on the rate of reaction $[Fe(salphen)]^+$ and H_2O_2 at $[Fe(salphen)^+] = 1.0 \times 10^{-4}$ mol dm^{-3}, $[H_2O_2] = 0.42$ mol dm^{-3}, $\mu = 0.6\ C^2$ mol dm^{-3}, $[H^+] = 2.0 \times 10^{-5}$ mol dm^{-3}, D = 78.12, T = 28 ± 1°C and $\lambda_{max} = 435$ nm

[X]	10^3 [X], mol dm^{-3}	$10^4 k_1$, s^{-1}	$10^4 k_2$, dm^3 mol^{-1} s^{-1}
Mg^{2+}	0.00	2.14	5.10
	1.00	2.21	5.26
	5.00	2.26	5.38
	10.00	2.42	5.76
	15.00	2.56	6.10
	20.00	2.88	6.86
	25.00	3.13	7.45
	30.00	3.34	7.95
Ca^{2+}	0.00	2.14	5.10
	1.00	2.24	5.33
	5.00	2.27	5.40
	10.00	2.35	5.60
	15.00	2.49	5.93
	20.00	2.81	6.69
	25.00	2.99	7.12
	30.00	3.22	7.67

Table 4.29: Effect of added cations on the rate of reaction $[Mn(salphen)]^+$ and TSH at $[Mn(salphen)^+] = 1.0 \times 10^{-4}$ mol dm^{-3}, [TSH] = 0.42 mol dm^{-3}, μ = 0.6 C^2 mol dm^{-3}, D = 77.98, T = 32 ± 1°C and λ_{max} = 450 nm

[X]	10^3 [X], mol dm^{-3}	10^4 k_1, s^{-1}	10^3 k_2, dm^3 mol^{-1} s^{-1}
Mg^{2+}	0.00	6.79	1.62
	1.00	7.09	1.69
	5.00	8.01	1.91
	10.00	8.36	1.99
	15.00	9.83	2.34
	20.00	10.78	2.57
	25.00	13.22	3.15
	30.00	14.32	3.41
Ca^{2+}	0.00	6.79	1.62
	1.00	6.86	1.63
	5.00	7.42	1.77
	10.00	7.88	1.88
	15.00	8.41	2.00
	20.00	9.70	2.31
	25.00	10.41	2.48
	30.00	11.20	2.67

Table 4.30: Effect of added cations on the rate of reaction $[Mn(salphen)]^+$ and $H_2NNHCSNH_2$ at $[Mn(salphen)^+] = 1.0 \times 10^{-4}$ mol dm^{-3}, $[H_2NNHCSNH_2] = 0.28$ mol dm^{-3}, $\mu = 0.6$ C^2 mol dm^{-3}, $[H^+] = 2.0 \times 10^{-5}$ mol dm^{-3}, D = 75.10, T = 28 ± 1°C and λ_{max} = 450 nm

[X]	10^3 [X], mol dm^{-3}	10^4 k_1, s^{-1}	10^3 k_2, dm^3 mol^{-1} s^{-1}
Mg^{2+}	0.00	11.33	4.05
	1.00	12.41	4.43
	5.00	15.42	5.51
	10.00	25.63	9.15
	15.00	33.41	11.93
	20.00	36.82	13.15
	25.00	44.13	15.76
	30.00	53.86	19.24
Ca^{2+}	0.00	11.33	4.05
	1.00	12.21	4.36
	5.00	15.96	5.70
	10.00	19.16	6.84
	15.00	25.49	9.10
	20.00	39.20	14.00
	25.00	45.16	16.13
	30.00	52.09	18.60

Table 4.31: Effect of added cations on the rate of reaction $[Mn(salphen)]^+$ and H_2O_2 at $[Mn(salphen)^+] = 1.0 \times 10^{-4}$ mol dm^{-3}, $[H_2O_2] = 0.15$ mol dm^{-3}, $\mu = 0.2$ C^2 mol dm^{-3}, $[H^+] = 2.0 \times 10^{-5}$ mol dm^{-3}, D = 76.82, T = 30 ± 1°C and $\lambda_{max} = 450$ nm

[X]	10^3 [X], mol dm^{-3}	10^3 k_1, s^{-1}	10^2 k_2, dm^3 mol^{-1} s^{-1}
Mg^{2+}	0.00	1.86	1.24
	2.00	1.61	1.07
	4.00	1.43	0.95
	6.00	1.22	0.81
	8.00	1.06	0.71
	1.00	0.90	0.60
	12.00	0.71	0.48
Ca^{2+}	0.00	1.86	1.24
	2.00	1.73	1.15
	4.00	1.59	1.06
	6.00	1.36	0.91
	8.00	1.17	0.78
	1.00	1.09	0.73
	12.00	0.83-	0.55

Table 4.32: Effect of added cations on the rate of reaction $[Mn(salphen)]^+$ and RSH at $[Mn(salphen)^+] = 1.0 \times 10^{-4}$ mol dm^{-3}, [RSH] = 0.4 mol dm^{-3}, $\mu = 0.6\ C^2$ mol dm^{-3}, $[H^+] = 4.0 \times 10^{-5}$ mol dm^{-3}, D = 78.19, T = 28 ± 1°C and λ_{max} = 450 nm

[X]	10^3 [X], mol dm^{-3}	$10^3\ k_1$, s^{-1}	$10^2\ k_2$, $dm^3\ mol^{-1}\ s^{-1}$
Mg^{2+}	0.00	5.02	1.26
	1.00	4.86	1.22
	5.00	4.24	1.06
	10.00	3.41	0.85
	15.00	2.67	0.67
	20.00	2.51	0.63
	25.00	1.70	0.43
	30.00	1.32	0.33
K^+	0.00	5.02	1.26
	1.00	4.91	1.23
	5.00	4.44	1.11
	10.00	3.80	0.95
	15.00	2.92	0.73
	20.00	2.21	0.55
	25.00	1.93	0.48
	30.00	1.45	0.36

Table 4.33: Effect of added cations on the rate of reaction $[Mn(salphen)]^+$ and SCN^- at $[Mn(salphen)^+] = 1.0 \times 10^{-4}$ mol dm^{-3}, $[SCN^-] = 0.42$ mol dm^{-3}, $\mu = 0.6$ C^2 mol dm^{-3}, $[H^+] = 4.0 \times 10^{-5}$ mol dm^{-3}, D = 78.12, T = 28 ± 1°C and λ_{max} = 450 nm

[X]	10^3 [X], mol dm^{-3}	10^4 k_1, s^{-1}	10^3 k_2, dm^3 mol^{-1} s^{-1}
Mg^{2+}	0.00	6.47	1.54
	1.00	6.40	1.52
	5.00	6.10	1.45
	10.00	5.62	1.34
	15.00	4.88	1.16
	20.00	3.98	0.95
	25.00	3.66	0.87
	30.00	3.22	0.77
Ca^{2+}	0.00	6.47	1.54
	1.00	6.43	1.53
	5.00	6.00	1.43
	10.00	5.44	1.30
	15.00	4.76	1.13
	20.00	4.50	1.07
	25.00	3.58	0.85
	30.00	3.14	0.75

Table 4.34: Effect of added cations on the rate of reaction of $[Mn(salphen)]^+$ and $S(CH_2CH_2OH)_2$ at $[Mn(salphen)^+] = 1.0 \times 10^{-4}$ mol dm^{-3}, $[S(CH_2CH_2OH)_2] = 0.40$ mol dm^{-3}, $\mu = 0.6$ C^2 mol dm^{-3}, $[H^+] = 2.0 \times 10^{-5}$ mol dm^{-3}, D = 66.60, T = 50 ± 1°C and λ_{max} = 450 nm

[X]	10^3 [X], mol dm^{-3}	10^3 k_1, s^{-1}	10^3 k_2, dm^3 mol^{-1} s^{-1}
Mg^{2+}	0.00	16.60	4.15
	1.00	16.00	4.00
	5.00	13.90	3.48
	10.00	13.00	3.25
	15.00	12.10	3.03
	20.00	11.20	2.80
	25.00	10.40	2.60
	30.00	9.50	2.38
Ca^{2+}	0.00	16.60	4.15
	1.00	15.50	3.88
	5.00	13.80	3.45
	10.00	11.60	2.90
	15.00	9.70	2.43
	20.00	8.60	2.15
	25.00	7.80	1.95
	30.00	6.70	1.68

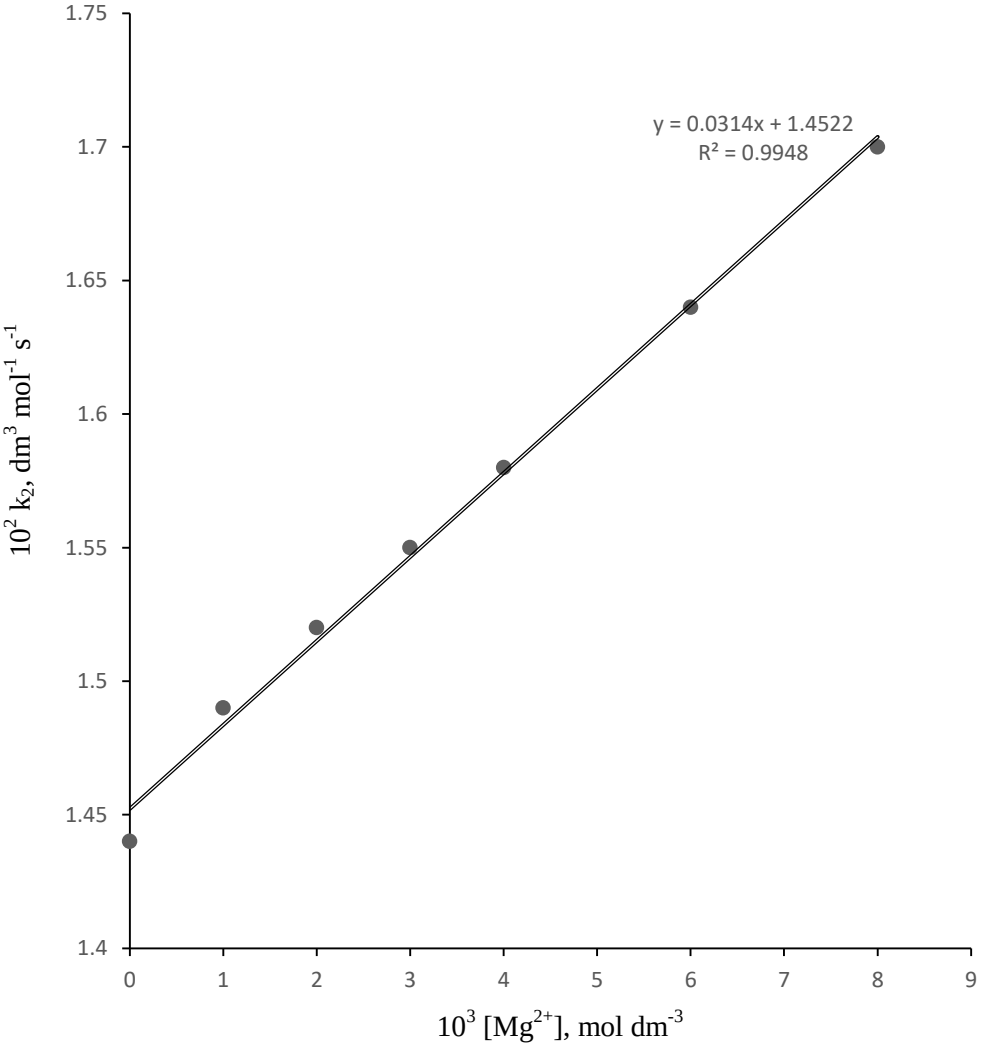


Figure 4.46: Plot of k_2 versus $[Mg^{2+}]$ for the redox reaction of $[Fe(salphen)]^+$ and TSH at $[Fe(salphen)^+] = 2.0 \times 10^{-4}$ mol dm^{-3}, [TSH] = 0.15 mol dm^{-3}, μ = 0.2 C^2 mol dm^{-3}, D = 76.88, T = 26 ± 1°C and λ_{max} = 435 nm

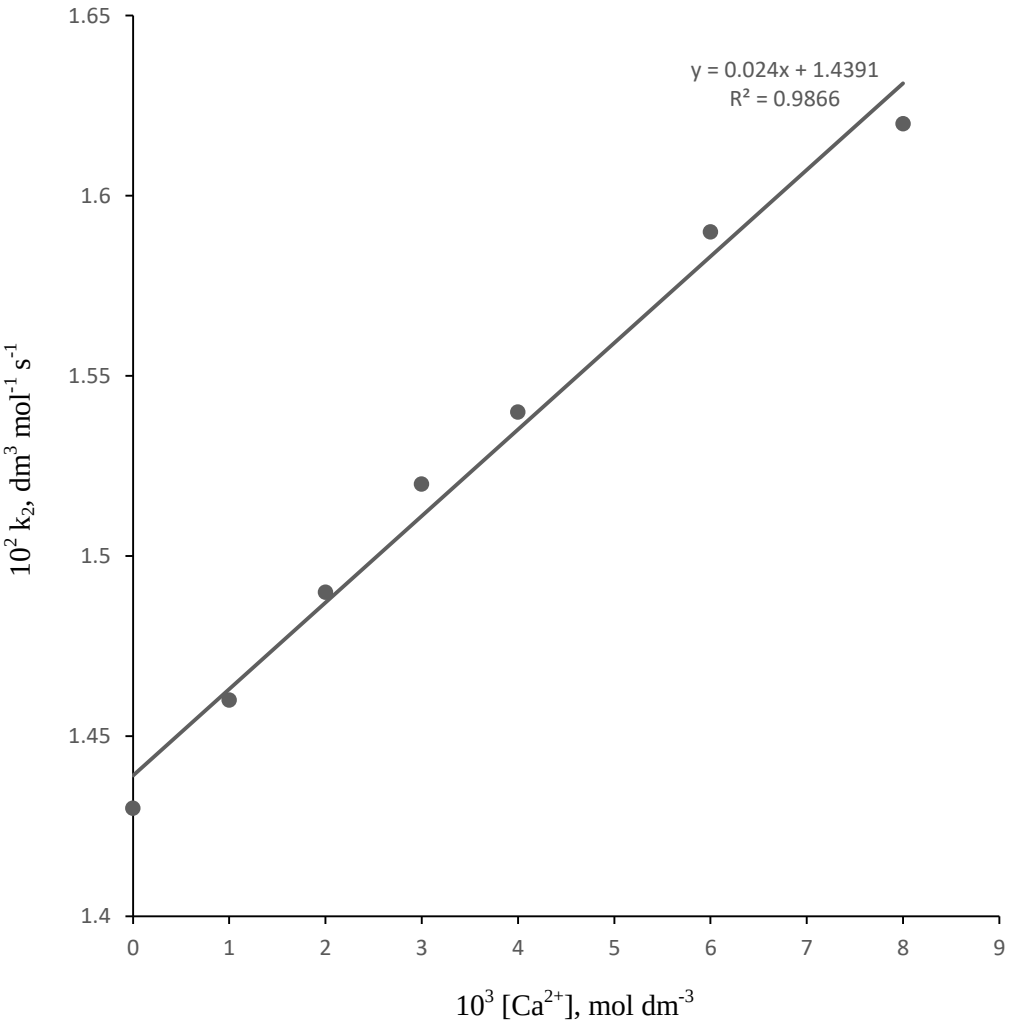


Figure 4.47: Plot of k_2 versus $[Ca^{2+}]$ for the redox reaction of $[Fe(salphen)]^+$ and TSH at $[Fe(salphen)^+] = 2.0 \times 10^{-4}$ mol dm^{-3}, [TSH] = 0.15 mol dm^{-3}, μ = 0.2 C^2 mol dm^{-3}, D = 76.88, T = 26 ± 1°C and λ_{max} = 435 nm

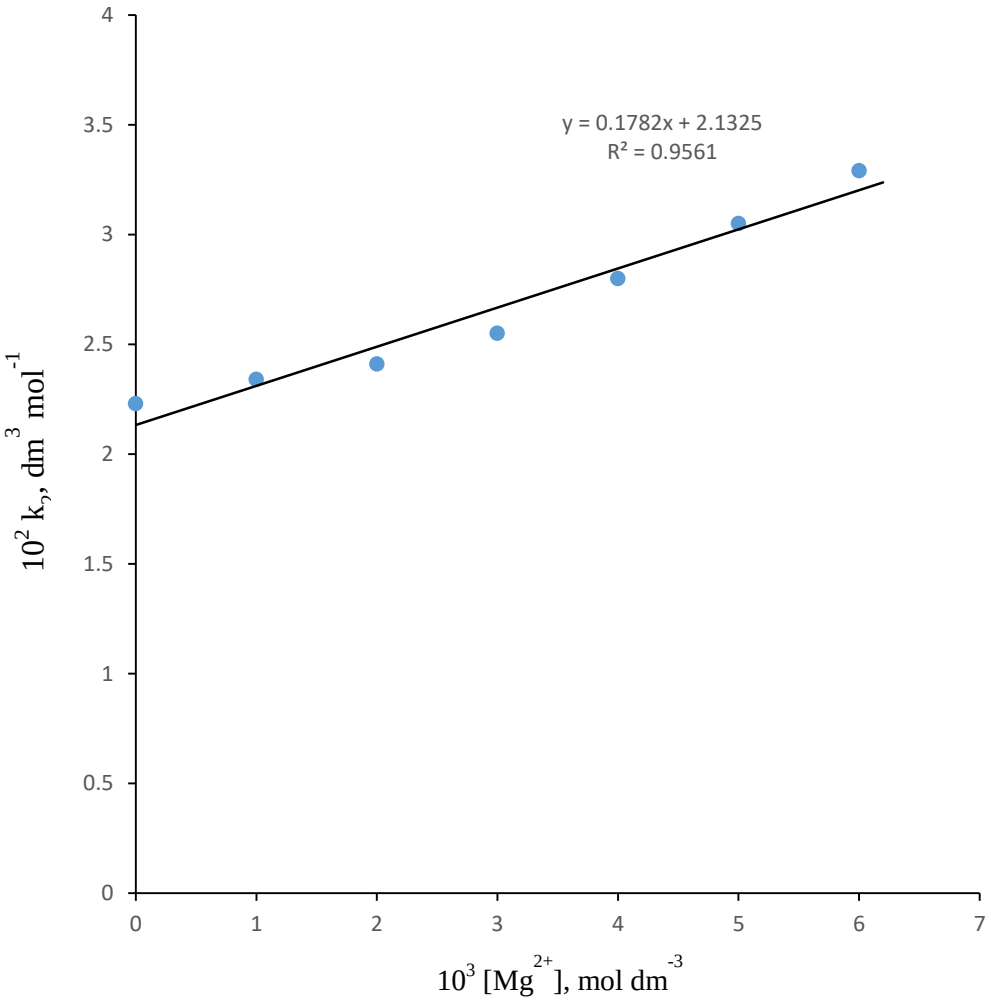


Figure 4.48: Plot of k_2 versus $[Mg^{2+}]$ for the redox reaction of $[Fe(salphen)]^+$ and H_3PO_2 at $[Fe(salphen)^+] = 2.0 \times 10^{-4}$ mol dm^{-3}, $[H_3PO_2] = 0.13$ mol dm^{-3}, $\mu = 0.2$ C^2 mol dm^{-3}, D = 76.68, T = 26 ± 1 °C and $\lambda_{max} = 435$ nm

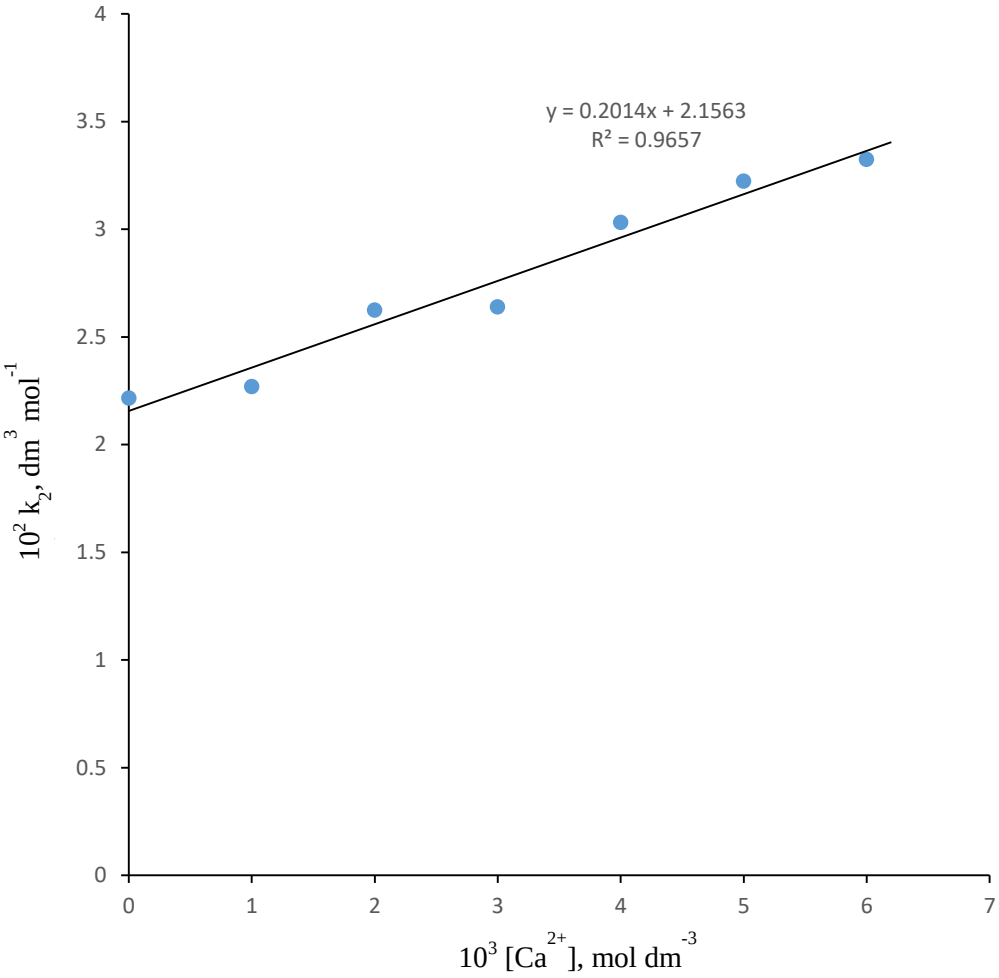


Figure 4.49: Plot of k_2 versus $[Ca^{2+}]$ for the redox reaction of $[Fe(salphen)]^+$ and H_3PO_2 at $[Fe(salphen)^+] = 2.0 \times 10^{-4}$ mol dm^{-3}, $[H_3PO_2] = 0.13$ mol dm^{-3}, $\mu = 0.2$ C^2 mol dm^{-3}, D = 76.68, T = 26 ± 1°C and $\lambda_{max} = 435$ nm

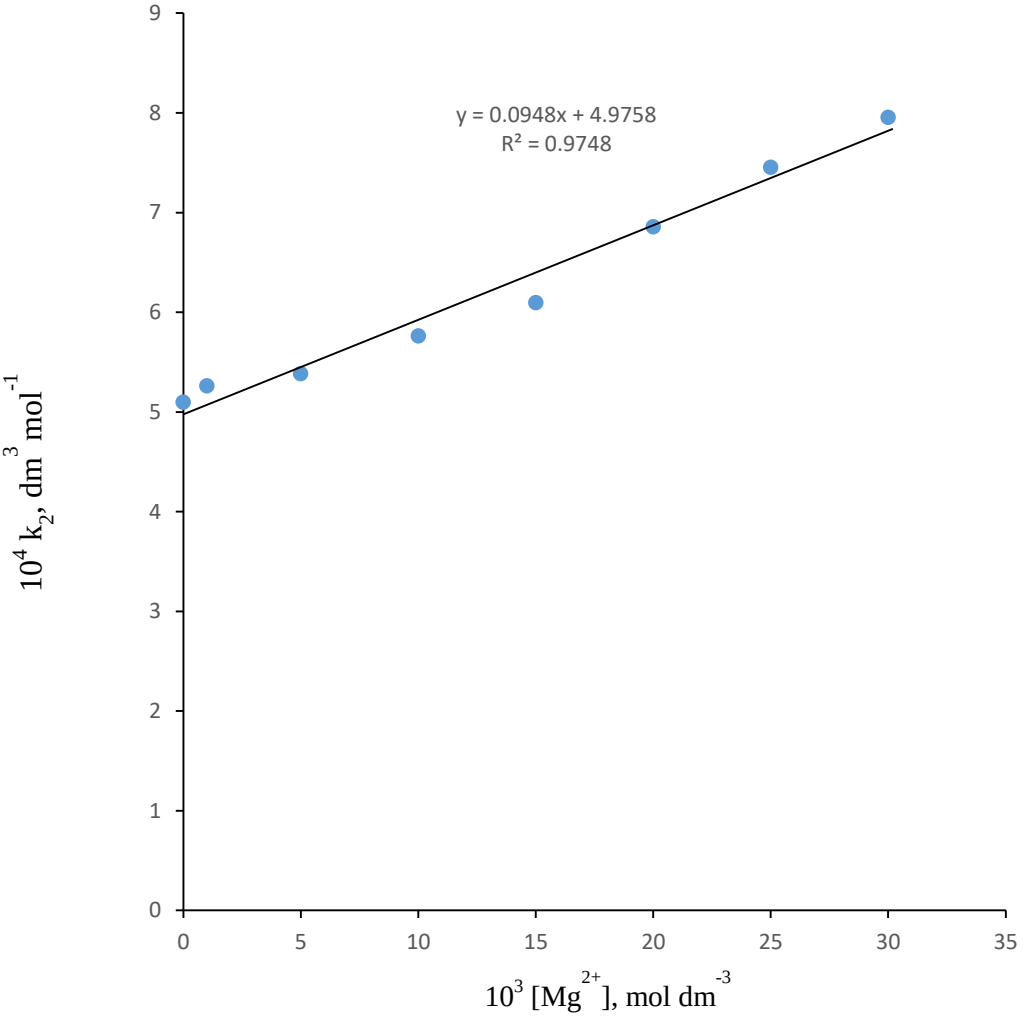


Figure 4.50: Plot of 10^4 k_2 versus 10^3 $[Mg^{2+}]$ for the redox reaction of $[Fe(salphen)]^+$ and H_2O_2 at $[Fe(salphen)^+] = 1.0 \times 10^{-4}$ mol dm^{-3}, $[H_2O_2] = 0.42$ mol dm^{-3}, $\mu = 0.6$ C^2 mol dm^{-3}, $[H^+] = 2.0 \times 10^{-5}$ mol dm^{-3}, D = 78.12, T = 28 ± 1 °C and λ_{max} = 435 nm

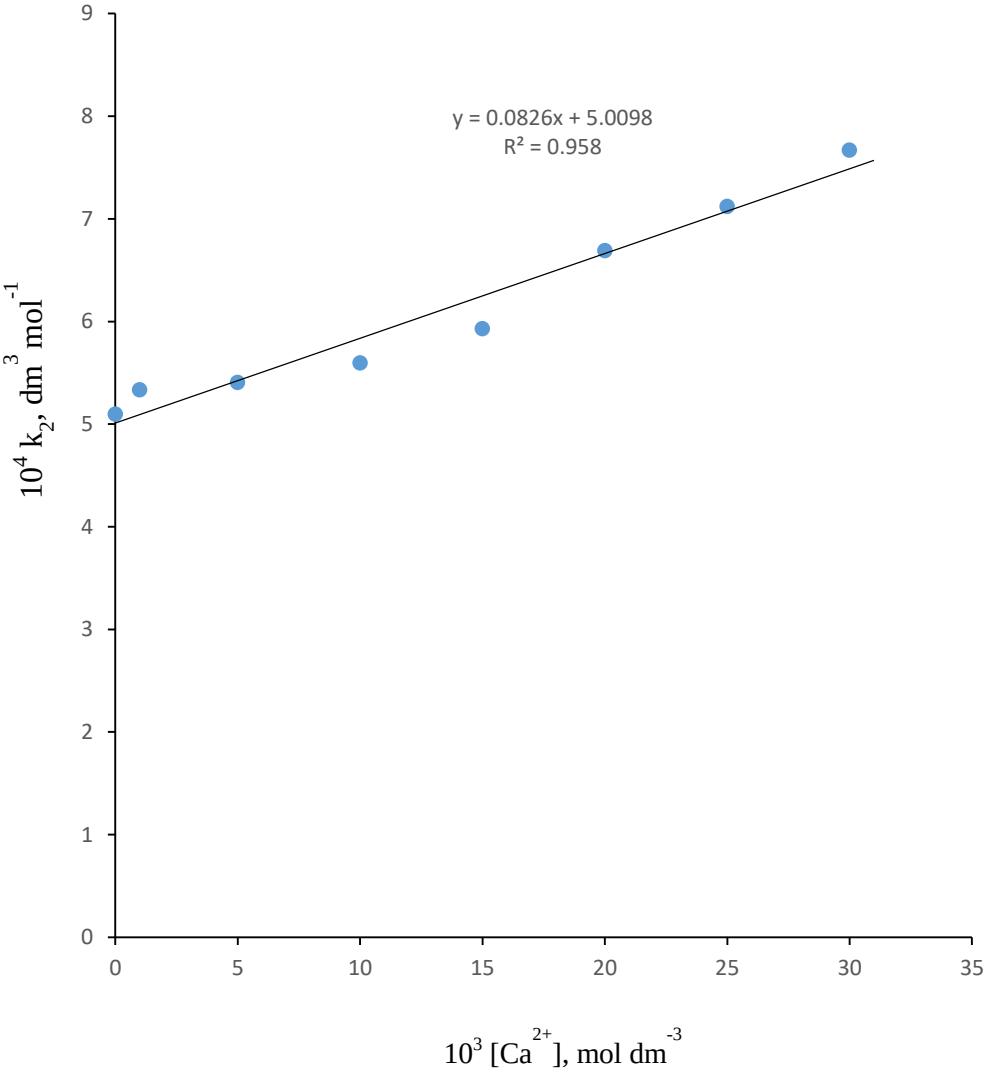


Figure 4.51: Plot of 10^4 k_2 versus 10^3 $[Ca^{2+}]$ for the redox reaction of $[Fe(salphen)]^+$ and H_2O_2 at $[Fe(salphen)^+] = 1.0 \times 10^{-4}$ mol dm^{-3}, $[H_2O_2]$ = 0.42 mol dm^{-3}, μ = 0.6 C^2 mol dm^{-3}, $[H^+] = 2.0 \times 10^{-5}$ mol dm^{-3}, D = 78.12, T = 28 ± 1°C and λ_{max} = 435 nm

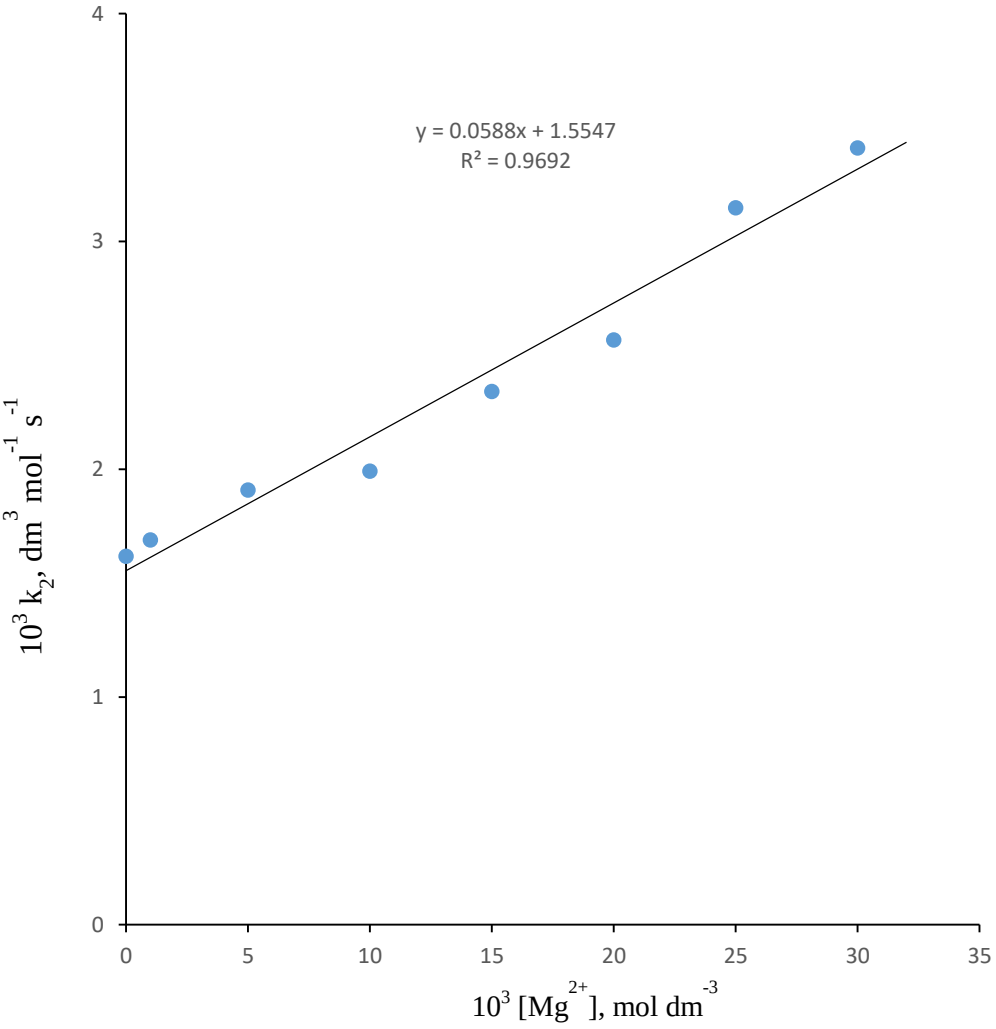


Figure 4.52: Plot of 10^3 k_2 versus 10^3 $[Mg^{2+}]$ for the redox reaction of $[Mn(salphen)]^+$ and TSH at $[Mn(salphen)^+]$ = 1.0 × 10^{-4} mol dm^{-3}, [TSH] = 0.42 mol dm^{-3}, μ = 0.6 C^2 mol dm^{-3}, D = 77.98, T = 32 ± 1°C and λ_{max} = 450 nm

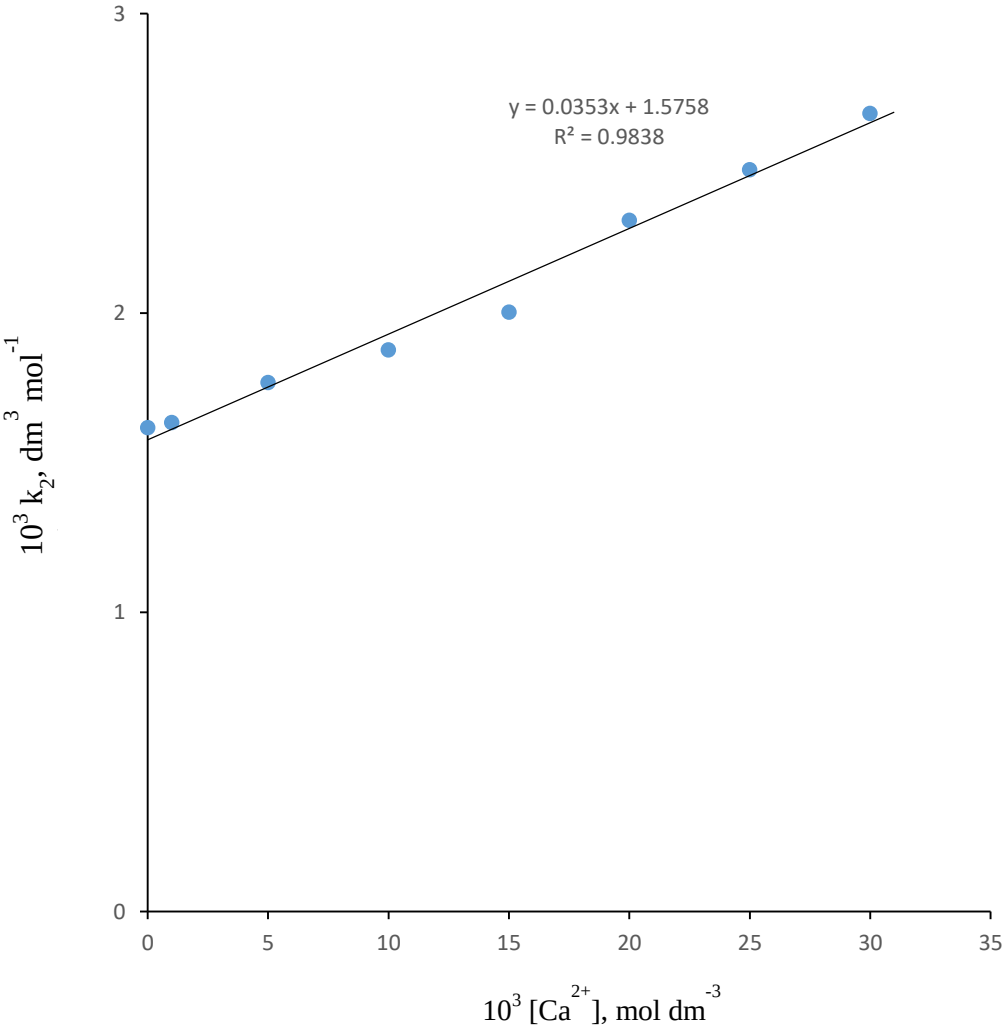


Figure 4.53: Plot of 10^3 k_2 versus 10^3 $[Ca^{2+}]$ for the redox reaction of $[Mn(salphen)]^+$ and TSH at $[Mn(salphen)^+] = 1.0 \times 10^{-4}$ mol dm^{-3}, [TSH] = 0.42 mol dm^{-3}, μ = 0.6 C^2 mol dm^{-3}, D = 77.98, T = 32 ± 1°C and λ_{max} = 450 nm

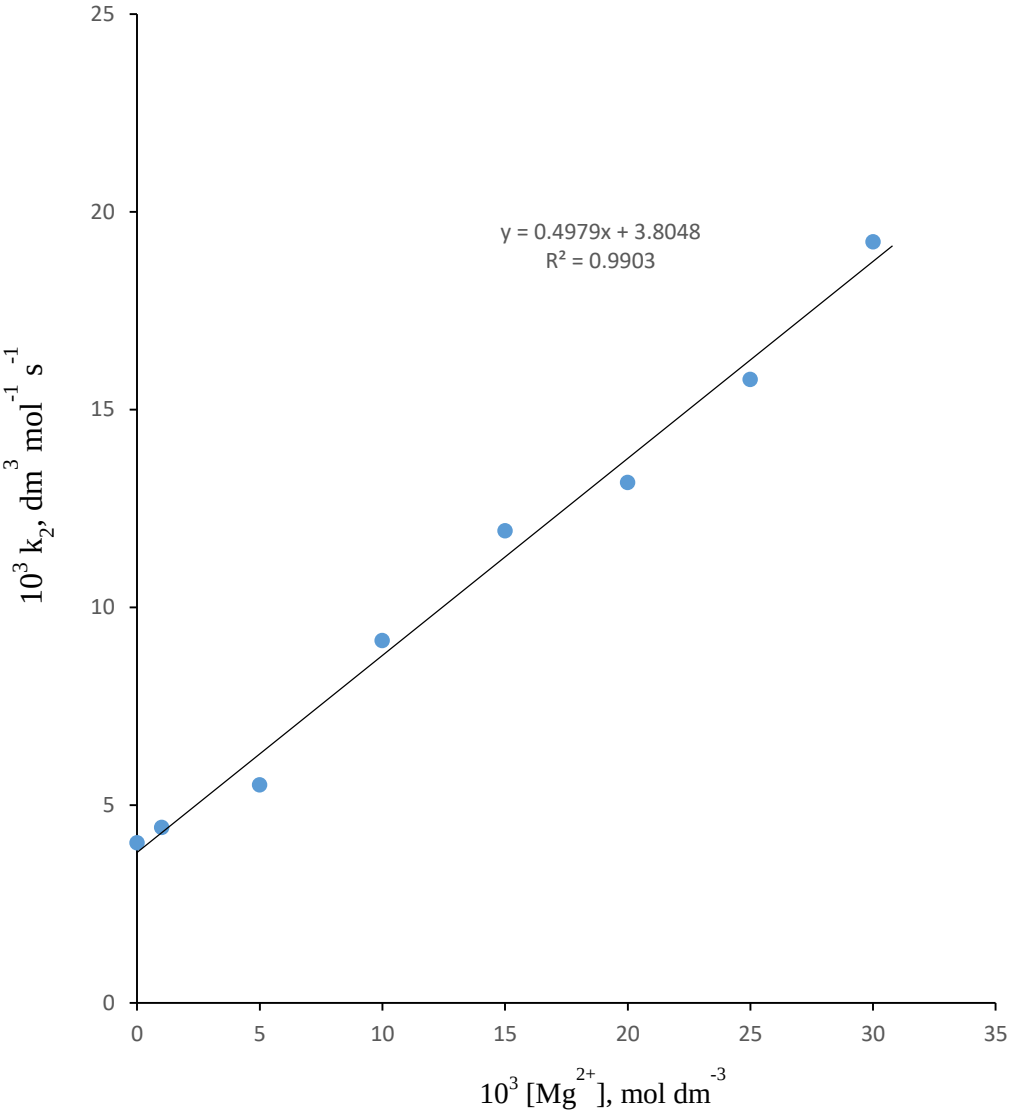


Figure 4.54: Plot of $10^3\ k_2$ versus $10^3\ [Mg^{2+}]$ for the redox reaction of $[Mn(salphen)]^+$ and $H_2NNHCSNH_2$ at $[Mn(salphen)^+] = 1.0 \times 10^{-4}$ mol dm^{-3}, $[H_2NNHCSNH_2] = 0.28$ mol dm^{-3}, $\mu = 0.6\ C^2$ mol dm^{-3}, $[H^+] = 2.0 \times 10^{-5}$ mol dm^{-3}, D = 75.10, T = 28 ± 1 °C and λ_{max} = 450 nm

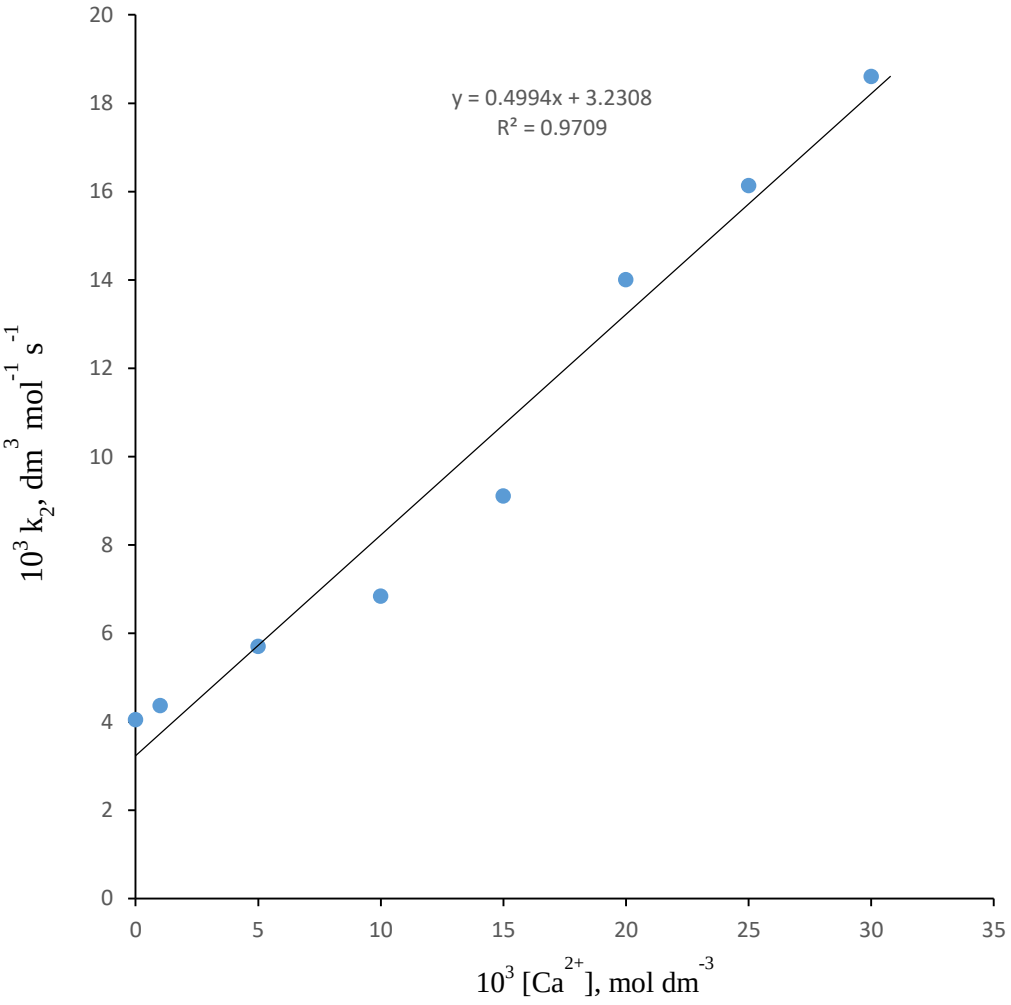


Figure 4.55: Plot of 10^3 k_2 versus 10^3 $[Ca^{2+}]$ for the redox reaction of $[Mn(salphen)]^+$ and $H_2NNHCSNH_2$ at $[Mn(salphen)^+]$ = 1.0 × 10^{-4} mol dm^{-3}, $[H_2NNHCSNH_2]$ = 0. 28 mol dm^{-3}, μ = 0.6 C^2 mol dm^{-3}, $[H^+]$ = 2.0 × 10^{-5} mol dm^{-3}, D = 75.10, T = 28 ± 1 °C and λ_{max} = 450 nm

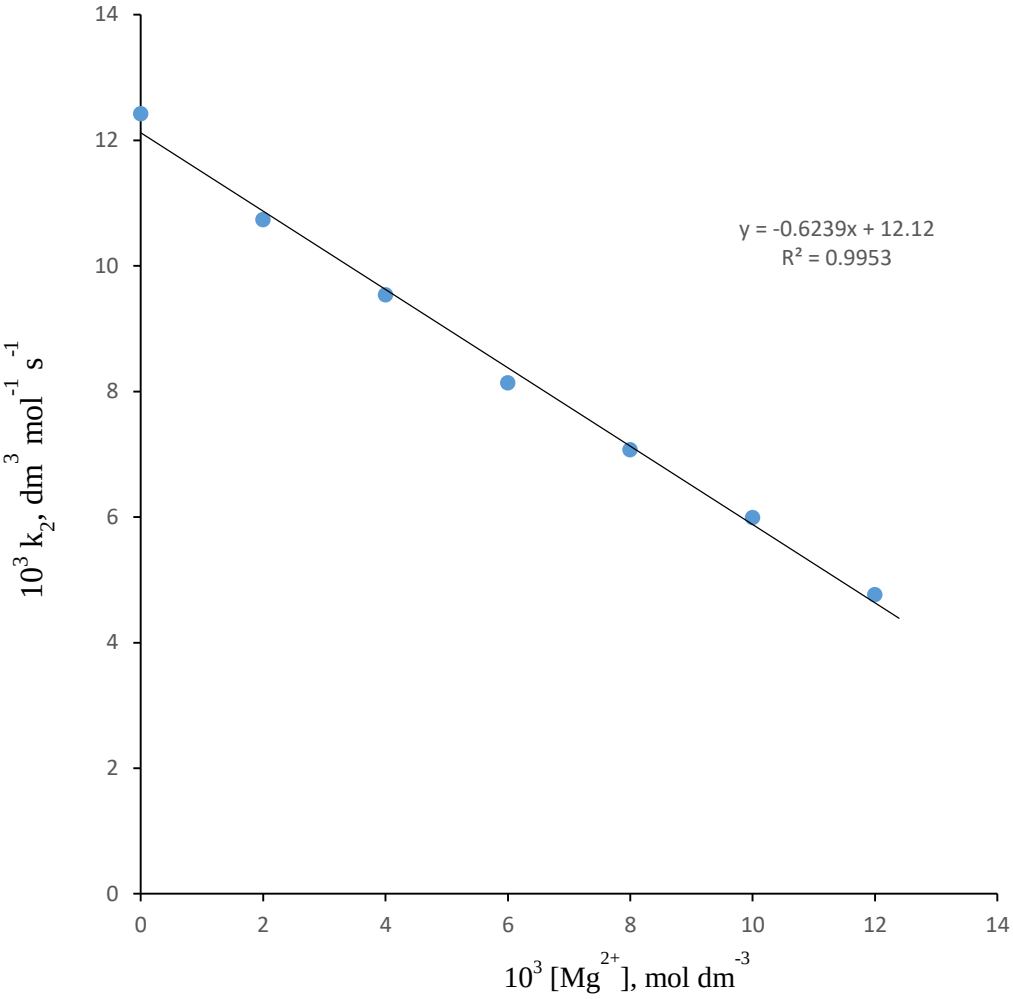


Figure 4.56: Plot of 10^3 k_2 versus 10^3 $[Mg^{2+}]$ for the redox reaction of $[Mn(salphen)]^+$ and H_2O_2 at $[Mn(salphen)^+] = 1.0 \times 10^{-4}$ mol dm^{-3}, $[H_2O_2] = 0.15$ mol dm^{-3}, $\mu = 0.2$ C^2 mol dm^{-3}, $[H^+] = 2.0 \times 10^{-5}$ mol dm^{-3}, D = 76.82, T = 30 ± 1 °C and λ_{max} = 450 nm

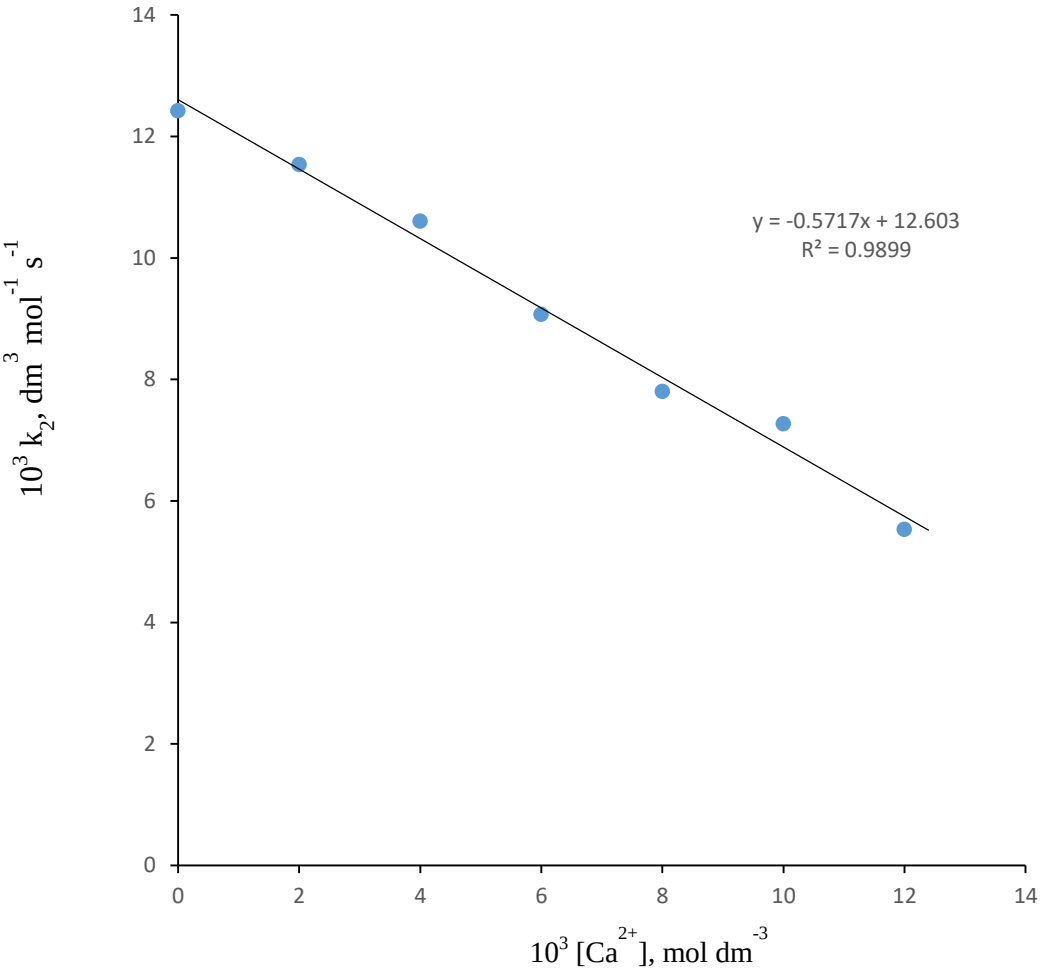


Figure 4.57: Plot of 10^3 k_2 versus 10^3 $[Ca^{2+}]$ for the redox reaction of $[Mn(salphen)]^+$ and H_2O_2 at $[Mn(salphen)^+] = 1.0 \times 10^{-4}$ mol dm^{-3}, $[H_2O_2] = 0.15$ mol dm^{-3}, $\mu = 0.2$ C^2 mol dm^{-3}, $[H^+] = 2.0 \times 10^{-5}$ mol dm^{-3}, D = 76.82, T = 30 ± 1°C and λ_{max} = 450 nm

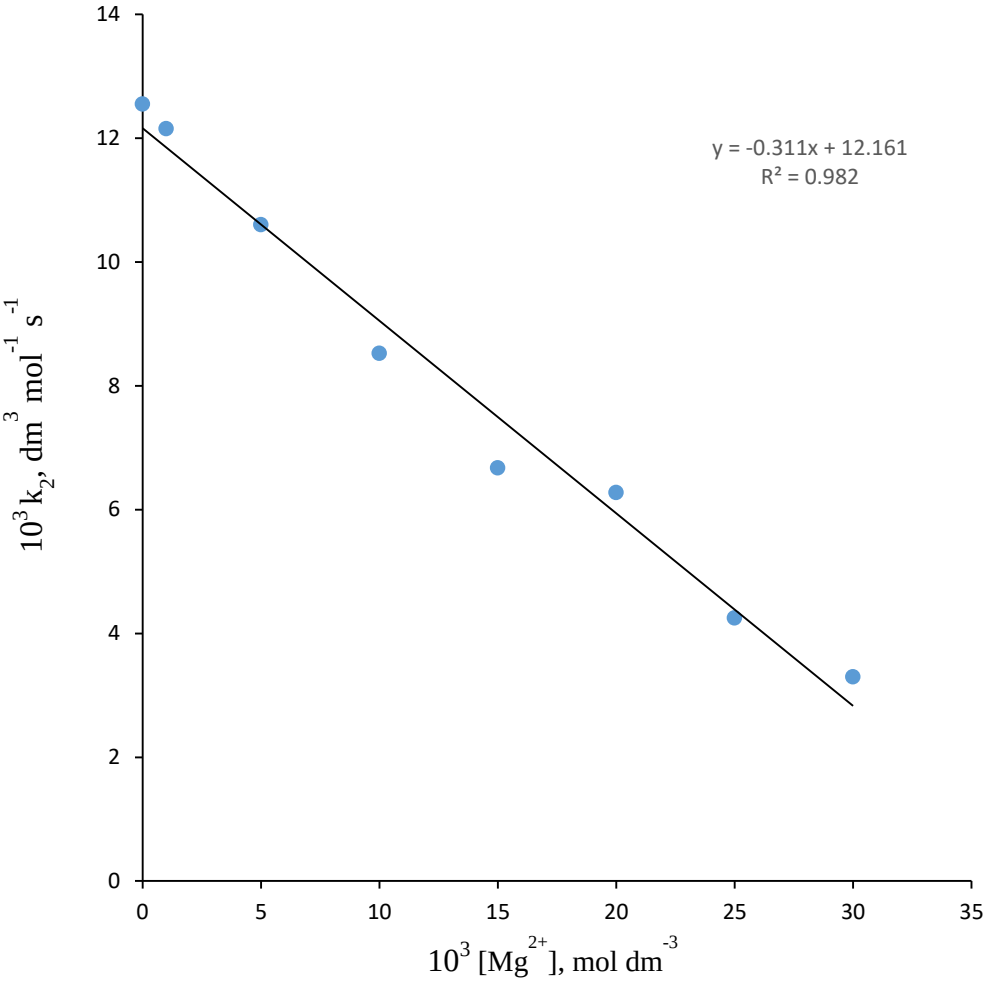


Figure 4.58: Plot of 10^3 k_2 versus 10^3 [Mg^{2+}] for the redox reaction of [Mn(salphen)]$^+$ and RSH at [Mn(salphen)$^+$] = 1.0×10^{-4} mol dm^{-3}, [RSH] = 0.4 mol dm^{-3}, μ = 0.6 C^2 mol dm^{-3}, [H^+] = 4.0×10^{-5} mol dm^{-3}, D = 78.19, T = 28 ± 1 °C and λ_{max} = 450 nm

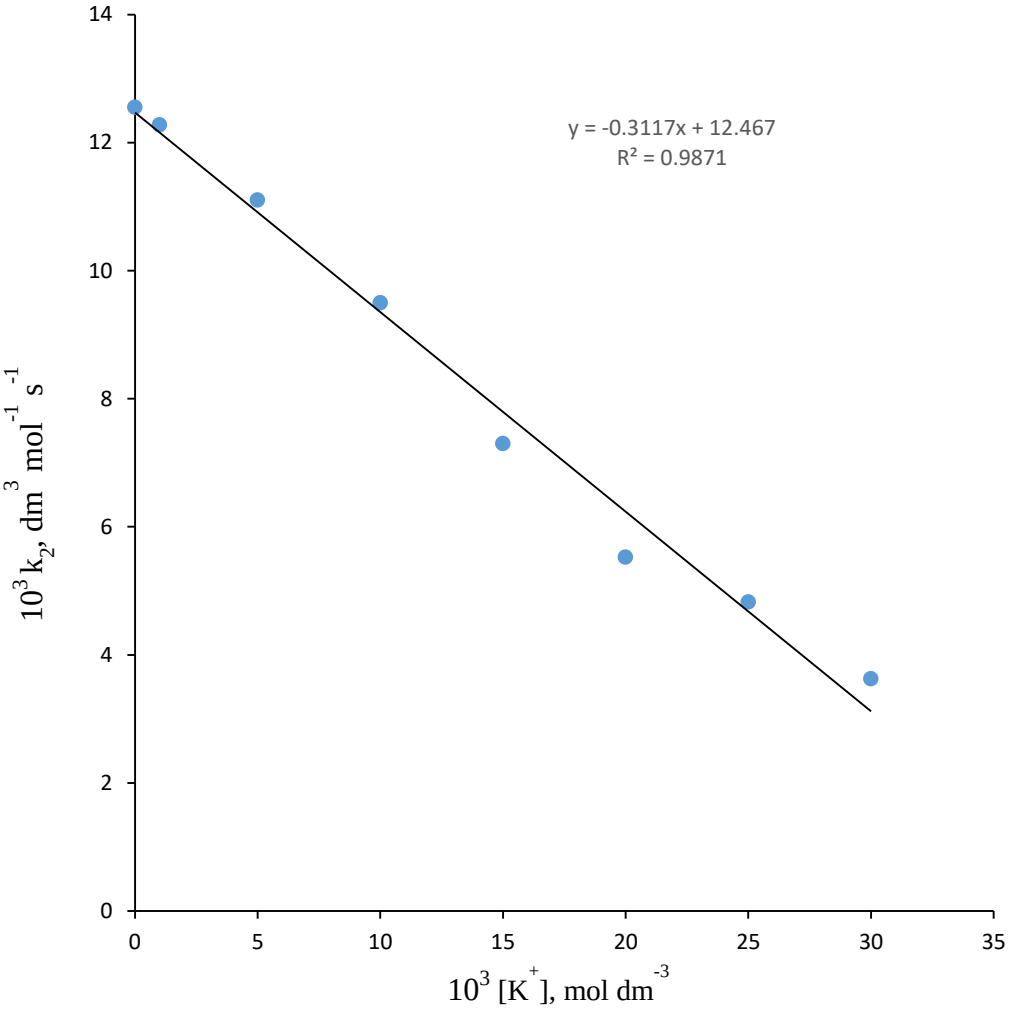


Figure 4.59: Plot of 10^3 k_2 versus 10^3 $[K^+]$ for the redox reaction of $[Mn(salphen)]^+$ and RSH at $[Mn(salphen)^+]$ = 1.0 × 10^{-4} mol dm^{-3}, [RSH] = 0.4 mol dm^{-3}, μ = 0.6 C^2 mol dm^{-3}, $[H^+]$ = 4.0 × 10^{-5} mol dm^{-3}, D = 78.19, T = 28 ± 1°C and λ_{max} = 450 nm

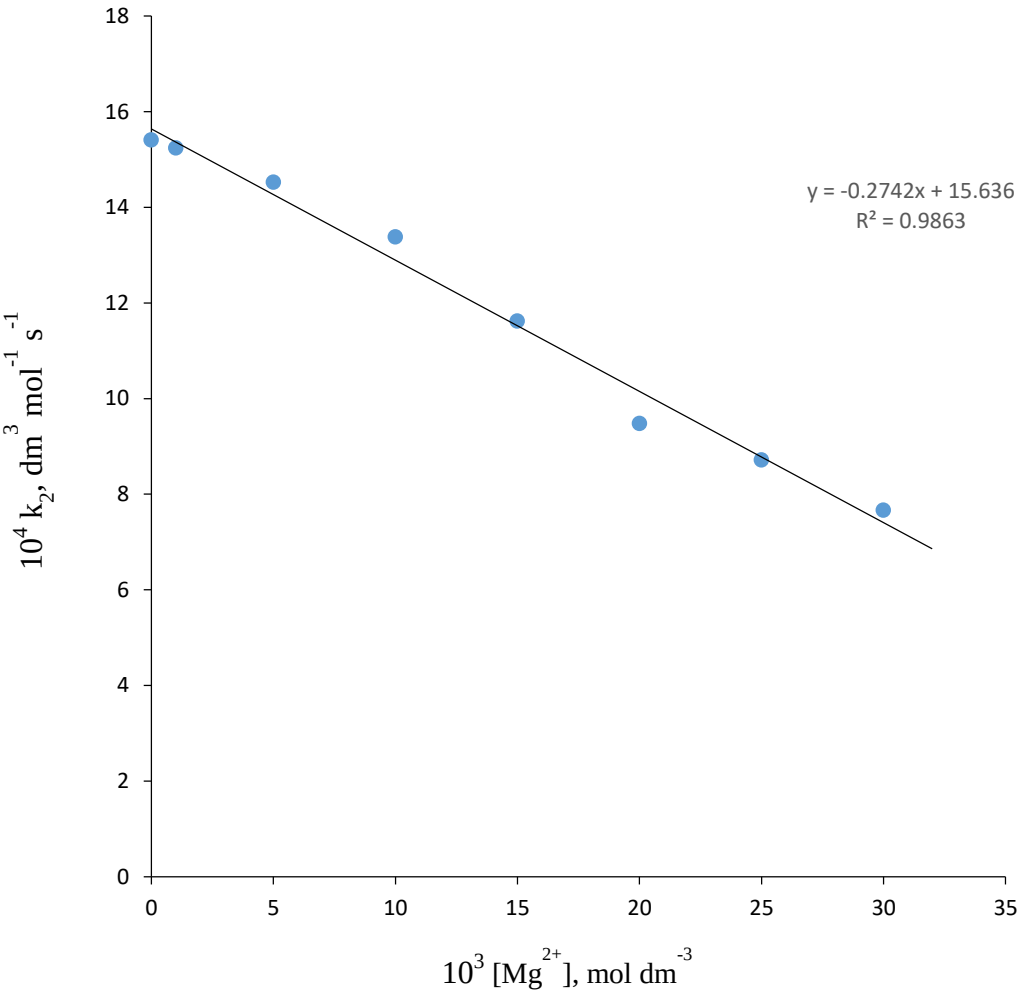


Figure 4.60: Plot of 10^4 k_2 versus 10^3 $[Mg^{2+}]$ for the redox reaction of $[Mn(salphen)]^+$ and SCN^- at $[Mn(salphen)^+]$ = 1.0 × 10^{-4} mol dm^{-3}, $[SCN^-]$ = 0.42 mol dm^{-3}, μ = 0.6 C^2 mol dm^{-3}, $[H^+]$ = 4.0 × 10^{-5} mol dm^{-3}, D = 78.12, T = 28 ± 1 °C and λ_{max} = 450 nm

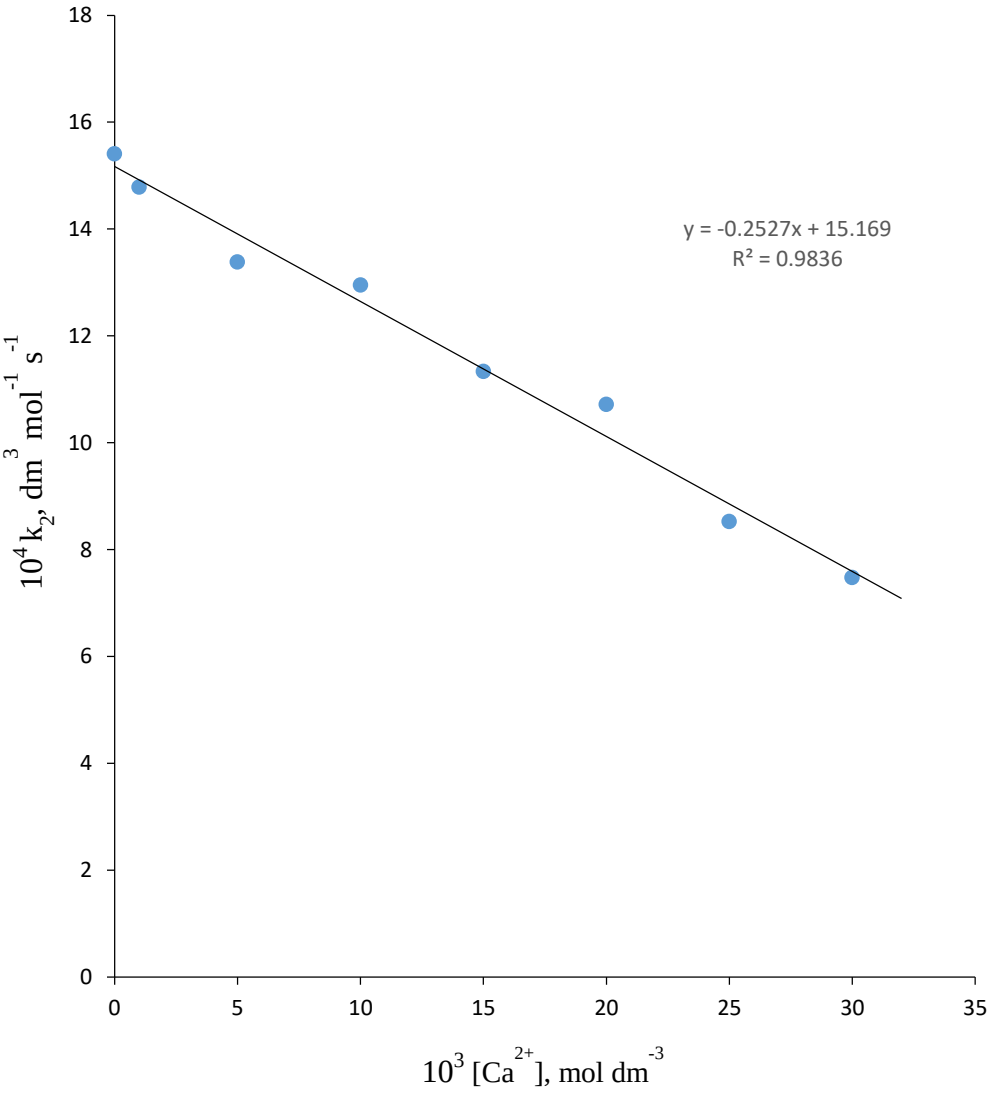


Figure 4.61: Plot of $10^4\,k_2$ versus $10^3\,[Ca^{2+}]$ for the redox reaction of $[Mn(salphen)]^+$ and SCN^- at $[Mn(salphen)^+] = 1.0 \times 10^{-4}$ mol dm^{-3}, $[SCN^-] = 0.42$ mol dm^{-3}, $\mu = 0.6\ C^2$ mol dm^{-3}, $[H^+] = 4.0 \times 10^{-5}$ mol dm^{-3}, D = 78.12, T = 28 ± 1°C and λ_{max} = 450 nm

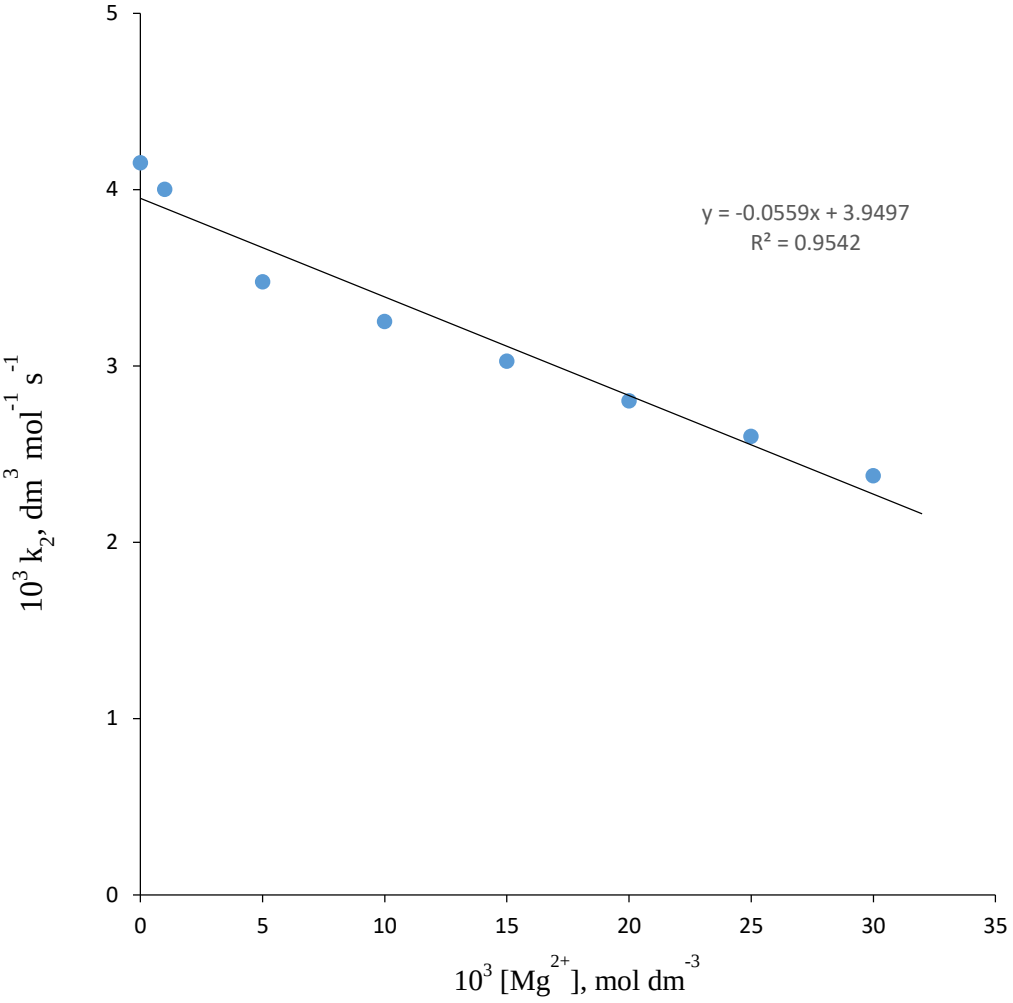


Figure 4.62: Plot of 10^3 k_2 versus 10^3 $[Mg^{2+}]$ for the redox reaction of $[Mn(salphen)]^+$ and $S(CH_2CH_2OH)_2$ at $[Mn(salphen)^+]$ = 1.0×10^{-4} mol dm^{-3}, $[S(CH_2CH_2OH)_2]$ = 0.40 mol dm^{-3}, μ = 0.6 C^2 mol dm^{-3}, $[H^+]$ = 2.0×10^{-5} mol dm^{-3}, D = 66.60, T = 50 ± 1°C and λ_{max} = 450 nm

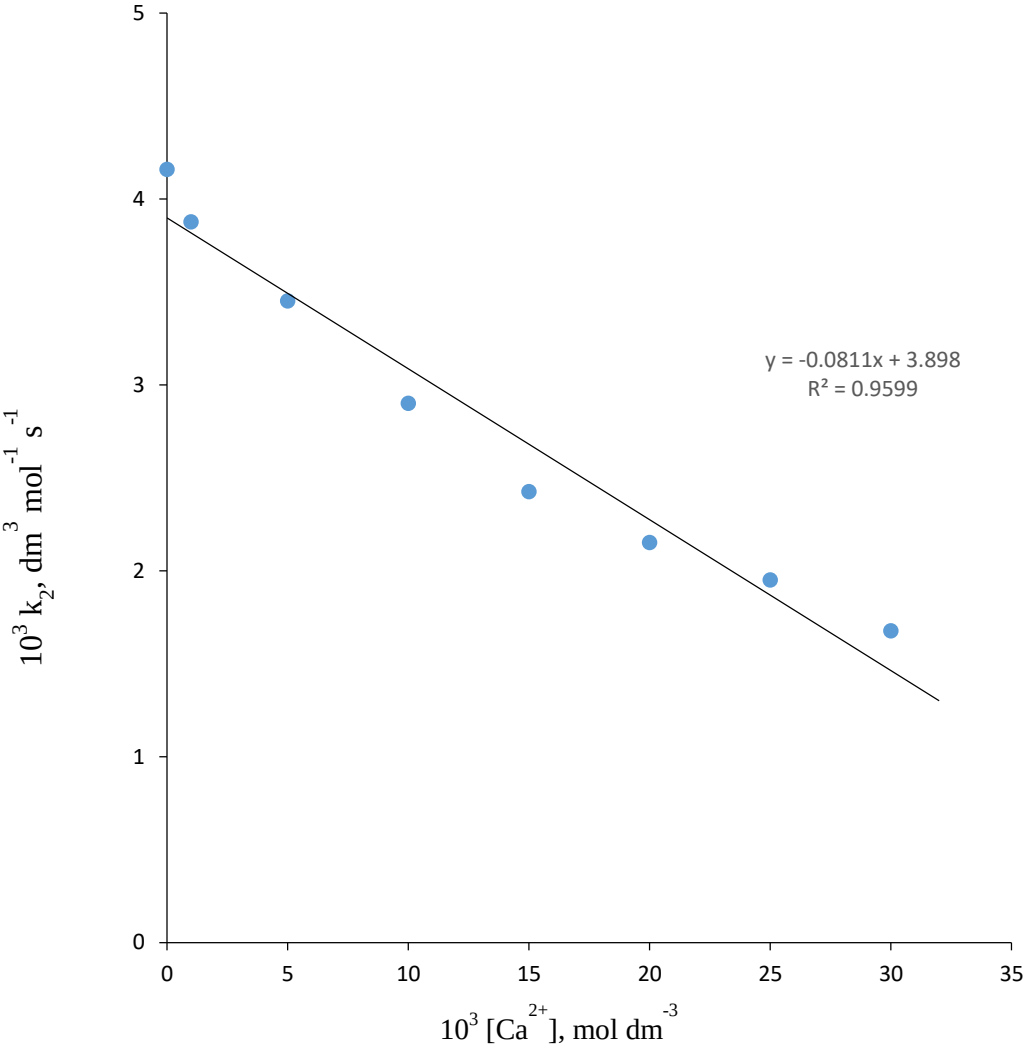


Figure 4.63: Plot of 10^3 k_2 versus 10^3 $[Ca^{2+}]$ for the redox reaction of $[Mn(salphen)]^+$ and $S(CH_2CH_2OH)_2$ at $[Mn(salphen)^+] = 1.0 \times 10^{-4}$ mol dm^{-3}, $[S(CH_2CH_2OH)_2] = 0.40$ mol dm^{-3}, $\mu = 0.6$ C^2 mol dm^{-3}, $[H^+] = 2.0 \times 10^{-5}$ mol dm^{-3}, D = 66.60, T = 50 ± 1°C and λ_{max} = 450 nm

Table 4.35: Effect of added anions on the rate of reaction $[Fe(salphen)]^+$ and $H_2C_2O_4$ at $[Fe(salphen)^+] = 2.0 \times 10^{-4}$ mol dm^{-3}, $[H_2C_2O_4] = 6.0 \times 10^{-3}$ mol dm^{-3}, $\mu = 0.2$ C^2 mol dm^{-3}, D = 76.06, T = 26 ± 1°C and λ_{max} = 435 nm

[X]	10^3 [X], mol dm^{-3}	$10^3 k_1$, s^{-1}	$10\ k_2$, dm^3 mol^{-1} s^{-1}
NO_3^-	0.00	4.27	7.12
	1.00	4.29	7.15
	2.00	4.28	7.13
	3.00	4.26	7.10
	4.00	4.29	7.15
	6.00	4.27	7.12
	8.00	4.28	7.13
CH_3COO^-	0.00	4.28	7.13
	1.00	4.26	7.10
	2.00	4.29	7.15
	3.00	4.27	7.12
	4.00	4.30	7.17
	6.00	4.29	7.15
	8.00	4.26	7.10

Table 4.36: Effect of added anions on the rate of reaction $[Fe(salphen)]^+$ and TSH at $[Fe(salphen)^+] = 2.0 \times 10^{-4}$ mol dm^{-3}, [TSH] = 0.15 mol dm^{-3}, μ = 0.2 C^2 mol dm^{-3}, D = 76.88, T = 26 ± 1 °C and λ_{max} = 435 nm

[X]	10^3 [X], mol dm^{-3}	$10^3 k_1$, s^{-1}	$10^2 k_2$, dm^3 mol^{-1} s^{-1}
NO_3^-	0.0	2.16	1.44
	1.0	2.18	1.45
	2.0	2.22	1.48
	3.0	2.26	1.51
	4.0	2.30	1.53
	6.0	2.36	1.57
	8.0	2.46	1.64
CH_3COO^-	0.0	2.16	1.44
	1.0	2.21	1.47
	2.0	2.25	1.50
	3.0	2.30	1.53
	4.0	2.34	1.56
	6.0	2.43	1.62
	8.0	2.49	1.66

Table 4.37: Effect of added anions on the rate of reaction $[Fe(salphen)]^+$ and H_3PO_2 at $[Fe(salphen)^+] = 2.0 \times 10^{-4}$ mol dm^{-3}, $[H_3PO_2] = 0.13$ mol dm^{-3}, $\mu = 0.2$ C^2 mol dm^{-3}, D = 76.68, T = 26 ± 1°C and $\lambda_{max} = 435$ nm

[X]	10^3 [X], mol dm^{-3}	$10^3 k_1$, s^{-1}	$10^2 k_2$, dm^3 mol^{-1} s^{-1}
NO_3^-	0.0	2.88	2.22
	1.0	3.21	2.47
	2.0	3.49	2.68
	3.0	3.61	2.78
	4.0	3.66	2.82
	5.0	4.06	3.12
	6.0	4.35	3.35
CH_3COO^-	0.0	2.86	2.20
	1.0	3.06	2.35
	2.0	3.20	2.46
	3.0	3.34	2.57
	4.0	3.59	2.76
	5.0	3.96	3.05
	6.0	4.26	3.28

Table 4.38: Effect of added anions on the rate of reaction $[Fe(salphen)]^+$ and H_2O_2 at $[Fe(salphen)^+] = 1.0 \times 10^{-4}$ mol dm^{-3}, $[H_2O_2] = 0.42$ mol dm^{-3}, $\mu = 0.6$ C^2 mol dm^{-3}, $[H^+] = 2.0 \times 10^{-5}$ mol dm^{-3}, D = 78.12, T = 28 ± 1°C and $\lambda_{max} = 435$ nm

[X]	10^3 [X], mol dm^{-3}	10^4 k_1, s^{-1}	10^4 k_2, dm^3 mol^{-1} s^{-1}
NO_3^-	0.00	2.15	5.12
	1.00	2.17	5.17
	5.00	2.40	5.71
	10.00	2.63	6.26
	15.00	2.67	6.36
	20.00	3.04	7.24
	25.00	3.22	7.67
	30.00	3.57	8.50
$HCOO^-$	0.00	2.14	5.10
	1.00	2.19	5.21
	5.00	2.28	5.43
	10.00	2.47	5.88
	15.00	2.78	6.62
	20.00	3.11	7.40
	25.00	3.41	8.12
	30.00	3.64	8.67

Table 4.39: Effect of added anions on the rate of reaction $[Mn(salphen)]^+$ and TSH at $[Mn(salphen)^+] = 1.0 \times 10^{-4}$ mol dm^{-3}, [TSH] = 0.42 mol dm^{-3}, μ = 0.6 C^2 mol dm^{-3}, D = 77.98, T = 32 ± 1°C and λ_{max} = 450 nm

[X]	10^3 [X], mol dm^{-3}	10^4 k_1, s^{-1}	10^3 k_2, dm^3 mol^{-1} s^{-1}
NO_3^-	0.00	6.79	1.62
	1.00	6.91	1.65
	5.00	7.23	1.72
	10.00	9.53	2.27
	15.00	11.79	2.81
	20.00	12.25	2.92
	25.00	16.24	3.87
	30.00	17.20	4.10
$HCOO^-$	0.00	6.79	1.62
	1.00	7.00	1.67
	5.00	7.58	1.80
	10.00	9.76	2.32
	15.00	12.02	2.86
	20.00	14.16	3.37
	25.00	17.83	4.25
	30.00	20.73	4.94

Table 4.40: Effect of added anions on the rate of reaction $[Mn(salphen)]^+$ and RSH at $[Mn(salphen)^+] = 1.0 \times 10^{-4}$ mol dm^{-3}, [RSH] = 0.40 mol dm^{-3}, μ = 0.6 C^2 mol dm^{-3}, $[H^+] = 4.0 \times 10^{-5}$ mol dm^{-3}, D = 78.19, T = 28 ± 1°C and λ_{max} = 450 nm

[X]	10^3 [X], mol dm^{-3}	10^3 k_1, s^{-1}	10^2 k_2, dm^3 mol^{-1} s^{-1}
NO_3^-	0.00	5.02	1.26
	1.00	5.32	1.33
	5.00	5.62	1.41
	10.00	6.91	1.73
	15.00	7.53	1.88
	20.00	9.04	2.26
	25.00	9.86	2.47
	30.00	11.68	2.92
SO_4^{2-}	0.00	5.02	1.26
	1.00	5.20	1.30
	5.00	5.57	1.39
	10.00	6.56	1.64
	15.00	7.46	1.87
	20.00	8.08	2.02
	25.00	9.74	2.44
	30.00	10.32	2.58

Table 4.41: Effect of added anions on the rate of reaction $[Mn(salphen)]^+$ and SCN^- at $[Mn(salphen)^+] = 1.0 \times 10^{-4}$ mol dm^{-3}, $[SCN^-] = 0.42$ mol dm^{-3}, $\mu = 0.6$ C^2 mol dm^{-3}, $[H^+] = 4.0 \times 10^{-5}$ mol dm^{-3}, D = 78.12, T = 28 ± 1°C and λ_{max} = 450 nm

[X]	10^3 [X], mol dm^{-3}	10^4 k_1, s^{-1}	10^3 k_2, dm^3 mol^{-1} s^{-1}
NO_3^-	0.00	6.47	1.54
	1.00	6.52	1.55
	5.00	6.68	1.59
	10.00	7.16	1.70
	15.00	8.29	1.97
	20.00	8.64	2.06
	25.00	9.40	2.24
	30.00	10.76	2.56
$HCOO^-$	0.00	6.47	1.54
	1.00	6.54	1.56
	5.00	6.88	1.64
	10.00	6.96	1.66
	15.00	7.74	1.84
	20.00	7.97	1.90
	25.00	8.98	2.14
	30.00	9.17	2.18

Table 4.42: Effect of added anions on the rate of reaction $[Mn(salphen)]^+$ and $H_2NNHCSNH_2$ at $[Mn(salphen)^+] = 1.0 \times 10^{-4}$ mol dm^{-3}, $[H_2NNHCSNH_2] = 0.28$ mol dm^{-3}, $\mu = 0.6$ C^2 mol dm^{-3}, $[H^+] = 2.0 \times 10^{-5}$ mol dm^{-3}, D = 75.10, T = 28 ± 1°C and λ_{max} = 450 nm

[X]	10^3 [X], mol dm^{-3}	10^4 k_1, s^{-1}	10^3 k_2, dm^3 mol^{-1} s^{-1}
NO_3^-	0.00	11.33	4.05
	1.00	11.93	4.26
	5.00	13.34	4.76
	10.00	16.91	6.04
	15.00	22.44	8.01
	20.00	23.58	8.42
	25.00	30.03	10.73
	30.00	35.79	12.78
$HCOO^-$	0.00	11.33	4.05
	1.00	11.98	4.28
	5.00	13.66	4.88
	10.00	17.87	6.38
	15.00	21.90	7.82
	20.00	27.89	9.96
	25.00	34.24	12.23
	30.00	38.55	13.77

However, the rate decreased with an increase in concentration of added anions in H_2O_2 and $S(CH_2CH_2OH)_2$ reactions with $[Mn(salphen)]^+$ (Tables 4.43 and 4.44). Plots of ion dependent second order rate constant, k_2, versus concentrations of anions, [X] are presented in Figures 4.64 – 4.81.

4.8 Effect of Temperature on the Reactions Rate

The results of temperature dependence on the reactions rate and activation parameters for the reactions are presented in Tables 4.45 – 4.54. Plots of $\ln\left(\frac{k_2}{T}\right)$ versus $\left(\frac{1}{T}\right)$ are presented in Figures 4.82 – 4.91 while the values of $\Delta H^{\ddagger}$, $\Delta S^{\ddagger}$, $\Delta G^{\ddagger}$ and E_a obtained are also presented in Tables 4.45 – 4.54.

4.9 Test for Intermediate Complex Formation

The results of test for intermediate complex are presented in sections 4.9.1 – 4.9.2.

4.9.1 Spectrophotometric test

There was no shift in λ_{max} recorded for all the reactions studied (Figures 4.92 – 4.100) except in the reaction of RSH with $[Mn(salphen)]^+$ where a slight shift was observed from 450 nm to 425 nm (Figure 4.101).

4.9.2 Michaelis – Menten plots

The Michaelis-Menten plots of $1/k_1$ versus 1/[reductant] were linear without an intercept in the reactions of TSH, $H_2C_2O_4$ and H_3PO_2 with $[Fe(salphen)]^+$ (Figures 4.102 – 4.104) and in the reactions of TSH, RSH, SCN^-, $H_2NNHCSNH_2$ and $S(CH_2CH_2OH)_2$ with $[Mn(salphen)]^+$ (Figures 4.105 – 4.109). However, intercepts were obtained from the plots of $1/k_1$ versus $1/[H_2O_2]$ in the reactions of H_2O_2 with $[Fe(salphen)]^+$ and $[Mn(salphen)]^+$ (Figures 4.110 and 4.111).

Table 4.43: Effect of added anions on the rate of reaction $[Mn(salphen)]^+$ and H_2O_2 at $[Mn(salphen)^+] = 1.0 \times 10^{-4}$ mol dm^{-3}, $[H_2O_2] = 0.15$ mol dm^{-3}, $\mu = 0.2$ C^2 mol dm^{-3}, $[H^+] = 2.0 \times 10^{-5}$ mol dm^{-3}, D = 76.82, T = 30 ± 1°C and $\lambda_{max} = 450$ nm

[X]	10^3 [X], mol dm^{-3}	10^3 k_1, s^{-1}	10^2 k_2, dm^3 mol^{-1} s^{-1}
NO_3^-	0.00	1.86	1.24
	2.00	1.68	1.12
	4.00	1.50	1.00
	6.00	1.40	0.93
	8.00	1.29	0.86
	10.00	1.12	0.75
	12.00	1.04	0.69
$HCOO^-$	0.00	1.86	1.24
	2.00	1.64	1.09
	4.00	1.45	0.97
	6.00	1.27	0.85
	8.00	1.11	0.74
	10.00	1.01	0.67
	12.00	0.92	0.61

Table 4.44: Effect of added anions on the rate of reaction of $[Mn(salphen)]^+$ and $S(CH_2CH_2OH)_2$ at $[Mn(salphen)^+] = 1.0 \times 10^{-4}$ mol dm^{-3}, $[S(CH_2CH_2OH)_2] = 0.40$ mol dm^{-3}, $\mu = 0.6$ C^2 mol dm^{-3}, $[H^+] = 2.0 \times 10^{-5}$ mol dm^{-3}, D = 66.60, T = 50 ± 1°C and λ_{max} = 450 nm

[X]	10^3 [X], mol dm^{-3}	10^4 k_1, s^{-1}	10^3 k_2, dm^3 mol^{-1} s^{-1}
SO_4^{2-}	0.00	16.60	4.15
	1.00	15.30	3.83
	5.00	12.80	3.20
	10.00	11.10	2.78
	15.00	9.50	2.38
	20.00	7.60	1.90
	25.00	6.38	1.60
	30.00	4.68	1.17
$HCOO^-$	0.00	16.60	4.15
	1.00	15.00	3.75
	5.00	12.30	3.08
	10.00	10.10	2.53
	15.00	7.89	1.97
	20.00	6.41	1.60
	25.00	3.34	0.84
	30.00	1.29	0.32

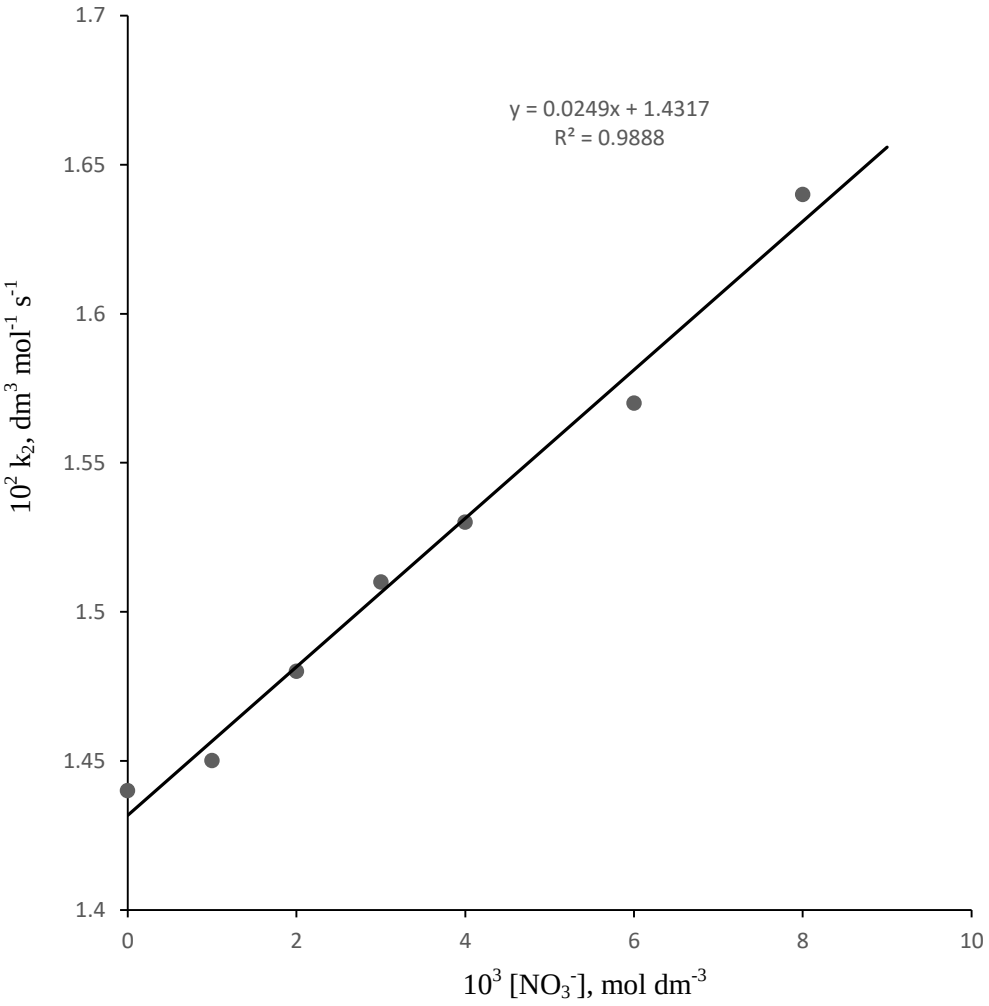


Figure 4.64: Plot of k_2 versus $[NO_3^-]$ for the redox reaction of $[Fe(salphen)]^+$ and TSH at $[Fe(salphen)^+] = 2.0 \times 10^{-4}$ mol dm^{-3}, [TSH] = 0.15 mol dm^{-3}, μ = 0.2 C^2 mol dm^{-3}, D = 76.88, T = 26 ± 1°C and λ_{max} = 435 nm

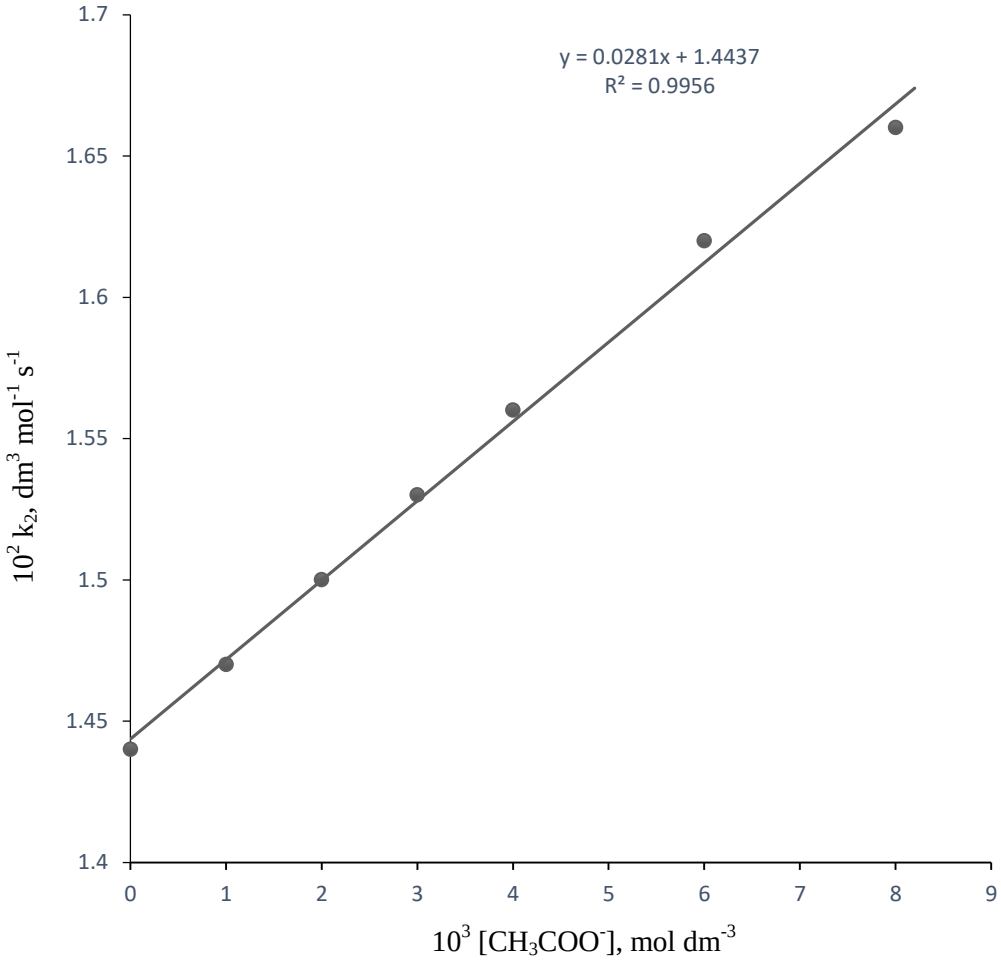


Figure 4.65: Plot of k_2 versus $[CH_3COO^-]$ for the redox reaction of $[Fe(salphen)]^+$ and TSH at $[Fe(salphen)^+] = 2.0 \times 10^{-4}$ mol dm^{-3}, [TSH] = 0.15 mol dm^{-3}, $\mu = 0.2$ C^2 mol dm^{-3}, D = 76.88, T = 26 ± 1°C and λ_{max} = 435 nm

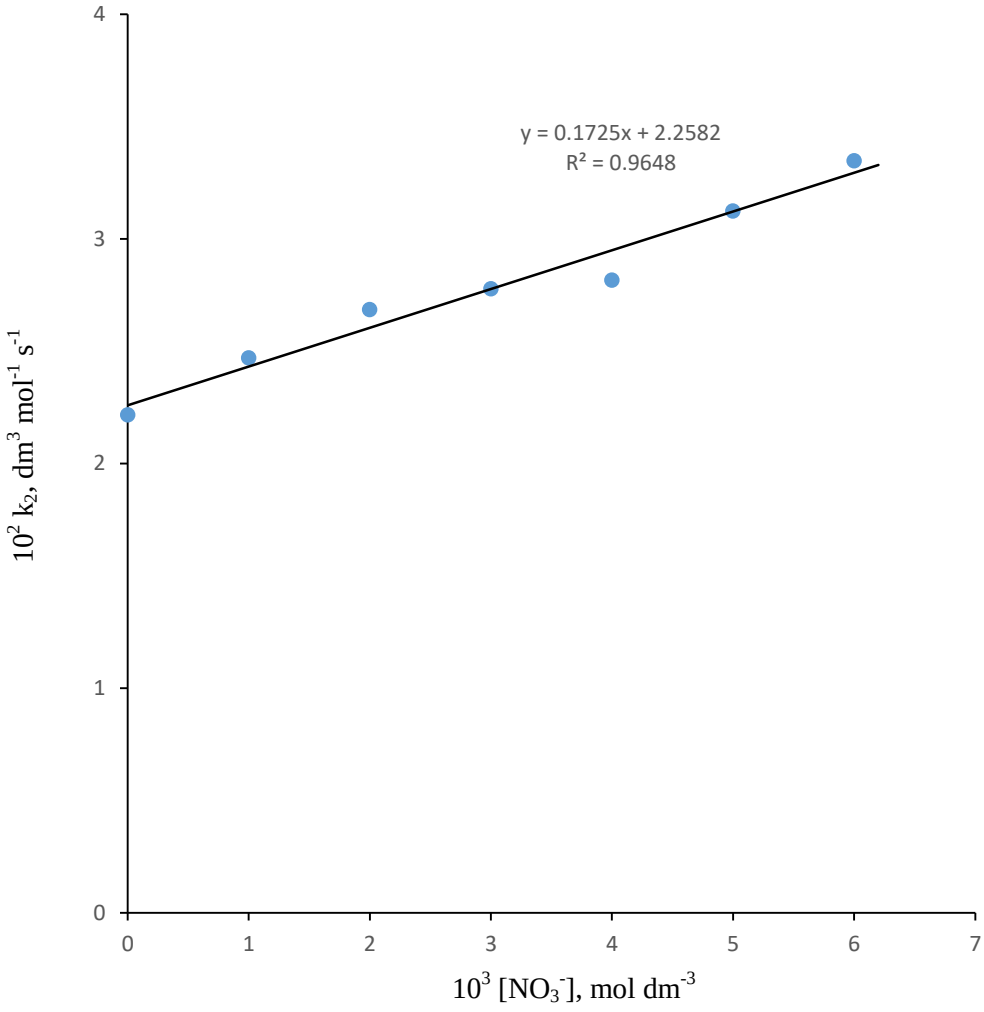


Figure 4.66: Plot of k_2 versus $[NO_3^-]$ for the redox reaction of $[Fe(salphen)]^+$ and H_3PO_2 at $[Fe(salphen)^+] = 2.0 \times 10^{-4}$ mol dm^{-3}, $[H_3PO_2] = 0.13$ mol dm^{-3}, $\mu = 0.2$ C^2 mol dm^{-3}, D = 76.68, T = 26 ± 1°C and $\lambda_{max} = 435$ nm

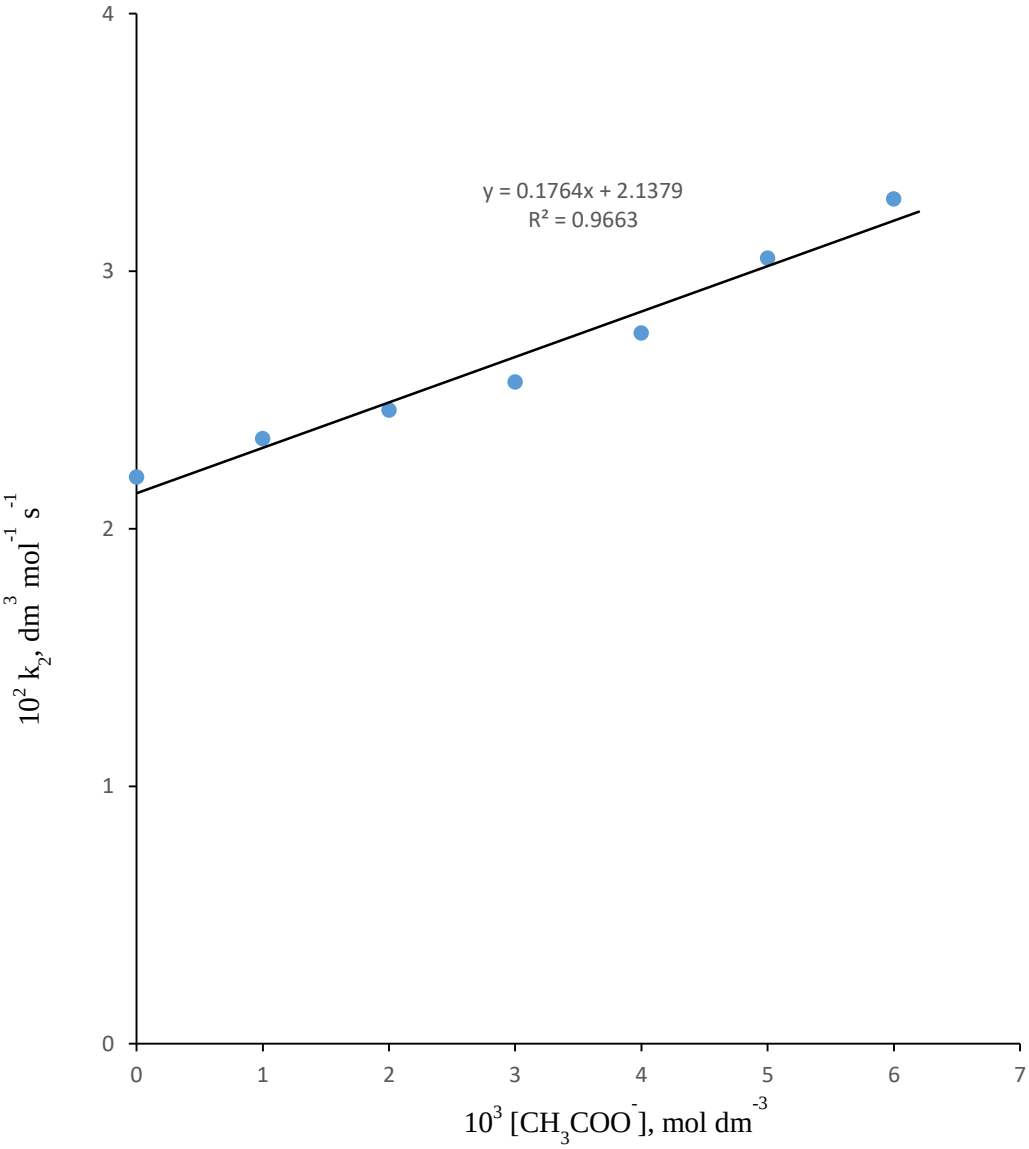


Figure 4.67: Plot of k_2 versus $[CH_3COO^-]$ for the redox reaction of $[Fe(salphen)]^+$ and H_3PO_2 at $[Fe(salphen)^+] = 2.0 \times 10^{-4}$ mol dm^{-3}, $[H_3PO_2] = 0.13$ mol dm^{-3}, $\mu = 0.2$ C^2 mol dm^{-3}, D = 76.68, T = 26 ± 1°C and $\lambda_{max} = 435$ nm

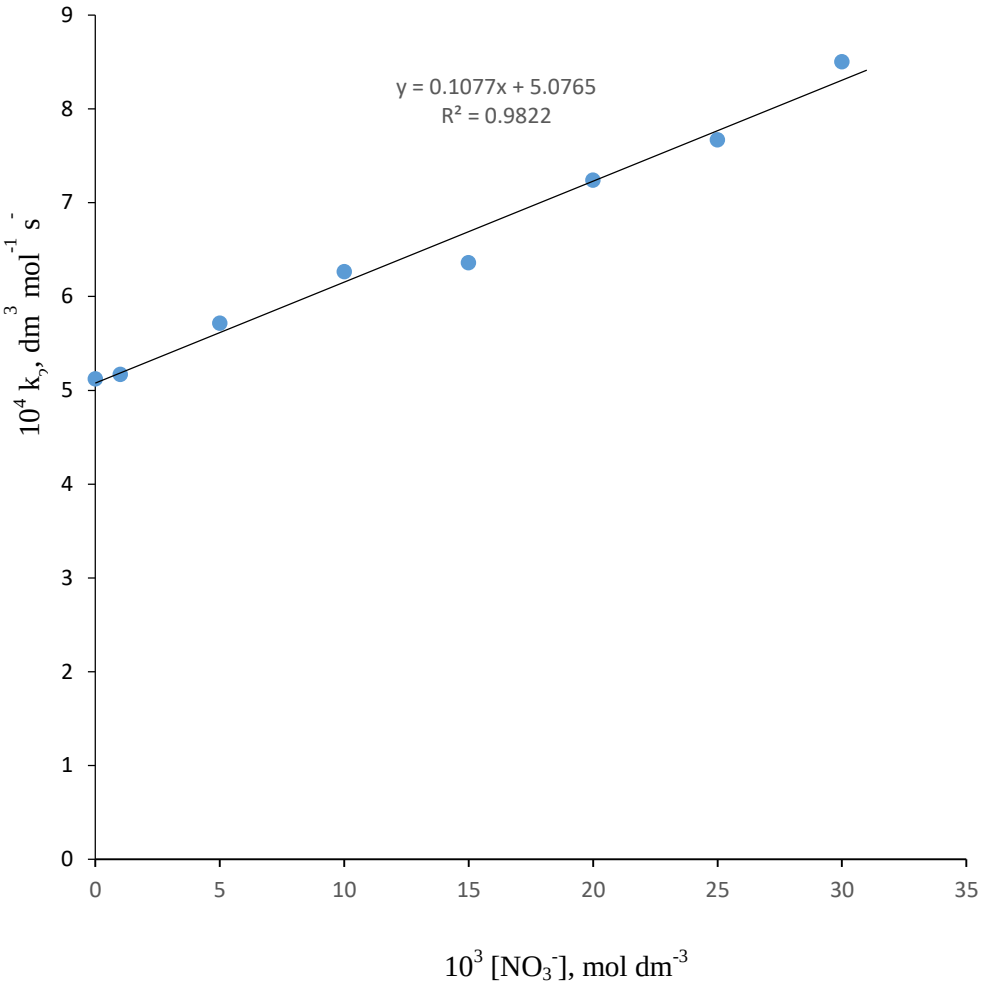


Figure 4.68: Plot of 10^4 k_2 versus 10^3 $[NO_3^-]$ for the redox reaction of $[Fe(salphen)]^+$ and H_2O_2 at $[Fe(salphen)^+] = 1.0 \times 10^{-4}$ mol dm^{-3}, $[H_2O_2] = 0.42$ mol dm^{-3}, $\mu = 0.6$ C^2 mol dm^{-3}, $[H^+] = 2.0 \times 10^{-5}$ mol dm^{-3}, D = 78.12, T = 28 ± 1°C and λ_{max} = 435 nm

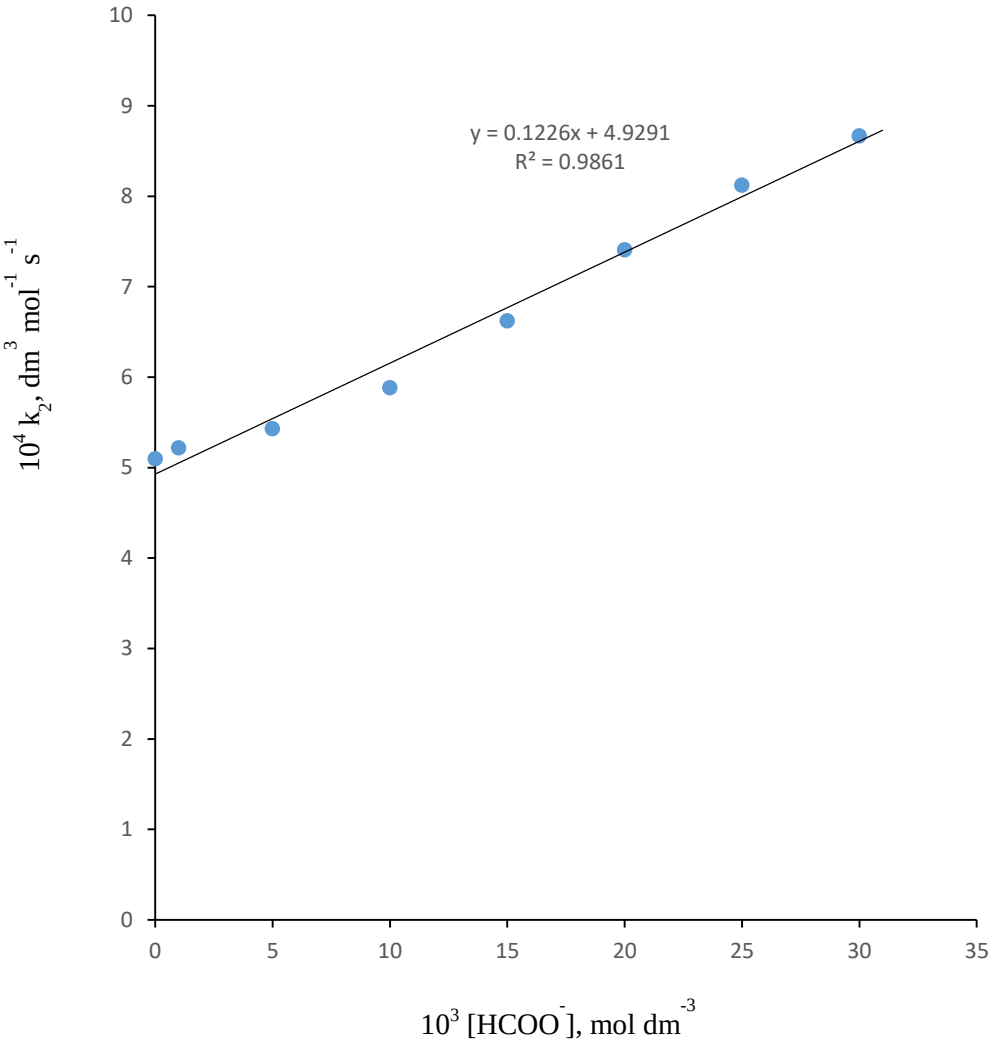


Figure 4.69: Plot of 10^4 k_2 versus 10^3 [HCOO$^-$] for the redox reaction of [Fe(salphen)]$^+$ and H_2O_2 at [Fe(salphen)$^+$] = 1.0×10^{-4} mol dm^{-3}, [H_2O_2] = 0.42 mol dm^{-3}, μ = 0.6 C^2 mol dm^{-3}, [H^+] = 2.0×10^{-5} mol dm^{-3}, D = 78.12, T = 28 ± 1 °C and λ_{max} = 435 nm

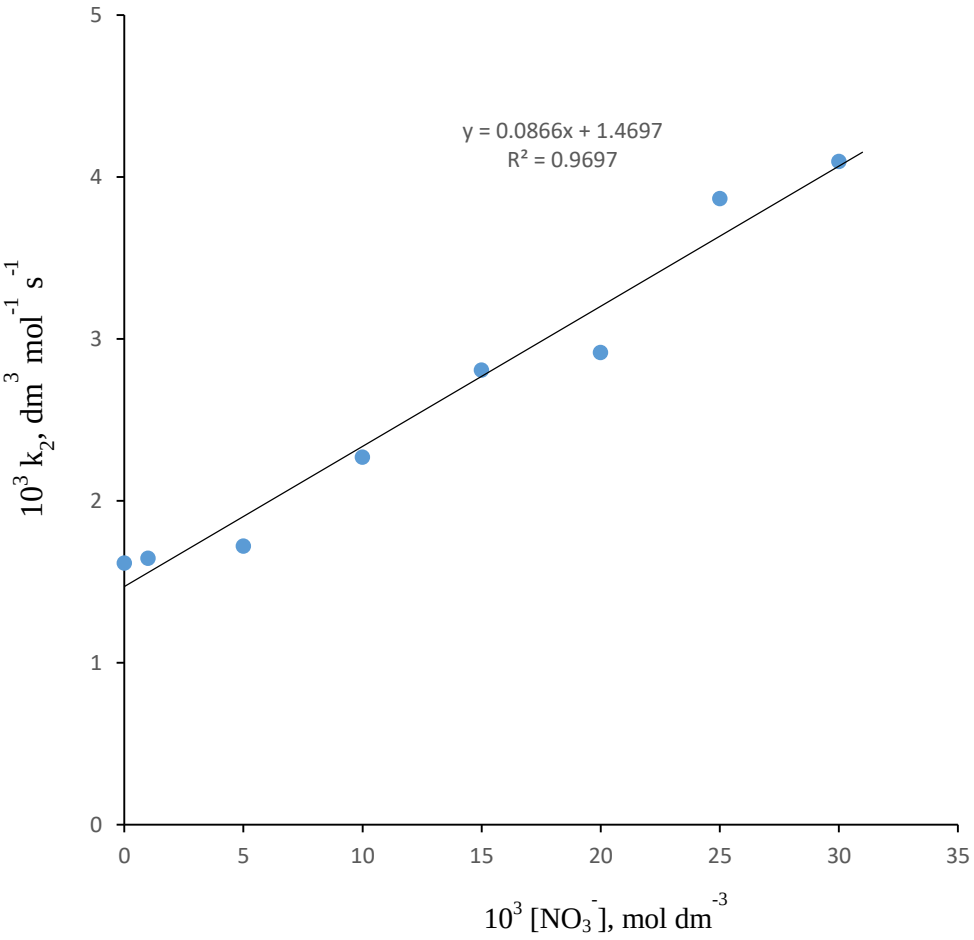


Figure 4.70: Plot of 10^3 k_2 versus 10^3 $[NO_3^-]$ for the redox reaction of $[Mn(salphen)]^+$ and TSH at $[Mn(salphen)^+]$ = 1.0 × 10^{-4} mol dm^{-3}, [TSH] = 0.42 mol dm^{-3}, μ = 0.6 C^2 mol dm^{-3}, D = 77.98, T = 32 ± 1°C and λ_{max} = 450 nm

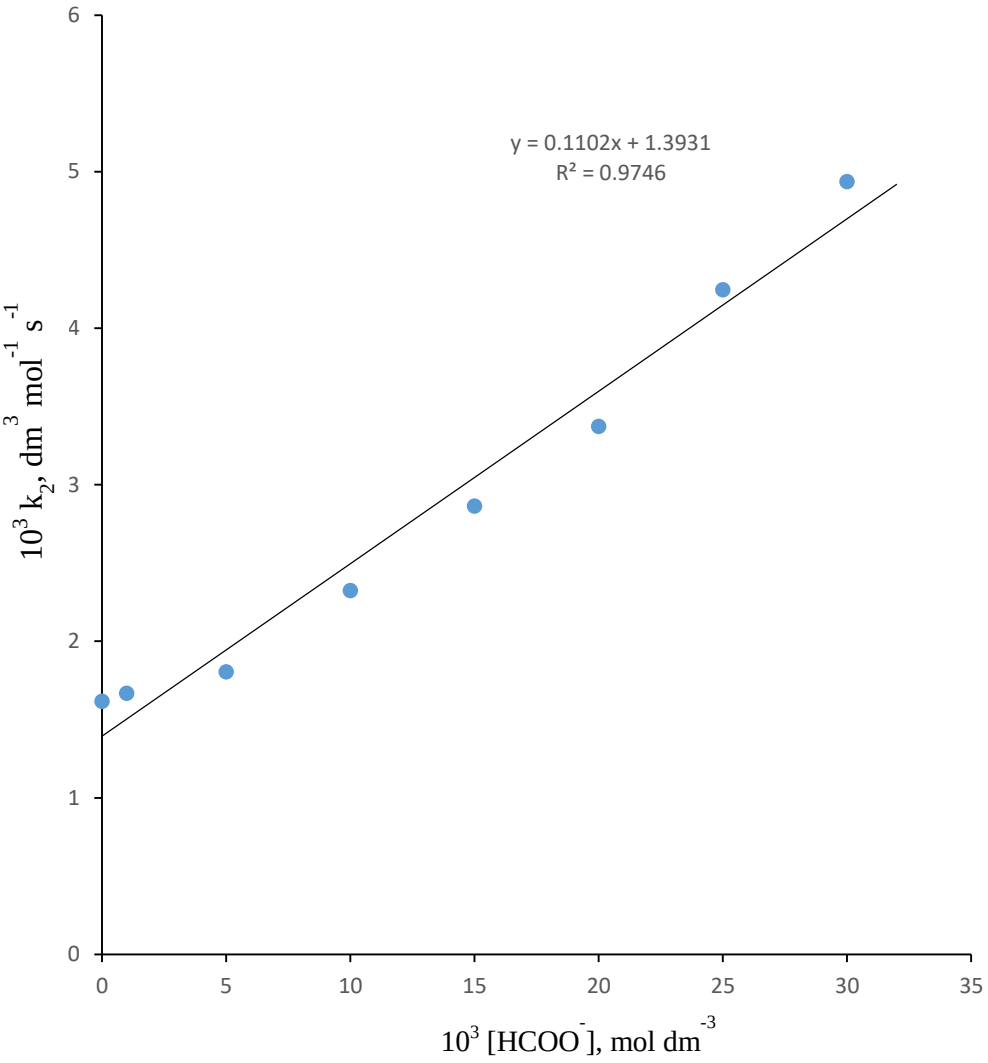


Figure 4.71: Plot of 10^3 k_2 versus 10^3 [$HCOO^-$] for the redox reaction of [Mn(salphen)]$^+$ and TSH at [Mn(salphen)$^+$] = 1.0 × 10^{-4} mol dm^{-3}, [TSH] = 0.42 mol dm^{-3}, μ = 0.6 C^2 mol dm^{-3}, D = 77.98, T = 32 ± 1°C and λ_{max} = 450 nm

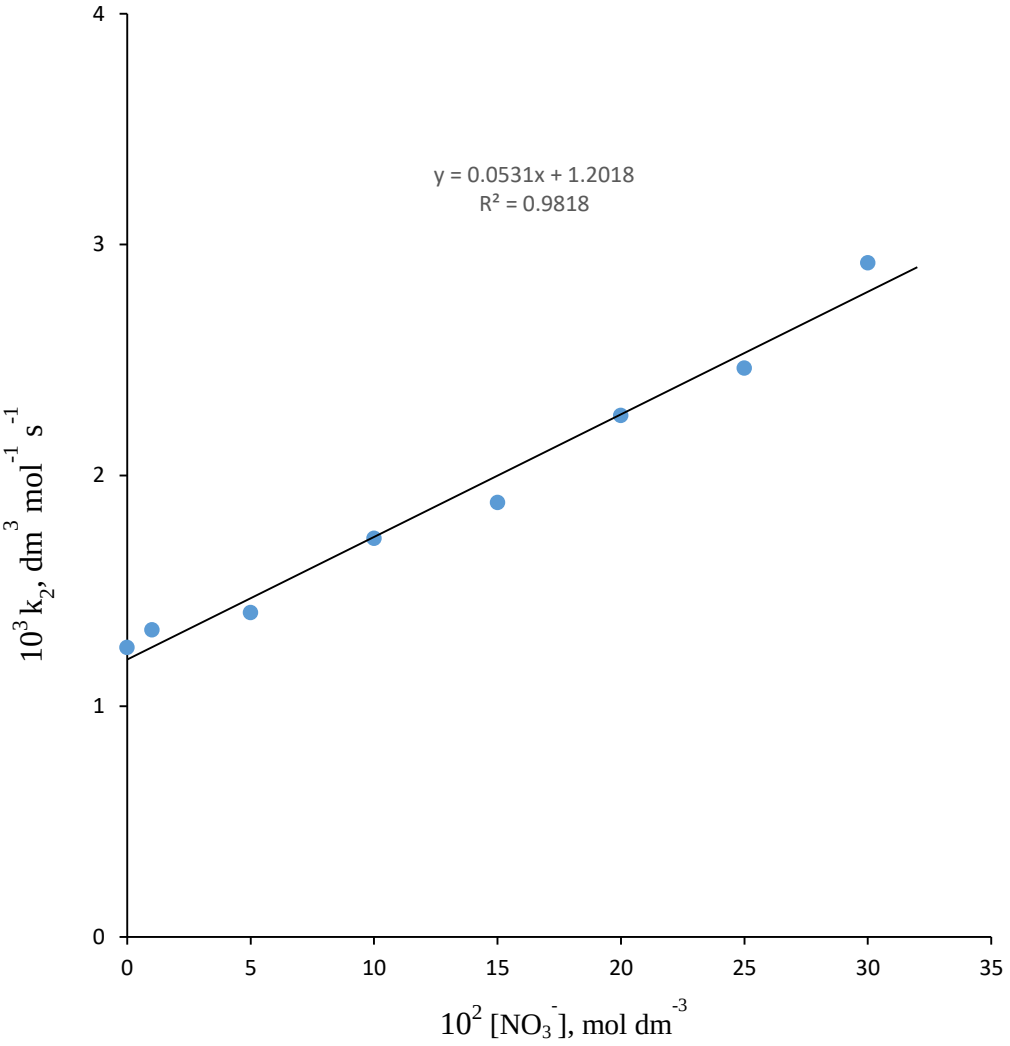


Figure 4.72: Plot of $10^3\ k_2$ versus $10^2\ [NO_3^-]$ for the redox reaction of $[Mn(salphen)]^+$ and RSH at $[Mn(salphen)^+] = 1.0 \times 10^{-4}$ mol dm^{-3}, [RSH] = 0.4 mol dm^{-3}, μ = 0.6 C^2 mol dm^{-3}, $[H^+] = 4.0 \times 10^{-5}$ mol dm^{-3}, D = 78.19, T = 28 ± 1°C and λ_{max} = 450 nm

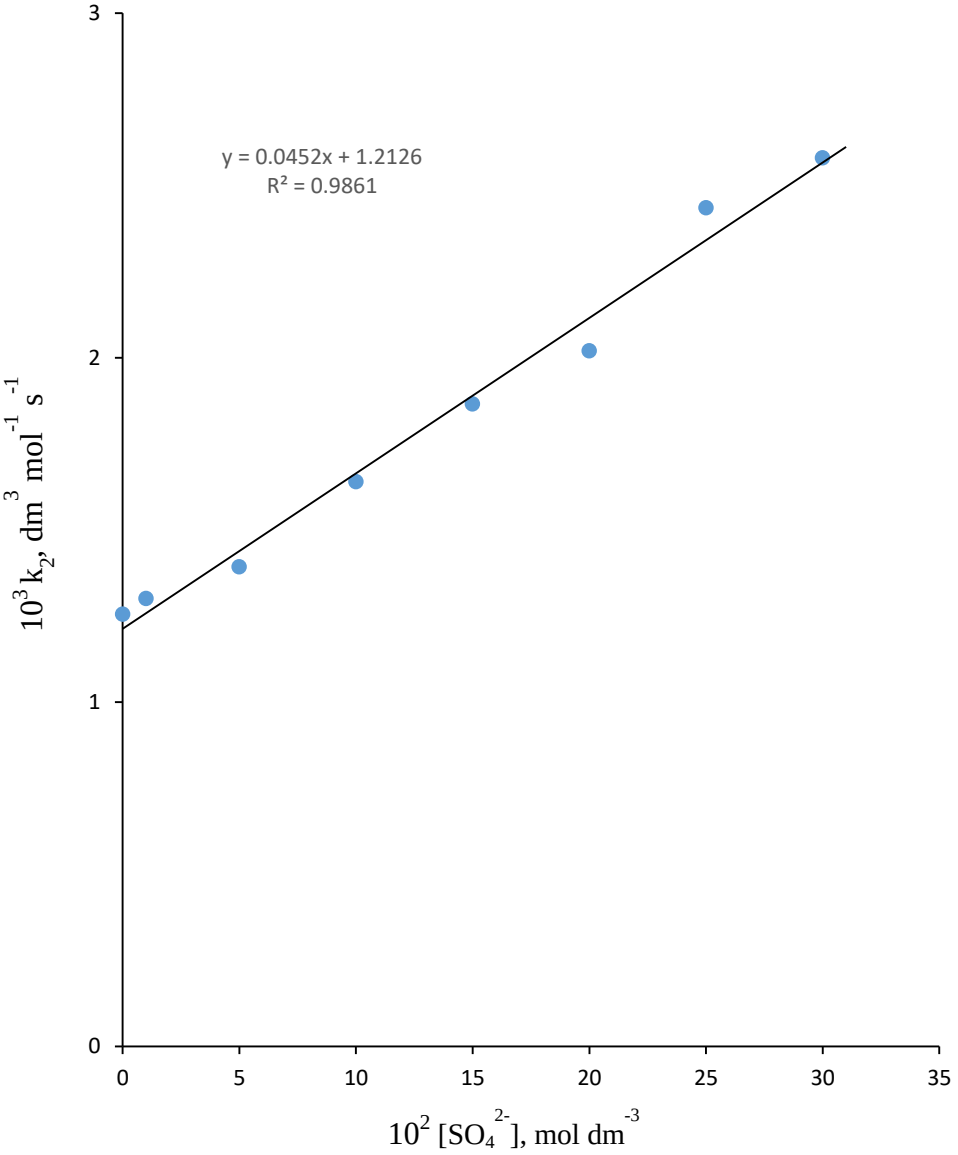


Figure 4.73: Plot of $10^3 k_2$ versus 10^2 $[SO_4^{2-}]$ for the redox reaction of $[Mn(salphen)]^+$ and RSH at $[Mn(salphen)^+] = 1.0 \times 10^{-4}$ mol dm^{-3}, [RSH] = 0.4 mol dm^{-3}, μ = 0.6 C^2 mol dm^{-3}, $[H^+] = 4.0 \times 10^{-5}$ mol dm^{-3}, D = 78.19, T = 28 ± 1°C and λ_{max} = 450 nm

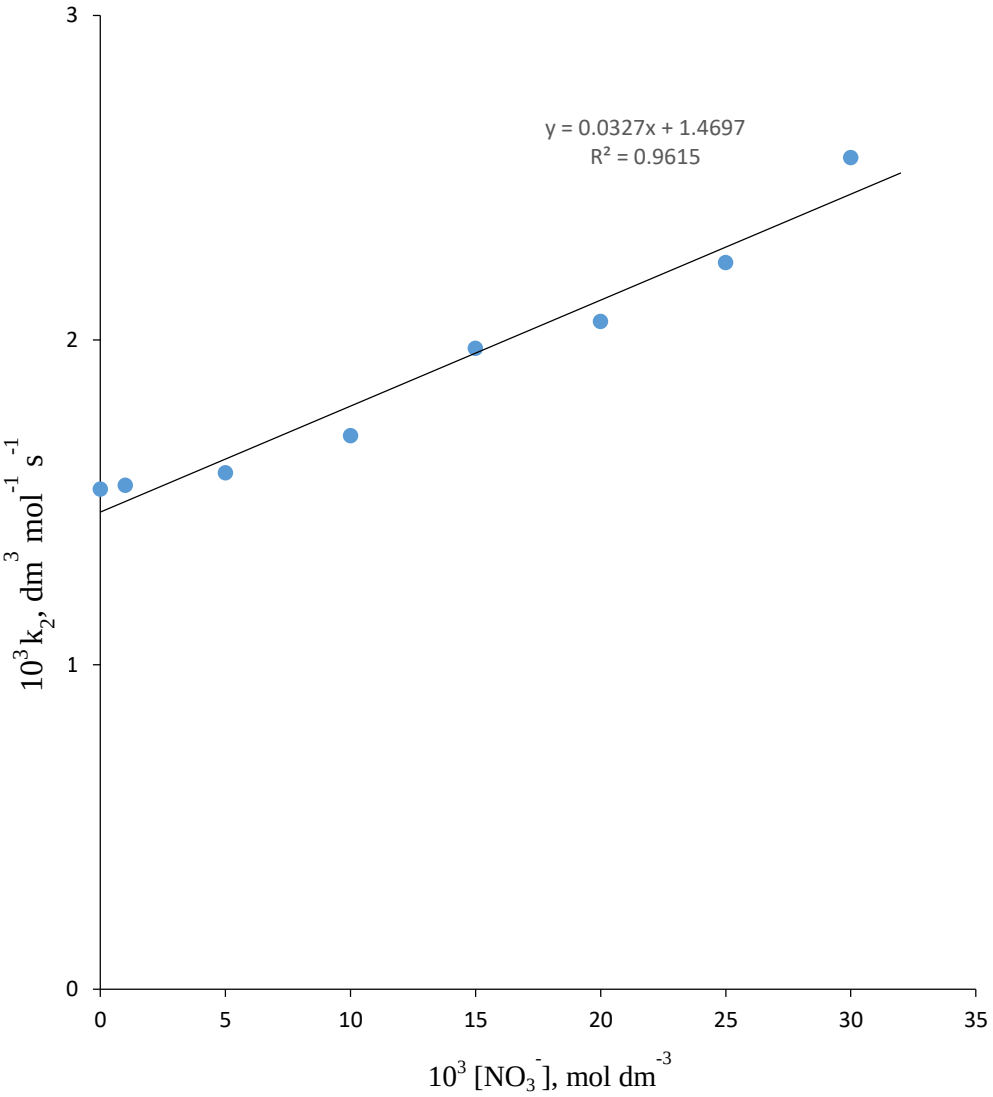


Figure 4.74: Plot of 10^3 k_2 versus 10^3 $[NO_3^-]$ for the redox reaction of $[Mn(salphen)]^+$ and SCN^- at $[Mn(salphen)^+] = 1.0 \times 10^{-4}$ mol dm^{-3}, $[SCN^-] = 0.42$ mol dm^{-3}, $\mu = 0.6$ C^2 mol dm^{-3}, $[H^+] = 4.0 \times 10^{-5}$ mol dm^{-3}, D = 78.12, T = 28 ± 1 °C and λ_{max} = 450 nm

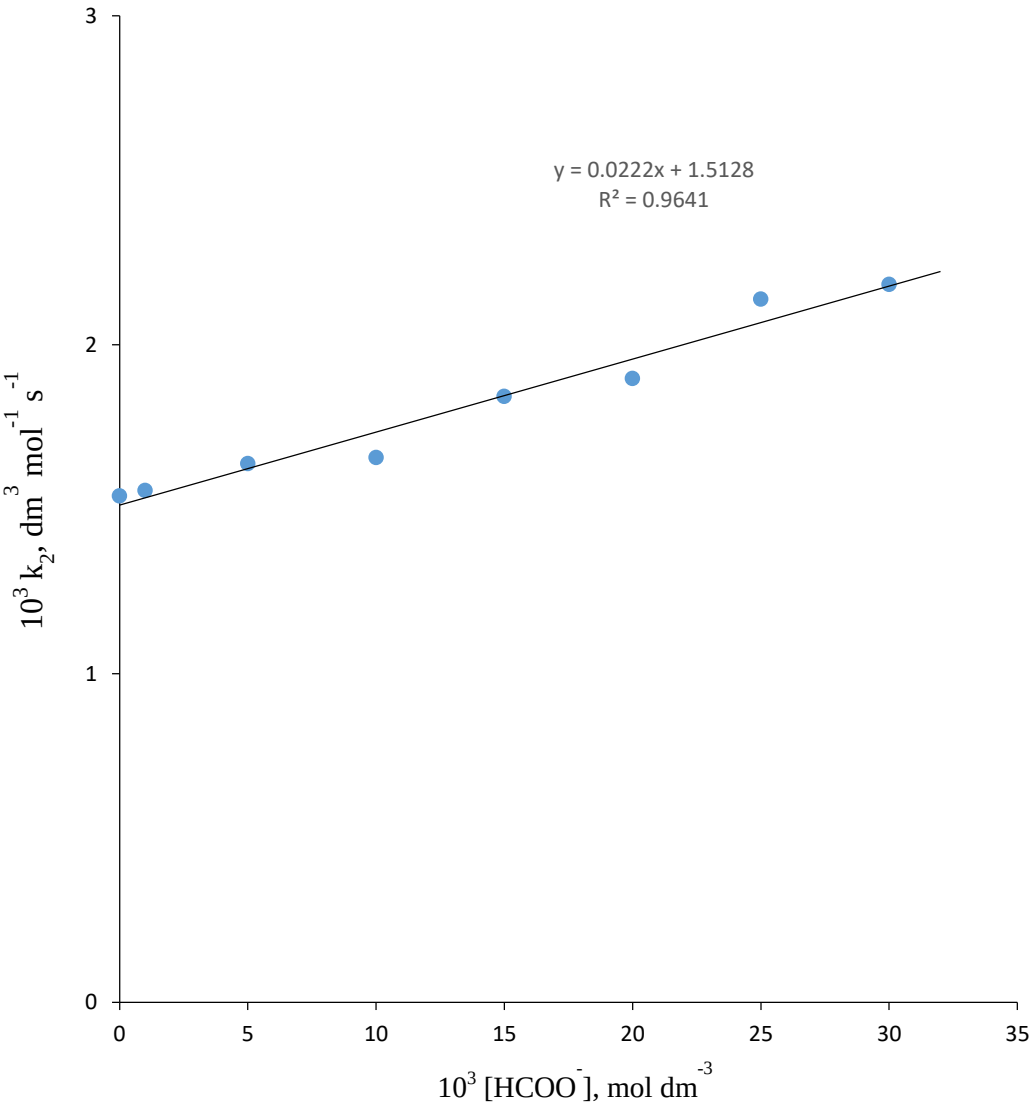


Figure 4.75: Plot of 10^3 k_2 versus 10^3 [$HCOO^-$] for the redox reaction of [Mn(salphen)]$^+$ and SCN^- at [Mn(salphen)$^+$] = 1.0×10^{-4} mol dm^{-3}, [SCN^-] = 0.42 mol dm^{-3}, μ = 0.6 C^2 mol dm^{-3}, [H^+] = 4.0×10^{-5} mol dm^{-3}, D = 78.12, T = 28 ± 1°C and λ_{max} = 450 nm

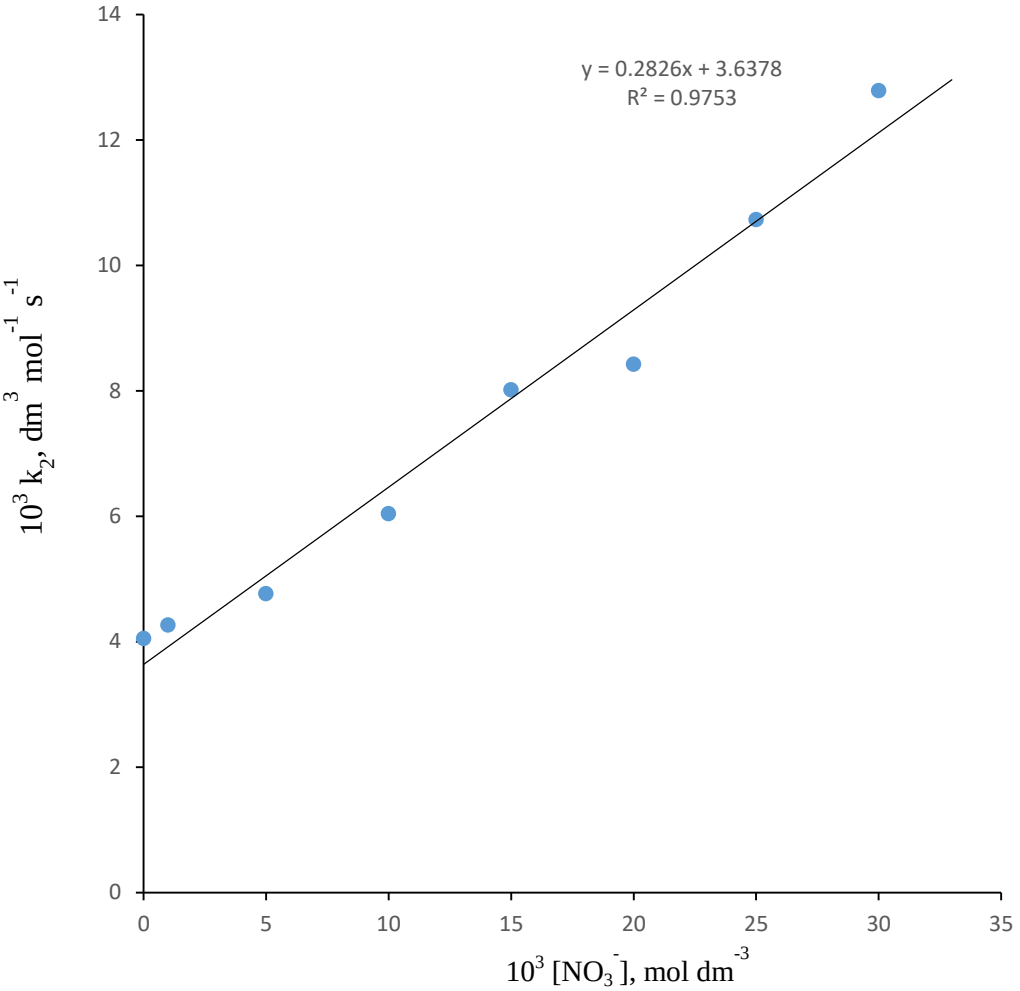


Figure 4.76: Plot of 10^3 k_2 versus 10^3 $[NO_3^-]$ for the redox reaction of $[Mn(salphen)]^+$ and $H_2NNHCSNH_2$ at $[Mn(salphen)^+]$ = 1.0 × 10^{-4} mol dm^{-3}, $[H_2NNHCSNH_2]$ = 0. 28 mol dm^{-3}, μ = 0.6 C^2 mol dm^{-3}, $[H^+]$ = 2.0 × 10^{-5} mol dm^{-3}, D = 75.10, T = 28 ± 1°C and λ_{max} = 450 nm

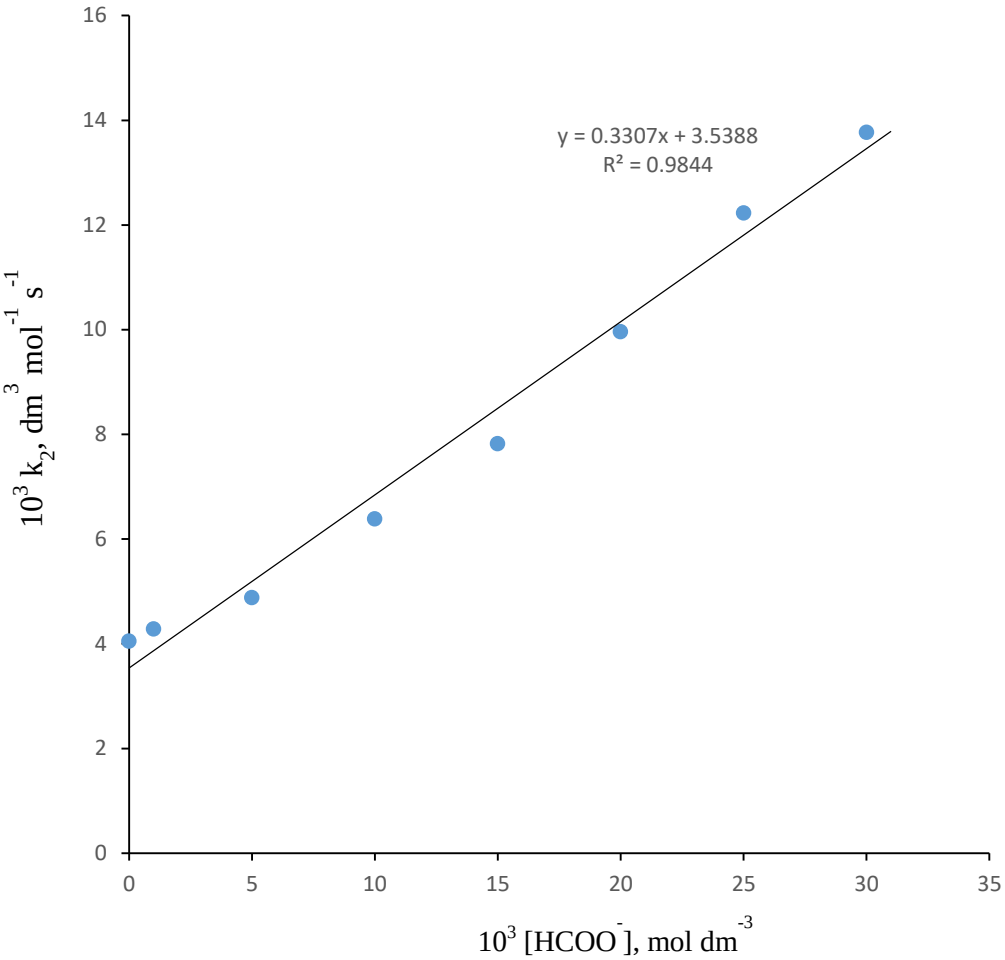


Figure 4.77: Plot of 10^3 k_2 versus 10^3 [$HCOO^-$] for the redox reaction of [Mn(salphen)]$^+$ and $H_2NNHCSNH_2$ at [Mn(salphen)$^+$] = 1.0 × 10^{-4} mol dm^{-3}, [$H_2NNHCSNH_2$] = 0. 28 mol dm^{-3}, μ = 0.6 C^2 mol dm^{-3}, [H^+] = 2.0 × 10^{-5} mol dm^{-3}, D = 75.10, T = 28 ± 1°C and λ_{max} = 450 nm

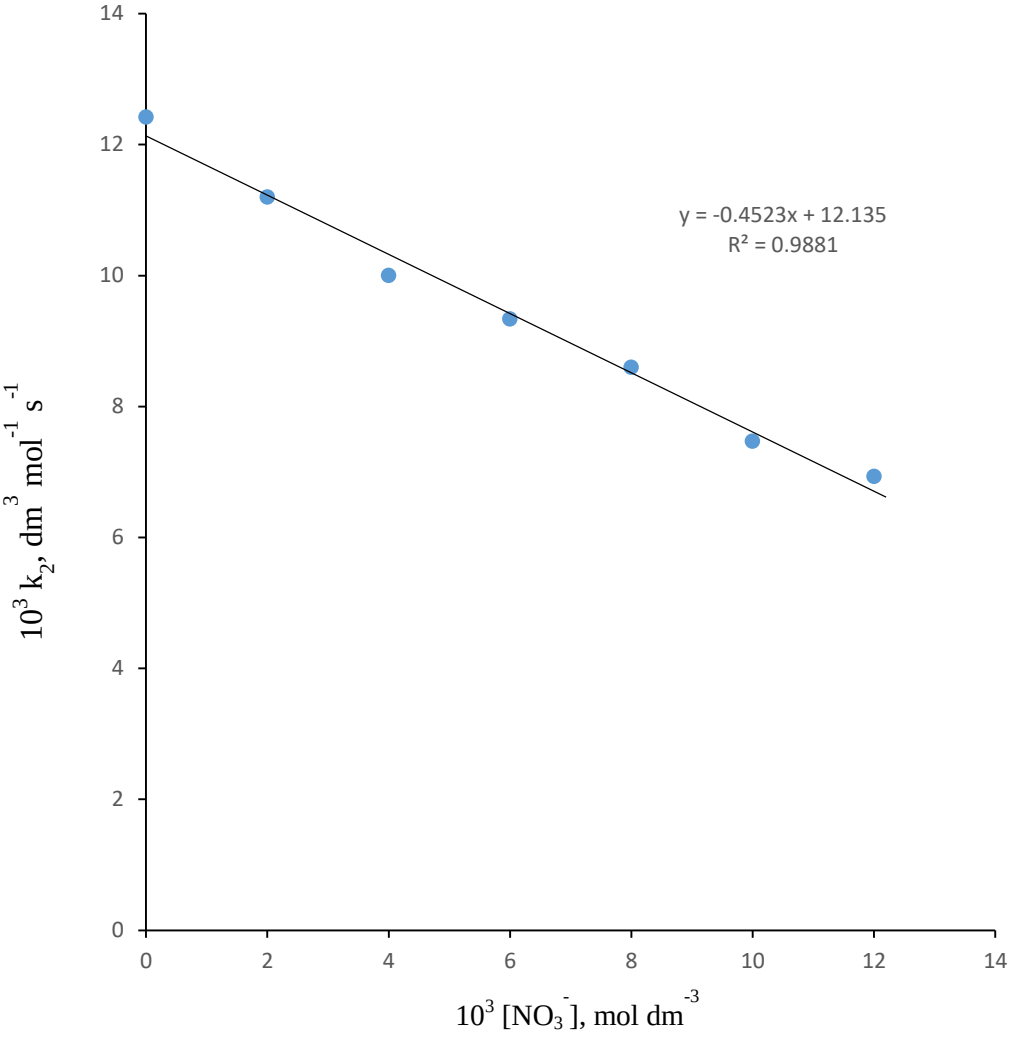


Figure 4.78: Plot of 10^3 k_2 versus 10^3 $[NO_3^-]$ for the redox reaction of $[Mn(salphen)]^+$ and H_2O_2 at $[Mn(salphen)^+] = 1.0 \times 10^{-4}$ mol dm^{-3}, $[H_2O_2] = 0.15$ mol dm^{-3}, $\mu = 0.2$ C^2 mol dm^{-3}, $[H^+] = 2.0 \times 10^{-5}$ mol dm^{-3}, D = 76.82, T = 30 ± 1°C and $\lambda_{max} = 450$ nm

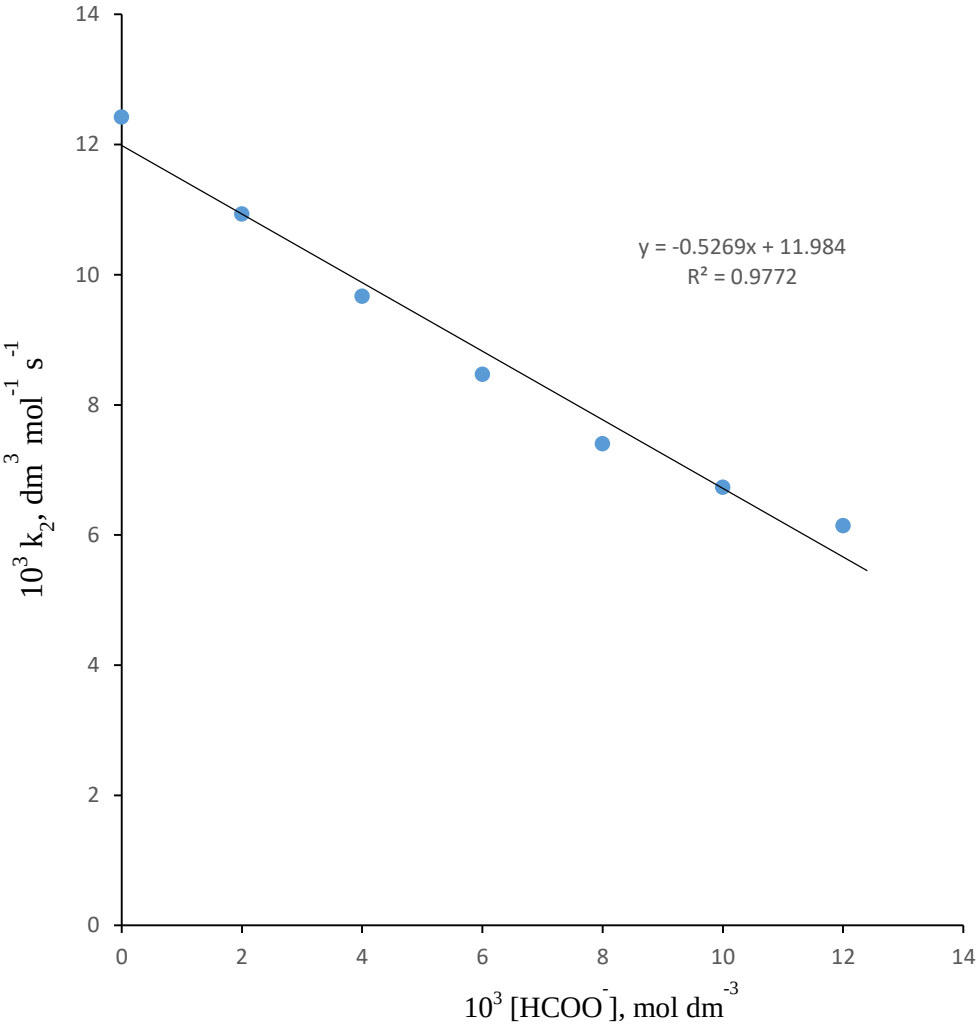


Figure 4.79: Plot of k_2 versus $[HCOO^-]$ for the redox reaction of $[Mn(salphen)]^+$ and H_2O_2 at $[Mn(salphen)^+] = 1.0 \times 10^{-4}$ mol dm^{-3}, $[H_2O_2] = 0.15$ mol dm^{-3}, $\mu = 0.2$ C^2 mol dm^{-3}, $[H^+] = 2.0 \times 10^{-5}$ mol dm^{-3}, D = 76.82, T = 30 ± 1°C and $\lambda_{max} = 450$ nm

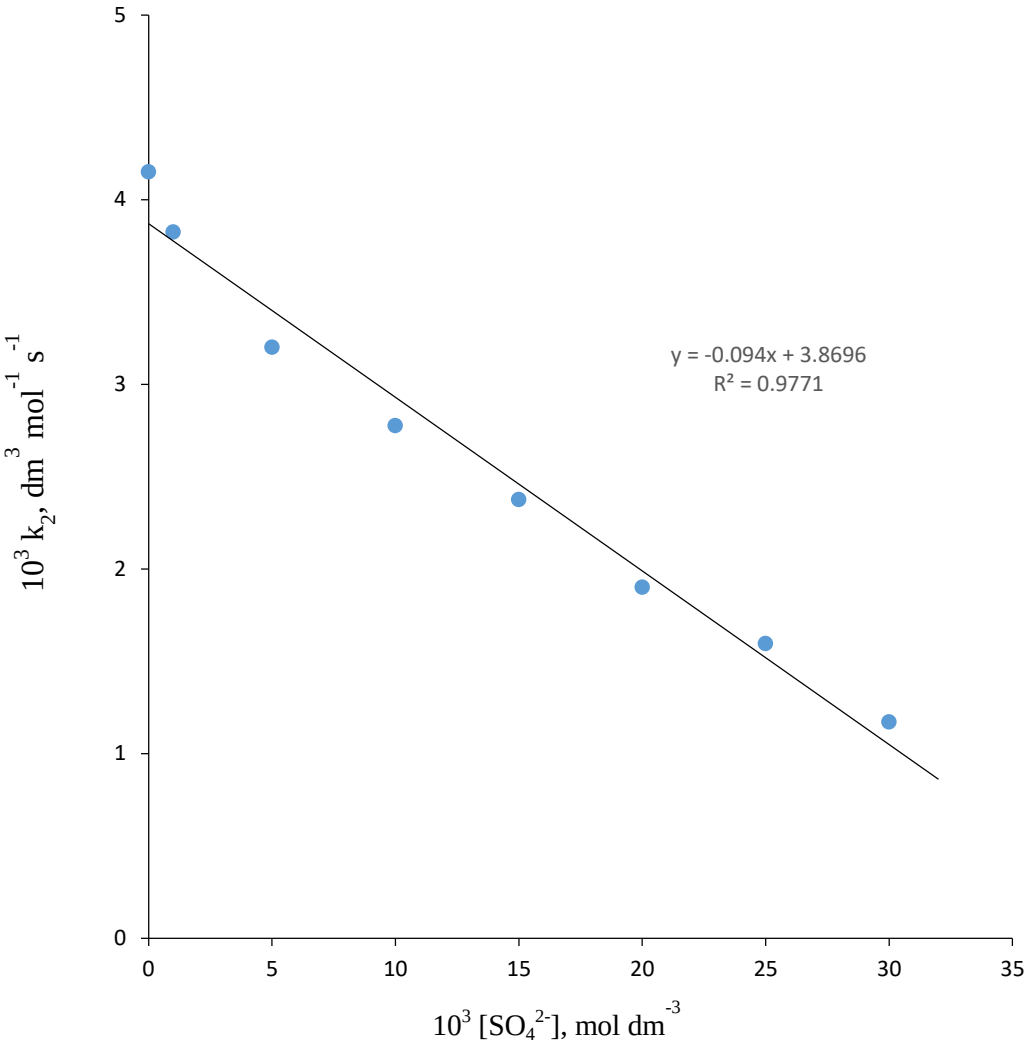


Figure 4.80: Plot of $10^3\ k_2$ versus $10^3\ [SO_4^{2-}]$ for the redox reaction of $[Mn(salphen)]^+$ and $S(CH_2CH_2OH)_2$ at $[Mn(salphen)^+] = 1.0 \times 10^{-4}$ mol dm^{-3}, $[S(CH_2CH_2OH)_2] = 0.40$ mol dm^{-3}, $\mu = 0.6\ C^2$ mol dm^{-3}, $[H^+] = 2.0 \times 10^{-5}$ mol dm^{-3}, D = 66.60, T = 50 ± 1 °C and λ_{max} = 450 nm

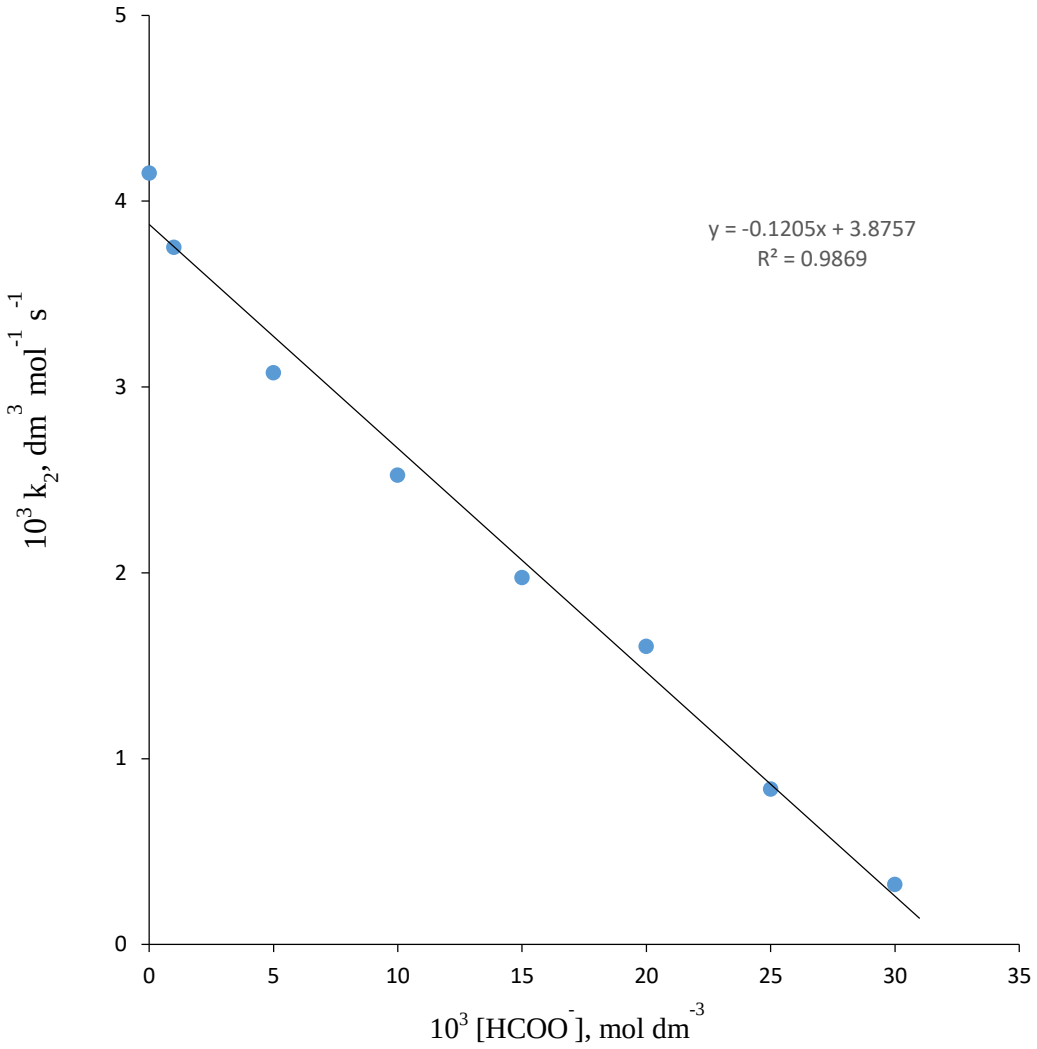


Figure 4.81: Plot of 10^3 k_2 versus 10^3 [$HCOO^-$] for the redox reaction of [Mn(salphen)]$^+$ and $S(CH_2CH_2OH)_2$ at [Mn(salphen)$^+$] = 1.0 × 10^{-4} mol dm^{-3}, [$S(CH_2CH_2OH)_2$] = 0.40 mol dm^{-3}, μ = 0.6 C^2 mol dm^{-3}, [H^+] = 2.0 × 10^{-5} mol dm^{-3}, D = 66.60, T = 50 ± 1 °C and λ_{max} = 450 nm

Table 4.45: Temperature dependent rate constants and activation parameters for the reaction of $[Fe(salphen)]^+$ and TSH at $[Fe(salphen)^+] = 2.0 \times 10^{-4}$ mol dm^{-3}, [TSH] = 0.15 mol dm^{-3}, μ = 0.2 C^2 mol dm^{-3}, D = 76.88 and λ_{max} = 435 nm

T, K	$10^3 k_1$, s^{-1}	$10^2 k_2$, dm^3 mol^{-1} s^{-1}
299	2.16	1.44
303	2.37	1.58
307	2.56	1.71
311	2.95	1.97
315	3.09	2.06

$\Delta H^{\ddagger}$ = +15.792 kJ mol^{-1}, $\Delta S^{\ddagger}$ = -227.393 J mol^{-1} K^{-1}, $\Delta G^{\ddagger}$ = +83.783 kJ mol^{-1} at 299K,

E_a = +18.344 kJ mol^{-1}

Table 4.46: Temperature dependent rate constants and activation parameters for the reaction of $[Fe(salphen)]^+$ and $H_2C_2O_4$ at $[Fe(salphen)^+] = 2.0 \times 10^{-4}$ mol dm^{-3}, $[H_2C_2O_4] = 6.0 \times 10^{-3}$ mol dm^{-3}, $\mu = 0.2$ C^2 mol dm^{-3}, D = 76.06 and λ_{max} = 435 nm

T, K	$10^3 k_1$, s^{-1}	10 k_2, dm^3 mol^{-1} s^{-1}
299	4.29	7.15
303	4.46	7.57
307	4.94	8.23
311	5.45	9.08
315	8.23	10.15
$\Delta H^{\ddagger}$ = +14.693 kJ mol^{-1},	$\Delta S^{\ddagger}$ = -198.756 J mol^{-1} K^{-1},	$\Delta G^{\ddagger}$ = +74.121 kJ mol^{-1} at 299K,
E_a = +17.224 kJ mol^{-1}		

Table 4.47: Temperature dependent rate constants and activation parameters for the reaction of $[Fe(salphen)]^+$ and H_3PO_2 at $[Fe(salphen)^+] = 2.0 \times 10^{-4}$ mol dm^{-3}, $[H_3PO_2] = 0.13$ mol dm^{-3}, $\mu = 0.2$ C^2 mol dm^{-3}, D = 76.68 and $\lambda_{max} = 435$ nm

T, K	$10^3 k_1$, s^{-1}	$10^2 k_2$, dm^3 mol^{-1} s^{-1}
299	2.90	2.23
303	3.71	2.85
307	4.17	3.21
311	5.21	4.01
315	6.93	5.33
$\Delta H^{\ddagger}$ = +38.152 kJ mol^{-1},	$\Delta S^{\ddagger}$ = -149.02 J mol^{-1} K^{-1},	$\Delta G^{\ddagger}$ = +82.71 kJ mol^{-1} at 299K,
E_a = +40.704 kJ mol^{-1}		

Table 4.48: Temperature dependent rate constants and activation parameters for the reaction of $[Fe(salphen)]^+$ and H_2O_2 at $[Fe(salphen)^+] = 1.0 \times 10^{-4}$ mol dm^{-3}, $[H_2O_2] = 0.42$ mol dm^{-3}, $[H^+] = 2.0 \times 10^{-5}$ mol dm^{-3}, $\mu = 0.6$ C^2 mol dm^{-3}, D = 78.12 and $\lambda_{max} = 435$ nm

T, K	$10^4 k_1$, s^{-1}	$10^4 k_2$, dm^3 mol^{-1} s^{-1}
301	2.15	5.12
305	3.00	7.14
307	3.59	8.55
311	4.58	10.90
315	5.70	13.57
$\Delta H^{\ddagger}$ = +52.2 kJ mol^{-1},	$\Delta S^{\ddagger}$ = -134 J mol^{-1} K^{-1},	$\Delta G^{\ddagger}$ = +92.5 kJ mol^{-1} at 301K,
E_a = +54.7 kJ mol^{-1}		

Table 4.49: Temperature dependent rate constants and activation parameters for the reaction of $[Mn(salphen)]^+$ and H_2O_2 at $[Mn(salphen)^+] = 1.0 \times 10^{-4}$ mol dm^{-3}, $[H_2O_2] = 0.15$ mol dm^{-3}, $\mu = 0.2$ C^2 mol dm^{-3}, $[H^+] = 2.0 \times 10^{-5}$ mol dm^{-3}, D = 76.82 and λ_{max} = 450 nm

T, K	$10^3 k_1$, s^{-1}	$10^2 k_2$, dm^3 mol^{-1} s^{-1}
303	1.87	1.25
307	2.20	1.47
309	2.46	1.64
311	2.76	1.84
315	3.16	2.12

$\Delta H^{\ddagger}$ = +33.36 kJ mol^{-1}, $\Delta S^{\ddagger}$ = -171.43 J mol^{-1} K^{-1}, $\Delta G^{\ddagger}$ = +85.30 kJ mol^{-1} at 303K,

E_a = +35.88 kJ mol^{-1}

Table 4.50: Temperature dependent rate constants and activation parameters for the reaction of $[Mn(salphen)]^+$ and TSH at $[Mn(salphen)^+] = 1.0 \times 10^{-4}$ mol dm^{-3}, [TSH] = 0.42 mol dm^{-3}, μ = 0.6 C^2 mol dm^{-3}, D = 77.98 and λ_{max} = 450 nm

T, K	$10^4 k_1$, s^{-1}	$10^3 k_2$, dm^3 mol^{-1} s^{-1}
305	6.87	1.64
308	9.14	2.18
311	10.25	2.44
315	12.52	2.98
318	14.23	3.39
$\Delta H^{\ddagger}$ = +40.58 kJ mol^{-1},	$\Delta S^{\ddagger}$ = -164.40 J mol^{-1} K^{-1},	$\Delta G^{\ddagger}$ = +90.72 kJ mol^{-1} at 305K,
E_a = +43.12 kJ mol^{-1}		

Table 4.51: Temperature dependent rate constants and activation parameters for the reaction of $[Mn(salphen)]^+$ and RSH at $[Mn(salphen)^+] = 1.0 \times 10^{-4}$ mol dm^{-3}, [RSH] = 0.40 mol dm^{-3}, μ = 0.6 C^2 mol dm^{-3}, $[H^+] = 4.0 \times 10^{-5}$ mol dm^{-3}, D = 78.19 and λ_{max} = 450 nm

T, K	$10^3 k_1$, s^{-1}	$10^2 k_2$, dm^3 mol^{-1} s^{-1}
301	5.07	1.27
303	5.57	1.39
307	6.15	1.54
311	7.35	1.84
315	8.24	2.06
$\Delta H^{\ddagger}$ = +24.3 kJ mol^{-1},	$\Delta S^{\ddagger}$ = -200.5 J mol^{-1} K^{-1},	$\Delta G^{\ddagger}$ = +84.7 kJ mol^{-1} at 301K,
E_a = +26.8 kJ mol^{-1}		

Table 4.52: Temperature dependent rate constants and activation parameters for the reaction of $[Mn(salphen)]^+$ and SCN^- at $[Mn(salphen)^+] = 1.0 \times 10^{-4}$ mol dm^{-3}, $[SCN^-] = 0.42$ mol dm^{-3}, $\mu = 0.6$ C^2 mol dm^{-3}, $[H^+] = 4.0 \times 10^{-5}$ mol dm^{-3}, D = 78.12 and λ_{max} = 450 nm

T, K	10^4 k_1, s^{-1}	10^3 k_2, dm^3 mol^{-1} s^{-1}
301	6.47	1.54
303	7.65	1.82
307	8.81	2.10
311	10.36	2.47
315	12.46	2.97
$\Delta H^{\ddagger}$ = +32.4 kJ mol^{-1},	$\Delta S^{\ddagger}$ = -191 J mol^{-1} K^{-1},	$\Delta G^{\ddagger}$ = +90 kJ mol^{-1} at 301K,
E_a = +34.9 kJ mol^{-1}		

Table 4.53: Temperature dependent rate constants and activation parameters for the reaction of $[Mn(salphen)]^+$ and $H_2NNHCSNH_2$ at $[Mn(salphen)^+] = 1.0 \times 10^{-4}$ mol dm^{-3}, $[H_2NNHCSNH_2] = 0.28$ mol dm^{-3}, $\mu = 0.6$ C^2 mol dm^{-3}, $[H^+] = 2.0 \times 10^{-5}$ mol dm^{-3}, D = 75.10 and $\lambda_{max} = 450$ nm

T, K	$10^4 k_1$, s^{-1}	$10^3 k_2$, $dm^3 mol^{-1} s^{-1}$
301	11.33	4.05
305	14.85	5.30
309	17.80	6.36
313	21.44	7.66
317	24.90	8.89
$\Delta H^{\ddagger}$ = +36.00 kJ mol^{-1},	$\Delta S^{\ddagger}$ = -170.89 J mol^{-1} K^{-1},	$\Delta G^{\ddagger}$ = +87.44 kJ mol^{-1} at 299K,
E_a = +38.45 kJ mol^{-1}		

Table 4.54: Temperature dependent rate constants and activation parameters for the reaction of $[Mn(salphen)]^+$ and $S(CH_2CH_2OH)_2$ at $[Mn(salphen)^+] = 1.0 \times 10^{-4}$ mol dm^{-3}, $[S(CH_2CH_2OH)_2] = 0.40$ mol dm^{-3}, $\mu = 0.6$ C^2 mol dm^{-3}, $[H^+] = 2.0 \times 10^{-5}$ mol dm^{-3}, D = 66.60 and $\lambda_{max} = 450$ nm

T, K	$10^4 k_1$, s^{-1}	$10^3 k_2$, $dm^3 mol^{-1} s^{-1}$
308	6.70	1.68
313	7.88	1.97
318	10.82	2.71
323	16.60	4.15
328	22.00	5.50
$\Delta H^{\ddagger}$ = +49.00 kJ mol^{-1},	$\Delta S^{\ddagger}$ = -137.6 J mol^{-1} K^{-1},	$\Delta G^{\ddagger}$ = +94.14 kJ mol^{-1} at 323K,
E_a = +52.39 kJ mol^{-1}		

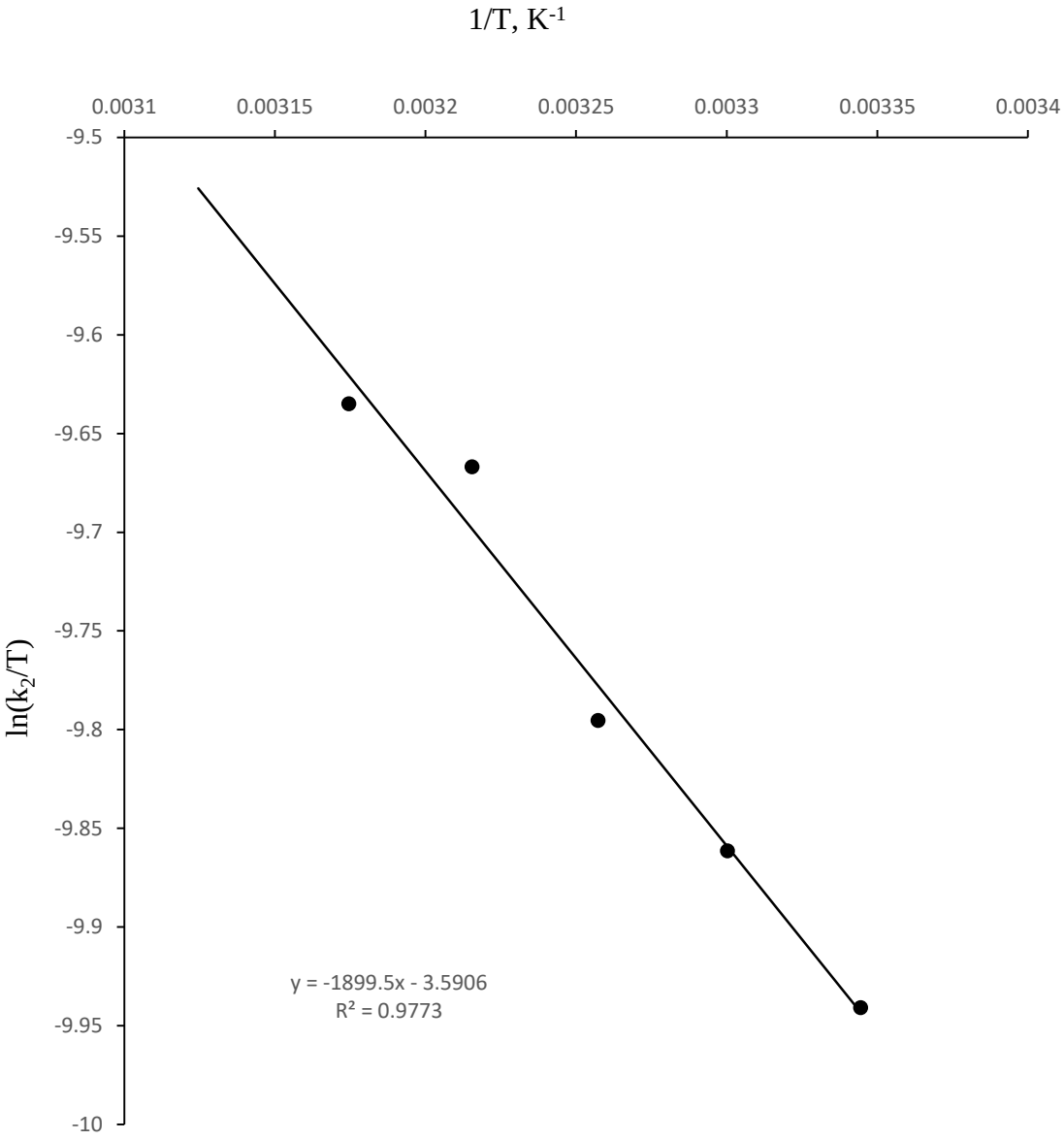


Figure 4.82: Plot of $\ln\left(\frac{k_2}{T}\right)$ versus $\left(\frac{1}{T}\right)$ for the reaction of $[Fe(salphen)]^+$ and TSH at $[Fe(salphen)^+] = 2.0 \times 10^{-4}$ mol dm^{-3}, [TSH] = 0.15 mol dm^{-3}, μ = 0.2 C^2 mol dm^{-3}, D = 76.88 and λ_{max} = 435 nm

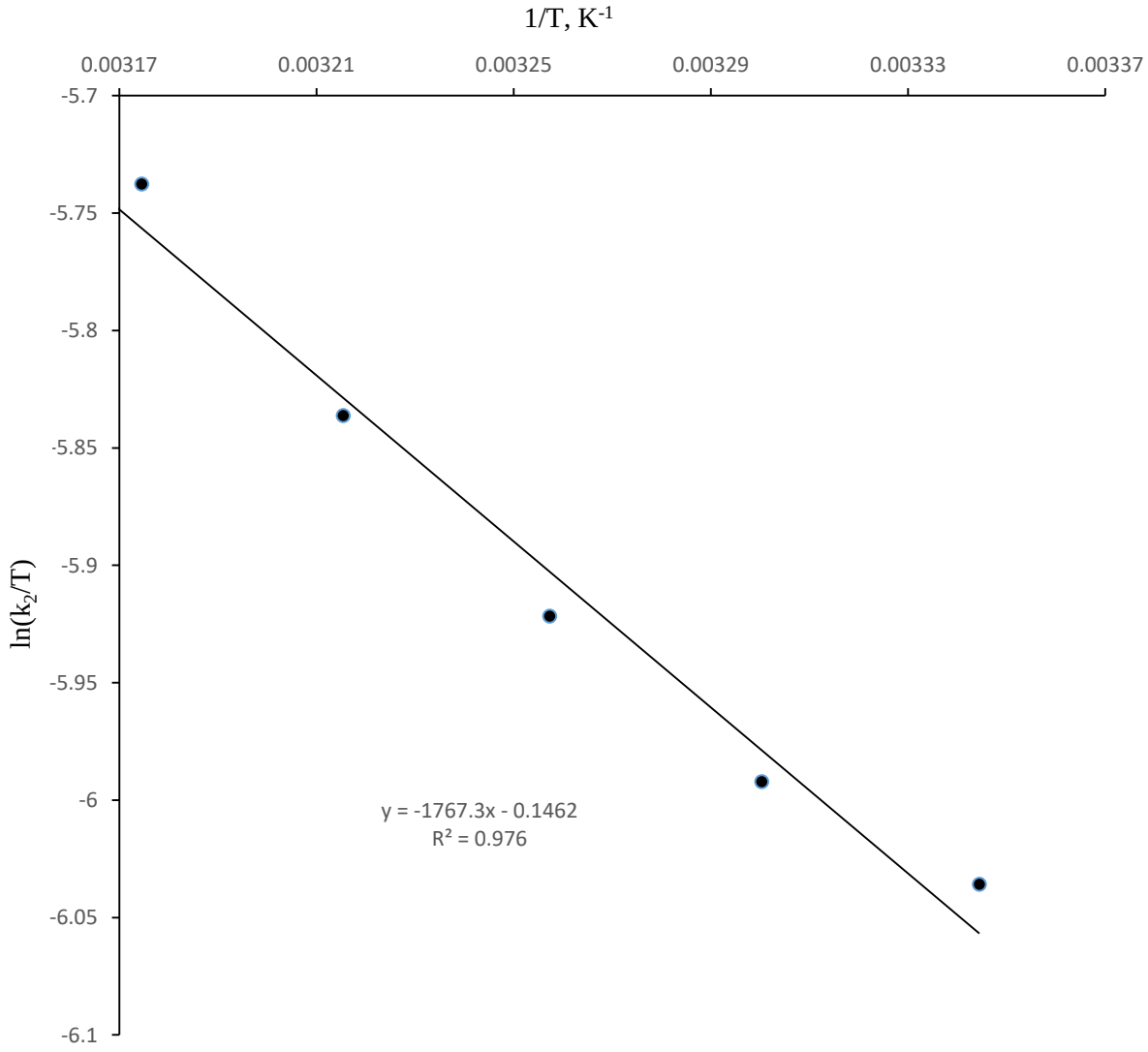


Figure 4.83: Plot of $\ln\left(\frac{k_2}{T}\right)$ versus $\left(\frac{1}{T}\right)$ for the reaction of $[Fe(salphen)]^+$ and $H_2C_2O_4$ at $[Fe(salphen)^+] = 2.0 \times 10^{-4}$ mol dm^{-3}, $[H_2C_2O_4] = 6.0 \times 10^{-3}$ mol dm^{-3}, μ = 0.2 C^2 mol dm^{-3}, D = 76.06 and λ_{max} = 435 nm

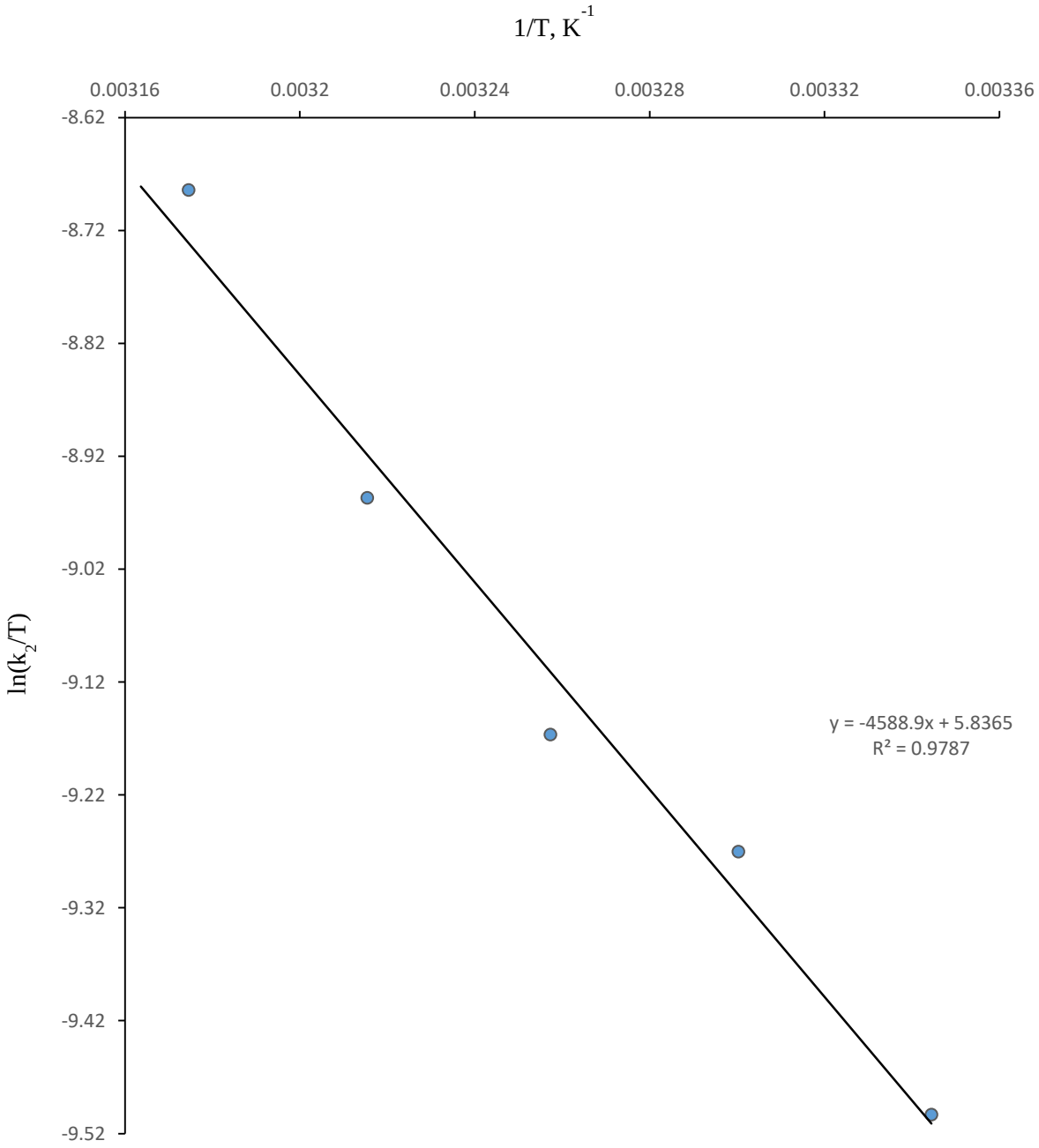


Figure 4.84: Plot of $\ln\left(\frac{k_2}{T}\right)$ versus $\left(\frac{1}{T}\right)$ for the reaction of $[Fe(salphen)]^+$ and H_3PO_2 at $[Fe(salphen)^+] = 2.0 \times 10^{-4}$ mol dm^{-3}, $[H_3PO_2] = 0.13$ mol dm^{-3}, $\mu = 0.2$ C^2 mol dm^{-3}, D = 76.68 and $\lambda_{max} = 435$ nm

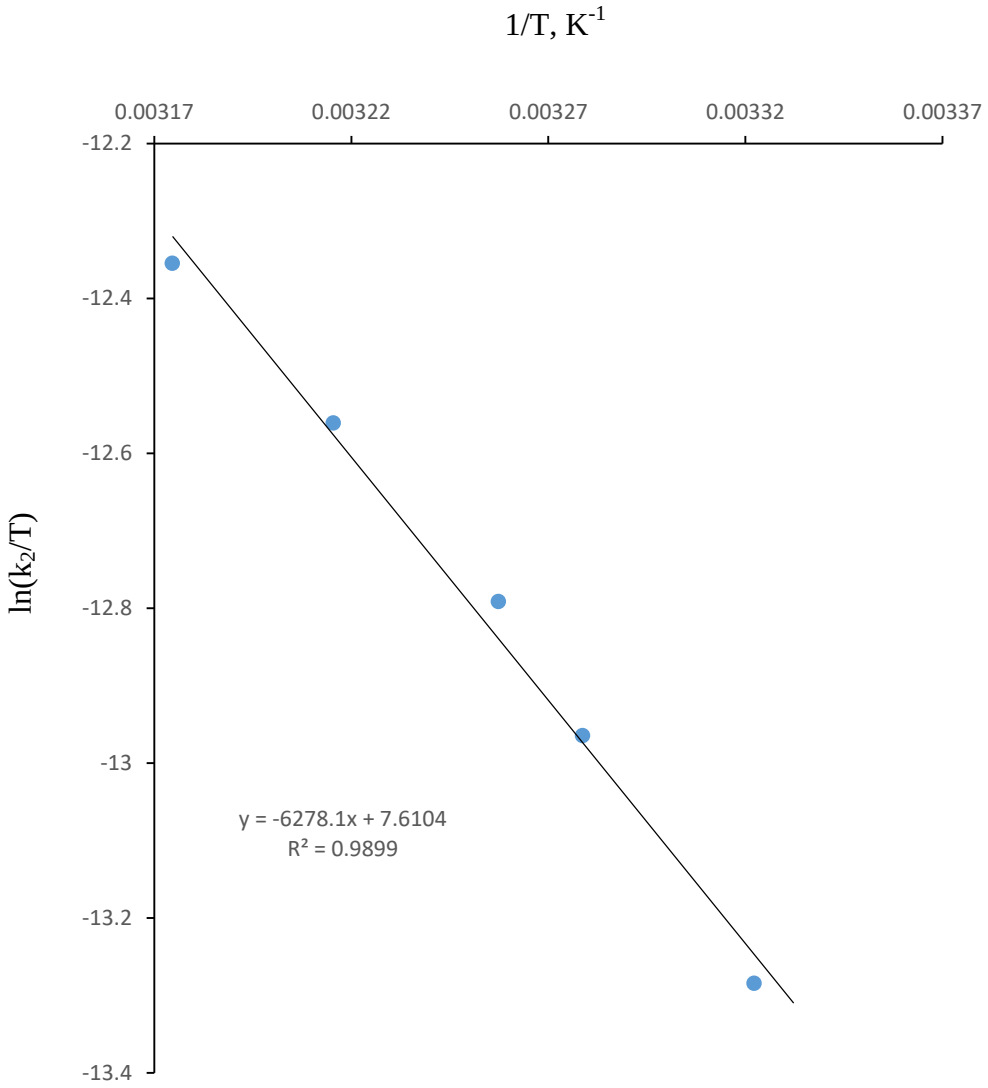


Figure 4.85: Plot of $\ln\left(\frac{k_2}{T}\right)$ versus $\left(\frac{1}{T}\right)$ for the reaction of $[Fe(salphen)]^+$ and H_2O_2 at $[Fe(salphen)^+] = 1.0 \times 10^{-4}$ mol dm^{-3}, $[H_2O_2] = 0.42$ mol dm^{-3}, $[H^+] = 2.0 \times 10^{-5}$ mol dm^{-3}, $\mu = 0.6$ C^2 mol dm^{-3}, D = 78.12 and $\lambda_{max} = 435$ nm

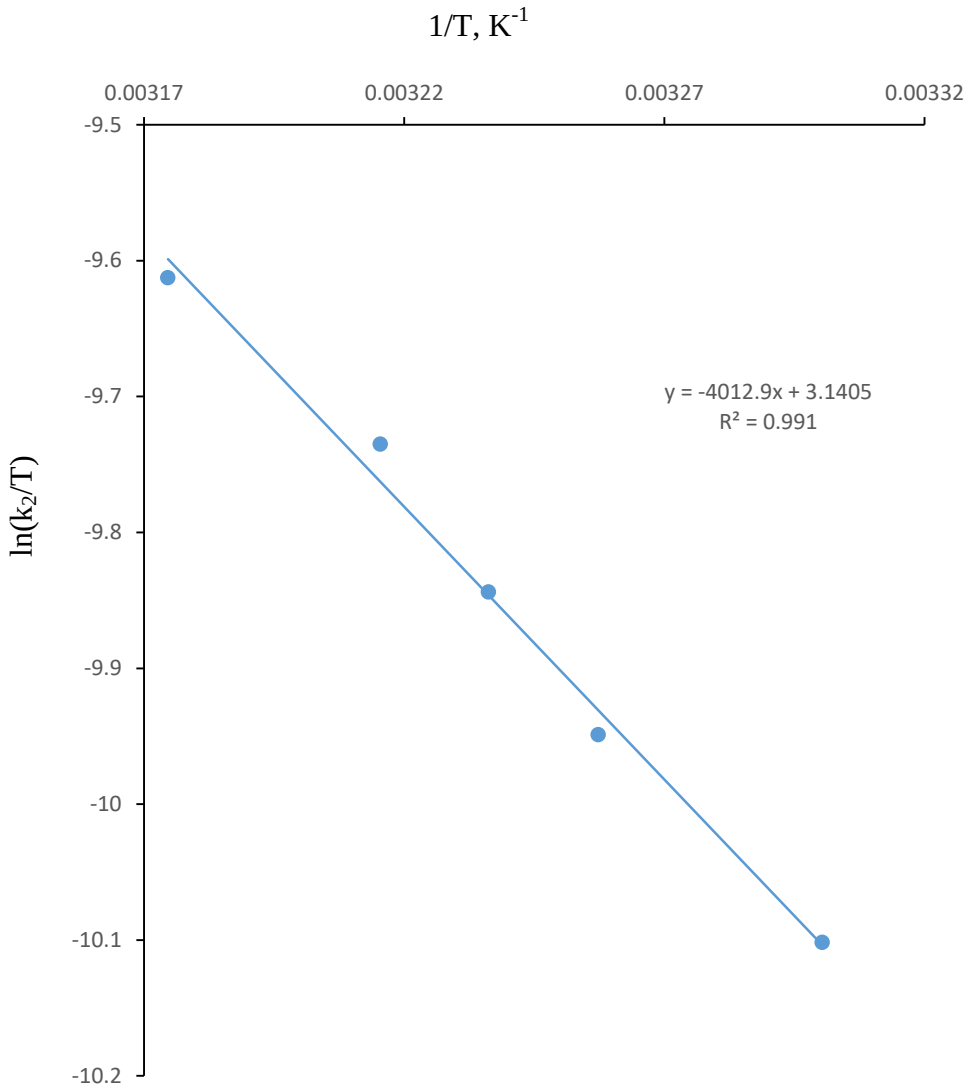


Figure 4.86: Plot of $\ln\left(\frac{k_2}{T}\right)$ versus $\left(\frac{1}{T}\right)$ for the reaction of $[Mn(salphen)]^+$ and H_2O_2 at $[Mn(salphen)^+] = 1.0 \times 10^{-4}$ mol dm^{-3}, $[H_2O_2] = 0.15$ mol dm^{-3}, $\mu = 0.2$ C^2 mol dm^{-3}, D = 76.82 and $\lambda_{max} = 450$ nm

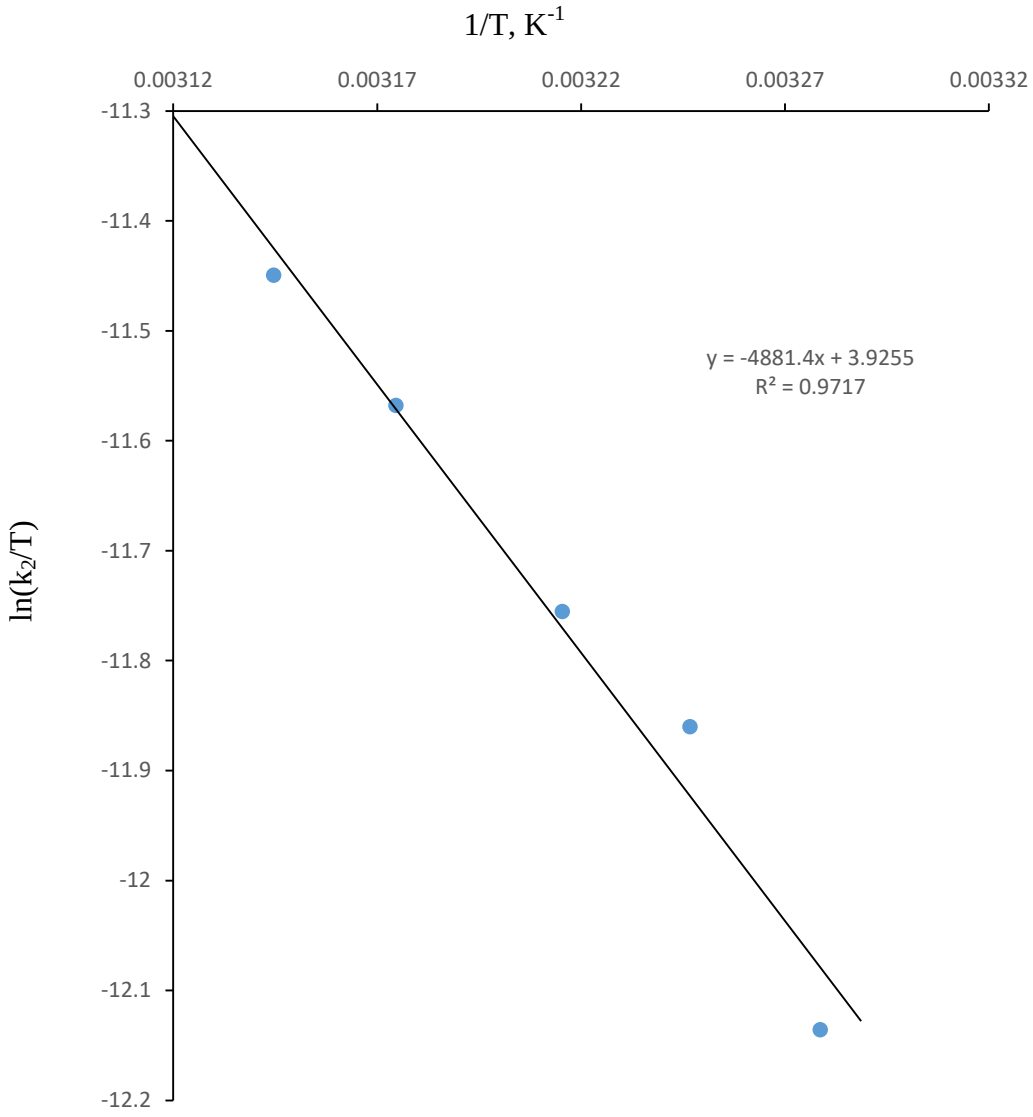


Figure 4.87: Plot of $\ln\left(\frac{k_2}{T}\right)$ versus $\left(\frac{1}{T}\right)$ for the reaction of $[Mn(salphen)]^+$ and TSH at $[Mn(salphen)^+] = 1.0 \times 10^{-4}$ mol dm^{-3}, [TSH] = 0.42 mol dm^{-3}, μ = 0.6 C^2 mol dm^{-3}, D = 77.98 and λ_{max} = 450 nm

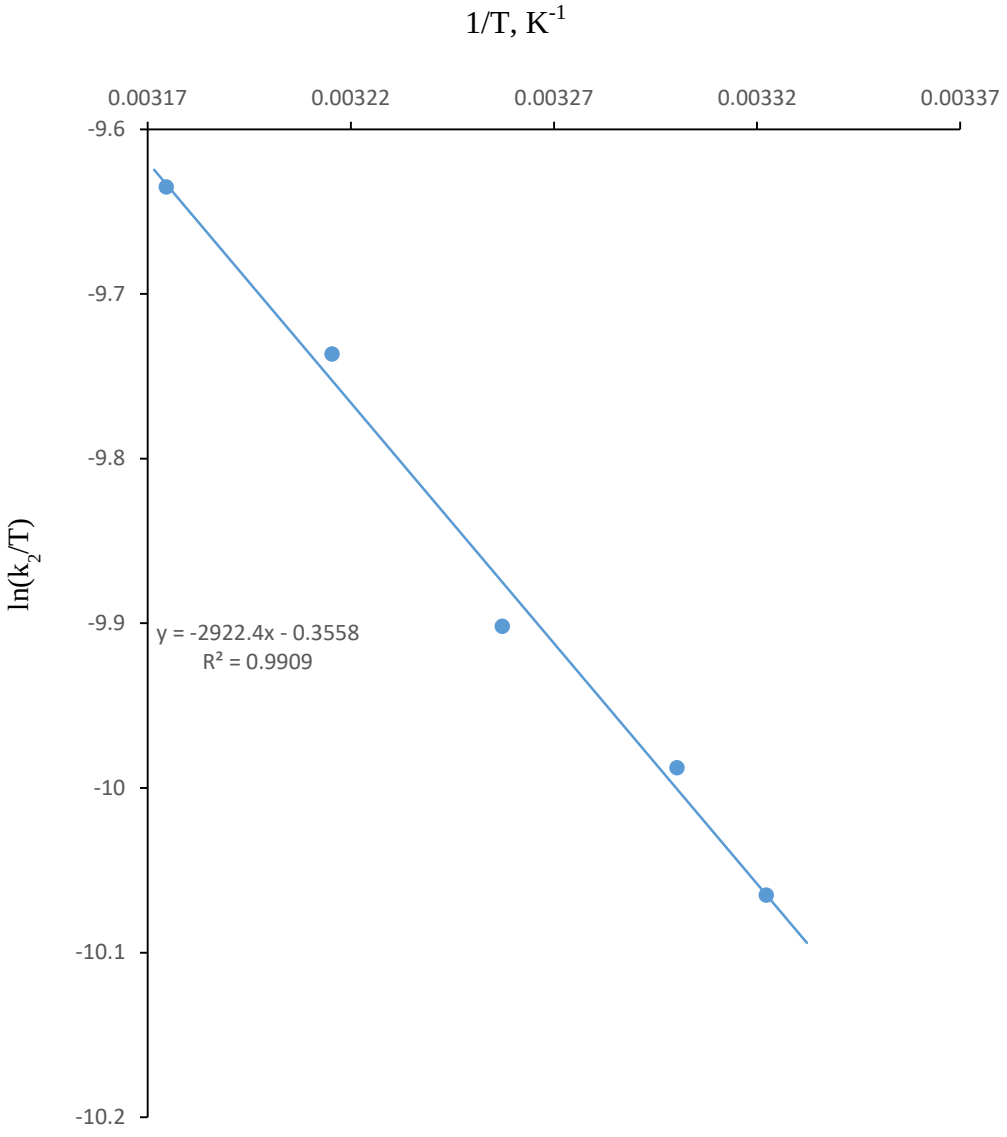


Figure 4.88: **Plot of $\ln\left(\frac{k_2}{T}\right)$ versus $\left(\frac{1}{T}\right)$ for the reaction of $[Mn(salphen)]^+$ and RSH at $[Mn(salphen)^+] = 1.0 \times 10^{-4}$ mol dm^{-3}, [RSH] = 0.40 mol dm^{-3}, μ = 0.6 C^2 mol dm^{-3}, D = 78.19 and λ_{max} = 450 nm**

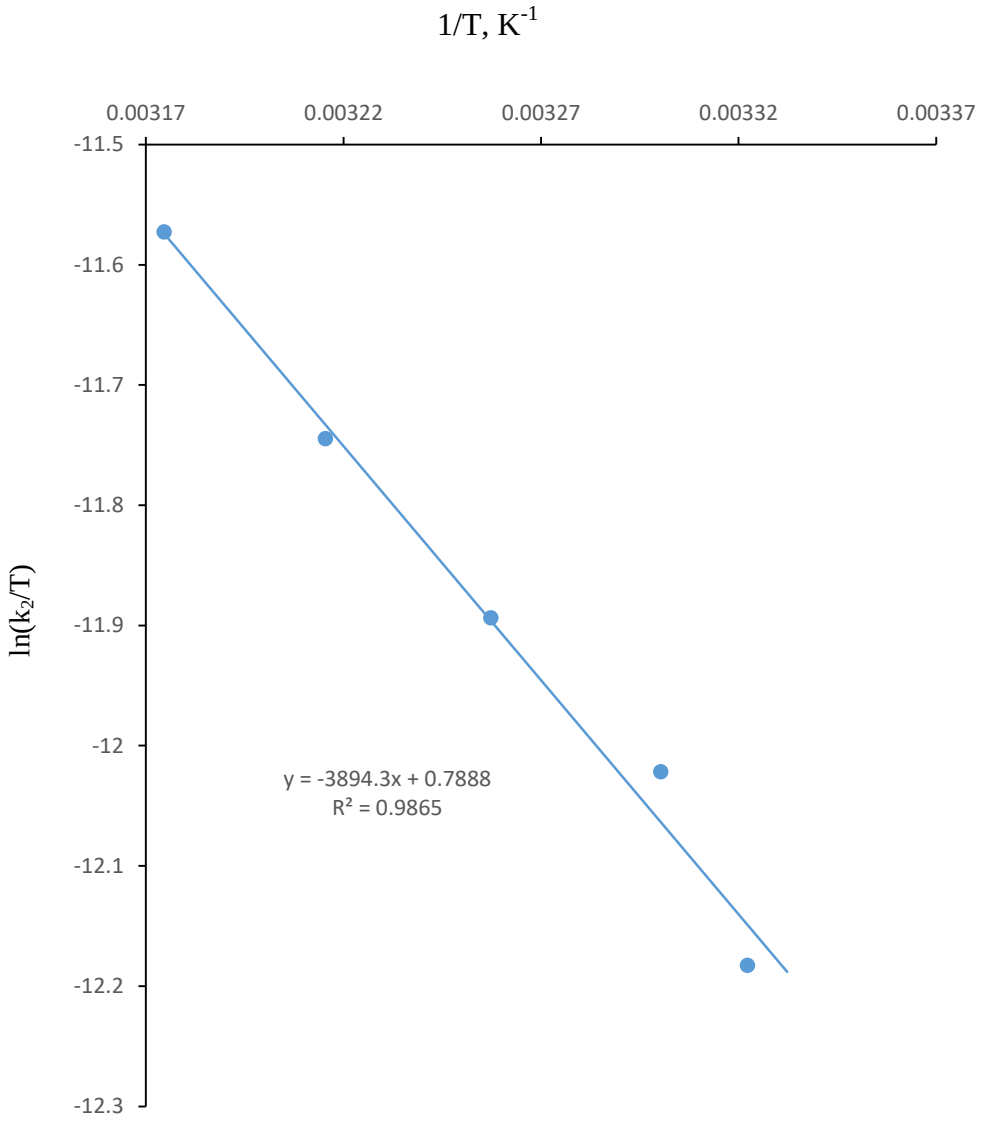


Figure 4.89: Plot of $\ln\left(\frac{k_2}{T}\right)$ versus $\left(\frac{1}{T}\right)$ for the reaction of $[Mn(salphen)]^+$ and SCN^- at $[Mn(salphen)^+] = 1.0 \times 10^{-4}$ mol dm^{-3}, $[SCN^-] = 0.42$ mol dm^{-3}, $\mu = 0.6$ C^2 mol dm^{-3}, D = 78.12 and $\lambda_{max} = 450$ nm

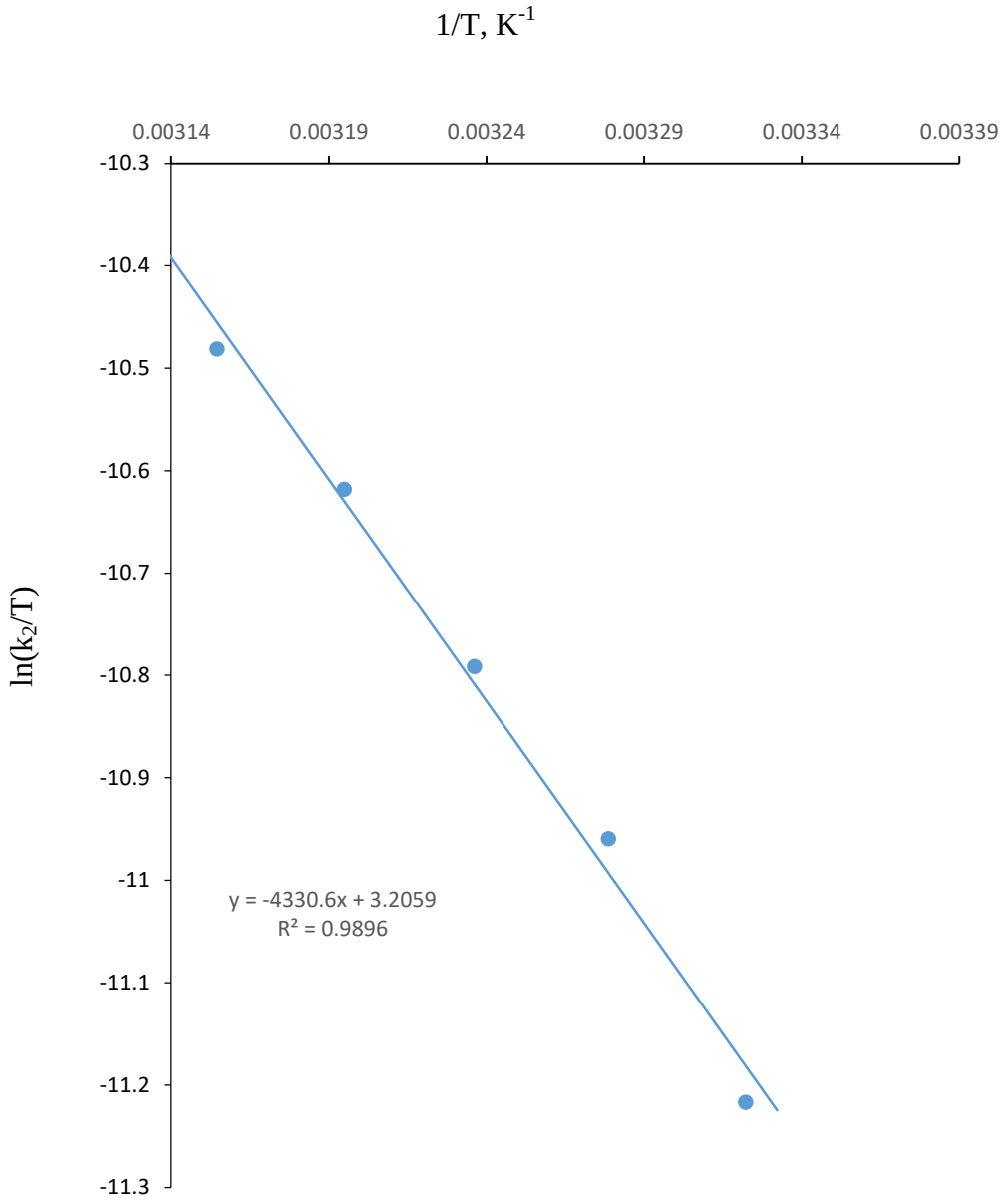


Figure 4.90: Plot of $\ln\left(\frac{k_2}{T}\right)$ versus $\left(\frac{1}{T}\right)$ for the reaction of $[Mn(salphen)]^+$ and $H_2NNHCSNH_2$ at $[Mn(salphen)^+] = 1.0 \times 10^{-4}$ mol dm^{-3}, $[H_2NNHCSNH_2] = 0.28$ mol dm^{-3}, $\mu = 0.6$ C^2 mol dm^{-3}, D = 75.10 and $\lambda_{max} = 450$ nm

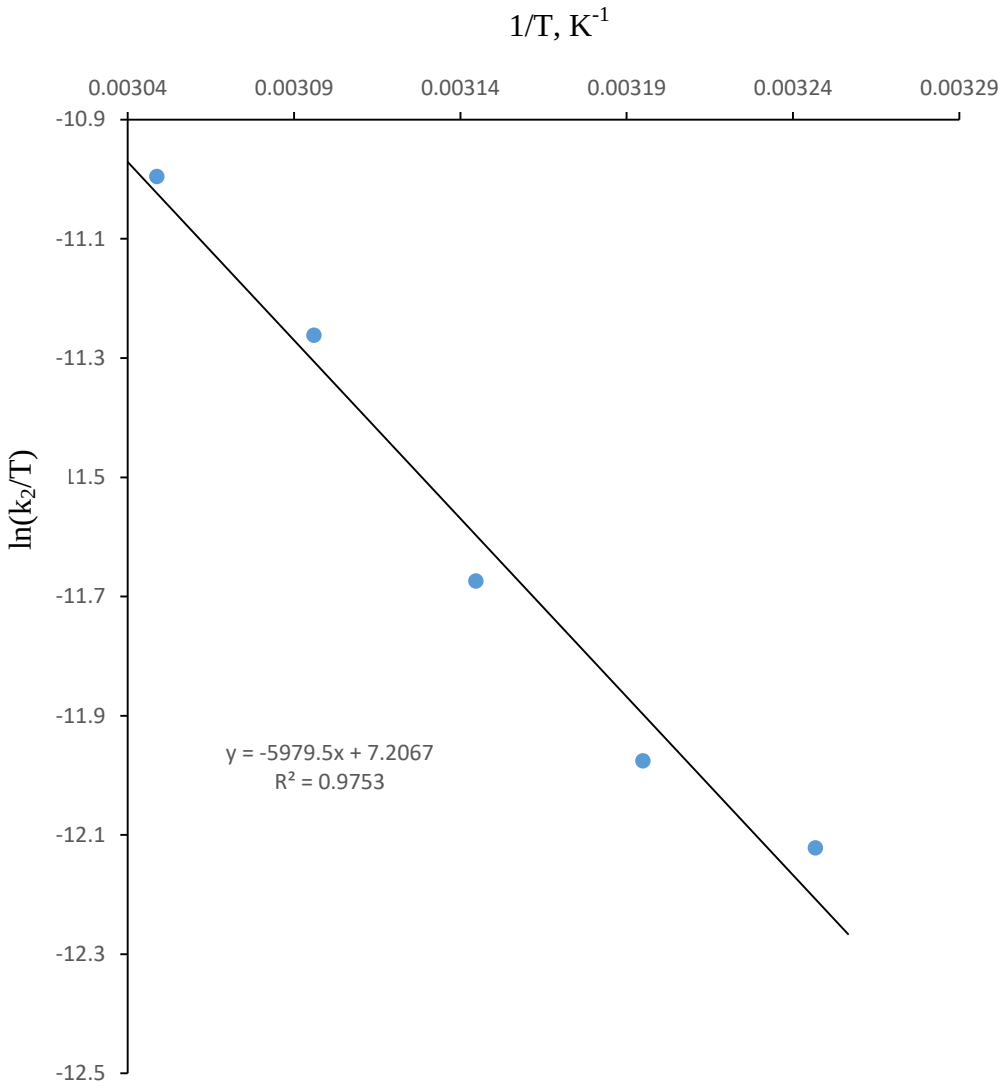


Figure 4.91: Plot of $\ln\left(\frac{k_2}{T}\right)$ versus $\left(\frac{1}{T}\right)$ for the reaction of $[Mn(salphen)]^+$ and $S(CH_2CH_2OH)_2$ at $[Mn(salphen)^+] = 1.0 \times 10^{-4}$ mol dm^{-3}, $[S(CH_2CH_2OH)_2] = 0.40$ mol dm^{-3}, $\mu = 0.6$ C^2 mol dm^{-3}, $[H^+] = 2.0 \times 10^{-5}$ mol dm^{-3}, D = 66.60 and λ_{max} = 450 nm

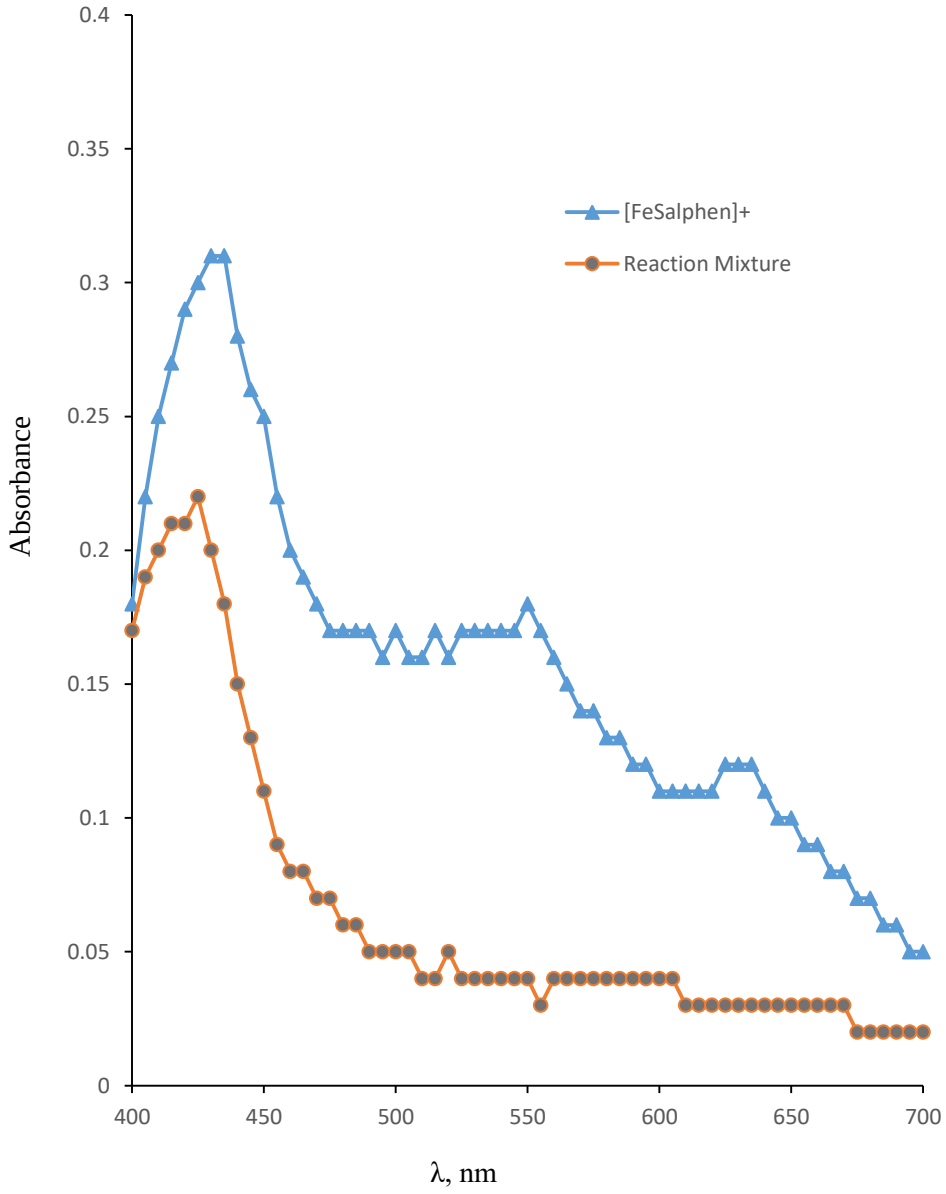


Figure 4.92: Plot for spectrophotometric test for the redox reaction of Fe(salphen)]$^{+}$ and TSH at [Fe(salphen)$^{+}$] = 2.0 × 10^{-4} mol dm^{-3}, [TSH] = 0.15 mol dm^{-3}, μ = 0.2 C^{2} mol dm^{-3}, D = 76.88, T = 26 ± 1°C and λ_{max} = 435 nm

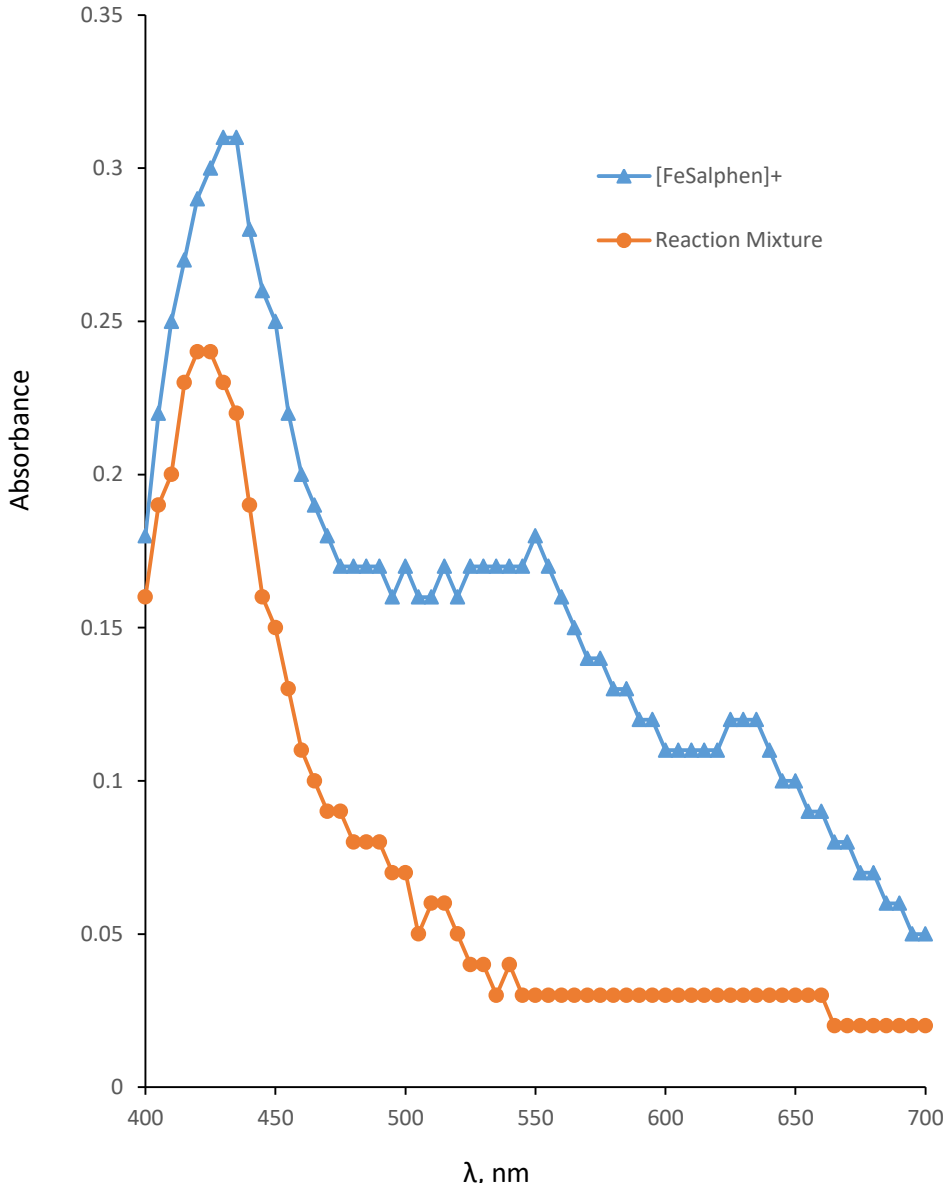


Figure 4.93: Plot for spectrophotometric test for the redox reaction of $Fe(salphen)]^{+}$ and $H_2C_2O_4$ at $[Fe(salphen)^{+}] = 2.0 \times 10^{-4}$ mol dm^{-3}, $[H_2C_2O_4] = 6.0 \times 10^{-3}$ mol dm^{-3}, $\mu = 0.2$ C^2 mol dm^{-3}, D = 76.06, T = 26 ± 1°C and λ_{max} = 435 nm

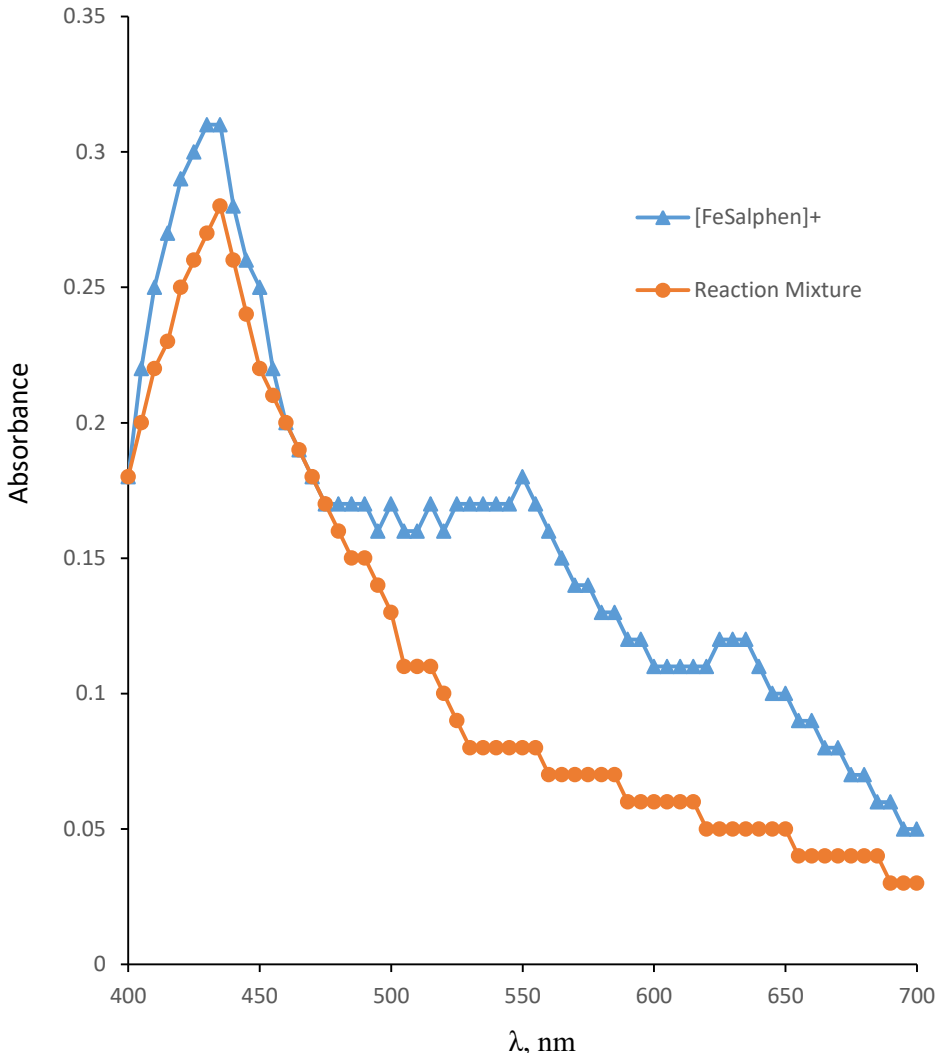


Figure 4.94: Plot for spectrophotometric test for the redox reaction of $[Fe(salphen)]^{+}$ and H_3PO_2 at $[Fe(salphen)^{+}] = 2.0 \times 10^{-4}$ mol dm^{-3}, $[H_3PO_2]$ = 0.13 mol dm^{-3}, μ = 0.2 C^2 mol dm^{-3}, D = 76.68, T = 26 ± 1°C and λ_{max} = 435 nm

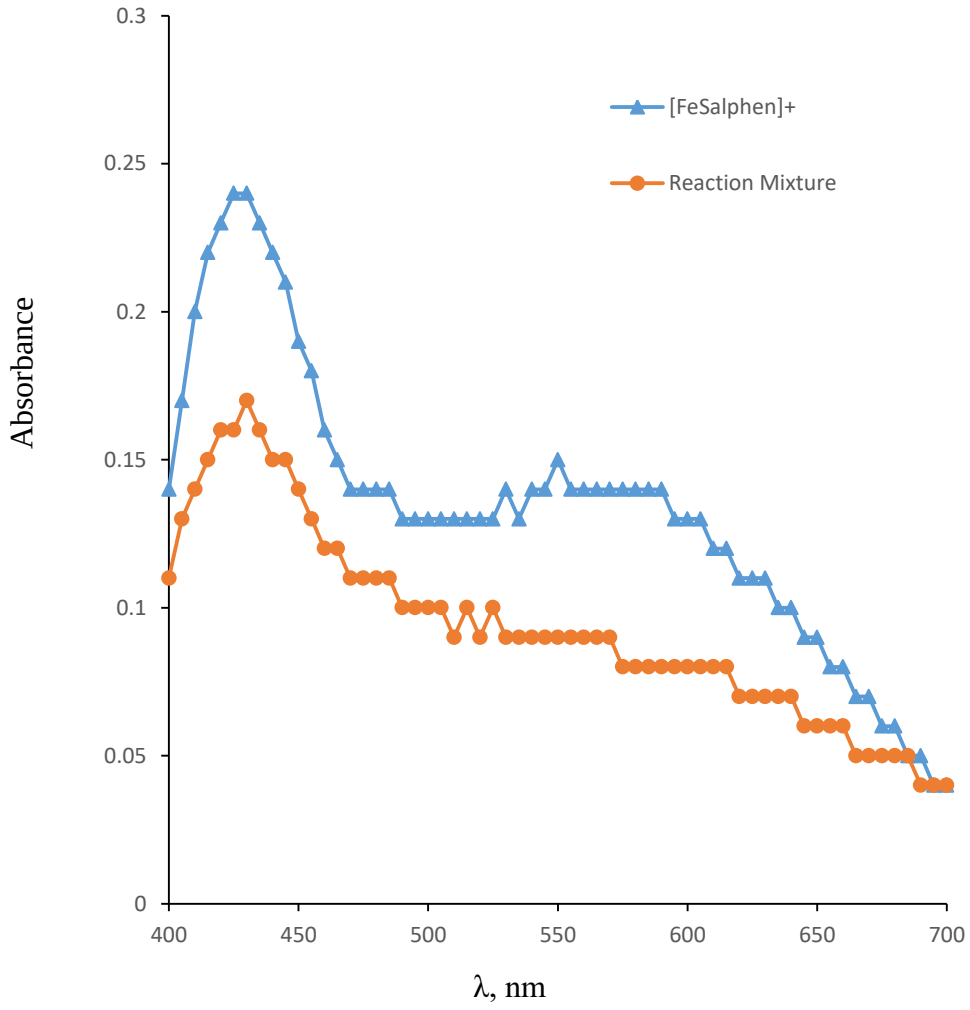


Figure 4.95: Plot for spectrophotometric test for the redox reaction of $[Fe(salphen)]^{+}$ and H_2O_2 at $[Fe(salphen)^{+}] = 1.0 \times 10^{-4}$ mol dm^{-3}, $[H_2O_2]$ = 0.42 mol dm^{-3}, $\mu = 0.6$ C^2 mol dm^{-3}, $[H^{+}] = 2.0 \times 10^{-5}$ mol dm^{-3}, D = 78.12, T = 28 ± 1°C and λ_{max} = 435 nm

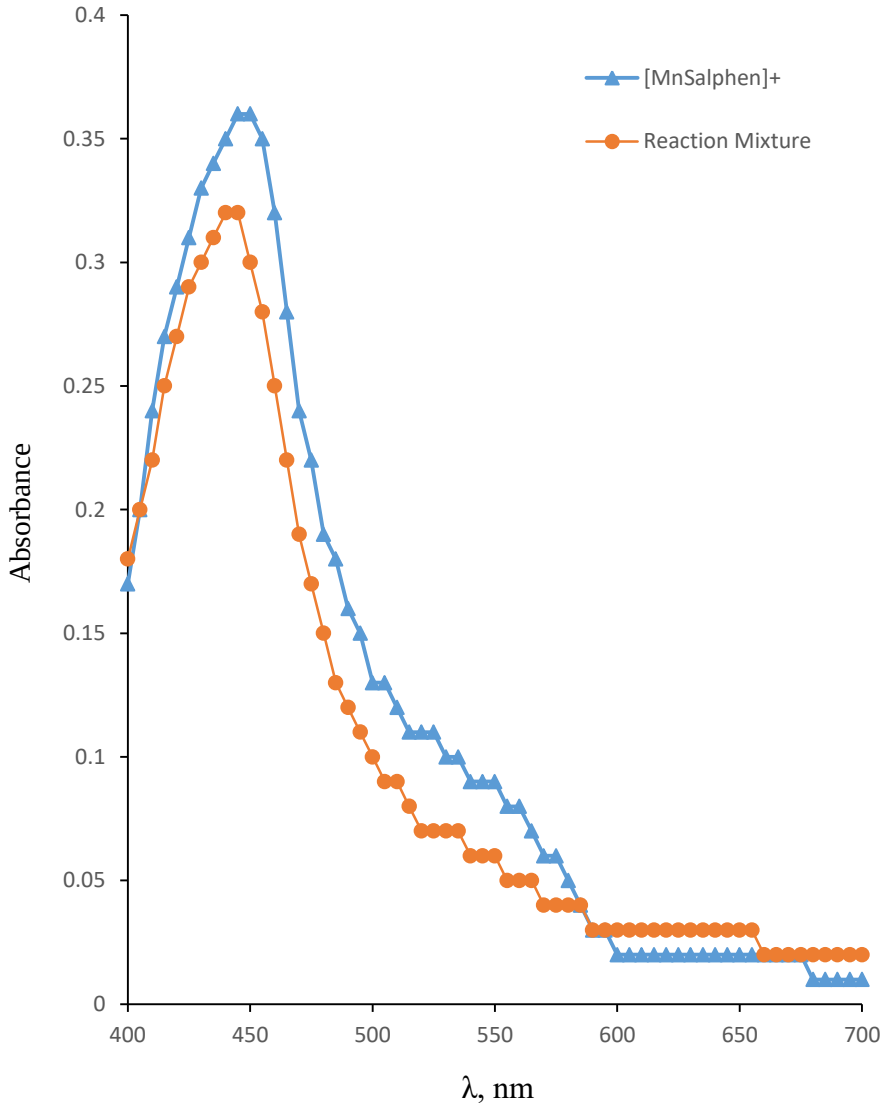


Figure 4.96: Plot for spectrophotometric test for the redox reaction of $[Mn(salphen)]^{+}$ and H_2O_2 at $[Mn(salphen)^{+}] = 1.0 \times 10^{-4}$ mol dm^{-3}, $[H_2O_2] = 0.15$ mol dm^{-3}, $\mu = 0.2$ C^2 mol dm^{-3}, $[H^{+}] = 2.0 \times 10^{-5}$ mol dm^{-3}, D = 76.82, T = 30 ± 1 °C and λ_{max} = 450 nm

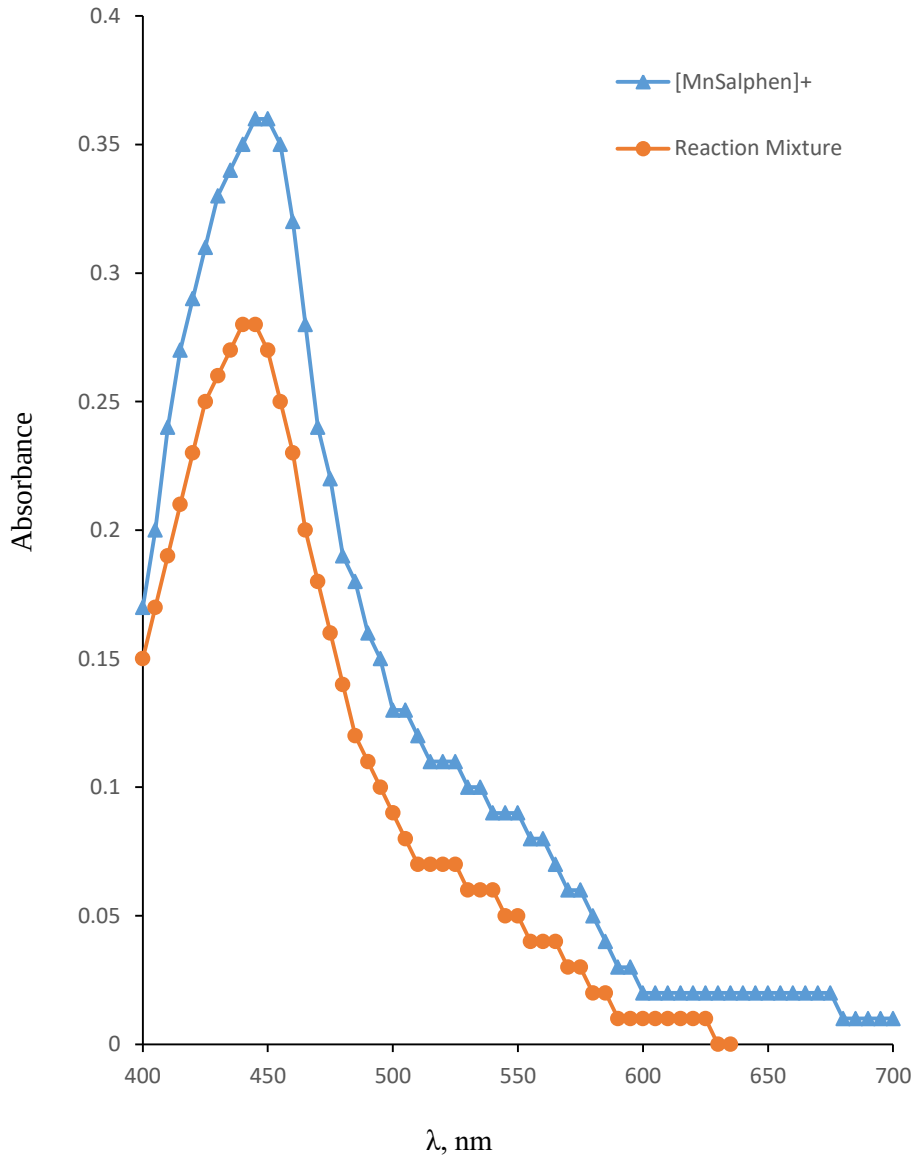


Figure 4.97: Plot for spectrophotometric test for the redox reaction of $[Mn(salphen)]^{+}$ and TSH at $[Mn(salphen)^{+}] = 1.0 \times 10^{-4}$ mol dm^{-3}, [TSH] = 0.42 mol dm^{-3}, $\mu = 0.6\ C^2$ mol dm^{-3}, D = 77.98, T = 32 ± 1°C and λ_{max} = 450 nm

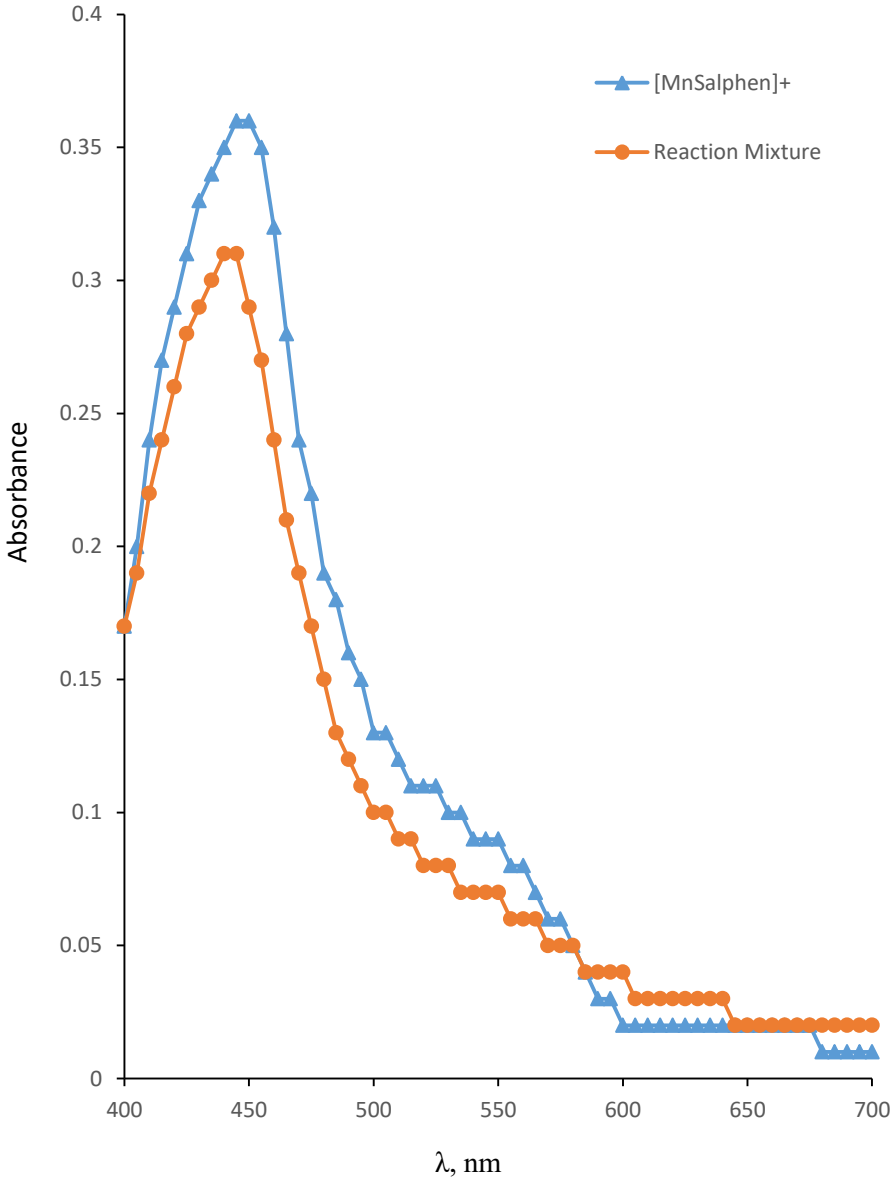


Figure 4.98: Plot for spectrophotometric test for the redox reaction of $[Mn(salphen)]^{+}$ and SCN^{-} at $[Mn(salphen)^{+}] = 1.0 \times 10^{-4}$ mol dm^{-3}, $[SCN^{-}] = 0.42$ mol dm^{-3}, $\mu = 0.6$ C^2 mol dm^{-3}, $[H^{+}] = 4.0 \times 10^{-5}$ mol dm^{-3}, D = 78.12, T = 28 ± 1 °C and λ_{max} = 450 nm

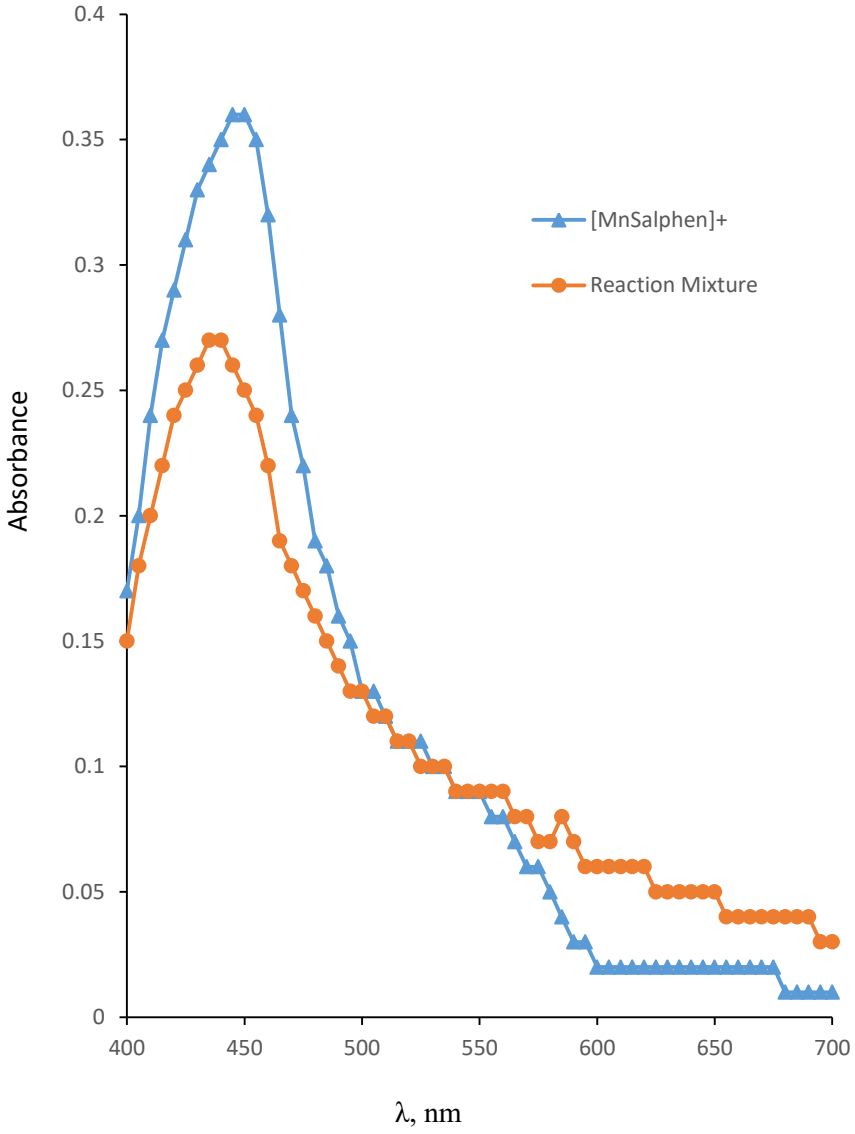


Figure 4.99: Plot for spectrophotometric test for the redox reaction of $[Mn(salphen)]^{+}$ and $H_2NNHCSNH_2$ at $[Mn(salphen)^{+}] = 1.0 \times 10^{-4}$ mol dm^{-3}, $[H_2NNHCSNH_2] = 0.28$ mol dm^{-3}, $\mu = 0.6$ C^2 mol dm^{-3}, $[H^{+}] = 2.0 \times 10^{-5}$ mol dm^{-3}, D = 75.10, T = 28 ± 1°C and λ_{max} = 450 nm

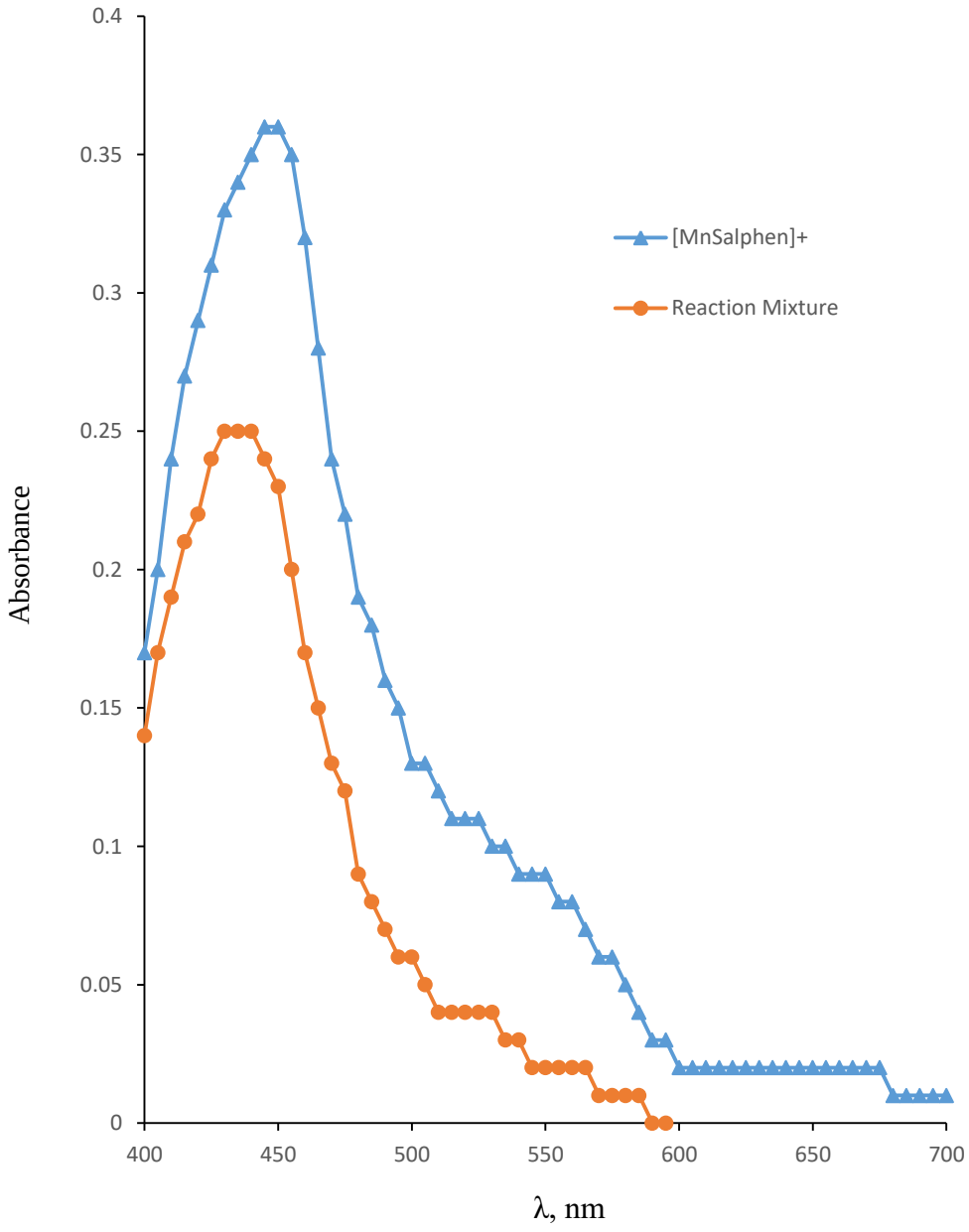


Figure 4.100: Plot for spectrophotometric test for the redox reaction of $[Mn(salphen)]^{+}$ and $S(CH_2CH_2OH)_2$ at $[Mn(salphen)^{+}] = 1.0 \times 10^{-4}$ mol dm^{-3}, $[S(CH_2CH_2OH)_2] = 0.40$ mol dm^{-3}, $\mu = 0.6$ C^2 mol dm^{-3}, $[H^{+}] = 2.0 \times 10^{-5}$ mol dm^{-3}, D = 66.60, T = 50 ± 1°C and λ_{max} = 450 nm

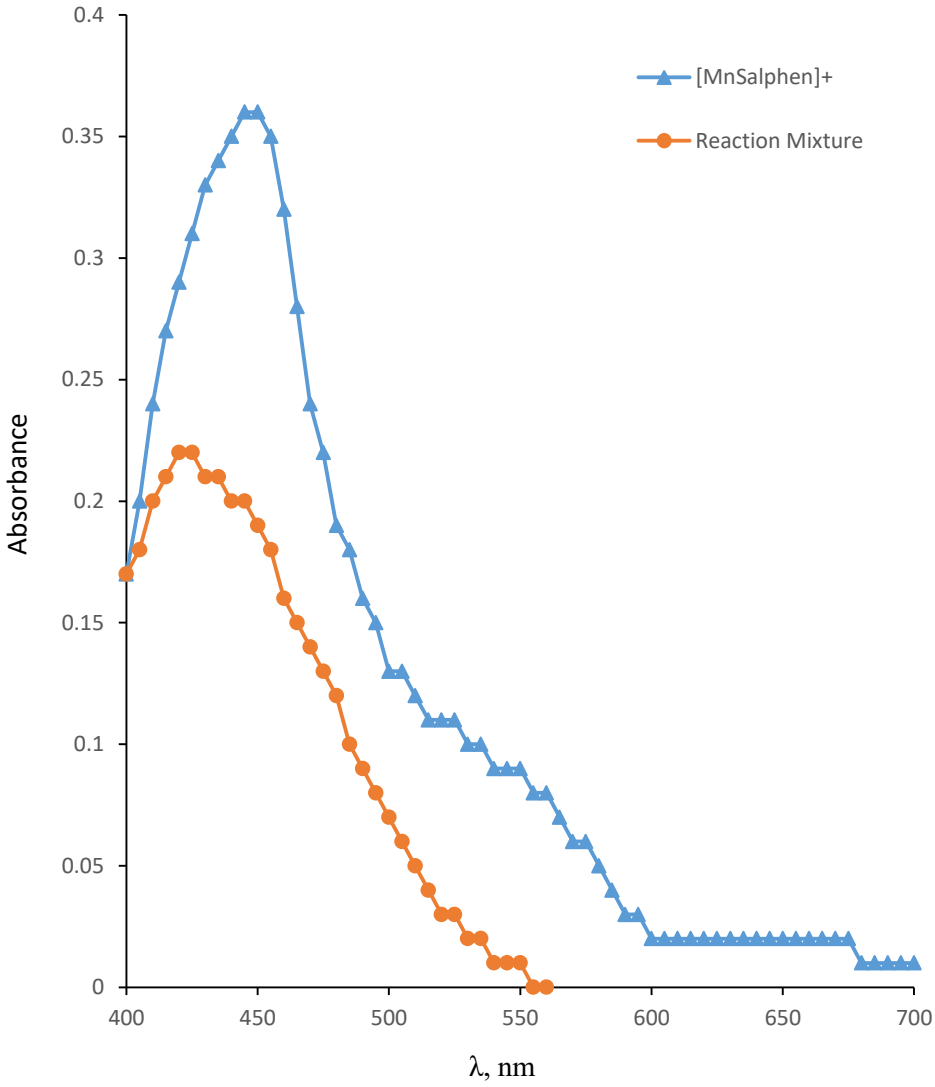


Figure 4.101: Plot for spectrophotometric test for the redox reaction of $[Mn(salphen)]^{+}$ and RSH at $[Mn(salphen)^{+}] = 1.0 \times 10^{-4}$ mol dm^{-3}, [RSH] = 0.40 mol dm^{-3}, $\mu = 0.6\ C^2$ mol dm^{-3}, D = 78.19, T = 28 ± 1°C and λ_{max} = 450 nm

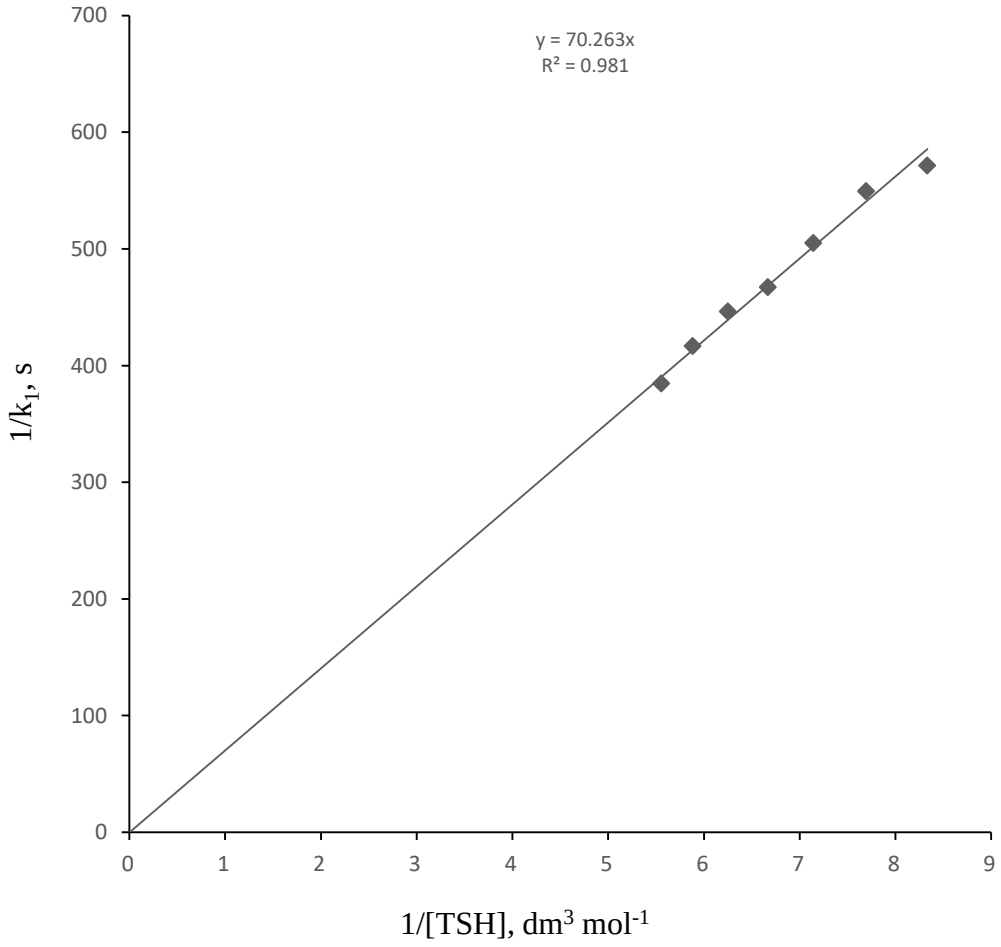


Figure 4.102: Michaelis-Menten plot for the redox reaction of $[Fe(salphen)]^+$ and TSH at $[Fe(salphen)^+] = 2.0 \times 10^{-4}$ mol dm^{-3}, μ = 0.2 C^2 mol dm^{-3}, D = 76.88, T = 26 ± 1°C and λ_{max} = 435 nm

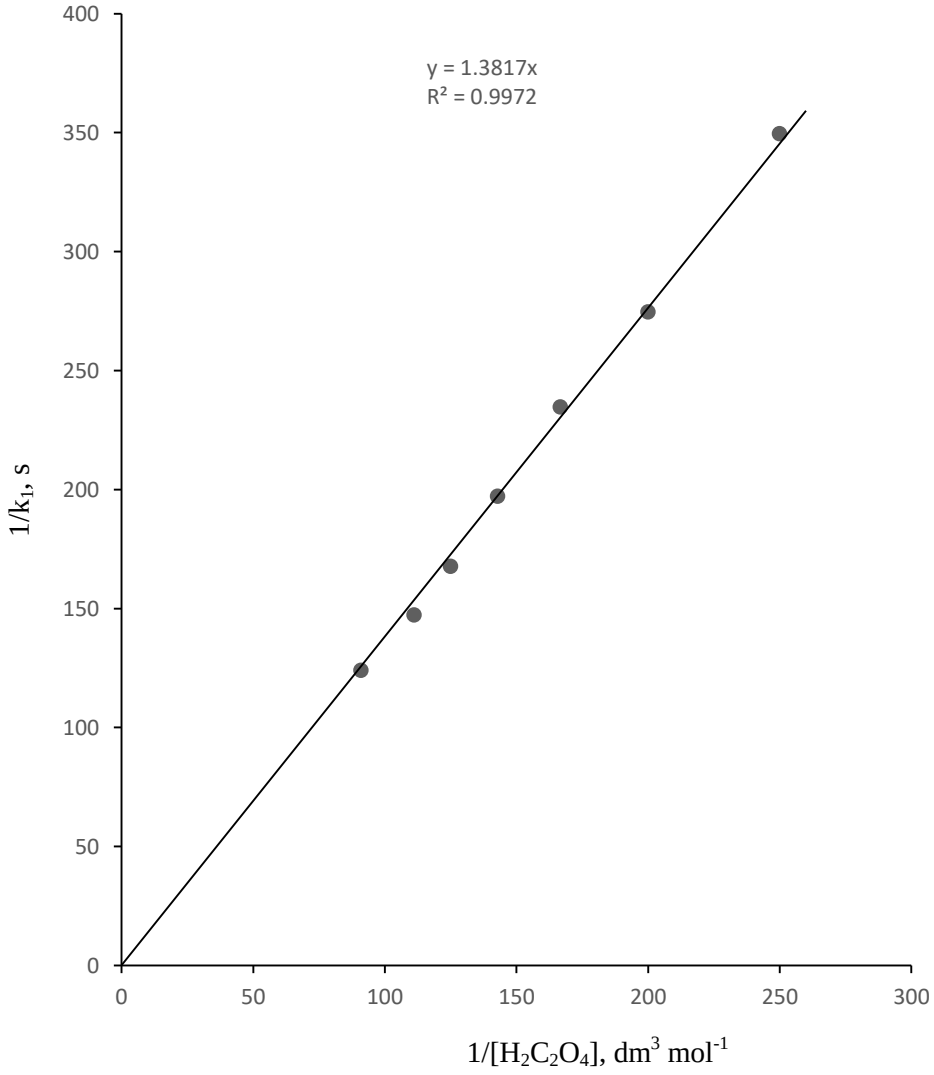


Figure 4.103: Michaelis-Menten plot for the redox reaction of $[Fe(salphen)]^+$ and $H_2C_2O_4$ at $[Fe(salphen)^+] = 2.0 \times 10^{-4}$ mol dm^{-3}, μ = 0.2 C^2 mol dm^{-3}, D = 76.06, T = 26 ± 1°C and λ_{max} = 435 nm

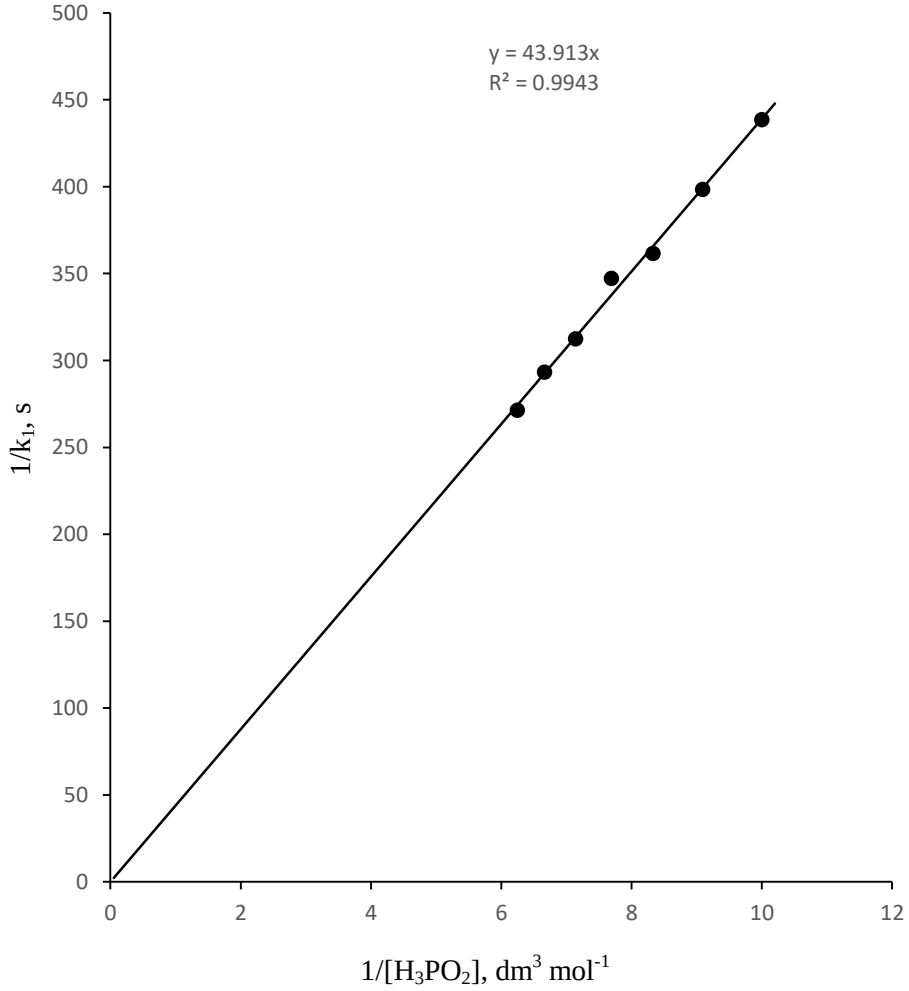


Figure 4.104: Michaelis-Menten plot for the redox reaction of $[Fe(salphen)]^{+}$ and H_3PO_2 at $[Fe(salphen)^{+}] = 2.0 \times 10^{-4}$ mol dm^{-3}, μ = 0.2 C^2 mol dm^{-3}, D = 76.68, T = 26 ± 1°C and λ_{max} = 435 nm

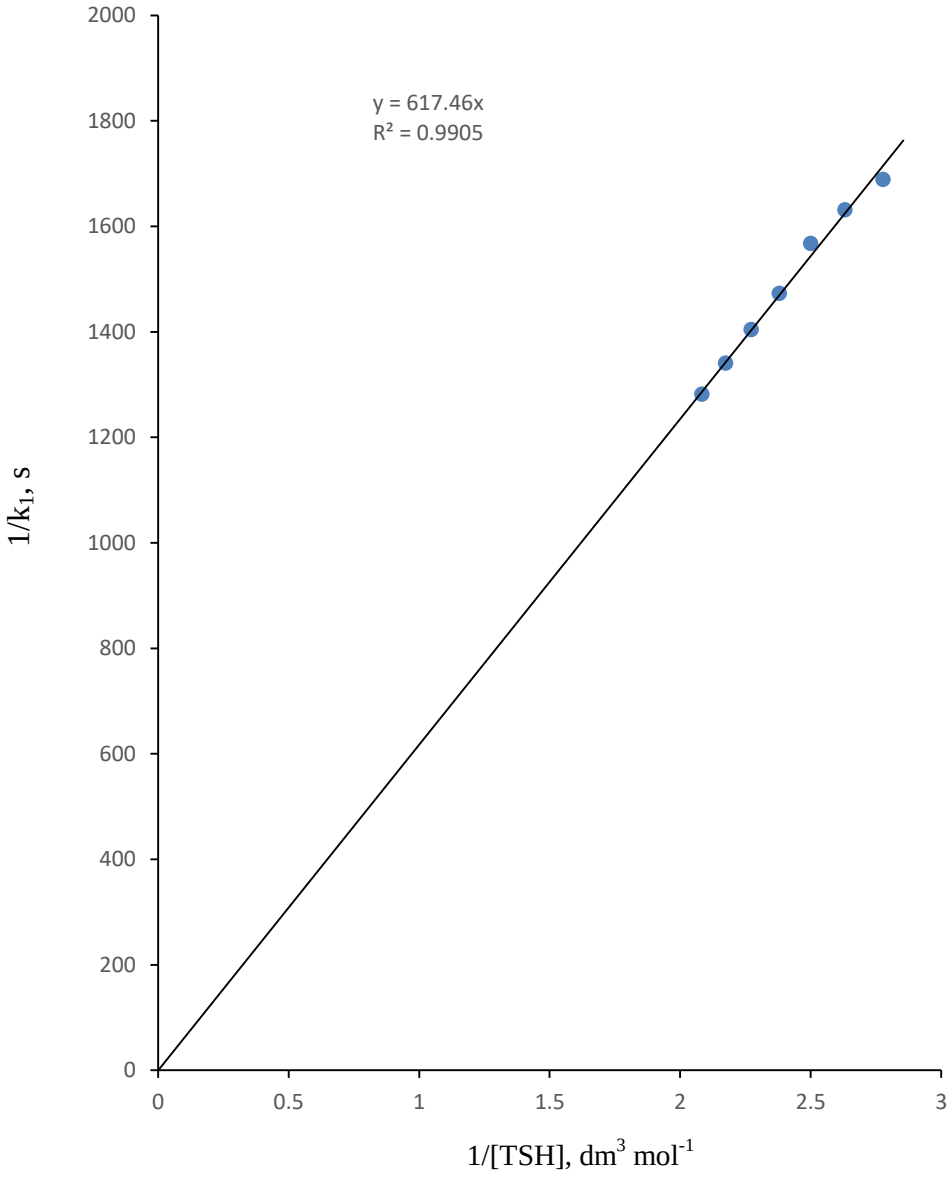


Figure 4.105: Michaelis-Menten plot for the redox reaction of $[Mn(salphen)]^+$ and TSH at $[Mn(salphen)^+] = 1.0 \times 10^{-4}$ mol dm^{-3}, μ = 0.6 C^2 mol dm^{-3}, D = 77.98, T = 32 ± 1°C and λ_{max} = 450 nm

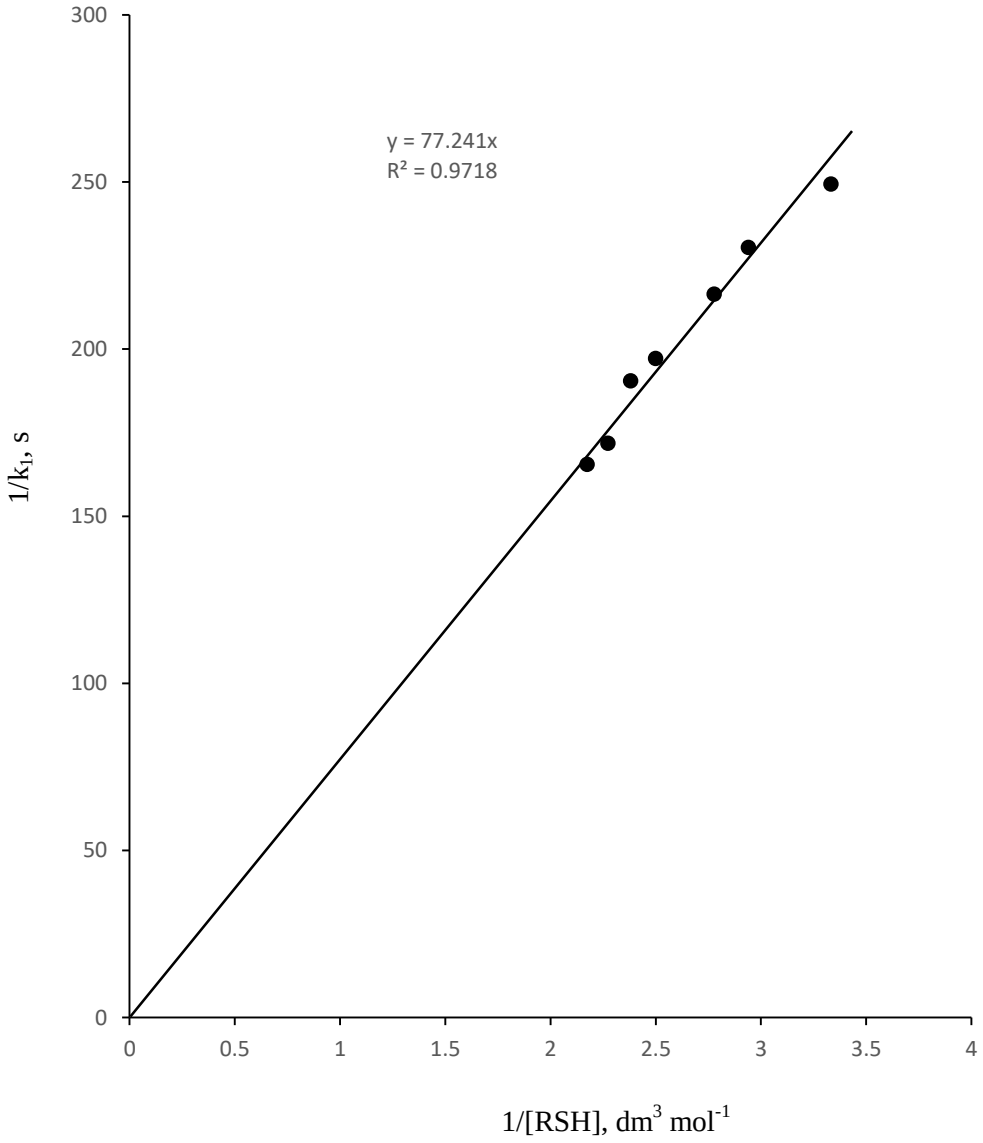


Figure 4.106: Michaelis-Menten plot for the redox reaction of $[Mn(salphen)]^+$ and RSH at $[Mn(salphen)^+] = 1.0 \times 10^{-4}$ mol dm^{-3}, $\mu = 0.6$ C^2 mol dm^{-3}, D = 78.19, T = 28 ± 1°C and λ_{max} = 450 nm

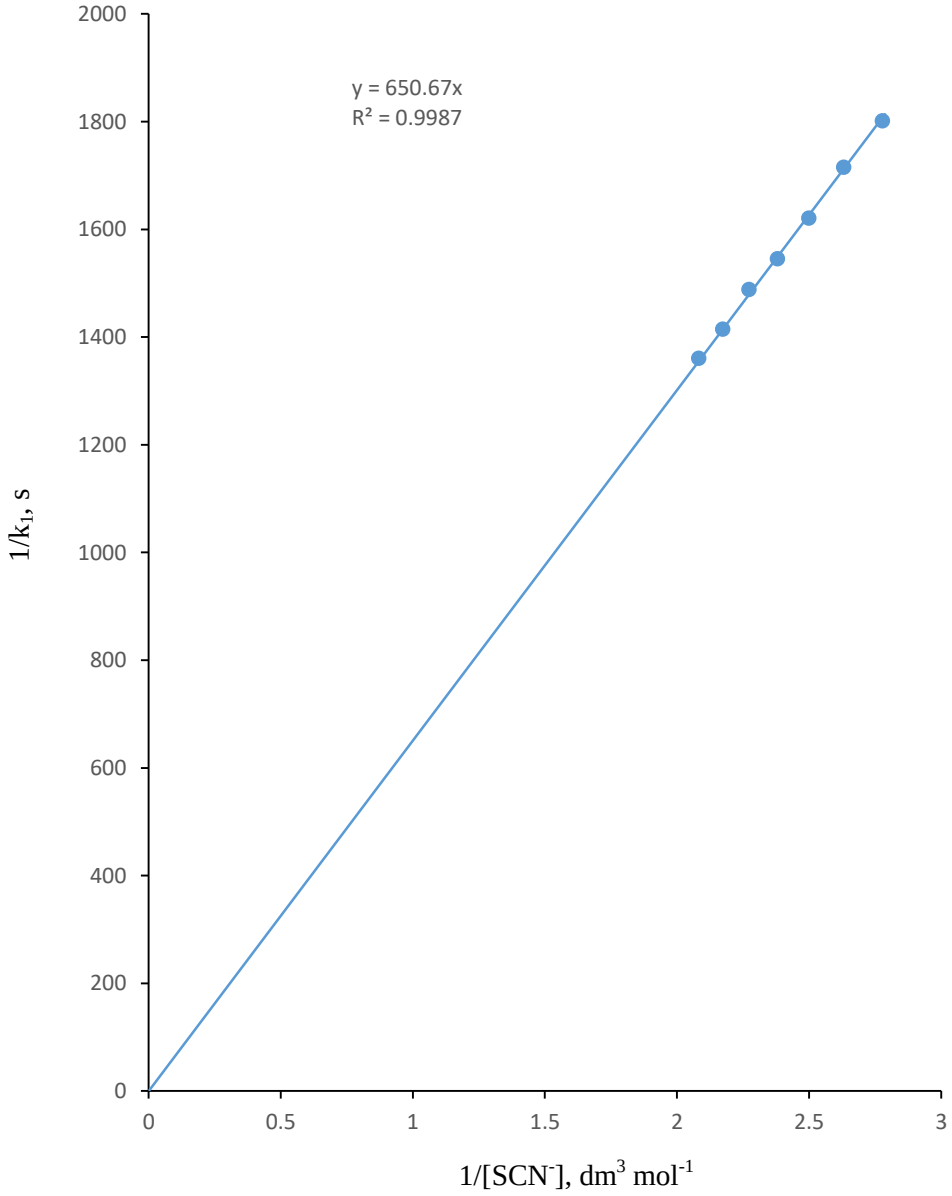


Figure 4.107: Michaelis-Menten plot for the redox reaction of $[Mn(salphen)]^+$ and SCN^- at $[Mn(salphen)^+] = 1.0 \times 10^{-4}$ mol dm^{-3}, μ = 0.6 C^2 mol dm^{-3}, $[H^+] = 4.0 \times 10^{-5}$ mol dm^{-3}, D = 78.12, T = 28 ± 1°C and λ_{max} = 450 nm

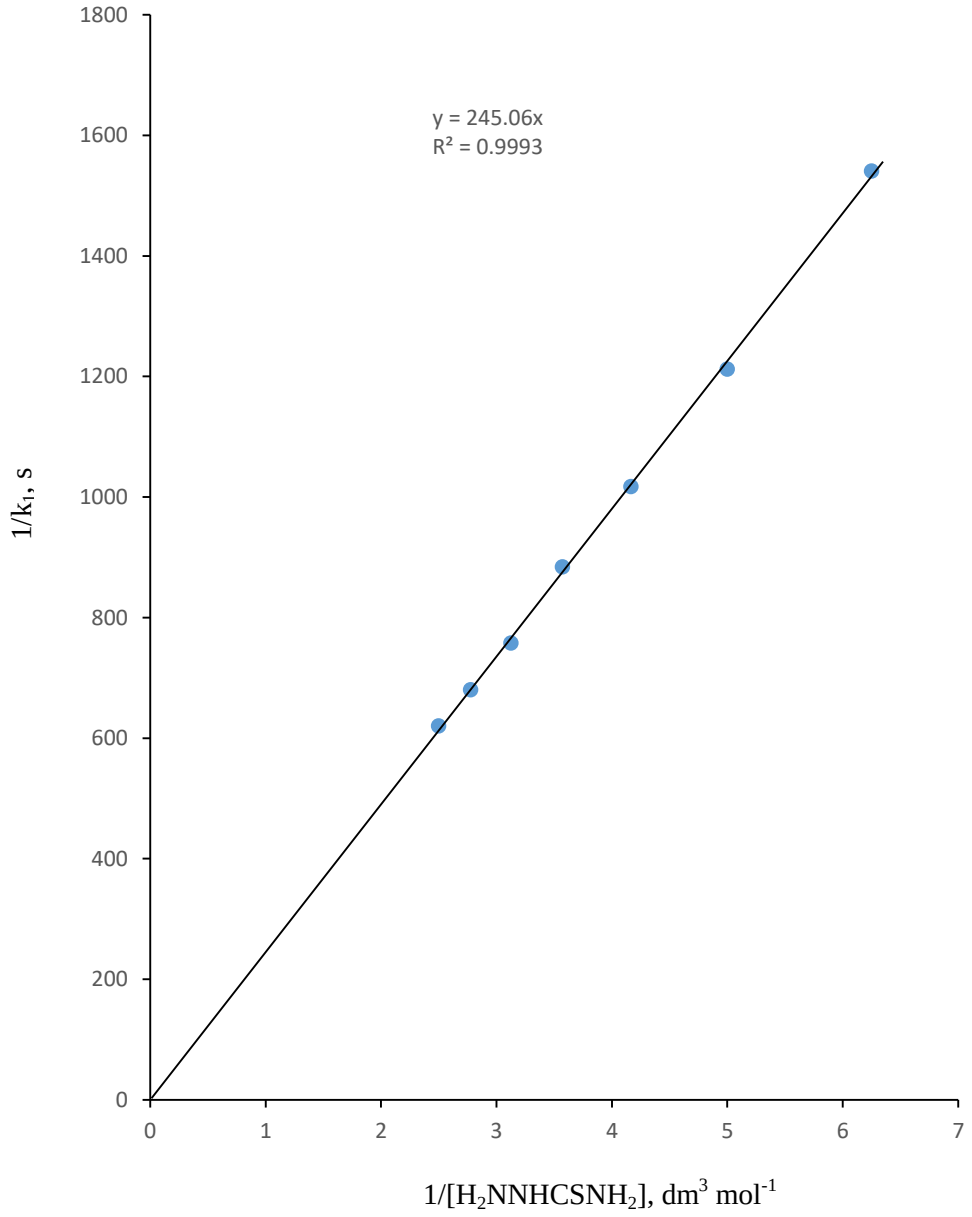


Figure 4.108: Michaelis-Menten plot for the redox reaction of $[Mn(salphen)]^+$ and $H_2NNHCSNH_2$ at $[Mn(salphen)^+] = 1.0 \times 10^{-4}$ mol dm^{-3}, μ = 0.6 C^2 mol dm^{-3}, $[H^+] = 2.0 \times 10^{-5}$ mol dm^{-3}, D = 75.10, T = 28 ± 1°C and λ_{max} = 450 nm

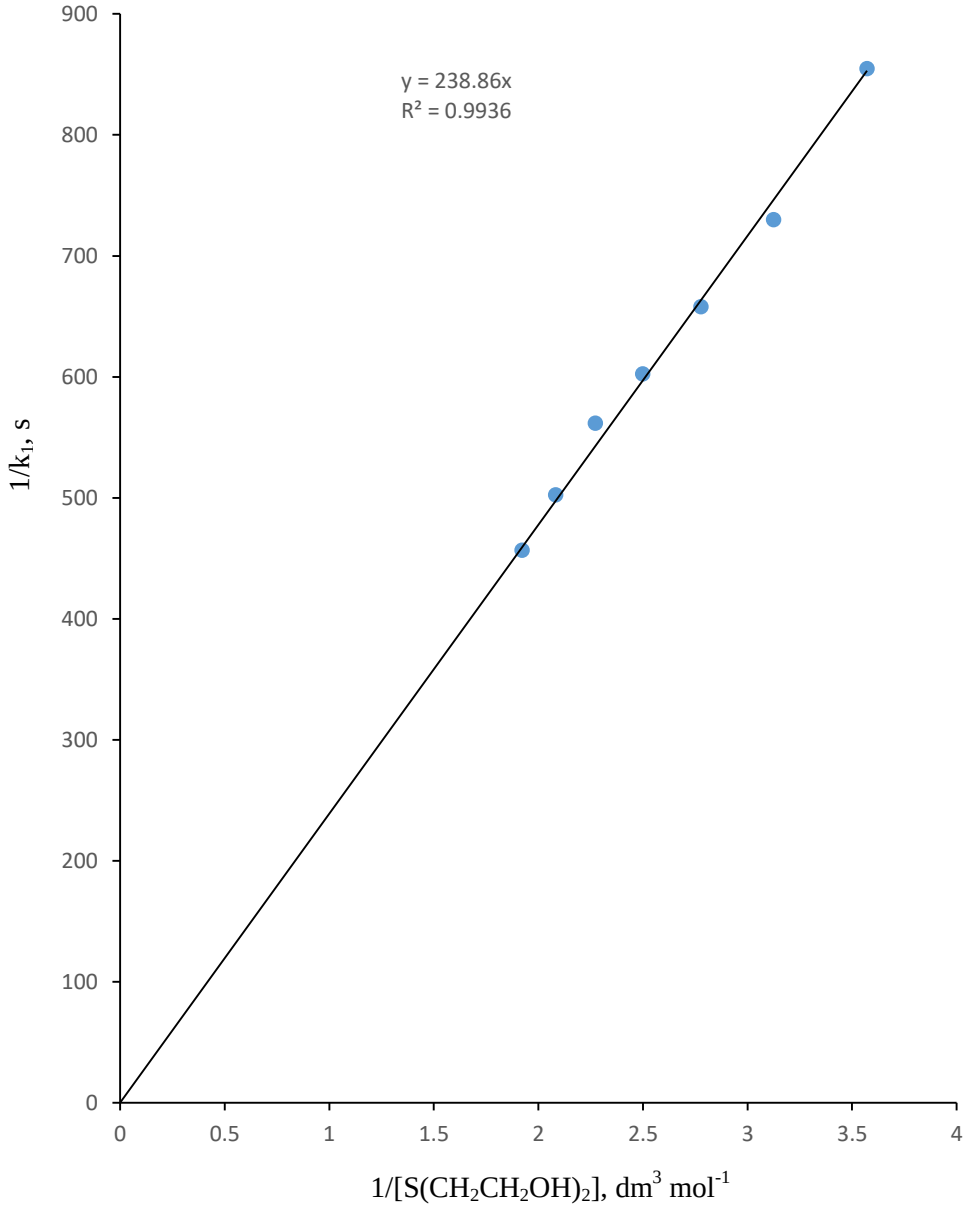


Figure 4.109: Michaelis-Menten plot for the redox reaction of $[Mn(salphen)]^+$ and $S(CH_2CH_2OH)_2$ at $[Mn(salphen)^+] = 1.0 \times 10^{-4}$ mol dm^{-3}, μ = 0.6 C^2 mol dm^{-3}, $[H^+] = 2.0 \times 10^{-5}$ mol dm^{-3}, D = 66.60, T = 50 ± 1°C and λ_{max} = 450 nm

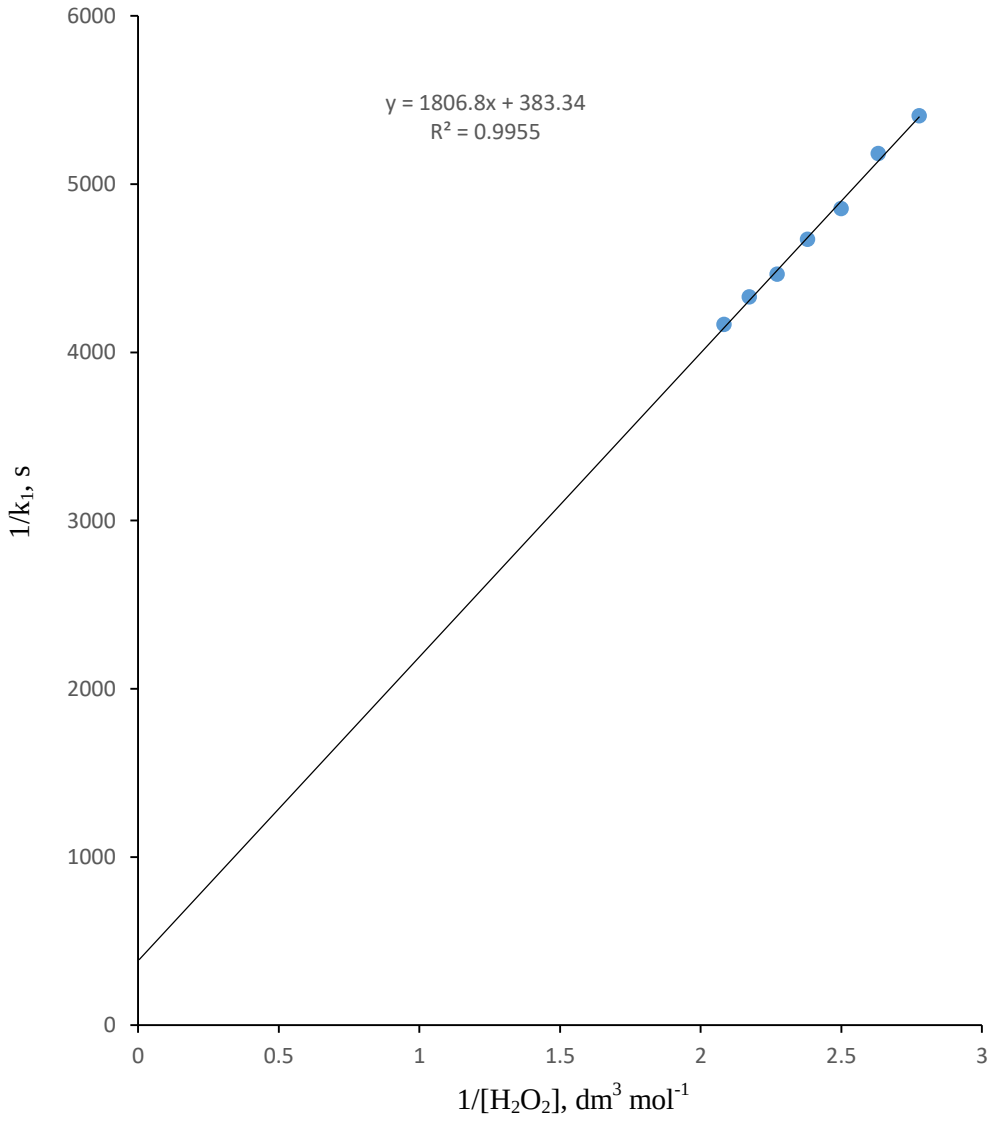


Figure 4.110: Michaelis-Menten plot for the redox reaction of $[Fe(salphen)]^+$ and H_2O_2 at $[Fe(salphen)^+] = 1.0 \times 10^{-4}$ mol dm^{-3}, μ = 0.6 C^2 mol dm^{-3}, $[H^+] = 2.0 \times 10^{-5}$ mol dm^{-3}, D = 78.12, T = 28 ± 1°C and λ_{max} = 435 nm

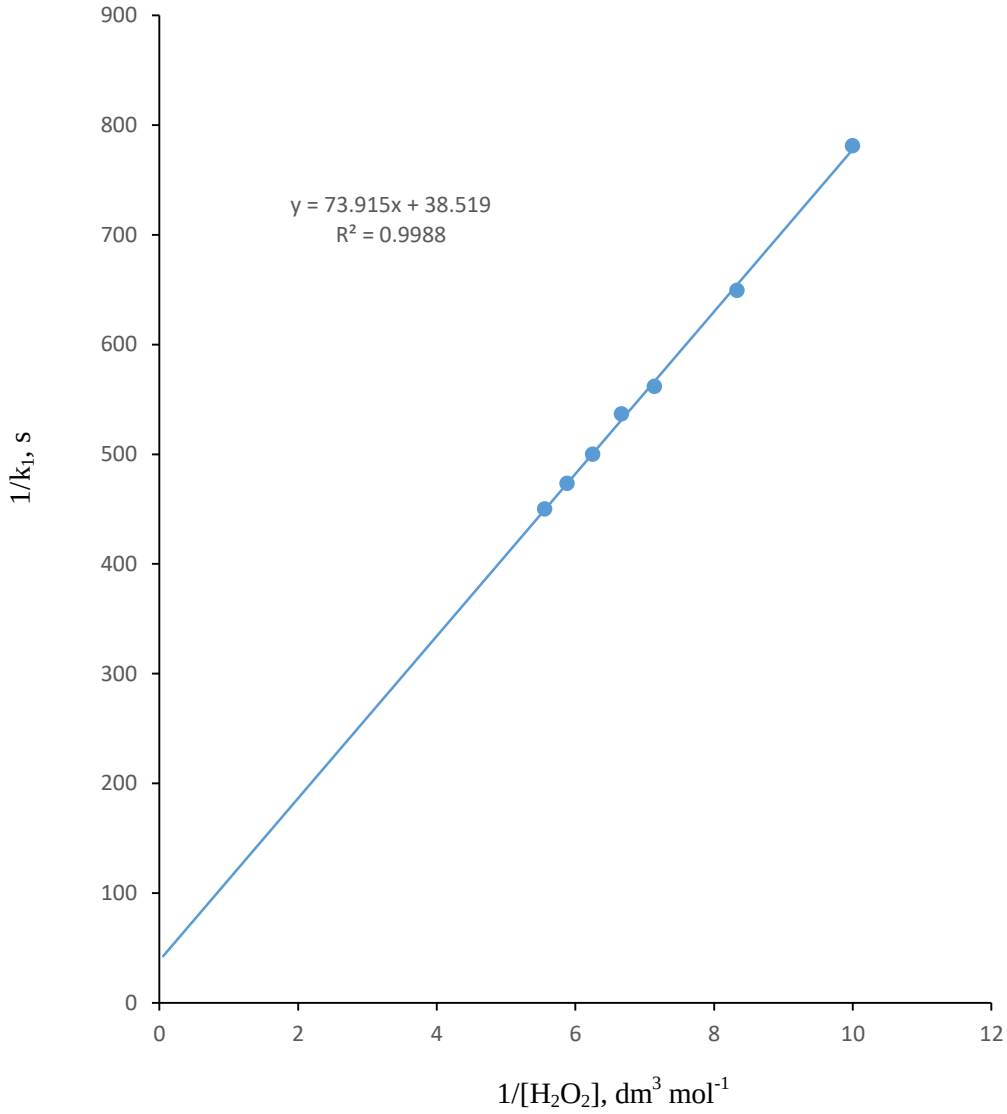


Figure 4.111: Michaelis-Menten plot for the redox reaction of $[Mn(salphen)]^+$ and H_2O_2 at $[Mn(salphen)^+] = 1.0 \times 10^{-4}$ mol dm^{-3}, μ = 0.2 C^2 mol dm^{-3}, $[H^+] = 2.0 \times 10^{-5}$ mol dm^{-3}, D = 76.82, T = 30 ± 1°C and λ_{max} = 450 nm

4.10 Free radicals

Addition of acrylamide, a known radical scavenger to the reaction mixtures in excess methanol produced a gelatinous precipitate in the reactions of TSH, H_3PO_2 and H_2O_2 with $[Fe(salphen)]^+$ and in H_2O_2, TSH, RSH, SCN^-, $H_2NNHCSNH_2$ and $S(CH_2CH_2OH)_2$ reactions with $[Mn(salphen)]^+$, while no gel was observed in the reaction of $H_2C_2O_4$ with $[Fe(salphen)]^+$.

4.11 Effect of Surfactants on the Reactions Rate

4.11.1 Critical micelle concentration

The variation of specific conductance (k, μS/cm) with surfactant concentrations ($[S_f]$) (where S_f = SDS or CTAB) are presented in Table 4.55 (where k_1, k_2 and k_3 = specific conductance of SDS in (i) water; (ii) H_2O/DMSO (4:1), 0.6 mol dm^{-3} NaCl and 1.0 × 10^{-4} mol dm^{-3} $[Fe(salphen)]^+$ and (iii) H_2O/DMSO (4:1), 0.6 mol dm^{-3} NaCl and 1.0 × 10^{-4} mol dm^{-3} $[Mn(salphen)]^+$ respectively, k_4, k_5, and k_6 = specific conductance of CTAB in (i) water; (ii) H_2O/DMSO (4:1), 0.6 mol dm^{-3} NaCl and 1.0 × 10^{-4} mol dm^{-3} $[Fe(salphen)]^+$; and (iii) H_2O/DMSO (4:1), 0.6 mol dm^{-3} NaCl and 1.0 × 10^{-4} mol dm^{-3} $[Mn(salphen)]^+$ respectively).

The CMCs of SDS determined from the plots of specific conductance (k, μS/cm) against $[S_f]$ in the various media as described (i – iii) are 8.0×10^{-3}, 3.3×10^{-3} and 2.8×10^{-4} mol dm^{-3} respectively (Figures 4.112 – 4.114) while that of CTAB are 2.0×10^{-3}, 2.8×10^{-3} and 4.0×10^{-4} mol dm^{-3} respectively (Figures 4.115 – 4.117).

4.11.2 Influence of surfactants on the reactions rate

Increasing SDS concentrations catalysed the reactions of TSH (Table 4.56) and $H_2C_2O_4$ with $[Fe(salphen)]^+$ (Table 4.57), the reactions of TSH (Table 4.58), SCN^- (Table

4.59) and $S(CH_2CH_2OH)_2$ (Table 4.60) with $[Mn(salphen)]^+$, while it inhibited the reaction

Table 4.55: Variation of specific conductance of surfactant with surfactant concentration

$10^4[S_f]$, mol dm^{-3}	k_1, µS/cm	k_2, µS/cm	k_3, µS/cm	k_4, µS/cm	k_5, µS/cm	k_6, µS/cm
0.00	-	-	28110	-	-	27510
1.00	-	-	28150	-	-	27590
2.00	85.74	8131	28190	38.13	8165	27670
4.00	101.00	8135	28160	65.26	8244	27810
6.00	112.10	8117	28140	86.34	8284	27780
8.00	126.70	8132	28110	112.78	8292	27740
10.00	136.00	8160	28090	135.32	8288	27710
12.00	140.30	8143	28100	152.80	8273	27670
14.00	157.60	8157	28030	169.45	8230	27660
16.00	166.00	8193	28030	186.50	8272	27620
18.00	176.00	8211	28000	213.50	8350	27620
20.00	183.10	8286	27940	233.50	8380	27600
24.00	200.40	8281	27940	243.00	8395	27490
28.00	223.90	8285	27860	250.20	8370	27470
32.00	234.00	8295	27750	262.00	8394	27420
36.00	268.60	8329	27710	269.20	8395	27360
40.00	288.60	8280	27620	278.30	8390	27300
44.00	304.00	8252	27540	285.00	8393	27240
48.00	326.40	8260	27480	288.50	8320	27180
52.00	343.20	8264	27400	298.00	8302	27120
56.00	357.60	8252	27300	306.10	8286	27070
60.00	374.00	8240	27260	314.50	8281	26980
80.00	474.70	8203	27140	346.00	8250	26640
100.00	503.80	8141	26960	382.80	8220	26360
140.00	604.30	8041	26630	443.10	8106	26000
200.00	726.40	7893	25900	535.10	7880	25480

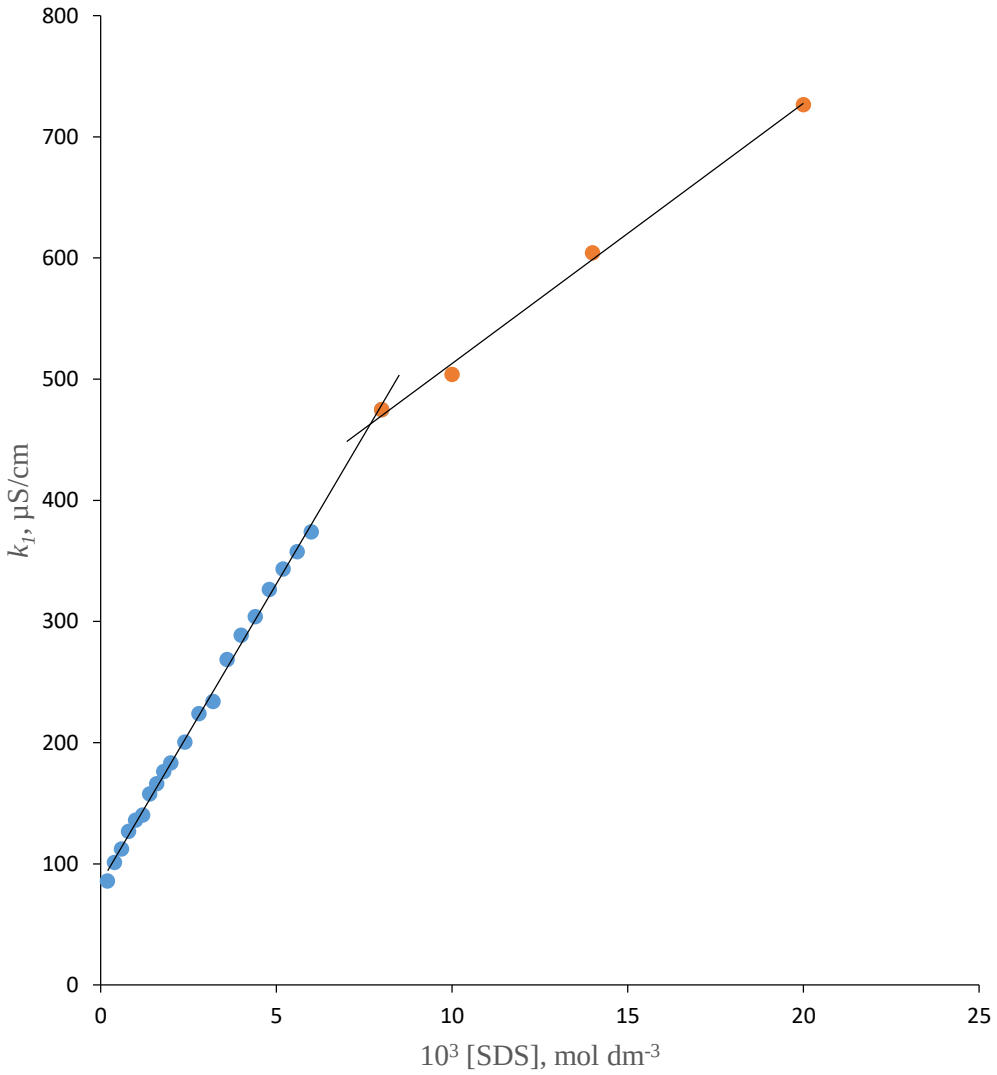


Figure 4.112: Plot of specific conductance against [SDS] in water

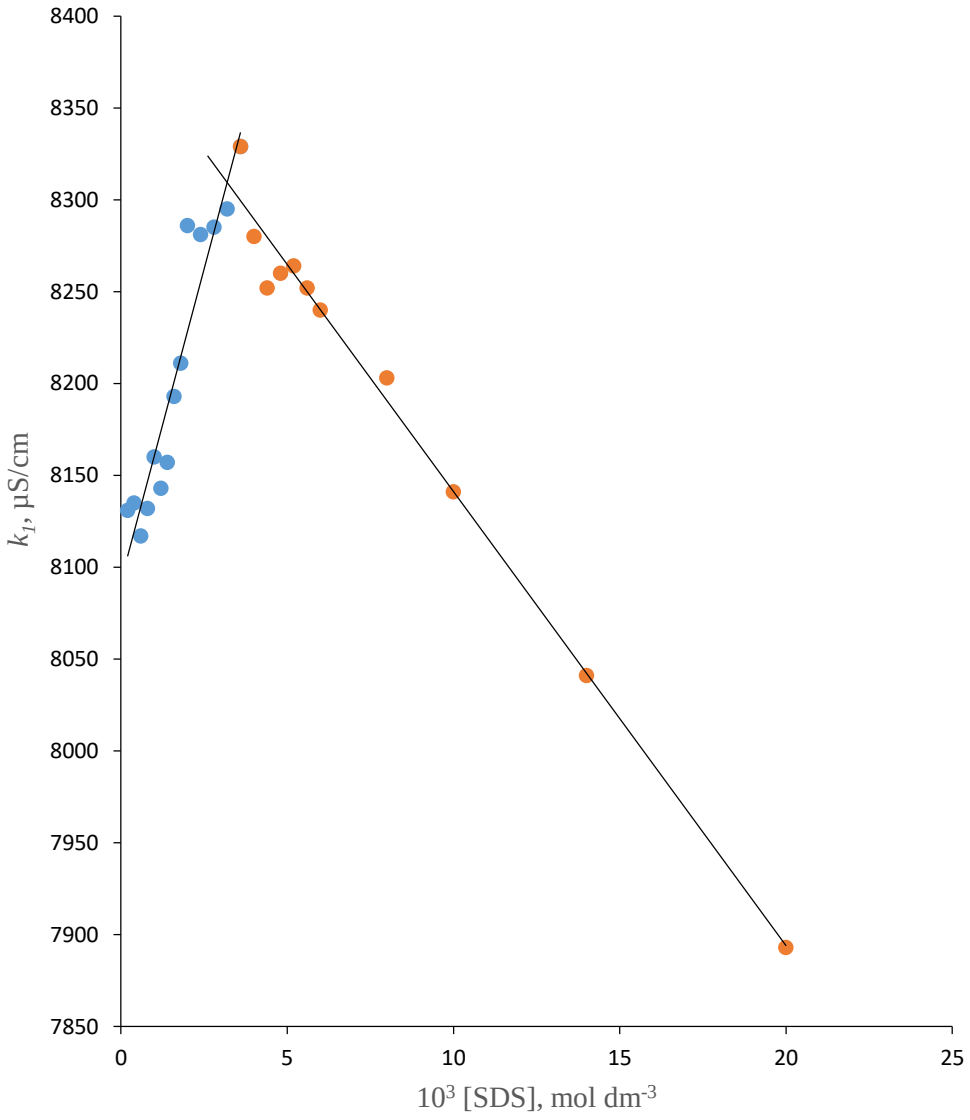


Figure 4.113: Plot of specific conductance against [SDS] in H_2O/DMSO (4:1), 0.6 mol dm^{-3} NaCl and 1×10^{-4} mol dm^{-3} $[Fe(salphen)]^+$

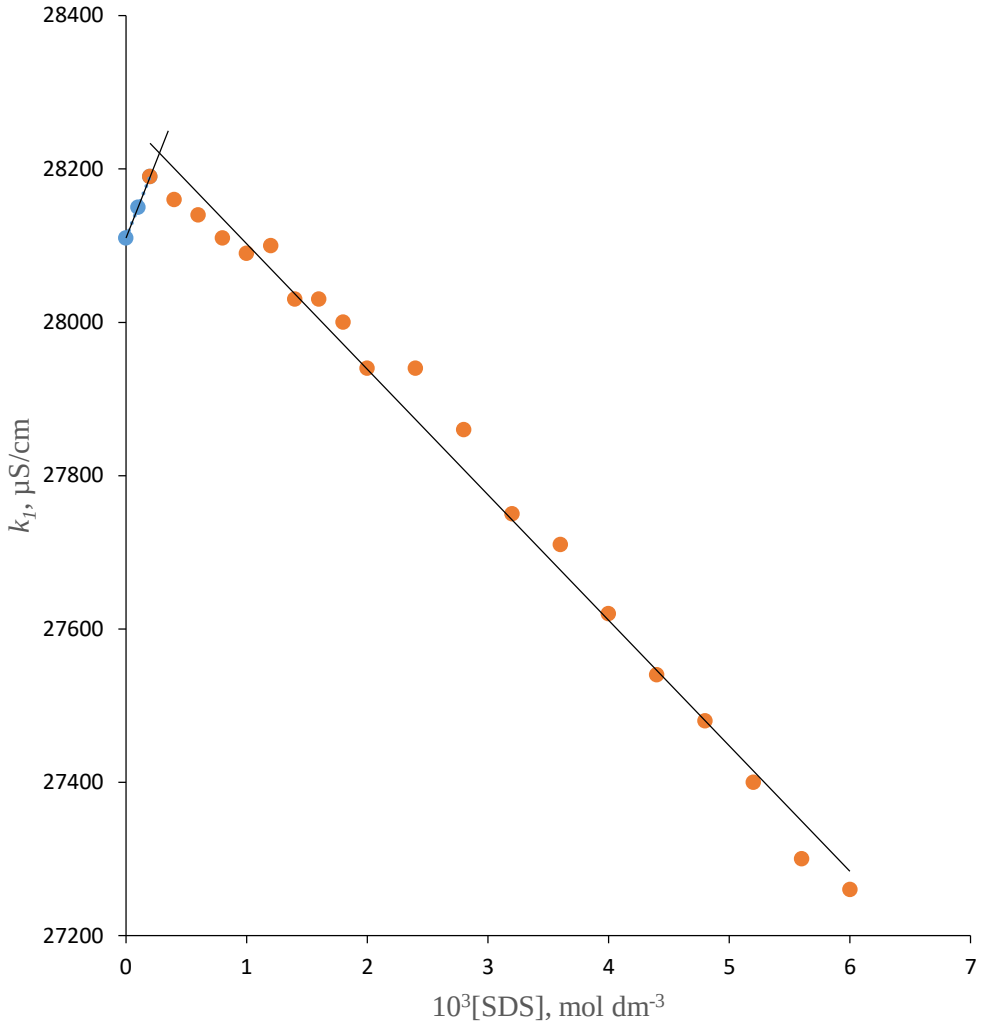


Figure 4.114: Plot of specific conductance against [SDS] in H_2O/DMSO (4:1), 0.6 mol dm^{-3} NaCl and 1×10^{-4} mol dm^{-3} [Mn(salphen)]$^+$

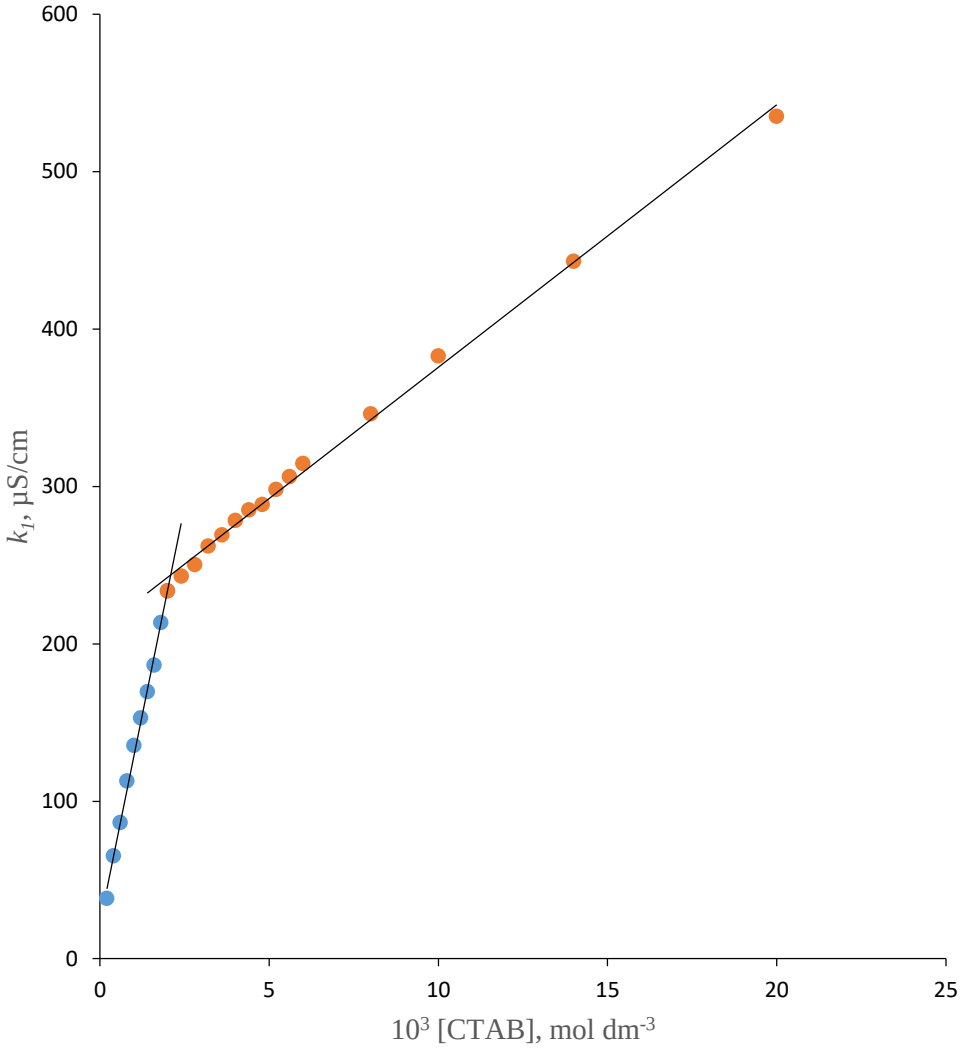


Figure 4.115: Plot of specific conductance against [CTAB] in water

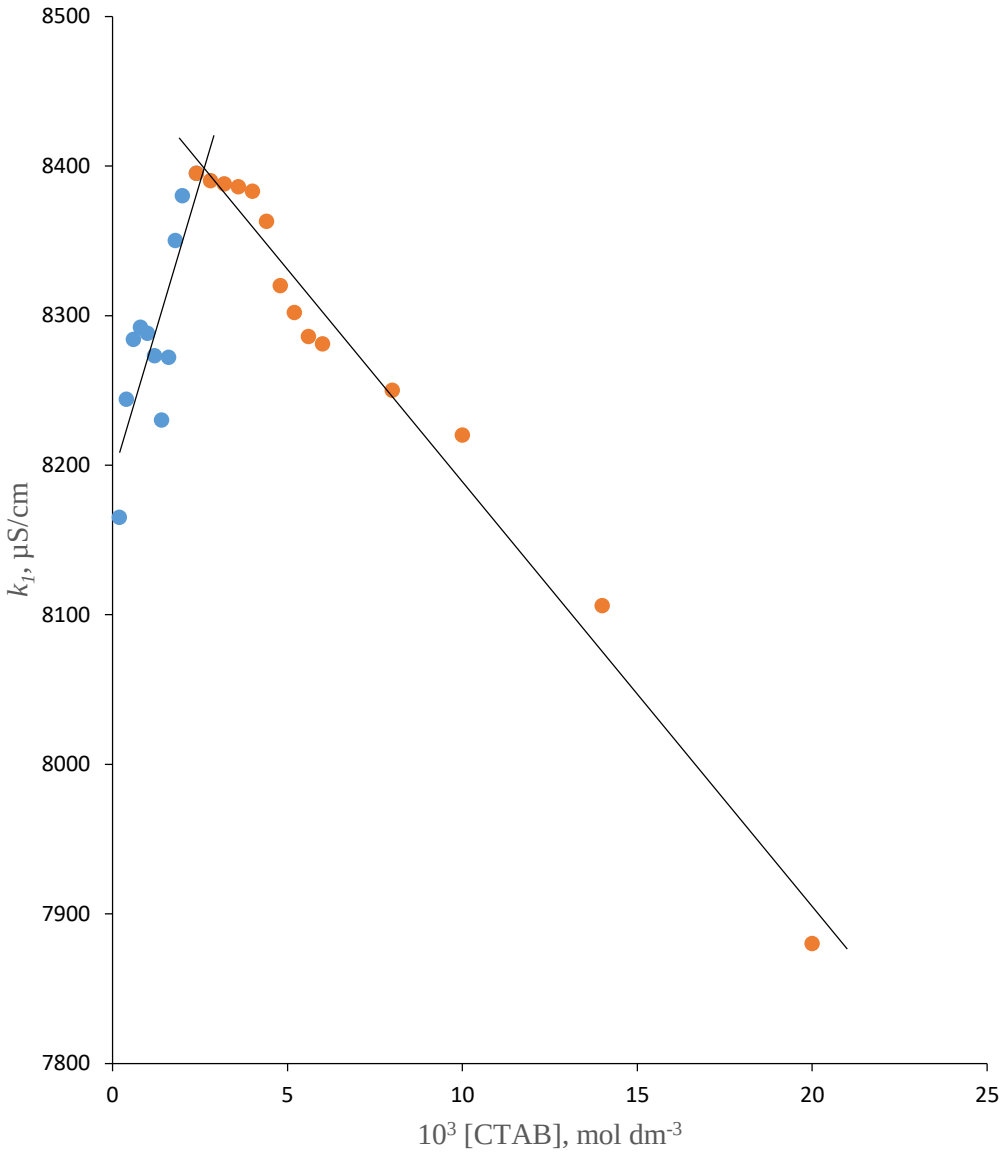


Figure 4.116: Plot of specific conductance against [CTAB] in H_2O/DMSO (4:1), 0.6 mol dm^{-3} NaCl and 1×10^{-4} mol dm^{-3} [Fe(salphen)]$^+$

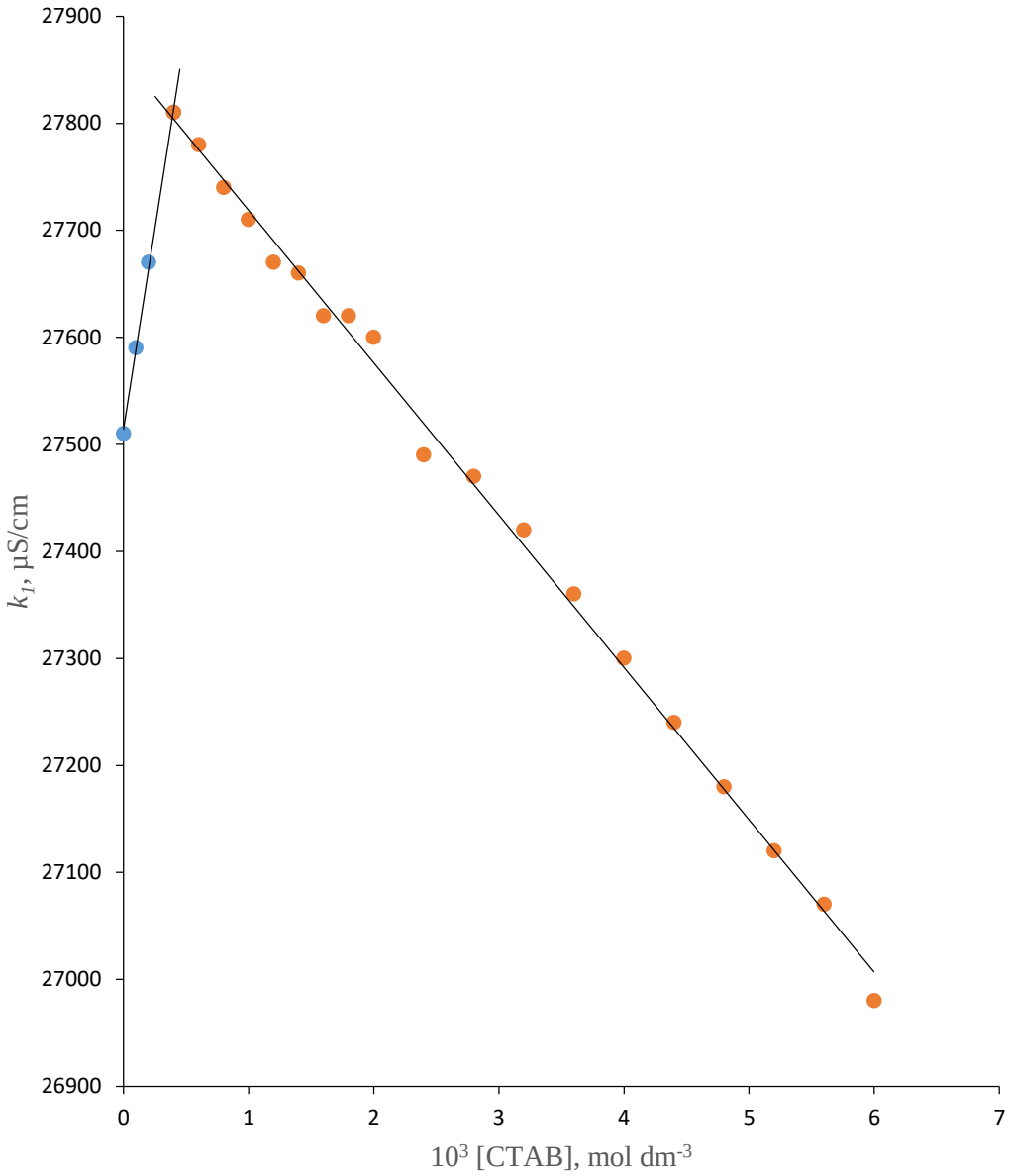


Figure 4.117: Plot of specific conductance against [CTAB] in H_2O/DMSO (4:1), 0.6 mol dm^{-3} NaCl and 1×10^{-4} mol dm^{-3} [Mn(salphen)]$^+$

Table 4.56: Surfactant dependent rate constants and Piszkiewicz parameters for the reaction of $[Fe(salphen)]^+$ and TSH at $[Fe(salphen)^+] = 2.0 \times 10^{-4}$ mol dm^{-3}, [TSH] = 0.15 mol dm^{-3}, μ = 0.2 C^2 mol dm^{-3}, D = 76.88, T = 26 ± 1 °C and λ_{max} = 435 nm

$[S_f]$	10^5 $[S_f]$, mol dm^{-3}	10^3 k_1, s^{-1}	10^2 $k_{\psi\ exp}$, dm^3 mol^{-1} s^{-1}	10^2 $k_{\psi\ cal}$, dm^3 mol^{-1} s^{-1}	k_ψ/k_2
[SDS]	0.00	2.13	1.42	1.42	1.00
	1.00	2.18	1.45	1.46	1.02
	2.00	2.25	1.52	1.51	1.07
	3.00	2.35	1.57	1.57	1.11
	4.00	2.42	1.61	1.62	1.13
	5.00	2.51	1.67	1.66	1.18
	6.00	2.55	1.70	1.71	1.20
	7.00	2.63	1.75	1.75	1.23
k_m = 2.54 × 10^{-2} dm^3 mol^{-1} s^{-1},			K_D = 2.09 × 10^{-5} mol dm^{-3},		
n = 1.22,			**K** = 4.78 × 10^4 dm^3 mol^{-1}		
$[S_f]$	10^5 $[S_f]$, mol dm^{-3}	10^3 k_1, s^{-1}	10^2 $k_{\psi\ exp}$, dm^3 mol^{-1} s^{-1}	10^2 $k_{\psi\ cal}$, dm^3 mol^{-1} s^{-1}	k_ψ/k_2
[CTAB]	0.00	2.13	1.42	1.42	1.00
	1.00	2.15	1.43	1.45	1.01
	2.00	2.22	1.48	1.50	1.04
	3.00	2.31	1.54	1.55	1.08
	4.00	2.36	1.57	1.59	1.11
	5.00	2.49	1.66	1.64	1.17
	6.00	2.52	1.68	1.69	1.18
	7.00	2.58	1.72	1.74	1.21
k_m = 3.02 × 10^{-2} dm^3 mol^{-1} s^{-1},			K_D = 2.20 × 10^{-5} mol dm^{-3},		
n = 1.27,			**K** = 4.55 × 10^4 dm^3 mol^{-1}		

Table 4.57: Surfactant dependent rate constants and Piszkiewicz parameters for the reaction of $[Fe(salphen)]^+$ and $H_2C_2O_4$ at $[Fe(salphen)^+] = 2.0 \times 10^{-4}$ mol dm^{-3}, $[H_2C_2O_4] = 6.0 \times 10^{-3}$ mol dm^{-3}, $\mu = 0.2$ C^2 mol dm^{-3}, D = 76.06, T = 26 ± 1°C and λ_{max} = 435 nm

$[S_f]$	10^5 $[S_f]$, mol dm^{-3}	10^3 k_1, s^{-1}	10 $k_{\Psi\ exp}$, dm^3 mol^{-1} s^{-1}	10 $k_{\Psi\ cal}$, dm^3 mol^{-1} s^{-1}	k_Ψ/k_2
[SDS]	0.00	4.26	7.10	7.10	1.00
	1.00	4.32	7.20	7.33	1.01
	2.00	4.57	7.62	7.69	1.07
	3.00	4.89	8.15	8.04	1.15
	4.00	5.01	8.35	8.34	1.18
	5.00	5.16	8.60	8.57	1.21
	6.00	5.25	8.75	8.75	1.23
	7.00	5.31	8.85	8.90	1.25
$k_m = 9.71 \times 10^{-1}$ dm^3 mol^{-1} s^{-1},			$K_D = 9.24 \times 10^{-8}$ mol dm^{-3},		
n = 1.61,			$K = 1.08 \times 10^7$ dm^3 mol^{-1}		
$[S_f]$	10^5 $[S_f]$, mol dm^{-3}	10^3 k_1, s^{-1}	10 $k_{\Psi\ exp}$, dm^3 mol^{-1} s^{-1}	10 $k_{\Psi\ cal}$, dm^3 mol^{-1} s^{-1}	k_Ψ/k_2
[CTAB]	0.00	4.26	7.10	7.10	1.00
	1.00	4.28	7.13	7.32	1.00
	2.00	4.48	7.47	7.75	1.05
	3.00	4.81	8.02	8.21	1.13
	4.00	5.14	8.57	8.64	1.21
	5.00	5.37	8.95	9.01	1.26
	6.00	5.52	9.20	9.32	1.30
	7.00	5.71	9.52	9.56	1.34
$k_m = 1.10$ dm^3 mol^{-1} s^{-1},			$K_D = 4.01 \times 10^{-8}$ mol dm^{-3},		
n = 1.72,			$K = 2.49 \times 10^7$ dm^3 mol^{-1}		

Table 4.58: Surfactant dependent rate constants and Piszkiewicz parameters for the reaction of $[Mn(salphen)]^+$ and TSH at $[Mn(salphen)^+] = 1.0 \times 10^{-4}$ mol dm^{-3}, [TSH] = 0.42 mol dm^{-3}, $\mu = 0.6$ C^2 mol dm^{-3}, D = 77.98, T = 32 ± 1 °C and λ_{max} = 450 nm

$[S_f]$	10^5 $[S_f]$, mol dm^{-3}	10^4 k_1, s^{-1}	10^3 $k_{\Psi\ exp}$, dm^3 mol^{-1} s^{-1}	10^3 $k_{\Psi\ cal}$, dm^3 mol^{-1} s^{-1}	k_Ψ/k_2
[SDS]	0.00	6.79	1.62	1.62	1.00
	1.00	7.48	1.78	1.79	1.10
	2.00	8.22	1.96	1.94	1.21
	3.00	8.84	2.11	2.08	1.30
	4.00	9.03	2.15	2.21	1.33
	5.00	9.88	2.35	2.33	1.45
	6.00	10.30	2.45	2.45	1.51
$k_m = 1.63 \times 10^{-2}$ dm^3 mol^{-1} s^{-1}, n = 0.889,			$K_D = 2.94 \times 10^{-3}$ mol dm^{-3}, $K = 3.40 \times 10^2$ dm^3 mol^{-1}		
$[S_f]$	10^5 $[S_f]$, mol dm^{-3}	10^4 k_1, s^{-1}	10^3 $k_{\Psi\ exp}$, dm^3 mol^{-1} s^{-1}	10^3 $k_{\Psi\ cal}$, dm^3 mol^{-1} s^{-1}	k_Ψ/k_2
[CTAB]	0.00	6.79	1.62	1.62	1.00
	1.00	6.84	1.63	1.69	1.01
	2.00	7.53	1.79	1.79	1.11
	3.00	7.99	1.90	1.89	1.17
	4.00	8.61	2.05	2.00	1.27
	5.00	8.77	2.09	2.11	1.29
	6.00	9.33	2.22	2.23	1.37
$k_m = 4.19 \times 10^{-2}$ dm^3 mol^{-1} s^{-1}, n = 1.17,			$K_D = 7.12 \times 10^{-4}$ mol dm^{-3}, $K = 1.41 \times 10^3$ dm^3 mol^{-1}		

Table 4.59: Surfactant dependent rate constants and Piszkiewicz parameters for the reaction of $[Mn(salphen)]^+$ and SCN^- at $[Mn(salphen)^+]$ = 1.0 × 10^{-4} mol dm^{-3}, $[SCN^-]$ = 0.42 mol dm^{-3}, μ = 0.6 C^2 mol dm^{-3}, $[H^+]$ = 4.0 × 10^{-5} mol dm^{-3}, D = 78.12, T = 28 ± 1 °C and λ_{max} = 450 nm

$[S_f]$	10^5 $[S_f]$, mol dm^{-3}	10^4 k_1, s^{-1}	10^3 $k_{\psi\ exp}$, dm^3 mol^{-1} s^{-1}	10^3 $k_{\psi\ cal}$, dm^3 mol^{-1} s^{-1}	k_ψ/k_2
[SDS]	0.00	6.47	1.54	1.54	1.00
	1.00	7.37	1.76	1.69	1.14
	2.00	7.83	1.86	1.91	1.21
	3.00	8.98	2.14	2.15	1.39
	4.00	9.90	2.36	2.41	1.53
	5.00	11.75	2.80	2.68	1.82
	6.00	12.21	2.91	2.96	1.89
	7.00	13.59	3.24	3.24	2.10
k_m = 1.50 × 10^{-2} dm^3 mol^{-1} s^{-1},			K_D = 2.51 × 10^{-5} mol dm^{-3},		
n = 1.31,			**K** = 3.98 × 10^4 dm^3 mol^{-1}		
$[S_f]$	10^5 $[S_f]$, mol dm^{-3}	10^4 k_1, s^{-1}	10^3 $k_{\psi\ exp}$, dm^3 mol^{-1} s^{-1}	10^3 $k_{\psi\ cal}$, dm^3 mol^{-1} s^{-1}	k_2/k_ψ
[CTAB]	0.00	6.47	1.54	1.54	1.00
	1.00	5.30	1.26	1.06	1.22
	2.00	3.22	0.77	0.79	2.01
	3.00	2.30	0.55	0.64	2.81
	4.00	2.14	0.51	0.54	3.02
	5.00	1.89	0.45	0.48	3.42
	6.00	1.77	0.42	0.44	3.65
k_m = 2.06 × 10^{-4} dm^3 mol^{-1} s^{-1},			K_D = 1.76 × 10^{-6} mol dm^{-3},		
n = 1.20,			**K** = 5.68 × 10^5 dm^3 mol^{-1}		

Table 4.60: Surfactant dependent rate constants and Piszkiewicz parameters for the reaction of $[Mn(salphen)]^+$ and $S(CH_2CH_2OH)_2$ at $[Mn(salphen)^+] = 1.0 \times 10^{-4}$ mol dm^{-3}, $[S(CH_2CH_2OH)_2] = 0.40$ mol dm^{-3}, $\mu = 0.6$ C^2 mol dm^{-3}, $[H^+] = 2.0 \times 10^{-5}$ mol dm^{-3}, D = 66.60, T = 50 ± 1°C and λ_{max} = 450 nm

$[S_f]$	10^5 $[S_f]$, mol dm^{-3}	10^4 k_1, s^{-1}	10^3 $k_{\psi\ exp}$, dm^3 mol^{-1} s^{-1}	10^3 $k_{\psi\ cal}$, dm^3 mol^{-1} s^{-1}	k_ψ/k_2
[SDS]	0.00	16.60	4.15	4.15	1.00
	5.00	17.20	4.30	4.44	1.04
	7.00	18.30	4.58	4.52	1.10
	10.00	18.90	4.73	4.63	1.14
	20.00	20.40	5.10	4.92	1.23
	40.00	20.80	5.20	5.35	1.25
	60.00	22.30	5.58	5.67	1.34
	80.00	22.80	5.70	5.93	1.37
	100.00	25.50	6.38	6.14	1.54
	200.00	27.80	6.95	6.85	1.67
	400.00	30.00	7.50	7.56	1.81
$k_m = 9.51 \times 10^{-3}$ dm^3 mol^{-1} s^{-1}, $n = 0.78$,			$K_D = 7.62 \times 10^{-3}$ mol dm^{-3}, $K = 1.31 \times 10^2$ dm^3 mol^{-1}		
$[S_f]$	10^5 $[S_f]$, mol dm^{-3}	10^4 k_1, s^{-1}	10^3 $k_{\psi\ exp}$, dm^3 mol^{-1} s^{-1}	10^3 $k_{\psi\ cal}$, dm^3 mol^{-1} s^{-1}	k_2/k_ψ
[CTAB]	0.00	16.60	4.15	4.15	1.00
	5.00	15.80	3.95	3.59	1.05
	7.00	14.20	3.55	3.40	1.17
	10.00	12.30	3.08	3.15	1.35
	20.00	9.51	2.38	2.62	1.75
	40.00	8.31	2.08	2.14	2.00
	60.00	7.78	1.95	1.92	2.13
	80.00	7.30	1.83	1.80	2.27
$k_m = 1.43 \times 10^{-3}$ dm^3 mol^{-1} s^{-1}, $n = 1.15$,			$K_D = 4.53 \times 10^{-5}$ mol dm^{-3}, $K = 2.21 \times 10^4$ dm^3 mol^{-1}		

of H_2O_2 with $[Fe(salphen)]^+$ (Table 4.61), H_2O_2 (Table 4.62) and RSH (Table 4.63) reactions with $[Mn(salphen)]^+$.

As for CTAB, increase in its concentration catalysed the reactions of TSH (Table 4.56) and $H_2C_2O_4$ (Table 4.57) with $[Fe(salphen)]^+$ as well as the reactions of H_2O_2 (Table 4.62) and TSH (Table 4.58) with $[Mn(salphen)]^+$ but inhibited the reaction of H_2O_2 with $[Fe(salphen)]^+$ (Table 4.61) and the reactions of SCN^- (Table 4.59), $S(CH_2CH_2OH)_2$ (Table 4.60) and RSH (Table 4.63) with $[Mn(salphen)]^+$.

The second order rate constants in the presence of surfactants, $k_{\Psi exp}$, were fitted into the Piszkiewicz equation (Piszkiewicz, 1977) and $k_{\Psi cal}$ (where $k_{\Psi cal}$ = calculated second order rate constants in the presence of surfactants) were determined. The catalytic factor, $k_{\Psi exp}/k_w$, or inhibition factor, $k_w/k_{\Psi exp}$, were also determined and the results are presented in Tables 4.56 – 4.63. Plots of k_Ψ against $[S_f]$ fitted into the Piszkiewicz's equation are presented in Figures 4.118 – 4.133.

Table 4.61: Surfactant dependent rate constants and Piszkiewicz parameters for the reaction of $[Fe(salphen)]^+$ and H_2O_2 at $[Fe(salphen)^+] = 1.0 \times 10^{-4}$ mol dm^{-3}, $[H_2O_2] = 0.42$ mol dm^{-3}, $\mu = 0.6$ C^2 mol dm^{-3}, $[H^+] = 2.0 \times 10^{-5}$ mol dm^{-3}, D = 78.12, T = 28 ± 1°C and $\lambda_{max} = 435$ nm

$[S_f]$	10^5 $[S_f]$, mol dm^{-3}	10^4 k_1, s^{-1}	10^4 $k_{\psi\ exp}$, dm^3 mol^{-1} s^{-1}	10^4 $k_{\psi\ cal}$, dm^3 mol^{-1} s^{-1}	k_2/k_ψ
[SDS]	0.00	2.14	5.10	5.10	1.00
	2.00	2.12	5.05	4.99	1.01
	4.00	2.05	4.88	4.88	1.04
	6.00	1.98	4.71	4.77	1.08
	10.00	1.87	4.45	4.57	1.15
	20.00	1.77	4.21	4.17	1.21
	40.00	1.66	3.95	3.70	1.29
	60.00	1.57	3.74	3.44	1.36
	80.00	1.43	3.40	3.28	1.50
	100.00	1.31	3.12	3.17	1.64
$k_m = 2.68 \times 10^{-4}$ dm^3 mol^{-1} s^{-1}, $n = 1.15$,			$K_D = 9.19 \times 10^{-5}$ mol dm^{-3}, $K = 1.09 \times 10^4$ dm^3 mol^{-1}		
$[S_f]$	10^5 $[S_f]$, mol dm^{-3}	10^3 k_1, s^{-1}	10^4 $k_{\psi\ exp}$, dm^3 mol^{-1} s^{-1}	10^4 $k_{\psi\ cal}$, dm^3 mol^{-1} s^{-1}	k_2/k_ψ
[CTAB]	0.00	2.14	5.10	5.10	1.00
	2.00	2.07	4.93	5.04	1.03
	4.00	2.05	4.88	4.94	1.04
	6.00	2.00	4.76	4.82	1.07
	10.00	1.93	4.60	4.56	1.11
	20.00	1.68	4.00	4.05	1.28
	40.00	1.54	3.67	3.54	1.39
	60.00	1.38	3.29	3.33	1.55
	80.00	1.27	3.02	3.22	1.69
	100.00	1.20	2.86	3.17	1.79
$k_m = 3.01 \times 10^{-4}$ dm^3 mol^{-1} s^{-1}, $n = 1.56$,			$K_D = 1.76 \times 10^{-6}$ mol dm^{-3}, $K = 5.68 \times 10^5$ dm^3 mol^{-1}		

Table 4.62: Surfactant dependent rate constants and Piszkiewicz parameters for the reaction of $[Mn(salphen)]^+$ and H_2O_2 at $[Mn(salphen)^+]$ = 1.0×10^{-4} mol dm^{-3}, $[H_2O_2]$ = 0.15 mol dm^{-3}, μ = 0.2 C^2 mol dm^{-3}, $[H^+] = 2.0 \times 10^{-5}$ mol dm^{-3}, D = 76.82, T = 30 ± 1 °C and λ_{max} = 450 nm

$[S_f]$	10^5 $[S_f]$, mol dm^{-3}	10^3 k_1, s^{-1}	10^2 $k_{\Psi\ exp}$, dm^3 mol^{-1} s^{-1}	10^2 $k_{\Psi\ cal}$, dm^3 mol^{-1} s^{-1}	k_2/k_Ψ
[SDS]	0.00	1.863	1.242	1.242	1.00
	1.00	1.640	1.093	1.042	1.14
	2.00	1.270	0.846	0.849	1.47
	3.00	1.016	0.677	0.704	1.83
	4.00	0.912	0.608	0.597	2.04
	5.00	0.785	0.523	0.517	2.37
	6.00	0.698	0.465	0.456	2.67
	7.00	0.569	0.379	0.409	3.27
k_m = 1.00×10^{-3} dm^3 mol^{-1} s^{-1},			K_D = 1.37×10^{-6} mol dm^{-3},		
n = 1.31,			**K** = 7.35×10^5 dm^3 mol^{-1}		
$[S_f]$	10^5 $[S_f]$, mol dm^{-3}	10^3 k_1, s^{-1}	10^2 $k_{\Psi\ exp}$, dm^3 mol^{-1} s^{-1}	10^2 $k_{\Psi\ cal}$, dm^3 mol^{-1} s^{-1}	k_Ψ/k_2
[CTAB]	0.00	1.86	1.24	1.24	1.00
	1.00	1.96	1.31	1.32	1.05
	2.00	2.06	1.37	1.46	1.11
	3.00	2.20	1.47	1.64	1.18
	4.00	2.59	1.73	1.83	1.39
	5.00	3.07	2.05	2.03	1.65
	6.00	3.52	2.35	2.24	1.89
	7.00	3.71	2.47	2.44	1.99
k_m = 6.00×10^{-2} dm^3 mol^{-1} s^{-1},			K_D = 1.08×10^{-6} mol dm^{-3},		
n = 1.55,			**K** = 9.26×10^5 dm^3 mol^{-1}		

Table 4.63: Surfactant dependent rate constants and Piszkiewicz parameters for the reaction of $[Mn(salphen)]^+$ and RSH at $[Mn(salphen)^+]$ = 1.0×10^{-4} mol dm^{-3}, [RSH] = 0.40 mol dm^{-3}, μ = 0.6 C^2 mol dm^{-3}, $[H^+] = 4.0 \times 10^{-5}$ mol dm^{-3}, D = 78.19, T = 28 ± 1°C and λ_{max} = 450 nm

$[S_f]$	10^5 $[S_f]$, mol dm^{-3}	10^3 k_1, s^{-1}	10^2 $k_{\psi\ exp}$, dm^3 mol^{-1} s^{-1}	10^2 $k_{\psi\ cal}$, dm^3 mol^{-1} s^{-1}	k_2/k_ψ
[SDS]	0.00	5.08	1.27	1.27	1.00
	1.00	4.96	1.24	1.23	1.02
	2.00	4.80	1.20	1.15	1.06
	3.00	4.53	1.13	1.05	1.12
	4.00	3.76	0.94	0.94	1.35
	5.00	3.24	0.81	0.84	1.57
	6.00	2.65	0.663	0.75	1.92
	8.00	2.63	0.658	0.61	1.93
$k_m = 2.00 \times 10^{-3}$ dm^3 mol^{-1} s^{-1},			$K_D = 1.62 \times 10^{-8}$ mol dm^{-3},		
n = 1.85,			$K = 6.17 \times 10^7$ dm^3 mol^{-1}		
$[S_f]$	10^5 $[S_f]$, mol dm^{-3}	10^3 k_1, s^{-1}	10^2 $k_{\psi\ exp}$, dm^3 mol^{-1} s^{-1}	10^2 $k_{\psi\ cal}$, dm^3 mol^{-1} s^{-1}	k_2/k_ψ
[CTAB]	0.00	5.08	1.27	1.27	1.00
	1.00	4.86	1.21	1.20	1.05
	2.00	4.08	1.02	1.09	1.25
	3.00	4.05	1.01	0.96	1.25
	4.00	3.52	0.88	0.86	1.44
	5.00	2.92	0.73	0.76	1.74
	6.00	2.58	0.65	0.69	1.97
	8.00	2.56	0.64	0.59	1.98
$k_m = 3.01 \times 10^{-3}$ dm^3 mol^{-1} s^{-1},			$K_D = 5.44 \times 10^{-8}$ mol dm^{-3},		
n = 1.68,			$K = 1.84 \times 10^7$ dm^3 mol^{-1}		

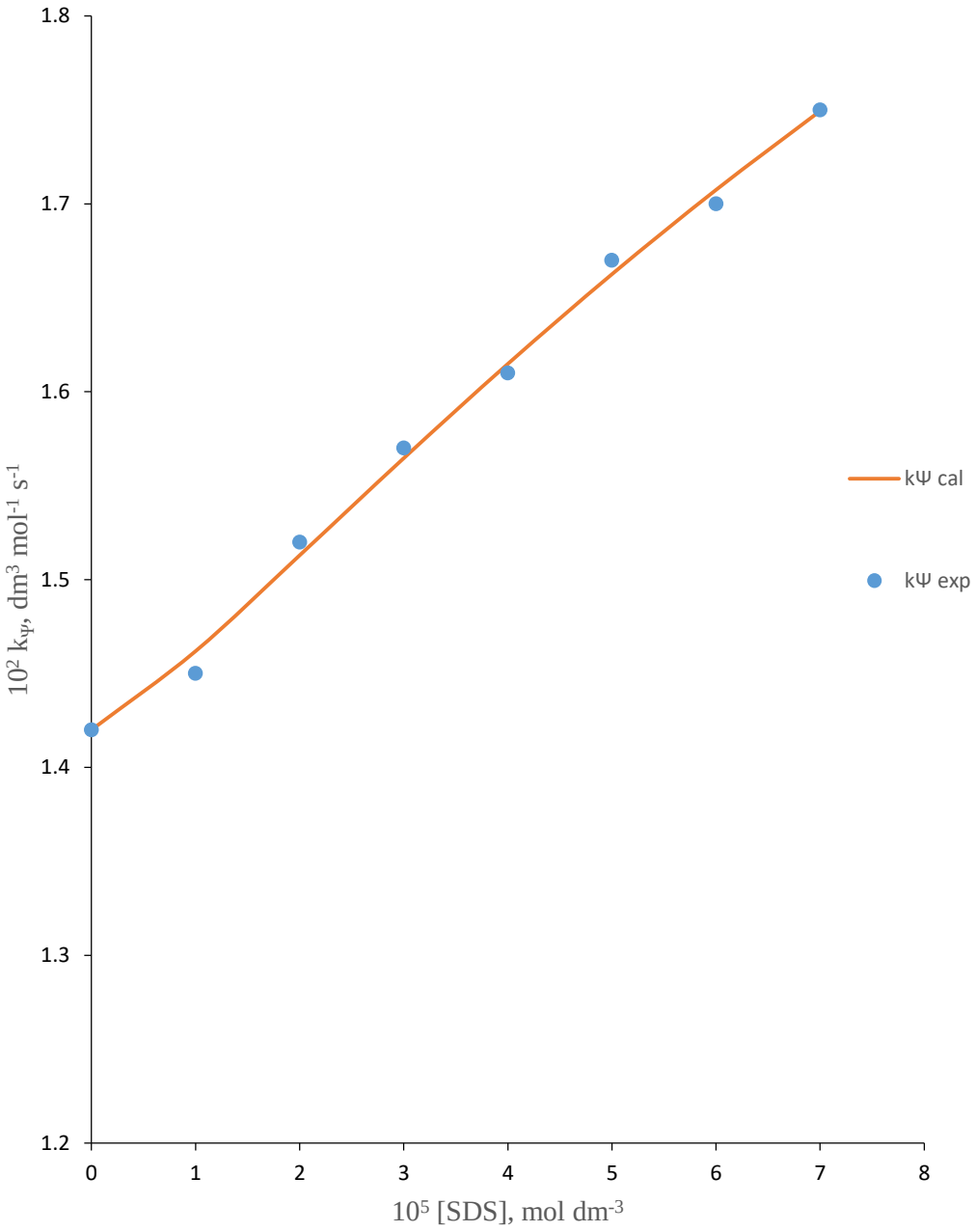


Figure 4.118: Plot of k_ψ against [SDS] fitted into the Piszkiewicz's equation for the reaction of $[Fe(salphen)]^+$ and TSH at $[Fe(salphen)^+]$ = 2.0×10^{-4} mol dm^{-3}, [TSH] = 0.15 mol dm^{-3}, μ = 0.2 C^2 mol dm^{-3}, D = 76.88, T = 26 ± 1°C and λ_{max} = 435 nm

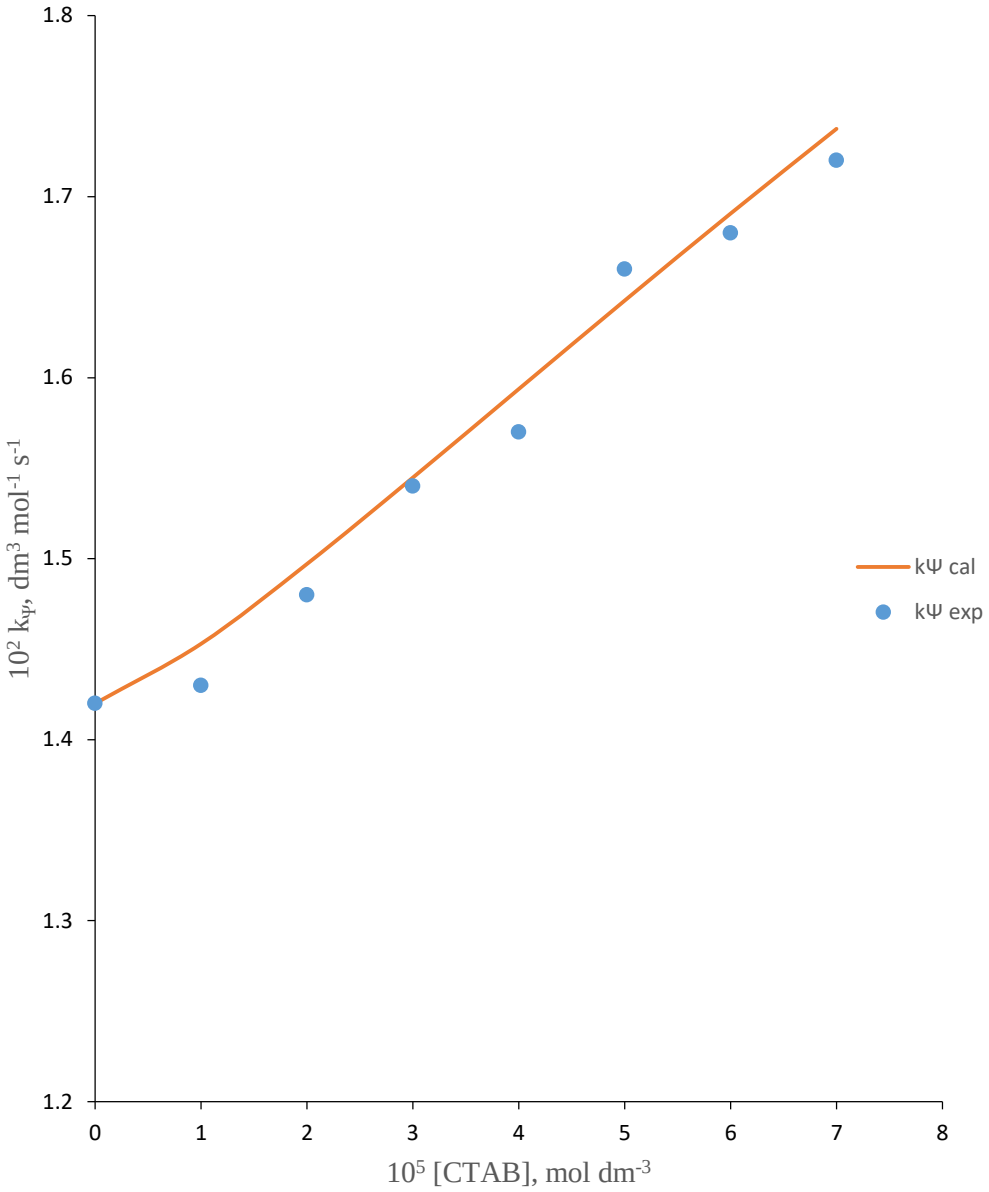


Figure 4.119: Plot of k_ψ against [CTAB] fitted into the Piszkiewicz's equation for the reaction of $[Fe(salphen)]^+$ and TSH at $[Fe(salphen)^+]$ = 2.0×10^{-4} mol dm^{-3}, [TSH] = 0.15 mol dm^{-3}, μ = 0.2 C^2 mol dm^{-3}, D = 76.88, T = 26 ± 1°C and λ_{max} = 435 nm

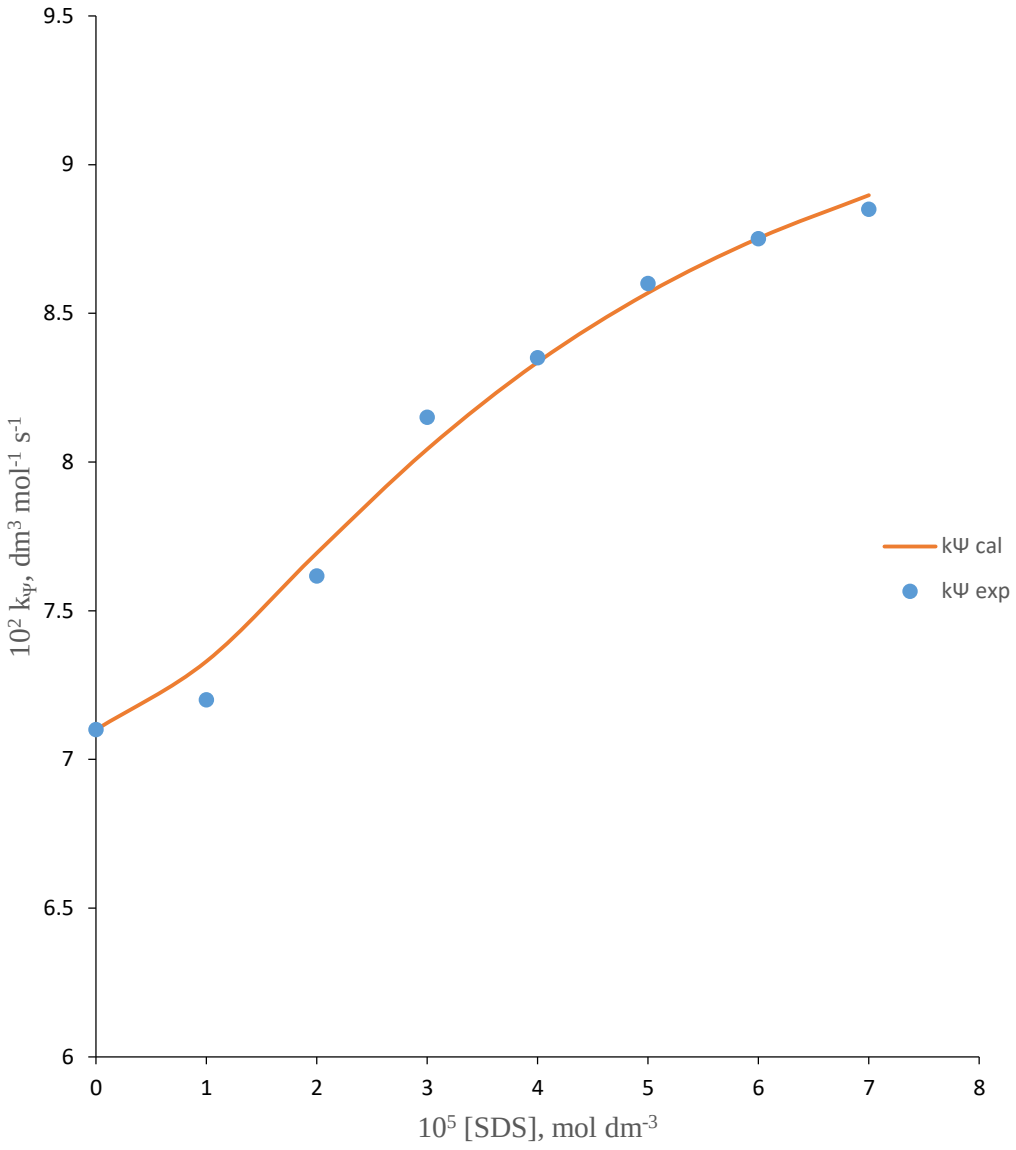


Figure 4.120: Plot of k_ψ against [SDS] fitted into the Piszkiewicz's equation for the reaction of $[Fe(salphen)]^+$ and $H_2C_2O_4$ at $[Fe(salphen)^+]$ = 2.0×10^{-4} mol dm^{-3}, $[H_2C_2O_4] = 6.0 \times 10^{-3}$ mol dm^{-3}, μ = 0.2 C^2 mol dm^{-3}, D = 76.06, T = 26 ± 1 °C and λ_{max} = 435 nm

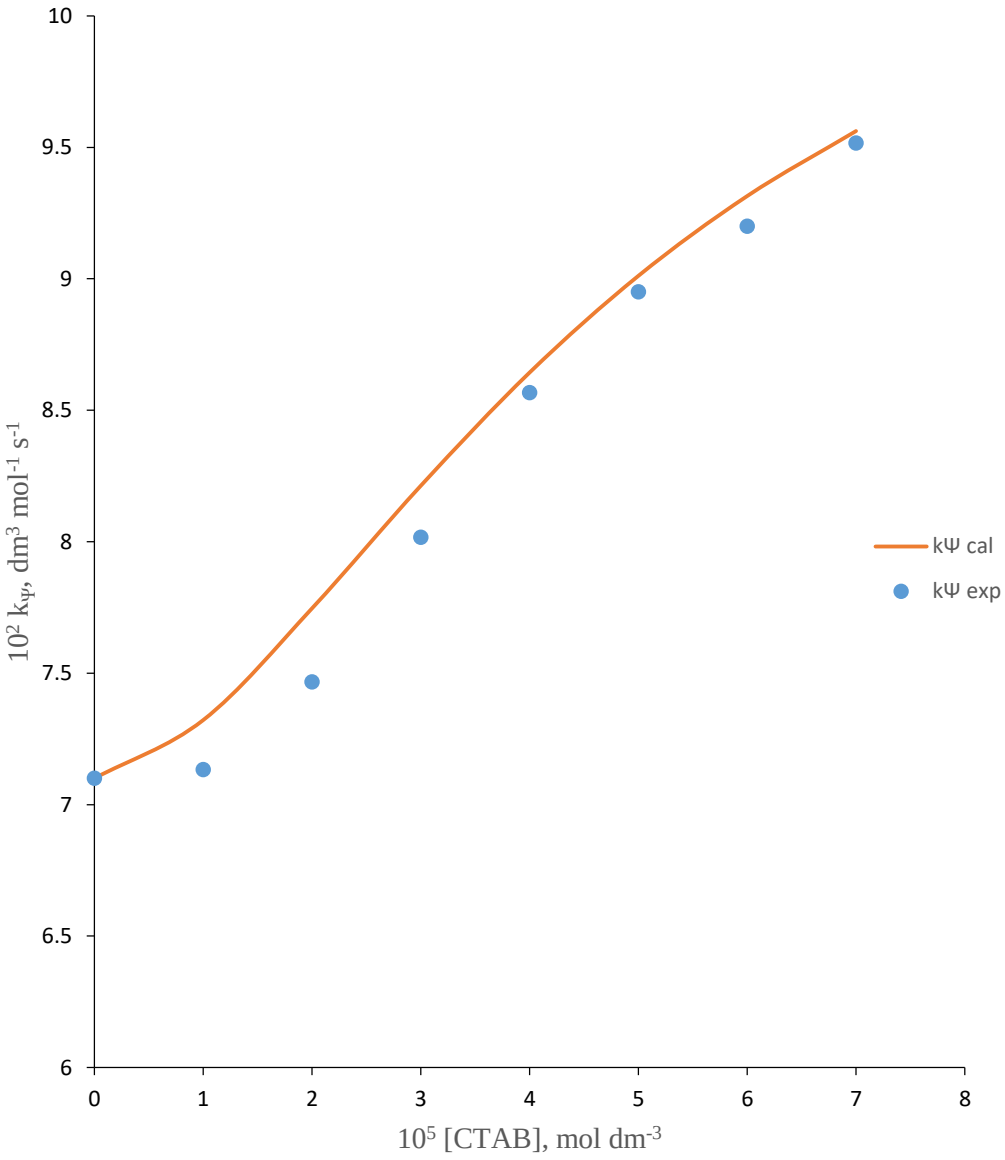


Figure 4.121: Plot of k_ψ against [CTAB] fitted into the Piszkiewicz's equation for the reaction of $[Fe(salphen)]^+$ and $H_2C_2O_4$ at $[Fe(salphen)^+] = 2.0 \times 10^{-4}$ mol dm^{-3}, $[H_2C_2O_4] = 6.0 \times 10^{-3}$ mol dm^{-3}, $\mu = 0.2$ C^2 mol dm^{-3}, D = 76.06, T = 26 ± 1 °C and λ_{max} = 435 nm

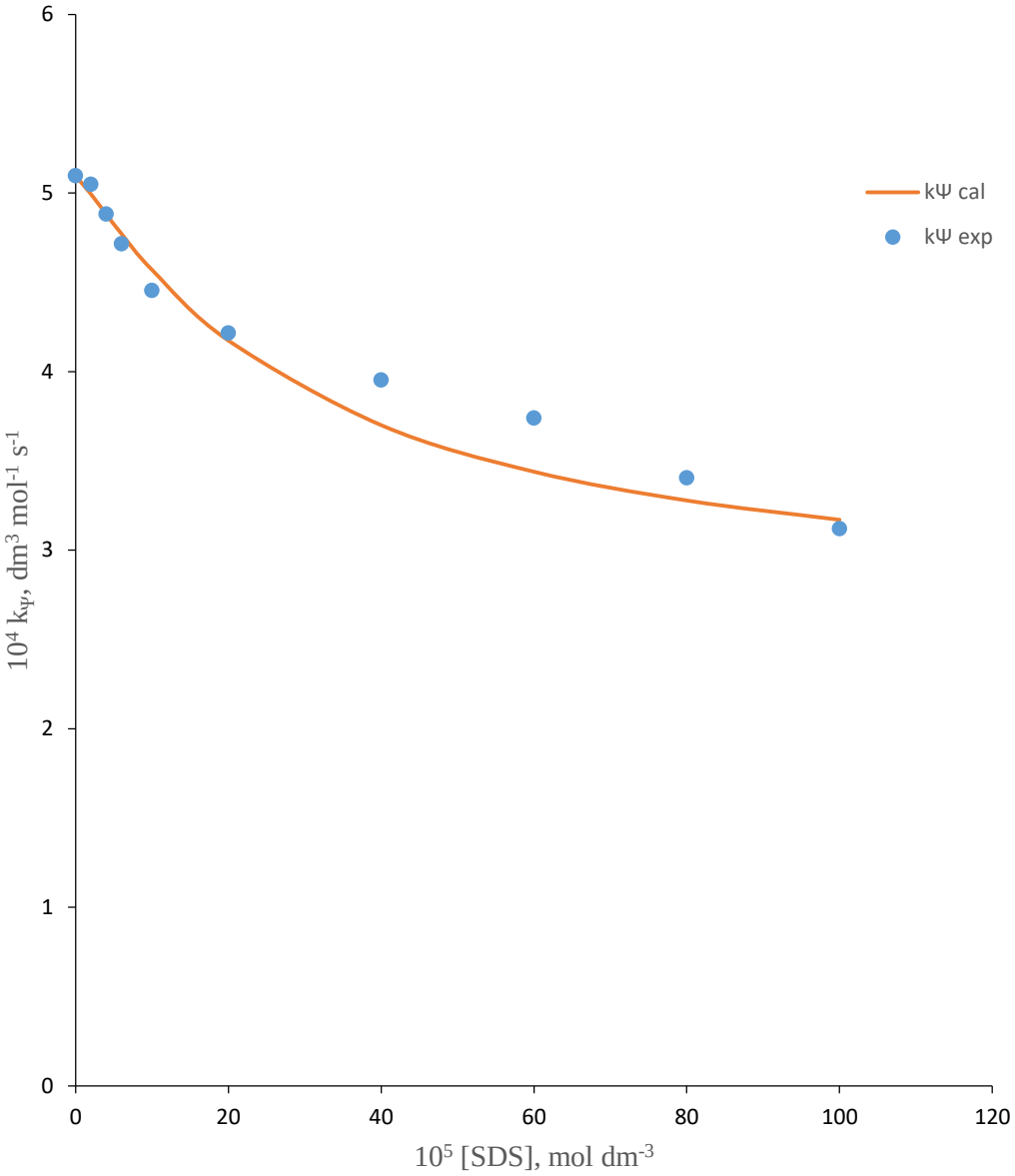


Figure 4.122: Plot of k_ψ against [SDS] fitted into the Piszkiewicz's equation for the reaction of $[Fe(salphen)]^+$ and H_2O_2 at $[Fe(salphen)^+] = 1.0 \times 10^{-4}$ mol dm^{-3}, $[H_2O_2] = 0.42$ mol dm^{-3}, $\mu = 0.6$ C^2 mol dm^{-3}, $[H^+] = 2.0 \times 10^{-5}$ mol dm^{-3}, D = 78.12, T = 28 ± 1°C and λ_{max} = 435 nm

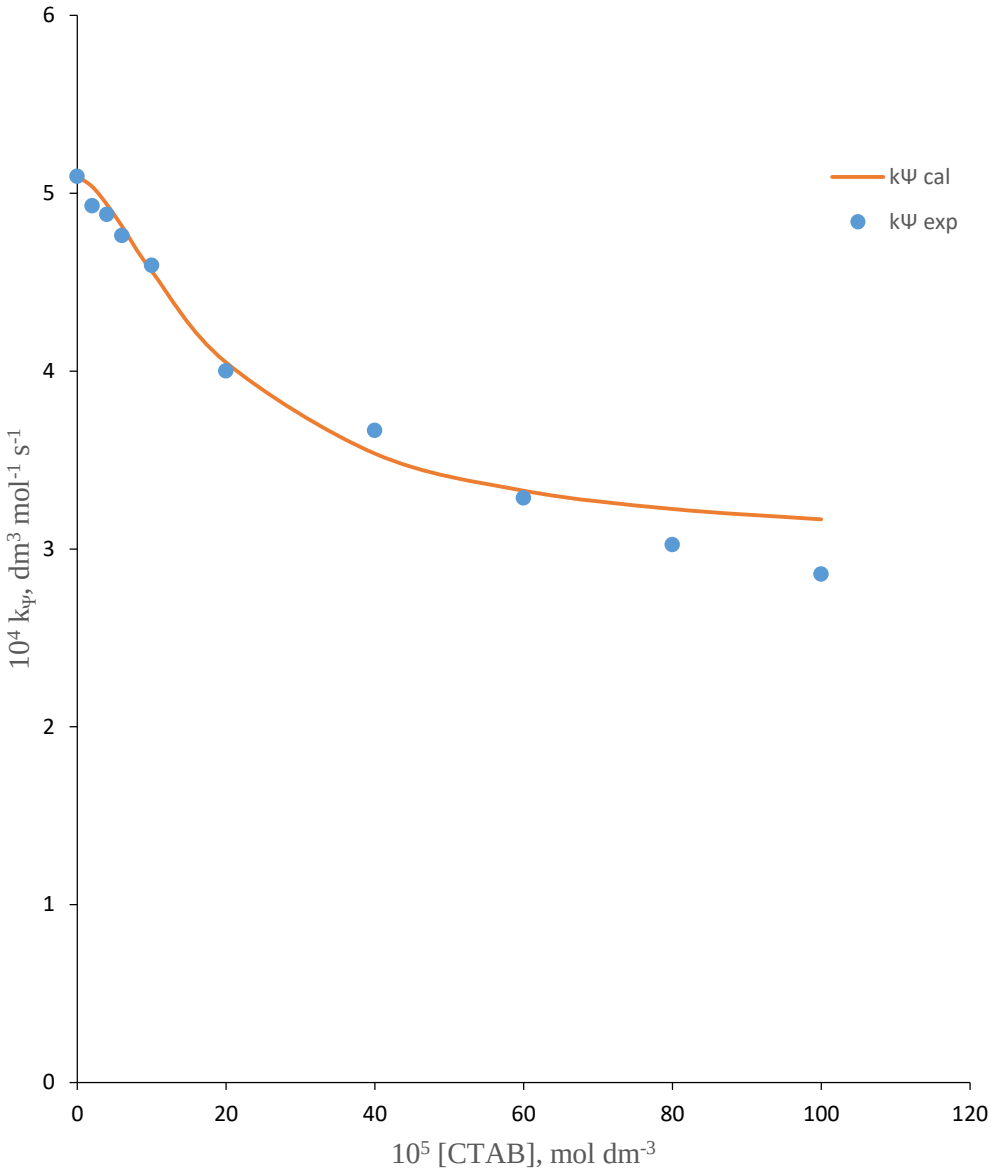


Figure 4.123: Plot of k_ψ against [CTAB] fitted into the Piszkiewicz's equation for the reaction of $[Fe(salphen)]^+$ and H_2O_2 at $[Fe(salphen)^+] = 1.0 \times 10^{-4}$ mol dm^{-3}, $[H_2O_2] = 0.42$ mol dm^{-3}, $\mu = 0.6$ C^2 mol dm^{-3}, $[H^+] = 2.0 \times 10^{-5}$ mol dm^{-3}, D = 78.12, T = 28 ± 1°C and λ_{max} = 435 nm

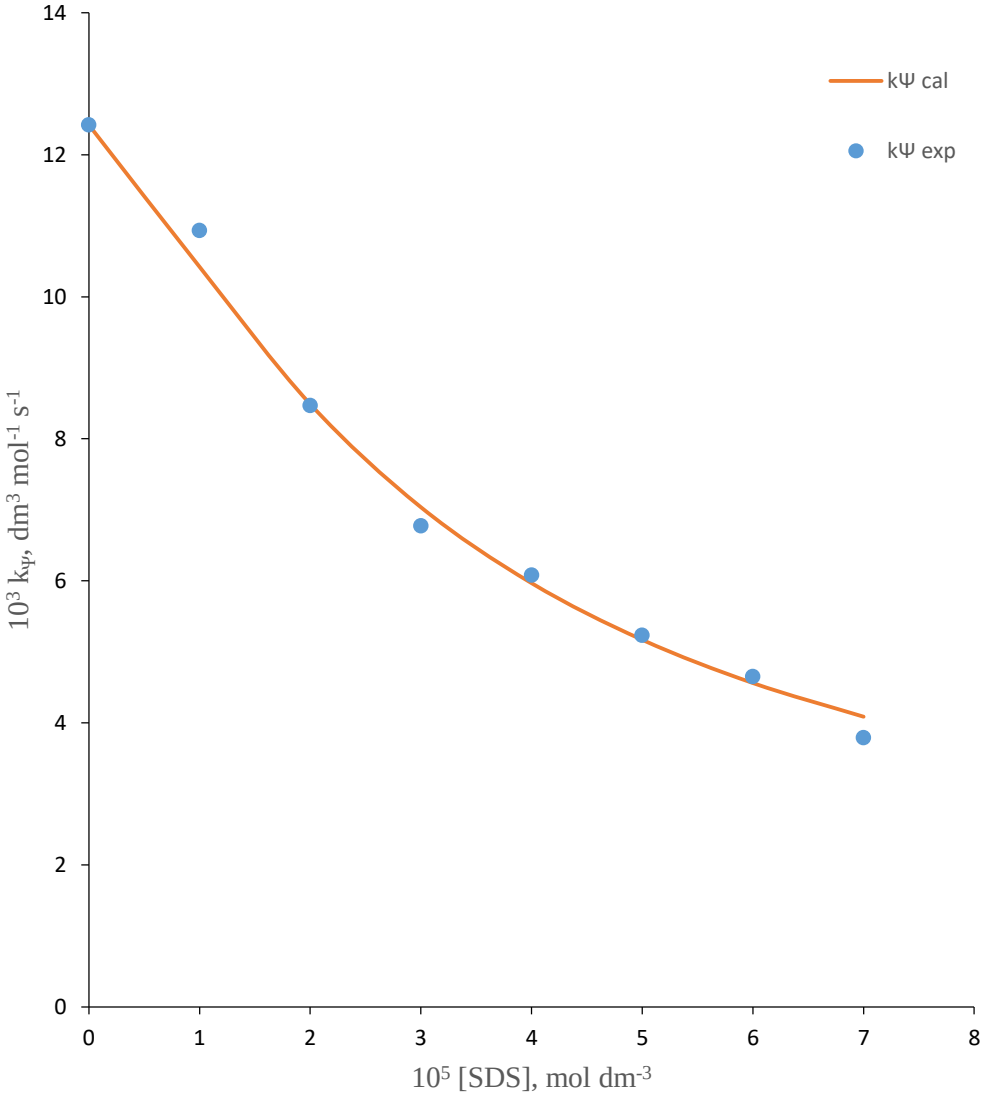


Figure 4.124: Plot of k_ψ against [SDS] fitted into the Piszkiewicz's equation for the reaction of $[Mn(salphen)]^+$ and H_2O_2 at $[Mn(salphen)^+]$ = 1.0×10^{-4} mol dm^{-3}, $[H_2O_2]$ = 0.15 mol dm^{-3}, μ = 0.2 C^2 mol dm^{-3}, $[H^+] = 2.0 \times 10^{-5}$ mol dm^{-3}, D = 76.82, T = 30 ± 1°C and λ_{max} = 450 nm

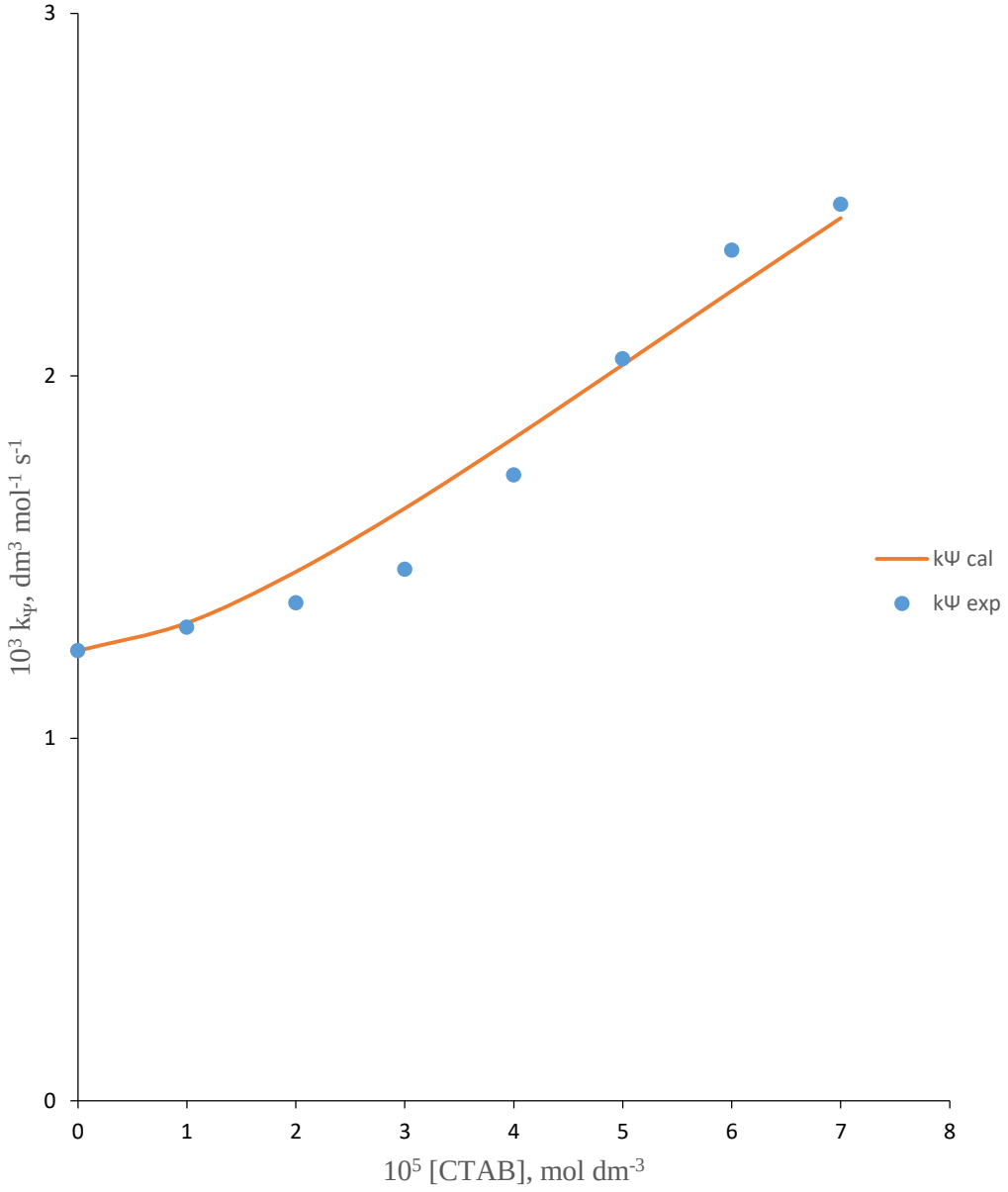


Figure 4.125: Plot of k_ψ against [CTAB] fitted into the Piszkiewicz's equation for the reaction of $[Mn(salphen)]^+$ and H_2O_2 at $[Mn(salphen)^+] = 1.0 \times 10^{-4}$ mol dm^{-3}, $[H_2O_2] = 0.15$ mol dm^{-3}, $\mu = 0.2$ C^2 mol dm^{-3}, $[H^+] = 2.0 \times 10^{-5}$ mol dm^{-3}, D = 76.82, T = 30 ± 1 °C and λ_{max} = 450 nm

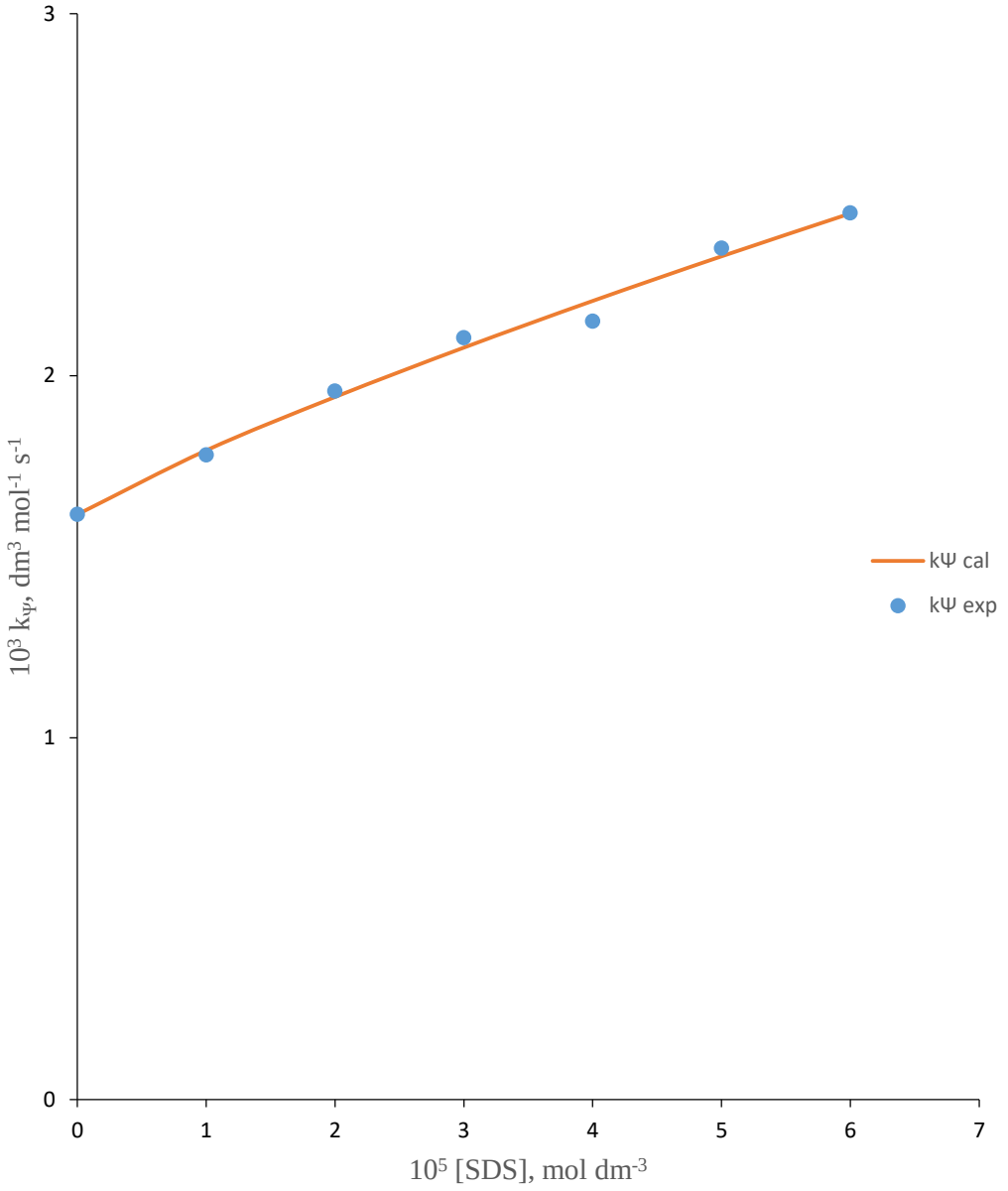


Figure 4.126: Plot of k_ψ against [SDS] fitted into the Piszkiewicz's equation for the reaction of $[Mn(salphen)]^+$ and TSH at $[Mn(salphen)^+] = 1.0 \times 10^{-4}$ mol dm^{-3}, [TSH] = 0.42 mol dm^{-3}, μ = 0.6 C^2 mol dm^{-3}, D = 77.98, T = 32 ± 1°C and λ_{max} = 450 nm

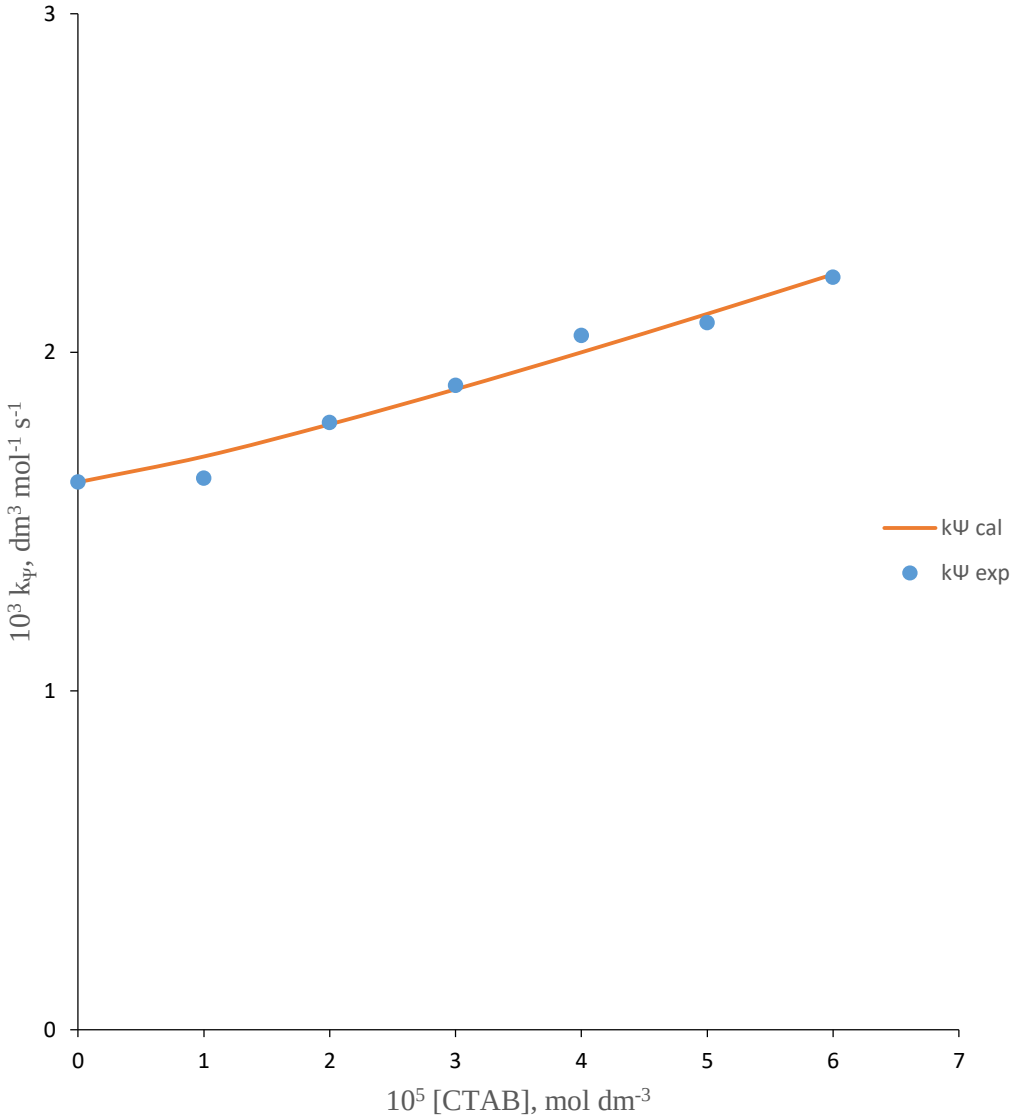


Figure 4.127: Plot of k_ψ against [CTAB] fitted into the Piszkiewicz's equation for the reaction of $[Mn(salphen)]^+$ and TSH at $[Mn(salphen)^+]$ = 1.0×10^{-4} mol dm^{-3}, [TSH] = 0.42 mol dm^{-3}, μ = 0.6 C^2 mol dm^{-3}, D = 77.98, T = 32 ± 1 °C and λ_{max} = 450 nm

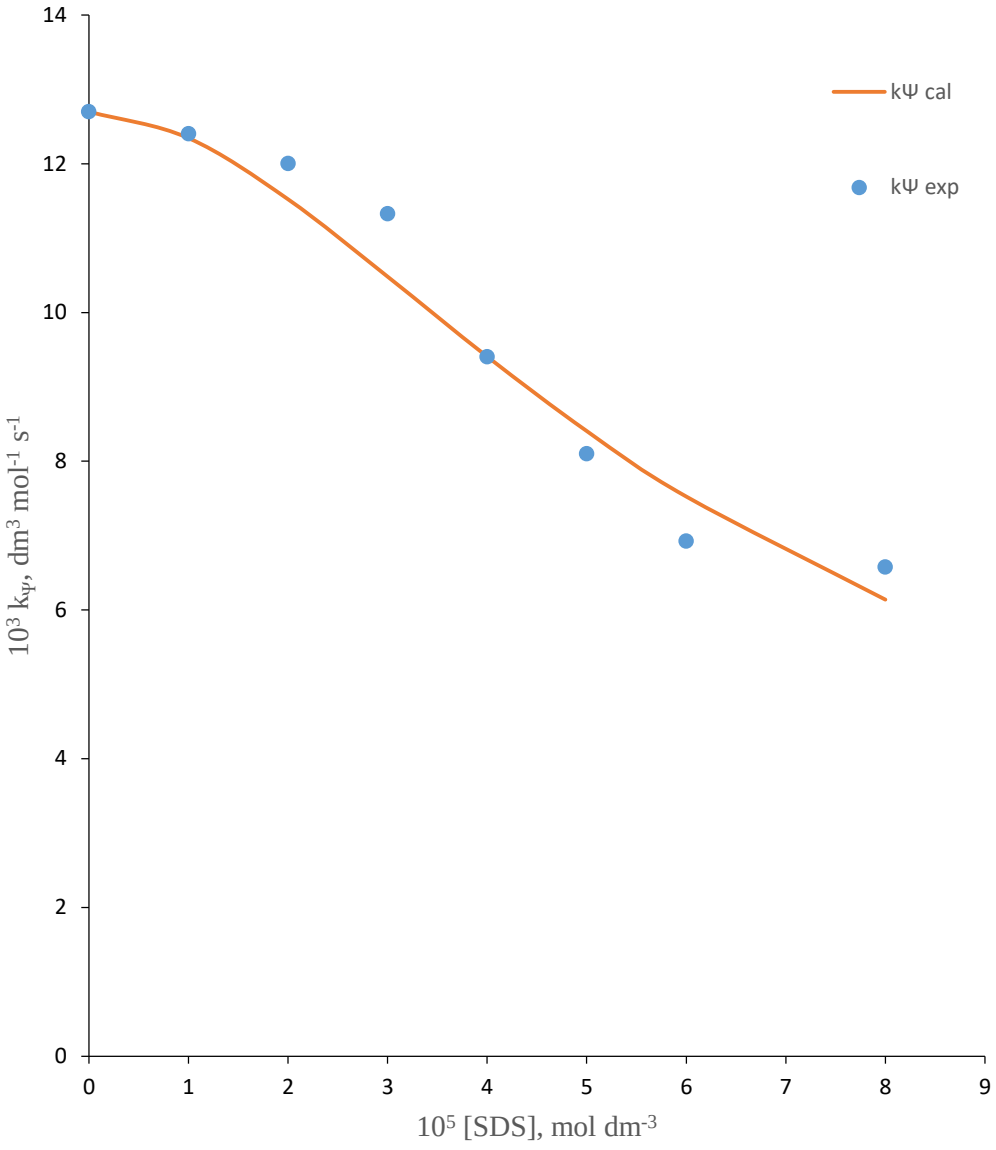


Figure 4.128: Plot of k_ψ against [SDS] fitted into the Piszkiewicz's equation for the reaction of $[Mn(salphen)]^+$ and RSH at $[Mn(salphen)^+] = 1.0 \times 10^{-4}$ mol dm^{-3}, [RSH] = 0.40 mol dm^{-3}, μ = 0.6 C^2 mol dm^{-3}, $[H^+] = 4.0 \times 10^{-5}$ mol dm^{-3}, D = 78.19, T = 28 ± 1 °C and λ_{max} = 450 nm

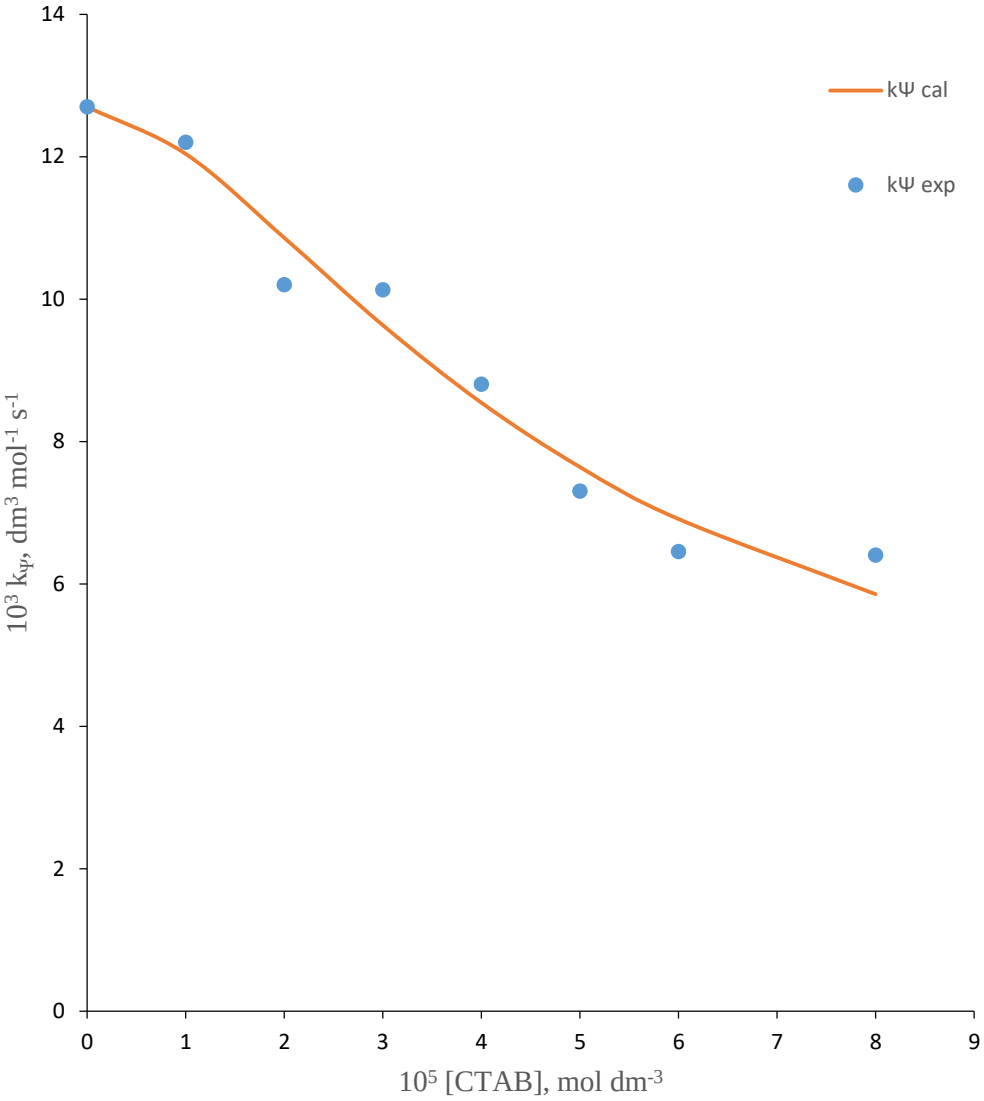


Figure 4.129: Plot of k_ψ against [CTAB] fitted into the Piszkiewicz's equation for the reaction of $[Mn(salphen)]^+$ and RSH at $[Mn(salphen)^+] = 1.0 \times 10^{-4}$ mol dm^{-3}, [RSH] = 0.40 mol dm^{-3}, $\mu = 0.6$ C^2 mol dm^{-3}, $[H^+] = 4.0 \times 10^{-5}$ mol dm^{-3}, D = 78.19, T = 28 ± 1 °C and λ_{max} = 450 nm

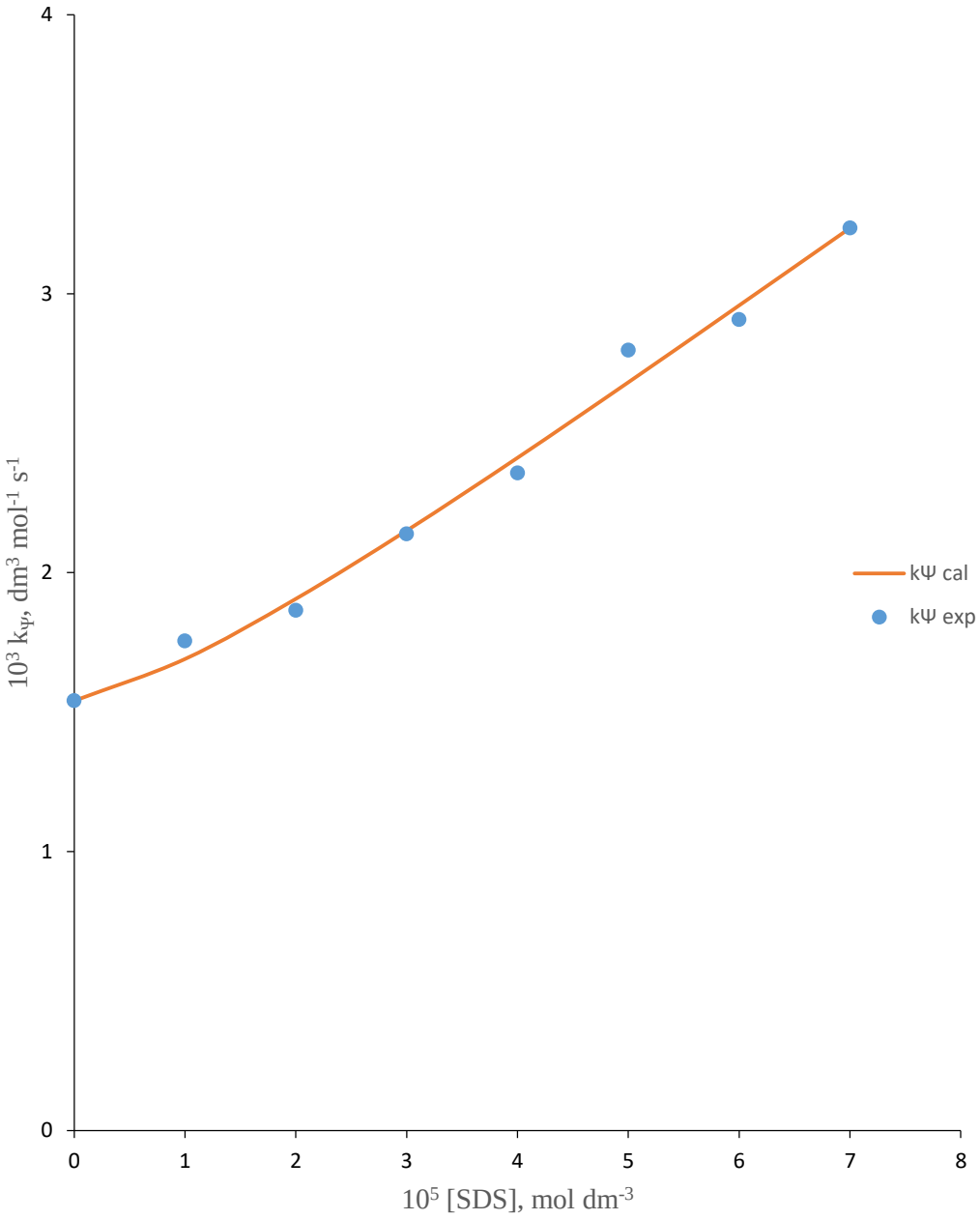


Figure 4.130: Plot of k_ψ against [SDS] fitted into the Piszkiewicz's equation for the reaction of $[Mn(salphen)]^+$ and SCN^- at $[Mn(salphen)^+]$ = 1.0×10^{-4} mol dm^{-3}, $[SCN^-]$ = 0.42 mol dm^{-3}, μ = 0.6 C^2 mol dm^{-3}, $[H^+]$ = 4.0×10^{-5} mol dm^{-3}, D = 78.12, T = 28 ± 1 °C and λ_{max} = 450 nm

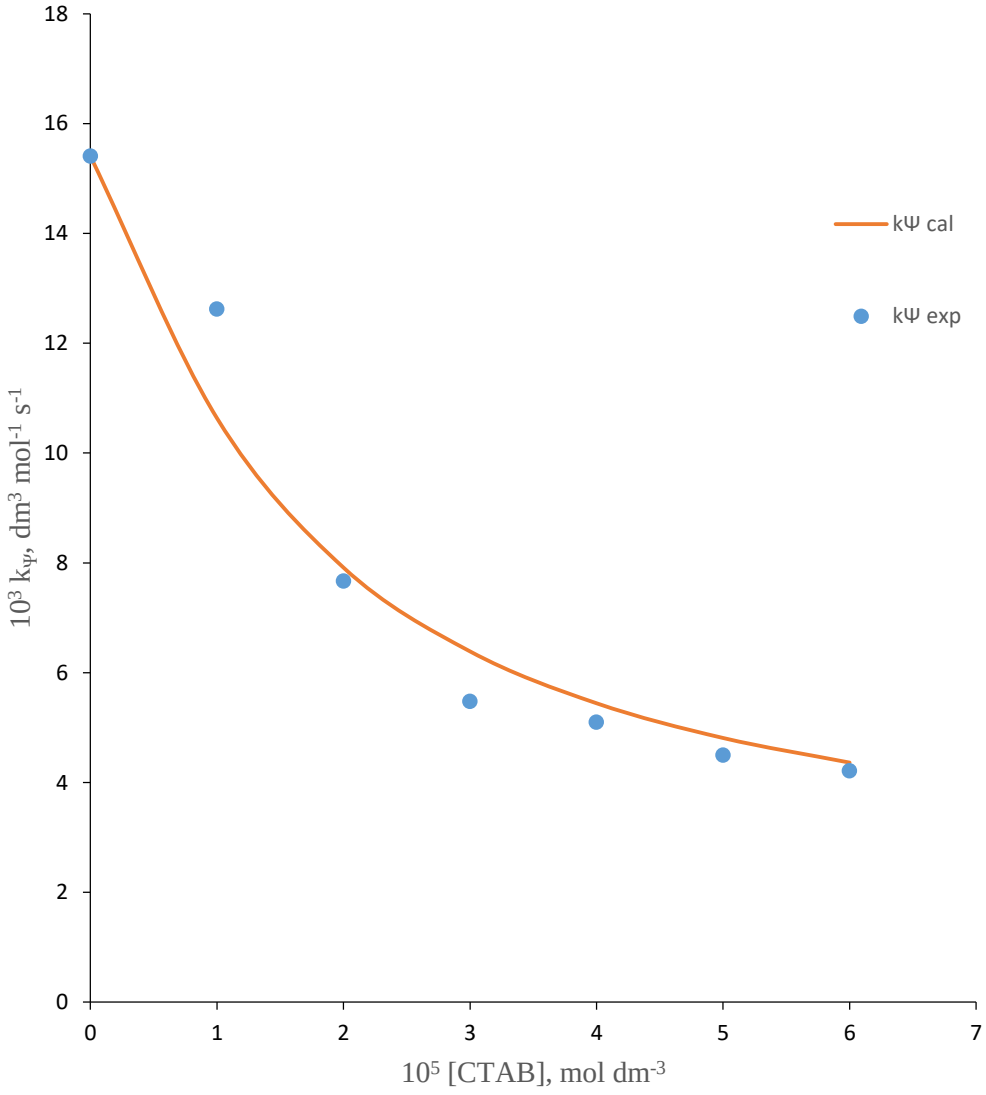


Figure 4.131: Plot of k_ψ against [CTAB] fitted into the Piszkiewicz's equation for the reaction of $[Mn(salphen)]^+$ and SCN^- at $[Mn(salphen)^+] = 1.0 \times 10^{-4}$ mol dm^{-3}, $[SCN^-] = 0.42$ mol dm^{-3}, $\mu = 0.6$ C^2 mol dm^{-3}, $[H^+] = 4.0 \times 10^{-5}$ mol dm^{-3}, D = 78.12, T = 28 ± 1 °C and λ_{max} = 450 nm

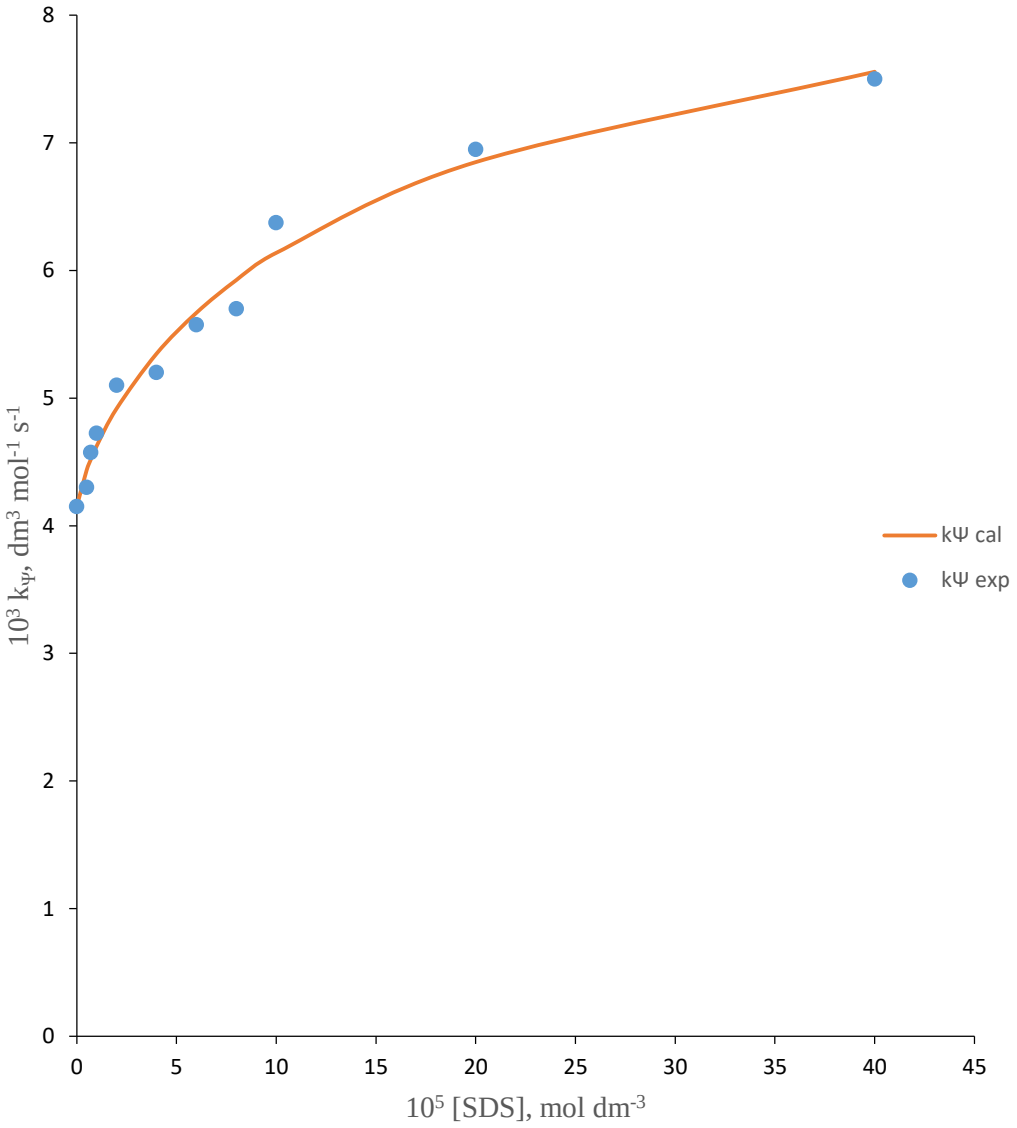


Figure 4.132: Plot of k_ψ against [SDS] fitted into the Piszkiewicz's equation for the reaction of $[Mn(salphen)]^+$ and $S(CH_2CH_2OH)_2$ at $[Mn(salphen)^+] = 1.0 \times 10^{-4}$ mol dm^{-3}, $[S(CH_2CH_2OH)_2] = 0.40$ mol dm^{-3}, $\mu = 0.6$ C^2 mol dm^{-3}, $[H^+] = 2.0 \times 10^{-5}$ mol dm^{-3}, D = 66.60, T = 50 ± 1°C and λ_{max} = 450 nm

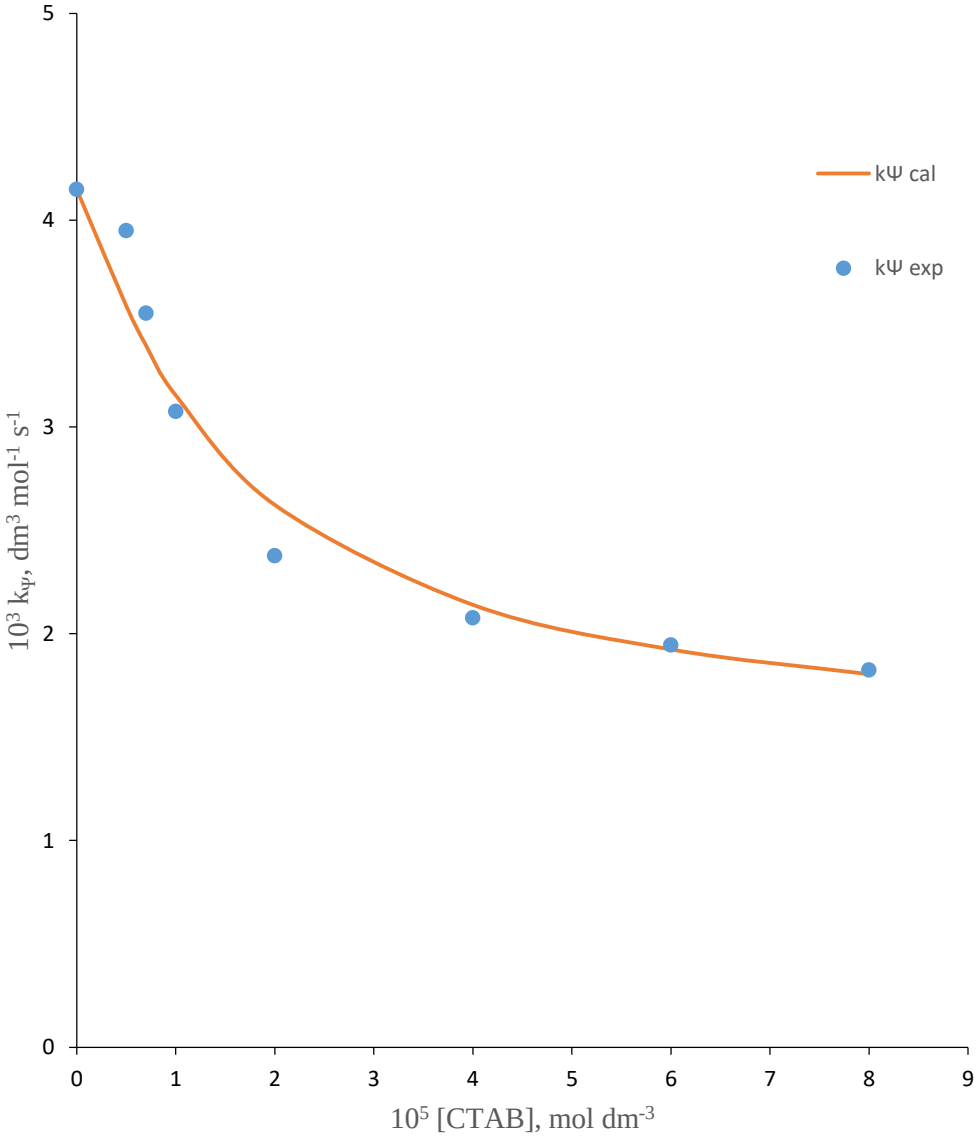


Figure 4.133: Plot of k_ψ against [CTAB] fitted into the Piszkiewicz's equation for the reaction of $[Mn(salphen)]^+$ and $S(CH_2CH_2OH)_2$ at $[Mn(salphen)^+] = 1.0 \times 10^{-4}$ mol dm^{-3}, $[S(CH_2CH_2OH)_2] = 0.40$ mol dm^{-3}, $\mu = 0.6$ C^2 mol dm^{-3}, $[H^+] = 2.0 \times 10^{-5}$ mol dm^{-3}, D = 66.60, T = 50 ± 1°C and λ_{max} = 450 nm

CHAPTER FIVE

5.0 DISCUSSION

5.1 Synthesis of $[Fe(salphen)]^+$ and $[Mn(salphen)]^+$ Ions

The band observed at 3050 cm^{-1} from the FTIR spectra of the ligand (Appendix I) was assigned to (*v*=C-H) stretching, whereas that observed at 1608 cm^{-1} was assigned to (*v*C=N) stretching which shifted to 1602 cm^{-1} in $[Fe(salphen)]^+$ complex (Appendix II) and 1604 cm^{-1} in $[Mn(salphen)]^+$ complex (Appendix III), an indication of complexation of the imine group with the central metal ions. Similarly, the band observed at 1274 cm^{-1} was assigned to (*v*C-O) stretching in the ligand which shifted to 1197 cm^{-1} in $[Fe(salphen)]^+$ and 1190 cm^{-1} in $[Mn(salphen)]^+$, indicating the involvement of the oxygen atom of the carbonyl group of the ligand in complex formation (Ansari *et al*., 2009a; Ansari *et al*., 2009b; Bashyal, 2013).

From the spectra of $[Fe(salphen)]^+$, the band appearing at 536 cm^{-1} was assigned to (*v*Fe-O) stretching while that at 475 cm^{-1} was assigned to (*v*Fe-N) stretching. Similarly, from the spectra of $[Mn(salphen)]^+$, the band at 539 cm^{-1} was ascribed to (*v*Mn-O) stretching while that at 446 cm^{-1} was ascribed to (*v*Mn-N) stretching (Appendix II and III) (Ansari *et al*., 2009a; Ansari *et al*., 2009b; Bashyal, 2013).

The UV-Vis spectrum of $[Fe(salphen)]^+$ showed a λ_{max} at 435 nm while that of $[Mn(salphen)]^+$ was at 450 nm. The observed molar conductivity of $[Fe(salphen)]^+$, 145 S cm^2 mol^{-1}, with specific conductance of 29.0×10^{-6} S cm^{-1} and $[Mn(salphen)]^+$ with a molar conductivity of 112 S cm^2 mol^{-1} and specific conductance of 11.20×10^{-6} S cm^{-1} are consistent with a 1:1 electrolyte (Ali *et al*., 2013). The existence of $[Fe(salen)]^+$ species

in DMSO–H_2O (4:1 v/v) and CH_3CN–H_2O (1:1 v/v) solvent systems have been reported previously (Liou and Wang, 2000; Subramaniam *et al*., 2014).

5.2 Reactions of TSH with $[Fe(salphen)]^+$ and $[Mn(salphen)]^+$

From the stoichiometric studies, the mole ratio of the reactions were found to be 1:1 (Figures 4.1 and 4.6) and is represented by equation 5.1.

$$2[M(salphen)]^+ + 2TSH \longrightarrow 2[M(salphen)] + TSST + 2H^+ \qquad 5.1$$

where M = Fe or Mn

A similar stoichiometry of 1:1 has been reported in the reactions of $[Co(ox)_3]^{3-}$ (Lawal *et al*., 1994), $[Mn^{III}(cdta)]^-$ (Gangopadhyay *et al*., 1994b), Ru_2O^{4+} (Musa *et al*., 1995), $[IrCl_6]^{2-}$ (Sun and Stanbury, 2002), Fe_2O^{4+} (Idris *et al*., 2007) and Co^{III} superoxide complex (Mandal *et al*., 2015) with TSH. However, in the reaction of TSH with $[Pt(CN)_4Cl_2]^{2-}$ (Shi *et al*., 1996), a mole ratio of 2:1 (TSH with $[Pt(CN)_4Cl_2]^{2-}$) was obtained. This is consistent with TSH being a 1 electron donor whereas Pt(IV) in the complex accepts two 2 electrons donated by 2 TSH molecules and is reduced to Pt(II).

The test for the Fe^{2+} product gave a brown precipitate of Fe_2O_3 as a result of the $KMnO_4$ oxidation of the Fe^{2+} complex that formed during the reduction of $[Fe(salphen)]^+$ (Misfud, 2009). The appearance of a purple colour of MnO_4^-, the oxidation product of Mn^{2+} by KIO_4 shows the presence of Mn^{2+} product (Nazarenko, 2004).

The presence of TSST, the oxidation product of TSH, was confirmed according to earlier published procedures (McAuley and Gomwalk, 1968; McAuley and Gomwalk, 1969). From the FTIR results, bands observed at 2916 cm^{-1}, 1679 cm^{-1}, 1257 cm^{-1} and 562 cm^{-1}, were assigned to (νO-H), (νC=O), (νC-O) and (νS-S) stretching respectively for

[Fe(salphen)]$^{+}$ reaction with TSH (Appendix IV). Similarly, bands appearing at 2917 cm^{-1}, 1681 cm^{-1}, 1258 cm^{-1} and 562 cm^{-1} were assigned to (νO-H), (νC=O), (νC-O) and (νS-S) stretching respectively for [Mn(salphen)]$^{+}$ reaction with TSH (Trofimov *et al*., 2009) (Appendix V). This result supports the formation of $HOOCCH_2S\text{-}SCH_2COOH$ as the organic product of TSH oxidation.

The results obtained from the plots of $\log(A_t\text{-}A_\infty)$ against time, t, (Figures 4.11 and 4.16) indicated first order dependence in [M(salphen)$^{+}$]. The reactions order with respect to [TSH] were determined by plotting log k_1 against log [TSH] and the gradient of the linear graphs obtained were 0.98 for TSH - [Fe(salphen)]$^{+}$ and 0.99 for TSH - [Mn(salphen)]$^{+}$ reactions (Figures 4.21 and 4.26) indicating first order dependence in [TSH]. The values of second order rate constants, k_2 were fairly constant (Tables 4.1 and 4.6), a confirmation that the reaction is second order overall. The rate equation for the reactions can be represented by equation 5.2.

$$\frac{-d[M(salphen)^+]}{dt} = k_2[M(salphen)^+][TSH] \qquad 5.2$$

where M = Fe^{3+} or Mn^{3+}

k_2 = $1.42 \pm 0.02 \times 10^{-2}$ dm^3 mol^{-1} s^{-1} for [Fe(salphen)]$^{+}$ reaction

= $1.62 \pm 0.02 \times 10^{-3}$ dm^3 mol^{-1} s^{-1} for [Mn(salphen)]$^{+}$ reaction

The observed first order dependence in [TSH] is similar to reported results in the redox reactions of TSH with $[Mn^{III}(cdta)]^-$ (Gangopadhyay et al., 1994b), trans-$[Pt(CN)_4Cl_2]^{2-}$ (Shi *et al*., 1996), $[IrCl_6]^{2-}$ (Sun and Stanbury, 2002), IO_3^- (Ukoha and Ibrahim, 2004) and Co^{III} superoxide complex (Mandal *et al*., 2015). However, a zero order

dependence in [TSH] has also been reported in the reaction of Fe_2O^{4+} with TSH (Idris *et al*., 2007).

The reaction rates were independent of $[H^+]$ as shown in Tables 4.11 and 4.12, suggesting that the undissociated thioglycolic acid, $HSCH_2COOH$ is involved in the reaction. Similar acid dependence has been established in the reaction of Fe_2O^{4+} with TSH (Idris *et al*., 2007). However, acid catalysis was reported in the reaction of trans-$[Pt(CN)_4Cl_2]^{2-}$ with TSH (Shi *et al*., 1996) while an inverse acid dependence was observed for Co^{III} superoxide complex reaction with TSH (Mandal *et al*., 2015).

Results from Tables 4.1 and 4.6 show that changes in ionic strength of the reaction medium had no effect on the reaction rate indicating zero Brønsted – Debye salt effect. Similar effect has been reported in the reaction of TSH and Fe_2O^{4+} (Idris *et al*., 2007). This implies that the activated complex is formed from reactants of charged ion ($[M(salphen)]^+$) and uncharged molecule (TSH) (Atkins and de Paula, 2018). This assertion was supported from the negligible effect on the reaction rate observed from changing the dielectric constants of the reaction medium (Tables 4.15 and 4.19).

Increase in concentrations of added ions (Mg^{2+}, Ca^{2+}, $HCOO^-$, CH_3COO^- and NO_3^-) catalysed the reactions (Tables 4.26, 4.29, 4.36 and 4.39). Previous investigation has shown reaction involving the ion, ($[M(salphen)]^+$) and dipole molecules (TSH) to be catalysed by added ions as observed in the reaction of $[Fe(salen)]^+$ with thiodiglycolic acid (Subramaniam *et al*., 2014). This catalytic effect is consistent with a reaction occurring through an outer-sphere pathway of electron transfer.

From the Eyring's plot of $\ln\left(\frac{k_2}{T}\right)$ versus $\left(\frac{1}{T}\right)$ (Figures 4.82 and 4.87) thermodynamic parameters were calculated and results are presented in Tables 4.45 and 4.50. The negative value of $\Delta S^{\ddagger}$ and positive $\Delta H^{\ddagger}$ shows that the species in the activated complex is more ordered, indicative of an associatively activated process (Ukoha *et al*., 2010) and that the transition state is highly solvated (Katre *et al*., 2012), suggesting bond formation during the process of activation.

There was no shift in λ_{max} at 435 nm for $[Fe(salphen)]^+$ and 450 nm for $[Mn(salphen)]^+$ when the spectra of the reaction mixtures were compared with that of the complexes alone (Figures 4.92 and 4.97) and the Michaelis-Menten plots of $\frac{1}{k_1}$ versus $\frac{1}{[TSH]}$ were linear with zero intercept. These two pieces of evidences support lack of formation of intermediate complex.

Addition of solution of acrylamide radical scavenger, to the partially reacted reaction mixture in the presence of large excess of methanol gave a gelatinous precipitate, indicating the involvement of free radicals in the reaction (Sun and Stanbury, 2002; Mandal *et al*., 2015).

On the basis of the results obtained from the investigation, the following reaction scheme is proposed for this reaction:

$$[M(salphen)]^+ + TSH \xrightarrow{k_3} [M(salphen)\text{–}TSH]^+ \qquad 5.3$$

$$[M(salphen)\text{–}TSH]^+ \xrightarrow[slow]{k_4} [M(salphen)] + TS^{\bullet} + H^+ \qquad 5.4$$

$$[M(salphen)]^+ + TSH \xrightarrow[slow]{k_5} [M(salphen)] + TS^{\bullet} + H^+ \qquad 5.5$$

$$TS^{\bullet} + TS^{\bullet} \xrightarrow{k_6} TSST \qquad 5.6$$

$$Rate = k_4 [M(salphen)\text{–}TSH]^+ + k_5 [M(salphen)^+][TSH] \qquad 5.7$$

Applying steady state approximation;

$$\frac{-d[Msalphen\text{–}TSH^+]}{dt} = k_3\,[M(salphen)^+][TSH] - k_{-3}\,[M(salphen)\text{–}TSH^+] - k_4[M(salphen)\text{–}TSH^+] \approx 0 \qquad 5.8$$

$$[M(salphen)\text{–}TSH^+] = \frac{k_3[M(salphen)^+][TSH]}{k_{-3} + k_4} \qquad 5.9$$

Substituting equation 5.9 into equation 5.7

$$\text{Rate} = \frac{k_4 k_3[M(salphen)^+][TSH]}{k_{-3} + k_4} + k_5\,[M(salphen)^+][TSH] \qquad 5.10$$

$$\text{Rate} = \left(\frac{k_4 k_3}{k_{-3} + k_4} + k_5\right)[M(salphen)^+][TSH] \qquad 5.11$$

Equation 5.11 is analogous to equation 5.2

where $k_2 = \left(\frac{k_4 k_3}{k_{-3} + k_4} + k_5\right) = 1.42 \pm 0.02 \times 10^{-2}$ dm^3 mol^{-1} s^{-1} for $[Fe(salphen)]^+$

$= 1.62 \pm 0.02 \times 10^{-3}$ dm^3 mol^{-1} s^{-1} for $[Mn(salphen)]^+$

A key point of interest in this discussion is whether this reaction occurs via the inner- or outer-sphere mechanism or a combination of both. Although, an outer-sphere mechanism has been reported for the reaction of TSH with $[IrCl_6]^{2-}$ (Sun and Stanbury, 2002), in the same view, an inner-sphere pathway has also been observed in the reactions of TSH with $[Mn^{III}(cdta)]^-$ (Gangopadhyay *et al*., 1994b) and $[Pt(CN)_4Cl_2]^{2-}$ (Shi *et al*., 1996). This issue for the reactions of $[Fe(salphen)]^+$ and $[Mn(salphen)]^+$ with TSH can be addressed as follows;

(a) The existence of ion catalysis is characteristic of reactions occurring via the outer-sphere mechanism.

(b) Spectroscopic evidence indicated no shift in λ_{max} suggesting that there was no inner-sphere complex formation. This observation suggests the occurrence of the outer-sphere mechanism.

(c) Michaelis - Menten plot of $\frac{1}{k_1}$ versus $\frac{1}{[TSH]}$ had zero intercept which suggests the absence of a detectable intermediate in the rate determining step. This observation also suggests the occurrence of the outer-sphere mechanism.

The points (a) – (c) overwhelmingly tilt the argument in favour of outer-sphere mechanism and is hereby proposed for the reaction.

5.3 Reaction of $H_2C_2O_4$ with $[Fe(salphen)]^+$

The stoichiometric studies indicated the consumption of 2 moles of $[Fe(salphen)]^+$ by 3 moles of $H_2C_2O_4$ (Figure 4.2) as represented by equation 4.2.

Earlier researchers have shown that the reactions of oxalic acid exhibited varying stoichiometries as reported in its reactions with N-bromophthalimide (Katre *et al*., 2012), Bi(V) (Prasad *et al*., 2007) and quinolinium fluorochromate (Khurana *et al*., 2000), where a stoichiometry of 1:1 was obtained. However, the consumption of 4 moles of oxalic acid per mole of chromic acid was observed in the reaction of chromic acid with oxalic acid (Khan *et al*., 1998) while a 2:1 stoichiometry (Mn^{III}:oxalate) was indicated in the reactions of tris(acetylacetonato)manganese(III) (Mukhopadhyay *et al*., 1993) and $[Mn(salphen)]^+$ (Jena *et al*., 2018) with oxalate ion.

The formation of CO_2 as the oxidation product of $H_2C_2O_4$, was confirmed using lime water ($Ca(OH)_2$) which turned milky (Svehla and Sivasankar, 2012) whereas a brown

precipitate of Fe_2O_3 was observed due to the $KMnO_4$ oxidation of the Fe^{2+} complex that formed during the reduction of $[Fe(salphen)]^+$ in the reaction (Misfud, 2009).

The straight line graph (Figure 4.12) obtained from the $\log(A_t - A_\infty)$ against time, t, plot suggested that the reaction is first order with respect to $[Fe(salphen)^+]$ while the slope of 1.04 obtained from the plot of log k_1 against log $[H_2C_2O_4]$ showed that the reaction was first order with respect to $[H_2C_2O_4]$. The value of the second order rate constant, k_2 were fairly constant for different $[H_2C_2O_4]$ at constant ionic strength (Table 4.2) indicating an overall second order reaction. The rate equation for the reaction is presented in equation 4.13.

The rate of reaction was independent of $[H^+]$, as shown in Table 4.13, indicating the unlikely deprotonation of oxalic acid molecule in the reaction. Previous studies have reported that undissociated oxalic acid molecule was involved in the rate determining step in the raction of the molecule with chromic acid (Bakore and Jian, 1969) and chromic acid reaction in different acidic media (Khan *et al*., 1998). Similarly, the protonation of $[Fe(salphen)]^+$ was not supported due to very low range of $[H^+]$ (1.0×10^{-5} mol $dm^{-3} \geq [H^+] \leq 1.0 \times 10^{-4}$ mol dm^{-3}) used in the reaction.

The results in Table 4.2 showed that variation in the ionic strength of the reaction medium had no effect on the rate suggesting zero Brønsted – Debye salt effect (Magarian, 2014). This implies that the activated complex is formed from the reactants of charged ion ($[Fe(salphen)]^+$) and undissociated molecule (HO_2CCO_2H) (Atkins and de Paula, 2018). Supporting this result is the insensitivity of the reaction to the change in dielectric constant of the reaction medium as presented in Table 4.16. The observed result is not unexpected as

the reactant species at the rate determining step are composed of charged and neutral species.

Equally, the reaction rate was unaffected by the presence of added ions (Mg^{2+}, K^{+}, $CH_3COO^{-}$and NO_3^{-}) as shown in Tables 4.25 and 4.35. The lack of ion catalysis could be attributed to the absence of coulombic interaction between $H_2C_2O_4$ and the added ions, hence the absence of attraction or repulsion towards $[Fe(salphen)]^{+}$. Ion catalysis is however ascribed to a reaction occurring through the outer-sphere pathway (Abdulsalam *et al*., 2020).

From the Eyring's plot of $\ln\left(\frac{k_2}{T}\right)$ versus $\left(\frac{1}{T}\right)$ (Figures 4.83), thermodynamic parameters were calculated and the results are presented in Tables 4.46. The negative values of $\Delta S^{\ddagger}$ and positive $\Delta H^{\ddagger}$ may suggest the formation of a more ordered activated complex and a highly solvated transition state (Katre *et al*., 2012).

The absence of a gelatinous precipitate when acrylamide was added to the reaction mixture indicates the unlikely involvement of free radicals in the reaction (Khurana *et al*., 2000; Jena *et al*., 2018) whereas no shift in λ_{max} (435 nm) was observed when the spectrum of the reaction mixture was compared with that of $[Fe(salphen)]^{+}$ (Figure 4.93), indicating lack of spectrophotometric evidence for the formation of intermediate complex or if formed had small formation constant. Similarly, Michaelis-Menten plot of $\frac{1}{k_1}$ versus $\frac{1}{[H_2C_2O_4]}$ was linear without an intercept, equally indicating the absence of an intermediate complex (Figure 4.103).

Therefore, taking recourse to the experimental data, the the following mechanistic steps have been posited for the reaction:

$$[Fe(salphen)]^{+} + H_2C_2O_4 \xrightarrow{k_3} [Fe(salphen)–H_2C_2O_4^{+}] \quad 5.12$$

$$[Fe(salphen)–H_2C_2O_4^{+}] \xrightarrow[slow]{k_4} [Fe(salphen)] + 2CO_2 + 2H^{+} + e^{-} \quad 5.13$$

$$[Fe(salphen)]^{+} + 2H_2C_2O_4 + O_2 + e^{-} \xrightarrow{k_5} [Fe(salphen)] + 4CO_2 + 2H_2O \quad 5.14$$

$$\text{Rate} = k_4 [Fe(salphen)–H_2C_2O_4^{+}] \quad 5.15$$

Applying steady state approximation to $[Fe(salphen)–H_2C_2O_4^{+}]$ gives

$$\frac{-d[Fe(salphen)-H_2C_2O_4^{+}]}{dt} = k_3 [Fe(salphen)^{+}][H_2C_2O_4] – k_{-3} [Fe(salphen)–H_2C_2O_4^{+}] – k_4[Fe(salphen)–H_2C_2O_4^{+}] \approx 0 \quad 5.16$$

$$[Fe(salphen)–H_2C_2O_4^{+}] = \frac{k_3[Fe(salphen)^{+}][H_2C_2O_4]}{k_{-3} + k_4} \quad 5.17$$

Substituting equation 5.17 into equation 5.15 gives

$$\text{Rate} = \frac{k_4 k_3 [Fe(salphen)^{+}][H_2C_2O_4]}{k_{-3} + k_4} \quad 5.18$$

Equation 5.18 is analogous to equation 4.13

where $k_2 = \frac{k_4 k_3}{k_{-3} + k_4} = 7.29 \pm 0.16 \times 10^{-1}$ dm^3 mol^{-1} s^{-1} (as indicated in Table 4.2)

Many reports have indicated the occurrence of inner-sphere mechanism in the reactions of oxalic acid (Mukhopadhyay *et al*., 1993; Khan *et al*., 1998, Khurana *et al*., 2000; Prasad *et al*., 2007; Banerji *et al*., 2009). However, an outer-sphere pathway has also been proposed (Bruyère *et al*., 2001). It is noteworthy to deduce the plausible mechanism for the reaction of $H_2C_2O_4$ and $[Fe(salphen)]^{+}$ from the following observed experimental data:

a) the rate of the reaction was unaffected in the presence of added ions, which might suggests that the reaction occurring via inner-sphere mechanism.

b) spectroscopic evidence indicated no shift in λ_{max} suggesting that there was no inner-sphere complex formation. This observation supports the occurrence of the outer-sphere mechanism.

c) Michaelis - Menten plot of $\frac{1}{k_1}$ versus $\frac{1}{[H_2C_2O_4]}$ had zero intercept which indicates the absence of a detectable intermediate in the rate determining step. This observation also suggests the occurrence of the outer-sphere mechanism.

Based on the findings, option (a) might suggest an inner-sphere pathway, options (b) and (c) are in support of the occurrence of outer-sphere mechanism and is hereby proposed for the reaction.

5.4 Reaction of H_3PO_2 with $[Fe(salphen)]^+$

The results of stoichiometric study and product analysis conform to equation 4.3 and represent the reduction of 2 moles of $[Fe(salphen)]^+$ per mole of H_3PO_2.

Yusuf *et al*. (2004) and Xiao-Juan *et al.* (2011) obtained similar results. However, Mohammed *et al.* (2017) obtained a stoichiometry of 1:1 in the reaction involving di-Ru^{III} ion and H_3PO_2 and Nkole *et al.* (2018) also obtained a mole ratio of 1:1 for the reaction of $[Fe(EDTA)]^-$ and thioglycolic acid.

The mole ratio of 2:1 in this reaction is not unusual for reactions involving Fe^{3+}. The varying mole ratios obtained in the reactions involving either the oxidant or reductant as reported can be appreciated in the context of the nature of the oxidant or reductant either as a one electron oxidant or reductant. In the case of Fe^{3+}, the electrochemical half-cell

reduction potential of Fe^{III}/Fe^{II} (Equation 5.19) (Atkins and de Paula, 2018) shows that Fe^{III} is a one electron strong oxidant.

$$Fe^{III} + e^{-} \longrightarrow Fe^{II} \qquad E_{Fe^{III}/Fe^{II}} = 0.71\ V \qquad 5.19$$

Therefore, the number of moles of Fe^{III} consumed in its redox reaction is dictated by the reductant. Where the reductant is also a one electron reducing agent, a mole ratio of 1:1 is obtained and if it is a two or more electron reducing agent, a mole ratio of 2:1 or higher is obtained.

On completion of the reaction, the product of oxidation of hypophosphorous acid was confirmed by the addition of saturated sodium molybdate solution to the reaction mixture. The presence of phosphorous acid was inferred from the absence of sodium phosphomolybdate precipitate indicating the absence of H_3PO_4 (Yusuf *et al*., 2004; Mohammed *et al*., 2017). Similarly, a brown precipitate was observed on addition of $KMnO_4$ indicating the formation of Fe_2O_3 from the $KMnO_4$ oxidation of the Fe^{2+} complex that formed during the reduction of $[Fe(salphen)]^+$ by H_3PO_2 (Misfud, 2009).

The result of the analysis of the kinetic data shows that the reaction is first order with respect to the concentration of $[Fe(salphen)^+]$ and $[H_3PO_2]$ and second order overall. The rate law for the reaction is given in equation 4.14.

As for the effect of acid concentration on the reaction, the rate of reaction was acid independent as shown in Table 4.14. From the acid stability studies, the complex was found to be stable within the range of acid (1.0×10^{-5} mol $dm^{-3} \geq [H^+] \leq 1.0 \times 10^{-4}$ mol dm^{-3}) used in this work. Therefore, the none-influence of acid concentration in this reaction further shows that the reductant was neither protonated nor deprotonated in the course of the

reaction. The work of Mohammed *et al*. (2017) involving H_3PO_2 with di-Ru^{III} ion also agreed to this acid pathway.

The compositon of the reactants at the rate determing step consisted of a charged ion ($[Fe(salphen)]^+$) and an uncharged molecule (H_3PO_2) (Atkins and de Paula, 2018), a feature observed when the reaction rate was unaffected by variation in ionic strength of the reaction medium (Table 4.3), indicating zero Brønsted – Debye salt effect (Magarian, 2014). Similarly, changing the dielectric constants of the reaction medium had no effect on the reaction rate (Table 4.17) which is in support of the previous assertion of the composition of the activated complex at the rate determing step in this study.

The reaction was catalysed by added ions (Mg^{2+}, Ca^{2+}, CH_3COO^- and NO_3^-), an indication of the redox partners consisting of an ion ($[Fe(salphen)]^+$) and a dipole molecule (H_3PO_2) as observed in the reaction of $[Fe(salen)]^+$ with thiodiglycolic acid (Subramaniam *et al*., 2014) where ion catalysis was also recorded. This catalytic effect is consistent with a reaction following an outer-sphere pathway of electron transfer.

A comparison of the spectrum of the reaction mixture with that of $[Fe(salphen)^+]$ indicated no shift in λ_{max} (435 nm) (Figure 4.94) and a Michaelis-Menten plot of $\frac{1}{k_1}$ versus $\frac{1}{[H_3PO_2]}$ was linear without an intercept (Figure 4.104). These observations suggest the absence of intermediate complex with significant stability in the reaction, which is in support of an outer sphere redox mechanism.

The observed gelatinous precipitate when acrylamide was added to the reaction mixture indicated the involvement of free radicals in the reaction whereas the values of

negative $\Delta S^{\ddagger}$ and positive $\Delta H^{\ddagger}$ suggest the formation of a more ordered activated complex and that the transition state is highly solvated (Katre *et al*., 2012).

The reaction mechanism proposed based on the results obtained from the experimental finding is as follows:

$$[Fe(salphen)]^{+} + H_3PO_2 \underset{k_{-3}}{\overset{k_3}{\rightleftharpoons}} [Fe(salphen)–H_3PO_2^{+}] \quad 5.20$$

$$[Fe(salphen)–H_3PO_2^{+}] \xrightarrow[slow]{k_4} [Fe(salphen)] + H_2PO_2^{\bullet} + H^{+} \quad 5.21$$

$$[Fe(salphen)]^{+} + H_2PO_2^{\bullet} + H_2O \xrightarrow{k_5} [Fe(salphen)] + H_3PO_3 + H^{+} \quad 5.22$$

For this mechanism,

$$\text{Rate} = k_4 [Fe(salphen)–H_3PO_2^{+}] \quad 5.23$$

Applying the steady state approximation to the complex, $[Fe(salphen)–H_3PO_2^{+}]$,

$$\frac{-d[Fe(salphen)-H_3PO_2^{+}]}{dt} = k_3 [Fe(salphen)^{+}][H_3PO_2] - k_{-3} [Fe(salphen)–H_3PO_2^{+}] - k_4[Fe(salphen)–H_3PO_2^{+}] = 0 \quad 5.24$$

Then

$$[\{Fe(salphen)–H_3PO_2\}^{+}] = \frac{k_3[Fe(salphen)^{+}][H_3PO_2]}{k_{-3}+ k_4} \quad 5.25$$

Substituting equation 5.25 into equation 5.23 gives

$$\text{Rate} = \frac{k_4k_3[Fe(salphen)^{+}][H_3PO_2]}{k_{-3}+ k_4} \quad 5.26$$

Equation 5.26 is analogous to equation 4.14

where $k_2 = \frac{k_4k_3}{k_{-3}+ k_4} = 2.28 \pm 0.03 \times 10^{-2}$ dm^3 mol^{-1} s^{-1}

Although, an outer-sphere mechanism was earlier reported in the reactions of neutral red (Ibrahim *et al.*, 2016) and diaquotetrakis-(2,2'-bipyridine)-μ-oxodiruthenium(III) ion (Mohammed *et al.*, 2017) with hypophosphorous, the following experimental findings can be used to assign mechanistic pathway to this reaction:

a) Added ions catalysis observed in the reaction is characteristic of reactions occurring via the outer-sphere mechanism.
b) Spectroscopic evidence indicated no shift in λ_{max} indicating that there was no inner-sphere complex formation. This observation also conforms to the occurrence of the outer-sphere mechanism.
c) Michaelis - Menten plot of $\frac{1}{k_1}$ versus $\frac{1}{[H_3PO_2]}$ had zero intercept, which further suggests the absence of a detectable intermediate in the rate determining step in support of the occurrence of the outer-sphere mechanism.

Therefore, outer-sphere mechanism is proposed for the reaction.

5.5 Reactions of H_2O_2 with $[Fe(salphen)]^+$ and $[Mn(salphen)]^+$

The stoichiometry of the reactions were found to be 2:1 (Figures 4.4 and 4.5) as represented by equation 5.27 indicating that 2 moles of the complexes were reduced each per mole of H_2O_2.

$$2[M(salphen)]^+ + H_2O_2 \longrightarrow 2[M(salphen)] + O_2 + 2H^+ \qquad 5.27$$

where M = Fe^{3+} or Mn^{3+}

A similar 2:1 stoichiometry is common in the reactions of H_2O_2 as reported in its reactions with cysteine (Luo *et al.*, 2005), $[(NH_3)_5Co^{III}(\mu\text{-}O_2)Co^{III}(NH_3)_5]^{5+}$ (Mishra *et al.*,

2009) and aminocarboxylactocobaltate(II) complex (Onu *et al*., 2015). However, a stoichiometry of 1:1 was implicated in the reaction of Tl^{III} with H_2O_2 (Rao *et al*., 1993).

The presence of Mn^{2+}, the reduction product of Mn^{3+} was ascertained by the appearance of a purple colour of MnO_4^-, which was as a result of Mn^{2+} oxidation by KIO_4 (Nazarenko, 2004). Similarly, a brown precipitate was observed indicating the formation of Fe_2O_3 from $KMnO_4$ oxidation of the Fe^{2+} complex that formed during the reduction of $[Fe(salphen)]^+$ (Misfud, 2009), confirming the presence of Fe^{2+}.

The kinetic analysis for the reaction indicated first order dependence in $[M(salphen)^+]$ and $[H_2O_2]$ and the values of second order rate constants, k_2 were fairly constant indicating and overall second order reaction.

First order dependence in $[H_2O_2]$ is common as reported in the reactions of H_2O_2 with Tl^{III} (Rao *et al*., 1993), N,N'-propylenebis(salicylideneiminato)manganese(III) (Salem, 1994), cysteine (Luo *et al*., 2005), $[(NH_3)_5Co^{III}(\mu\text{-}O_2)Co^{III}(NH_3)_5]^{5+}$ (Mishra *et al*., 2009), Cu^{II} (Skounas *et al*., 2010), trispicolinatoruthenate(II) (Impert *et al*., 2012), aminocarboxylactocobaltate(II) (Onu *et al*., 2015) and Cu-buserite complex (Feng *et al*., 2020).

Equation 5.28 describes the rate equation for the reactions as:

$$\frac{-1}{2}\frac{d[Fe(salphen)^+]}{dt} = k_2[M(salphen)^+][H_2O_2] \qquad 5.28$$

where $k_2 = 5.08 \pm 0.06 \times 10^{-4}$ dm^3 mol^{-1} s^{-1} for $[Fe(salphen)^+]$

$= 1.26 \pm 0.02 \times 10^{-2}$ dm^3 mol^{-1} s^{-1} for $[Mn(salphen)^+]$

The reactions were inhibited in the presence of $[H^+]$ as shown in Tables 4.4 and 4.5. A plot of k_2 against $\frac{1}{[H^+]}$ gave a straight line with an intercept (Figures 4.31 and 4.32). Acid dependence of this nature suggests deprotonation of H_2O_2 during the reaction as represented by equation 5.29, with both deprotonated and neutral molecule being reactive (Rao *et al*., 1993; Mishra *et al*., 2009).

$$H_2O_2 \rightleftharpoons HO_2^- + H^+ \qquad 5.29$$

However, Onu *et al*. (2015) presented a straight line graph of a plot of k_2 against $\frac{1}{[H^+]}$ in the reaction of Co^{II} and H_2O_2 where no intercept was obtained, an indication that only the deprotonated form of H_2O_2 was reactive (Onu *et al*., 2015). Similarly, it was reported that $[H^+]$ catalysed the reaction of H_2O_2 with trispicolinatoruthenate(II) complex. This result was explained in terms of the protonation of trispicolinatoruthenate(II) complex (Impert *et al*., 2012).

Results from Tables 4.4 and 4.5 show that increase in ionic strength of reaction medium decreased the reaction rate. Plot of log k_2 against $\sqrt{\mu}$ gave a slope of -0.91 and -1.37 for $[Fe(salphen)]^+$ and $[Mn(salphen)]^+$ respectively (Figures 4.35 and 4.36), suggesting negative Brønsted – Debye salt effect (Magarian, 2014) and that the product of the charges at the rate determining step is about unity. This implies that the activated complex is composed of reactants with oppositely charged ions ($[M(salphen)]^+$ and HO_2^-) (Atkins and de Paula, 2018). However, lack of dependence of rate on ionic strength was reported for the reactions of H_2O_2 with Tl^{III} (Rao *et al*., 1993), cysteine (Luo *et al*., 2005) and aminocarboxylactocobaltate(II) complex (Onu *et al*., 2015), corresponding to the presence of a neutral molecule (H_2O_2) at the rate determining step.

Results from Tables 4.18 and 4.20 also show that decreasing the dielectric constants of the reaction medium decreased the reaction rate, implying decreased mobility of one or the two oppositely charged ions at the rate determing step.

The reaction of H_2O_2 with $[Fe(salphen)]^+$ was catalysed by added ions (Mg^{2+}, Ca^{2+}, $HCOO^-$ and NO_3^-) (Tables 4.28 and 4.38) due to the probable existence of couloumbic attractions between the redox parteners and the ions at the rate determining step prior to electron transfer. However, the ions inhibited the reaction of H_2O_2 with $[Mn(salphen)]^+$ (Tables 4.31 and 4.43), an indication of the existence of couloumbic repulsions between the redox partners. The observed ion catalysis or inhibition shows probable occurrence of reactions occurring via outer-sphere mechanism as reported in the reaction of H_2O_2 with aminocarboxylactocobaltate(II) complex (Onu *et al*., 2015).

From the thermodynamic parameters evaluated, the negative value of $\Delta S^{\ddagger}$ and positive $\Delta H^{\ddagger}$ indicated a more ordered activated complex, indicative of an associatively activated process (Anis *et al*., 1987; Rao *et al*., 1993) and that the transition state is highly solvated (Katre *et al*., 2012) as a result of arrangement of solvent molecules around the transition state (Anis *et al*., 1987).

Lack of spectrophotometric evidence for the formation of intermediate complex was inferred when no shift in λ_{max} at 435 nm for $[Fe(salphen)]^+$ and 450 nm for $[Mn(salphen)]^+$ was observed when the spectra of the reaction mixtures were compared with that of the complexes alone (Figures 4.95 and 4.96) suggesting the absence of an intermediate and a probable outer sphere mechanism. However, the presence of intermediates in the reactions were inferred from intercepts obtained from Michaelis-Menten plots of $\frac{1}{k_1}$ versus $\frac{1}{[H_2O_2]}$

(Figures 4.110 and 4.111) suggesting formation of intermediates and probable inner-sphere mechanisms for the reactions (Salem, 1994; Mishra *et al*., 2009; Impert *et al*., 2012).

The addition of acrylamide to the partially reacted solutions gave a gelatinous precipitate indicating the involvement of free radicals in the reactions (Salem, 1994; De-Laat and Gallard, 1999; Perez-Benito, 2004; Mishra *et al*., 2009; Impert *et al*., 2012; Kremer, 2017).

With recourse to the experimental data, the proposed mechanism for the reactions is as follows:

$$H_2O_2 \underset{}{\overset{K_H^+}{\rightleftharpoons}} HO_2^- + H^+ \qquad 5.30$$

$$[M(salphen)]^+ + HO_2^- \xrightarrow[slow]{k_4} [M(salphen)] + HO_2^{\bullet} \qquad 5.31$$

$$[M(salphen)]^+ + HO_2^{\bullet} \xrightarrow{k_5} [M(salphen)] + O_2 + H^+ \qquad 5.32$$

$$[M(salphen)^+] + H_2O_2 \xrightarrow{k_6} [M(salphen)–H_2O_2^+] \qquad 5.33$$

$$[M(salphen)–H_2O_2^+] \xrightarrow[slow]{k_7} [M(salphen)] + HO_2^{\bullet} + H^+ \qquad 5.34$$

$$[M(salphen)]^+ + HO_2^{\bullet} \xrightarrow{k_8} [M(salphen)] + O_2 + H^+ \qquad 5.35$$

$$\text{Rate} = k_4\,[M(salphen)^+][HO_2^-] + k_7\,[M(salphen)–H_2O_2^+] \qquad 5.36$$

Applying steady state approximation to the intermediate $[M(salphen)–H_2O_2^+]$;

$$\frac{-d[M(salphen)-H_2O_2^+]}{dt} = k_6\,[M(salphen)^+][H_2O_2] - k_{-6}\,[M(salphen)–H_2O_2^+] - k_7\,[M(salphen)–H_2O_2^+] \approx 0 \qquad 5.37$$

$$[M(salphen)–H_2O_2^+] = \frac{k_6[M(salphen)^+][H_2O_2]}{k_{-6}+k_7} \qquad 5.38$$

But

$$K_{H^+} = \frac{[HO_2^-][H^+]}{[H_2O_2]} \quad 5.39$$

Therefore;

$$[HO_2^-] = \frac{K_H^+[H_2O_2]}{[H^+]} \quad 5.40$$

Substituting equations 5.38 and 5.40 into equation 5.36 gives equation 5.41

$$\text{Rate} = \frac{K_H^+ k_4[M(\text{salphen})^+][H_2O_2]}{[H^+]} + \frac{k_6 k_7[M(\text{salphen})^+][H_2O_2]}{k_{-6} + k_7} \quad 5.41$$

$$\text{Rate} = \left(\frac{K_H^+ k_4}{[H^+]} + \frac{k_6 k_7}{k_{-6} + k_7}\right)[M(\text{salphen})^+][H_2O_2] \quad 5.42$$

Equation 5.42 is analogous to equation 5.28

where M = Fe^{3+} or Mn^{3+}

$k_2 = \left(\frac{K_H^+ k_4}{[H^+]} + \frac{k_6 k_7}{k_{-6} + k_7}\right) = 5.08 \pm 0.06 \times 10^{-4}$ dm^3 mol^{-1} s^{-1} for $[Fe(\text{salphen})]^+$

$= 1.26 \pm 0.02 \times 10^{-2}$ dm^3 mol^{-1} s^{-1} for $[Mn(\text{salphen})]^+$

Various mechanistic pathways have been proposed for the reactions of H_2O_2 such as an outer-sphere pathway in its reaction with aminocarboxylactocobaltate(II) complex (Onu *et al*., 2015), while an inner-sphere mechanism has also been proposed in its reactions with cysteine (Luo *et al*., 2005), Cu^{II} (Skounas *et al*., 2010) and trispicolinatoruthenate(II) (Impert *et al*., 2012). An analysis of the experimental data in terms of mechanistic pathway for the reactions of H_2O_2 with $[M(\text{salphen})]^+$ is provided as follows:

a) Added ions catalysis was observed in the reaction of H_2O_2 with $[Fe(salphen)]^+$ whereas inhibition was observed in the reaction of H_2O_2 with $[Mn(salphen)]^+$, a characteristic feature of reactions occurring via the outer-sphere mechanism.

b) Spectroscopic evidence indicated no shift in λ_{max} suggesting the absence of intermediates, which is in support of an outer-sphere mechanism.

c) Michaelis - Menten plots of $\frac{1}{k_1}$ versus $\frac{1}{[H_2O_2]}$ had intercepts, which suggest the presence of intermediates in the rate determining steps. This observation supports the occurrence of the inner-sphere mechanism.

Although option (c) suggests an inner-sphere pathway, however, options (a) and (b) are in favour of the outer-sphere mechanism and is hereby proposed for the reactions.

5.6 Reaction of RSH with $[Mn(salphen)]^+$

The stoichiometry of the reaction was found to be 1:1 (Figure 4.7) and conforms to equation 4.7.

A similar stoichiometry of 1:1 has been reported in the reactions of RSH with $[Mn^{III}(O)_2Mn^{IV}]$ (Goswami *et al*., 2004), Co^{III} superoxide (Mandal *et al*., 2015), $[(bpy)_2H_2ORu^{III}]_2O^{4+}$ (Iyun and Musa, 1995) and heteropoly-11-tungsto-1-vanadophosphate (Shanmugaprabha *et al*., 2016). However, 2 moles of RSH have been reduced by a mole of Co^{II} histimine (Rafiquee *et al*., 2016) whereas 6 moles of RSH consumed 1 mole of $[Mn_3(\mu\text{-}O)_4(phen)_4(H_2O)_2]^{4+}$ (Chakraborty *et al*., 2013).

The presence of Mn^{2+}, the reduction product of Mn^{3+} was obtained by the appearance of purple colour of MnO_4^- as a result of Mn^{2+} oxidation by KIO_4 (Nazarenko, 2004) while the oxidation product of RSH, was confirmed according to earlier published

procedures (McAuley and Gomwalk, 1968; McAuley and Gomwalk, 1969). From the FTIR results, bands observed at 3309 cm^{-1}, 1042 cm^{-1} and 481 cm^{-1} were assigned to (νO-H), (νC-O) and (νS-S) stretching respectively (Trofimov *et al*., 2009) (Appendix VI). The data obtained from the results support the formation of $HOCH_2CH_2S\text{-}SCH_2CH_2OH$ as the organic product of the oxidation of thioglycol.

The kinetic analysis indicated first order dependence in [Mn(salphen)$^+$] and [RSH] with fairly constant values of second order rate constants, k_2 (Table 4.7) indicating that the reaction is second order overall. The rate equation for the reaction is depicted by equation 4.18.

The observed first order dependence in [RSH] is similar to earlier results obtained in the reactions of RSH with $[(bpy)_2H_2ORu^{III}]_2O^{4+}$ (Iyun and Musa, 1995), $[Mn^{III}(O)_2Mn^{IV}]$ (Goswami *et al*., 2004), $[Mn_3(\mu\text{-}O)_4(phen)_4(H_2O)_2]^{4+}$ (Chakraborty *et al*., 2013), $[MnV_{13}O_{38}]^{7-}$ (Chakrabarty and Banerjee, 2014), Co^{II}histimine (Rafiquee *et al*., 2015), Co^{III} complex (Mandal *et al*., 2015) and heteropoly-11-tungsto-1-vanadophosphate (Shanmugaprabha *et al*., 2016).

The rate of reaction was catalysed in the presence of [H^+] as shown in Table 4.7. A plot of k_2 versus [H^+] gave a straight line graph with an intercept (Figure 4.34). Acid dependence of this nature suggests protonation of RSH during the reaction as shown in equation 5.43, with both protonated and neutral forms being reactive. Similar acid dependence has been established in the reaction of RSH with $[MnV_{13}O_{38}]^{7-}$, but $[MnV_{13}O_{38}]^{7-}$ was reported to have been protonated and not RSH (Chakrabarty and Banerjee, 2014). A deprotonation of RSH was however reported in its reactions with $[(bpy)_2H_2ORu^{III}]_2O^{4+}$ (Iyun and Musa, 1995), $[Mn_3(\mu\text{-}O)_4(phen)_4(H_2O)_2]^{4+}$ (Chakraborty *et*

al., 2013), Co(III) complex (Mandal *et al*., 2015) and heteropoly 11-tungsto-1-vanadophosphate (Shanmugaprabha *et al*., 2016).

The results from Table 4.7 shows that increase in ionic strength of reaction medium increased the reaction rate. Plot of log k_2 against $\sqrt{\mu}$ gave a slope of +0.92 (Figure 4.39), suggesting a positive Brønsted – Debye salt effect (Magarian, 2014). This implies that the activated complex is formed from reactants of similar charged ions ($[Mn(salphen)]^+$ and $HRSH^+$) of unit magnitude (Atkins and de Paula, 2018). Results from Table 4.24 also show that decreasing the dielectric constants of the reaction medium increased the reaction rate, an indication that the reaction is favoured with decreasing polarity of the medium.

The reaction was inhibited by increasing concentrations of added cations (Mg^{2+} and K^+) (Table 4.32), an indication of the existence of coulombic repulsions between the redox partners and the added cations at the rate determining step. This could happen if both the redox partners are positively charged species. However, increase in concentrations of added anions (NO_3^- and SO_4^{2-}) catalysed the reaction (Table 4.40) suggesting the presence of positively charged ions at the rate determining step and the probable existence of coulombic attractions between the redox partners and the anions. Ion catalysis or inhibition supports reactions occurring via outer-sphere mechanism.

The slight decrease in λ_{max} observed from 450 nm to 425 nm when the spectrum of the reaction mixture was compared with that of $[Mn(salphen)^+]$ (4.101) indicates the possible formation of an intermediate complex in the reaction. However, Michaelis-Menten plot of $\frac{1}{k_1}$ versus $\frac{1}{[RSH]}$ was linear without intercept suggesting the absence of an intermediate complex (Figure 4.106) (Iyun and Musa, 1995, Nkole *et al*., 2018). Similarly, the involvement of free radicals in the reaction was inferred from the gelatinous precipitate

obtained when acrylamide was added to the partially reacted solution (Goswami *et al*., 2004; Chakrabarty and Banerjee, 2014; Mandal *et al*., 2015; Rafiquee *et al*., 2016; Shanmugaprabha *et al*., 2016).

Based on the experimental findings, the mechanism of reaction is rationalized to outer-sphere pathway, and the following mechanism is proposed:

$$RSH + H^+ \underset{}{\overset{K_H^+}{\rightleftharpoons}} HRSH^+ \qquad 5.43$$

$$[Mn(salphen)]^+ + HRSH^+ \xrightarrow[slow]{k_3} [Mn(salphen)] + RS^{\bullet} + 2H^+ \qquad 5.44$$

$$[Mn(salphen)]^+ + RSH \xrightarrow[slow]{k_4} [Mn(salphen)] + RS^{\bullet} + H^+ \qquad 5.45$$

$$RS^{\bullet} + RS^{\bullet} \xrightarrow{k_5} RSSR \qquad 5.46$$

$$Rate = k_3 [Mn(salphen)^+][HRSH^+] + k_4[Mn(salphen)^+][RSH] \qquad 5.47$$

From equation 5.43;

$$[HRSH^+] = K_H^+[RSH][H^+] \qquad 5.48$$

Therefore;

$$Rate = k_3K_H^+[Mn(salphen)^+][RSH][H^+] + k_4 [Mn(salphen)^+][RSH] \qquad 5.49$$

$$Rate = (k_4 + k_3K_H^+[H^+])[Mn(salphen)^+][RSH] \qquad 5.50$$

Equation 5.50 is analogous to equation 4.18

where $k_2 = (k_4 + k_3K_H[H^+]) = 1.29 \pm 0.03 \times 10^{-2}$ dm^3 mol^{-1} s^{-1}

The proposition of outer-sphere mechanism for this reaction is similar to that reported in the reactions of RSH with $[(bpy)_2H_2ORu^{III}]_2O^{4+}$ (Iyun and Musa, 1995), $[Mn^{III}(O)_2Mn^{IV}]$ (Goswami *et al*., 2004), heteropoly-11-tungsto-1-vanadophosphate (Shanmugaprabha, *et al*., 2016) and $[Fe^{III}HEDTAOH_2]$ (Nkole *et al*., 2018). However, the occurrence of inner-sphere mechanism in the reactions of RSH have also been reported in

its reactions with $[Mn_3(\mu\text{-}O)_4(phen)_4(H_2O)_2]^{4+}$ (Chakraborty *et al*., 2013) and $[MnV_{13}O_{38}]^{7-}$ (Chakrabarty and Banerjee, 2014).

5.7 Reaction of SCN^- with $[Mn(salphen)]^+$

The consumption of 1 mole of $[Mn(salphen)]^+$ per mole of SCN^- was inferred from the stoichiometric studies (Figure 4.8) as shown in equation 4.8.

A similar stoichiometry of 1:1 has been reported in the reactions of SCN^- with $Mn_4(P_2O_7)_3$ (Bhat *et al*., 1993) and peroxomonosulphate ion (Kalmar *et al*., 2013). However, different results of reaction stoichiometry were recorded in the reaction of IO_4^- and SCN^- where Nandibewoor *et al*. (2000) reported the consumption of 4 moles of IO_4^- per mole of SCN^- and Lohdip and Iyun (2003) showed the reduction of 1 mole of $[Mn^{III}O_2Mn^{IV}]^{3+}$ by 3 moles of SCN^-.

Although thiocyanogen, $(SCN)_2$, is known to be formed as one of the reaction products in the redox reaction involving SCN^- (Aune and Thomas, 1977; Bhat *et al*., 1993; Lohdip and Iyun, 2003), this can undergo further hydrolysis according to equation 5.51 to give the final products (Lohdip and Iyun, 2003).

$$4H_2O + 3(SCN)_2 \longrightarrow 7H^+ + 5SCN^- + HCN + SO_4^{2-} \qquad 5.51$$

Formation of white precipitate of $BaSO_4$ insoluble in excess dilute HCl indicated the presence of SO_4^{2-} ion and the formation of a blood red complex of $Fe(SCN)_3$ confirmed the presence of CN^- ion (Svehla and Sivasankar, 2012). The presence of Mn^{2+} was determined by the appearance of characteristic purple colour of MnO_4^-, which was as a result of Mn^{2+} oxidation by KIO_4 (Nazarenko, 2004).

The reaction kinetics indicated first order dependence with respect to [Mn(salphen)$^{+}$] and [SCN^{-}] and the rate equation for the reaction is given as equation 4.19.

The observed first order dependence in [SCN^{-}] is similar to the results shown in the reactions of SCN^{-} with $Mn_4(P_2O_7)_3$ (Bhat *et al*., 1993) and $[Mn^{III}O_2Mn^{IV}]^{3+}$ (Lohdip and Iyun, 2003). However, a half order dependence in [SCN^{-}] was reported in the aqueous polymerisation of methyl methacrylate initiated by manganese(III) pyrophosphate (Sherigara *et al*., 2001) while Ghosh and De (1992) indicated a zero order dependence in [SCN^{-}] in its reaction with $[Rh(H_2O)_6]^{3+}$.

The rate of reaction was independent of [H^{+}] as shown in Table 4.8. Acid dependence of this nature suggests that none of the reactants was protonated or deprotonated during the reaction. In the reaction of $Mn_4(P_2O_7)_3$ with SCN^{-}, the reaction was [H^{+}] catalysed and this observation was explained in terms of protonation of SCN^{-} (Bhat *et al*., 1993) while in the reaction of $[Mn^{III}O_2Mn^{IV}]^{3+}$ with SCN^{-}, catalysis by [H^{+}] was as a result of the protonation of the complex, $[Mn^{III}O_2Mn^{IV}]^{3+}$ (Lohdip and Iyun, 2003).

Results from Table 4.8 also show that increase in ionic strength of reaction medium decreased the reaction rate. Plot of log k_2 against $\sqrt{\mu}$ gave a slope of -0.75 (Figure 4.37), suggesting a negative Brønsted – Debye salt effect (Nandibewoor *et al*., 2000; Magarian, 2014). This implies that the activated complex is formed from reactants of oppositely charged ions ([Mn(salphen)]$^{+}$ and SCN^{-}) with a charge magnitude of unity (Atkins and de Paula, 2018). However, a zero Brønsted – Debye salt effect has been observed in the reaction of $[Mn^{III}O_2Mn^{IV}]^{3+}$ with SCN^{-} (Lohdip and Iyun, 2003). The decrease in the reaction rate with decreasing dielectric constants of the reaction medium (Table 4.21) also

supports the interaction of oppositely charged ions at the rate determing step as indicated earlier.

Increase in concentrations of added cations (Mg^{2+} and Ca^{2+}) retarded the reaction (Table 4.33) while an increase in concentrations of added anions ($HCOO^-$ and NO_3^-) catalysed it (Table 4.41). This is as a result of the ions interacting with the redox partners at the rate determing step, either bringing them closer together (coulombic attraction) or setting them far apart (coulombic repulsion) prior to electron transfer. Ion catalysis or inhibition are typical for reactions occurring via outer-sphere mechanism.

The participation of free radicals in the reaction was inferred from the observed gelatinous precipitate formed when acrylamide was added to the partially reacted solution of SCN^- with $[Mn(salphen)]^+$. Similar result was obtained in the reactions of SCN^- with $Mn_4(P_2O_7)_3$ (Bhat *et al*., 1993) and manganese(III) pyrophosphate (Sherigara *et al*., 2001). However, the involvement of free radicals in the reaction of $[Mn^{III}O_2Mn^{IV}]^{3+}$ with SCN^- was unlikely due to the absence gel formation in the reaction (Lohdip and Iyun, 2003).

From the thermodynamic parameters evaluated, a large negative value of $\Delta S^{\ddagger}$ supports a more ordered activated complex, indicative of an associatively activated process. A similar result was reported in the reactions of SCN^- with HSO_5^- (Kalmar *et al*., 2013), manganese(III) complex (Bhat *et al*., 1993), and in the aqueous polymerisation of methyl methacrylate initiated by manganese(III) pyrophosphate (Sherigara *et al*., 2001). In another report, a positive $\Delta S^{\ddagger}$ recorded in the reaction of thiocyanate ion with $[Rh(H_2O)_6]^{3+}$ was indicative of a dissociative mode of activation (Ghosh and De, 1992). The positive $\Delta H^{\ddagger}$ obtained suggests that the transition state is highly solvated (Katre *et al*., 2012).

Lack of spectrophotometric evidence for the formation of intermediate complex was observed since there was no shift in λ_{max} (450 nm) when the spectrum of the reaction mixture was compared with that of $[Mn(salphen)^{+}]$ (Figure 4.98), suggesting an outer sphere mechanism. A similar result was obtained in the reaction of $[Mn^{III}O_2Mn^{IV}]^{3+}$ with SCN^- (Lohdip and Iyun, 2003). The Michaelis-Menten plot of $\frac{1}{k_1}$ versus $\frac{1}{[SCN^-]}$ was linear with no intercept indicating the absence of an intermediate complex (Figure 4.107).

On the basis of the results obtained from the investigation, the following reaction scheme is proposed:

$$[Mn(salphen)]^{+} + SCN^- \xrightarrow[slow]{k_3} [Mn(salphen)] + SCN^{\bullet} \qquad 5.52$$

$$SCN^{\bullet} + SCN^- \xrightarrow{k_4} (SCN)_2^{-\bullet} \qquad 5.53$$

$$[Mn(salphen)]^{+} + (SCN)_2^{-\bullet} \xrightarrow{k_5} [Mn(salphen)] + (SCN)_2 \qquad 5.54$$

$$Rate = k_3 [Mn(salphen)^{+}][SCN^-] \qquad 5.55$$

Equation 5.55 is analogous to equation 4.19

where $k_2 = k_3 = (1.54 \pm 0.01) \times 10^{-3}$ dm^3 mol^{-1} s^{-1}

Although Nandibewoor *et al*. (2000) reported an inner-sphere pathway in the reaction of SCN^- with IO_4^-, the experimental data obtained for the reaction of $[Mn(salphen)]^{+}$ and SCN^- are in favour of the occurrence of outer-sphere mechanism and is proposed for the reaction.

5.8 Reaction of $H_2NNHCSNH_2$ with $[Mn(salphen)]^{+}$

From the stoichiometric study, two moles of $[Mn(salphen)]^{+}$ were reduced per mole of $H_2NNHCSNH_2$ (Figure 4.9) as represented in equation 4.10.

Reactions of $H_2NNHCSNH_2$ have shown varying reaction stoichiometries. For example, a 1:1 mole ratio was reported in the reduction of Fe^{3+} by thiosemicarbize and a disulphide, $(H_2NN{=}C(NH_2)S)_2$, was confirmed as the reaction product (Ratnam and Anipindi, 2012). A 2:1 stoichiometry (2 moles of complex to 1 mole of thiosemicarbize) was reported in the reaction of $[(H_2O)(tap)_2RuORu(tap)_2(H_2O)]^{2+}$ with $H_2NNHCSNH_2$ and confirmed a bridged product, $[(tap)_2Ru(\mu\text{-}O)(\mu\text{-}tsc)Ru(tap)_2]^{2+}$, as one of the reaction products (Das-Karfa *et al*., 2010). More *et al*. (2018) reported a 1:2 stoichiometry (1 mole of complex to 2 moles of thiosemicarbize) in the reaction of $[Mn^{IV}Mo_9O_{32}]^{6-}$ with $H_2NNHCSNH_2$ and confirmed the formation of a disulphide product, $H_2N(HN)_2CSSC(NH)_2NH_2$.

A 3:1 mole ratio (3 moles of bromate or H_2O_2 to 1 mole of thiosemicarbize) has been reported in the reactions of $H_2NNHCSNH_2$ with bromate (Jonnalagadda *et al*., 2002) and H_2O_2 (Gowda and Vasireddy, 1990) with reaction products of SO_4^{2-}, CO_2, NH_4^+, N_2, N_2H_4 and CN^-. A stoichiometry of 4:1 (4 moles of complex to 1 mole of thiosemicarbize) was however reported in the reaction of $H_2NNHCSNH_2$ with $Mn(P_2H_2O_7)_3^{3-}$, where reaction products consisting of NH_3, N_2 and COS were reported. The obtained COS hydrolysed to give CO_2 and H_2S (Sherigara *et al*., 1994).

A 5:1 mole ratio (5 moles of compound to 1 mole of thiosemicarbize) has been reported in the reactions of $H_2NNHCSNH_2$ with N-chlorobenzamide (Nayak and Gowda, 1992) and V^{5+} (Kandpal *et al*., 1996) and the reaction products include N_2, SO_4^{2-} and CN^-. A 6:1 mole ratio (6 moles of compounds to 1 mole of thiosemicarbize) were implicated in the reactions of $H_2NNHCSNH_2$ with chloramine-B, bromamine-B and dichloramine-B (Gowda and Bhat, 1987), chloramine T, bromamine T, and dichloramine T (Gowda and

Rao, 1988) and Co^{3+} (Prakash *et al*., 1993) and the reaction products of SO_4^{2-}, CNO^-, NH_4^+ and CNBr (cyanogen bromide) were confirmed.

The observed formation of a white precipitate of $BaSO_4$ which was insoluble in excess dilute HCl indicated the presence of SO_4^{2-} ion and the formation of a blood red complex of $Fe(SCN)_3$ indicated the presence of CN^- ion (Svehla and Sivasankar, 2012). Similarly, the presence of Mn^{2+}, was inferred from the appearance of purple colour of MnO_4^- (Nazarenko, 2004).

The result of the kinetic studies indicated first order dependence in $[Mn(salphen)^+]$ and $[H_2NNHCSNH_2]$. The values of second order rate constants, k_2 were fairly constant (Table 4.9) an indication that reaction is second order overall. Equation 4.20 represents the rate equation for the reaction.

The observed first order in $[H_2NNHCSNH_2]$ is similar to results reported in the reactions of $H_2NNHCSNH_2$ with $[Mn^{IV}Mo_9O_{32}]^{6-}$ (More *et al*., 2018), vanadium(V) (Kandpal *et al*., 1996), H_2O_2 (Gowda, and Vasireddy, 1990), bromate (Jonnalagadda *et al*., 2002) and Fe^{3+} (Ratnam and Anipindi, 2012). However, a half order dependence in $[H_2NNHCSNH_2]$ was observed in the reactions of $H_2NNHCSNH_2$ with chloramine-B, bromamine-B and dichloramine-B (Gowda and Bhat, 1987), chloramine T, bromamine T, and dichloramine T (Gowda and Rao, 1988) and N-chlorobenzamide (Nayak *et al*., 1992).

The reaction was independent of $[H^+]$ as shown in Table 4.9. Acid dependence of this nature suggests that none of the reactants was protonated during the reaction (Das-Karfa *et al*., 2010). Reports have shown that the rate of the reactions of $H_2NNHCSNH_2$ with $[Mn^{IV}Mo_9O_{32}]^{6-}$ (More *et al*., 2018) and Vanadium(V) (Kandpal *et al*., 1996) to be

catalysed by [H^+] and a first order dependence in [H^+] was obtained. This was explained in terms of the protonation of $H_2NNHCSNH_2$ as shown in equation 5.56 (Kandpal *et al*., 1996; More *et al*., 2018).

$$H_2NNHCSNH_2 + H^+ \rightleftharpoons H_2NNHCSNH_3^+ \qquad 5.56$$

However, a second order acid dependence was reported in the reaction of $H_2NNHCSNH_2$ with bromate, which was explained on the basis of the bromate ion being protonated (Jonnalagadda *et al*., 2002).

An inverse acid dependence was reported in the reactions of $H_2NNHCSNH_2$ with chloramine-B, bromamine-B and dichloramine-B (Gowda and Bhat, 1987), chloramine T, bromamine T and dichloramine T (Gowda and Rao, 1988) and were explained based on the deprotonation of the amines as shown in equation 5.57.

$$RNH_2Cl \rightleftharpoons RNHCl + H^+ \qquad 5.57$$

Similarly, an inverse acid dependence was also reported in the reactions of $H_2NNHCSNH_2$ with H_2O_2 (Gowda and Vasireddy, 1990) and the deprotonation of $H_2NNHCSNH_2$ before the rate determining step was expressed as the possible explanation for the nature of the acid dependence as shown in equation 5.58.

$$H_2NNHC(S{-}H)=NH \rightleftharpoons H_2NNHC(S^-)=NH + H^+ \qquad 5.58$$

Results from Table 4.9 shows that increase in ionic strength of reaction medium had no effect on the reaction rate indicating zero Brønsted – Debye salt effect (Magarian, 2014). This indicates that the reaction is independent of ionic strength in this concentration limit (More *et al*., 2018) and that the activated complex is formed from a charged ion

($[Mn(salphen)]^+$) and an uncharged molecule ($H_2NNHCSNH_2$) (Atkins and de Paula, 2018). However, results from Table 4.22 show that decreasing the dielectric constants of the reaction medium decreased the reaction rate, similar to earlier studies in the reaction of $H_2NNHCSNH_2$ with $[Mn^{IV}Mo_9O_{32}]^{6-}$ (More *et al*., 2018), indicating that the activated complex is formed from a charged ion ($[Mn(salphen)]^+$) and an uncharged molecule ($H_2NNHCSNH_2$) (Atkins and de Paula, 2018).

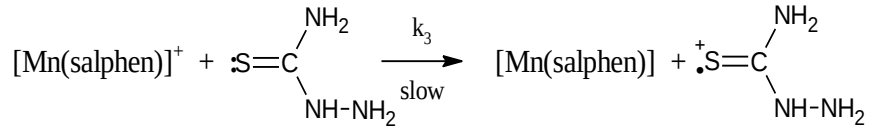
Increase in concentration of added ions (Mg^{2+}, Ca^{2+}, $HCOO^-$ and NO_3^-) catalysed the reaction (Tables 4.30 and 4.42) which supports the occurrence of outer-sphere mechanism. Reactions involving ion ($[Mn(salphen)]^+$) and dipole molecules ($H_2NNHCSNH_2$) have been reported to be catalysed by added ions (Subramaniam *et al*., 2014).

The formation of an inner-sphere complex in the reaction of $H_2NNHCSNH_2$ with $[Mn(salphen)]^+$ was rulled out from Michaelis-Menten plot of $\frac{1}{k_1}$ versus $\frac{1}{[H_2NNHCSNH_2]}$ which was linear without intercept (Figure 4.108) (Gowda and Rao, 1988) and from spectrophotometric test which indicated no observable shift in λ_{max} (450 nm) (Figure 99). This lack of spectrophotometric evidence for the formation of intermediate complex suggests an outer sphere mechanism for the reaction. An intercept was, however, reported in the reactions of $H_2NNHCSNH_2$ with $[(H_2O)(tap)_2RuORu(tap)_2(H_2O)]^{2+}$ (Das-Karfa *et al*., 2010) and vanadium(V) (Kandpal *et al*., 1996), suggesting that innersphere mechanism was likely in operation in the reactions.

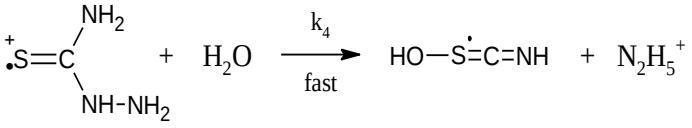
Addition of acrylamide to the partially reacted solution to serve as radical scavenger in the presence of large excess of methanol gave a gelatinous precipitate. This indicates the involvement of free radicals in the reaction (Ratnam and Anipindi, 2012).

From the thermodynamic parameters calculated, the positive $\Delta H^{\ddagger}$ indicates a highly solvated transition state (Katre *et al*., 2012) whereas the negative value of $\Delta \mathbf{S}^{\ddagger}$ indicates that the species in the activated complex are more ordered (Gowda and Vasireddy, 1990).

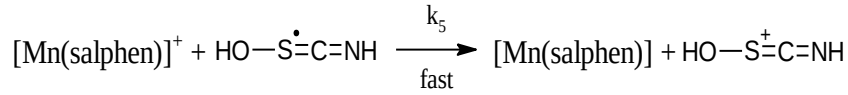
The following reaction scheme is proposed for this reaction based on the results obtained:



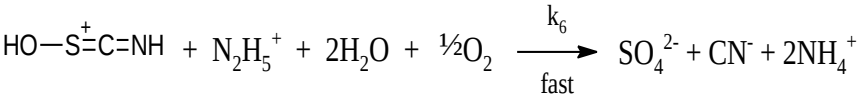
5.59



5.60



5.61



5.62

Rate = k_3 [Mn(salphen)$^+$][$H_2NNHCSNH_2$] 5.63

Equation 5.63 is analogous to equation 4.20

where $k_2 = k_3 = (4.08 \pm 0.04) \times 10^{-3}$ dm^3 mol^{-1} s^{-1}

Although most reactions of $H_2NNHCSNH_2$ have been reported to occur via inner-sphere mechanism (Gowda and Rao, 1988; Kandpal *et al*., 1996; Ratnam and Anipindi,

2012; More *et al*., 2018), an outer-sphere pathway has also been reported (Das-Karfa *et al*., 2010). The experimental results obtained for the reaction of $H_2NNHCSNH_2$ with $[Mn(salphen)]^+$ are in support of the occurrence of outer-sphere mechanism, which is therefore proposed for this reaction.

5.9 Reaction of $S(CH_2CH_2OH)_2$ with $[Mn(salphen)]^+$

The results of the stoichiometric study indicates that for every mole of $S(CH_2CH_2OH)_2$, two moles of $[Mn(salphen)]^+$ were reduced (Figure 4.10) and the stoichiometric reaction is given in equation 4.11.

Ross (1946) and Ogata and Sawaki (1963) have observed a 1:1 stoichiometry in the reaction of $S(CH_2CH_2OH)_2$ with hydrogen peroxide, and thiodiglycol sulphoxide was proposed as the reaction product. However, Veriansyah *et al*. (2005) reported the reaction of 7 moles of oxygen per mole of $S(CH_2CH_2OH)_2$ in the reaction of $S(CH_2CH_2OH)_2$ with oxygen, and proposed CO_2 and H_2SO_4 as the reaction products.

At the completion of the reaction, the appearance of purple colour of MnO_4^- after addition of KIO_4 indicated the presence of Mn^{2+} after oxidation by KIO_4 (Nazarenko, 2004). From the FTIR results, bands observed at 3334 cm^{-1}, 1040 cm^{-1} and 1007 cm^{-1} were assigned to (νO-H), (νC-O) and (νS=O) stretching respectively (Hampton *et al*., 2010) (Appendix VII). This observation is in support of the formation of $O=S(CH_2CH_2OH)_2$ as the organic product of the reaction.

Kinetic study results showed first order dependence in $[Mn(salphen)^+]$ and $[S(CH_2CH_2OH)_2]$, which is overall second order as observed from relatively constant values of second order rate constants, k_2 (Table 4.10) for the reaction.

Ross, (1946) and Ogata and Sawaki, (1963) have also observed similar first order dependence in $[S(CH_2CH_2OH)_2]$ in the reaction of $S(CH_2CH_2OH)_2$ with H_2O_2.

The reaction was also inhibited in the presence of $[H^+]$ as shown in Table 4.10 and a plot of k_2 against $\frac{1}{[H^+]}$ gave a straight line with an intercept (Figure 4.33). Acid dependence of this nature suggests the deprotonation of $S(CH_2CH_2OH)_2$ before or at the rate determing step of the reaction with an indication of both deprotonated and neutral forms being reactive as shown in equation 5.64 (Abdulsalam *et al*., 2020). However, acid catalysis that was reported in the reaction of $S(CH_2CH_2OH)_2$ with H_2O_2 and was due to the protonation of H_2O_2 to give $HOOH_2^+$ (Ross, 1946).

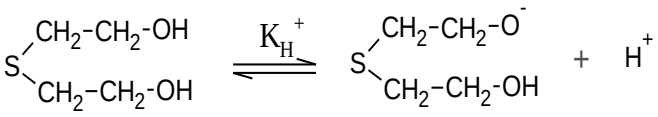
Results from Table 4.10 show that increase in ionic strength of reaction medium decreased the reaction rate. Plot of log k_2 against $\sqrt{\mu}$ gave a slope of -1.35 (Figure 4.38), suggesting negative Brønsted – Debye salt effect (Magarian, 2014). This implies that the activated complex is formed from reactants of oppositely charged ions ($[Mn(salphen)]^+$ and $HOCH_2CH_2SCH_2CH_2O^-$) of unit magnitude (Atkins and de Paula, 2018). Results from Table 4.23 also show that decreasing the dielectric constants of the reaction medium decreased the reaction rate. A decrease in solvent polarity decreased the reaction rate due to the decreasing mobility of participating ions at the rate determing step. The low values of dielectric constant reported in this work is due to the fact that at 25˚ C, the dielectric constant of DMSO and water are 46.7 and 80.1 respectively (Lide, 2007) which decreased to 43.51 (Hunger *et al*., 2010) and 69.91 (Malmberg and Maryott, 1956) respectively at 50˚ C.

The rate of reaction of $S(CH_2CH_2OH)_2$ with $[Mn(salphen)]^+$ was inhibited in the presence of ions such as Mg^{2+}, Ca^{2+}, SO_4^{2-} and $HCOO^-$ (Tables 4.34 and 4.44), due to the probable coulombic repulsions that exist between the ions and the redox partners. This observation is typical of reactions occurring via outer-sphere mechanism.

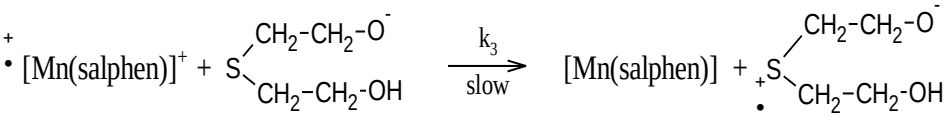
The values of negative $\Delta S^{\ddagger}$ and positive $\Delta H^{\ddagger}$ suggest the formation of a more ordered activated complex and a highly solvated transition state (Katre *et al*., 2012) while the involvement of free radicals in the reaction was inferred from the observed gelatinous precipitate formed when acrylamide was added to partially reacted solution of $[Mn(salphen)]^+$ and $S(CH_2CH_2OH)_2$.

Similarly, no shift in λ_{max} (450 nm) was obtained when the spectrum of the reaction mixture was compared with that of $[Mn(salphen)]^+$ (Figure 4.100). Lack of spectrophotometric evidence for the formation of intermediate complex was supported by the Michaelis-Menten plot of $\frac{1}{k_1}$ versus $\frac{1}{[S(CH_2CH_2OH)_2]}$. This was linear without intercept suggesting the absence of an intermediate complex (Figure 4.109).

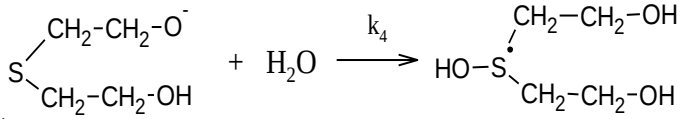
Although Ogata and Sawaki (1963) reported an inner-sphere mechanism in the reaction of $S(CH_2CH_2OH)_2$ with hydrogen peroxide, the experimental data obtained for the reaction of $[Mn(salphen)]^+$ with $S(CH_2CH_2OH)_2$ supports outer-sphere mechanistic pathway of electron transfer in accordance the with following proposed mechanism.



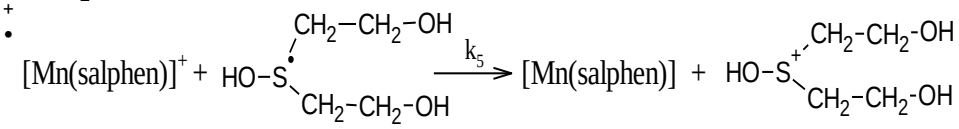
5.64



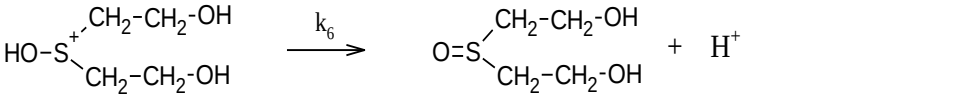
5.65



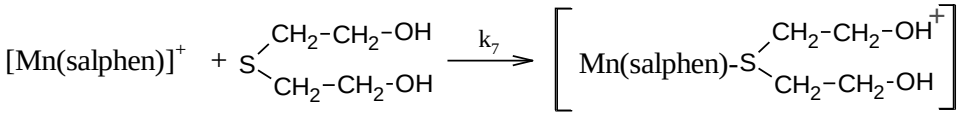
5.66



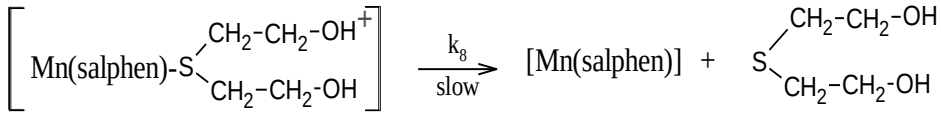
5.67



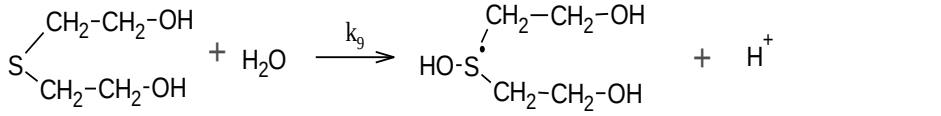
5.68



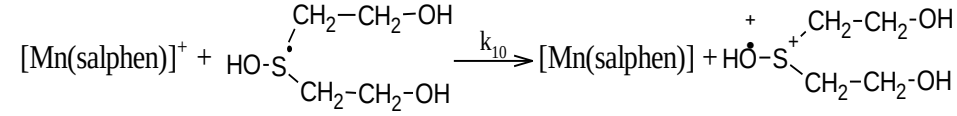
5.69



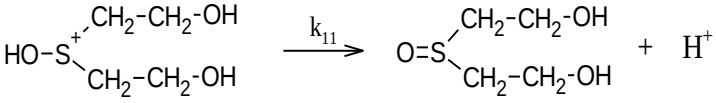
5.70



5.71



5.72



5.73

$$\text{Rate} = k_3[\text{Mn(salphen)}^+][\text{HOCH}_2\text{CH}_2\text{SCH}_2\text{CH}_2\text{O}^-] + k_8[\text{Mn(salphen)–S(CH}_2\text{CH}_2\text{OH)}_2{}^+] \quad 5.74$$

Applying steady state approximation to the intermediate $[\text{Mn(salphen)–S(CH}_2\text{CH}_2\text{OH)}_2{}^+]$;

$$\frac{-d[\{\text{Mn(salphen)}--\text{S(CH}_2\text{CH}_2\text{OH)}_2\}^+]}{dt} = k_7[\text{Mn(salphen)}^+][\text{S(CH}_2\text{CH}_2\text{OH)}_2] - k_{-7}[\text{Mn(salphen)–S(CH}_2\text{CH}_2\text{OH)}_2{}^+] - k_8[\text{Mn(salphen)–S(CH}_2\text{CH}_2\text{OH)}_2{}^+] \approx 0 \quad 5.75$$

$$[\text{Mn(salphen)–S(CH}_2\text{CH}_2\text{OH)}_2{}^+] = \frac{k_7[\text{Mnsalphen}^+][\text{S(CH}_2\text{CH}_2\text{OH)}_2]}{k_{-7}+k_8} \quad 5.76$$

But

$$K_H^+ = \frac{[HOCH_2CH_2SCH_2CH_2O^-][H^+]}{[S(CH_2CH_2OH)_2]} \quad 5.77$$

Therefore;

$$[HOCH_2CH_2SCH_2CH_2O^-] = \frac{K_H^+[S(CH_2CH_2OH)_2]}{[H^+]} \quad 5.78$$

Substituting equations 5.77 and 5.78 into equation 5.74 gives equation 5.79

$$\text{Rate} = \frac{K_3K_H^+[Mn(salphen)^+][S(CH_2CH_2OH)_2]}{[H^+]} + \frac{k_7k_8[Mnsalphen^+][S(CH_2CH_2OH)_2]}{k_{-7}+k_8} \quad 5.79$$

$$\text{Rate} = \left(\frac{K_3K_H^+}{[H^+]} + \frac{k_7k_8}{k_{-7}+k_8}\right)[Mn(salphen)^+][S(CH_2CH_2OH)_2] \quad 5.80$$

Equation 5.80 is analogous to equation 4.21

where $k_2 = \left(\frac{K_3K_H^+}{[H^+]} + \frac{k_7k_8}{k_{-7}+k_8}\right) = 4.18 \pm 0.07 \times 10^{-3}$ dm^3 mol^{-1} s^{-1}

5.10 Reaction Rate in the Presence of Surfactants

5.10.1 Critical micelle concentration of surfactants

The variation of specific conductance with surfactant concentration ([S_f]) is presented in Table 4.55 and the plots of specific conductance versus [S_f] are presented in Figures 4.112 – 4.117. The breaking points on the graphs were taken as the critical micelle concentration (CMC).

The CMC of SDS obtained in water, 8.0×10^{-3} mol dm^{-3}, is in good agreement with previously reported values of 8.64×10^{-3} mol dm^{-3} (Jiang *et al*., 2003), 8.1×10^{-3} mol dm^{-3} (Kumari, 2004; Chauhan *et al*., 2007), 8.2×10^{-3} mol dm^{-3} (Markarian *et al*., 2005) and 8.0×10^{-3} mol dm^{-3} (Demissie and Duraisamy, 2016), while that of CTAB, 2.0×10^{-3}

mol dm^{-3}, is similar to previously reported values of 1.005×10^{-3} (Sood and Sharma, 2016), 9.7×10^{-4} mol dm^{-3} (Modaressi *et al*., 2007; Dubey, 2013), 9.6×10^{-4} mol dm^{-3} (Kumari, 2004), 9.5×10^{-4} mol dm^{-3} (Jalali and Gerandaneh, 2011; Olaseni *et al*., 2012) and 9.0×10^{-4} mol dm^{-3} (Jiang *et al*., 2003).

The presence of electrolytes has a great effect on micelle formation and micelle stabilization (Lin *et al*., 2003; Vautier-Giongo and Pastore, 2006). As a result, a lower CMC of surfactants is observed in the presence of electrolytes. For instance, in the presence of 0.1 mol dm^{-3} KNO_3, a CMC of 4.0×10^{-3} mol dm^{-3} and 7.0×10^{-4} mol dm^{-3} were reported for SDS and CTAB respectively (Jiang *et al*., 2003). Similarly, in 0.1 mol dm^{-3} NaCl, a CMC of 1.6×10^{-3} mol dm^{-3} (Ogunlusi *et al*., 2013) and 6.8×10^{-5} mol dm^{-3} (Ogunlusi *et al*., 2016) were reported for SDS and CTAB respectively. Micellization is favoured in the presence of electrolytes due to decreased repulsion between surfactant head groups (Shamsipur *et al*., 1997; Kumar *et al*., 2012).

On the other hand, the addition of co-solvents leads to an inhibition of the micellization of surfactant process due to dehydratation of the micelle surface which leads to an increase in CMC (Markarian *et al*., 2005). For instance, in the presence of 20 % DMSO, a CMC of 1.5×10^{-2} mol dm^{-3} and 4.25×10^{-3} mol dm^{-3} were reported for SDS and CTAB respectively (Kumari, 2004).

This increase in CMC in the presence of DMSO can be attributed to a decrease in the dielectric constant of the solvent (Peyre *et al*., 2013). This can be due to the fact that the ions on the surfactant head group are strongly solvated by DMSO which results in weak counter-ion binding on the micellar surface, and a strong intermolecular interaction occurs between DMSO and water molecules, leading to significant dehydration of the micellar

surface. As a result of these effects, the aggregation of surfactant molecules is inhibited (Chauhan *et al*., 2001; Markarian *et al*., 2005; Chauhan *et al*., 2007).

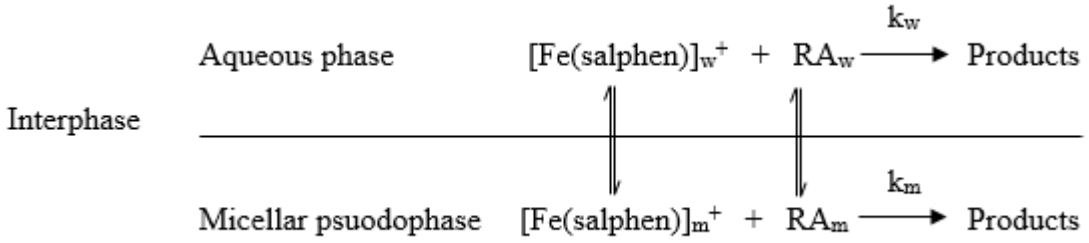
The observed values of CMC in this study could be attributed to the overall effect of a decrease in CMC in the presence of ions (NaCl and $[M(salphen)]^+$) and an increase in CMC in the presence of co-solvent (20 % DMSO).

5.10.3 Kinetic model for the effect of surfactants on the reactions rate

From the results, an increase in k_ψ at $[S_f]$ < CMC was observed when SDS was added to the reaction medium in the reactions of TSH and $H_2C_2O_4$ with $[Fe(salphen)]^+$ and in the reactions of TSH, SCN^- and $S(CH_2CH_2OH)_2$ with $[Mn(salphen)]^+$ whereas a decrease in k_ψ was observed in the reaction of H_2O_2 with $[Fe(salphen)]^+$ and RSH with $[Mn(salphen)]^+$. Similarly, an increase in k_ψ at $[S_f]$ < CMC was observed in the presence of CTAB, in the reactions of TSH and $H_2C_2O_4$ with $[Fe(salphen)]^+$ and in the reactions of H_2O_2 and TSH with $[Mn(salphen)]^+$, whereas a decrease in k_ψ was observed in the reaction of H_2O_2 with $[Fe(salphen)]^+$ and the reactions of SCN^-, $S(CH_2CH_2OH)_2$ and RSH with $[Mn(salphen)]^+$.

This is interpreted as reactants inducing micelle formation (surfactant molecules start aggregating below CMC). This catalysis/inhibition below CMC is termed as sub-micellar or pre-micellar catalysis/inhibition. This is because small aggregates of the surfactants (such as dimers, trimers and tetramers) exist below CMC. These small pre-micellar aggregates can interact physically with the reactants forming catalytically active entities (Katre *et al*., 2013; Ogunlusi *et al*., 2016).

In the micellar solution of a surfactant, the complex ion and the reducing agents (RA) are distributed between aqueous phase and micellar pseudophase according to Scheme 5.1 (Romsted, 2012).



Scheme 5.1: Distribution of reactants between aqueous phase and micellar pseudophase

The reaction rate in the presence of surfactants was analyzed using the kinetic model of Piszkiewicz (Piszkiewicz, 1977) which is analogous to the Hill model (Pandey and Upadhyay, 2005) for enzymatic reactions. According to this model, a substrate (S) associates with (n) number of surfactant molecules (D) to form aggregates (D_nS), which may react to yield products as represented by equations 5.81 – 5.83.

$$S + RA \xrightarrow{k_w} \text{Products} \qquad 5.81$$

$$S + nD \underset{K_D}{\overset{K}{\rightleftharpoons}} D_nS \qquad 5.82$$

$$D_nS + RA \xrightarrow{k_m} \text{Products} \qquad 5.83$$

where S = $[Fe(salphen)]^+$ or $[Mn(salphen)]^+$, RA = reducing agent, K is the binding constant of substrate to micelle, K_D is the dissociation constant of substrate bound micelle, k_m is the rate constant for the reaction between RA and D_nS aggregates and k_w is the rate constant in water.

From equations 5.81 – 5.83, the second order rate constant at low surfactant concentration is presented in equation 5.84

$$k_{\psi} = \frac{k_w K_D + k_m [D]^n}{K_D + [D]^n} \qquad 5.84$$

The parameters in equation 5.84 were obtained by non-linear least squares method (Ogunlusi *et al*., 2013; Ogunlusi *et al*., 2016; Laguta *et al*., 2018b) and the results are shown in Tables 4.56 – 4.63.

The large values of binding constant (K) is in agreement with the observed significant catalysis/inhibition of the electron transfer rate in surfactant media (Ogunlusi *et al*., 2013; Ogunlusi *et al*., 2016).

The obtained values of n > 1 are in agreement with earlier observation of Piszkiewicz, as indices of positive cooperativity. These values have previously been interpreted as indicative of existence of premicellar aggregates (Pandey and Upadhyay, 2005; Ogunlusi *et al*., 2013; Ogunlusi *et al*., 2016). The obtained non-integer values of the n parameter values imply multiple equilibria in the formation of a catalytic micelle (Piszkiewicz, 1977; Laguta *et al*., 2018b).

5.10.3 Reaction mechanism in the presence of surfactants

In determining the mechanism of the reaction catalysis/inhibition by surfactants, the possible factors to be considered include:

a) coulombic attraction/repulsion between the positively charged salphen metal complexes and the anionic/cationic surfactants respectively,
b) electrostatic attraction/repulsion between the RA and the charged head groups of the surfactants,

c) electrostatic attraction due to the interaction between the aromatic π-electrons of salphen ligands of the metal complex and the positive charge density on the nitrogen of the quartenary ammonium ion of the head group of CTAB (Aschia *et al*., 2002; Wang *et al*., 2006) or repulsion due to the interaction between the aromatic π-electrons of the salphen ligands of the metal complex and the negative charge of sulphur ion on the head group of SDS (Schottel *et al*., 2008; Geronimo *et al*., 2011),

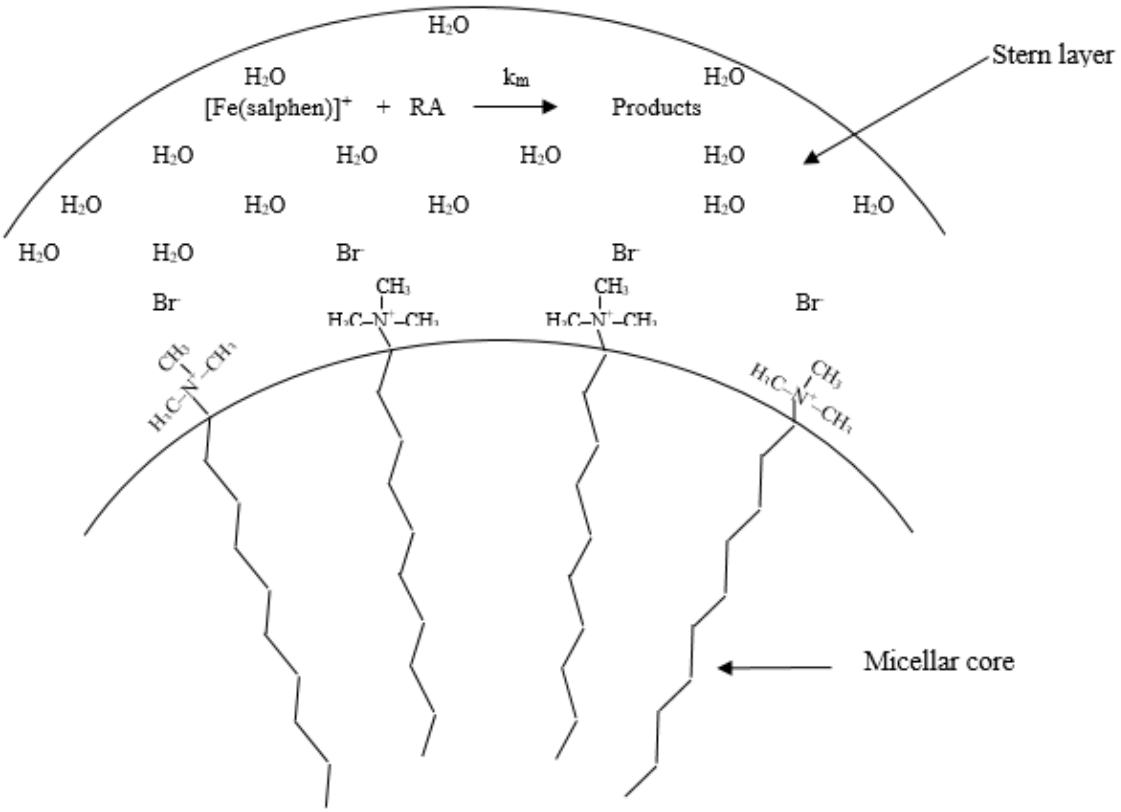
d) hydrophobic interaction between the hydrophobic ligands of the salphen complexes and the hydrophobic region of the surfactants, and

e) a possible hydrophobic interaction between the RA and the hydrophobic region of the surfactants (Ogunlusi *et al*., 2016).

A possible arrangement of the reactants is depicted in Scheme 5.2 indicating the probable reaction site in the stern layer of a micelle (Singh, 2014).

If both S and RA are more hydrophobic, they are retained just under the stern layer in the micelle, and as such, the observed reaction catalysis. Catalysis is also observed when both S and RA are attracted to the micellar surface and hence confined within the stern layer (Olanrewaju *et al*., 2011).

However, if S is more hydrophobic than RA, the later is retained in the stern layer, or much more in the aqueous phase outside the micelle while the former is just below the stern layer. This partitioning of RA and S in different layers with increased inter-nuclear distance results in the observed reaction inhibition (Ogunlusi *et al*., 2016).



Scheme 5.2: Model showing probable location of reactants in micellar pseudophase

The reaction rate was catalysed in the presence of CTAB and SDS in the reactions of TSH with $[Fe(salphen)]^+$ and $[Mn(salphen)]^+$ respectively. From electrostatic interaction, it is expected that $[Fe(salphen)]^+$ and $[Mn(salphen)]^+$ will be repelled by the positively charged head group of CTAB and attracted by the negatively charged head group of SDS. However, the hydrophobic interactions between the salphen ligand of the metal complexes and the hydrophobic region of the surfactants is much higher than their electrostatic interactions.

Also, the existence of hydrophobic interactions between TSH and the surfactants leads to the reactants (TSH and $[Fe(salphen)]^+$ or TSH and $[Mn(salphen)]^+$) being confined in the region around the stern layer, just below it (Scheme 5.2). This reduced internuclear

distance between (TSH and $[Fe(salphen)]^+$ or TSH and $[Mn(salphen)]^+$) will lead to the reaction catalysis observed in this reaction.

The reaction rate was inhibited in the presence of SDS in the reactions of H_2O_2 with $[Fe(salphen)]^+$ and $[Mn(salphen)]^+$. Also, CTAB inhibited the reaction rate of H_2O_2 reaction with $[Fe(salphen)]^+$ while it catalysed the reaction of H_2O_2 with $[Mn(salphen)]^+$. However, the proposed reactive species of H_2O_2 in this reaction from the experimental results is the HO_2^- anion. Therefore, from electrostatic interaction, $[Fe(salphen)]^+$ and $[Mn(salphen)]^+$ should be repelled by the positively charged head group of CTAB while HO_2^- will be attracted by it. Also, $[Fe(salphen)]^+$ and $[Mn(salphen)]^+$ will be attracted by the negatively charged head group of SDS while HO_2^- will be repelled by it.

However, the hydrophobic interactions between the salphen ligand of the metal complexes and the hydrophobic region of the surfactants is much higher than their electrostatic interactions, while no hydrophobic interaction exists between the HO_2^- anion and the surfactants. As such, the HO_2^- anion is partitioned far away from the stern layer, possibly in the bulk aqueous phase while $[Fe(salphen)]^+$ and $[Mn(salphen)]^+$ are retained in the stern layer (Scheme 5.2). This partitioning of the HO_2^- anion and $[Fe(salphen)]^+$ and $[Mn(salphen)]^+$ respectively in different layers with increased internuclear distance results in the reaction inhibition observed in the presence of SDS.

However, the catalysis observed in the presence of CTAB for the reaction of HO_2^- anion and $[Mn(salphen)]^+$ could be as a result of the electrostatic attraction that exists between the HO_2^- anion and the positively charged head group of CTAB which retains both the HO_2^- anion and $[Mn(salphen)]^+$ in the stern layer. This reduced internuclear distance between $[Mn(salphen)]^+$ and HO_2^- led to the observed reaction catalysis.

The reaction rate was catalysed in the presence of CTAB and SDS in the reaction of $[Fe(salphen)]^+$ with $H_2C_2O_4$. It is expected from the view point of electrostatic interaction that $[Fe(salphen)]^+$ will be repelled by the positive charged head group of CTAB and attracted by the negative charged head group of SDS. However, the hydrophobic interactions between the salphen ligand of the metal complex and the hydrophobic region of the surfactants is much higher than their electrostatic interactions. Also the existence of hydrophobic interactions between $H_2C_2O_4$ and the surfactants causes the two reactants to be confined in the region around the stern layer, just below it (Scheme 5.2). This led to the observed reaction catalysis.

The reaction rate was catalysed in the presence of SDS in the reaction of $[Mn(salphen)]^+$ with SCN^- while CTAB inhibited it. When coulombic interaction is considered, $[Mn(salphen)]^+$ will be repelled by the positively charged head group of CTAB and attracted by the negatively charged head group of SDS. However, the hydrophobic interactions between the salphen ligand of the metal complex and the hydrophobic region of the surfactants is much higher than their electrostatic interactions. Also, a repulsion should exist between SCN^- and SDS head group while an attraction should occur between the ion and the head group of CTAB. The possible absence of hydrophobic interactions between SCN^- and the surfactants indicates that the SCN^- ion is partitioned far away from the stern layer, possibly in the bulk aqueous phase while $[Mn(salphen)]^+$ is retained in the stern layer (Scheme 5.2).

This partitioning of SCN^- ion and $[Mn(salphen)]^+$ in different layers with increased internuclear distance results in the observed reaction rate inhibition in CTAB. However, in the presence of SDS, $[Mn(salphen)]^+$ interacts considerably with the head group of SDS

and in the stern layer together with the SCN^- ion. This leads to the two reactants being confined in the stern layer (Scheme 5.2) and hence the observed reaction rate catalysis.

The reaction rate was inhibited in the presence of CTAB and SDS in the reaction of $[Mn(salphen)]^+$ with RSH. Recall that the proposed reactive species of RSH in this reaction from the experimental results is $HRSH^+$ ion. Therefore, considering electrostatic interaction, $[Mn(salphen)]^+$ will be repelled by the positive charged head group of CTAB and attracted by the negative charged head group of SDS. However, the hydrophobic interactions between the salphen ligand of the metal complex and the hydrophobic region of the surfactants is much higher than their electrostatic interactions.

Also the possible absence of hydrophobic interactions between $HRSH^+$ and the surfactants indicates that the $HRSH^+$ ion is partitioned far away from the stern layer, possibly in the bulk aqueous phase while $[Mn(salphen)]^+$ is retained in the stern layer (Scheme 5.2). This partitioning of the $HRSH^+$ ion and $[Mn(salphen)]^+$ in different layers with increased internuclear distance results in the observed reaction inhibition.

The reaction was catalysed in the presence of SDS in the reaction of $[Mn(salphen)]^+$ with $S(CH_2CH_2OH)_2$ while CTAB inhibited the reaction. Also recall that the reactive species of $S(CH_2CH_2OH)_2$ proposed earlier from the experimental results is $HOCH_2CH_2SCH_2CH_2O^-$ ion. Therefore, from the consideration of electrostatic interaction, $[Mn(salphen)]^+$ will be repelled by the positively charged head group of CTAB and attracted by the negatively charged head group of SDS. However, the hydrophobic interactions between the salphen ligand of the metal complex and the hydrophobic region of the surfactants is much higher than their electrostatic interactions. Also, a repulsion

should exist between $HOCH_2CH_2SCH_2CH_2O^-$ and SDS head group while an attraction should occur between the ion and the head group of CTAB.

The possible absence of hydrophobic interactions between $HOCH_2CH_2SCH_2CH_2O^-$ and the surfactants indicates that the $HOCH_2CH_2SCH_2CH_2O^-$ ion is partitioned far away from the stern layer, possibly in the bulk aqueous phase while $[Mn(salphen)]^+$ is retained in the stern layer (Scheme 5.2). The partitioning of $HOCH_2CH_2SCH_2CH_2O^-$ ion and $[Mn(salphen)]^+$ in different layers with increased internuclear distance results in the reaction rate inhibition observed in CTAB. However, in the presence of SDS, $[Mn(salphen)]^+$ interacts considerably with the head group of SDS and in the stern layer together with the $HOCH_2CH_2SCH_2CH_2O^-$ ion. This causes the confinement of the two reactants in the stern layer (Scheme 5.2) and hence the observed reaction catalysis.

CHAPTER SIX

6.0 SUMMARY, CONCLUSION AND RECOMMENDATIONS

6.1 Summary

The kinetics of the reduction of $[Fe(salphen)]^+$ by TSH, $H_2C_2O_4$, H_3PO_2 and H_2O_2 and $[Mn(salphen)]^+$ by H_2O_2, TSH, RSH, SCN^-, $H_2NNHCSNH_2$ and $S(CH_2CH_2OH)_2$ were studied in mixed aqueous medium (DMSO:H_2O; 1:4 v/v). For the reactions involving $[Fe(salphen)]^+$, the stoichiometric studies showed that one mole of $[Fe(salphen)]^+$ was consumed per mole of TSH whereas two moles of $[Fe(salphen)]^+$ were consumed by one mole each of H_3PO_2 and H_2O_2 and two moles of $[Fe(salphen)]^+$ by three moles of $H_2C_2O_4$. The results also showed that one mole of $[Mn(salphen)]^+$ was consumed per mole each of TSH, RSH and SCN^- whereas two moles of $[Mn(salphen)]^+$ were consumed by one mole each of H_2O_2, $H_2NNHCSNH_2$ and $S(CH_2CH_2OH)_2$.

The kinetic study showed a first order dependence in both [oxidant] and [reductant] for all the reactions and therefore, second order overall. The reaction rates were independent of $[H^+]$ in the reactions of TSH, $H_2C_2O_4$ and H_3PO_2 with $[Fe(salphen)]^+$ and in the reactions of TSH, SCN^- and $H_2NNHCSNH_2$ with $[Mn(salphen)]^+$ while for the reactions involving H_2O_2 and $S(CH_2CH_2OH)_2$, inverse acid dependence was obtained whereas RSH – $[Mn(salphen)]^+$ reaction showed a linear dependence.

The ionic strength of the reaction medium had no effect on the reactions of TSH, $H_2C_2O_4$ and H_3PO_2 with $[Fe(salphen)]^+$ as well as that of TSH and $H_2NNHCSNH_2$ with $[Mn(salphen)]^+$ but were found to be dependent on the rate of H_2O_2 – $[Fe(salphen)]^+$ reaction and the rate of H_2O_2, RSH, SCN^- and $S(CH_2CH_2OH)_2$ reactions with $[Mn(salphen)]^+$. Dielectric constant of the reaction medium had an effect on the reaction

rate of all the reactions except in the reactions of TSH, $H_2C_2O_4$ and H_3PO_2 with $[Fe(salphen)]^+$ and in the reaction of TSH with $[Mn(salphen)]^+$, where no effect was observed.

Added ion catalysis or inhibition was observed in all the reactions except in $H_2C_2O_4$ - $[Fe(salphen)]^+$ reaction where none was observed. Free radical polymerisation was observed in all the reactions except in $H_2C_2O_4$ - $[Fe(salphen)]^+$ reaction. Also, spectroscopic evidence showed no shift in λ_{max} in all the reactions except in the reaction of RSH with $[Mn(salphen)]^+$ where a slight shift was observed and Michaelis – Menten plot of $\frac{1}{k_1}$ versus $\frac{1}{[\text{reductant}]}$ had zero intercept for all the reactions except in H_2O_2 reactions, where an intercept was obtained. The results indicated the probable occurrence of outer sphere mechanism in all the reactions.

The reaction rates were affected by the presence of surfactants (SDS and CTAB) and the results were analyzed using the kinetic model of Piszkiewicz, which indicated the existence of pre-micellar aggregates in the reactions. In addition, electrostatic and hydrophobic interactions exist between the metal complexes and the micellar aggregate of the surfactants.

The metal complexes are largely resistant to reduction due to the presence of salphen ligand containing π-electrons which stabilizes the metals in their +3 oxidation states. This stability is consistent with hard acid – hard base interactions.

In addition, the large binding constants observed and the positive cooperativities indicate the existence of a substantial interaction between the complexes and the micelles.

6.2 Conclusion

The reduction of iron(III) and manganese(III) complexes of bis(salicylidene)phenylenediamine by some reductants in mixed aqueous and surfactant medium have been studied. From the findings, the reactions were second order overall and first order with respect to the concentrations of the oxidants and reductants. Also, all the reactions occurred through the outer-sphere mechanism. The findings of the Piszkiewicz model analysis of the kinetic data in the presence of surfactants predicted the existence of pre-micellar aggregates. The findings from the study also established the existence of significant electrostatic and hydrophobic interaction between the metal complexes and the micellar aggregates of the surfactants, hence, the observed catalysis or inhibition. The study also gives an alternative route to the generation of thiyl ($TS^{\bullet}$), hydroperoxide ($HO_2^{\bullet}$) and hypophosphite ($H_2PO_2^{\bullet}$) radicals which are important in the formation of the deoxyribonucleic acids, Fenton process and in organic syntheses respectively.

6.3 Recommendations

The following recommendations are made:

i) Further studies should be carried out on other metal-salphen complexes such as $[Cr(salphen)]^+$ and [Ni(salphen)].

ii) The effect of non-ionic, zwitter-ionic and mixed surfactants should be studied in order to understand other modes of complex-surfactant interactions.

iii) The use of other kinetic models such as Berezin, Pseudophase ion exchange (PIE) and Raghavan and Srinivasan models should also be used for possible interpretation of the reaction rate in the presence of surfactants.

iv) Further studies should be carried out by the application of computational techniques to support the experimental data.

REFERENCES

Abdulsalam, S and Idris, S.O. (2016). Kinetic approach to the mechanism of oxidation of hexamethylpararosaniline chloride by bromate ion in acidic medium. *FUW Trends in Science &Technology Journal,* 1(2):546-553.

Abdulsalam, S., Idris, S.O., Shallangwa, G.A. and Onu, A.D. (2020). A kinetic study and mechanisms of reduction of N,N'-phenylenebis(salicyalideneiminato)cobalt(III) by L-ascorbic acid in DMSO-water medium. *Heliyon,* 6: e04621. https://doi.org/10.1016/j.heliyon.2020.e04621.

Ahmad, N., Anouar, E.H., Tajuddin, A.M., Ramasamy, K., Yamin, B.M. and Bahron, H. (2020). Synthesis, characterization, quantum chemical calculations and anticancer activity of a Schiff base NNOO chelate ligand and Pd(II) complex. *Plosone,* 15(4):e0231147. https://doi.org/10.1371/journal.pone.0231147

Akram, M., Saeed, A.A.M. and Kabir-ud-Din (2014). Cationic micellar effect on the reaction between dipeptide glycyl-alanine (gly-ala) and ninhydrin with and without salt additives. *European Chemical Bulletin*, 3: 119-126.

Ali, M.A., Mirza, A.H., Monsur, A., Hossain, S. and Nazimuddin, M. (2001). Synthesis, characterization, antifungal properties and X-ray crystal structures of five- and six-coordinate copper(II) complexes of the 6-methyl-2-formylpyridine-4-N dimethylthiosemicarbazone. *Polyhedron*, 20: 1045-1052.

Ali, I., Wani, W.A. and Saleem, K. (2013). Empirical formulae to molecular structures of metal complexes by molar conductance. *Synthesis and Reactivity in Inorganic, Metal-Organic, and Nano-Metal Chemistry*, 43(9): 1162-1170.

Alioke C.U., Ukoha, P.O., Ukwueze, N.N., Ujam, O.T. and Jonnie N.A. (2012). Kinetics and mechanism of the reduction of N, N'-salicylideneiminationiron(III) complex ion by L-ascorbic acid in aqueous acid medium. *Chemistry and Materials Research*, 2(7):48-57.

Alsop, L., Cowly, A.R., Dilworth, J.R., Donnely, P.S., Peach, J.M. and Rider, J.T. (2005). Investigations into some aryl substituted bis(thiosemicarbazones) and their copper complexes. *Inorganica Chimica Acta*, 358: 2770-2780.

Anis, S.S., Hanna, W.G. and Stefan, S.L. (1987). Kinetics and mechanism of catalysed decomposition of hydrogen peroxide by ethylenebis(oxyethylenedinitrilo)tetraacetate complex of iron(III). *Microchemical Journal*, 36: 326-338.

Ansari, K.I, Grant, J.D., Woldemariam, G.A., Kasiri, S. and Mandal, S.S. (2009a). Iron(III) salen complexes with less DNA cleavage activity exhibit more efficient apoptosis in MCF7 cells. *Organic and Biomolecular Chemistry*, 7: 926-932.

Ansari, K.I., Kasiri, S., Grant, J.D. and Mandal, S.S. (2009b). Apoptosis and anti-tumour activities of manganese(III)-salen and –salphen complexes. *Dalton Transactions*, 8525-8531.

Ansari K.I., Kasiri, S., Grant, J.D. and Mandal, S.S. (2011). Fe(III) salen and salphen complexes induce caspase activation and apoptosis in human cells. *Journal of Biomolecular Screening*, 16: 26-35.

Anweting, I.B., Idris, S.O. and Onu, A.D. (2017). Kinetics and mechanism of oxidation of thiourea by tetrakis (2,2ˈ- bipyridine)-µ-oxodiiron(III) complex in aqueous acidic media. *FUW Trends in Science & Technology Journal*, 2(2): 856-860.

Anweting, I.B., Idris, S.O. and Onu, A.D. (2020). Kinetics and mechanism of redox reaction of tetrakis (2,2'- bipyridine)-µ- oxodiiron(III) complex and glutathione in aqueous hydrochloric acid. *FUW Trends in Science & Technology Journal*, 6(1): 161-165.

Aschia, M., Mazzaa, F. and Di-Nola, A. (2002). Cation–π interactions between ammonium ion and aromatic rings: an energy decomposition study. *Journal of Molecular Structure*, 587: 177-188.

Ashmore, M.H. and Nathanail, C.P. (2008). A critical evaluation of the implications for risk based land management of the environmental chemistry of sulphur mustard. *Environment International*, 34: 1192-1203.

Astray, G., Cid, A., Manso, J.A., Mejuto, J.C., Moldes, O. and Morales, J. (2011). Influence of anionic and nonionic micelles upon hydrolysis of 3-hydroxy-carbofuran. *International Journal of Chemical Kinetics*, 43(8): 402–408.

Atiga, S., Ukoha, P.O., Ujam, O.T. and Okpareke, O.C. (2014). Kinetics and mechanism of the reduction of µ-adi-di[N,N′- bis(salicylidene)ethylenediaminatoiron(III) by dithionate ion. *Transition Metal Chemistry*, 39: 189–194.

Atkins, P.W. and de Paula, J. (2018). *Physical chemistry* (11th ed.). Oxford University Press, Oxford, p. 798.

Aune, T.M. and Thomas, E.L. (1977). Accumulation of hypothiocyanite ion during peroxidase catalysed oxidation of thiocyanate ion. *European Journal of Biochemistry*, 80: 209-214.

Ayoko, G.A. (1990). Oxidation of hypophosphorous and arsenious acids by 12-tungstocobaltate(III) ion in aqueous solution. *Transition Metal Chemistry*, 15: 421-

431.

Bakore, G.V. and Jian, C.L. (1969). Chromic acid oxidation of oxalic acid: Kinetic investigation of the uncatalysed oxidation of oxalic acid by chromic acid. *Journal of Inorganic and Nuclear Chemistry*, 31: 805-810.

Banerji, J., Kotai, L. and Banerji, K.K. (2009). Kinetics and mechanisms of oxidation of formic and oxalic acids by bis(pyridine) silver permanganate. *Indian Journal of Chemistry*, 48(A): 789-800.

Barnes, K.R. and Lippard, S. J. (2004). Cisplatin and related anticancer drugs: recent advances and insights. *Metal Ions in Biological Systems*, 42:143-177.

Bashyal, A. (2013). *Synthesis and biochemical characterization of novel metallo-salphen derivatives* (Unpublished master's thesis). The University of Texas, Arlington. Retrieved September 10, 2018 from http://hdl.handle.net/10106/26658

Beckwith, A.L.J. (1972). Phosphorous and hypophosphorous acid derived radicals and their reactions-an E.P.R. study. *Australian Journal of Chemistry*, 25: 1887-1905.

Bhat, I.K., Sherigara, B.S. and Pinto, I. (1993). Kinetics of oxidation of thiocyanate ion by manganese(III) in pyrophosphate medium. *Transition Metal Chemistry*, 18: 163-166.

Bhattacharya, S. and Mandal, S.S. (1996). DNA cleavage by intercalatable cobalt bispicolylamine complexes activated by visible light. *Chemical Communication*, (13): 1515-1516.

Boerner, L.J.K. and Zaleski, J.M. (2005). Metal complex–DNA interactions: from transcription inhibition to photoactivated cleavage. *Current Opinion in Chemical Biology*, 9(2):135-144.

Boronin, A.M., Ermakova, I.T., Sakharovsky, V.G., Grechkina, G.M., Starovoitov, I.I., Autenrieth, R.L. and Wild, J.R. (2000). Ecologically safe destruction of the detoxification products of mustard- lewisite mixtures from the Russian chemical stockpile. *Journal of Chemical Technology and Biotechnology*, 75: 82–88.

Brausam, A. and Van-Eldik, R. (2004). Further mechanistic information on the reaction between Fe(III) (EDTA) and hydrogen peroxide: observation of a second step and importance of pH. *Inorganic Chemistry*, 43(17): 5351-5359.

Brevett, C.A.S., Sumpter, K.B., Nickol, R.G. (2009). Kinetics of the degradation of sulphur mustard on ambient and moist concrete. *Journal of Hazardous Materials*, 162(1): 281-291.

Bruyère, V.I.E., Rodenas, L.A.G., Morando, P.J. and Blesa, M.A. (2001). Reduction of vanadium(V) by oxalic acid in aqueous acid solutions. *Journal of the Chemical Society, Dalton Transactions*, 24:3593–3597.

Busari, A., Idris, S.O. Onu, A.D. and Abdulkadir, I. (2019). Reaction of $S_2O_5^{2-}$ ion and µ-oxo–tetrakis(1, 10–phenanthroline)diiron(III) complex ion in aqueous phenanthrolinium buffer: A kinetic study. *FUW Trends in Science & Technology Journal*, 4(3): 651-656.

Busari, A., Idris, S.O. Onu, A.D. and Abdulkadir, I. (2021). Comparative study of the kinetics of µ-oxo-tetrakis(1,10-phenanthroline) diiron(III) complex ion reduction by N-methylthiourea and N-allylthiourea in aqueous phenanthrolinium buffer. *Science Forum (Journal of Pure and Applied Sciences)*, 21:28–37

Buurma, N.J. (2009). Kinetic medium effects on organic reactions in aqueous colloidal solutions. *Advances in Physical* Organic Chemistry, 43:1–36.

Caballero, E.G., Alvarez, R.M. and Sierra, M.A. (2018). Unexpected reaction pathways leadingto thiodiglycol during the degradation of long-chain sulphur mustards. *Journal of Organic Chemistry*, 83(20): 12432-12439.

Canali, L. and Sherrington, D.C. (1999). Utilisation of homogeneous and supported chiral metal(salen) complexes in asymmetric catalysis. *Chemical Society Reviews*, 28(2): 85-93.

Castanheiro, T., Suffert, J., Donnard, M. and Gulea, M. (2016). "Recent advances in the chemistry of organic thiocyanates". *Chemical Society Reviews*, 45(3): 494–505.

Chakraborty, M., Mandal, P.C. and Mukhopadhyay, S. (2013). Kinetic studies on oxidation of L-cysteine and 2-mercaptoethanol by a trinuclear Mn(IV) species in aqueous acidic media. *Inorganica Chimica Acta*, 398:77–82.

Chakrabarty, S. and Banerjee, R. (2014). Kinetics and mechanism of oxidation of 2-mercaptoethanol by the heteropolyoxovanadate $[MnV_{13}O_{38}]^{7-}$. *International Journal of Chemical Kinetics*, DOI: 10.1002/kin.20887.

Chattopadhyay, S.K. and Mak, T.C.W. (2000). Study of Cu^{2+} mediated oxidation of thiosemicarbazide, thiocarbohydrazide and thiourea. *Inorganic Chemistry Communications*, 3: 111–113.

Chauhan, M.S., Kumar, G., Kumar, A., Sharma, K. and Chauhan, S. (2001). Conductance and viscosity studies of sodium dodecylsulphatein aqueous solutions of dimethylsulphoxide and methanol. *Colloids and Surfaces A: Physicochemical and Engineering Aspects*, 180: 111-119.

Chauhan, M.S., Kumari, N., Pathania, S., Sharma, K. and Kumar, G. (2007). A conductometric study of interactions between gelatin and sodium dodecyl sulphate (SDS) in aqueous-richmixtures of dimethylsulphoxide. *Colloids and Surfaces A: Physicochemical and Engineering Aspects*, 293: 157–161.

Clarke, J.D. (2009). Cetyltrimethylammonium bromide (CTAB) DNA miniprep for plant DNA isolation. *Cold Spring Harbor Protocols*, 3: 51-77.

Cohen, S. M. and Lippard, S. J. (2001). Cisplatin: from DNA damage to cancer chemotherapy. *Progress in Nucleic Acid Research and Molecular Biology,* 67: 93-130.

Conner, G. E., Wijkstrom-Frei, C., Randell, S.H., Fernandez, V.E. and Salathe, M. (2007). "The lactoperoxidase system links anion transport to host defense in cystic fibrosis". *Federation of European Biochemical Societies Letters*, 581(2): 271–278.

Costes, J.P., Shova, S. and Wernsdorfer, W. (2008). Tetranuclear $[Cu–Ln]_2$ single molecule magnets: synthesis, structural and magnetic studies. *Daltons Transactions*, 14: 1843 -1849.

Cozzi, P.G. (2004). Metal–Salen Schiff base complexes in catalysis: practical aspects. *Chemical Society Reviews*, 33(7): 410-421.

Czlapinski, J.L. and Sheppard, T.L., (2001). Nucleic acid template-directed assembly of metallosalen DNA conjugates. *Journal of the American Chemical Society*, 123: 8618- 8619.

Danford, A. J., Wang, D., Wang, Q., Tullius, T.D. and Lippard, S. J. (2005). Platinum anticancer drug damage enforces a particular rotational setting of DNA in nucleosomes, *Proceedings of the National Academy of Sciences of the United States of America*, 102(35): 12311-12316.

Das-Karfa, T., Bera, B.K., Mallick, S., Karmakar, P., Mandal, A., Mondal, S., … Ghosh, A.K. (2010). Kinetic and mechanistic studies on the reaction of thiosemicarbazide with $[(H_2O)(tap)_2RuORu(tap)_2(H_2O)]^{2+}$. *Transition Metal Chemistry*, 35: 885–890.

De-Laat, J. and Gallard H. (1999). Catalytic decomposition of hydrogen peroxide by Fe(III) in homogeneous aqueous solution: Mechanism and kinetic modeling. *EnvironmentalScience and Technology*, 33: 2726-2732.

Dell'Amico, E., Bernasconi, S., Cavalca, L., Magni, C., Prinsi, B. and Andreoni, V. (2009). New insights into the biodegradation of thiodiglycol, the hydrolysis product of Yperite(sulphur mustard gas). *Journal of Applied Microbiology*, 106: 1111-1121.

Demissie, H. and Duraisamy, R. (2016). Effects of electrolytes on the surface and micellar characteristics of Sodium dodecyl sulphate surfactant solution. *Journal of Scientific and Innovative Research*, 5(6): 208-214.

Doctrow, S.R., Huffman, K., Marcus, C.B., Tocco, G., Malfroy, E., Adinolfi, C.A., … Malfroy, B. (2002). Salen-manganese complexes as catalytic scavengers of hydrogen peroxide and cytoprotective agents: structure-activity relationship studies. *Journal of Medical Chemistry,* 45(20): 4549-4558.

Dubey N. (2013). CTAB aggregation in solutions of higher alcohols: thermodynamic and spectroscopic studies. *Journal of Molecular Liquids*, 184: 60–67.

Dwars, T., Paetzold, E. and Oehme, G. (2005). Reactions in micellar systems. *Angewandte Chemie, International Edition*, 44:7174–7199.

Ehrsson, H., Wallin, I., Yachnin, J. (2002). Pharmacokinetics of oxaliplatin in humans. *Medical Oncology*, 19(4): 261–265.

El-Gammal, O.A., Al-Gader, I.M.A., El-Asmy, A.A. (2014). Synthesis, characterization, biological activity of binuclear Co(II), Cu(II) and mononuclear Ni(II) complexes of bulky multi-dentate thiosemicarbazide. *Spectrochimica Acta. Part A, Molecular and Biomolecular Spectroscopy*, 128: 759-772.

Espenson, J.H. (1981). *Chemical kinetics and reaction mechanisms*. McGraw-Hill. p. 117. ISBN 0-07-019667-2.

Feng, L., Lu, S., Qi, L., Fang, M. and Song, Y. (2020). Kinetics of hydrogen peroxide decomposition catalysed by Cu-buserite over a well-sealed and thermostated kinetics assembly. *International Journal of Chemical Kinetics,* 2020: 1–8.

Fernandez, O.B., Lorkovic, I.M. and Ford, C.P. (2004). Mechanisms of ferriheme reduction by nitric oxide: nitrite and general base catalysis. *Inorganic Chemistry*, 43(17): 5393- 5402.

Ferrari, M.B., Capacchi, S., Pelosi, G., Reffo, G., Tarasconi, P., Albertini, R., … Lunghi, P. (1999). Synthesis, structural characterization and biological activity of helicon thiosemicarbazone monohydrate and a copper(II) complex of salicylaldehyde thiosemicarbazone. *Inorganica Chimica Acta*, 286: 134-141.

Ferrari, M.B., Bisceglie, F., Pelosi, G., Tarasconi, P., Albertini, R. and Pinelli, S. (2001). New methyl pyruvate thiosemicarbazones and their copper and zinccomplexes: synthesis, characterization, X-ray structures and biologicalactivity. *Journal of Inorganic Biochemistry*, 87: 137-147.

Friedman, M. (1973). *The chemistry and biochemistry of the sulphhydryl group in amino acids, peptides and proteins*. Pergamon, New York, pp. 52-87.

Gangopadhyay, S., Ali, M. and Banerjee, P. (1994a). Oxidation reactions of mononuclear manganese(III) complexes. *Coordination Chemistry Reviews*, 135: 399-427.

Gangopadhyay, S., Ali, M., Dutta, A. and Banerjee, P. (1994b). Oxidation of thioglycolic acid and glutathione by (trans-cyclohexane-1,2-diamine-N,N,N',N'-tetraacetato)manganate(III) inaqueous media. *Journal of the Chemistry Society, Dalton Transactions*, 6: 841-845.

Geronimo, I., Singh, N.J. and Kim, K.S. (2011). Can electron-rich π systems bind anions? *Journal of Chemical Theory and Computation*, 7: 825–829.

Ghosh, A.K. and De, G.S. (1992). Kinetics and mechanism of the reaction of thiocyanate ion with hexaaquo rhodium(Ill) ion. *Transition Metal Chemistry*, 17: 435-437.

Gielen, M. (2003). An overview of forty years organotin chemistry developed at the free universities of Brussels ULB and VUB. *Journal of the Brazilian Chemical Society*, 14(6): 870-877.

Goswami, S., Shaikh, N., Panja, A. and Banerjee, P. (2004). A comparative kinetic study for the oxidation of 2-mercaptoethanol by di-μ-oxo-bis(1,4,7,10-tetraazacyclododecane)- dimanganese(III,IV) and di-μ-oxo-bis(1,4,8,11-tetraazacyclotetradecane)- dimanganese(III,IV) complexes: Influence of copper(II). *International Journal* of *Chemical Kinetics*, 36: 129–137.

Gowda, B.T. and Bhat, J.I. (1987). Mechanistic investigations with positive halogens; kinetics of oxidation of thiosemicarbazide by chloramine-B, bromamine-B and dichloramine-B in acid medium. *Tetrahedron*, 43(9): 2119-2128.

Gowda, B.T. and Rao, R.V. (1988). Kinetics and mechanism of oxidation of thiosemicarbazide in the pure state and in its metal complex by chloramine T, bromamine T, and dichloramine T in acid medium. *Journal of the Chemical Society Perkin Transactions*, 2(3): 355-361.

Gowda, B.T. and Sherigara, B.S. (1989). Kinetic investigations of positive halogen reactions. oxidation of thiosemicarbazide by chlroramine-T and dichloramine-T. *Journal of the Indian Chemical Society*, 66(2): 91-98.

Gowda, B.T. and Vasireddy, P. (1990). Kinetics of oxidation of S-N donor ligands by hydrogen peroxide. *Proceedings of the Indian Academy of Sciences, Chemical Sciences*, 102(4): 463-469.

Gowda, B.T., Kumar, P.S.K. and Bhat, J. (1991). Kinetics of oxidation of thiocyanate and thiosemicarbazide in the free and metal-bound states by potassium iodate in aqueous perchloric acid medium. *Journal of the Indian Chemical Society*, 68(4): 215-220.

Greenwood, N.N. and Earnshaw, A. (1997). *Chemistry of the Elements* (2nd ed.). Butterworth Heinemann. pp. 461-464. ISBN 0080379419

Gündüz, T., Gündüz, N. and Şakiyan, I. (1994): A new method for synthesis of manganese(III) acetate dehydrate. *Synthesis and Reactivity in Inorganic and Metal Organic Chemistry*, 24(4): 519-524.

Gupta, K.C. and Sutar, A.K. (2008). Catalytic activities of schiff base transition metal complexes. *Coordination Chemistry Reviews*, 252: 1420-1450.

Guy, R. G. (1977). Syntheses and preparative applications of thiocyanates. In Patai, S. (ed.). *Chemistry of cyanates and their derivatives* 2. John Wiley, New York.

Hadgiivanova, R. and Diamant, H. (2007). Premicellar aggregation of amphiphilic molecules. *Journal of Physical Chemistry B*, 111(30): 8854–8859.

Hampton, C., Demoin, D. and Glaser, R.E. (2010). Vibrational spectroscopy tutorial: sulphur and phosphorus. In Glaser, R.E. (ed). *Fall 2010 Organic Spectroscopy*. University of Missouri. Retrieved November 23rd, 2020 from https://faculty.missouri.edu/~glaserr/8160f10/A03_Silver.pdf

Hamza, S.A., Iyun, J.F. and Idris, S. O. (2012). Kinetics and mechanism of the redox reaction of toluidine blue and nitrite ions in aqueous acidic medium. *Archives of Applied Science Research*, 4(1): 10-18.

Harvey, S.P., Szafraniec, L.L., Beaudry, W.T., Earley, J.T. and Irvine, R.L. (1997). *Neutralization and biodegradation of sulphur mustard*. Aberdeen Proving Ground, MD. U.S. Department of the Army.

Harvey, S.P., Szafraniec, L.L. and Beaudry, W.T. (1998). Hydrolysis and biodegradation of the vesicant agent HT: Two potential approaches. *Bioremediation Journal*, 3: 191-203.

Herold, S. (2004). The outer-sphere oxidation of nitrosyliron (ll) hemeghobin by peroxynitrite leads to the release of nitrogen monoxide. *Inorganic Chemistry*, 43(13): 3783-3785.

Hill, C. N. (2001). *A vertical empire: the history of the UK rocket launch and space programme*. Imperial College Press, London, pp.1950–1971. ISBN 978-1-86094-268-6.

Hong, W.S., Wu, C.Y., Lee, C.S., Hwang, W.S. and Chiang, M.Y. (2004). Novel iron carbonyl complexes from thiophene-2-carboxaldehyde thiosemicarbazone. *Journal of Organometallic Chemistry*, 689: 277-285.

Hoshino, N. (1998). Liquid crystal properties of metal–salicylaldimine complexes: Chemical modifications towards lower symmetry. *Coordination Chemistry Reviews*, 174(1):77-108.

Housecroft, Catherine E. and Sharpe, Alan G. (2005). *Inorganic chemistry* (2nd ed.). Pearson Prentice-Hall. p. 443. ISBN 0130-39913-2.

Hunger, J., Buchner, R., Kandil, M.E., May, E.F., Marsh, K.N. and Glenn, H. (2010). Relative permittivity of dimethylsulphoxide and N,N-dimethylformamide at temperatures from 278 K to 328 K and pressures from 0.1 MPa to 5 MPa. *Journal of Chemical & Engineering Data*, 55: 2055-2065.

Huynh, M.H.V. and Meyer, T.J. (2007). Proton-coupled electron transfer, *Chemical Reviews,*107(11)**:** 5004-5064

Ibrahim, I., Idris, S.O., Onu, A.D. (2016). Kinetics and mechanism of the oxidation of neutral red by hypophosphorous acid in aqueous acidic medium. *Gashua Journal of Sciences and Humanities*, 2(2): 1 – 7.

Idris, S.O., Iyun, J.F. and Agbaji, E.B. (2007). Kinetics of the reduction of tetrakis(2,2' bipyridine)-µ-oxodiiron(III) ion by mercaptoacetic acid in aqueous hydrochloric acid medium. *African Journal of Natural Sciences*, 10: 35-39.

Idris, S.O., Samson, V.O. and Myek, B. (2015). Kinetics of the oxidation of bromopyrogallol red by nitrite ion in aqueous acidic medium. *International Frontier Science Letters*, 3: 32-38.

Ige, J. and Soriyan, O. (1986). Micellar inhibition of the aquation of tris-(3,4,7,8-tetramethyl 1,10 phenanthroline)iron(II) by sodium dodecyl sulphate in aqueous acid medium. *Journal of the Chemical Society, Faraday Transactions 1*, 82: 2011-2023.

Impert, O., Katafias, A., Fenska, J. and Kita, P. (2012). Kinetics and mechanism of electron transfer processes in a hydrogen peroxide—trispicolinatoruthenate(II) system. *Transition Metal Chemistry*, 37: 7–16.

Islam, M.F. (2003). High weight fraction surfactant solubilization of single-wall carbon nanotubes in water. *Nano Letters*, 3(2): 269–273.

Iyun, J.F. and Musa, K.Y. (1995). Oxidation of 2-mercaptoethanol and 2 mercaptoethylamine by $[(bpy)_2H_2ORu^{III}]_2O^{4+}$ in aqueous media. *Indian Journal of Chemistry*, 34A: 635-638.

Jacobsen, E.N. (2000). Asymmetric catalysis of epoxide ring-opening reactions. *Accounts of Chemical Research*, 33(6): 421-431.

Jacobsen, E.N., Zhang, W. and Guler, M.L. (1991). Electronic tuning of asymmetric catalysts. *Journal of the American Chemical Society*, 113: 6703-6704.

Jacobsen, E.N., Zhang, W., Muci, A.R., Ecker, J.R. and Deng, L. (1990). Highly enantioselective epoxidation catalysts derived from 1,2-diaminocyclohexane. *Journal of the American Chemical Society*, 113(18): 7063-7064.

Jalali, F. and Gerandaneh, A. (2011). Micellization of cetyltrimethylammonium bromide (CTAB) in mixed solvents and in the presence of potassium bromide, *Journal of Dispersion Science and Technology*, 32(5): 659-666.

Jena, P., Acharya, A.N., Mundlapati, V.R., Dash, A.C. and Biswal, H.S. (2018). Kinetics and mechanistic study of the reduction of Mn^{III} by oxalate in Salophen scaffold: relevance to oxalate oxidase. *Journal of Chemical Sciences*, 130: 123-136.

Jiang, B., Du, J., Cheng, S., Wang, Q. and Zeng, X. (2003). Effects of amine additives on critical micelle concentration of ionic surfactants. *Journal of Dispersion Science and Technology*, 24(6): 755-760.

Jocelyn, P.C. (1972). *Biochemistry of the SH group*. Academic Press, New York, p. 94.

Jonnalagadda, S.B., Chinake, C.R., Olojo, R. and Simoyi, R.H. (2002). Kinetics and mechanism of the oxidation of 4-methyl-3-thiosemicarbazide by acidic bromate. *International Journal of Chemical Kinetics*, 34(4): 237-247.

Jonnalagadda, S.B. and Gollapalli, N.R. (2008). Speciation and stability of methylene blue-metal-thiocyanate ion-association complexes. *Bulleting of the Chemical Society of Ethiopia*, 22(1): 85-91.

Joshi, N., Rawat, K. and Bohidar, H.B. (2016). Influence of structure, charge, and concentration on the pectin–calcium–surfactant complexes. *Journal of Physical Chemistry B*, 120(18): 4249–4257.

Joshua D.C. and Brian J.D. (2012). Thiocyanate: A potentially useful therapeutic agent with host defense and antioxidant properties. *Biochemical Pharmacology*, 84: 1381–1387.

Kalmar, J., Lente, G. and Fabian, I. (2013). Detailed kinetics and mechanism of the oxidation of thiocyanate ion (SCN^-) by peroxomonosulphate ion (HSO_5^-). Formation and subsequent oxidation of hypothiocyanite ion ($OSCN^-$). *Inorganic chemistry*, 52: 2150-2156.

Kandpal, N.D., Joshi, S.K. and Mishra, V.N. (1996). The oxidation of thiosemicarbazide by vanadium (V) in perchloric acid. *Chemica Acta Turcica*, 24: 189-194.

Kar, A.K., Acharyab, A., Pradhana, G.C. and Dash, A.C. (2014). Glyoxylate as a reducing agent for manganese(III) in salen scaffold: A kinetics and mechanistic study. *Journal of Chemical Sciences*, 126(3): 547–559.

Katre, Y., Mudliar, S.R., Joshi, G.K. and Singh, A.K. (2012). Catalytic effect of cetyltrimethylammonium bromide on the oxidation of oxalic acid by N-bromophthalimide in acidic medium. *Journal of Dispersion Science and Technology*,33: 1038–1045.

Katre, Y., Goyal, N. and Singh, A.K. (2013). Impact of micelle media on the kinetics of oxidation of l-lysine (an essential amino acid) by N-bromophthalimide. *Journal of Dispersion Science and Technology*, 34(10): 1421-1428.

Khan, Z., Hashimi, A.A., Ahmed, L. and Haq, M.M. (1998). Kinetics and mechanism of chromic acid oxidation of oxalic acid in absence and presence of different acid media. A kinetic study. *International Journal of Chemical Kinetics*, 30: 335–340.

Khurana, M., Sharma, P.K. and Banerji, K.K. (2000). Kinetics and mechanism of the oxidation of formic and oxalic acids by quinolinium fluorochromate. *Proceedings of the Indian Academy of Sciences: Chemical Sciences*, 112(2): 73-81.

Kim, J.W., Rainina, E.I., Efremenko, E., Engler, C.R. and Wild, J.R. (1997). Degradation of thiodiglycol, the hydrolysis product of sulphur mustard, with bacteria immobilized within poly(vinyl) alcohol cryogels. *Biotechnology Letters*, 19(11): 1067-1071.

Klaassen, C.D. (2001). *Casarett and Doull's toxicology. The basic science of poisons* (6^{th} ed.). McGraw-Hill, New York, p. 726.

Komiyama, M., Takeda, N. and Shigekawa, H. (1999). Hydrolysis of DNA and RNA by lanthanide ions: Mechanistic studies leading to new applications. *Chemical Communication*, 16: 1443 -1451.

Kovacs, K.A., Grof, P., Burai, L., and Riedel, M. (2004). Revising the mechanism of the permanganate/oxalate reaction. *Journal of Physical Chemistry A*, 108(50): 11026-11031.

Kremer, M.L. (2017). Strong inhibition of the Fe^{3+} - H_2O_2 reaction by ethanol: Evidence against the free radical theory. *Progress in Reaction Kinetics and Mechanism*, 42(4): 397-413.

Kumar, B., Tikariha, D. and Ghosh, K.K. (2012). Effects of electrolytes on micellar and surface properties of some monomeric surfactants, *Journal of Dispersion Science and Technology*, 33(2): 265-271.

Kumar, D., Neo, K., and Rub, M.A. (2016). Effect of alkanediyl-α,ω-type cationic dimeric (gemini) surfactants on the reaction rate of ninhydrin with $[Cu(II)\text{-}Gly\text{-}Tyr]^+$ Complex. *Journal of Surfactants and Detergents*, 19(1): 101-109.

Kumari, N. (2004). *Physicochemical studies of protein interaction with ionic surfactants* (Unpublished PhD Dissertation). Himachal Pradesh University. pp. 30-31. Retrieved October 29, 2020, from https://sg.inflibnet.ac.in/bitstream/10603/127767/15/09_chapter%203.pdf

Laemmli, U.K. (1970). Cleavage of structural proteins during the assembly of the head of bacteriophage T4. *Nature*, 227(5259): 680–685.

Laguta, A.N., Eltsov, S.V., Mchedlov-Petrossyan, N.O. (2018a). Kinetics of alkaline fading of methyl violet in micellar solutions of surfactants: Comparing Piszkiewicz's, Berezin's, and Pseudophase Ion-Exchange models. *International Journal of Chemical Kinetics*, 1–12. https://doi.org/10.1002/kin.21231

Laguta, A.N., Eltsov, S.V. and Mchedlov-Petrossyan, N.O. (2018b). Quantitative analysis of micellar effect on the reaction rate of alkaline fading of phenolphthalein. *Kharkov University Bulletin. Chemical Series*, 30(53): 18-26.

Larson, R.A., Jafvert, C.T., Bosc´a, F., Marley, K.A. and Miller, P.L. (2000). Effects of surfactants on reduction and photolysis (>290 nm) of nitroaromatic compounds. *EnvironmentalScience and Technology*, 34(3): 505–508.

Lawal, H.M., Olagbemiro O.T. and Iyun J.F. (1994). Oxidation of mercaptoacetic acid by trioxalatocobaltate(III) ion in aqueous perchloric acid. *Journal of Chemical Society of Nigeria*, 19: 118-122.

Lee, K.P. and Allen, H.E. (1998). Environmental transformation mechanisms of thiodiglycol. *Environmental Toxicology and Chemistry*, 17: 1720–1726.

Lide, D.R. (2007). *CRC handbook of chemistry and physics* (87th ed.). CRC Press, Boca Raton, 2006–2007.

Lin, B., Mohanty, S., McCormick, A.V., and Davis, H.T. (2003). Study of the Effects of Added Salts on Micellization of Cetyltrimethylammonium Bromide Surfactant. *American Chemical Society Symposium Series*, 861:313–326.

Linley, E., Denyer, S.P., McDonnell, G., Simons, C. and Maillard, J.Y. (2012). Use of hydrogen peroxide as a biocide: new consideration of its mechanisms of biocidal action. *Journal of Antimicrobial Chemotherapy*, 67(7): 1589-1596.

Liou, Y.W. and Wang, C.M. (2000). Peroxidase mimicking: Fe(Salen)Cl modified electrodes, fundamental properties and applications for biosensing. *Journal of Electroanalytical Chemistry*, 481(1): 102-109.

Llewellyn, B.D. (2014). Thiosemicarbazide-ferricyanide reduction for the histochemical demonstration of aldehydes in tissue sections. *Biotechnic and Histochemistry*, 89(3): 228-231.

Löffler G. and Petrides, P. E. (1988). *Physiological chemist*ry (4 ed.). Springer, Berlin, p. 288, DOI:10.1007/978-3-642-87858-9

Lohdip, Y.N. and Iyun, J.F. (2003). Kinetics and mechanism of the oxidation of thiocyanate ion by di-μ-oxo-tetrakis(1,10-phenanthroline)-dimanganese(III,IV) ion in acid medium. *Global Journal of Pure and Applied Sciences*, 9(1): 105-112.

Lombardo, R., Sbriziolo, C. and Turco-Liveri, M.L. (2006). Rate-retarding effects of mixed anionic/non-ionic micelles on the alkaline hydrolysis of the chloropentamminocobalt(III) complex: Role of the anionic surfactant chain nature**.** *Colloids and Surfaces A,* 273: 1–9.

Lu, C.P., Lin, C.T., Chang, C.M., Wu, S.H. and Lo, L.C. (2011). Nitrophenylboronic acids as highly chemoselective probes to detect hydrogen peroxide in foods and agricultural products. *Journal of Agricultural and Food Chemistry,* 59(21): 11403-11406.

Luo, D., Smith, S.W. and Anderson, B.D. (2005). Kinetics and mechanism of the reaction of cysteine and hydrogen peroxide in aqueous solution. *Journal of Pharmaceutical Sciences*, 94: 304–316.

Magarian, N.J. (2014). *Mechanistic studies of salt effects on bimolecular electron-transfer reactions of pentaamine ruthenium pyridyl complexes studied by 19F NMR line-broadening and T2 spin-echo techniques* (Unpublished Masters Thesis). The University of San Francisco. https://repository.usfca.edu/thes/101

Malmberg, C.G. and Maryott, A.A. (1956). Dielectric constant of water from 0˚ to 100˚ C. *Journal of Research of the National Bureau of Standards*, 56(1): 1-8.

Mandal, A., Das, R.S., Singh, B., Banerjeeb, R. and Mukhopadhay, S. (2015). Kinetic and mechanistic studies of the reactions of 2-mercaptoethanol and thioglycolic acid with Co(III)-bound superoxide complex. *Canadian Journal of Chemistry*, *93*(11): 1276-1282.

Markarian, S.A., Harutyunyan, L.R. and Harutyunyan, R.S. (2005). The properties of mixtures of sodium dodecylsulphate and diethylsulphoxide in water. *Journal of Solution Chemistry*, 34(3): 361-368.

Matsushita, T and Shono, T. (1981). Reactions of manganese(III) schiff base complexes with superoxide ion in dimethyl sulphoxide. *Bulletin of the Chemical Society of Japan,* 54: 3743-3748.

McAuley, A. and Gomwalk, U.D. (1968). Metal ion oxidations in solution. Part V. Cerium(IV) oxidation of thiourea and its N – substituted derivatives. *Journal of the Chemical Society A*: 2948– 2951.

McAuley, A. and Gomwalk, U.D. (1969). Metal ion oxidations in solution. Part VI. Oxidation of thiourea and its N–substituted derivatives by cobalt(III). *Journal of the Chemical Society A*: 977–980.

Medvedeva, N., Polyak, Y., Kuzikova, I., Orlova, O., Zharikov, G. (2008). The effect of mustard gas on the biological activity of soil. *Environmental Research,* 106: 289-295.

Mehrotra, R.N. (2013). Three oxyacids of phosphorus: tautomerism and oxidation mechanism. *European Chemical Bulletin,* 2(10): 758 – 776.

Metwally, M.A., Bondock, S., El-Azap, H. and Kandeel, E.M. (2011). Thiosemicarbazides: synthesis and reactions. *Journal of Sulphur Chemistry*, 32(5): 489-519.

Mifsud, S. (2009). *Metal cation identification*. Retrieved August 31, 2018, from http://www.marz-kreations.com/Chemistry/Cation-ID/162k-Iron.html

Minarowski, Ł., Sands, D., Minarowska, A., Karwowska, A., Sulewska, A., Gacko, M. and Chyczewska, E. (2008). Thiocyanate concentration in saliva of cystic fibrosis patients. *Folia Histochemica et Cytobiologica*, 46(2): 245–246.

Mishra, R., Mukhopadhyay S. and Banerjee, R. (2009). Reaction of hydrogen peroxide with coordinated superoxide in $[(NH_3)_5Co^{III}(\mu\text{-}O_2)Co^{III}(NH_3)_5]^{5+}$: A mechanistic study. *Journal of the Chemical Society Daltons Transaction*s, 5469-5473.

Miyasaka, H., Ieda, H., Mastumoto, N., Crescenzi, R. and Floriani, C. (1998). Assembling bi-, tri and pentanuclear complexes into extended structures using a desolvation reaction: synthesis, structure, and magnetic properties of manganese(III)−schiff-base−hexacyanoferrate polymeric compounds and their derived extended structures. *Inorganic Chemistry*, 37(2): 255-263.

Modaressi, A., Sifaoui, H., Grzesiak, B., Solimando, R., Domanska, U. and Rogalski, M. (2007). CTAB aggregation in aqueous solutions of ammonium based ionic liquids; conductimetricstudies. *Colloids and Surfaces A: Physicochemical and Engineering Aspects*, 296(3): 104- 108.

Mohammed, Y., Idris, S.O., Onu, A.D. and Iyun, J.F. (2016). Studies of the kinetics and mechanism of the electron transfer reaction of diaquotetrakis(2,2ˈ-bipyridine-µ-oxodiruthenium(III) ion and dithionite in aqueous medium. *FUW Trends in Science & Technology Journal,* 1(1):11-23.

Mohammed, Y., Idris, S. O. and Onu, A. D. (2017). Kinetics and mechanism of the reduction of diaquotetrakis-(2,2'-bipyridine)- µ-oxodiruthenium(III) ion by hypophosphorous acid in acidicmedium. *Transition Metal Chemistry*, 42: 323–329.

Mohareb, M.M., Ghosh, K.K. and Palepu, R.M. (2006). Kinetics of the reaction of methyl-4 nitrobenzenesulphonate + Br^- in ethanol amine based surfactants, *International Journal of Chemical Kinetics*, 38(5): 303–308.

More, S.S., Gurame, V.M. and Gokavi, G.S. (2018). Kinetics and mechanism of oxidation of thiosemicarbazide by waugh-type 9-molybdomanganate(IV) in aqueous perchloric acid. *Journal of Applicable Chemistry,* 7(3): 686-694.

Moskwa, P., Lorentzen, D., Excoffon, K.J., Zabner, J., McCray, P.B.J., Nauseef, W.M., … Bánfi, B. (2007). A Novel Host Defense System of Airways is Defective in Cystic Fibrosis. *American Journal of Respiratory and Critical Care Medicine,* 175(2): 174-183.

Mukhopadhyay, S., Rinadas, S. and Banerjee, R. (1993). Kinetics and mechanism of the oxidation of oxalate ion by tris(acetylacetonato)-manganese(III) and its hydrolytic derivatives in aqueous perchlorate media. *Canadian Journal of Chemistry,* 71: 2155-2159.

Muller, J.G., Kayser, L.A., Paikoff, S.J., Duarte, V., Tang, N., Perez, R.J., … Burrows, C.J. (1999). Formation of DNA adducts using nickel(II) complexes of redox active ligands: a comparison of salen and peptide complexes. *Coordination Chemistry Reviews,* 186: 761-774.

Munro, N.B., Talmage, S.S., Griffin, G.D., Waters, L.C., Watson, A.P., King, J.F. and Hauschild, V. (1999). The sources, fate, and toxicity of chemical warfare agent degradation products. *Environmental Health Perspectives*, 107(12): 933-974.

Musa, K.Y., Iyun, J.F. and Ayoko G.A. (1995). Mechanism of the reduction of diaquotetrakis(2,2'bipyridine)-µ-oxodiruthenium(III) ion by L-cysteine and mercaptoacetic acid. *Bulletin of the Science Association of Nigeria*, 19: 212-216.

Myek, B., Idris, S.O. and Iyun, J.F. (2017). Kinetics and mechanism of the redox reaction of naphthol green b with hyydrazine dihydrochloride in aqueous acidic medium. *Science Journal of Chemistry,* 5(6):76-79.

Nagarajan, R. and Ruckenstein, E. (1991). Theory of surfactant self-assembly: a predictive molecular thermodynamic approach, *Langmuir,* 7(12): 2934-2969.

Nandibewoor, S.T., Hiremath, G.A. and Timmanagoudar, P.L. (2000). Ruthenium(III) catalysed oxidation of thiocyanate by periodate in aqueous alkaline medium; autocatalysis in catalysis. *Transition Metal Chemistry*, 25: 394–399.

Natarajan, S.V., Kuppuraj, G. and Rajagopal, S. (2005). Metal–salen complexes as efficient catalysts for the oxygenation of heteroatom containing organic compounds-synthetic and mechanistic aspects. *Coordination Chemistry Reviews*, 249: 1249–1268.

Nayak, S.P. and Gowda, B.T. (1992). Kinetics and mechanisms of oxidation of thiosemicarbazide, its metal complex and hydrazones by N-chlorobenzamide in water methanol medium. *Journal of Physical Organic Chemistry*, 5: 755-763.

Nazarenko, A. (2004). *Qualitative tests on 3d-metal ions*. Retrieved September 16, 2020, from http://staff.buffalostate.edu/nazareay/che112/ex9.htm.

Nkole, I.U., Osunkwo, C.R., Onu, A.D. and Idris, S.O. (2018). Kinetics and mechanism of the reduction of N-(2-hydroxyethyl)ethylenediaminetriacetatoiron(III) complex by thioglycol in bicarbonate buffer medium. *International Journal of Advanced Chemistry*, 6(1): 102- 107.

Nkole, I.U., Abdulsalam, S., Ibrahim, I. and Arthur, D.E. (2021a). Micellar effect on electron transfer reaction of 2-(hydroxyethyl)ethylenediaminetriacetatoiron(III) complex with thiocarbonate ion: Kinetic model. *Chemistry Africa* 4: 525–533.

Nkole, I.U., Idris, S.O. and Onu, A.D. (2021b). Redox reactions of tris-(1,10 phenanthroline)iron(III) complex with thiourea and N-methylthiourea in an aqueous acidic medium: Kinetics and mechanism. *Inorganic Chemistry Communications*, 133: 108930. https://doi.org/10.1016/j.inoche.2021.108930.

Ogata, Y. and Sawaki, Y. (1963). Kinetics of the catalytic hydrogen peroxide oxidation of thiodiglycol in aqueous solutions. *Bulletin of the Chemical Society of Japan*, 36(11): 1453-1459.

Ogunlusi, G.O., Ige, J., Oyetunji, A.O. and Owoyomi, O. (2013). Effects of SDS, Triton X-100, and the binary mixture of Triton X-100/SDS surfactants on the electron transfer reaction between Tris-2,20-bipyridyl iron(II) and azidopentacyanocobaltate(III)complexes. *Journal of Dispersion Science and Technology*, 34: 941–946.

Ogunlusi, G.O., Oyetunji, O.A., Owoyomi, O. and Ige, J. (2016). Effects of alkyltrimethylammonium bromide surfactants on the kinetics of the oxidation of tris(1,10-phenanthroline)iron(II) by azido-pentacyanocobaltate(III) complex. *Journal of Dispersion Science and Technology*, 1-21. DOI:10.1080/01932691.2016.1225218

Olanrewaju, O., Ige, J. and Soriyan O.O. (2011). Alkaline hydrolysis of brilliant green in mixed cationic surfactant systems. *Central European Journal of Chemistry*, 9(1): 106-111.

Olaseni, S.E., Oladoja, N.A., Ololade, I.A., Aboluwoye, C.O. and Osundiya, M.O. (2012). Micellisation of cetyltrimethyl ammonium bromide in aqueous-organic media. *Chemical Sciences Journal*, 52: 1-11.

O'Neil, M.J. (ed.). (2013). *The merck index - An encyclopedia of chemicals, drugs, and biologicals*. Royal Society of Chemistry, Cambridge, UK, p. 889.

Onu, A.D, Iyun, J.F and Idris, S.O. (2015). Kinetics and stoichiometry of the reduction of hydrogen peroxide by an aminocarboxylactocobaltate(II) complex in aqueous medium. *OpenJournal of Inorganic Chemistry*, 5: 75-82.

Onu, A.D. Idris, S.O. and Iyun, J.F. (2016). Oxidation of ethylenediamine-tetraacetatocobaltate(II) complex by hydrogen peroxide in aqueous acidic medium: A kinetic study. *Journal of Chemical Society of Nigeria,* 41(2):81-86.

Orio, M., Jarjayes, O., Kanso, H., Philouze, C., Neese, F. and Thomas, F. (2010). X-ray structures of copper(II) and nickel(II) radical salen complexes: The preference of galactose oxidase for copper(II). *Angewandte Chemie International Edition*, 49(29): 4989-4992.

Ott, I. and Gust, R. (2007). Non platinum metal complexes as anti-cancer drugs, *Archiv de Pharmazie (Weinheim),* 340(3): 117-126.

Owoyomi O., Ige, J., Soriyan, O., Ogunlusi G., Olaseni S.E. and Oladimeji O. (2007). Kinetics and Mechanism of the Alkaline Fading of Brilliant Green in Aqueous Solutions of a Double-tailed and Some Single-tailed Cationic Surfactants. *Acta Chimica Slovenica,* 54: 370–374.

Pandey, E. and Upadhyay, S.K. (2005). Effect of micellar aggregates on the kinetics of oxidation of α-aminoacids by chloramine-T in perchloric acid medium. *Colloids and Surfaces A,* 269: 7–15.

Patist, A., Oh, S.G., Leung. R., and Shah, D.O. (2001). Kinetics of micellization: its significance to technological processes, *Colloids and Surfaces A,* 176(1): 3–16.

Pecoraro, V.L., Baldwin, M.J. and Gelasco, A. (1994). Interaction of manganese with dioxygen and its reduced derivatives. *Chemical Reviews,* 94(3): 807-826.

Pedemonte, N., Caci, E., Sondo, E., Caputo, A., Rhoden, K., Pfeffer, U., … Galietta, L.J. (2007).Thiocyanate transport in resting and IL-4-stimulated human bronchial epithelial cells: role of pendrin and anion channels. *Journal of Immunology*. 178(8): 5144–5153.

Peng, H. and Guo, J. (2020). Reduction behavior of chromium(VI) with oxalic acid in aqueous solution. *Scientific Reports*, 10:17732. https://doi.org/10.1038/s41598-020-74928-7

Perez-Benito, J.F. (2004). Iron(III)-hydrogen peroxide reaction: kinetic evidence of a hydroxyl mediated chain mechanism. *Journal of Physical Chemistry A,* 108: 4853-4858.

Peyre, V., Bouguerra, S. and Testard, F. (2013). Micellization of dodecyltrimethylammonium bromide in water–dimethylsulphoxide mixtures: A multi-length scale approach in a model system. *Journal of Colloid and Interface Science*, 389(1): 164-174.

Pinkowicz, D., Southerland, H.I., Avendaño, C., Prosvirin, A., Sanders, C., Wernsdorfer, W.,… Dunbar, K.R. (2015). Cyanide single molecule magnets exhibiting solvent dependent reversible "on" and "off" exchange bias behavior. *Journal of the American ChemicalSociety*, 137(45): 14406–14422.

Piszkiewicz, D. (1977). Positive cooperativity in micelle-catalysed reactions. *Journal of the American Chemical Society*, 99(5): 1550–1557.

Prakash S.D.V., Sherigara, B.S. and Khader, A.M.A. (1993). Oxidation of semicarbazide, thiosemicarbazide, carbohydrazide, thiocyanate, thiourea and its derivatives with aquocobaltic ions in acid media. *Indian Journal of Chemistry*, 32(A): 921-924.

Prasad, C.M., Mishra, P.M. and Jha, C.S. (2007). Kinetics and mechanism of oxidation of oxalic acid with Bi(V) in $HClO_4$-HF mixture. *Asian Journal of Chemistry*, 19(2): 1103-1108.

Prema, D., Wiznycia, A.V., Scott, B.M.T., Hilborn, J., Desper. J. and Levy, C.J. (2007). Dinuclear zinc(II) complexes of symmetric Schiff-base ligands with extended quinoline sidearms. *Daltons Transactions*, 42: 4788-4796.

Rafiquee, M.Z.A., Siddiqui, M.R., Haque, H.N., Ola, M.S., Al-Lohedan, H.A., Al-Othman, Z.A. and Wabaidur, S.M. (2015). Activation of molecular oxygen for the oxidation of 2-mercaptoethanol: A kinetic and mechanistic approach. *Journal of Industrial and Engineering Chemistry*, http://dx.doi.org/10.1016/j.jiec.2015.10.039

Rajendran, T., Rajagopal, S., Srinivasan, C. and Ramamurthy, P. (1997). Micellar effect on the photoinduced electron-transfer reactions of ruthenium(II)–polypyridyl complexes with phenolate ions. Effect of cetyltrimethylammonium chloride. *Journal of the Chemical Society, Faraday Transactions*, 93:3155-3160.

Ramade, I., Khan, O., Jennin, Y. and Robert, F. (1997). Design and Magnetic Properties of a Magnetically Isolated $Gd^{III}Cu^{II}$ Pair. Crystal Structures of $[Gd(hfa)_3Cu(salen)]$, $[Y(hfa)_3Cu(salen)]$, $[Gd(hfa)_3Cu(salen)(Meim)]$, and $[La(hfa)_3(H_2O)Cu(salen)]$. *Inorganic Chemistry*, 36(5): 930-936.

Ramalingam, G., Jayanthi, S. and Gopalakrishnan, M. (2009). Kinetics and mechanistic study of oxidation of thiosemicarbazide and its hydrazones by N-chloro-3-methyl-2,6-diphenyl piperidin-4-one (NCP) in water–methanol medium. *Oxidation Communication*, 32(2): 335-348.

Ran, X., Wang, L., Lin, Y., Hao, J. and Cao, D. (2010). Syntheses, characterization and biological studies of zinc(II), copper(II) and cobalt(II) complexes with Schiff base

ligand derived from 2-hydroxy-1-naphthaldehyde and selenomethionine. *Applied Organometallic Chemistry*, 24: 741-747.

Rao, M.S.P., Rao, A.R.M., Kalavathi, R., Rao, T.S. and Vani, P. (1993). Kinetics and mechanism complexes by hydrogen of reduction of bromothallium(III) peroxide in perchloric acidmedia. *Journal of the Chemical Society, Daltons Transaction*, 2283-2287.

Ratnam, S. and Anipindi, N. R. (2012). Kinetic and mechanistic studies on the oxidation of hydroxylamine, semicarbazide, and thiosemicarbazide by iron(III) in the presence of triazines. *Transition Metal Chemistry*, 37: 453–462.

Ribeiro da Silva, M.D.M.C., Goncalves, J.M., Silva, A.L.R., Oliveira, P.C.F.C., Schroder, B. and Ribeiro da Silva, M.A.V. (2004). Molecular thermochemical study of Ni(II), Cu(II) and Zn(II) complexes with *N,N*-bis(salicylaldehydo)ethylenediamine. *Journal of Molecular Catalysis A,* 224: 207–212.

Rippel, R. and Hoechst, A.G. (2012). *Mercaptoacetic acid and derivatives*. *Ullmann's encyclopedia of industrial chemistry*. Wiley-VCH Verlag GmbH & Co. KGaA, Weinheim, Germany, (22):555-557.

Rodriguez, B.C.O., Bailey, N.A., Fenton, D.E. and He, Q.Y. (1997). Zinc(II) complexes derivedfrom potentially hexadentate (N_4O_2) acyclic ligands containing pyridinyl and phenolic groups. *Journal of the Chemical Society, Dalton Transactions*, 161-166.

Rokita, S. E. and Burrows, C. J. (2001). Nickel- and cobalt-dependent oxidation and crosslinking of proteins. *Metal Ions in Biological Systems,* 38: 289-311.

Romsted, L.S. (2012). *Introduction to surfactant self-assembly*. In: *Supramolecular Chemistry: From Molecules to Nanomaterials*. Hoboken, NJ: Wiley; 1–23 https://doi.org/10.1002/9780470661345.smc013

Ross, S.D. (1946). The rate of oxidation of thiodiglycol and triethylamine by hydrogen peroxide. *Journal of the American Chemical Society*, 68: 1484-1485.

Routier, S., Bernier, J.L., Waring, M.J., Colson, P., Houssier, C. and Bailly, C. (1996). Synthesis of a functionalized salen copper complex and its interaction with DNA. *Journal of Organic Chemistry,* 61: 2326-2331.

Routier, S., Vezin, H., Lamour, E., Bernier, J.L., Catteau, J.P. and Bailly, C. (1999). DNA cleavage by hydroxy-salicylidene-ethylendiamine-iron complexes. *Nucleic Acids Research*, 27: 4160-4166.

Roy, K. (2005). *Thiols and organic sulphides. Ullmann's Encyclopedia of Industrial Chemistry*. Wiley-VCH, Weinheim, doi:10.1002/14356007.a26_767

Salem, I.A. (1994). A kinetic approach for the homogeneous reaction between N,N'-propylenebis (salicylideneiminato)manganese(III) complex and hydrogen peroxide in aqueous solution, *Polyhedron,* 13(10): 1547-1551.

Sánchez, F., Moyá, M.L., Jime′nez, R., Gómez-Herrera, C., Carmona, M.C. and López Cornejo, P. (1997). Effect of surfactant addition on the kinetics of the reaction $Fe(bpy)_3^{2+}$ - $S_2O_8^{2-}$**.** *Journal of the Chemical Society, Faraday Transactions,* 93: 2181-2184.

Schottel, B.L., Chifotides, H.T. and Dunbar, K.R. (2008). Anion- π interactions. *Chemical Society Reviews,* 37: 68–83.

Senapati, S., Das, S., Mohanty, P. and Patnaik, A. (2011). Kinetics and mechanism of electron transfer to pyridinium chlorochromate (VI) from sulphur containing amino acid, L-cysteine in aqueous and micellar media. *Polish Journal of Chemical Technology,* 13(2): 6-10.

Shamsipur, M., Alizadeh, N. and Gharibi, H. (1997). Physicochemical studies of the hexadecylpyridinium bromide micellar system in the presence of various concentrations of sodium bromide using a surfactant-selective electrode. *Indian Journal of Chemistry*, 36A: 1031–1037.

Shanmugaprabha, T., Selvakumar, K., Rajasekaran, K. and Sami, P. (2016). A kinetic study of the oxidations of 2-mercaptoethanol and 2-mercaptoethylamine by heteropoly-11-tungsto-1-vanadophosphate in aqueous acidic medium. *Transition Metal Chemistry*, 41: 71-85.

Shen, Y.H. (2001). Preparations of organobentonite using nonionic surfactants. *Chemosphere,* 44(5): 989-995.

Shen, Y., Zhong, L., Markwell, S. and Cao, D. (2010). Thiol-disulphide exchanges modulate aldo-keto reductase family 1 member B10 activity and sensitivity to inhibitors *Biochimie*, 92(5): 530–537.

Sherigara, B.S., Pinto, I. and Bhat, K.I. (1994). Manganese(III) oxidations of benzoylhydrazine, aroxyacetylhydrazine, semicarbazide, thiosemicarbazide and their derivatives in pyrophosphate media. *Mikrochimica Acta*, 113(2): 61-69.

Sherigara, B.S., Rai, S.K. and Shivakumar, K. (2001). Aqueous polymerisation of methyl methacrylate initiated by manganese(III) pyrophosphate – potassium thiocyanate redox system: A kinetic study. *Indian Journal of Chemistry,* 40(A): 46-52.

Shi, T., Berglund, J. and Elding, L.I. (1996). Kinetics and mechanism for reduction of *trans* dichlorotetracyanoplatinate(IV) by thioglycolic acid, l-cysteine, dl-penicillamine, and glutathione in aqueous solution. *Inorganic Chemistry,* 35: 3498-3503.

Shrivastava, H.Y., Devaraj, S.N. and Nair, B.U. (2004). A Schiff base complex of chromium(III): an efficient inhibitor for the pathogenic and invasive potential of Shigella dysenteriae. *Journal of Inorganic Biochemistry*, 98(2): 387-392.

Singh, M. (2014). Kinetic treatment of the reaction of fructose and N-bromosuccinimide in cationic/anionic/nonionic micelles. *Journal of Soft Matter*, 2014: 1-10.

Singh, S., Athar, F., Maurya, M.R. and Azam, A. (2006). Cyclooctadiene Ru(II) complexes of thiophene-2-carboxaldehyde-derived thiosemicarbazones: synthesis, characterization and antiamoebic activity. *European journal of medicinal chemistry*, 41(5): 592-598.

Skounas, S., Methenitis, C., Pneumatikakis, G. and Michel Morcellet, M., (2010). Kinetic studies and mechanism of hydrogen peroxide catalytic decomposition by Cu(II) complexes with polyelectrolytes derived from L-alanine and glycylglycine. *Bioinorganic Chemistry and Applications*, 2010: 1-9.

Smelkal, Z., Biezina, F., Sindelar, Z. and Klicka, R. (1996). Binuclear iron(III) – iron(III) complexes with teradentate Schiff base N,N'-bis(salicylidene)ethylenediamine and dicarboxylic acids or dithiooxamide as bridging ligands. *Transition Metal Chemistry*, 21: 49-51.

Sokołowski, M.S. and Konopski, L. (2007). Reaction of lewisite-1 with alcohols, diols, and thiols in water-A simple method of derivatization of thiodiglycol. *Phosphorus, Sulphur, and Silicon*, 182: 2311–2327.

Sood, A.K. and Sharma, S. (2016). Influence of organic solvents and temperature on the micellization of conventional and gemini surfactants: A conductometric study. *Physics and Chemistry of Liquids*, 2016: 1-15. DOI:10.1080/00319104.2016.1139711

Soriyan, O.O., Owoyomi, O. and Bamgbose, J.T. (2009). The effect of mixed surfactants of sodium dodecyl sulphate and Triton X-100 on the base hydrolysis of Malachite green. *Reaction Kinetics and Catalysis Letters*, 98: 77–82.

Soriyan, O.O., Owoyomi, O. and Ige, J. (2008). Periodate oxidation of dicyano-bis-(1, 10 phenanthroline) iron(II) dihydrate in aqueous sodium dodecyl sulphate (SDS). *Transition Metal Chemistry*, 33: 121–126.

Sorouraddin, M.H., Manzoori, J.L. and Iranifam, M. (2005). Determination of copper(II) based on its catalytic effect on thiosemicarbazide–H_2O_2–CTMAB chemiluminescence reaction. *Talanta*, 66: 1117–1121.

Srinivasan, K., Michaud, P. and Kochi, J.K. (1986). Epoxidation of olefins with cationic (salen)manganese(III) complexes. The modulation of catalytic activity by substituents. *Journal of the American Chemical Society*, 108(9): 2309-2320.

Subramaniam, P., Vanitha, T., Kodispathi, T. and Sundari, C.R.S. (2014). Role of iron(III)-salen chloride as oxidising agent with thiodiglycolic acid: the effect of axial ligands. *Journal of the Mexican Chemical Society*, 58(2): 211–217.

Subrata, J., Chatterjee, S. and Chattopadhyay, S. (2012). Syntheses, characterization and X-ray crystal structures of hexa-coordinated monomeric and oxo-bridged dimeric Fe(III) compounds with salen-type Schiff bases. *Polyhedron*, 48: 189–198.

Sugumar, K., Nagaraj, K., Murugan, K.S., Thangamuniyandi, P., Sakthinathan, S. and Vijayakumar, P. (2015). A Comparative study on the electron transfer reaction (ETR) of surfactant cobalt (III) complexes of aliphatic/aromatic ligands in microheterogeneous media: A thermodynamic approach. *RSC Advances*, 5: 48079- 48085.

Sukhikh, T.S and Vostrikova, K.E. (2017). Assembly of Mn(III) schiff base complexes with heptacyanorhenate(IV). Inorganics, 5(3): 59-75.

Sun, J. and Stanbury, D.M. (2002). Kinetics and mechanism of oxidation of thioglycolic acid by hexachloroiridate(IV). *Journal of the Chemical Society, Dalton Transaction*, 24: 785-791.

Svehla, G. and Sivasankar, B. (2012). *Vogel's Qualitative Inorganic Analysis* (Seventh Edition). Pearson, New Delhi, India. ISBN-13: 978-8131773710

Tachiyashiki, S. and Yamatera, H. (1986). Micellar effects on the kinetics of the aquation and the base hydrolysis of tris(1,10-phenanthroline)iron(II) and chloropentaamminecobalt(III) ions. *Inorganic Chemistry*, 25(17): 3043–3047.

Tanaka, F.S., Wien, R.G. and Mansager, E.R. (1979). Effect of nonionic surfactants on the photochemistry of 3-(4-chlorphenyl)-1,1-urea in aqueous solution. *Journal of Agricultural and Food Chemistry*, 27: 774–779.

Toups, M., Wubbeler, J.H., Steinbuchel, A. (2010). Microbial utilization of the industrial wastewater pollutants 2-ethylhexylthioglycolic acid and iso-octylthioglycolic acid by aerobic Gram-negative bacteria. *Biodegradation*, 21(2): 309–319.

Trofimov, B.A., Sinegovskaya, L.M. and Gusarova, N.K. (2009). Vibrations of the S–S bond in elemental sulphur and organic polysulphides: a structural guide, Journal of Sulphur Chemistry, 30(5): 518-554.

U.S. Arms Control and Disarmament Agency (1993). Convention on the prohibition of the development, production, stockpiling and use of chemical weapons and on their destruction. Washington, DC: The U.S. Government Printing Office.

U.S. Food and Drug Administration (2011). 21 CFR 184.1366: Hydrogen peroxide. http://www.accessdata.fda.gov/scripts/cdrh/cfdocs/cfcfr/CFRSearch.cfm?fr=184.1366. Accessed 12/07/2021 by 4.20 pm.

Ukoha, P.O. and Ibrahim, E. (2004). Mechanism of the oxidation of β– mercaptoacetic acid by trioxoiodate(V) in aqueous acid medium. *Chemclass Journal,* 138-141.

Ukoha, P.O., Asegbeloyin, J.N., Alioke, C. and Ujam, O.T. (2010). Kinetics and mechanism of the oxidation of dithionate ion by N,N′-ethylenebis-[Salicylideneiminato] iron (III) complex in aqueous percloric acid medium. *Journal of the Chemical Society of Nigeria*, 35(1): 163-170.

Ukoha, P.O., Atiga, S., Ujam, O.T., Asegbeloyin, J.N., Okpareke, O.C. and Okereke, S.O.E. (2015). Kinetics and mechanism of electron transfer reaction of an adipato bridged iron(III)-salen complex with dithionite ion in perchloric acid medium. *Croatica Chemica Acta*, 88(3): 259–266.

Umena, Y., Kawakami, K., Shen, J.R. and Kamiya, N. (2011). Crystal structure of oxygen evolving photosystem II at a resolution of 1.9 Å. *Nature*, 473: 55-60.

Valko, M., Izakovic, M., Mazur, M., Rhodes, C. J. and Telser, J. (2004). Role of oxygen radicals in DNA damage and cancer incidence. *Molecular and Cellular Biochemistry*, 266: 37-56.

Vautier-Giongo, C. and Pastore, H.O. (2006). Micellization of CTAB in the presence of silicate anions and the exchange between bromide and silicate at the micelle surface: A step to understand the formation of mesoporous molecular sieves at extremely low surfactant and silicate concentrations. *Journal of Colloid and Interface Science*, 299(2): 874–882.

Veriansyah, B., Kim, J.D and Lee, J.C. (2005). Supercritical water oxidation of thiodiglycol. *Industrial & Engineering Chemistry Research,* 44: 9014-9019.

Veriansyah, B. Kim, J., Lee, J. and Hong, D. (2006). Hydrothermal decomposition rate of thiodiglycol in supercritical water. *Journal of Industrial and Engineering Chemistry*, 12(3): 395-400.

Vogel A.I. (2000). *Vogel's Text Book of Quantitative Chemical Analysis* (Sixth Edition). Pearson Education Limited, Harlow, England. p. 350. ISBN: 978-0-582-22628-9.

Waldo, G.S. and Penner-Hahn, J.E. (1995). Mechanism of manganese catalase peroxide disproportionation: determination of manganese oxidation states during turnover. *Biochemistry*, 34(5): 1507-1512.

Wang, J. (2001). DNA damage and apoptosis. *Cell Death and Differentiation,* 8: 1047-1048.

Wang, Z., Zhang, J. and Cao, W. (2006). Study on the cation-π interactions between ammonium ion and aromatic π systems. *Chinese Journal of Chemistry*, 24: 1523-1530.

Warren, D.B., Grieser, F., Perera, J.M. and Stevens, G.W. (2006). Effect of surfactants on the kinetics of nickel(II) extraction by 2-hydroxy-5-nonylacetophenone oxime (LIX 84) in an N-heptane/water system. *Langmuir*, 22: 213-218.

Watson, A.P. and Griffin, G.D. (1992). Toxicity of vesicant agents scheduled for destruction by the Chemical Stockpile Disposal Program. *Environmental Health Perspectives*, 98: 259-280.

Wiznycia, A.V., Desper, J. and Levy, C.J. (2005). Iron(II) and zinc(II) monohelical binaphthyl salen complexes. *Chemical Communications*, 37: 4693-4695.

Woldemariam, G.A. and Mandal, S.S. (2008). Iron(III)-salen damages DNA and induces apoptosis in human cell via mitochondrial pathway. *Journal of Inorganic Biochemistry*, 102: 740-747.

Xiao-Juan, Y., Lin, Y., Li, D., Xian-Li L. and Wei-Kang Yuan (2011). Kinetics of the $[Fe^{III}$- EDTA$]^-$ reduction by sulphite under the catalysis of activated carbon *Journal of the American Chemical Society*, 25: 4248-4255.

Xu, Y., Szep, S. and Lu, Z. (2009). The antioxidant role of thiocyanate in the pathogenesis of cystic fibrosis and other inflammation-related diseases. *Proceedings of the National Academy of Sciences*, 106(48), 20515–20519.

Yadav, H., Bhoite, S.A. and Singh, A.K. (2016). Effect of surfactants on hydrolysis of mono- N-ethyl-O-toluidine phosphate. *Tenside Surfactants Detergents*, 53(2): 182-194.

Yamaguchi, M.U., Da Silva, A.P.B., UedaNakamura, T., Filho, B.P.D., Da Silva, C.C. and Nakamura, C.V. (2009). Effects of a thiosemicarbazide camphene derivative on Trichophyton mentagrophytes. *Molecules*, 14: 1796-1807.

Yokoyama, H., Shinozaki, K., Hattori, S., Miyazaki, F., Goto, M. (1995). Conductometric study of hydrophobic properties of tris(1,10-phenanthroline) and tris(2,2′-bipyridine) complexes. *Journal of Molecular Liquids*, 65/66:357-360.

Yusuf, U.F., Iyun, J.F. and Ayoko, G.A. (2004). Oxidation of hypophosphorous acid by poly(pyridine)iron(III) complexes. *ChemClass Journal*, 2: 118–122.

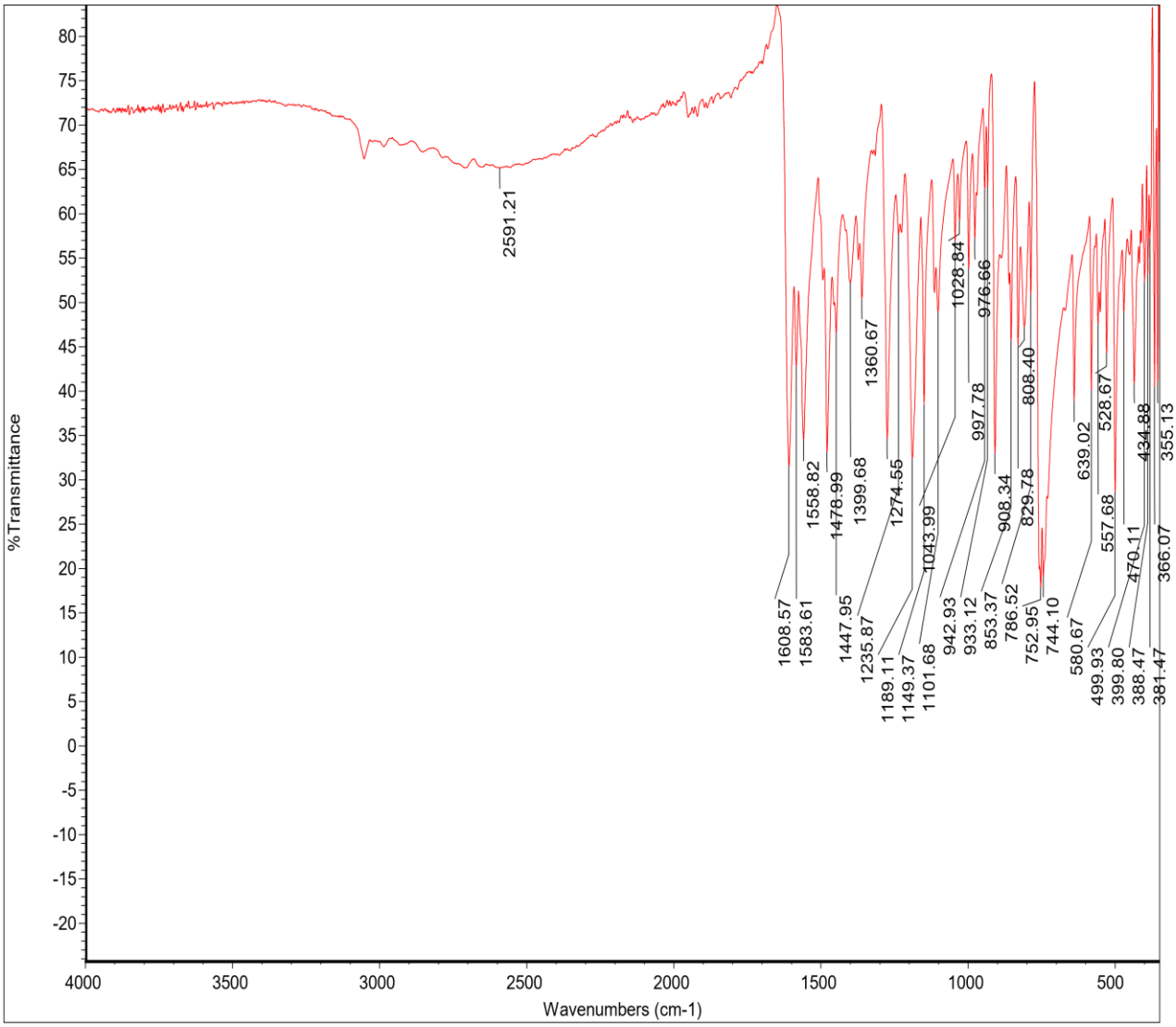
Zaheer, Z.R. (2009). Sub- and post-micellar catalytic and inhibitory effects of cetyltrimethylammonium bromide in the permanganate oxidation of phenylalanine. *Colloids and Surfaces B*, 69(2): 251–256.

Ziessel, R. (2001). Schiff-based bipyridine ligands. Unusual coordination features and mesomorphic behaviour. *Coordination Chemistry Reviews*, 216: 195-223.

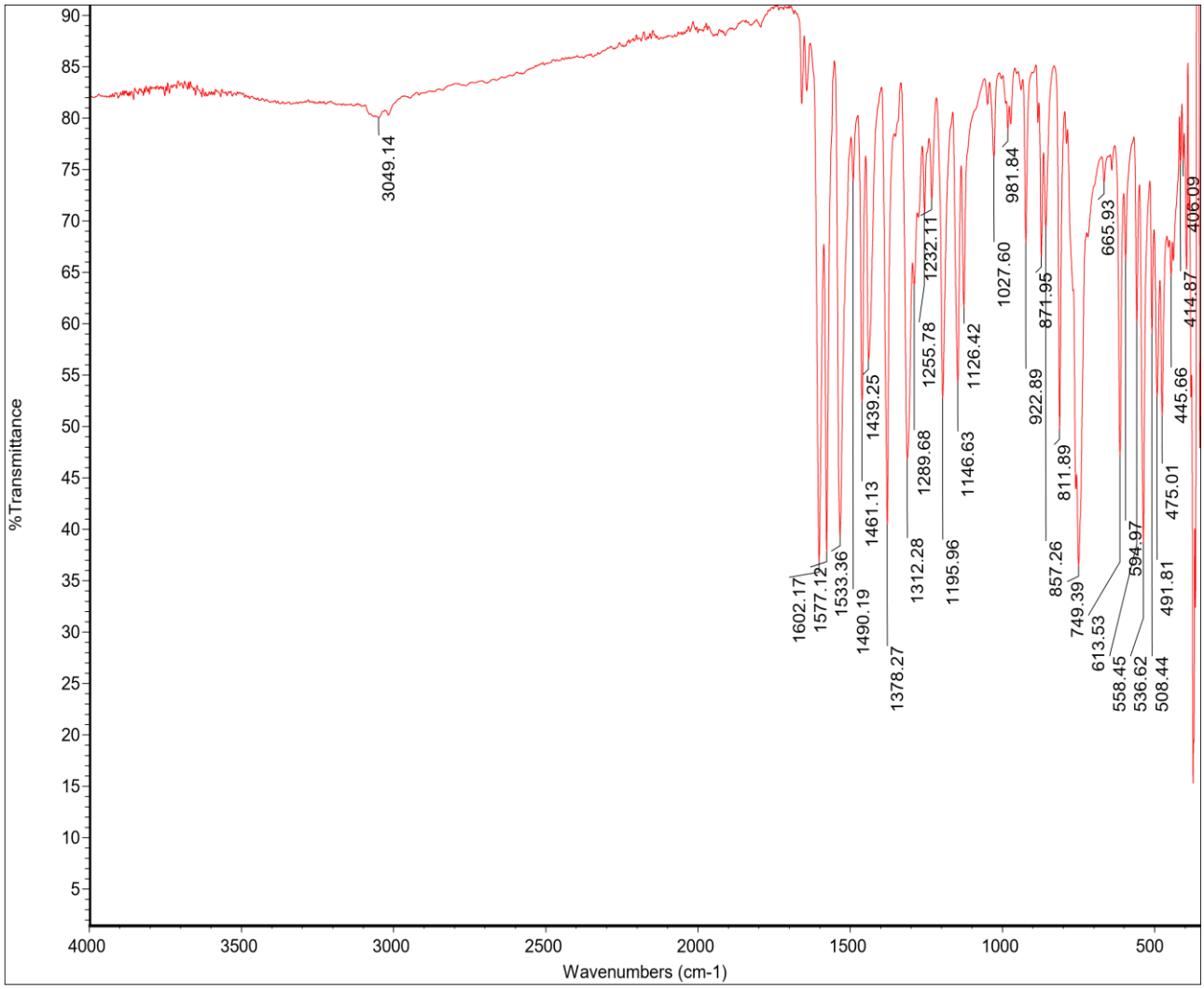
Zouni, A., Witt, H.T., Kern, J., Fromme, P., Krauss, N., Saenger, W. and Orth, P. (2001). Crystal structure of photosystem II from Synechococcus elongatus at 3.8 Å resolution. *Nature*, 409: 739-743.

APPENDICES

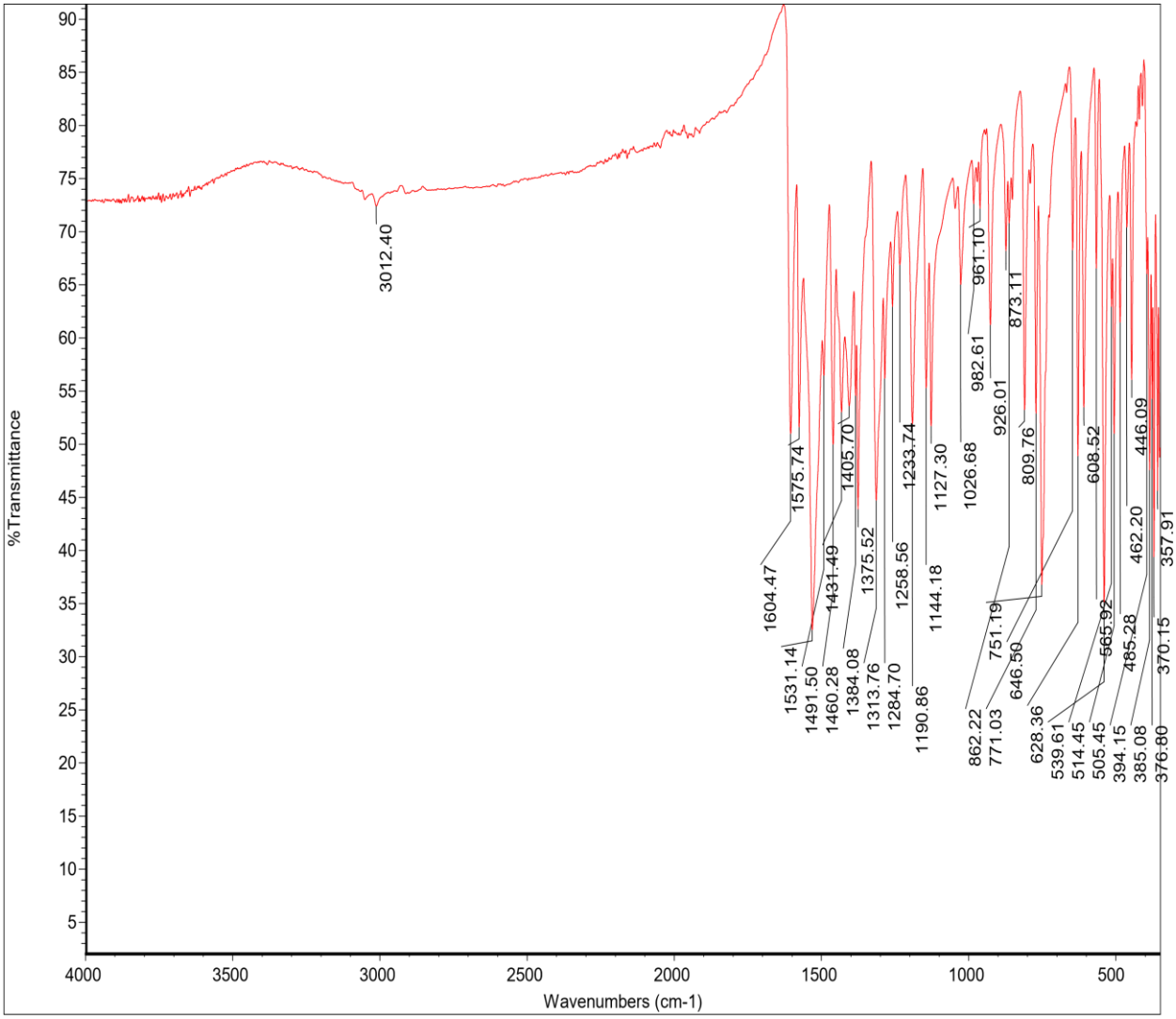
Appendix I: FTIR spectrum of salphen



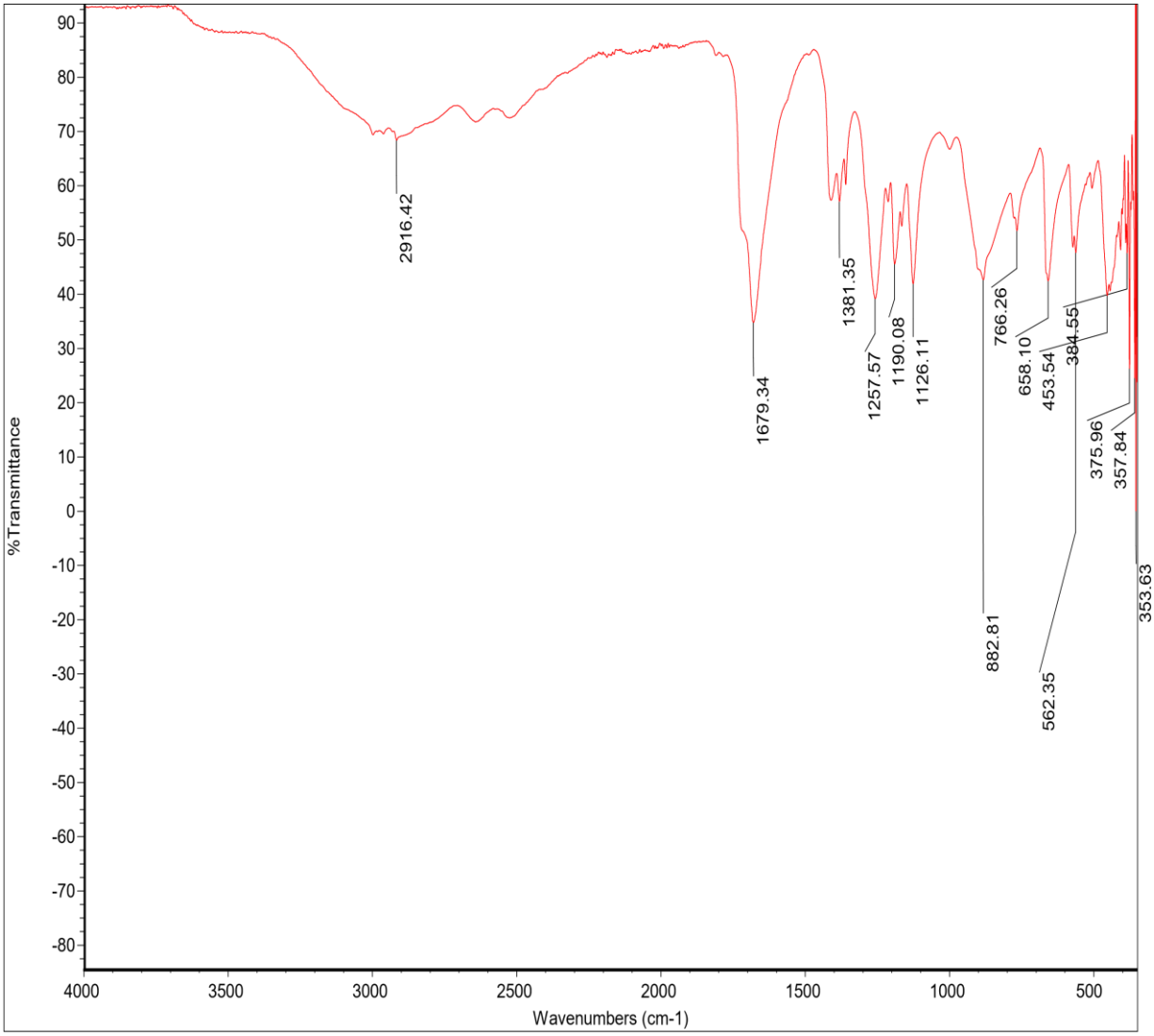
Appendix II: FTIR spectrum of $[Fe(salphen)]^+$



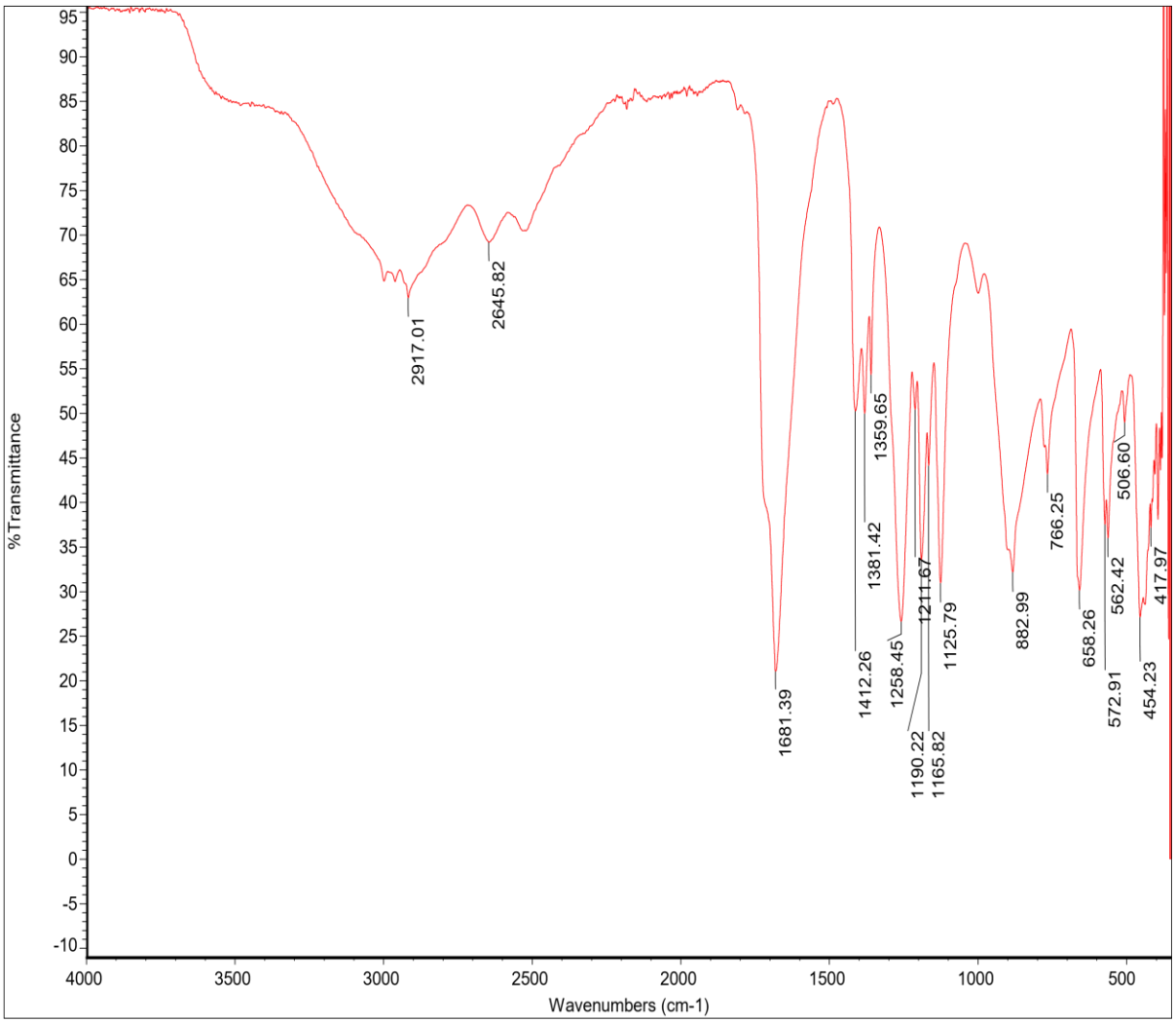
Appendix III: FTIR spectrum of $[Mn(salphen)]^+$



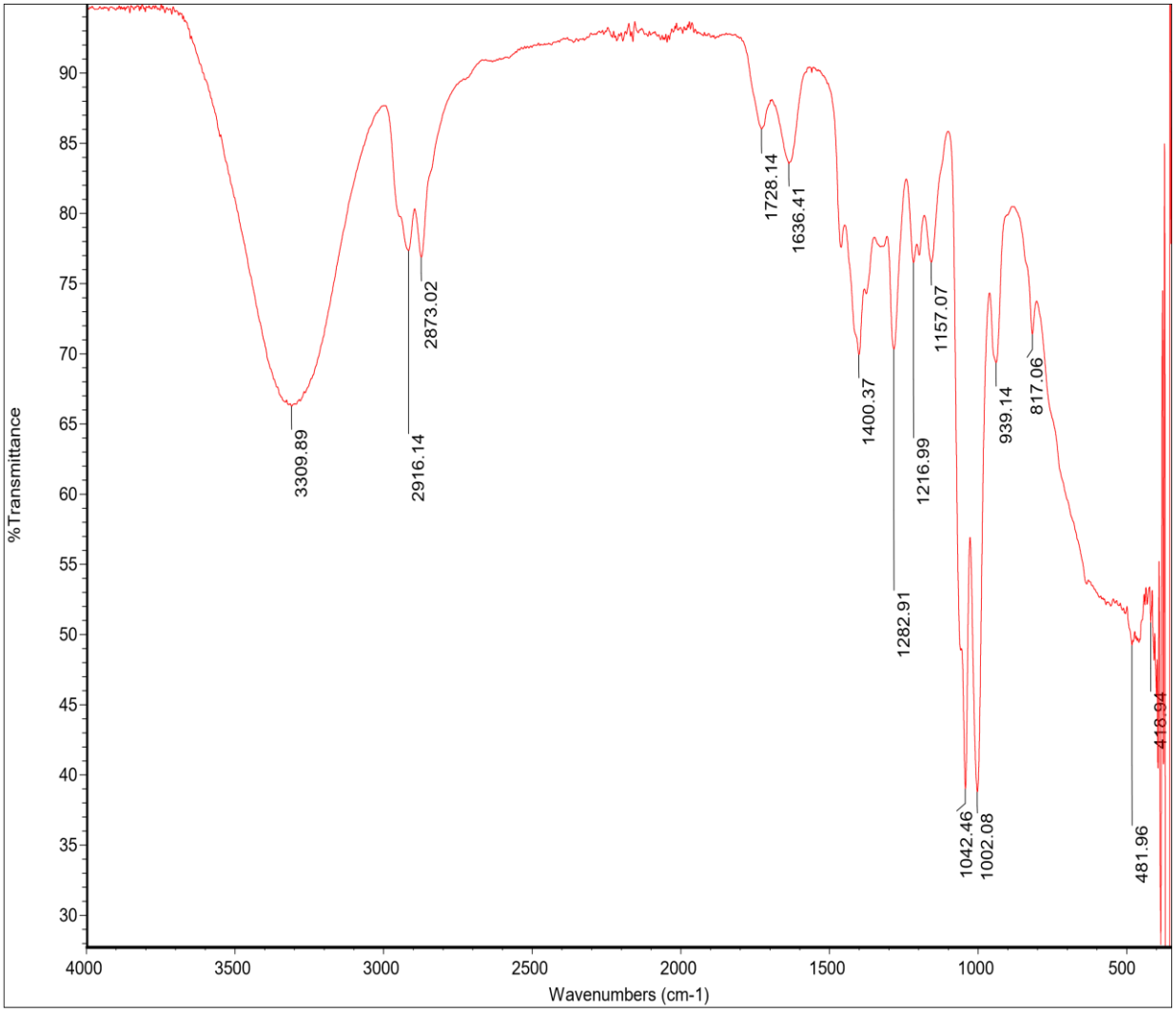
Appendix IV: FTIR spectrum of the product of reaction of TSH and [Fe(salphen)]$^{+}$



Appendix V: FTIR spectrum of the product of reaction of TSH and $[Mn(salphen)]^+$



Appendix VI: FTIR spectrum of the product of reaction of RSH and $[Mn(salphen)]^+$



Appendix VII: FTIR spectrum of the product of reaction of $S(CH_2CH_2OH)_2$ and $[Mn(salphen)]^+$

